A THREE-DIMENSIONAL TECHNIQUE FOR PREDICTING FIRST- AND SECOND-ORDER HYDRODYNAMIC FORCES ON A MARINE VEHICLE ADVANCING IN WAVES

by

HOI SANG CHAN, B.Sc.

Submitted as a Thesis for the Degree of Doctor of Philosophy,

Department of Naval Architecture and Ocean Engineering, University of Glasgow.

August 1990

DECLARATION

Except where reference is made to the work of others, this thesis is believed to be original.

DEDICATION

To my parents and my sister.

ACKNOWLEDGEMENTS

I would like to express my sincere gratitude to Professor D. Faulkner, Head of Department, for his help in making this research possible, especially with regard to obtaining financial support through the Froude Research Scholarship of the Royal Institute of Naval Architects and the Overseas Research Student Award, for which I am grateful.

I wish to express my sincere thanks to Dr.A.Incecik for his supervision, valuable advice and encouragement throughout this research. My special thanks go to Mr.N.S.Miller, formerly senior lecturer in the Department, who has carefully read my thesis and given valuable comments. My thanks also go to the researchers and staff of the Department for their assistance and friendship.

Finally I am deeply indebted forever to my parents for their continuous encouragement and support.

NOMENCLATURE

Symbols not included in the list below are only used at a specific place and are explained when they occur.

A	Area of waterplane.
A_y	First moment of waterplane area about y-axis.
A_{yy}	Second moment of waterplane area about y-axis.
A_{jk}	Hydrodynamic added mass in the j-th direction due to the k-th mode of motion; expressed in the system o–xyz.
B	Characteristic breadth of the body.
B_{jk}	Hydrodynamic damping coefficient in the j-th direction due to the k-th mode of motion; expressed in the system o–xyz.
C_B	Block coefficient of the body $C_B = V/(L \,.\, B.\, T)$
C_w	Waterplane area coefficient $C_w = A/(L \,.\, B)$
C_{jk}	Hydrostatic restoring coefficient in the j-th direction due to the k-th mode of motion; express in the system o–xyz.
D	Characteristic depth of the body.
	Draught of the body.
D	Fluid domain exterior of the body.
$\hat{D}$	Fluid domain interior of the body.
$E_1(Z)$	Exponential integral.
$\vec{F}$	Force vector.
F_j^{δ}	Hydrostatic restoring force in j-th direction.
F_j^{R}	Hydrodynamic reactive force in j-th direction.
F_j^{W}	Wave exciting force in j-th direction.
$\lvert F'_j \rvert$	Non-dimensional wave exciting force in j-th direction.
$\bar{F}_j^{(2)}$	Mean second-order force in j-th direction.

F_n	Froude number $F_n = U/\sqrt{(gL)}$.
$G(\vec{x}; \vec{\xi})$	Green function.
GM_T	Transverse metacentric height.
H	water depth.
$H(\vec{x}; \vec{\xi})$	Regular harmonic function.
	Inverse Fourier transform operator.
$H^{**}(\vec{x}; \vec{\xi})$	Fourier transform operator.
H(x)	Heaviside step function.
Im	Imaginary part of a complex quantity.
$J_o(x)$	Bessel function of the first kind of zero order.
$J_1(x)$	Bessel function of the first kind of first order.
L	Characteristic length of the body.
L_o	Intersection line of the body surface S_o and the undisturbed free surface S_F.
L_∞	Simple closed curve on the undisturbed free surface S_F at far-field.
LCB	Longitudinal distance of the centre of buoyancy from midship.
M_{ij}	Element of mass matrix.
$\vec{M}$	Moment vector.
$N(\vec{x}; \vec{\xi})$	Near-field function.
PV	Principal-value of a integral.
Re	Real part of a complex quantity.
$S, \hat{S}$	Fluid boundary surfaces exterior and interior of the body respectively.
$S_F, \hat{S}_F$	Undisturbed free surfaces exterior and interior of the body respectively.
S_H	Sea bottom surface at water depth h (h may be infinite).
S_o	Mean wetted body surface.
S_w	Wetted body surface in steady flow (mean wetted body surface).
S_w	Wetted body surface in unsteady flow.
S_∞	Control boundary surface at far-field.
T	Draught of the body.
U	Mean forward speed of the body.
V	Volume of the body.

$\vec{V}$	Velocity field of total fluid flow.
$\vec{V}_s$	Local velocity of a point on the surface S_w.
VCG	Vertical distance of the centre of gravity about base.
$W(\vec{x};\vec{\xi})$	Far-field function.
$\vec{W}$	Velocity field of steady flow.
Z	Complex variable.
a_{jk}	Non-dimensional hydrodynamic coefficient of the mass term in the j-th force equation due to motion in the k-th mode; expressed in the system o–xyz.
b_{jk}	Non-dimensional hydrodynamic coefficient of the damping term in the j-th force equation due to motion in the k-th mode; expressed in the system o–xyz.
f	Frequency number $f = \omega\sqrt{(L/g)}$.
g	Gravitational constant.
h	Water depth.
i	$\sqrt{(-1)}$
$\vec{i}, \vec{j}, \vec{k}$	Unit vectors in x,y and z directions respectively.
k_{xx}	Radius of gyration of the body about x-axis.
k_{yy}	Radius of gyration of the body about y-axis.
k_{zz}	Radius of gyration of the body about z-axis.
$\vec{n}(n_1,n_2,n_3)$	Normal vector outward the boundary surface.
$o–x_oy_oz_o$	Space-fixed coordinate system.
o–xyz	Steady translating coordinate system.
	Global coordinate system for body discretisation.
o–x'y'z'	Body-fixed coordinate system.
$\bar{o} - \bar{x}\bar{y}\bar{z}$	Local coordinate system for surface element.
p	Fluid pressure.
r	Magnitude of $\vec{x} - \vec{\xi}$.
r'	Magnitude of $\vec{x} - \vec{\xi}'$.
$\vec{r}'$	Position vector of a fluid particle on the surface S_w.
–1/r	Source singularity.

$1/r'$	Image sink.
$-1/r_h$	Finite depth source.
$\vec{s}$	Unit tangent vector along the curve L_o.
t	A time variable.
	A parameter.
$\vec{x}(x, y, z)$	Coordinates of a field point.
$\vec{x}'$	Resultant vector of $\vec{x} - \vec{\xi}'$.
(α,β)	Fourier transform coordinates.
$\dot{\alpha}$	Local velocity of a point on the surface S_w.
$\vec{\alpha}$	Local oscillatory displacement vector.
β	Angle of incident wave with x-axis (180° at head sea).
γ	Angle at which the pole $k_1 = k_2$.
$\delta(x)$	Dirac delta function.
$\vec{\delta}$	Unsteady translational displacement vector.
δ_{ij}	Kronecker delta symbol.
ε	Rayleigh artificial viscosity.
	Perturbation parameter.
Φ	Total velocity potential of fluid flow in the fluid domain D.
$\hat{\Phi}$	Total velocity potential inside the domain D.
$\bar{\Phi}$	Velocity potential of steady flow.
$\tilde{\Phi}$	Velocity potential of unsteady flow.
$\bar{\phi}$	Steady perturbation potential.
ϕ_o	Incident wave potential per unit amplitude.
ϕ_j	Radiation wave potential per unit amplitude.
ϕ_7	Diffraction wave potential per unit amplitude.
λ	Wave length.
μ	Dipole strength.
	Finite depth parameter.
υ	Wave number = $2\pi/\lambda$.
θ_j	Phase angle in agrees of wave exciting force or motion in the j-th mode with respect to the origin of the system o–xyz.

ρ	Density of fluid.
	Horizontal distance between source and field points.
ρ_B	Density of body material.
σ	Source strength.
τ	Correlation parameter $\tau = f F_n$.
$\vec{\tau}$	Unit vector tangential to surface S_o and normal to the curve L_o.
$\vec{\Omega}$	Unsteady rotational displacement vector.
ω	Wave encounter frequency.
	Frequency of oscillation.
ω_o	Incident wave frequency.
ξ_o	Incident wave amplitude.
ξ_r	Relative wave elevation.
$\lvert\xi'_j\rvert$	Non-dimensional motion amplitude response in j-th mode of motion.
$\vec{\xi}(\xi, \eta, \zeta)$	Coordinates of a source point in the system o–xyz.
$\vec{\xi}'(\xi, \eta, -\zeta)$	Coordinates of mirror image of the source with respect to the plane $z = 0$
	in the system o-xyz.
ζ	Exact free surface elevation.
ζ_i	Incident wave profile.
$\bar{\zeta}$	Steady free surface elevation.
∇	Grad operator.
∇^2	Laplace's operator.

CONTENTS

PAGE NUMBERING AS ORIGINAL

LIST OF FIGURES

LIST OF TABLES

SUMMARY

This thesis presents theoretical formulations and numerical computations for predicting first- and second-order hydrodynamic forces on a marine vehicle advancing in waves. The theoretical formulation starts with the derivation of the governing equations for the boundary-value problem of potential flow and its consequence leads to linearised radiation and diffraction problems using the perturbation expansion technique. Solutions of these two problems are obtained by solving the three-dimensional Green function integral equations over the mean wetted body surface. The forward speed free surface Green function representing a translating pulsating source potential for infinite water depth and finite water depth is derived using double Fourier transformation technique. This source potential reduces to an oscillating source at zero speed or to a Kelvin source at zero frequency. In order to solve the three-dimensional Green function integral equations efficiently, symmetry properties of the Green function and the body surface are exploited in the numerical implementation.

Using a fully submerged ellipsoid and a half-submerged ellipsoid as examples, the free surface and forward speed effects on hydrodynamic coefficients are investigated. Their cross coupled hydrodynamic coefficients calculated by the present theory satisfy with Timman-Newman relationships. Numerical results for the first-order hydrodynamic coefficients, the wave excitation loads and the resulting motion responses of surface ships are presented. For zero speed case excellent correlations between the calculated and experimental results are found. For the forward speed case, the three-dimensional translating pulsating source modelling and three-dimensional oscillating source modelling with simple speed corrections on the linearised body boundary condition for pitch and yaw motions are used for a realistic ship. When the calculated results are compared with available experimental data, the three-dimensional translating pulsating source modelling gives better correlations than the three-dimensional oscillating source modelling.

Based on the first-order solutions, the mean second-order forces and moments are obtained by direct integrating second-order pressures over the mean wetted body surface. Using zero speed horizontal drifting forces and mean yaw moment as examples, the predictions of the mean second-order forces and moments are compared with available experimental results and found good agreement. For forward speed case the numerical computations for the added resistances of surface ships in head waves are performed by the three-dimensional translating pulsating source modelling and three-dimensional oscillating source modelling. The performance of the former is much better than the latter in comparison with available experimental results. It is found that the successful prediction of the peak of the added resistance is critically dependent upon the motion response results, especially in pitch. Effects of ship heading, forward speed, water depth on the first-order and second-order hydrodynamic forces are investigated.

CHAPTER 1
INTRODUCTION

The first attempt to study unsteady wave forces on a ship was made by Froude (1861) and subsequently by Krylov (1896). This resulted in the Froude-Krylov hypotheses which calculates the pressure field of the undisturbed incident waves. In parallel with the study of unsteady wave forces Kelvin (1887) and Michell (1898) opened a door to study the steady-state wave resistance theory. The Froude-Krylov approach dominated ship dynamics for almost half a century and had been refined by the inclusion of the added mass terms (but neglecting the free surface effects) initiated by Lewis (1929) and Lockwood-Taylor (1930), the Doppler effects due to forward speed (Manning 1939) and the development of numerical procedures to include the effect of wave profile (the Smith effect). In the same period very significant analytical foundations in the theory of ship motions were laid down by Kochin (1939), Havelock (1940) (1942), and Haskind (1946). Haskind made use of Green's identities to construct the velocity potential due to the presence of a ship hull and derived the necessary Green's function. The resulting integral equation was solved by using a thin ship approximation. A notable feature of Haskind's work was to separate the complete linearised problem into the diffraction problem and radiation problem and find their solutions. Some years later John (1949) (1950) presented a rigorous mathematical analysis for the motions of floating bodies and Peters & Stoker (1957) introduced the perturbation expansion technique to naval hydrodynamics and derived a thin ship theory of motion. Their thin ship approach was not successful from the practical applications point of view, but the methodology opened new and fertile grounds.

Naval Architects have not awaited a three-dimensional theory of ship motions which is both rigorous and practical. Instead the numerical solutions of a simpler class

of two-dimensional problems for free floating bodies without forward speed have been utilised. This type of problem was first solved rigorously by Ursell (1949) who used a series of multipoles to present the radiation potential for the heaving motions of a half immersed circular cylinder in deep water. The method was extended by Tasai (1959), Porter (1960) and De Jong (1969) to other shapes using conformal mapping transformation. The method of integral equations in the form of source distributions for two-dimensional problems was first used by Ursell (1953) to calculate the hydrodynamic coefficients of a half immersed circular cylinder in short waves. The practical use of the source distribution method for a two-dimensional ship shaped section is due to Frank (1967), which is often referred to as the 'Frank Close Fit' method.

The utilisation of two-dimensional methods coupled with the strip theory approximation for ship motions was initiated by Korvin-Kroukovsky (1955) as an extension of the slender body theory in aerodynamics. Some refinements were provided by Korvin-Kroukovsky & Jacobs (1957). Since then more systematic derivations were given by Ursell (1962) and Newman & Tuck (1964) for the long wave slender body theory and Ogilvie & Tuck (1969) and Salvesen et al (1970) for the short wave strip theory. These theories are based on the assumptions of potential flow, slender ship and small amplitude motions (motion amplitudes are assumed to be small compared to the transverse dimensions of the ship). Radiation wave length is assumed to be of the same order as ship length for the long wave slender body theory but it is in the same order as ship beam for the short wave strip theory. The long wave slender body theory is applicable for the zero speed case only and the short wave strip theory for high frequency of oscillation and low forward speed only. The strip theory does not have any three-dimensional interactions between sections nor any forward speed effects on the free surface although Ogilvie and Tuck provided a higher order approximation for the forward speed effect.

For radiation problem, Newman (1978) proposed a unified strip theory that

improves the short wave strip theory of Salvesen et al (1970) in the high frequency regime and reduces to the long wave slender body theory in the low frequency limit. The unified strip theory starts with the solution of the two-dimensional near-field problem and the solution of the three-dimensional far-field problem. The near-field solution includes the ordinary strip theory solution supplemented with an unknown longitudinal interaction function. The three-dimensional far-field solution is represented by a line distribution of sources and dipoles. The unknown longitudinal interaction function is solved by analysing the near-field behavior of the far-field solution and matching with the outer behavior of the near-field solution. In the unified theory the inner and outer wave fields are compatible for the case of zero forward speed. However, in the case of forward speed, these wave fields are not compatible since the inner solution of the two-dimensional problem is still basically one corresponding to a single wave length. The diffraction problem was solved by Newman & Sclavounos (1980). Later Børrsen & Faltinsen (1984) extended the unified strip theory to finite water depth.

In spite of the unified strip theory which brings in a certain amount of three-dimensional correction to the basic strip solution, a number of unsettling questions of a hydrodynamic nature remain. Firstly, in three-dimensional flow, the interaction of the uniform flow and oscillatory flow generates complex free surface waves in the near-field as well as in the far-field. Secondly strip theories can produce only two-dimensional waves which are unaffected by the forward motion and so some restrictions must apply to the forward speed.

In order to place no restrictions on the frequency of oscillation and the forward speed of the ship, the author is going to solve the three-dimensional unsteady forward motion problem. In the present work the author develops a method of computing the three-dimensional flows generated by a translating pulsating source disturbance to investigate the effects of interaction between the forward speed and the frequency of oscillation and also the water depth effects on these flows. The first-order radiation and

diffraction problems are solved by means of three-dimensional source distributions over the mean wetted body surface. Once the first-order velocity potentials for these two problems and the resulting motion responses are obtained, the mean second-order wave forces are pursued by directly integrating second-order pressures over the mean wetted body surface. The content and order of presentation of this thesis is briefly summarised below.

Chapter 2 presents a theoretical formulation of the three-dimensional potential flows due to steady and unsteady forward motions of a marine vehicle in waves. The exact boundary conditions in the formulation lead to a non-linear problem which is intractable in analytical or numerical computations. In order to make the problem amenable for solution, the problem must be simplified through linearisation. It is shown that the complete linearised free surface condition requires the assumption that the steady perturbation potential due to steady forward motion is of higher order and so can be neglected in the unsteady free surface flows away from the body which is thin, slender or fully submerged. If the steady flows around the body are as small as those on the free surface, all convective effects of the steady perturbation flows on the body surface are negligible.

In Chapter 3 the three-dimensional Green function integral equation method is derived from Green's identities to find the velocity potential of the three-dimensional flows in the presence of a body. Due to numerical difficulties in the integral equations for external flows created by forward motion, the integral equations are modified by combination of external and internal fictitious flows. This modification leads to dipole and source distribution methods. For the unsteady forward motion problem the dipole distribution method is not attractive since the free surface integral is present and some convective terms are unknown a priori. Therefore the source distribution method is employed in the present work to obtain the velocity potential. Methods of avoiding or removing the irregular frequencies present in integral equations are discussed.

In Chapter 4 the Green function representing a translating pulsating source beneath the free surface of infinite water depth and finite water depth is derived by using a double Fourier transform technique. Single integral representation of the Green function for infinite water depth is obtained while the Green function for finite water depth consists of the finite depth part and infinite depth part. The characteristics of this Green function are discussed and illustrated for various combinations of forward speed and frequency of oscillation. The interaction effects of the forward speed and the frequency of oscillation, and the water depth effects on the free surface wave patterns are demonstrated.

Chapter 5 describes the numerical implementation of the Green function method by first introducing the discretisation of boundary integral equations and wetted body surface. The description of integration over surface elements then follows. In order to reduce computing time in the evaluation of the forward speed free surface Green function, the symmetry properties of the Green function are exploited. Furthermore, the symmetry of body is utilised to save the computing storage and time.

In Chapter 6 a theoretical formulation of hydrodynamic forces on a body moving in regular waves is presented. Numerical computations are carried out to predict hydrodynamic loads on a fully submerged ellipsoid, a half-submerged ellipsoid, a Series-60 ship and a 200,000 dwt tanker. For a body having two planes of symmetry such as an ellipsoid the translating pulsating source modelling technique is validated by the well known Timman-Newman relationships. Forward speed computations for the Series-60 ship are performed by using the three-dimensional translating pulsating source modelling and three-dimensional oscillating source modelling with simple speed correction on the linearised body condition for pitch and yaw motions. When the calculated results are compared with the available experimental data the three-dimensional translating pulsating source modelling gives better agreement than the three-dimensional oscillating source modelling. Both mathematical models give poor correlations in predicting roll and pitch damping coefficients. The reasons for these

discrepancies are discussed. Effects of ship heading, forward speed and water depth on the hydrodynamic forces and ship motions are discussed.

Chapter 7 presents a theoretical formulation of the second-order forces and moments acting on a body with a forward speed in regular waves. Without solving the second-order velocity potential numerical calculations for the mean second-order forces and moments on an ocean-going barge, a 200,000 dwt tanker and three Series-60 ships with different block coefficients are carried out by using the three-dimensional source distribution technique coupled with the near-field method. Zero speed computations for the barge and tanker show good agreement with available experimental data. Forward speed computations for the added resistance of three Series-60 ships in head waves are carried out by using the three-dimensional translating pulsating source modelling and three-dimensional oscillating source modelling with simple speed correction on the linearised body boundary condition for pitch and yaw motions. In comparison with the available experimental data of added resistance, the performance of the translating pulsating source modelling is much better than the oscillating source modelling, especially at the peak value of the added resistance and in short wave region where a similar asymptotic trend is obtained by the translating pulsating source modelling. Effects of ship heading, forward speed and water depth on the mean second-order forces and moments are discussed.

Finally, a review of main conclusions is given in Chapter 8.

CHAPTER 2

FORMULATION OF THREE-DIMENSIONAL FLOW

2.1 Introduction

This chapter is devoted to describing the formulation of three-dimensional flow, which forms the basis for the computation of a boundary-value problem for a rigid body travelling at a constant velocity on the surface of sea. The problem of determining a particular flow caused by the presence and forward motion of the body amounts mathematically to finding a velocity potential which is based on the assumptions of an inviscid and incompressible fluid. The flow field of this ideal fluid is known as 'Potential Flow' or 'Irrotational Flow'. The velocity field of an irrotational flow is always expressible in terms of the gradient of some scalar function Φ (i.e. the velocity potential) which must satisfy not only the equation of continuity (i.e. the Laplace's equation) but also the prescribed boundary conditions of the given problem. It will be noted in the first part of this chapter that the exact formulation of these conditions leads to a non-linear problem which is so complicated that no solution of practical application can be found. Therefore, a theoretical formulation of a linear boundary-value problem in steady and unsteady flows induced by forward and oscillatory motions of the moving body will be carried out in the second part of this chapter by means of a perturbation expansion.

2.2 Assumptions of fluid properties

The first step in solving a boundary value problem is to set up differential equations such as Laplace's equation which will describe the flow field. The degree of complexity of these equations depends very largely on the mathematical description of

fluid properties and flow field. These differential equations are usually difficult to solve if one insists on the exact mathematical description of the fluid properties and the flow field involved in the problem. It is necessary to introduce certain simplifying assumptions in order to make the formulation of the problem amenable to analysis.

In order to represent a possible case of potential flow, we assume that there exists a scalar function which must conform to the equation of continuity at every point in the flow field except singular points. This scalar function is well known as 'the velocity potential'. A velocity potential does exist if the following assumptions can be made

1. The fluid is homogeneous.
2. The fluid is incompressible.
3. The fluid is inviscid.
4. Surface tension is neglected.

Although the density of water in ocean varies with both position and time, these variations are small enough to assume homogeneous sea water in ocean. Water can be regarded incompressible since it has a bulk modulus high enough to make this assumption. Moreover in an ocean surface waves generated by wind and gravitational effects cannot produce extremely high acceleration, as in the phenomenon of water hammer in which the effect of compressibility of water should be taken into consideration. It can be shown that an incompressible and homogeneous fluid leads to zero divergence of the velocity field from the conservation of mass. The requirement for the existence of a velocity potential is that the flow be irrotational to an extent that the vorticity of the fluid is zero throughout the fluid domain. The vorticity of a fluid element cannot be changed except through the action of viscosity and non-uniform dissipative effects. The assumption of inviscid fluid is reasonable since we are dealing with water of small viscosity and regions of irrotational flow constitute a large portion of the flow field. The zero divergence of velocity field and the irrotational or inviscid flow leads to Laplace's equation. The main advantage of introducing the concept of velocity potential from irrotational flow is that the problem is reduced to a scalar field problem rather than

a vector field problem. Once the velocity potential is solved from the governing equations of motion, the velocity field can be determined by taking the gradient of the velocity potential and the pressure field can in turn be calculated from Bernoulli's equation.

In most cases, the viscous effects may be neglected on motions such as heave and pitch, which can be well predicted by a velocity potential based theoretical approach, due to the small amplitudes and large inertia effects of these modes. On the other hand, the modes of surge, sway and yaw may be influenced significantly by nonlinear and viscous effects where restoring forces do not exist if the body travels with a forward speed and these forces are weak for a stationary body with mooring arrangements. In the case of roll, the radiation damping of a ship is weak, especially at low frequencies near resonance. Thus roll motion is extremely sensitive to viscosity effects especially at the resonant frequency where a large amplitude occurs. Consequently, nonlinear effects on roll damping are significant in terms of energy dissipation. At present there exists no satisfactory method of predicting the roll motion of ships with engineering accuracy. For marine vehicles travelling with forward speed, the viscous effects becomes significant because of the growth of the boundary layer toward the aft end of the body and the rotational flow in the boundary layer will leave the body at the trailing edge in the form of a narrow wake. In order to superpose the effects of viscosity on the solutions of the potential flow, empirical formula may be helpful.

The surface of water acts, in some ways, like a stretched membrane. When very short waves such as capillary waves curve the 'membrane' a great deal, the surface tension tries to flatten it out again. Capillary waves occur in the period range from zero to 0.1 sec, which is not interesting in engineering practice. We are dealing with ocean waves of period greater than 1 sec. where longer waves produce much less curvature per unit wave length, so that the water surface is not distorted so much. In this case the major force acting to flatten the sea surface is gravity, not surface tension. Thus it is reasonable to neglect surface tension effect except in model experiments where scale effects make surface tension significant.

2.3 Coordinate systems

To describe flow fields and motions of a rigid body travelling at a constant mean forward velocity $U\vec{i}$, it is convenient to refer the rigid body motion to various types of moving coordinate systems as well as to a fixed coordinate system. Let us consider three right-handed orthogonal coordinate systems as shown in Fig.2.1. The first is the space-fixed system $o\text{-}x_o y_o z_o$, the second is the steady translating system o-xyz with the same mean forward velocity as the body and the third is the oscillatory and translating system o'-x'y'z' fixed with respect to the body.

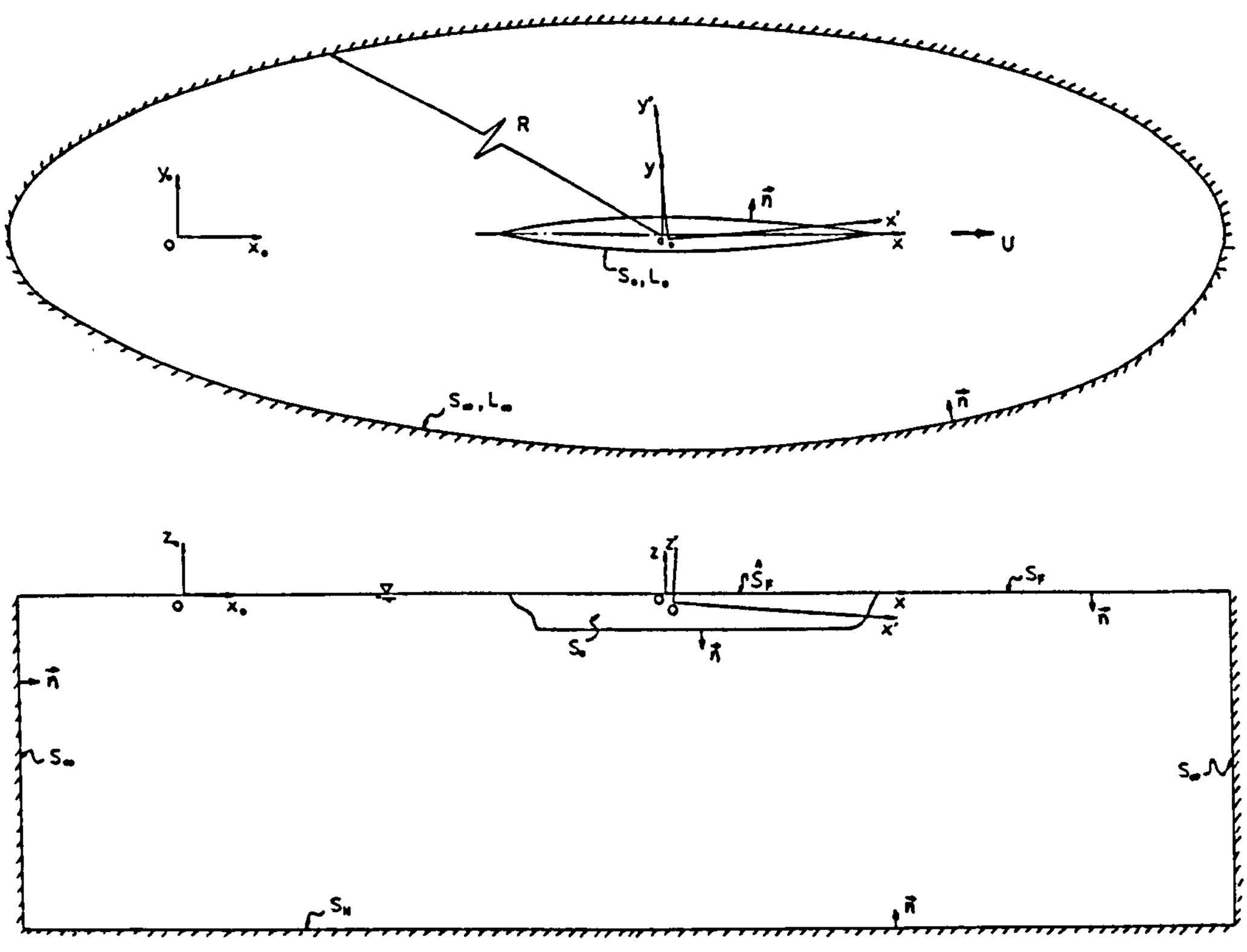

Fig.2.1 Coordinate Systems

The orientation of the space-fixed system $o\text{-}x_o y_o z_o$ is such that $o\text{-}x_o y_o$ plane coincides with the undisturbed free surface, the x_o-axis in the direction of the body's forward velocity and the z_o-axis vertically upward. This system facilitates the description of the free surface boundary condition.

The steady-translating system o-xyz is an inertia frame with the x-axis translating on the undisturbed free surface with the same mean forward velocity $U\vec{i}$ as that of the body. The axes of this system are always parallel to that of the space-fixed system $o\text{-}x_o y_o z_o$. The steady-translating system o-xyz is therefore related to the space-fixed system $o\text{-}x_o y_o z_o$ by the linear transformation

$$\vec{x} = (x, y, z) = (x_o - Ut, y_o, z_o) \qquad (2.1)$$

From the foregoing equation (2.1), it can be shown that the space-fixed system $o\text{-}x_o y_o z_o$ and the steady-translating system o-xyz coincide when the forward velocity of the body is zero. The steady-translating system o-xyz is used to describe the body motions in six degrees of freedom with complex amplitudes ξ_j (j=1,2,...6). Here j=1,2,3,4,5,6 refer to surge, sway, heave, roll, pitch and yaw motions respectively as shown in Fig.2.2.

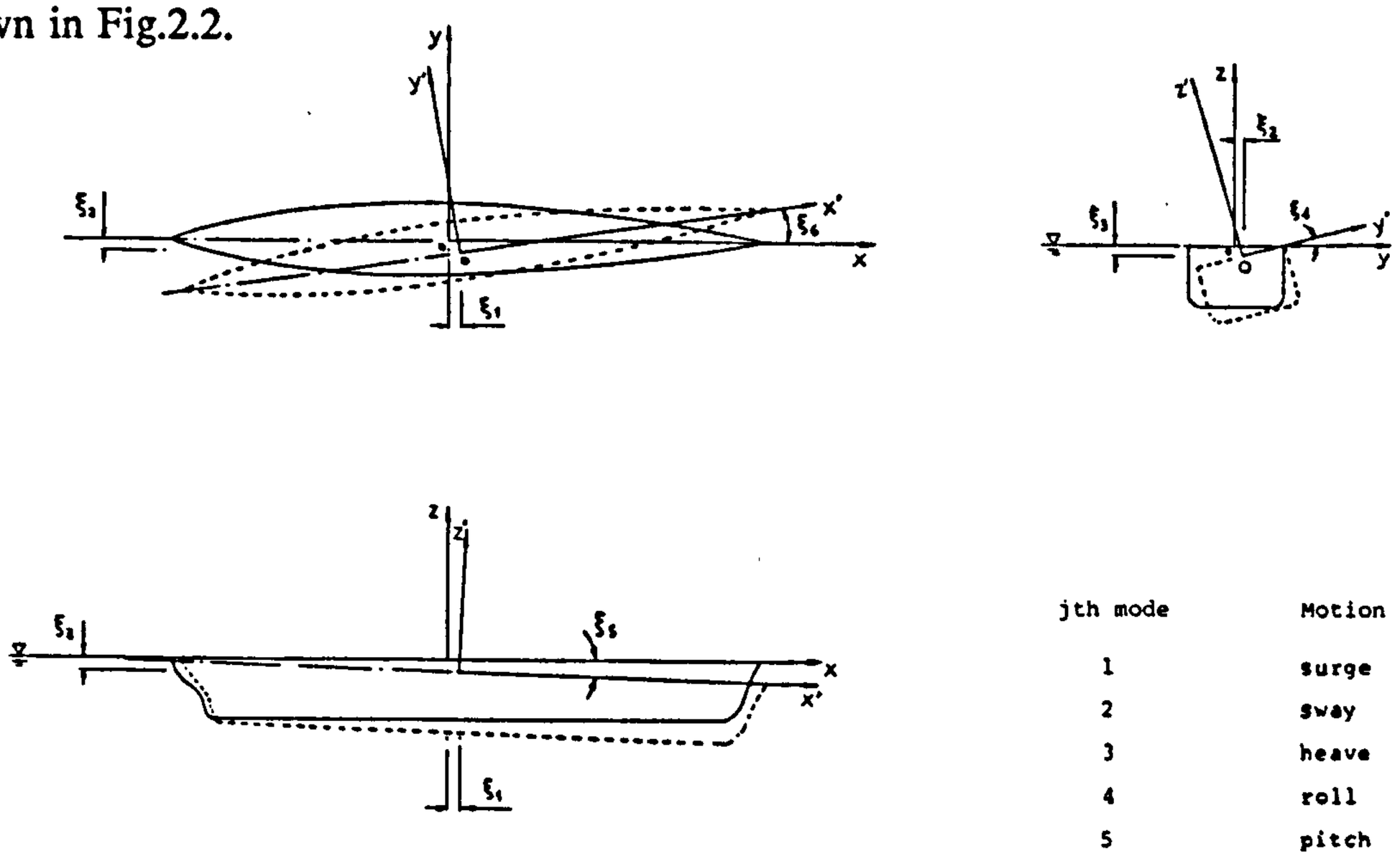

Fig.2.2 Orientation of Motions

The oscillatory and translating system o'-x'y'z' is the body-fixed frame which fluctuates with respect to the steady-translating system o-xyz. Therefore, the local oscillatory displacement $\vec{\alpha}$ of a point on the body's surface S_w is defined by

$$\vec{\alpha} = \vec{x} - \vec{x}' \tag{2.2a}$$

or
$$\vec{\alpha} = \vec{\delta} + \vec{\Omega} \times \vec{r}' \tag{2.2b}$$

where $\vec{\delta}=(\xi_1,\xi_2,\xi_3)$ and $\vec{\Omega}=(\xi_4,\xi_5,\xi_6)$ are the unsteady translational and rotational displacement vectors respectively. $\vec{r}'$ is the position vector of the point on the surface S_w relative to body-fixed frame o'-x'y'z'. In the steady equilibrium state $\vec{\alpha}$ is a constant, the body-fixed frame o'-x'y'z' and the steady-translating system o-xyz coincide. If the origin o' is at the centre of gravity which is on the undisturbed free surface, $\vec{\alpha}$ is equal to zero in a steady equilibrium state. The body-fixed frame o'-x'y'z' is the best way to describe the body boundary condition on the wetted body surface.

2.4 Formulation of non-linear problem

Based on our assumptions of an homogeneous, incompressible and inviscid fluid, there exists a velocity potential denoted by $\Phi(x_o,t)$ in the fluid domain D, which satisfies the Laplace's equation

$$\nabla^2\Phi(\vec{x}_o, t) = 0 \tag{2.3}$$

The velocity field of the flow is given by

$$\vec{V}(\vec{x}_o, t) = \nabla\Phi(\vec{x}_o, t) \tag{2.4}$$

Since Laplace's equation, due to its elliptic nature, has many solutions, some prescribed boundary conditions should be defined in the fluid domain in order to obtain the exact solution of a given problem. We deal with the motions of a rigid body travelling on/below the surface of an ocean which is assumed to be infinite in all horizontal directions and the boundaries enclosing the fluid domain consist of the free surface, the wetted body surface, the sea bed and a control surface at far-field. Sufficient conditions must be known concerning all boundaries on which the fluid encounters. These boundary conditions will be discussed in the following sections.

2.4.1 Free surface condition

The free surface is defined by its elevation

$$z_o = \zeta(x_o, y_o; t) \tag{2.5}$$

On the free surface, the kinematic and dynamic conditions must be satisfied. The kinematic condition is that a fluid particle at the surface always remains at the surface whereas the dynamic condition specifies that the pressure p on the free surface must conform to Bernoulli's equation. Thus, the kinematic and dynamic conditions can be written respectively as

$$\frac{D}{Dt}(\zeta - z_o) = 0 \tag{2.6}$$

$$\Phi_t + \tfrac{1}{2}|\nabla\Phi|^2 + g z_o = 0 \tag{2.7}$$

where the total derivative $D/Dt = \partial/\partial t + \vec{V} \bullet \nabla$ in the space-fixed frame and the pressure p has been taken as zero without loss of generality.

Substituting equation (2.7) with $z_o=\zeta$ into (2.6), we have

$$(\frac{\partial}{\partial t} + \vec{V} \bullet \nabla)(\Phi_t + \tfrac{1}{2}|\nabla\Phi|^2 + g z_o) = 0 \qquad (2.8)$$

After some manipulations, we may get the following free surface condition on the exact free surface ζ

$$\Phi_{tt} + g\Phi_{z_o} + 2\nabla\Phi \bullet \nabla\Phi_t + \tfrac{1}{2}\nabla\Phi \bullet \nabla(\nabla\Phi \bullet \nabla\Phi) = 0 \qquad \text{on } z_o=\zeta \qquad (2.9)$$

This free surface condition, as it stands, is non-linear because it includes the last two quadratic terms. It is realised how difficult it is to solve this exact condition analytically because not only is the problem non-linear but also the elevation of the free surface ζ is not known a priori. Therefore we shall formulate a linear free surface condition in section 2.5.2 by means of a perturbation expansion.

2.4.2 Body boundary condition

When fluid is in contact with a rigid body boundary, kinematic conditions require that the fluid does not penetrate the boundary and that there no gaps between the fluid and the boundary.

For the body in motion, the prescribed statement implies that the fluid velocity component normal to the wetted body surface S_w equals the velocity component of the surface normal to itself. Then we have

$$\vec{V} \bullet \vec{n} = \vec{V}_s \bullet \vec{n} \qquad \text{on } S_w \qquad (2.10)$$

where $\vec{V}_s$ denotes the local velocity of the wetted body surface S_w relative to the body-fixed frame o'-x'y'z' and $\vec{n}$ is the unit normal vector outward to the fluid domain D.

$$\vec{V}_s = \dot{\alpha} \qquad \text{on } S_w \qquad (2.11)$$

In fact, the body boundary condition in equation (2.10) must be satisfied on the exact oscillating surfaceS_w. Since the exact oscillating surface S_w makes the condition mathematically intractable, we must expand the body boundary condition onto the steady surface $\bar{S}_w$ in a systematic manner so as to include the oscillatory flow induced on the body surface by its change of position in the steady-state field. We shall discuss the expansion of the body boundary condition in section 2.5.3.

2.4.3 Sea bed condition

The sea bottom S_H is, to some extent, irregular but we may assume the bottom to be horizontal at a finite depth h in the fluid domain. Since the sea bottom, unlike the wetted body surface, is a stationary boundary, the fluid particle on the bottom has zero velocity normal to the boundary, that is

$$\frac{\partial \Phi}{\partial n} = \frac{\partial \Phi}{\partial z} = 0 \qquad \text{on } z = -h \qquad (2.12)$$

Equation (2.12) is the sea bed condition for finite depth h. From an oceangrapher's point of view (Kinsman 1965), the deep water approximation to incident wave is justifiable only when the ratio of water depth h to wave length λ is greater than 1/2. Ocean wavelengths over 180 m are commonly found in heavy gales and swell has been observed with lengths of 800 m in the equatorial Atlantic. On this occasion, the sea bed condition for deep water is defined by

$$\frac{\partial \Phi}{\partial z} = 0 \qquad \text{at } z \to \infty \qquad (2.13)$$

2.4.4 Far field radiation condition

The boundary conditions on all the physical boundaries, namely, the free surface, the wetted body surface and the sea bed, given in the previous sections are not sufficient to ensure a unique solution to the problems in which the fluid domain occupies an unbounded region. Since the ocean is assumed to be infinite in all horizontal directions, the remaining boundary condition must be imposed on the flow field at infinity. This condition known as ' the far field radiation condition' is described by a fictitious boundary surface S_∞, at infinity, extending from the free surface to the sea bed.

The far field radiation condition, in certain cases, is clear from the physical problem. For example, the fluid motion produced by a stationary but steadily oscillating body seems to be outgoing waves at infinity in all horizontal radial directions and vanishes at infinity. This type of radiation condition was originally used in the study of acoustics by Sommerfeld (1949) and is often called the Sommerfeld condition : the waves must behave at infinity like progressing waves moving away from the source of disturbance. The Sommerfeld condition is specified for a cylindrical wave in the form

$$\lim_{r \to \infty} \sqrt{r}\left(\frac{\partial \Phi}{\partial r} - i\upsilon\Phi\right) = 0 \qquad (2.14)$$

where r is the horizontal radial distance away from the body and υ is a wave number. The Sommerfeld radiation condition given by equation (2.14) may be obtained by using Green's third identity associated with the velocity potential Φ and a circular wave potential on the far field enclosed surface. The quantity $\sqrt{r}$ in equation (2.14) is used to make the potential Φ regular everywhere in the fluid domain.

For the case of Kelvin waves due to a body moving steadily in positive x-direction in calm water, the wave disturbance is generated downstream only. The far field radiation condition for the Kelvin wave problem is defined by

$$\lim_{x \to +\infty} \Phi = 0 \tag{2.15}$$

It is apparent that equation (2.15) cannot be described by the Sommerfeld condition because the Kelvin wave disturbance is not in cylindrical form.

For the unsteady flow due to forward and oscillatory motions of the body moving with constant speed in waves, the far field radiation condition is hardly defined. This is because the propagation of surface waves generated by the interaction of the body motions and incident wave depends on two parameters, namely the forward speed and the frequency of oscillation. The steady waves (Kelvin waves) due to the forward speed motion interact with the unsteady waves generated by the diffraction of the incident waves and the radiation of the oscillatory body. As a consequence of these interactions, if the forward speed of the body is less than the group velocity of the diffracted waves and the radiated waves, the resultant waves will propagate upstream, otherwise they are confined to the downstream. Although the nature of the unsteady flows is complicated, we may assume that the potential Φ vanishes at infinity as no energy is radiated from infinity into the source singularities of the flow field.

$$\lim_{r \to \infty} \sqrt{r}\,\Phi = 0 \tag{2.16}$$

Equation (2.16) is not an obvious far field radiation condition. Apart from the specified far field radiation condition, the unique solution of the potential Φ in the boundary-value problem can be obtained by the treatment of initial-value problem or the proper interpretation of improper integral through Rayleigh's artificial viscosity ε. If the solution begins with determining the velocity potential as an initial-value problem, the far field radiation condition is not needed. The steady state of the solution, as time increases to infinity, is obtained and the final solution indeed satisfies the far radiation condition. The limit of time to infinity is introduced to choose an appropriate path of integration in the evaluation of the improper integral. A similar idea is used in the concept of Rayleigh's artificial viscosity ε.

2.5 Formulation of linearised problem

From the previous sections, we have shown that the boundary-value problem needs to be solved to determine a velocity potential which satisfies not only the Laplace's equation but also the prescribed conditions. It has been noted that the exact formulation of the boundary conditions leads to the non-linear free surface condition on $z_o=\zeta$ and the body boundary condition on unsteady body surface S_w. These two conditions make the problem mathematically intractable because not only the free surface condition is non-linear but also both the free surface ζ and the unsteady body surface S_w interact and are not known a priori. In order to solve the problem, we shall simplify it through linearisation. The linearisation means that all the quadratic terms appearing in the boundary conditions are assumed to be sufficiently small to be negligible. In developing a linearised boundary-value problem, we should realise that the mathematical description loses contact with reality to a great extent, but it gains the capacity to construct new solutions from the old ones by addition. For linearised problems the principle of superposition is applicable, any linear combination of solutions being itself a solution. The application of the principle of superposition to the ship motion problem is a powerful tool so that the responses of a ship to an irregular wave spectrum can be considered as the summation of the responses to regular waves of all frequencies present in the spectrum (St.Denis & Pierson 1953). By linearisation the flow field may be separated into steady and unsteady flows due to forward and oscillatory motions of a moving body. In the following sections, we shall derive linearised boundary conditions for steady flow and unsteady flow problems by means of perturbation expansions.

2.5.1 Perturbation expansion

The principle of perturbation expansion in classical hydrodynamic problems is that any functions entering into the problems may be expanded in a convergent power

series with respect to a small and dimensionless parameter ε. Then the velocity potential of the flow and all quantities derivable from the flow, such as wave elevation, fluid velocity, pressure, hydrodynamic forces and the motions of the body can be represented by convergent power series, for example :

- the total velocity potential Φ

$$\Phi(\vec{x}_o, t; \varepsilon) = \Phi^{(0)} + \varepsilon\Phi^{(1)} + \varepsilon^2\Phi^{(2)} + \ldots \tag{2.17}$$

- the free surface elevation ζ

$$\zeta(x_o, y_o, t; \varepsilon) = \zeta^{(0)} + \varepsilon\zeta^{(1)} + \varepsilon^2\zeta^{(2)} + \ldots \tag{2.18}$$

where the superscript denotes the order of variations. The zero order terms mean the static-state value associated with the time t=0. The series are substituted into the governing equation as well as the boundary conditions, and the like terms with respect to the powers of ε are grouped. Then the coefficients of each power yield a sequence of equations and boundary conditions, the coefficients of ε giving the first-order solution, those of ε^2 the second-order solution, etc. The perturbation expansion solves the problem systematically step by step starting from an exact initial solution to any required order solution. The discrepancy between the linearised problem and non-linear problem may be expected to be eliminated if the order of the solution is taken as high as possible. The higher the order is, the more complicated and expensive in computation the problem will become.

The power series in the perturbation expansion are convergent if and only if the perturbation parameter ε exists and is less than unity. There are various ways to choose the dimensionless parameter ε which help to determine the exact physical problem. In our fluid flow problem, we may separate the flow field into two special cases through linearisation. One is the steady perturbation flow due to the forward motion of the body

moving in calm water and the other is the unsteady flow due to the disturbances of the incident waves, diffraction waves and radiation waves caused by the presence and motions of the body in the steady field. We may express the total velocity potential Φ in the form

$$\Phi(\vec{x}_o, t) = \Phi(x + Ut, y, z, t) = \bar{\Phi}(\vec{x}) + \tilde{\Phi}(\vec{x}, t) \qquad (2.19)$$

where $\bar{\Phi}$ and $\tilde{\Phi}$ denote steady and unsteady potential respectively. Moreover each potential satisfies the Laplace's equation

$$\nabla^2\bar{\Phi}(\vec{x}) = 0 \qquad (2.20)$$

$$\nabla^2\tilde{\Phi}(\vec{x}, t) = 0 \qquad (2.21)$$

The dimensionless parameter ε attached to the steady potential $\bar{\Phi}$ assumes the disturbance of the free surface due to the forward motion of the body to be small. The assumption of small disturbance due to the forward motion implies that certain constraints must be imposed on the geometric dimensions of the body and on the speed of advance. In our engineering practice, the hull form of a high speed vessel is fine since the fine form causes small disturbance and, as a result, runs economically. The fine form relates the parameter ε to thinness, slenderness, or flatness. On the other hand, a full form vessel only runs at slow speed, which also causes small disturbance. This results in the slow speed assumption that the ratio of disturbance velocity to the mean forward speed U is small. Regardless of the physical nature of the parameter ε with respect to the steady potential $\bar{\Phi}$, it is reasonable to assume that the parameter ε is small enough to make the expansion of the steady potential $\bar{\Phi}$ valid.

In the linearised problem, the possible profiles of incident waves are restricted to small amplitudes. The parameter ε attached to the unsteady potential $\tilde{\Phi}$ is then related to the incident wave steepness which is much smaller than unity. Consequently, diffraction waves, radiation waves and the motion responses of the body are also considered to be of small amplitudes because they are created by the disturbance of

small amplitude incident waves due to the presence and motions of the body.

No mention is made of the existence of the perturbation expansions for other quantities such as the free surface elevation ζ because these quantities may be derivable from the velocity potentials.

2.5.2 Linearised free surface condition

If one insists on using the non-linear free surface condition given by equation (2.9), a possible method of solving this free surface condition on the exact free surface elevation ζ is iterative procedures using Rankine sources distributed on the wetted body surface as well as on the exact free surface. The iterative procedures start with an initial estimation of the free surface and of the velocity potential and then new solutions replace old ones until the exact boundary conditions are satisfied. Moreover, the Rankine sources do not satisfy the far-field radiation condition and as a result the source distributions must cover the infinite free surface which makes numerical calculations difficult. However, the iterative procedures suffer serious problems in the stability and convergence of solutions as well as being expensive in computation time.

On the other hand, we can employ the perturbation expansion to linearise the free surface condition to the first-order, as seems to be sufficient, and use Taylor series expansion to transform the exact free surface ζ to some known surface such as the undisturbed free surface. Since the flow field has been considered to be the combination of steady and unsteady flows, we must linearise both the steady and unsteady flow problems. If the disturbance on the free surface due to the steady forward motion is small, the unsteady velocity potential $\tilde{\Phi}$ is an order of magnitude greater than the steady velocity potential $\bar{\Phi}$. Before obtaining the expression of free surface condition for unsteady flow problem, we firstly consider the steady flow problem.

For a steady flow, the velocity potential $\bar{\Phi}$ due to the steady forward motion of the body is

$$\bar{\Phi}(\vec{x}) = -Ux + \bar{\phi}(\vec{x}) \tag{2.22}$$

where $\bar{\phi}$ is the steady perturbation potential. The velocity field of the steady flow relative to the steady-translating frame o-xyz is

$$\vec{W}(\vec{x}) = \nabla\bar{\Phi}(\vec{x}) = \nabla(-Ux + \bar{\phi}) \tag{2.23}$$

The kinematic and dynamic conditions on the steady free surface elevation $\bar{\zeta}$ can be written as

$$\frac{D}{Dt}(\bar{\zeta} - z) = 0 \tag{2.24}$$

$$(\frac{\partial}{\partial t} - U\frac{\partial}{\partial x})\bar{\phi} + \frac{1}{2}|\nabla\bar{\phi}|^2 + gz = 0 \tag{2.25}$$

where the total derivative is

$$\frac{D}{Dt} = \frac{\partial}{\partial t} + (\nabla\bar{\phi} - U\vec{i})\bullet\nabla = \frac{\partial}{\partial t} + \nabla\bar{\Phi}\bullet\nabla$$

with respect to the steady-translating frame o-xyz.

Re-arranging equation (2.25) with $\bar{\Phi}_t$=0, we have

$$gz = U\bar{\phi}_x - \frac{1}{2}\nabla\bar{\phi}\bullet\nabla\bar{\phi} \qquad \text{on} \quad z = \bar{\zeta}$$

Substituting $\bar{\phi} = \bar{\Phi} + Ux$ into the foregoing equation yields

$$\bar{\zeta} = -\frac{1}{2g}(|\nabla\bar{\Phi}|^2 - U^2) \qquad \text{on} \quad z = \bar{\zeta} \tag{2.26}$$

Equation (2.26) is called the steady free surface elevation. Putting this expression into equation (2.24) and omitting the local time derivative $\partial/\partial t$, we have

$$(\nabla\bar{\Phi}\bullet\nabla)[\tfrac{1}{2}(|\nabla\bar{\Phi}|^2-U^2)+gz]=0$$

$$\tfrac{1}{2}\nabla\bar{\Phi}\bullet\nabla(\nabla\bar{\Phi}\bullet\nabla\bar{\Phi})+g\bar{\Phi}_z=0 \qquad \text{on } z=\bar{\zeta} \quad (2.27)$$

Equation (2.27) is called the non-linear free surface condition for the steady flow problem. It is noted that this equation is analogous to equation (2.9) by deleting the time dependent terms. Substituting equation (2.22) into (2.27) and retaining the first-order terms of $\bar{\Phi}$ in ε yields the linear free surface condition for the steady flow problem.

$$U^2\bar{\Phi}_{xx}+g\bar{\Phi}_z=0 \qquad \text{on } z=0 \quad (2.28)$$

For an unsteady flow problem, the free surface condition may be derived by putting equation (2.19) into (2.8) as follows

$$[\frac{\partial}{\partial t}+(\nabla\bar{\Phi}+\nabla\tilde{\Phi})\bullet\nabla][\tilde{\Phi}_t+\tfrac{1}{2}(\nabla\bar{\Phi}+\nabla\tilde{\Phi})\bullet(\nabla\bar{\Phi}+\nabla\tilde{\Phi})+gz]=0 \quad \text{on } z=\zeta$$

After some manipulation through neglecting the quadratic terms of $\tilde{\Phi}$, i.e. coefficients of $O(\varepsilon^2)$ in $\tilde{\Phi}$, we get the free surface condition of the unsteady flow

$$\begin{aligned}&\tfrac{1}{2}\nabla\bar{\Phi}\bullet\nabla(\nabla\bar{\Phi}\bullet\nabla\bar{\Phi})+g\bar{\Phi}_z\\&+\tilde{\Phi}_{tt}+2\nabla\bar{\Phi}\bullet\nabla\tilde{\Phi}_t+\nabla\bar{\Phi}\bullet\nabla(\nabla\bar{\Phi}\bullet\nabla\tilde{\Phi})\\&+\tfrac{1}{2}\nabla\tilde{\Phi}\bullet\nabla(\nabla\bar{\Phi}\bullet\nabla\bar{\Phi})+g\tilde{\Phi}_z=0 \qquad \text{on } z=\zeta \quad (2.29)\end{aligned}$$

The free surface elevation of the unsteady flow is obtained by superposing $\tilde{\Phi}$ over $\bar{\Phi}$ in equation (2.25) as follows

$$(\frac{\partial}{\partial t} - U\frac{\partial}{\partial x})(\bar{\phi} + \tilde{\Phi}) + \frac{1}{2}(\nabla\bar{\phi} + \nabla\tilde{\Phi}) \bullet (\nabla\bar{\phi} + \nabla\tilde{\Phi}) + gz = 0 \qquad \text{on } z = \zeta$$

Substituting $\bar{\phi} = \bar{\Phi} + Ux$ into the foregoing equation and retaining only the first-order terms of $\tilde{\Phi}$ in ε yields the free surface of unsteady flow in the form

$$\zeta = -\frac{1}{g}[\tilde{\Phi}_t + \frac{1}{2}(|\nabla\bar{\Phi}|^2 - U^2) + \nabla\bar{\Phi} \bullet \nabla\tilde{\Phi}] \qquad \text{on } z = \zeta \quad (2.30)$$

In order to transform the free surface ζ to $\bar{\zeta}$, we may carry out a Taylor series expansion for equation (2.30). The first two terms of the expansion can be shown to be

$$\zeta = -\frac{1}{g}[\tilde{\Phi}_t + \frac{1}{2}(|\nabla\bar{\Phi}|^2 - U^2) + \nabla\bar{\Phi} \bullet \nabla\tilde{\Phi}]_{z=\zeta}$$

$$-(\zeta - \bar{\zeta})\frac{1}{g}\frac{\partial}{\partial z}[\tilde{\Phi}_t + \frac{1}{2}(|\nabla\bar{\Phi}|^2 - U^2) + \nabla\bar{\Phi} \bullet \nabla\tilde{\Phi}]_{z=\zeta}$$

$$= \bar{\zeta} - \frac{1}{g}[\tilde{\Phi}_t + \nabla\bar{\Phi} \bullet \nabla\tilde{\Phi}]_{z=\zeta} - \frac{1}{g}(\zeta - \bar{\zeta})[\tilde{\Phi}_{zt} + \nabla\bar{\Phi} \bullet \nabla\bar{\Phi}_z + (\nabla\bar{\Phi} \bullet \nabla\tilde{\Phi})_z]_{z=\zeta}$$

Substituting the perturbation series expansion of ζ, $\bar{\zeta}$ and $\tilde{\Phi}$ into this expression and truncating the error to $O(\varepsilon^2)$ reduces to

$$\zeta = \bar{\zeta} - \frac{1}{g}[\tilde{\Phi}_t + \nabla\bar{\Phi} \bullet \nabla\tilde{\Phi}]_{z=\zeta} - \frac{1}{g}(\zeta - \bar{\zeta})(\nabla\bar{\Phi} \bullet \nabla\bar{\Phi}_z)_{z=\zeta}$$

Then the difference (ζ- $\bar{\zeta}$) can be written as

$$\zeta - \bar{\zeta} = -(\tilde{\Phi}_t + \nabla\bar{\Phi} \bullet \nabla\tilde{\Phi}) / (g + \nabla\bar{\Phi} \bullet \nabla\bar{\Phi}_z) \qquad \text{on } z = \zeta \quad (2.31)$$

By using Taylor series expansion and perturbation series expansion of ζ, $\bar{\zeta}$ and $\tilde{\Phi}$, similar procedures may be carried out to expand the free surface condition given by equation (2.29) from unsteady position ζ to steady position $\bar{\zeta}$. This produces

$$[\tfrac{1}{2}\nabla\bar{\Phi}\bullet\nabla(\nabla\bar{\Phi}\bullet\nabla\bar{\Phi})+g\bar{\Phi}_z$$

$$+\tilde{\Phi}_{tt}+2\nabla\bar{\Phi}\bullet\nabla\tilde{\Phi}_t+\nabla\bar{\Phi}\bullet\nabla(\nabla\bar{\Phi}\bullet\nabla\tilde{\Phi})+\tfrac{1}{2}\nabla\tilde{\Phi}\bullet\nabla(\nabla\bar{\Phi}\bullet\nabla\bar{\Phi})+g\tilde{\Phi}_z]_{z=\zeta}$$

$$+(\zeta-\bar{\zeta})\frac{\partial}{\partial z}[\tfrac{1}{2}\nabla\bar{\Phi}\bullet\nabla(\nabla\bar{\Phi}\bullet\nabla\bar{\Phi})+g\bar{\Phi}_z]_{z=\zeta}=0$$

The first line of the above equation is identical to zero as given in equation (2.27) and the expression of difference (ζ- $\bar{\zeta}$) can be obtained from equation (2.31). Thus, the first-order free surface condition for the unsteady flow problem is

$$\tilde{\Phi}_{tt}+2\nabla\bar{\Phi}\bullet\nabla\tilde{\Phi}_t+\nabla\bar{\Phi}\bullet\nabla(\nabla\bar{\Phi}\bullet\nabla\tilde{\Phi})+\tfrac{1}{2}\nabla\tilde{\Phi}\bullet\nabla(\nabla\bar{\Phi}\bullet\nabla\bar{\Phi})+g\tilde{\Phi}_z$$

$$-(\tilde{\Phi}_t+\nabla\bar{\Phi}\bullet\nabla\tilde{\Phi})[\tfrac{1}{2}\frac{\partial}{\partial z}(\nabla\bar{\Phi}\bullet\nabla|\nabla\bar{\Phi}|^2)+g\bar{\Phi}_{zz}]/(g+\nabla\bar{\Phi}\bullet\nabla\bar{\Phi}_z)=0$$

$$\text{on } z=\bar{\zeta} \qquad (2.32)$$

If the steady flow problem is firstly solved, equation (2.32) for the unsteady flow problem on $z=\bar{\zeta}$ becomes a linear free surface condition associated with steady potential terms. Nevertheless, the general solution of this equation, at the present state of the art, is impossible. One obvious simplification is to reduce the effects of steady flow by the assumption of small steady perturbation flow due to a forward motion. Small steady perturbation is implicitly assumed in equation (2.32) and that all terms associated with the steady potential are of higher order and may be neglected in the first order free surface condition for the unsteady flow. Therefore, we assume

$$\vec{W}=\nabla\bar{\Phi}=(-U,0,0) \qquad (2.33)$$

Equation (2.32) reduces to

$$\tilde{\Phi}_{tt}-2U\tilde{\Phi}_{xt}+U^2\tilde{\Phi}_{xx}+g\tilde{\Phi}_z=0 \qquad \text{on } z=0 \quad (2.34a)$$

or

$$(\frac{\partial}{\partial t}-U\frac{\partial}{\partial x})^2\tilde{\Phi}+g\tilde{\Phi}_z=0 \qquad \text{on } z=0 \quad (2.34b)$$

2.5.3 Linearised body boundary condition

Having specified the body boundary condition given by equation (2.10) on the oscillatory wetted body surface S_w, we next turn to transform this exact surface S_w to the mean wetted body surface $\bar{S}_w$. Before doing this, we may consider that the body boundary condition in the steady surface $\bar{S}_w$ is known such that

$$\vec{W} \bullet \vec{n} = 0 \qquad \text{on } \bar{S}_w \qquad (2.35)$$

From the foregoing equations (2.10),(2.11) ,(2.19) and (2.22) we can write

$$(\nabla\bar{\phi} + \nabla\tilde{\Phi} - U\vec{i}) \bullet \vec{n} = \dot{\alpha} \bullet \vec{n}$$

Using equation (2.23) results

$$\tilde{\Phi}_n = \dot{\alpha} \bullet \vec{n} - \vec{W} \bullet \vec{n} \qquad \text{on } S_w \qquad (2.36)$$

The instantaneous normal vector $\vec{n}$ may be expanded through perturbation series as

$$\vec{n} = \vec{n}^{(0)} + \varepsilon\vec{n}^{(1)} + O(\varepsilon^2) \qquad (2.37)$$

where $\vec{n}^{(0)} = \vec{n}$ and $\vec{n}^{(1)} = \vec{\Omega} \times \vec{n}$

The definition of $\vec{\Omega}$ has been given in equation (2.2b). Similarly, the perturbation expansion of $\vec{W}$ may be written as

$$\vec{W} = \vec{W}^{(0)} + \varepsilon\vec{W}^{(1)} + O(\varepsilon^2) \qquad (2.38)$$

where $\vec{W}^{(0)} = \vec{W} = (u, v, w)$ and $\vec{W}^{(1)} = \delta\vec{W} = (\vec{\alpha} \bullet \nabla)\vec{W}$

Hence the dot product of $\vec{W}$ and $\vec{n}$ given by equations (2.38) and (2.37) respectively yields

$$\{\vec{W} \bullet \vec{n}\}_S = \{[\vec{W} - \vec{\Omega} \times \vec{W} + (\vec{\alpha} \bullet \nabla)\vec{W}] \bullet \vec{n}\}_S \quad \text{on } S_w, \bar{S}_w \qquad (2.39)$$

Substituting equation (2.39) into (2.36) and invoking equation (2.35) it follows that

$$\Phi_n = [\dot{\alpha} + \vec{\Omega} \times \vec{W} - (\vec{\alpha} \bullet \nabla)\vec{W}] \bullet \vec{n} \qquad \text{on } S_w, \bar{S}_w \qquad (2.40)$$

An alternative expression to equation (2.40) can be derived by making use of equation (2.2b) and the following vector identity

$$(\vec{W} \bullet \nabla)\vec{\alpha} = (\vec{W} \bullet \nabla)\vec{\delta} + [(\vec{W} \bullet \nabla)\vec{\Omega}] \times \vec{r}' + \vec{\Omega} \times [(\vec{W} \bullet \nabla)\vec{r}'] \quad (2.41)$$

The first two terms on the right hand side of equation (2.41) are zero because both $\vec{\delta}$ and $\vec{\Omega}$ are independent of the spatial coordinate. Then equation (2.41) reduces to

$$(\vec{W} \bullet \nabla)\vec{\alpha} = \vec{\Omega} \times \vec{W}$$

Substituting this expression into equation (2.40) produces

$$\Phi_n = [\dot{\alpha} + (\vec{W} \bullet \nabla)\vec{\alpha} - (\vec{\alpha} \bullet \nabla)\vec{W}] \bullet \vec{n} \qquad \text{on } S_w, \bar{S}_w \qquad (2.42a)$$

or

$$\Phi_n = [(\frac{\partial}{\partial t} + \vec{W} \bullet \nabla)\vec{\alpha} - (\vec{\alpha} \bullet \nabla)\vec{W}] \bullet \vec{n} \qquad \text{on } S_w, \bar{S}_w \qquad (2.42b)$$

The first term in the right hand side of equation (2.42b) gives the rate of change of oscillatory displacement $\vec{\alpha}$ in a reference frame moving with the steady flow. A simplified form of equation (2.42a) can also be derived by using the following vector identity

$$\nabla \times (\vec{\alpha} \times \vec{W}) = (\vec{W} \bullet \nabla)\vec{\alpha} - (\vec{\alpha} \bullet \nabla)\vec{W} + \vec{\alpha}(\nabla \bullet \vec{W}) - \vec{W}(\nabla \bullet \vec{\alpha})$$

Since $\vec{\alpha}$ and $\vec{W}$ have zero divergence, the last two terms on the right hand side of the foregoing equation are identical to zero. Hence, equation (2.40) can be written in a simplified form as

$$\tilde{\Phi}_n = [\dot{\alpha} + \nabla \times (\vec{\alpha} \times \vec{W})] \bullet \vec{n} \qquad \text{on } S_w, \overline{S}_w \qquad (2.42c)$$

The boundary condition given by equation (2.42c) is identical to the condition derived by Timman & Newman (1962). It is evident that the body boundary condition due to a forward motion highlights the interaction between steady and unsteady flow fields. This interaction causes the problem to become complicated. If further simplification such as slender body or low speed is made to the assumption that the steady perturbation potential $\bar{\Phi}$ is small, then equation (2.33) is acceptable and equation (2.42b) can be read as

$$\begin{aligned} \tilde{\Phi}_n &= [(\frac{\partial}{\partial t} - U\frac{\partial}{\partial x})\vec{\alpha}] \bullet \vec{n} \\ &= (\dot{\alpha} - U(\vec{\Omega} \times \vec{i})] \bullet \vec{n} \qquad \text{on } S_o \qquad (2.43) \end{aligned}$$

The term $\vec{\Omega} \times \vec{i}$ is the angle of attack due to pitch and yaw.

2.5.4 Decomposition of velocity potential

By linearisation, we have separated the total potential Φ into steady potential $\bar{\Phi}$ and unsteady potential $\tilde{\Phi}$ and further divided the steady part into the uniform stream and the steady perturbation flows. Our assumption in perturbation expansion restricts the unsteady flow as well as the resulting motions to be of small amplitudes and hence the unsteady potential $\tilde{\Phi}$ can be decomposed linearly into separate components due to the incident waves, diffraction waves and radiation waves. The profiles of small amplitude incident waves are sinusoidal and harmonic in time. This

means that the diffraction waves, radiation waves and motion responses are harmonic in time with frequency of encounter ω. Then the unsteady velocity potential $\tilde{\Phi}$ can be written as

$$\tilde{\Phi}(\vec{x}, t) = [\xi_0(\phi_0 + \phi_7) + \sum_{j=1}^{6} \xi_j \phi_j]e^{-i\omega t} \qquad (2.44)$$

where ϕ_0 is the incident wave potential of amplitude ξ_0, ϕ_7 the diffraction wave potential and ϕ_j the radiation wave potential in j^{th} mode of motion, having amplitude ξ_j. The diffraction waves are generated by the diffraction of the incident waves as if the body is restrained to produce no motion with respect to the body-fixed frame o-x'y'z'. The radiation waves are the results of radiation from the body motion in calm water.

The incident wave potential of unit amplitude which satisfies the Laplace's equation (2.21), the free surface condition in equation (2.34) and the sea bed condition in equation (2.13) can be represented by

$$\phi_0 = -i\frac{g}{\omega_o}\frac{\cosh[\upsilon(z+h)]}{\cosh \upsilon h}e^{i\upsilon(x\cos\beta + y\sin\beta)} \qquad (2.45)$$

where ω_o = wave frequency

υ = wave number

β = angle of incidence with x-axis (180° at head sea)

The wave number υ is given by the dispersion relation

$$\frac{\omega_o^2}{g} = \upsilon \tanh \upsilon h \qquad (2.46)$$

and the frequency of encounter is

$$\omega = |\omega_o - U\upsilon\cos\beta| \qquad (2.47)$$

The body boundary condition given by equation (2.42a) for the components of the unsteady velocity potential $\tilde{\Phi}$ can be expressed as

$$[\xi_0 \frac{\partial}{\partial n}(\phi_0 + \phi_7) + \sum_{j=1}^{6} \xi_j \frac{\partial \phi_j}{\partial n}] e^{-i\omega t}$$

$$= [\dot{\vec{\alpha}} + (\vec{W} \bullet \nabla)\vec{\alpha} - (\vec{\alpha} \bullet \nabla)\vec{W}] \bullet \vec{n} \qquad \text{on } S_w, \bar{S}_w \qquad (2.48)$$

In the diffraction problem the body is assumed to be fixed with respect to the body-fixed frame o-x'y'z' as $\vec{\alpha}=0$ and $\xi_j=0$. Thus, the unsteady potential $\tilde{\Phi}$ in the free surface condition given by equation (2.32) can be written as $\tilde{\Phi}=\phi_0+\phi_7$. Consequently, the diffraction potential ϕ_7 satisfies an inhomogeneous free surface conditon similar to equation (2.32) with ϕ_7 instead of $\tilde{\Phi}$ and the linear differential form $D(\phi_0)$ on the right hand side of equation (2.32). Since this inhomogeneous free surface condition for diffraction potential ϕ_7 is complicated to an extent that no practical solution is obtained, the only way to simplify this condition is to make an assumption on a steady flow of small disturbance such that equation (2.33) remains valid. Then this assumption reduces the inhomogeneous free surface condition to the same form as equation (2.34). On the body boundary of no oscillatory motions, equation (2.48) simply becomes

$$\frac{\partial}{\partial n}(\phi_0 + \phi_7) = 0 \qquad \text{on } S_w \qquad (2.49)$$

On the other hand, the radiation problem occurs as if the flow field is produced by the forced oscillation of the body in j^{th} degree of freedom with the absence of incident waves such that $\xi_0=0$. The free surface condition for the radiation potential ϕ_j has the same form as equation (2.32) or the linearised form in equation (2.34). The body boundary condition given by equation (2.48) reduces to

$$\sum_{j=1}^{6} \xi_j \frac{\partial \phi_j}{\partial n} = [\dot{\vec{\alpha}} + (\vec{W} \bullet \nabla)\vec{\alpha} - (\vec{\alpha} \bullet \nabla)\vec{W}] \bullet \vec{n} \qquad \text{on } S_w, \bar{S}_w \qquad (2.50)$$

Considering each mode of translatory displacement, $\alpha=\xi_j\vec{i}_j e^{-i\omega t}$ in which $\vec{i}_j$ denotes the unit vector $\vec{i}, \vec{j}$ and $\vec{k}$ for j=1,2,3 respectively, the general expression of the normal derivative of ϕ_j in translational modes of motions can be derived as follows

$$\xi_j \frac{\partial \phi_j}{\partial n} e^{-i\omega t} = \xi_j e^{-i\omega t}[-i\omega\vec{i}_j + (\vec{W}\bullet\nabla)\vec{i}_j - (\vec{i}_j\bullet\nabla)\vec{W}]\bullet\vec{n} \quad ; j=1,2,3$$

Since the unit vector $\vec{i}_j$ and the amplitude ξ_j are independent of spatial coordinates, the second term in the bracket is identical to zero. The above expression reduces to

$$\frac{\partial \phi_j}{\partial n} = -i\omega\vec{n}\bullet\vec{i}_j - \vec{n}\bullet\frac{\partial\vec{W}}{\partial x_j} \qquad ; j=1,2,3 \qquad \text{on } S_w, \bar{S}_w \qquad (2.51)$$

where $x_j = x,y,z$ for j=1,2,3 respectively.

For a rotational motion, the oscillatory displacement for each mode can be written as $\alpha = \xi_j\vec{i}_{j-3}\times\vec{r}\,e^{-i\omega t}$ for j=4,5,6 respectively. The expression of the normal derivative of ϕ_j for rotational mode can be derived as

$$\xi_j \frac{\partial \phi_j}{\partial n} e^{-i\omega t} = \xi_j e^{-i\omega t}\{-i\omega\vec{i}_{j-3}\times\vec{r} + [(\vec{W}\bullet\nabla)\vec{i}_{j-3}]\times\vec{r} + \vec{i}_{j-3}\times(\vec{W}\bullet\nabla)\vec{r} - (\vec{i}_{j-3}\times\vec{r}\bullet\nabla)\vec{W}\}\bullet\vec{n} \qquad ; j=4,5,6$$

Further simplification gives

$$\frac{\partial \phi_j}{\partial n} = -i\omega\vec{r}\times\vec{n}\bullet\vec{i}_{j-3} + \vec{W}\times\vec{n}\bullet\vec{i}_{j-3} - [(\vec{i}_{j-3}\times\vec{r}\bullet\nabla)\vec{W}]\bullet\vec{n} \qquad ; j=4,5,6 \quad \text{on } S_w, \bar{S}_w \qquad (2.52)$$

If $\vec{W}$ is the velocity vector per unit speed of mean forward speed U, then we can write the general expression of the normal derivative of ϕ_j by using equations (2.51) and (2.52) in the form

$$\frac{\partial \phi_j}{\partial n} = -i\omega n_j + U m_j \qquad ; j=1,2,...6 \quad \text{on } S_w, \bar{S}_w \qquad (2.53)$$

where the components n_j are defined as

$$(n_1, n_2, n_3) = \vec{n} \qquad (2.54)$$

$$(n_4, n_5, n_6) = \vec{r} \times \vec{n} \qquad (2.55)$$

and the forward speed related coefficients m_j are

$$(m_1, m_2, m_3) = -(\vec{n} \bullet \frac{\partial}{\partial x}, \vec{n} \bullet \frac{\partial}{\partial y}, \vec{n} \bullet \frac{\partial}{\partial z})\vec{W} \qquad (2.56)$$

$$(m_4, m_5, m_6) = \sum_{j=4}^{6} \{\vec{W} \times \vec{n} \bullet \vec{i}_{j-3} - [(\vec{i}_{j-3} \times \vec{r} \bullet \nabla)\vec{W}] \bullet \vec{n}\}\vec{i}_{j-3} \qquad (2.57)$$

After some manipulation and using $\nabla \times \vec{W} = 0$, we have

$$(m_1, m_2, m_3) = \vec{m} = -\vec{n} \bullet (\nabla \vec{W}) = -(\vec{n} \bullet \nabla)\vec{W} \qquad (2.58)$$

$$(m_4, m_5, m_6) = \vec{W} \times \vec{n} + \vec{r} \times \vec{m} = -(\vec{n} \bullet \nabla)(\vec{r} \times \vec{W}) \qquad (2.59)$$

The linearised body boundary conditions given by equation (2.53) associated with equations (2.54) through (2.59) are identical to the results obtained by Ogilvie &

Tuck (1969). These body boundary conditions involve the steady velocity field. If the body is thin, slender or the mean forward speed is low, $\bar{\Phi}$ is small enough to be negligible in the unsteady flow and equation (2.33) remains valid. Then m_j term becomes

$$\left.\begin{aligned} m_j &= 0 \qquad \text{for } j=1,2,3,4 \\ m_5 &= n_3 \\ m_6 &= -n_2 \end{aligned}\right\} \quad (2.60)$$

Equations (2.49) and (2.53) associated with (2.60) are the linearised body boundary conditions for the diffraction and radiation problems respectively. These two equations can also be obtained from equation (2.43). In comparison with equations (2.43) and (2.53), the speed effects on the radiation potential ϕ_5 and ϕ_6 are proportional to the angle of attack due to pitch and yaw motions respectively.

2.6 Conclusions

A theoretical formulation for the steady and unsteady forward motion problems has been presented in the context of the potential theory. It has been noted that not only non-linear effects on the free surface boundary and body boundary conditions make the problems mathematically intractable but also the instantaneous surfaces of these two boundaries are not known a priori. These two boundary conditions must be linearised by means of perturbation expansions to an extent that practical solutions can be obtained.

The linearised free surface condition associated with the steady perturbation potential in the unsteady forward motion problem is still unsolvable analytically. A further simplification is to assume that the steady perturbation potential is of higher order and neglected in the linearised free surface condition for the unsteady flow.

Hence, only the combined effects of oscillating frequency and forward speed are retained in the linearised free surface condition, which leads to the use of a translating pulsating source to simulate the transverse and divergent waves swept downstream.

Due to oscillatory motions the linearised body boundary condition contains the convective effects of the steady velocity field due to forward speed. This steady velocity field can be found by solving the Neumann-Kelvin problem for the steady forward motion. On the other hand if the body is thin, slender or fully submerged, the steady disturbance is small around the body surface. This assumption leads to a simple speed correction, due to the angle of attack in pitch and yaw motions, on the linearised body boundary condition.

CHAPTER 3

THREE-DIMENSIONAL GREEN FUNCTION METHOD

3.1 Introduction

The three-dimensional Green function method is an integral equation used in solving a linearised boundary-value problem for steady and unsteady flow conditions induced by forward and oscillatory motions of a moving body. The formulation of the Green function method is based on Green's second identity to define a velocity potential using a Green function on the boundary of the fluid domain. This results in a surface integral equation of a complicated kernel function. The kernel function represents the Green function which satisfies Laplace's equation and nearly all the boundary conditions except that on the body surface. In order to fulfill the linearised free surface condition of the boundary-value problem, the Green function may be defined by a source submerged below the free surface. This source is represented by a translating source for a steady forward motion and a translating pulsating source for an unsteady forward motion of the moving body. For a stationary but oscillating body, the Green function is simply represented by a pulsating source.

A distinct feature of the Green function integral equation method is the irregular frequencies where the integral equation becomes ill-conditioned. Methods of avoiding and removing irregular frequencies are discussed in the literature.

3.2 Existence of Green function

The solution of an integral equation for potential flow problems is based on the existence of the Green function. The concept of Green's theorem is now applied to

define the Green function used in a surface integral to be evaluated over the fluid domain. Let us denote by D the fluid domain outside the mean wetted body surface S_o and by $\hat{D}$ the interior of the body. The fluid domain D of volume $\tilde{V}$ is bounded by the fluid boundary surface S consisting of the mean wetted body surface S_o, the undisturbed free surface S_F, the sea bed S_H and the control surface S_∞ at far-field as shown in Fig.2.1. The mean wetted body surface S_o is the lowest order of the mean wetted surface $\overline{S}_w$ in steady flow field. The undisturbed free surface S_F is enclosed by two simple closed curves. One is the intersection line L_o of the mean wetted body surface S_o and the undisturbed free surface S_F, and the other is the simple closed curve L_∞ at far-field.

Let us denote $\Phi(\vec{x}, t)$ as an unknown velocity potential and $G(\vec{x}, t; \vec{\xi})$ as a Green function of known harmonic nature, where $\vec{x}$ and $\vec{\xi}$ are a field point and a source point respectively in the fluid domain D. The Green function $G(\vec{x}, t; \vec{\xi})$ is defined by

$$G(\vec{x}, t; \vec{\xi}) = [-\frac{1}{r} + H(\vec{x}; \vec{\xi})]e^{-i\omega t} \qquad (3.1)$$

where $$r = \sqrt{[(x-\xi)^2 + (y-\eta)^2 + (z-\zeta)^2]} \quad ; \quad z \le 0 \qquad (3.2)$$

$-1/r$ is a source singularity and $H(\vec{x}; \vec{\xi})$ is a regular function. If both the velocity potential function Φ and the Green function G have continuous derivatives of the first and second orders, Green's second identity is written as

$$\iint_S (\Phi \frac{\partial G}{\partial n} - G \frac{\partial \Phi}{\partial n})\, ds = \iiint_{\tilde{V}} (\Phi \nabla^2 G - G \nabla^2 \Phi)\, dv \qquad (3.3)$$

where $\partial/\partial n$ is the normal derivative with respect to the source point $\vec{\xi}$ and the normal vector $\vec{n}$ is pointing inside the fluid domain.

Since both Φ and G are harmonic everywhere except at a singular point in the fluid volume $\tilde{V}$, i.e. they satisfy Laplace's equation, and equation (3.3) reduces to

$$\iint_S (\Phi \frac{\partial G}{\partial n} - G \frac{\partial \Phi}{\partial n}) \, ds = 0 \qquad (3.4)$$

The surface integral over the closed surface *S* has three different characteristics which depend on the position of the field point $\vec{x}$ relative to the source point $\vec{\xi}$. The source point $\vec{\xi}$ lies in the fluid domain in all cases but the field point $\vec{x}$ can be placed outside the domain.

Firstly, consider the field point $\vec{x}$ outside the fluid volume*V*. Since the source point $\vec{\xi}$ never coincides with the field point $\vec{x}$, equation (3.4) is valid.

Secondly, if the field point $\vec{x}$ lies inside the fluid volume *V* but not on the boundary *S*, concurrence of the field point $\vec{x}$ and the source point $\vec{\xi}$ may occur. When $\vec{x} = \vec{\xi}$, the singularity of the Green function G makes equation (3.4) invalid. In order to circumvent this singularity, consider a small sphere of radius ε whose origin is at $\vec{x}$. If we denote V_ε the volume of the sphere enclosed by surface S_ε, the fluid boundary surface becomes $S+S_\varepsilon$. We can write

$$\iint_{s_\varepsilon} \left[\Phi \frac{\partial}{\partial n} (-\frac{1}{r}) + (\frac{1}{r}) \frac{\partial \Phi}{\partial n} + \Phi \frac{\partial H}{\partial n} - H \frac{\partial \Phi}{\partial n} \right] ds(\vec{x}) + \iint_S (\Phi \frac{\partial G}{\partial n} - G \frac{\partial \Phi}{\partial n}) \, ds(\vec{\xi}) = 0 \qquad (3.5)$$

Using Gauss's theorem one obtains the following results

$$\iint_{s_\varepsilon} \frac{1}{r} \frac{\partial \Phi}{\partial n} ds = \frac{1}{\varepsilon} \iint_{s_\varepsilon} n \bullet \nabla \Phi \, ds = \iiint_{v_\varepsilon} \nabla^2 \Phi \, ds = 0$$

Then equation (3.5) reduces to

$$\iint_S (\Phi \frac{\partial G}{\partial n} - G \frac{\partial \Phi}{\partial n}) \, ds(\vec{\xi}) = - \iint_{s_\varepsilon} \left[\Phi \frac{\partial}{\partial n} (-\frac{1}{r}) + \Phi \frac{\partial H}{\partial n} - H \frac{\partial \Phi}{\partial n} \right] ds(\vec{x}) \qquad (3.6)$$

Since the surface area of the sphere V_ε is $4\pi\varepsilon^2$ and $\frac{\partial}{\partial n} = \frac{\partial}{\partial r}$, equation (3.6) becomes

$$\iint_s (\Phi\frac{\partial G}{\partial n} - G\frac{\partial \Phi}{\partial n})\, ds(\vec{\xi}) = \lim_{\varepsilon \to 0} \iint_{s_\varepsilon} (-\frac{\Phi}{\varepsilon^2} - \Phi\frac{\partial H}{\partial n} + H\frac{\partial \Phi}{\partial n}) ds(\vec{x})$$

$$= \lim_{\varepsilon \to 0} [-4\pi\Phi(\vec{x}) - 4\pi\varepsilon^2(\Phi\frac{\partial H}{\partial n} - H\frac{\partial \Phi}{\partial n})]$$

$$= -4\pi\Phi(\vec{x}) \qquad \text{for } \vec{x} \text{ inside } D \quad (3.7)$$

Finally, if the field point $\vec{x}$ lies on the boundary surface S, singularity is avoided by imposing the field point $\vec{x}$ inside a hemisphere and then the factor of 4π in equation (3.7) becomes 2π. We can write

$$\iint_s (\Phi\frac{\partial G}{\partial n} - G\frac{\partial \Phi}{\partial n})\, ds(\vec{\xi}) = -2\pi\Phi(\vec{x}) \qquad \text{for } \vec{x} \text{ on } S \qquad (3.8)$$

Now we amalgmate the results given by equations (3.4),(3.7) and (3.8) as

$$\iint_s [\Phi(\vec{\xi})\frac{\partial G(\vec{x};\vec{\xi})}{\partial n} - G(\vec{x};\vec{\xi})\frac{\partial \Phi(\vec{\xi})}{\partial n}] ds(\vec{\xi}) = \left\{ \begin{array}{c} 0 \\ -2\pi\Phi(\vec{x}) \\ -4\pi\Phi(\vec{x}) \end{array} \right\} \begin{array}{l} \vec{x} \text{ outside } D \quad (3.9a) \\ \text{if } \vec{x} \text{ on } S \qquad (3.9b) \\ \vec{x} \text{ inside } D \quad (3.9c) \end{array}$$

The corresponding two-dimensional problem is similarly dealt with and the coefficients of $\Phi(y,z)$ are reduced by a factor of 1/2 and $G(y,z;\eta,\zeta) = \log r + H(y,z;\eta,\zeta)$ whereas $r = \sqrt{[(y-\eta)^2+(z-\zeta)^2]}$. One can also obtain similar representations for an interior domain $\hat{D}$. Let us define $\hat{\Phi}$ the interior potential inside the domain $\hat{D}$ whose volume$V$ is the interior of the body. The interior volume V is enclosed by $\hat{S}_F$ which is a part of the plane z=0 within the body and S_o is the interior surface of the body as shown in Fig.2.1. If we designate $\hat{S}$ the interior boundary surface such that $\hat{S} = \hat{S}_F + S_o$, then

$$\iint_S [\hat{\Phi}(\xi)\frac{\partial G(\vec{x};\vec{\xi})}{\partial n} - G(\vec{x};\vec{\xi})\frac{\partial \hat{\Phi}(\vec{\xi})}{\partial n}]ds(\vec{\xi}) = \begin{cases} 0 & \vec{x} \text{ outside } \hat{D} \quad (3.10a) \\ \mp 2\pi\hat{\Phi}(\vec{x}) & \text{if } \vec{x} \text{ on } \hat{S} \quad (3.10b) \\ -4\pi\hat{\Phi}(\vec{x}) & \vec{x} \text{ inside } \hat{D} \quad (3.10c) \end{cases}$$

The sign of the factor 2π in equation (3.10b) may be taken as negative if the surface integral S is evaluated over the interior body surface S_o whose normal vector $\vec{n}$ is outward into the fluid domain $\hat{D}$. The existence of the Green function G may be proved by the theory of the Fredholm integral equation. If the fluid velocity is specified on the boundary surface S in equations (3.9a,b,c), then equation (3.9a) becomes a Fredholm integral equation of the first kind and (3.9b) and (3.9c) change to the Fredholm integral equations of the second kind.

3.3 Governing equation and boundary conditions

Before we develop the integral equation based on the Green function, we have to recall those governing equation and boundary conditions for the boundary-value problem as discussed in Chapter 2. The Green function $G(\vec{x}, t; \vec{\xi})$ based on the assumptions of an homogeneous, incompressible and inviscid fluid must satisfy the following equations

Laplace's equation

$$\nabla^2 G(\vec{x}, t; \vec{\xi}) = \delta(\vec{x} - \vec{\xi}) \quad ; \ z < 0 \quad (3.11)$$

Linearised free surface condition

$$[(\frac{\partial}{\partial t} - U\frac{\partial}{\partial x})^2 + g\frac{\partial}{\partial z}]G = 0 \quad ; \ z = 0 \quad (3.12)$$

Sea bed condition

$$G_z = 0 \qquad ;\ z = -h \quad (3.13a)$$

$$G_z = 0 \qquad ;\ z \to -\infty \quad (3.13b)$$

Far-field radiation condition

$$\lim_{r \to \infty} G = 0 \qquad (3.14)$$

where $\delta(\vec{x} - \vec{\xi})$ is a Dirac delta function in equation (3.11) such that $\delta(\vec{x} - \vec{\xi}) = 0$ if $\vec{x} - \vec{\xi} \neq 0$. Equation (3.13a) and (3.13b) are used for water of finite depth h and of infinite depth respectively.

3.4 Formulation of integral equation based on Green function

In the fluid domain D, we consider the contributions to the surface integral S from the boundary surfaces S_F, S_o, S_H and S_∞ in equations (3.9a,b,c). The integrand of equations (3.9a,b,c) has the normal derivatives of Φ and G which satisfy the sea bed condition given by equation (3.13) and the integrand becomes zero at z=−h (h may be infinity). This results in the surface integral over S_H being zero. On the far-field control surface S_∞, both Φ and G vanish at $r \to \infty$ as given by equation (3.14). Therefore the surface integral over S_∞ has no contribution.

On the free surface S_F, both Φ and G satisfy the linearised free surface conditon given by equation (3.12) as

$$-\omega^2\Phi + i2\omega U\Phi_x + U^2\Phi_{xx} + g\Phi_z = 0 \qquad \text{on } z=0 \qquad (3.15)$$

$$-\omega^2 G + i2\omega UG_x + U^2 G_{xx} + gG_z = 0 \qquad \text{on } z=0 \qquad (3.16)$$

After substituting equations (3.15) and (3.16) into the integrand of equations (3.9a,b,c) and making some manipulation, we may write

$$\begin{Bmatrix} 0 \\ 2\pi \\ 4\pi \end{Bmatrix} \Phi(\vec{x}) + \iint_{S_o} \Phi(\vec{\xi}) \frac{\partial G(\vec{x};\vec{\xi})}{\partial n} ds(\vec{\xi}) + \frac{U^2}{g} \oint_{L_o} \Phi(\vec{\xi}) \frac{\partial G(\vec{x};\vec{\xi})}{\partial x} dy(\vec{\xi})$$

$$- i\frac{2\omega U}{g} \oint_{L_o} \Phi(\vec{\xi}) G(\vec{x};\vec{\xi}) dy(\vec{\xi}) + i\frac{4\omega U}{g} \iint_{S_F} \Phi(\vec{\xi}) \frac{\partial G(\vec{x};\vec{\xi})}{\partial x} ds(\vec{\xi})$$

$$= \iint_{S_o} G(\vec{x};\vec{\xi}) \frac{\partial \Phi(\vec{\xi})}{\partial n} ds(\vec{\xi}) + \frac{U^2}{g} \oint_{L_o} G(\vec{x};\vec{\xi}) \frac{\partial \Phi(\vec{\xi})}{\partial x} dy(\vec{\xi})$$

$$\text{if} \begin{cases} \vec{x} \text{ outside } D & \text{(3.17a)} \\ \vec{x} \text{ on } S_o & \text{(3.17b)} \\ \vec{x} \text{ inside } D & \text{(3.17c)} \end{cases}$$

Application of equations (3.17a,b,c) is known as "direct method". For the motion problem of a body at zero Froude number, the line integrals along the waterline L_o and the surface integral over the free surface S_F in equations (3.17a,b,c) vanish. Although the normal velocity $\partial\Phi/\partial n$ in the right hand side of equations (3.17a,b,c) is specified by the body boundary condition, numerical implementation of equations (3.17a,b,c) in solving the unknown potential Φ is impossible to cover the entire free surface. Moreover, the x-derivative of Φ is unknown a priori. Hence, the direct method of using the integral equations (3.17a,b,c) is not recommended in the boundary-value problem of ship motion with forward speed but may be applied for the motion problem of a stationary body. It is necessary to use an alternative method in constructing integral equations by employing the interior domain $\hat{D}$. The resultant of surface integral over S_F and S_o in equations (3.10a,b,c) is analogous to that of equations (3.9a,b,c) in the form

$$\begin{Bmatrix} 0 \\ \pm 2\pi \\ 4\pi \end{Bmatrix}\hat{\Phi}(\vec{x}) + \iint_{S_o}\hat{\Phi}(\vec{\xi})\frac{\partial G(\vec{x};\vec{\xi})}{\partial n}ds(\vec{\xi}) + \frac{U^2}{g}\oint_{L_o}\hat{\Phi}(\vec{\xi})\frac{\partial G(\vec{x};\vec{\xi})}{\partial x}dy(\vec{\xi})$$

$$- i\frac{2\omega U}{g}\oint_{L_o}\hat{\Phi}(\vec{\xi})G(\vec{x};\vec{\xi})dy(\vec{\xi}) + i\frac{4\omega U}{g}\iint_{S_F}\hat{\Phi}(\vec{\xi})\frac{\partial G(\vec{x};\vec{\xi})}{\partial x}ds(\vec{\xi})$$

$$= \iint_{S_o}G(\vec{x};\vec{\xi})\frac{\partial\hat{\Phi}(\vec{\xi})}{\partial n}ds(\vec{\xi}) + \frac{U^2}{g}\oint_{L_o}G(\vec{x};\vec{\xi})\frac{\partial\hat{\Phi}(\vec{\xi})}{\partial x}dy(\vec{\xi})$$

$$\text{if}\begin{cases} \vec{x} \text{ outside } \hat{D} & (3.18a) \\ \vec{x} \text{ on } \hat{S} & (3.18b) \\ \vec{x} \text{ inside } \hat{D} & (3.18c) \end{cases}$$

The x-derivative of Φ and $\hat{\Phi}$ in equations (3.17a,b,c) and (3.18a,b,c) can be expressed in the form

$$\frac{\partial\Phi}{\partial x} = (\vec{s}\frac{\partial\Phi}{\partial s} + \vec{\tau}\frac{\partial\Phi}{\partial\tau} + \vec{n}\frac{\partial\Phi}{\partial n})\bullet\vec{i}$$

where $(\vec{s}, \vec{\tau}, \vec{n})$ is a dextral set of orthogonal unit vectors such that $\vec{s}$ is a unit tangent vector along the curve L_o, $\vec{\tau}$ a unit vector tangent to the body surface S_o and normal to the curve L_o, and $\vec{n}$ a unit normal vector outward the body surfaceS_o. Then $\vec{n}\times\vec{s} = \vec{\tau}$ forms a dextral set of orthogonal unit vector at each point of the curve L_o. On the curve L_o, $\vec{s}=(s_1,s_2,0)$ and $\vec{n}=(n_1,n_2,n_3)$. Thus, we can write

$$\frac{\partial\Phi}{\partial x} = s_1\frac{\partial\Phi}{\partial s} - n_3 s_2\frac{\partial\Phi}{\partial\tau} + n_1\frac{\partial\Phi}{\partial n} \qquad (3.19)$$

$$\frac{\partial\hat{\Phi}}{\partial x} = s_1\frac{\partial\hat{\Phi}}{\partial s} - n_3 s_2\frac{\partial\hat{\Phi}}{\partial\tau} + n_1\frac{\partial\hat{\Phi}}{\partial n} \qquad (3.20)$$

At certain point of the curve L_o, the second terms in the right hand side of equations (3.19) and (3.20) will vanish if the body surface at this point is a vertical wall side or if the curve L_o at this point is parallel to x-axis.

Subtracting equation (3.18a) from (3.17c) for $\vec{x}$ inside D or (3.18b) from (3.17b) for $\vec{x}$ on S_o and using equations (3.19) and (3.20), we get

$$4\pi\Phi(\vec{x}) + \iint_{S_o} \mu(\vec{\xi}) \frac{\partial G(\vec{x};\vec{\xi})}{\partial n}\, ds(\vec{\xi}) + \frac{U^2}{g} \oint_{L_o} \mu(\vec{\xi}) \frac{\partial G(\vec{x};\vec{\xi})}{\partial x} dy(\vec{\xi})$$

$$- i\frac{2\omega U}{g} \oint_{L_o} \mu(\vec{\xi}) G(\vec{x};\vec{\xi}) dy(\vec{\xi}) + i\frac{4\omega U}{g} \iint_{S_F} \mu(\vec{\xi}) \frac{\partial G(\vec{x};\vec{\xi})}{\partial x} ds(\vec{\xi}) = \iint_{S_o} \sigma(\vec{\xi}) G(\vec{x};\vec{\xi}) ds(\vec{\xi})$$

$$+ \frac{U^2}{g} \oint_{L_o} [s_1 \frac{\partial \mu(\vec{\xi})}{\partial s} - n_3 s_2 \frac{\partial \mu(\vec{\xi})}{\partial \tau} + n_1 \sigma(\vec{\xi})] G(\vec{x};\vec{\xi}) dy(\vec{\xi}) \quad (3.21)$$

where
$$\mu(\vec{\xi}) = \Phi(\vec{\xi}) - \hat{\Phi}(\vec{\xi}) \quad (3.22)$$

$$\sigma(\vec{\xi}) = \frac{\partial \Phi(\vec{\xi})}{\partial n} - \frac{\partial \hat{\Phi}(\vec{\xi})}{\partial n} \quad (3.23)$$

μ and σ can be interpreted as the dipole strength and the source strength respectively. The velocity potential $\Phi(\vec{x})$ can be described by either dipole or source distribution over the wetted body surface S_o. For the dipole distribution method, we simply take σ=0 such that the normal velocities are continuous across the wetted body surface S_o while the value of Φ undergoes a jump. On the other hand, the source distribution method requires the continuity of Φ across S_o. Then we may write

$$\mu(\vec{\xi}) = \Phi(\vec{\xi}) - \hat{\Phi}(\vec{\xi}) \quad \text{for dipole distribution method} \quad (3.24a)$$

$$\sigma(\vec{\xi}) = 0 \quad (3.24b)$$

$$\mu(\vec{\xi}) = 0 \quad \text{for source distribution method} \quad (3.25a)$$

$$\sigma(\vec{\xi}) = \frac{\partial \Phi(\vec{\xi})}{\partial n} - \frac{\partial \hat{\Phi}(\vec{\xi})}{\partial n} \quad (3.25b)$$

Substituting equations (3.24a,b) and (3.25a,b) respectively into (3.21), we may obtain

for dipole distribution method:-

$$\iint_{S_\bullet}\mu(\vec{\xi})\frac{\partial G(\vec{x};\vec{\xi})}{\partial n}ds(\vec{\xi})+\frac{U^2}{g}\oint_{L_\bullet}[\mu(\vec{\xi})\frac{\partial G(\vec{x};\vec{\xi})}{\partial x}-(s_1\frac{\partial\mu(\vec{\xi})}{\partial s}-n_3s_2\frac{\partial\mu(\vec{\xi})}{\partial\tau})G(\vec{x};\vec{\xi})]dy(\vec{\xi})$$

$$-i\frac{2\omega U}{g}\oint_{L_\bullet}\mu(\vec{\xi})G(\vec{x};\vec{\xi})dy(\vec{\xi})+i\frac{4\omega U}{g}\iint_{S_F}\mu(\vec{\xi})\frac{\partial G(\vec{x};\vec{\xi})}{\partial x}ds(\vec{\xi})=-4\pi\Phi(\vec{x})$$

$$;\ \vec{x}\ \text{in}\ D,\ \text{on}\ S_o \qquad (3.26)$$

for source distribution method:-

$$\iint_{S_\bullet}\sigma(\vec{\xi})G(\vec{x};\vec{\xi})ds(\vec{\xi})+\frac{U^2}{g}\oint_{L_\bullet}n_1\sigma(\vec{\xi})G(\vec{x};\vec{\xi})dy(\vec{\xi})=4\pi\Phi(\vec{x})$$

$$;\ \vec{x}\ \text{in}\ D,\ \text{on}\ S_o \qquad (3.27)$$

If we apply the body boundary condition in equation (3.26), it is apparent that the second normal derivative of the Green function G would be present. This second derivative of the Green function G is highly oscillatory and more complicated. Furthermore, the derivatives of μ along the waterline L_o is unknown a priori and the evaluation of the integral over the free surface S_F is impossible. Hence, the application of the dipole distribution method is not recommended for a surface piercing body with steady or unsteady forward motion but may be useful for a submerged body with steady forward motion. In contrast, the source distribution method is more convenient. In order to solve equation (3.27), we take the normal derivative of $\Phi(\vec{x})$ with respect to the field point $\vec{x}$ and let the field point $\vec{x}$ lie on the wetted body surface S_o. Then we get

$$2\pi\sigma(\vec{x})+\iint_{S_\bullet}\sigma(\vec{\xi})\frac{\partial G(\vec{x};\vec{\xi})}{\partial n}ds(\vec{\xi})+\frac{U^2}{g}\oint_{L_\bullet}n_1\sigma(\vec{\xi})\frac{\partial G(\vec{x};\vec{\xi})}{\partial n}dy(\vec{\xi})$$

$$=4\pi\frac{\partial\Phi(\vec{x})}{\partial n} \qquad ;\vec{x}\ \text{on}\ S_o \qquad (3.28)$$

The first term in the left hand side of equation (3.28) is depicted the isolation of singulaties for the validity of equation (3.3). When $\vec{x} = \vec{\xi}$, the singular part of the normal derivative of the Green function in equation (3.28) is taken by the first term. It is noted here that the normal derivative given in equation (3.28) is the differentiation of the equation (3.27) with respect to the field point $\vec{x}$ but the normal derivatives in those equations except (3.28) throughout this Chapter are with respect to the source point $\vec{\xi}$ since they are obtained from the dot product of the gradients of the functions and the normal vectors of the source element surfaces.

The derivations of equations (3.15) through (3.28) are made by using the linearised free surface condition in equation (3.12) for the unsteady flow problem. In the steady flow problem, the linearised free surface condition given by equation (2.28) is to be used, which is time independent. Consequently, the integral equations for steady flow problem is simply obtained by cancelling the time dependent terms in equations (3.15) through (3.28). For source distribution method, equations (3.27) and (3.28) can also be applied for a steady flow problem.

Through the known body boundary conditions and the Green function G, the unknown source strength σ can be solved in equation (3.28). The representation of the integral equations (3.27) and (3.28) can be simulated by means of the source distribution over the body surface which is discretised by a finite but a large number of panels to form a system of algebraic equations.

For the special case of zero forward speed problem, the application of the direct method given by equation (3.17) may be competitive with the source distribution method since the free surface integrals vanish. Nevertheless, the direct method cannot provide the source strength which is very useful in the evaluation of higher order derivatives of the Green function.

3.5 Irregular frequencies

One defect of the boundary integral equation method associated with the free surface Green function is the existence of irregular frequencies which correspond to the eignfrequencies of the interior Dirichlet problem (John 1950). At these discrete frequencies no unique solution of the Fredholm equation exists even though the solution of the corresponding boundary value problem is unique. As a result, the discretised integral equation is ill-conditioned over a finite bandwidth.

The existence of irregular frequencies was first recognised by Lamb (1932) when he applied Green function for studing acoustical scattering by a sphere. In the free surface flow problem John (1950) pointed out that an integral equation with the free surface Green function admits non-trivial solutions at the eignfrequencies defined by the interior eignvalue problem as follows

$$\nabla^2 \hat{\Phi}_m = 0 \qquad \text{inside } \hat{D} \qquad m = 1,2,3,... \qquad (3.29)$$

$$\frac{\partial \hat{\Phi}_m}{\partial z} - f_m^2 \hat{\Phi}_m = 0 \qquad \text{on } \hat{S}_F \qquad (3.30)$$

$$\hat{\Phi}_m = 0 \qquad \text{on } S_o \qquad (3.31)$$

For a free floating body without forward speed in waves, the integral equation is a surface integral which is obtained through direct consequence of Green's theorem or through the use of dipole / source distribution. The representation based on either the direct Green's integral equation or source distribution imposes a Dirichlet condition on the body surface and that the dipole distribution imposes a Neumann condition on the body surface. The homogeneous solutions of the direct Green's integral equation and dipole / source distribution method, associated with the interior eignvalue problem are unbounded, which happens at a discrete set of resonant frequencies. These interior

resonant frequencies are called the irregular frequencies. It is noted that the direct Green's integral equation and source distribution method have the same irregular frequencies since the kernel of one is the transponse of the other.

For linearised steady or unsteady forward motion problem the integral equation is supplemented by a free surface line integral. The Green function in the line integral is a weakly singular pressure point because the source point of the Green function is on the free surface. The presence of the free surface line integral causes numerical difficulties and might magnify the ill-conditioning in the vicinity of irregular frequencies. The bandwidth of irregular frequencies could be manifested by substantial errors due to numerical inaccuracy in the evaluations of the Green function or from the poor modelling of the body surface. Sclavounos & Lee (1985) showed that the errors and frequency bandwidth of the irregular frequencies decrease with increasing number of elements.

The irregular frequencies problem may be tackled by two possible approaches. They are

(i) to predict the irregular frequencies precisely and avoid computation around these discrete frequencies.

(ii) to modify the integral equation which ensure a unique solution at all frequencies.

For simple geometries analytical formulae to predict the occurrence of irregular frequencies are available. Frank (1967) identified the irregular frequencies of circular and rectangular cross-sections and found that the solutions become ill-conditioned within a region close to these frequencies. Inglis & Price (1981b) used the eignfrequencies of interior solution of a rectangular box as a guide to the position of irregular frequencies for a ship shaped body. Later Wu & Price (1986) generalised an equivalent box approximation based on the form coefficients of a body. Since this approximation is empirical, it is uncertain to hit the irregular frequencies for an arbitrarily floating structure. After all, the irregular frequencies are unknown a priori for

a complicated geometries and therefore alterative means are required to eliminate the irregular frequencies.

Unique solution of exterior problems at any frequencies has been shown by Ursell (1973). The difficulty of irregular frequencies arises from the method of solution and not from the nature of the boundary value problem. Therefore the irregular frequencies can be avoided by modifying the integral equation. The general spirit of eliminating the irregular frequencies is to impose extra constraints and unknowns to render the discreted integral equation well-conditioned. Ursell (1953) modified the kernel of the integral equation by adding a series of multipoles in the study of short surface waves due to an oscillating cylinder. In the field of acoustics Ursell (1973) showed that the modified Green function which satisfies a dissipative boundary condition on a circle lying inside the body produces a unique solution at all frequencies. This modified Green function is expressed in terms of a series of multipoles. The number of multipoles will determine the range of frequencies which are free of irregular frequencies. Although the multipole method of solution is valid at any frequencies, it becomes less and less convenient as frequency increases.

In the free surface problem the resonant wave pheonomana of the interior Dirichlet problem causes non-trivial solutions of the integral equation. This pheonomana can be thought of as a kind of fluid sloshing inside the body and thus the irregular frequencies can be suppressed by adding an artificial lid on the interior free surface, where a rigid wall boundary condition is applied. Ohmatsu (1975) proved that this approach does remove the irregular frequencies. Unfortunately, it leads to a substantial increases in the computational effort, especially in three-dimensions. The lid on the interior free surface introduces extra equations to the original integral equation. Consequently, the equation becomes overdetermined since the total number of equations is larger than that of unknowns. Another possible overdetermined scheme is the integral equation of second kind on the body surface combined by another integral equation of first kind in the interior domain. Numerical results presented by Lau (1987) showed that the combined boundary integral equation method for zero speed problem is

effective in the first few irregular frequencies but becomes less satisfactory at high frequency. From his numerical results for forward speed case this method fails at some frequencies where both direct Green's integral and source distribution have not detected errors.

Another way to remove the sloshing modes is to add a source singularity inside the body so that the energy associated with the interior Dirichlet eignsolutions is absorbed by the source. Sayer & Ursell (1977) and Ogilvie & Shin (1978) illustrated that this approach successfully removes the first two irregular frequencies of two-dimensional problem. Ursell (1981) proved that any number of irregular frequencies can be removed if a sufficient number of singularities are added inside the body.

In the field of acoustics Burton and Miller (1971) proposed a method which explorits the different location of the irregular frequencies of integral equations of the first and second kind. They showed that the linear combination of two such equations for the exterior Neumann problem has a unique solution at all frequencies provided that one of the two equations must be multiplied by an imaginary constant. Sclavounos & Lee (1985) adopted this method to the two-dimensional radiation problem and found that the error due to irregular frequencies is reduced.

3.6 Conclusions

Different approaches in the applications of the three-dimensional Green function integral equation have been presented. These approaches are the direct Green's integral equation method and the indirect method which consists of dipole and source distribution techniques. It seems that the source distribution technique is more versatile than the other method. For the free floating body without forward speed the applicablity of the direct Green's integral equation may be competitive with the source distribution method since the free surface integrals vanish. However the direct Green's integral equation and dipole distribution method are less attractive for the body translating and

oscillating in waves.

Various methods for avoiding or removing irregular frequencies have been discussed. These methods are either modifying the kernel of the integral equation or modifying the domain of the integral equation. However all the methods for eliminating irregular frequencies increase substantially computer time, especially in three-dimensional problems.

CHAPTER 4

GREEN FUNCTION

IN THE THEORY OF UNSTEADY FORWARD MOTION

4.1 Introduction

In the unsteady flow field due to the forward and oscillatory motions of a marine vehicle moving with a constant horizontal velocity in waves, the interaction between the steady waves (Kelvin waves) and the unsteady waves (radiation waves) makes the ship motion problem complicated to an extent that the numerical evaluation of the velocity potential representing the flow field is prone to difficulties because of the complex mathematical form of the Green function defining the velocity potential. This interaction depends on the magnitudes of the forward speed U and the frequency of oscillation ω. In the usual linearised formulation, the Green function satisfies the Laplace's equation, the linearised free surface condition, the sea bed condition and the far-field radiation condition. For the fully three-dimensional problem of a moving ship in waves, the complete linearised free surface condition is exactly satisfied without further assumption in terms of the forward speed. This three-dimensional Green function for a unit oscillating source moving beneath the undisturbed free surface of an infinite lateral extent of ocean is a function of forward speed, frequency of oscillation and spatial positions of source and field points for infinite water depth. Water depth must be added in the expression for the Green function in shallow water.

The computation of the potential of any kind of source depends on the expression for the Green function. With the advent of fast electronic computers, a great deal of research has been carried out examining modifications to the expressions for the Green function. Nevertheless, these modified expressions for the Green function are applicable for deep water only and they lack generality of application. In the present

study, a method for the calculation of a translating pulsating source for finite water depth is presented. The derivations of this source function will be described in the first part of this Chapter for infinite water depth and in the second part for finite water depth.

4.2 Formulation of the problem

In the linearised unsteady forward motion problem the flow disturbance may be represented by a translating pulsating source submerged below the free surface of the undisturbed fluid of infinite lateral extent. This source of unit strength is moving with a constant speed U and oscillating with a frequency of oscillation ω.

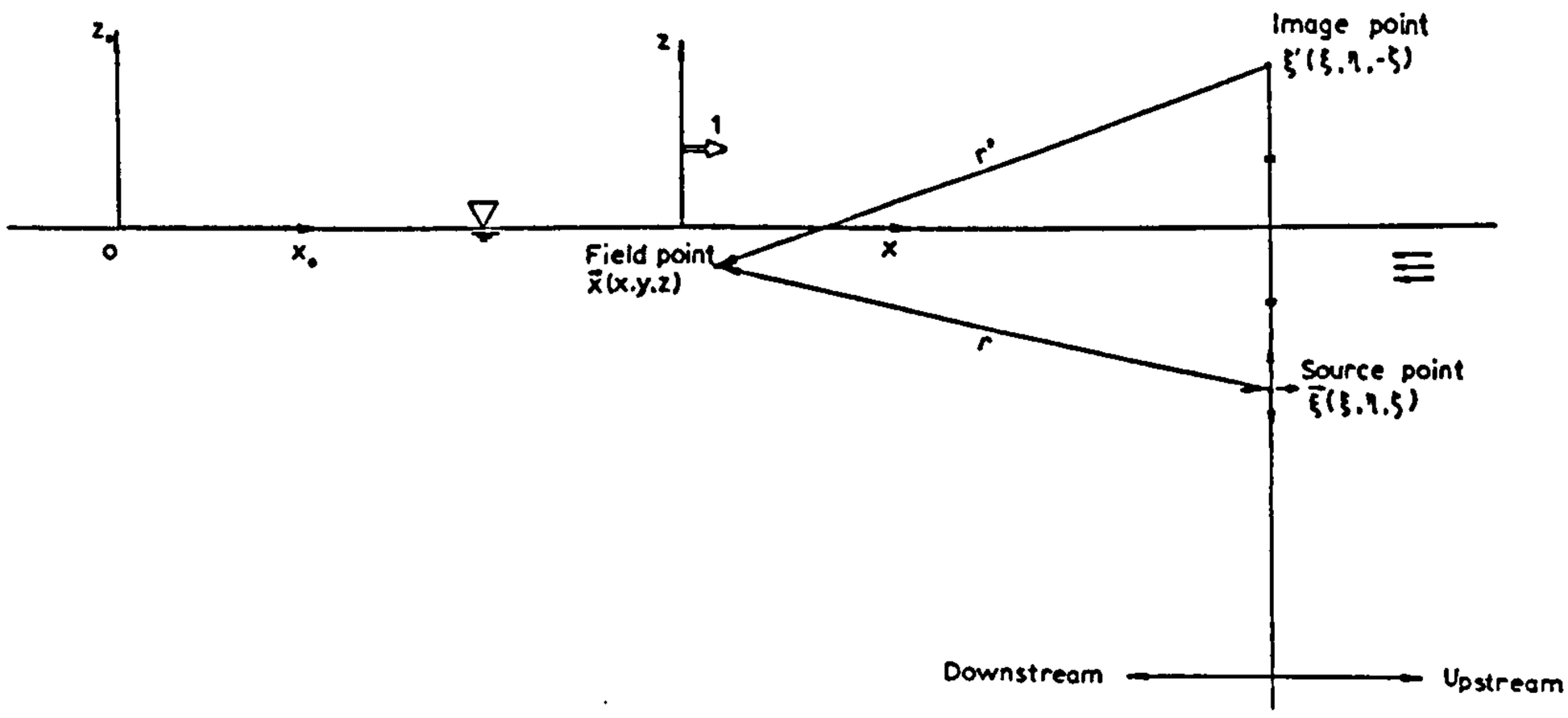

Fig.4.1 Sketch for Flow Field

It is convenient to use a right-handed system of coordinates 0-XYZ moving along with the source. The X-axis is taken in the same direction to the movement of the source, that is, pointing upstream while the Z-axis is vertically pointing upward with the plane z = 0 on the undisturbed free surface. In order to facilitate the study of the unsteady flow problem, it is conventional to non-dimensionalise the system of coordinates with a characteristic length L such that

$$\vec{x} = \vec{X} / L \quad ; \quad f = \omega\sqrt{(L/g)} \quad ; \quad F_n = U/\sqrt{(gL)} \quad ; \quad \tau = f F_n = \omega U/g$$

in which f is a non-dimensional frequency, F_n is a Froude number and τ gives the correlation of f and F_n. The flow at a field point $\vec{x}$ is being observed by an observer

from the translating system of coordinates o-xyz as shown in Fig.4.1 so that the observer perceives the unsteady flow disturbance caused by the submerged source at a fixed position $\vec{\xi}$ in an oncoming stream of velocity equal but opposite direction to that of the source. The coordinates of the source point $\vec{\xi}$ is denoted by $(\xi,\eta,\zeta<0)$, while the coordinates of the field point $\vec{x}$, where the flow is being observed, is denoted by $(x,y,z \leq 0)$. The vector joining the mirror image $\vec{\xi}'$ of the source with respect to the undisturbed free surface to the field point $\vec{x}$ is denoted by $\vec{x}'$, with $x' = x-\xi$, $y' = y-\eta$ and $z' = z+\zeta$. The magnitude of the vector $\vec{x} - \vec{\xi}$ is r while the magnitude of $\vec{x}'$ is r'. By making use of the non-dimensional system of coordinates, the governing equation and boundary conditions for the unsteady flow problem in association with the Green function $G(\vec{x}; \vec{\xi})$ as discussed in Chapter 2 can be shown in the form

Laplace's equation

$$\nabla^2 G(\vec{x}; \vec{\xi}, f, F_n, \varepsilon) = \delta(\vec{x} - \vec{\xi}) \qquad ; z<0 \quad (4.1)$$

Linearised free surface condition

$$-(f + i\varepsilon - iF_n \frac{\partial}{\partial x})^2 G + G_z = 0 \qquad ; z=0 \quad (4.2)$$

Sea bed condition

$$G_z = 0 \qquad ; z=-h \quad (4.3a)$$

$$G_z = 0 \qquad ; z \to \infty \quad (4.3b)$$

Far-field radiation condition

$$\lim_{r \to \infty} G = 0 \qquad (4.4)$$

where $\delta(\vec{x} - \vec{\xi})$ in equation (4.1) is a Dirac delta function such that $\delta(\vec{x} - \vec{\xi}) \neq 0$ if

$\vec{x} = \vec{\xi}$. The parameter ε in equation (4.2) is the Rayleigh artificial viscosity which provides a convenient alternative approach instead of using the exact far-field radiation condition. On the other hand, equation (4.4) is not an obvious far-field radiation condition. The concept of the Rayleigh artificial viscosity is to seek a steady-state solution at the zero limit of the parameter ε (Lighthill 1967) as the flow is initiated by the time dependent velocity potential $\phi(\vec{x}, t) = \varphi(\vec{x}) \exp[-i\omega(1 + i\varepsilon)t]$. Equations (4.3a) and (4.3b) represent the sea bed condition for finite depth h and infinite depth respectively. The general solutions of the unsteady flow problems for infinite and finite depth cases given by equations (4.1) through (4.4) can be shown in the following form

$$G(\vec{x}; \vec{\xi}, f, F_n, \varepsilon) = -\frac{1}{r} + H(\vec{x}; \vec{\xi}, f, F_n, \varepsilon) \qquad \text{for infinite depth} \quad (4.5)$$

$$G(\vec{x}; \vec{\xi}, h, f, F_n, \varepsilon) = -\frac{1}{r} - \frac{1}{r_h} + H(\vec{x}; \vec{\xi}, h, f, F_n, \varepsilon) \qquad \text{for finite depth} \quad (4.6)$$

The terms $-1/r$ and H in equations (4.5) and (4.6) are a source singularity and a regular harmonic function respectively. The term $-1/r_h$ in equation (4.6) is a finite depth source defined by

$$r_h = \sqrt{(x-\xi)^2 + (y-\eta)^2 + (z+2h+\zeta)^2} \qquad (4.7)$$

which is used to simplify the application of the sea bed condition for the finite depth case. After substituting equations (4.5) and (4.6) respectively into equations (4.1) through (4.4) for infinite and finite water depth cases, we obtain

for infinite depth : -

$$\nabla^2 H(\vec{x}; \vec{\xi}, f, F_n, \varepsilon) = 0 \qquad ; \ z < 0 \quad (4.8)$$

$$[-(f + i\varepsilon - iF_n \frac{\partial}{\partial x})^2 + \frac{\partial}{\partial z}]H$$

$$= [-(f + i\varepsilon - iF_n \frac{\partial}{\partial x})^2 + \frac{\partial}{\partial z}]\frac{1}{r} \qquad ; \ z = 0 \quad (4.9)$$

$$H_z = 0 \qquad ; \ z \to \infty \quad (4.10)$$

$$H = 0 \qquad ; \ r \to \infty \quad (4.11)$$

for finite depth : -

$$\nabla^2 H(\vec{x}; \vec{\xi}, h, f, F_n, \varepsilon) = 0 \qquad ; z < 0 \quad (4.12)$$

$$[-(f + i\varepsilon - iF_n \frac{\partial}{\partial x})^2 + \frac{\partial}{\partial z}]H$$

$$= [-(f + i\varepsilon - iF_n \frac{\partial}{\partial x})^2 + \frac{\partial}{\partial z}](\frac{1}{r} + \frac{1}{r_h}) \qquad ; z = 0 \quad (4.13)$$

$$H_z = 0 \qquad ; z = -h \quad (4.14)$$

$$H = 0 \qquad ; r \to \infty \quad (4.15)$$

The boundary-value problems defined by the above equations for infinite depth and finite depth cases can be solved by using a double Fourier transform of the function H with respect to the horizontal coordinates x and y, which is defined as

$$H^{**}(\alpha, \beta, z; \vec{\xi}, f, F_n, \varepsilon) = \frac{1}{2\pi} \int_{-\infty}^{\infty} dy \int_{-\infty}^{\infty} dx\, e^{-i(\alpha x + \beta y)} H(\vec{x}; \vec{\xi}, f, F_n, \varepsilon)$$

and its inverse Fourier transform as

$$H(\vec{x}; \vec{\xi}, f, F_n, \varepsilon) = \frac{1}{2\pi} \int_{-\infty}^{\infty} d\beta \int_{-\infty}^{\infty} d\alpha\, e^{i(\alpha x + \beta y)} H^{**}(\alpha, \beta, z; \vec{\xi}, f, F_n, \varepsilon)$$

in which $\alpha = k\cos\theta$ and $\beta = k\sin\theta$.

Since the general solutions of the boundary-value problems for infinite depth and finite depth cases are quite different, we shall derive these solutions for infinite depth in section 4.3 and for finite depth in section 4.4.

4.3 Derivation of Green function for infinite water depth

By taking the double Fourier transform of equations (4.8) through (4.10) defined for infinite depth boundary-value problem with respect to the horizontal coordinates x and y, we obtain

$$H_{zz}^{**} - k^2 H^{**} = 0 \quad ; \ z < 0 \quad (4.16)$$

$$-(f+i\varepsilon+F_n\alpha)^2 H^{**} + H_z^{**} = -\frac{k+(f+i\varepsilon+F_n\alpha)^2}{k} e^{k\zeta - i(\alpha\xi+\beta\eta)} \ ; \ z = 0 \quad (4.17)$$

$$H_z^{**} = 0 \quad ; \ z \to \infty \quad (4.18)$$

The general solution of the ordinary differential equation (4.16) is $H^{**} = Ae^{kz} + Be^{-kz}$ in which A and B are constant. By using the Fourier transform for the sea bed condition given in equation (4.18), we deduce that the constant B is identical to zero and

$$H^{**}(\alpha, \beta, z; \vec{\xi}, f, F_n, \varepsilon) = A(\alpha, \beta; \vec{\xi}, f, F_n, \varepsilon) e^{kz}$$

The constant A can be solved by the Fourier transform free surface condition in equation (4.17) and then we have

$$H^{**}(\alpha,\beta,z;\vec{\xi},f,F_n,\varepsilon) = -\frac{k+(f+i\varepsilon+F_n\alpha)^2}{k[k-(f+i\varepsilon+F_n\alpha)^2]} e^{kz' - i(\alpha\xi+\beta\eta)}$$

The inverse Fourier Transform of the foregoing expression yields

$$H(\vec{x};\vec{\xi}, f, F_n, \varepsilon) = \frac{1}{r'} - \frac{1}{\pi}\int_{-\infty}^{\infty} d\beta \int_{-\infty}^{\infty} d\alpha \frac{e^{kz' + i(\alpha x' + \beta y')}}{k - (f + i\varepsilon + F_n\alpha)^2}$$

Substituting the foregoing expression in equation (4.5), we get

$$G(\vec{x};\vec{\xi}, f, F_n, \varepsilon) = -\frac{1}{r} + \frac{1}{r'} - \frac{1}{\pi}\int_{-\infty}^{\infty} d\beta \int_{-\infty}^{\infty} d\alpha \frac{e^{kz' + i(\alpha x' + \beta y')}}{k-(f+i\varepsilon+F_n\alpha)^2} \quad (4.19a)$$

It is more convenient to use $G(\vec{x};\vec{\xi}, f, F_n, \varepsilon)$ in polar coordinates rather than

Fourier transform Cartesian coordinates. Thus equation (4.19a) becomes

$$G(\vec{x};\vec{\xi}, f, F_n, \varepsilon) = -\frac{1}{r} + \frac{1}{r'} - \frac{1}{\pi}\int_0^{2\pi} d\theta \int_0^{\infty} dk \frac{k e^{-k[|z'|-i(x'\cos\theta+y'\sin\theta)]}}{k-(f+i\varepsilon+F_n k\cos\theta)^2} \quad (4.19b)$$

Considering the integration limit of outer integral in the bound $[0,\pi]$, we may get

$$G(\vec{x};\vec{\xi}, f, F_n, \varepsilon) = -\frac{1}{r} + \frac{1}{r'} - D(\vec{x}'; f, F_n, \varepsilon) \quad (4.20)$$

where

$$D(\vec{x}'; f, F_n, \varepsilon) = \frac{1}{\pi}\sum_{j=1}^{2}\int_0^{\pi} d\theta \int_0^{\infty} dk \frac{k\exp(-kw_j)}{k-(f+i\varepsilon+F_n k\cos\theta)^2} \quad (4.21)$$

$$w_j = |z| - it_j \quad (4.22)$$

$$t_1 = x'\cos\theta + y'\sin\theta \quad (4.23a)$$

$$t_2 = x'\cos\theta - y'\sin\theta \quad (4.23b)$$

Let us designate

$$\gamma = \left\{\begin{array}{c} 0 \\ \\ \cos^{-1}(1/4\tau) \end{array}\right\} \text{ if } \left\{\begin{array}{l} \tau < 1/4 \\ \\ \tau \geq 1/4 \end{array}\right. \quad (4.24)$$

The integrand of the integral D given by equation (4.21) has two poles when the value of k satisfies

$$k = \frac{(1-2\tau\cos\theta) \mp \sqrt{1-4\tau\cos\theta}}{2F_n^2\cos^2\theta} - \frac{i\varepsilon(\sqrt{1-4\tau\cos\theta} \mp 1)}{F_n\cos\theta\sqrt{1-4\tau\cos\theta}} \quad (4.25)$$

After taking the limit of the Rayleigh artificial viscosity ε equal to zero, we may deduce the following results from equation (4.25)

$$k_1 = \frac{1 - 2\tau\cos\theta \mp i\sqrt{4\tau\cos\theta - 1}}{2F_n^2\cos^2\theta} \qquad \text{for} \quad 0 \le \theta \le \gamma \qquad (4.26a)$$

k_2

$$k_1 = \frac{1 - 2\tau\cos\theta \mp \sqrt{1 - 4\tau\cos\theta}}{2F_n^2\cos^2\theta} + \begin{matrix} i\,0^+ \\ -i\,0^+ \end{matrix} \qquad \text{for} \quad \gamma \le \theta \le \frac{\pi}{2} \qquad (4.26b)$$

k_2

$$k_1 = \frac{1 - 2\tau\cos\theta \mp \sqrt{1 - 4\tau\cos\theta}}{2F_n^2\cos^2\theta} + i0^+ \qquad \text{for} \quad \frac{\pi}{2} \le \theta \le \pi \qquad (4.26c)$$

k_2

In the range $0 \le \theta \le \gamma$, the values of the pole k are complex for $4\tau\cos\theta - 1 > 0$; $\tau > 1/4$ and $\theta < \gamma$. The complex poles which are conjugate to each other lie in the first and fourth quadrant of the complex κ-plane as shown in Fig.4.2a respectively. On the other hand, the values of the pole k are always real in the range $\gamma \le \theta \le \frac{\pi}{2}$ for $1 - 4\tau\cos\theta > 0$. Equation (4.26b) suggests that the path of integration along the real k-axis is deformed above to by-pass the pole k_1 and below to by-pass the pole k_2 in the range $\gamma \le \theta \le \frac{\pi}{2}$ as shown in Fig.4.2b. Meanwhile, equation (4.26c) suggests that both the poles k_1 and k_2 are by-passed by indenting the path above the real k-axis as shown in Fig.4.2c for $\theta > \pi/2$.

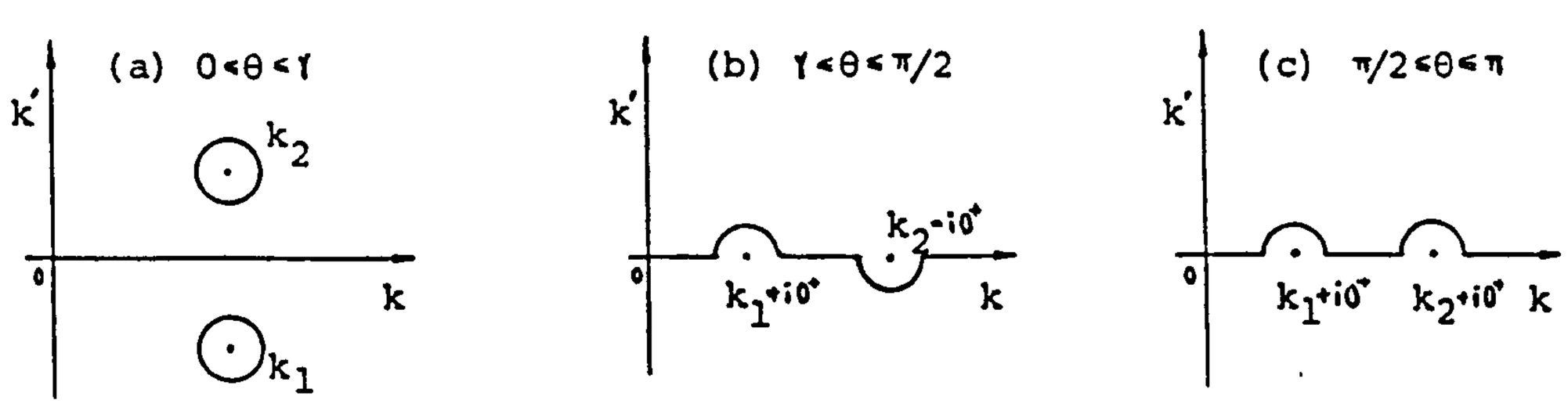

Fig.4.2 Path of integration in complex K-plane

Noting that the denominator of the integrand of the integral D in equation (4.21) can be expressed in the form

$$k-(f+F_n k\cos\theta)^2 = -F_n\cos^2\theta\,(k-k_1)(k-k_2)$$

in which the values of k_1 and k_2 are given by equations (4.26a,b,c). After some manipulation, the foregoing equation may be written as

$$\frac{1}{k-(f+F_n k\cos\theta)^2} = \begin{cases} \dfrac{-i}{\sqrt{4\tau\cos\theta-1}} \\ \\ \dfrac{1}{\sqrt{1-4\tau\cos\theta}} \end{cases} \left(\frac{1}{k-k_1}-\frac{1}{k-k_2}\right) \quad \text{if} \begin{cases} 0\le\theta\le\gamma \\ \\ \gamma\le\theta\le\pi \end{cases}$$

By invoking the foregoing expression into equation (4.21), it follows

$$D(\vec{x}';f,F_n,0^+) = \frac{1}{\pi}\sum_{j=1}^{2}(D_{1j}+D_{2j}+D_{3j}) \qquad (4.27)$$

where

$$D_{1j} = -i\int_0^{\gamma}\frac{M_j}{\sqrt{4\tau\cos\theta-1}}d\theta \qquad (4.28a)$$

$$D_{2j} = \int_{\gamma}^{\frac{\pi}{2}}\frac{M_j}{\sqrt{1-4\tau\cos\theta}}d\theta \qquad (4.28b)$$

$$D_{3j} = \int_{\frac{\pi}{2}}^{\pi}\frac{M_j}{\sqrt{1-4\tau\cos\theta}}d\theta \qquad (4.28c)$$

$$M_j = \int_0^{\infty}\left(\frac{1}{k-k_1}-\frac{1}{k-k_2}\right)k\exp(-kw_j)dk \quad \text{for } 0\le\theta\le\gamma \qquad (4.29a)$$

$$M_j = PV\int_0^{\infty}\left(\frac{1}{k-k_1}-\frac{1}{k-k_2}\right)k\exp(-kw_j)dk + i\pi[k_1\exp(-k_1w_j)+k_2\exp(-k_2w_j)]$$

$$\text{for } \gamma\le\theta\le\frac{\pi}{2} \qquad (4.29b)$$

$$M_j = PV\int_0^{\infty}\left(\frac{1}{k-k_1} - \frac{1}{k-k_2}\right)k\exp(-kw_j)dk$$

$$+ i\pi\left[k_1\exp(-k_1 w_j) - k_2\exp(-k_2 w_j)\right]$$

$$\text{for } \frac{\pi}{2} \le \theta \le \pi \quad (4.29c)$$

If $\tau < 1/4$, γ becomes zero and then the integral D_{1j} is identical to zero. When $\tau \geq 1/4$, the values of k_1 and k_2 are complex for $\theta < \gamma$ whereas they become purely real and equal, and the integrand M_j is identical to zero at $\theta = \gamma$. However, singularity occurs at the lower limit of the integral D_{2j} when $\theta = \gamma$. Special treatment will be applied to avoid this singularity.

The residue terms appearing in equations (4.29b,c) are the far-field wave like disturbances. The signs of these terms have been reversed in opposition to the directions shown in Fig.4.2b,c in order to satisfy the far-field condition that no energy feed into the source singularity from far-field.

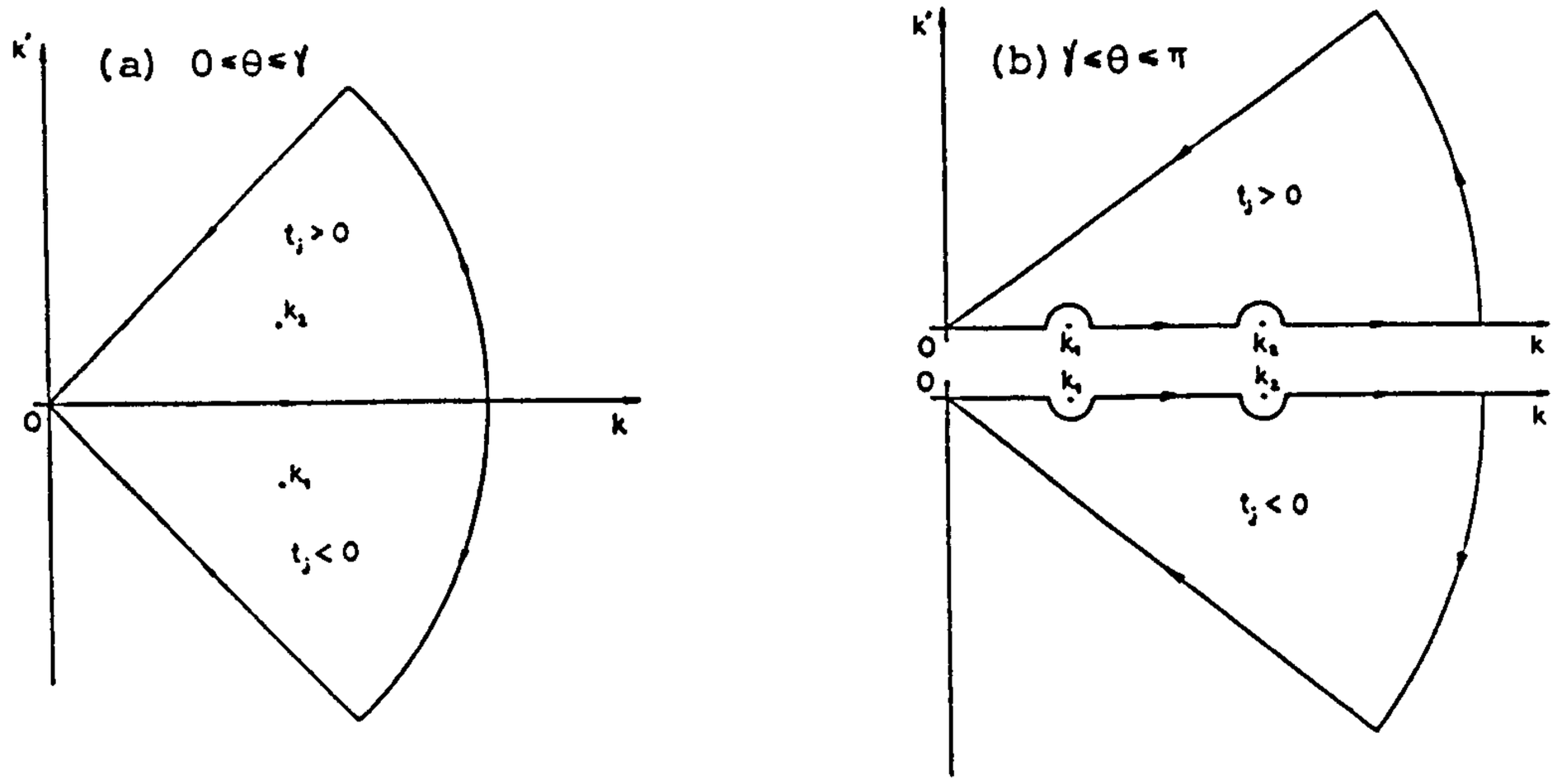

Fig.4.3 Contour integration in complex κ-plane

After evaluating those integrals, on the right-hand side of equations (4.29a,b,c), along a path as shown in Fig.4.3a,b, we may get the following equations (4.30a,b,c) in which H(x) is a Heaviside step function defined as H(x) = 0 for x < 0 and H(x) = 1 for x > 0. The residue terms arising in equation (4.30a) are the results of the contour integration whose path is taken as shown in Fig.4.3a and the poles lie inside the contour. These terms are not the far-field function since the complex poles k_1 and k_2 which are conjugate to each other contribute to the near-field integral M_j.

$$M_j = Q_j - i2\pi[H(-\mathrm{Im}\ Z_{1j})k_1 \exp(Z_{1j}) + H(\mathrm{Im}\ Z_{2j})k_2 \exp(Z_{2j})]$$

$$\text{for } 0 \le \theta \le \gamma \qquad (4.30a)$$

$$M_j = Q_j + i2\pi[H(t_j)k_1 \exp(Z_{1j}) + H(-t_j)k_2 \exp(Z_{2j})]$$

$$\text{for } \gamma \le \theta \le \frac{\pi}{2} \qquad (4.30b)$$

$$M_j = Q_j + i2\pi H(t_j)[k_1 \exp(Z_{1j}) - k_2 \exp(Z_{2j})]$$

$$\text{for } \frac{\pi}{2} \le \theta \le \pi \qquad (4.30c)$$

$$Q_j = k_1 \exp(Z_{1j}) E_1(Z_{1j}) - \frac{k_1}{Z_{1j}} - k_2 \exp(Z_{2j}) E_1(Z_{2j}) + \frac{k_2}{Z_{2j}} \qquad (4.31)$$

$$Z_{ij} = -k_i w_j \qquad ;\ i, j = 1, 2 \qquad (4.32)$$

The exponential integral $E_1(Z)$ given in equation (4.31) is defined by Abramowitz and Stegun (1972). The values of the poles k_1 and k_2 are complex in equation (4.30a) but real in (4.30b,c). In order to understand the physical meaning of those residue terms in equations (4.30b,c), it is convenient to consider the wave disturbances for two special cases, that is, zero Froude number (pulsating with zero forward speed) and zero frequency (steady translating).

For the case of zero Froude number, the results of the poles k_1 and k_2 in equation (4.26) are zero and infinite respectively. The infinite value of the pole k_2 causes the disappearance of the far-field waves. The zero value of the pole k_1 is meaningless. Therefore equations (4.26b,c) are not applicable for zero Froude number. However, we can find that the root of zero denominator in the integrand of the integral D for $F_n = 0$ is the square of the non-dimensional frequency f. At this moment we do not know whether this root belongs to either the pole k_1 or k_2 but the fact we understand is that the nature of this root is a cylindrical wave-like disturbance; waves radiate from the source in all horizontal directions. In any case, we have to ensure that this root belongs to the pole k_1 since the pole k_2 is Kelvin wave-like disturbance as will be noted later. Hence, we conclude that the pole k_1 is cylindrical wave-like disturbance.

On the other hand, if the frequency of oscillation ω is equal to zero, the values of the poles k_1 and k_2 in equations (4.26b,c) become zero and the reciprocal of $F_n^2\cos^2\theta$ respectively. The pole k_2 behaves as a Kelvin wave-like disturbance, that is, wave trailing downstream but zero upstream.

The interaction between cylindrical waves (unsteady waves) and Kelvin waves (steady waves) depends upon the magnitudes of the frequency ω and the forward speed U. They are correlated with the parameter τ. We can distinguish different wave patterns for subcritical regime $\tau < 1/4$, critical regime $\tau = 1/4$ and supercritical regime $\tau > 1/4$. It is convenient to consider wave patterns in the plane $y' = 0$, that is, the centre-plane of the moving object, in order to define different regimes. In the subcritical regime $\tau < 1/4$, the integral D_{1j} vanishes and the two wave trains obtained from equations (4.28b) associated with (4.30b) are fully developed. In addition to these two wave trains, two more wave trains also appear in equation (4.28c) associated with (4.30c). The two wave trains due to the pole k_2 are present only for $x' < 0$ as may be seen in equations (4.30b,c). Meanwhile, the wave train generated from the pole k_1 in equation (4.30b) is propagating upstream for $x' > 0$ and the remaining wave train generated from the pole k_1 in equation (4.30c) is propagating downstream for $x' < 0$. As a result, there are four wave trains generated in the subcritical regime $\tau < 1/4$; three behind the source and one

in advance. It may be shown that the group velocity of the radiation waves upstream is greater than the forward speed U. When the forward speed is equal to zero, the wave trains trailing downstream due to the pole k_2 disappear and all waves associated with the pole k_1 radiate from the source in all horizontal directions. In contrary, if the frequency of oscillation is equal to zero, the cylindrical wave trains due to the pole k_1 vanish and all waves become a pure Kelvin wave disturbance. In the critical regime $\tau = 1/4$, the group velocity of the wave trains due to the pole k_1 is equal to forward speed and these wave trains become standing waves. Therefore, the resultant wave trains from the pole k_1 and k_2 are propagating downstream. In the supercritical regime $\tau > 1/4$, no wave propagates upstream since the wave trains due to the pole k_1 for $x' > 0$ are constrained and cannot be fully developed. Consequently, upstream waves disappear and all waves leave downstream.

Substituting those results obtained in equations (4.27) through (4.32) into (4.20), we can write

$$G(\vec{x};\vec{\xi}, f, F_n) = -\frac{1}{r} + \frac{1}{r'} - N(\vec{x}'; f, F_n) - W(\vec{x}'; f, F_n) \qquad (4.33)$$

where

$$N(\vec{x}'; f, F_n) = \sum_{j=1}^{2} \{ \frac{1}{\pi} [-i \int_0^{\gamma} \frac{Q_j}{\sqrt{4\tau \cos\theta - 1}} d\theta + \int_{\gamma}^{\pi} \frac{Q_j}{\sqrt{1 - 4\tau \cos\theta}} d\theta]$$
$$- 2 \int_0^{\gamma} \frac{H(-\mathrm{Im}\, Z_{1j}) k_1 \exp(Z_{1j}) + H(\mathrm{Im}\, Z_{2j}) k_2 \exp(Z_{2j})}{\sqrt{4\tau \cos\theta - 1}} d\theta \} \qquad (4.34)$$

$$W(\vec{x}'; f, F_n) = \sum_{j=1}^{2} i 2 \{ \int_{\gamma}^{\frac{\pi}{2}} \frac{H(t_j) k_1 \exp(Z_{1j}) + H(-t_j) k_2 \exp(Z_{2j})}{\sqrt{1 - 4\tau \cos\theta}} d\theta$$
$$+ \int_{\frac{\pi}{2}}^{\pi} \frac{H(t_j) [k_1 \exp(Z_{1j}) - k_2 \exp(Z_{2j})]}{\sqrt{1 - 4\tau \cos\theta}} d\theta \} \qquad (4.35)$$

$$Q_j = k_1 \exp(Z_{1j}) E_1(Z_{1j}) - k_2 \exp(Z_{2j}) E_1(Z_{2j}) \qquad (4.36a)$$

or
$$Q_j = k_1 \exp(Z_{1j}) E_1(Z_{1j}) - \frac{k_1}{Z_{1j}} - k_2 \exp(Z_{2j}) E_1(Z_{2j}) + \frac{k_2}{Z_{2j}} \qquad (4.36b)$$

The expression for $N(\vec{x}'; f, F_n)$ given by equation (4.34) is the local disturbance function which is symmetric in all horizontal radial directions while the expression for $W(\vec{x}'; f, F_n)$ given by equation (4.35) is a wave-like far-field function which is symmetric only in transverse direction.

The expression for the Green function given by equation (4.33) which is associated with equations (4.34), (4.35), (4.36) and (4.32), is an alternative form derived independently by Havelock (1958) and Inglis & Price (1981) and is similar to that given by Wu & Eatock-Taylor (1987). Evaluation of the Green function given by equation (4.33) is straightforward. The exponential integral $E_1(Z)$ can be evaluated efficiently by means of an ascending series or an asymptotic expansion for small or large arguments respectively as given by Abramowitz and Stegun (1972). For moderate values of the argument an approximation of the exponential integral $E_1(Z)$ proposed by Hess & Smith (1967) may be used as a complementary expression for the ascending series and asymptotic expansion.

4.3.1 Generalisation of Green function at zero frequency

It is apparent that the expression (4.33) for Green function representing a translating pulsating source can generalise the Green function for translating source with zero frequency, that is, the Kelvin source. When the frequency of oscillation ω is equal to zero, $\tau = 0$ and $k_1 = 0$. Thus equation (4.33) which is associated with equations (4.34), (4.35) and (4.36a) reduces to

$$G(\vec{x}; \vec{\xi}, F_n) = -\frac{1}{r} + \frac{1}{r'} + N(\vec{x}'; F_n) + W(\vec{x}'; F_n) \qquad (4.37)$$

where

$$N(\vec{x}'; F_n) = \sum_{j=1}^{2} \{ \frac{1}{\pi} \int_0^{\pi} k_2 \exp(Z_{2j}) E_1(Z_{2j}) d\theta \} \tag{4.38}$$

$$W(\vec{x}'; F_n) = \sum_{j=1}^{2} \{ -i\, 2[\int_0^{\frac{\pi}{2}} H(-t_j) k_2 \exp(Z_{2j}) d\theta - \int_{\frac{\pi}{2}}^{\pi} H(t_j) k_2 \exp(Z_{2j}) d\theta] \} \tag{4.39}$$

$$k_2 = \frac{1}{F_n^2 \cos^2 \theta} \tag{4.40}$$

The expression (4.37) which is associated with equations (4.38), (4.39) and (4.40) for the Green function representing the Kelvin source is identical to the Havelock single representation as discussed by Chan (1989). It may be proved numerically that the order of the imaginary part of the expressions (4.38) and (4.39) is about 10^{-6} and is much less than that of the real part which is in the order 10^{-1}. In other words, the imaginary part does not contribute to the Kelvin source which is time-independent. The expression (4.39) is the wave disturbance trailing downstream for $x' < 0$ but zero upstream for $x' > 0$.

4.3.2 Generalisation of Green function at zero Froude number

It is evident that the quadratic denominator in the integrand of the integral D given in equation (4.21) reduces to one degree when the Froude number F_n is equal to zero. As a consequence, the value of the pole k_1 is the square of the non-dimensional frequency f and the pole k_2 vanishes. Hence,the expression (4.33) which is associated with equations (4.34),(4.35) and (4.36b) reduces to

$$G(\vec{x}; \vec{\xi}, f) = -\frac{1}{r} + \frac{1}{r'} - N(\vec{x}'; f) - W(\vec{x}'; f) \tag{4.41}$$

where

$$N(\vec{x}';f) = \sum_{j=1}^{2}\{\frac{1}{\pi}\int_0^{\pi}\left[k_1 \exp(Z_{1j})E_1(Z_{1j}) - \frac{k_1}{Z_{1j}}\right]d\theta\} \qquad (4.42)$$

$$W(\vec{x}';f) = \sum_{j=1}^{2}\{\, i2\int_0^{\pi}H(t_j)k_1\exp(Z_{1j})d\theta\,\} \qquad (4.43)$$

$$k_1 = f^2 \qquad (4.44)$$

The expression (4.41) which is associated with equations (4.42), (4.43) and (4.44) represents the Green function for an oscillating source. The expression (4.43) for $W(\vec{x}';f)$ is the far-field radiating wave propagating in all horizontal directions to infinity.

4.3.3 Derivatives of Green function

In the theory of ship motions the derivatives of the Green function are utilised to form a system of algebraic equations which represent integral equations in relation to body boundary condition as discussed in Chapters 2 and 3. Formulations of the Green function due to a unit oscillating source moving beneath the undisturbed free surface of infinite water depth have been obtained. The derivatives of the Green function $G(\vec{x};\vec{\xi},f,F_n)$ can be obtained by differentiating equation (4.33) with respect to x, y and z respectively. Thus, we may obtain

$$\nabla G(\vec{x};\vec{\xi},f,F_n) = \frac{\vec{x}-\vec{\xi}}{r^3} - \frac{\vec{x}'}{r'^3} - \nabla N(\vec{x}';f,F_n) - \nabla W(\vec{x}';f,F_n) \qquad (4.45)$$

where $N_x(\vec{x}';f,F_n) = \sum_{j=1}^{2}\{\frac{1}{\pi}[\int_0^{\gamma}\frac{T_j\cos\theta}{\sqrt{4\tau\cos\theta-1}}d\theta + i\int_{\gamma}^{\pi}\frac{T_j\cos\theta}{\sqrt{1-4\tau\cos\theta}}d\theta\,]$

$$-i2\int_0^{\gamma}\frac{H(-\mathrm{Im}\ Z_{1j})k_1^2\exp(Z_{1j}) + H(\mathrm{Im}\ Z_{2j})k_2^2\exp(Z_{2j})}{\sqrt{4\tau\cos\theta-1}}\cos\theta\,d\theta\,\} \qquad (4.46a)$$

$$N_y(\vec{x}';f,F_n)=\sum_{j=1}^{2}\mathrm{sig}(2/j-j)\{\frac{1}{\pi}[\int_0^{\gamma}\frac{T_j\sin\theta}{\sqrt{4\tau\cos\theta-1}}d\theta+i\int_{\gamma}^{\pi}\frac{T_j\sin\theta}{\sqrt{1-4\tau\cos\theta}}d\theta]$$

$$-i2\int_0^{\gamma}\frac{H(-\mathrm{Im}\ Z_{1j})k_1^2\exp(Z_{1j})+H(\mathrm{Im}\ Z_{2j})k_2^2\exp(Z_{2j})}{\sqrt{4\tau\cos\theta-1}}\sin\theta\,d\theta\} \quad (4.46b)$$

$$N_z(\vec{x}';f,F_n)=\sum_{j=1}^{2}\{\frac{1}{\pi}[-i\int_0^{\gamma}\frac{T_j}{\sqrt{4\tau\cos\theta-1}}d\theta+\int_{\gamma}^{\pi}\frac{T_j}{\sqrt{1-4\tau\cos\theta}}d\theta]$$

$$-2\int_0^{\gamma}\frac{H(-\mathrm{Im}\ Z_{1j})k_1^2\exp(Z_{1j})+H(\mathrm{Im}\ Z_{2j})k_2^2\exp(Z_{2j})}{\sqrt{4\tau\cos\theta-1}}d\theta\} \quad (4.46c)$$

$$W_x(\vec{x}',f,F_n)=-2\sum_{j=1}^{2}\{\int_{\gamma}^{\frac{\pi}{2}}\frac{H(t_j)k_1^2\exp(Z_{1j})+H(-t_j)k_2^2\exp(Z_{2j})}{\sqrt{1-4\tau\cos\theta}}\cos\theta\,d\theta$$

$$+\int_{\frac{\pi}{2}}^{\pi}\frac{H(t_j)[k_1^2\exp(Z_{1j})-k_2^2\exp(Z_{2j})]}{\sqrt{1-4\tau\cos\theta}}\cos\theta\,d\theta\} \quad (4.47a)$$

$$W_y(\vec{x}';f,F_n)=-2\sum_{j=1}^{2}\mathrm{sig}(2/j-j)\{\int_{\gamma}^{\frac{\pi}{2}}\frac{H(t_j)k_1^2\exp(Z_{1j})+H(-t_j)k_2^2\exp(Z_{2j})}{\sqrt{1-4\tau\cos\theta}}\sin\theta\,d\theta$$

$$+\int_{\frac{\pi}{2}}^{\pi}\frac{H(t_j)[k_1^2\exp(Z_{1j})-k_2^2\exp(Z_{2j})]}{\sqrt{1-4\tau\cos\theta}}\sin\theta\,d\theta\} \quad (4.47b)$$

$$W_z(\vec{x}';f,F_n)=i2\sum_{j=1}^{2}\{\int_{\gamma}^{\frac{\pi}{2}}\frac{H(t_j)k_1^2\exp(Z_{1j})+H(-t_j)k_2^2\exp(Z_{2j})}{\sqrt{1-4\tau\cos\theta}}d\theta$$

$$+\int_{\frac{\pi}{2}}^{\pi}\frac{H(t_j)[k_1^2\exp(Z_{1j})-k_2^2\exp(Z_{2j})]}{\sqrt{1-4\tau\cos\theta}}d\theta\} \quad (4.47c)$$

$$T_j=k_1^2\exp(Z_{1j})E_1(Z_{1j})-\frac{k_1^2}{Z_{1j}}+\frac{k_1^2}{Z_{1j}^2}-k_2^2\exp(Z_{2j})E_1(Z_{2j})+\frac{k_2^2}{Z_{2j}}-\frac{k_2^2}{Z_{2j}^2} \quad (4.48)$$

4.4 Derivations of Green function for finite water depth

By taking the double Fourier transform with respect to the horizontal coordinates x and y in equations (4.12) through (4.14) derived for the finite depth boundary-value problem, we may obtain

$$H_{zz}^{**} - k^2 H^{**} = 0 \qquad ; \ z < 0 \qquad (4.49)$$

$$-(f+i\varepsilon+F_n\alpha)^2 H^{**} + H_z^{**} = -\frac{2[k+(f+i\varepsilon+F_n\alpha)^2]}{k} e^{-kh}\cosh k(\zeta+h) e^{-i(\alpha\xi+\beta\eta)} \qquad ; \ z = 0 \qquad (4.50)$$

$$H_z^{**} = 0 \qquad ; \ z = -h \qquad (4.51)$$

The general solution of the ordinary differential equation (4.49) is $H^{**} = Ae^{kz} + Be^{-kz}$ in which A and B are constant. Making use of the Fourier transform sea bed condition given by equation (4.51), we deduce that $B = Ae^{-2kh}$ and

$$H^{**}(\alpha,\beta,z;\vec{\xi},h,f,F_n,\varepsilon) = A(\alpha,\beta;\vec{\xi},h,f,F_n,\varepsilon)\cosh k(z+h)$$

Substituting the foregoing equation into the free surface condition defined by the Fourier transform in equation (4.50), we can solve the constant A and have

$$H^{**}(\alpha,\beta,z;\vec{\xi},h,f,F_n,\varepsilon) = -\frac{2[k+(f+i\varepsilon+F_n\alpha)^2]e^{-kh}\cosh k(\zeta+h)\cosh k(z+h)}{k[k\tanh kh - (f+i\varepsilon+F_n)^2]\cosh kh} e^{-i(\alpha\xi+\beta\eta)}$$

The inverse Fourier transform of the foregoing expression yields

$$H(\vec{x};\vec{\xi},h,f,F_n,\varepsilon) = -\frac{1}{\pi}\int_{-\infty}^{\infty} d\beta \int_{-\infty}^{\infty} d\alpha \frac{[k+(f+i\varepsilon+F_n\alpha)^2]e^{-kh}\cosh k(\zeta+h)\cosh k(z+h)}{k[k\tanh kh - (f+i\varepsilon+F_n)^2]\cosh kh} e^{i(\alpha x'+\beta y')}$$

Substituting this expression into equation (4.6), we obtain

$$G(\vec{x};\vec{\xi}, h, f, F_n, \varepsilon) = -\frac{1}{r} - \frac{1}{r_h}$$

$$-\frac{1}{\pi}\int_{-\infty}^{\infty} d\beta \int_{-\infty}^{\infty} d\alpha \frac{[k+(f+i\varepsilon+F_n\alpha)^2]e^{-kh}\cosh k(\zeta+h)\cosh k(z+h)}{k[k\tanh kh-(f+i\varepsilon+F_n)^2]\cosh kh} e^{i(\alpha x'+\beta y')} \qquad (4.52a)$$

It may be seen that the integrand of the double integral in equation (4.52a) is so complicated, due to the square root term $\sqrt{(\alpha^2+\beta^2)}$ in the variable k, that cumbersome expression will involve after Rayleigh's artificial viscosity ε is taken to the limit as zero. It is therefore convenient to change the Fourier transform Cartesian coordinates (α,β) to polar coordinates as $\alpha = k\cos\theta$ and $\beta = k\sin\theta$. Thus equation (4.52a) becomes

$$G(\vec{x};\vec{\xi}, h, f, F_n, \varepsilon) = -\frac{1}{r} - \frac{1}{r_h}$$

$$-\frac{1}{\pi}\int_0^{2\pi} d\theta \int_0^{\infty} dk \left[\frac{k(1+\tanh kh)}{k\tanh kh-(f+i\varepsilon+F_n k\cos\theta)^2} - 1\right] \bullet$$

$$e^{-kh}\frac{\cosh k(\zeta+h)}{\cosh kh}\cosh k(z+h)e^{ik(x'\cos\theta+y'\sin\theta)} \qquad (4.52b)$$

By decomposing the double integral into two terms, equation (4.52b) reduces to

$$G(\vec{x};\vec{\xi}, h, f, F_n, \varepsilon) = -\frac{1}{r} - \frac{1}{r_h} + M(\vec{x};\vec{\xi}, h) - D(\vec{x};\vec{\xi}, h, f, F_n, \varepsilon)$$

or $$G(\vec{x};\vec{\xi}, h, f, F_n) = -\frac{1}{r} - \frac{1}{r_h} + M(\vec{x};\vec{\xi}, h) - D(\vec{x};\vec{\xi}, h, f, F_n, 0^+) \qquad (4.53)$$

where

$$M(\vec{x};\vec{\xi}, h) = \frac{2}{\pi}\,\mathrm{Re}\int_0^{\pi} d\theta \int_0^{\infty} dk\; e^{-kh}\frac{\cosh k(\zeta+h)}{\cosh kh}\cosh k(z+h)e^{ik\rho\cos\theta} \qquad (4.54)$$

$$D(\vec{x};\vec{\xi},h,f,F_n,\varepsilon) = \sum_{j=1}^{2} \frac{1}{\pi}\int_0^{\pi} d\theta \int_0^{\infty} I(k;\theta,\varepsilon)\,dk \tag{4.55}$$

$$I(k;\theta,\varepsilon) = e^{-kh}\,\frac{k(1+\tanh kh)\cosh\, k(\zeta+h)\cosh\, k(z+h)}{[k\tanh kh-(f+i\varepsilon+F_n k\cos\theta)^2]\cosh kh}\exp(ikt_j) \tag{4.56}$$

The variable ρ in equation (4.54) is defined as the horizontal dimensionless distance between the source point $\vec{\xi}$ and the field point $\vec{x}$ such that $\rho = \sqrt{(x'^2+y'^2)}$. t_1 and t_2 in equation (4.55) have been defined by equations (4.23a) and (4.23b) respectively. The real part taken in expression (4.54) for $M(\vec{x};\vec{\xi},h)$ is due to the fact that $M(\vec{x};\vec{\xi},h)$ does not contribute to the far-field radiation condition since it behaves like an image sink $1/r'$ as h tends to infinity and the integrand in equation (4.54) is analytical throughout the fluid domain. By making use of the approximation for a hyperbolic function for a large argument, equation (4.54) reduces to

$$M(\vec{x};\vec{\xi},h) = \frac{1}{r'} + 2\int_0^{\mu} e^{-kh}\,\frac{\cosh\, k(\zeta+h)}{\cosh\, kh}\cosh\, k(z+h)J_o(k\rho)dk - \int_0^{\mu} e^{kz'}J_o(k\rho)dk \tag{4.57}$$

provided that

$$\mu > 4.5/h \tag{4.58}$$

The integrand $I(k;\theta,\varepsilon)$ in the integral D given by equation (4.55) has two poles because the denominator of this integrand is an implicit quadratic equation which has two zeros such that

$$k\tanh\, kh - (f + i\varepsilon + F_n k\cos\,\theta)^2 = 0 \tag{4.59}$$

The foregoing implicit quadratic equation may be solved by considering the following two curves

$$F_n^2\cos^2\theta k^2 + (2\tau\cos\theta - p + i\,2\varepsilon F_n\cos\theta)k + (f^2 + i\,2\varepsilon f - \varepsilon^2) = 0$$

$$p = \tanh kh$$

These two curves meet at two positions when the values of k satisfy

$$k = \frac{p - 2\tau\cos\theta \mp \sqrt{p^2 - 4\tau\cos\theta}}{2F_n^2\cos^2\theta} - \frac{i\varepsilon(\sqrt{p^2 - 4\tau\cos\theta} \mp 1)}{F_n\cos\theta\sqrt{p^2 - 4\tau\cos\theta}}$$

It may be seen that the deformations of the path of integration in the complex κ-plane for finite depth are the same as that for infinite depth as justified by the Rayleigh artificial viscosity ε. This implies that the wave patterns for finite depth and infinite depth are similar, that is, four wave trains would be generated in association with the poles k_1 and k_2. However, apart from the values of the poles themselves, there are some differences between finite depth and infinite depth for far-field waves since the far-field waves as well as near-field waves are influenced by water depth. The value of the variable p is less than unity if the product of k and h is approximately less than 4.5. As a consequence of $p < 1$, the square of the variable p may be less than $4\tau\cos\theta$ even though the parameter τ is less than 1/4. When $p^2 < 4\tau\cos\theta$, the upstream wave trains may not be fully developed in the subcritical regime $\tau < 1/4$. This implies that the far-field wave patterns for finite depth shift a little bit towards supercritical regime when the water depth is not high. In any case, we may write

$$\left.\begin{matrix} k_1 \\ \\ k_2 \end{matrix}\right\} = \frac{p - 2\tau\cos\theta \mp i\sqrt{4\tau\cos\theta - p^2}}{2F_n^2\cos^2\theta} \qquad \text{for } 0 \le \theta \le \gamma \quad (4.60a)$$

$$\left.\begin{matrix} k_1 \\ \\ k_2 \end{matrix}\right\} = \frac{p - 2\tau\cos\theta \mp \sqrt{p^2 - 4\tau\cos\theta}}{2F_n^2\cos^2\theta} + \begin{cases} i\,0^+ \\ \\ -i\,0^+ \end{cases} \qquad \text{for } \gamma \le \theta \le \frac{\pi}{2} \quad (4.60b)$$

$$\left.\begin{matrix} k_1 \\ k_2 \end{matrix}\right\} = \frac{p - 2\tau\cos\theta \mp \sqrt{p^2 - 4\tau\cos\theta}}{2F_n^2\cos^2\theta} + i0^+ \qquad \text{for } \frac{\pi}{2} \le \theta \le \pi \qquad (4.60c)$$

The value of γ in equation (4.60b) is defined at $k_1=k_2$. The residue of the integrand $I(k;\theta,0^+)$ given by equation (4.56) may be found by means of Laurent series in the form

$$Res(I;k) = \frac{e^{-kh}k(1+\tanh kh)\cosh k(\zeta+h)\cosh k(z+h)}{\sinh kh - 2(f+F_n k\cos\theta)F_n\cos\theta\cosh kh + kh\,\mathrm{sech}\,kh}\exp(ikt_j) \qquad (4.61)$$

in which k is equal to k_1 or k_2.

By taking the limit of Rayleigh's artificial viscosity ε to zero, the expression (4.53) for the Green function will automatically satisfy the far-field radiation condition given by equation (4.4). As $\varepsilon \to 0$, we may express the inner integral in the right hand side of equation (4.56) in the Cauchy Principal-value form as

$$\int_0^\infty I(k;\theta,0^+)dk = PV\int_0^\infty I(k;\theta)dk + i\pi[Res(I,k_1) - Res(I,k_2)] \quad ;\ \gamma < \theta \le \frac{\pi}{2}$$

$$\int_0^\infty I(k;\theta,0^+)dk = PV\int_0^\infty I(k;\theta)dk + i\pi[Res(I,k_1) + Res(I,k_2)] \quad ;\ \frac{\pi}{2} \le \theta \le \pi$$

Substituting the foregoing two expressions into equation (4.55), we obtain

$$\begin{aligned} D(\vec{x};\vec{\xi},h,f,F_n,0^+) = \sum_{j=1}^{2}\{ & \frac{1}{\pi}\int_0^\pi d\theta\, PV\int_0^\infty I(k;\theta)dk \\ & + i\int_\gamma^{\frac{\pi}{2}}[Res(I;k_1) - Res(I;k_2)]d\theta \\ & + i\int_{\frac{\pi}{2}}^{\pi}[Res(I;k_1) + Res(I;k_2)]d\theta \ \} \end{aligned} \qquad (4.62)$$

PAGE NUMBERING AS ORIGINAL

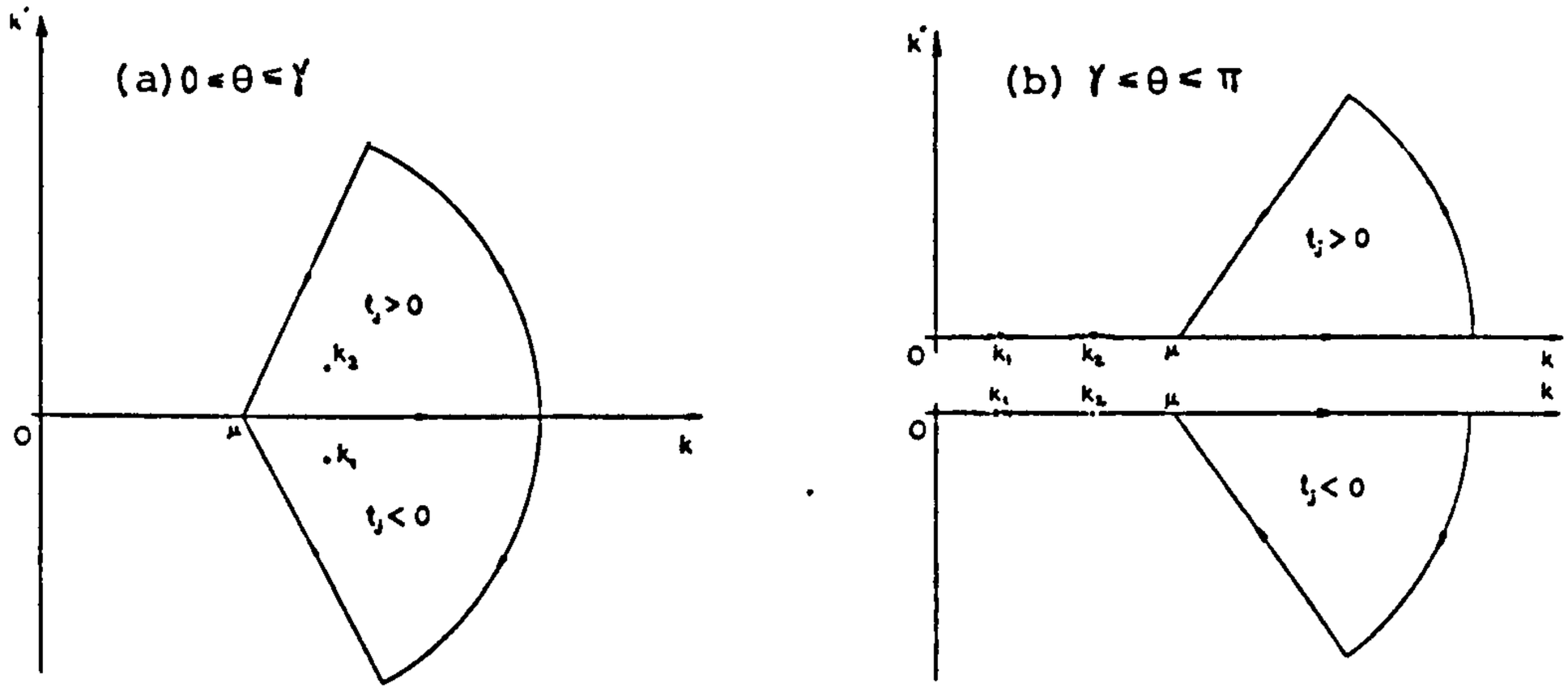

Fig.4.4 Contour integration in complex K-plane

The Principal-value still exists in the finite-depth integral if the integrand has a singularity. However, this singularity can easily be eliminated as will be discussed in section 4.5. The expression (4.53) defined with equations (4.57),(4.63) through (4.66) for the Green function representing a translating pulsating source beneath the free surface of water depth h is a special treatment of this complicated source function in terms of spatial coordinates, forward speed, frequency of oscillation and water depth. It is apparent that the expression (4.53) for finite depth can reduce to (4.33) for infinite depth as h approaches infinity. Meanwhile, the finite-depth source $-1/r_h$ vanishes, the image sink-like function $M(\vec{x}; \vec{\xi}, h)$ becomes an image sink $1/r'$ and the wave functions N and W given by equations (4.64) and (4.65) changes to (4.34) and (4.35) respectively as h tends to infinity.

4.4.1 Generalisation of Green function at zero frequency

In the supercritical regime $\tau < 1/4$, there are four wave trains associated with the poles k_1 and k_2; three leave behind the source and one in advance. On the other hand, the upstream wave trains disappear as the frequency of oscillation tends to zero even if

the parameter τ is less than 1/4. Once the frequency of oscillation becomes zero, the wave patterns are purely Kelvin-waves. Therefore the expression (4.53) defined with equations (4.57),(4.63) through (4.66) reduces to that for Kelvin-source function at f = 0 in the form

$$G(\vec{x};\vec{\xi},h,F_n) = -\frac{1}{r} - \frac{1}{r_h} + M(\vec{x};\vec{\xi},h) - N(\vec{x};\vec{\xi},h,F_n) - W(\vec{x};\vec{\xi},h,F_n) \quad (4.67)$$

where

$$N(\vec{x};\vec{\xi},h,F_n) = \sum_{j=1}^{2}\{\frac{1}{\pi}\int_0^{\pi} d\theta PV\int_0^{\mu}\frac{e^{-kh}(1+\tanh\ kh)\cosh\ k(\zeta+h)\cosh\ k(z+h)}{[\tanh\ kh - F_n^2 k\cos^2\theta]\cosh\ kh}\exp(ikt_j)dk$$

$$-\frac{1}{\pi}\int_0^{\pi} k_2\exp(Z_{2j})E_1(Z_{2j}+\mu w_j)d\theta\} \quad (4.68)$$

$$W(\vec{x};\vec{\xi},h,f,F_n) = -i2\sum_{j=1}^{2}[\int_0^{\frac{\pi}{2}} H_2(-t_j)\,Res(I;k_2)\,d\theta - \int_{\frac{\pi}{2}}^{\pi} H_2(t_j)\,Res(I;k_2)\,d\theta] \quad (4.69)$$

$$Res(I;k_2) = \frac{(1+\tanh\ k_2h)\cosh\ k_2(\zeta+h)\cosh\ k_2(z+h)}{[-F_n^2\cos^2\theta + h\,sech^2 k_2h]\cosh\ k_2h}\exp[-k_2(h-it_j)] \quad (4.70)$$

in which the value of k_2 satisfies

$$(F_n^2\cos^2\theta)k_2 - \tanh\ k_2h = 0 \quad (4.71)$$

The expression (4.67) associated with equations (4.57), (4.68) and (4.69) for the Green function represents a unit source with zero frequency moving steadily beneath the free surface of water depth h and is identical to the finite-depth Green function in terms of Havelock's single integral as discussed by Chan (1989). As h tends to infinity, the expression (4.67) associated with (4.57), (4.68) and (4.69) for finite depth reduces to that for infinite depth as given in section 4.3.1.

4.4.2 Generalisation of Green function with zero Froude number

When the forward speed is equal to zero, all waves radiate from the source in all horizontal directions to infinity. These radiation waves are depicted from the pole k_1 while the pole k_2 disappears. By taking $F_n = 0$, the expression (4.53) associated with equations (4.57),(4.63) through (4.66) reduces to the oscillating source function in the form

$$G(\vec{x};\vec{\xi},h,f) = -\frac{1}{r} - \frac{1}{r_h} + M(\vec{x};\vec{\xi},h) - N(\vec{x};\vec{\xi},h,f) - W(\vec{x};\vec{\xi},h,f) \quad (4.72)$$

where

$$N(\vec{x};\vec{\xi},h,f) = PV\int_0^{\mu} \frac{2e^{-kh}\,k(1+\tanh\,kh)\cosh\,k(\zeta+h)\cosh\,k(z+h)}{(k\tanh\,kh - f^2)\cosh\,kh} J_o(k\rho)\,dk$$

$$+ \sum_{j=1}^{2}\left(\frac{1}{\pi}\int_0^{\pi}\left[k_1\exp(Z_{1j})E_1(Z_{1j}+\mu w_j) - \frac{k_1\exp(-\mu w_j)}{Z_{1j}}\right]d\theta \right. \quad (4.73)$$

$$W(\vec{x};\vec{\xi},h,f) = i\,2\int_0^{\pi} H_1(t_j)\,Res(I;k_1)\,d\theta \quad (4.74)$$

$$Res(I;k_1) = \frac{k_1(1+\tanh\,k_1h)\cosh\,k_1(\zeta+h)\cosh\,k_1(z+h)}{\sinh\,k_1h + k_1h\,\mathrm{sech}\,k_1h}\exp\left[-k_1(h-it_j)\right] \quad (4.75)$$

in which the value of the pole k_1 satisfies

$$k_1\tanh k_1h - f^2 = 0 \quad (4.76)$$

The Green function for a unit oscillating source below the free surface of water depth h is represented by the expression (4.72) associated with (4.57), (4.73) and (4.74). These expressions are an alternative form derived by Faltinsen & Michelsen (1974) and can reduce to a form identical to that given in section 4.3.2 for infinite depth as h tends to infinity. For the purpose of numerical computation the series form of the oscillating source obtained by John (1950) should be used except where ρ tends to zero.

4.4.3 Derivatives of Green function

In order to set up a system of algebraic equations which represent the integral equations in relation to the body boundary condition for the ship motion problem, we must first evaluate the derivatives of the Green function. Based on the results of the Green function given by equation (4.53) defined together with equations (4.57) and (4.63) for a unit translating pulsating source below the undisturbed free surface of water depth h, the derivatives of the Green function with respect to x, y and z are easily obtained by direct differentiation of these equations. Then we get

$$\nabla G(\vec{x};\vec{\xi},h,f,F_n) = \frac{\vec{x}-\vec{\xi}}{r^3} + \frac{(x';y';z'+2h)}{r_h^3} + \nabla M(\vec{x};\vec{\xi},h) - \nabla N(\vec{x};\vec{\xi},h,f,F_n) - \nabla W(\vec{x};\vec{\xi},h,f,F_n) \tag{4.77}$$

where

for image-like function :-

$$M_x(\vec{x};\vec{\xi},h) = -\frac{x'}{r'^3} - \frac{x'}{\rho}\Big[2\int_0^{\mu} e^{-kh}\frac{\cosh k(\zeta+h)}{\cosh kh}\cosh k(z+h)J_1(k\rho)kdk - \int_0^{\mu} e^{kz'}J_1(k\rho)kdk\Big] \tag{4.78a}$$

$$M_y(\vec{x};\vec{\xi},h) = -\frac{y'}{r'^3} - \frac{y'}{\rho}\Big[2\int_0^{\mu} e^{-kh}\frac{\cosh k(\zeta+h)}{\cosh kh}\cosh k(z+h)J_1(k\rho)kdk - \int_0^{\mu} e^{kz'}J_1(k\rho)kdk\Big] \tag{4.78b}$$

$$M_z(\vec{x};\vec{\xi},h) = -\frac{z'}{r'^3} + 2\int_0^{\mu} e^{-kh}\frac{\cosh k(\zeta+h)}{\cosh kh}\sinh k(z+h)J_0(k\rho)kdk - \int_0^{\mu} e^{kz'}J_0(k\rho)kdk\Big] \tag{4.78c}$$

for local disturbance function N :-

$$N_x(\vec{x};\vec{\xi},h,f,F_n) =$$

$$\sum_{j=1}^{2}\{\frac{i}{\pi}\int_0^{\pi}\cos\theta d\theta PV\int_0^{\mu}\frac{e^{-kh}k^2(1+\tanh kh)\cosh k(\zeta+h)\cosh k(z+h)}{[k\tanh kh-(f+F_n k\cos\theta)^2]\cosh kh}\exp(ikt_j)dk$$

$$+\frac{1}{\pi}[\int_0^{\gamma}\frac{T_j\cos\theta}{\sqrt{4\tau\cos\theta-1}}d\theta+i\int_{\gamma}^{\pi}\frac{T_j\cos\theta}{\sqrt{1-4\tau\cos\theta}}d\theta]$$

$$-H[Re(k_1)-\mu]\,i\,2\int_0^{\gamma}\frac{H(-Im\ Z'_{1j})k_1^2\exp(Z_{1j})+H(Im\ Z'_{2j})k_2^2\exp(Z_{2j})}{\sqrt{4\tau\cos\theta-1}}\cos\theta d\theta\}$$

(4.79a)

$$N_y(\vec{x};\vec{\xi},h,f,F_n)=\sum_{j=1}^{2}sig(2/j-j)\{\frac{i}{\pi}\int_0^{\pi}\sin\theta d\theta\bullet$$

$$PV\int_0^{\mu}\frac{e^{-kh}k^2(1+\tanh kh)\cosh k(\zeta+h)\cosh k(z+h)}{[k\tanh kh-(f+F_n k\cos\theta)^2]\cosh kh}\exp(ikt_j)dk$$

$$+\frac{1}{\pi}[\int_0^{\gamma}\frac{T_j\sin\theta}{\sqrt{4\tau\cos\theta-1}}d\theta+i\int_{\gamma}^{\pi}\frac{T_j\sin\theta}{\sqrt{1-4\tau\cos\theta}}d\theta]$$

$$-H[Re(k_1)-\mu]\,i\,2\int_0^{\gamma}\frac{H(-Im\ Z'_{1j})k_1^2\exp(Z_{1j})+H(Im\ Z'_{2j})k_2^2\exp(Z_{2j})}{\sqrt{4\tau\cos\theta-1}}\sin\theta d\theta\}$$

(4.79b)

$$N_z(\vec{x};\vec{\xi},h,f,F_n)=\sum_{j=1}^{2}\{\frac{1}{\pi}\int_0^{\pi}d\theta PV\int_0^{\mu}\frac{e^{-kh}k^2(1+\tanh kh)\cosh k(\zeta+h)\sinh k(z+h)}{[k\tanh kh-(f+F_n k\cos\theta)^2]\cosh kh}\exp(ikt_j)dk$$

$$+\frac{1}{\pi}[-i\int_0^{\gamma}\frac{T_j}{\sqrt{4\tau\cos\theta-1}}d\theta+\int_{\gamma}^{\pi}\frac{T_j}{\sqrt{1-4\tau\cos\theta}}d\theta]$$

$$-H[Re(k_1)-\mu]\,2\int_0^{\gamma}\frac{H(-Im\ Z'_{1j})k_1^2\exp(Z_{1j})+H(Im\ Z'_{2j})k_2^2\exp(Z_{2j})}{\sqrt{4\tau\cos\theta-1}}d\theta\}\quad(4.79c)$$

for wave-like function W :-

$$W_x(\vec{x};\vec{\xi},h,f,F_n) = -2\sum_{j=1}^{2}\{\int_{\gamma}^{\frac{\pi}{2}}[H_1(t_j)k_1\,\mathrm{Res}(I;k_1) - H_2(-t_j)k_2\,\mathrm{Res}(I;k_2)]\cos\theta\,d\theta$$
$$+\int_{\frac{\pi}{2}}^{\pi}[H_1(t_j)k_1\,\mathrm{Res}(I;k_1) + H_2(t_j)k_2\,\mathrm{Res}(I;k_2)]\cos\theta\,d\theta\} \quad (4.80a)$$

$$W_y(\vec{x};\vec{\xi},h,f,F_n) = -2\sum_{j=1}^{2}\mathrm{sig}\,(2/j-j)\{\int_{\gamma}^{\frac{\pi}{2}}[H_1(t_j)k_1\mathrm{Res}(I;k_1)$$
$$-H_2(-t_j)k_2\,\mathrm{Res}(I;k_2)]\sin\theta\,d\theta$$
$$+\int_{\frac{\pi}{2}}^{\pi}[H_1(t_j)k_1\,\mathrm{Res}(I;k_1) + H_2(t_j)k_2\,\mathrm{Res}(I;k_2)]\sin\theta\,d\theta\} \quad (4.80b)$$

$$W_z(\vec{x};\vec{\xi},h,f,F_n) = i2\sum_{j=1}^{2}\{\int_{\gamma}^{\frac{\pi}{2}}[H_1(t_j)k_1\,\mathrm{Res}(I;k_1)\tanh k_1(z+h)$$
$$-H_2(-t_j)k_2\,\mathrm{Res}(I;k_2)\tanh k_2(z+h)]d\theta$$
$$+\int_{\frac{\pi}{2}}^{\pi}[H_1(t_j)k_1\mathrm{Res}(I;k_1)\tanh k_1(z+h) + H_2(t_j)k_2\mathrm{Res}(I;k_2)\tanh k_2(z+h)]\,d\theta\}$$

(4.80c)

$$T_j = k_1^2\exp(Z_{1j})E_1(Z_{1j}+\mu w_j) - \left[\frac{k_1-\mu}{Z_{1j}+\mu w_j} + \frac{\mu}{Z_{1j}} - \frac{k_1}{Z_{1j}^2}\right]k_1\exp(-\mu w_j)$$
$$-k_2^2\exp(Z_{2j})E_1(Z_{2j}+\mu w_j) + \left[\frac{k_2-\mu}{Z_{2j}+\mu w_j} + \frac{\mu}{Z_{2j}} - \frac{k_2}{Z_{2j}^2}\right]k_2\exp(-\mu w_j) \quad (4.81)$$

4.5 Elimination of singularities

It has been noted in the previous section that the finite-depth integral still has a singularity if the real part of the singularity is less than the parameter μ. Furthermore, the far-field integral also has a singularity at its lower limit of integration, that is, $\theta = \gamma$. By the definition of a Principal-value integral, the solution of the integral with singular integrand is unique if such an integral is defined. In other words, the Principal-value integral converges to a unique solution no matter how the singularities are eliminated.

The integral with an integrand f(k)/g(k) which has a simple pole at $k = \upsilon$ in the range of integration may be handled conveniently by a method developed by Monacella (1966). A modification of Monacella's method was used by Hogben & Standing (1974), and Endo (1983). Generally speaking, the singularity of the integrand is eliminated by cancellation of the singularity itself with a function approximate to the singularity. This approximated function is analytically evaluated. Then we may write

$$PV\int_0^{\mu}\frac{f(k)}{g(k)}dk=\int_0^{\mu}\left[\frac{f(k)}{g(k)}-\frac{f(\upsilon)}{g'(\upsilon)(k-\upsilon)}\right]dk+\frac{f(\upsilon)}{g'(\upsilon)}\ln\left|\frac{\mu-\upsilon}{\upsilon}\right| \qquad (4.82)$$

or $$PV\int_0^{\mu}\frac{f(k)}{g(k)}e^{ikw}\,dk=\int_0^{\mu}\left[\frac{f(k)}{g(k)}-\frac{f(\upsilon)}{g'(\upsilon)(k-\upsilon)}\right]e^{ikw}\,dk$$

$$+\frac{f(\upsilon)e^{i\upsilon w}}{g'(\upsilon)}\{E_1(i\upsilon w)-E_1[i(\upsilon-\mu)w]\} \qquad (4.83)$$

Essentially, equation (4.82) is the same as (4.83) but the exponential function e^{ikw} is incorporated in the numerator f(k) in equation (4.82). The singularity has been eliminated in these two equations provided that the first derivative of the denominator g(k) is not equal to zero at $k = \upsilon$. In the vicinity of the singularity, the integrand of the first integral in the right hand side of equation (4.82) or (4.83) approaches to zero. When $k = \upsilon$, the integrand vanishes.

If an integral has an end point singularity which occurs at the limit of integration, equations (4.82) and (4.83) are not applicable since a logarithmic singularity appears. In order to avoid this difficulty, a transformation is required. Since the far-field integral of the infinite water depth expressions described in section 4.3 has the end point singularity at the zero value of $\sqrt{(1-4\tau\cos\theta)}$, the change of variable $u^2=1-4\tau\cos\theta$ is used for the transformation. Then we may write

$$\int_{\gamma}^{\frac{\pi}{2}}\frac{F(\theta)}{\sqrt{1-4\tau\cos\theta}}d\theta=2\int_0^1\frac{F(u)}{\sqrt{16\tau^2-(1-u^2)^2}}du \qquad (4.84)$$

The transformed integrand in equation (4.84) is well behaved everywhere except at the critical value $\tau=1/4$. Therefore any combination of the non-dimensional frequency f and the Froude number F_n giving $\tau=1/4$ must be avoided.

On the other hand the transformation equation (4.84) is not applicable for the end point singularity in the finite water depth expressions mentioned in section 4.4. Alternatively, this difficulty can be circumvented in such a way that the transformation is to push the singularity to infinity and to ensure that the transformed integrand decays rapidly as the singularity approaches. The change of variable $\theta=\gamma+u^{-n}$ is used and equation (4.84) can be written as

$$\int_{\gamma}^{\frac{\pi}{2}} F(\theta)d\theta = \int_{(\pi/2-\gamma)^{-1/n}}^{\infty} \frac{nF(\gamma+u^{-n})}{u^{n+1}}du \qquad (4.85)$$

The value of n is always a positive integer which can be chosen so that the transformed integrand very quickly decreases as u increases. Satisfactory results were obtained for n=9.

4.6 Characteristics of the Green Function

The Green function given by equation (4.33) associated with equations (4.34),(4.35), (4.36) and (4.32) is a function of forward speed, frequency of oscillation and the spatial positions of source and field points for unsteady flow for infinite water depth. The Green function given by equation (4.53) defined by equations (4.57), (4.63) through (4.66) is expressed in terms of water depth for finite depth. The characteristics of this Green function depends upon the interaction between the steady waves (Kelvin waves) and unsteady waves (radiation waves). The steady and unsteady waves are the free surface disturbances due to the forward motion and oscillatory motions of the body. The steady waves are generated by the body moving with a constant forward speed in calm water while the unsteady waves are radiated from the

oscillating body. The influence of the water depth on the Green function is significant for those field points near the sea bottom. In order to illustrate the coupling effects of the forward speed and the frequency of oscillation on the free surface waves, the potential and its derivatives given by equations (4.33) and (4.53) respectively for a unit translating pulsating source have been calculated for various combinations of forward speeds and oscillation frequencies. The unit source located at the position (0., 0., −1.0) is travelling uniformly in the positive x-direction as shown in Fig.4.5. The potential and its derivatives are evaluated at equally spaced free surface grid points extending from x=10.0 (upstream) to x=−10.0 (downstream) and from y=10.0 to y=−10.0 in transverse direction. The computation covers the subcritical regime $\tau < 1/4$ and supercritical regime $\tau > 1/4$ for constant non-dimensional frequency $f = \omega\sqrt{(L/g)} = 0.5$ with varying Froude numbers $F_n = U/\sqrt{(gL)}$, where L is the depth of submergence of the source. Two limit cases for the translating pulsating source are also evaluated. They are the pulsating source with zero Froude number and the translating source with zero frequency. The water depth effects on the free surface disturbances are evaluated for the translating pulsating source at $U/\sqrt{(gh)}=0.0365$. The results of the free surface disturbances are presented in the form of three-dimensional isometric view. It will be noted that the potential and its x- and z-derivative in all cases are symmetric in x-z plane and the y-derivative is skew-symmetric in x-z plane.

4.6.1 Oscillating source with zero Froude number

The potential and its derivatives for the free surface disturbances due to the unit oscillating source potential at zero forward speed are illustrated in Fig.4.6 to Fig.4.10. It may be seen that the free surface patterns at any frequency due to the potential and its z-derivative are symmetric in all radial horizontal directions while the x-derivative and the y-derivative are symmetric only in the x-z plane and the y-z plane respectively and are skew-symmetric in the y-z plane and the x-z plane respectively.

It may be noted that the imaginary parts of the oscillating source potential and its

derivatives increase from low frequency to high frequency in Fig.4.6 to Fig.4.10. At the vanishing non-dimensional frequency, the imaginary parts of the potential and its derivatives are of the order 10^{-6} which is much less than the order of the real parts which is about 10^{-1}. On the other hand, the real parts of the oscillating source potential and its derivatives at the vanishing frequency number are approximately equal to the results of the following equations respectively.

$$G(\vec{x};\vec{\xi}) = -\frac{1}{r} - \frac{1}{r'} \qquad ; \ f \to 0 \qquad (4.85)$$

$$\nabla G(\vec{x};\vec{\xi}) = \frac{\vec{x}}{r} + \frac{\vec{x}'}{r'} \qquad ; \ f \to 0 \qquad (4.86)$$

Equations (4.85) and (4.86) satisfy the rigid wall free surface condition at zero frequency. For the frequency number f below 0.5, no significant change occurs in the overall free surface patterns with the exception that the surfaces due to the imaginary parts of x-derivative and y-derivative as shown in Fig.4.7 and Fig.4.8 are distorted to skew surfaces. As the frequency number is increased to 0.6, the radiating sinusoidal wave patterns start to spread outward from the source. When the frequency number is about 0.8, the radiating sinusoidal waves become more visible in Fig.4.10. It may be expected that these outward waves vanishes in remote field points.

4.6.2 Translating source at Zero Frequency

Fig.4.11 and Fig.4.12 illustrate the free surface disturbances due to the unit translating source at zero frequency. It may be seen that the translating source potential and its x-derivative and z-derivative are symmetric in x-z plane whereas the y-derivative is skew symmetric in x-z plane. The imaginary parts are indeed extremely small and are not presented.

At Froude numbers below 0.4, the local disturbances are dominant and the far-

field wave patterns do not appear on the free surface flow patterns due to the potential and its derivatives. At the zero speed case, the Kelvin wave patterns do not appear and the free surface condition becomes the rigid wall condition. As the speed approaches zero, the translating source potential and its derivatives satisfy the following two equations respectively.

$$G(\vec{x};\vec{\xi}) = -\frac{1}{r} - \frac{1}{r'} \qquad ; \; U \to 0 \qquad (4.87)$$

$$\nabla G(\vec{x};\vec{\xi}) = \frac{\vec{x}}{r} + \frac{\vec{x}'}{r'} \qquad ; \; U \to 0 \qquad (4.88)$$

As the speed is increased to about F_n=0.4, the far-field wave disturbances appear in x- and z-derivatives as shown in Fig.4.11. When the speed is progressively increased to about F_n=0.6, the waves trailing behind the source potential and its derivatives appear in Fig.4.12.

4.6.3 Translating pulsating source

In order to illustrate the forward speed effects on the oscillating body, the free surface disturbances due to the unit translating pulsating source potential and its derivatives at constant frequency number f=0.5 but varying Froude numbers are shown in Fig.4.13 through Fig.4.18.

At the vanishing speed (F_n=0.05), the free surface flow patterns behave like a pure oscillating source. Such a source potential has been discussed in section 4.6.1 indicate that the surface waves are simply the ring waves radiating outward in all horizontal directions. The effects of forward speed are clearly absent in Fig.4.13. When the forward speed is increased to F_n=0.2, the local disturbances and the frequency are still dominant. Therefore, the upstream and the downstream symmetry in potential and its z-derivative are still noticeable in Fig.4.14. As the speed is progressively increased,

the forward speed effects on the free surface patterns become more visible and the upstream and the downstream symmetry disappear. At the Froude number F_n=0.4, the wave-like patterns appear closely behind the source as shown in Fig.4.15.

The transition from subcritical regime to supercritical regime is illustrated in Fig.4.16 and Fig.4.17 for constant frequency number f=0.5 with two Froude numbers F_n=0.48 and 0.52. The Froude numbers F_n=0.48 (τ=0.24) and 0.52 (τ=0.26) correspond to the subcritical and supercritical regime respectively. It may be seen that the free surface disturbances are sensitive to small adjustment at the critical regime at which the Green function becomes singular.

As the speed further increases, the Kelvin wave patterns grow behind the source as shown in Fig.4.18. The effects of the forward speed become more dominant.

4.6.4 Water depth effects on free surface flows

Apart from the significant water depth effects on the flow fields near the sea bottom as noted in the finite depth source $-1/r_h$, the water depth effects on the free surface disturbances may be visible in some cases.

As discussed in section 4.4 the far-field wave pattern in the subcritical regime may be shifted a little bit towards the supercritical regime if the water depth is not high. Fig.4.19 represents the free surface disturbances due to the translating pulsating source with frequency number f=0.5 and Froude number F_n=0.2 at $U/\sqrt{(gh)} = 0.0365$. It may be seen that the upstream and downstream symmetry disappear on the surfaces due to the potential and its z-derivative in Fig.4.19 but this symmetry is noticeable in Fig.4.14 for infinite water depth.

4.7 Contours of free surface waves generated by a source

The wave patterns generated by anoscillating source moving beneath the free surface are governed by the far-field wave function W. It has been noted that the far-field wave function W is the result of the residues due to the poles k_1 and k_2. The influence of these two poles on the free surface waves depends on the frequency of oscillation ω and the forward speed U. In order to demonstrate this influence on the free surface waves, the contours of these wave disturbances due to a pulsating source located at the point (0., 0., −1) with respect to the moving system o-xyz are shown in Fig.4.20 through Fig.4.22 for different combination of the dimensionless frequency $f=\omega/\sqrt{(L/g)}$ and the Froude number $F_n=U/\sqrt{(gL)}$ at infinite water depth, where L is the depth of submergence of the source.

When the forward speed U is equal to zero, only the pole k_1 which is frequency dependent exists in the far-field wave function W. As a result the wave contours due to the oscillating source at zero Froude number are ring waves as shown in Fig.4.20. It is seen that the contours become closer as the dimensionless frequency f increases. This reveals that the oscillation of high frequency produces short wave length. Near the source point the contours are also closer because the steepness is high.

If the Froude number F_n is small the residue due to pole k_1 becomes dominant. Fig.4.21 shows the wave contours of the translating pulsating source at constant low Froude number $F_n=0.2$ with various dimensionless frequencies. At dimensionless frequency f=1.1 the corresponding parameter τ is equal to 0.22 which is less than one quarter. In this situation wave propagating ahead of the source appears. Meanwhile wave contours in front of the source are closer than those in the rear. As the dimensionless frequency increases to, say, f=1.5, the progressing wave in front of the source disappears at the same Froude number $F_n=0.2$, where $\tau=0.3$ exceeds 1/4. With a further increase in dimensionless frequency to f=1.75, the angle of the wedge in which waves are swept downstream is reduced.

For the source travelling at constant high Froude number F_n=0.6 with low frequency number the residue due to the pole k_2 is large. At the limit case the frequency number f is equal to zero, the wave contours become Kelvin wave group as shown in the top of Fig.4.22a. It is seen that the all the wave contours are contained within a wedge making the angle about 19°28' with the line of motion. Moreover the transverse waves are more visible than the divergent waves in the illustrated contours. As the frequency number is increasing to f=0.1 (τ=0.06) the waves radiating in front of the source are noticeable. At a further increase in the frequency number the wave length of the radiated wave becomes shorter as seen for f=0.2 (τ=0.12) in the bottom of Fig.4.22a and f=0.3 (τ=0.18) in the top of Fig.4.22b. It is observed that the Kelvin wave patterns are still visible for f=0.3 and F_n=0.6 since the residue due to the pole k_2 is the dominant component in the far-field wave function W. At the dimensionless frequency f=0.5 and the Froude number F_n=0.6 (τ=0.3) the wave patterns are less definite since the residues due to the poles k_1 and k_2 are comparable to each other. However for high frequency number f=1.1 (τ=0.66) all waves are cut moon-like and swept downstream.

Fig.4.23 shows the wave contours due to the translating pulsating source at various water depths. It is evident that similar wave patterns generated by the translating pulsating source are visible for finite water depth and infinite water depth. Nevertheless the wave length of the radiated wave in front of the source becomes shorter at shallow water as seen in the top of the Fig.4.23 for the frequency number f=0.3, Froude number F_n=0.6 and $U/\sqrt{(gh)}$=0.268. This implies that the flow regime shifts towards supercritical.

4.8 Conclusions

In the present study, a method to calculate the Green function representing a translating pulsating source for infinite depth and finite depth is described. The expression for the finite depth Green function consists of two parts. One is the finite

depth part and the other is the infinite depth part. Since the finite depth part is expressed in the double integral of finite integration limits, the computation effort is greatly reduced. Moreover, the infinite depth part is efficiently evaluated.

For the fully three-dimensional problem of a moving ship in waves, the translating pulsating source exactly satisfies the linearised free surface condition without further assumption in terms of the forward speed. The behaviour of this source potential and its derivatives depend largely on the interaction between the forward speed and the frequency of oscillation. Furthermore, if the water depth is not high, the water depth effects on the flow fields are significant for those field points near the sea bottom as well as on the free surface.

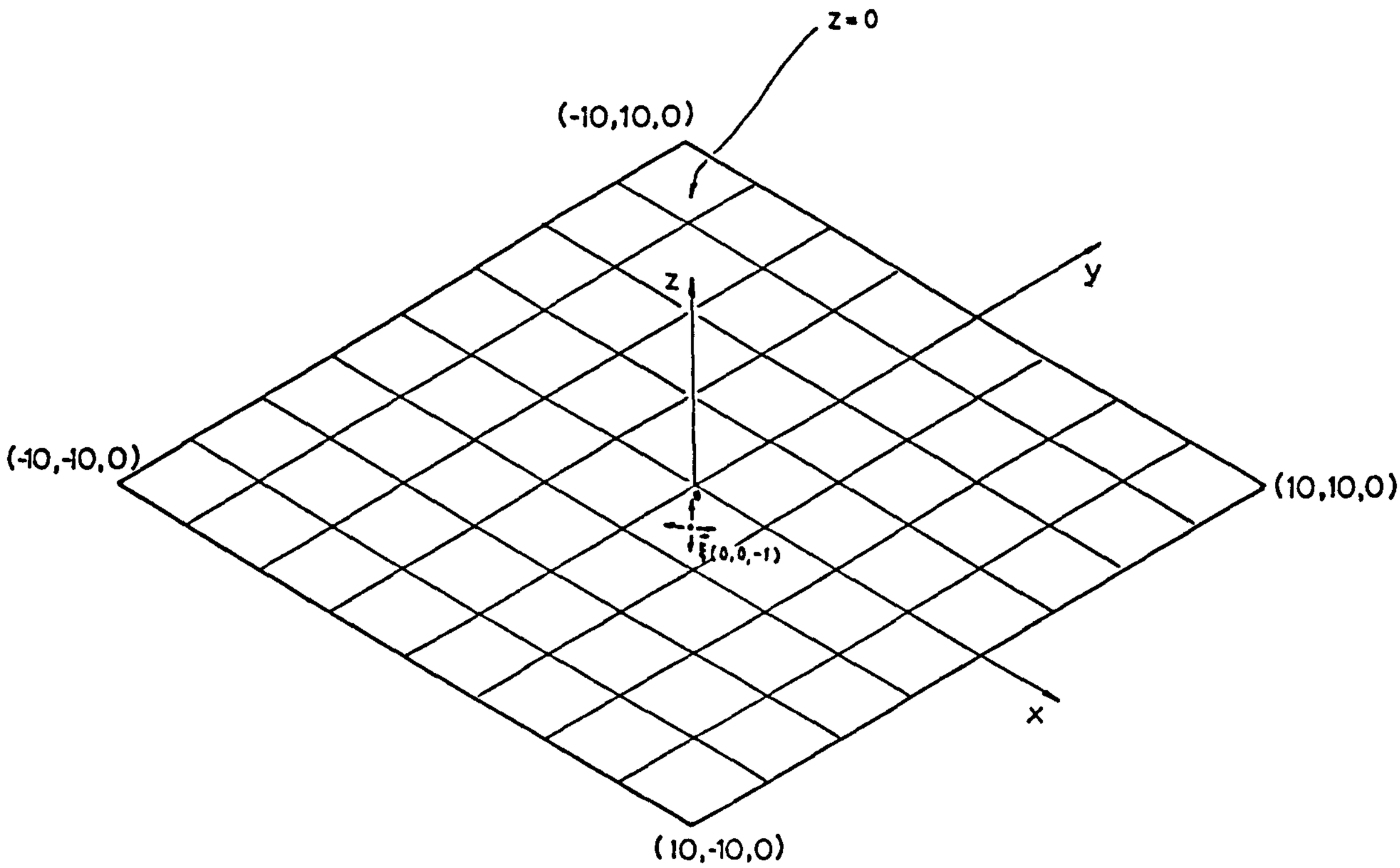

Fig.4.5 Locations of Surface Grid Points

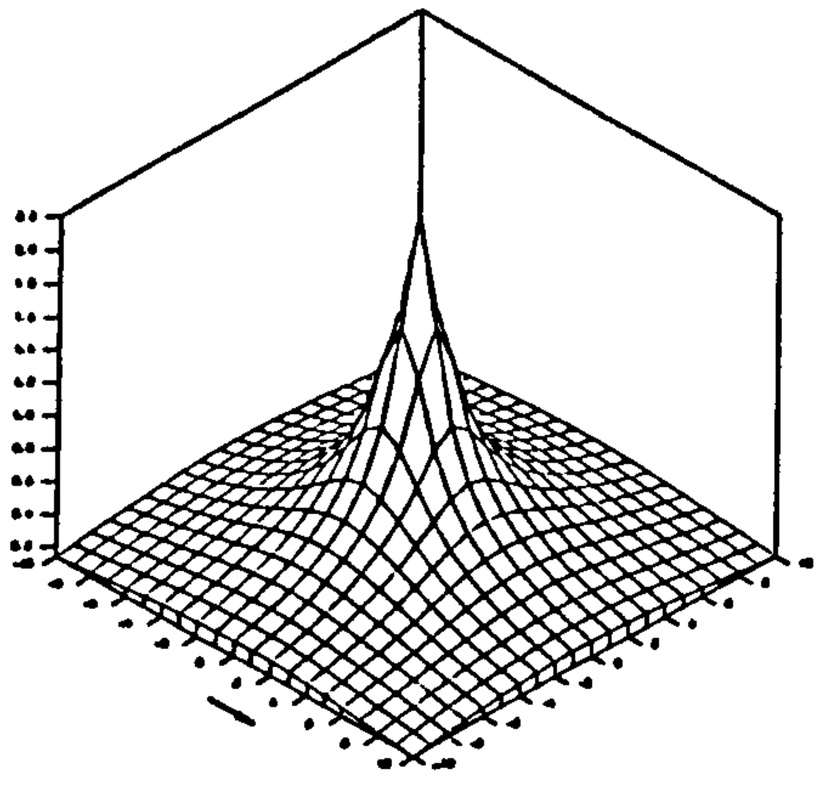

Potential Real Part

FREQ. NO. F=.2 FROUDE NO. FN=0.

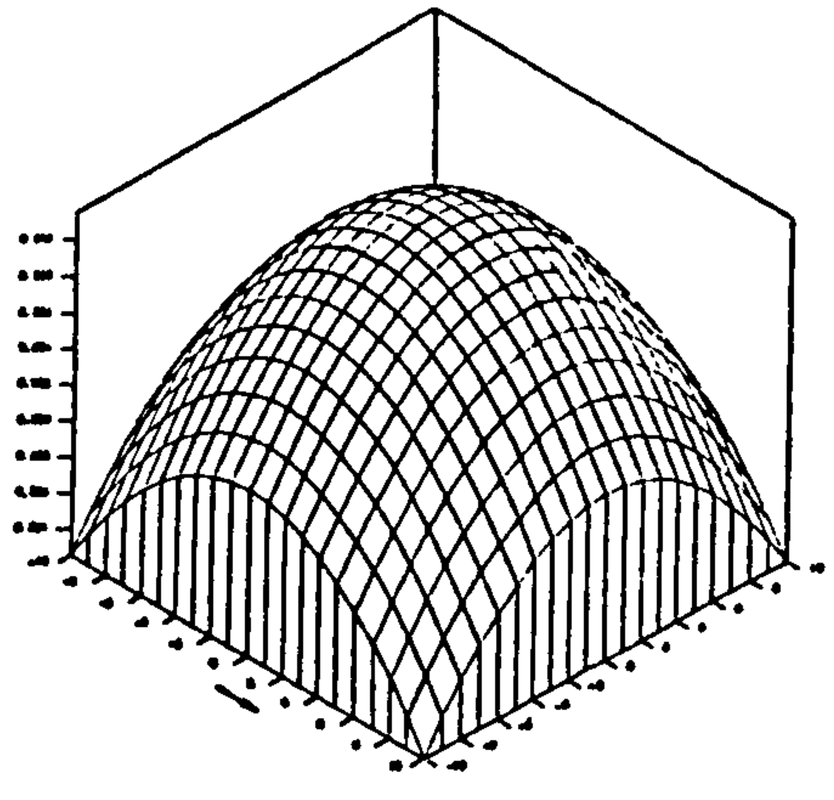

Potential Imaginary Part

FREQ. NO. F=.2 FROUDE NO. FN=0.

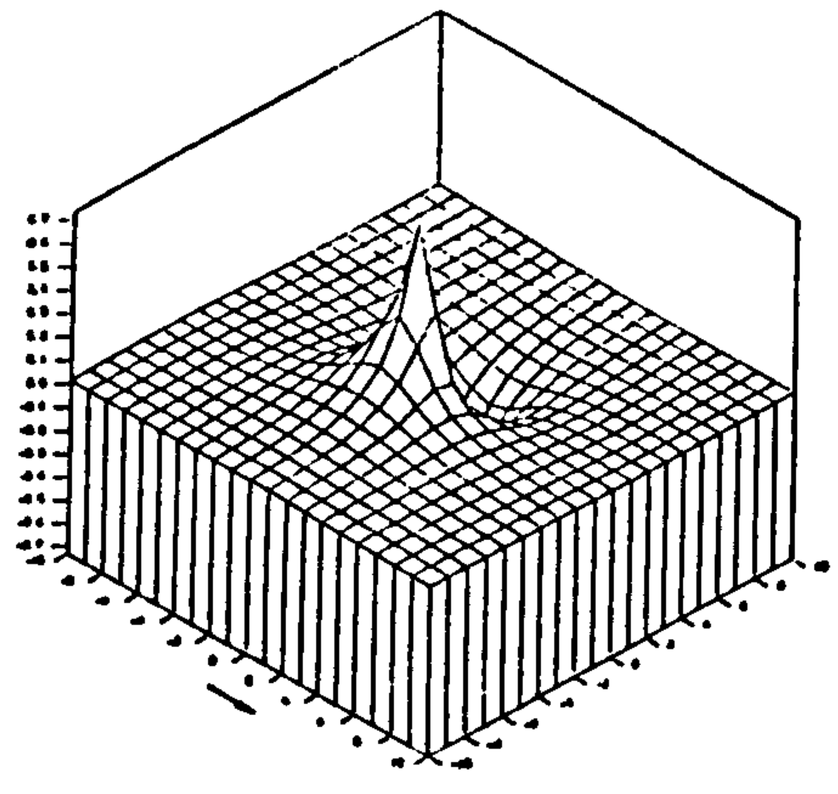

Y-derivative Real Part

FREQ. NO. F=.2 FROUDE NO. FN=0.

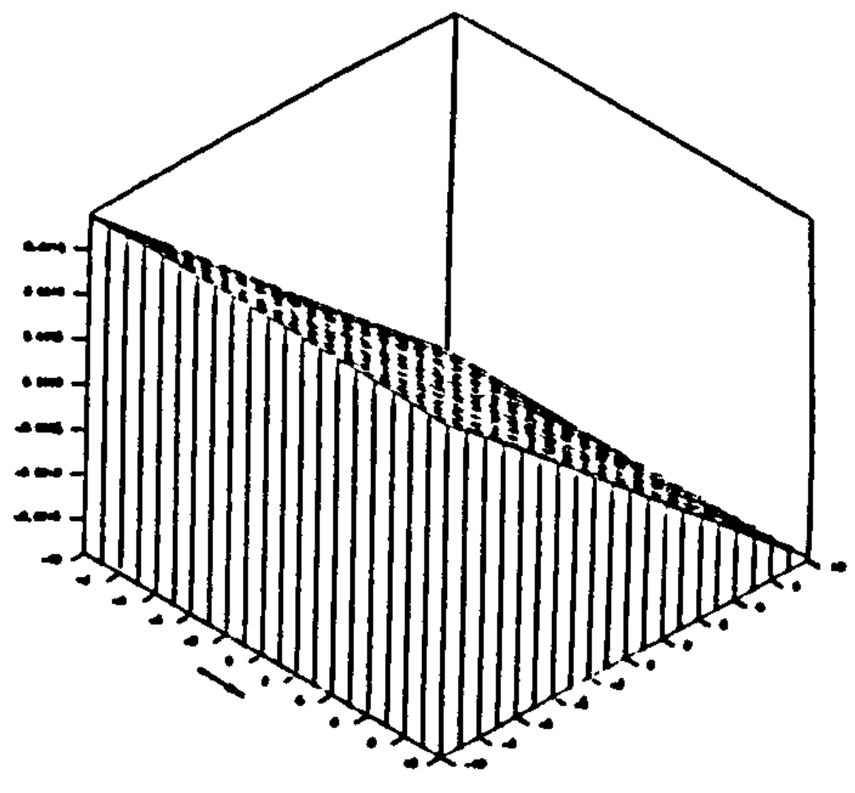

Y-derivative Imaginary Part

FREQ. NO. F=.2 FROUDE NO. FN=0.

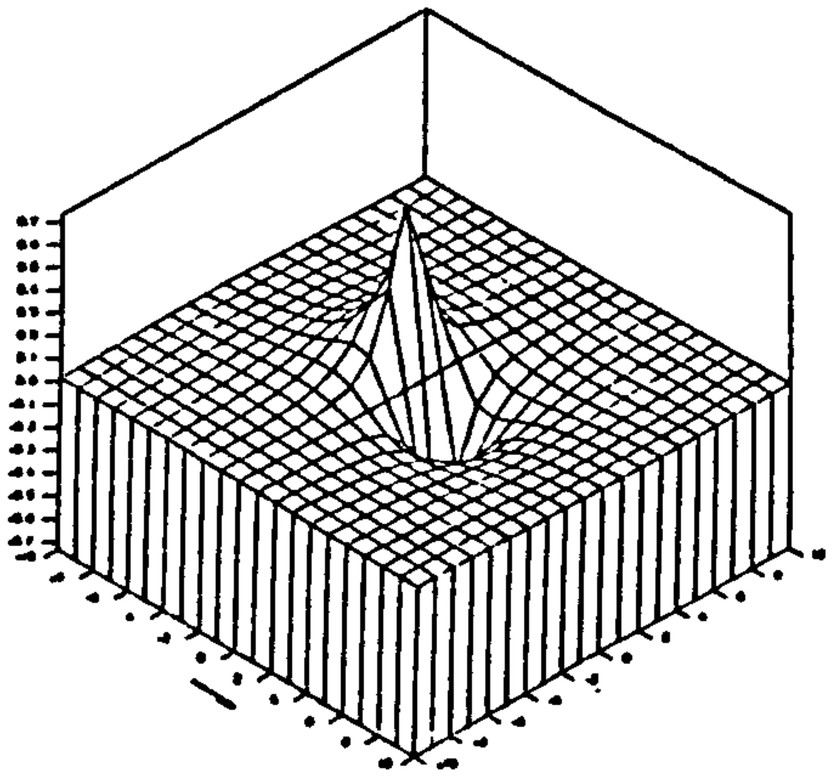

X-derivative Real Part

FREQ. NO. F=.2 FROUDE NO. FN=0.

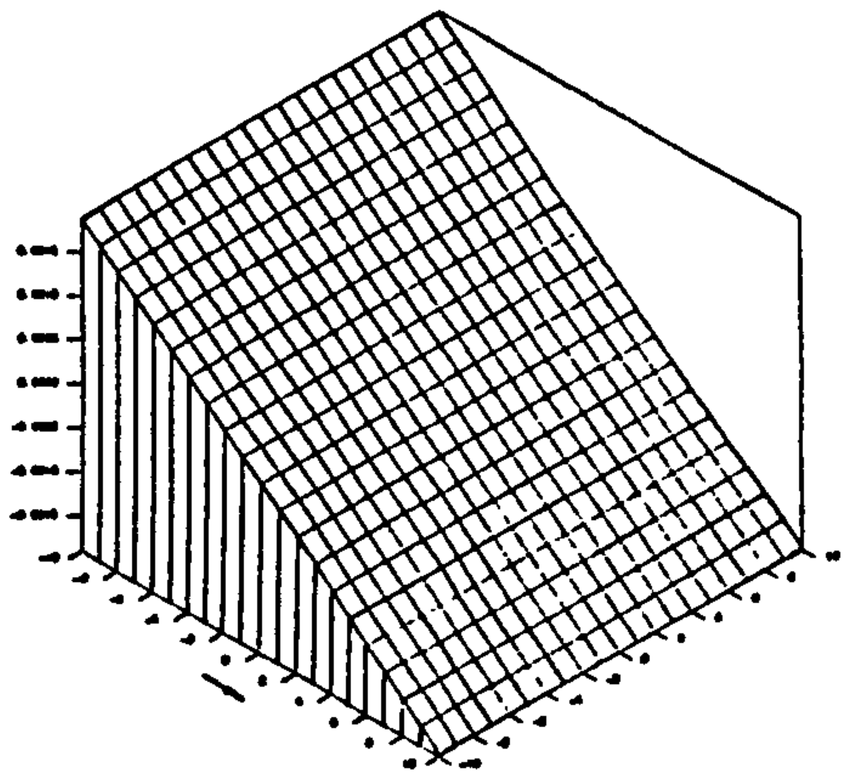

X-derivative Imaginary Part

FREQ. NO. F=.2 FROUDE NO. FN=0.

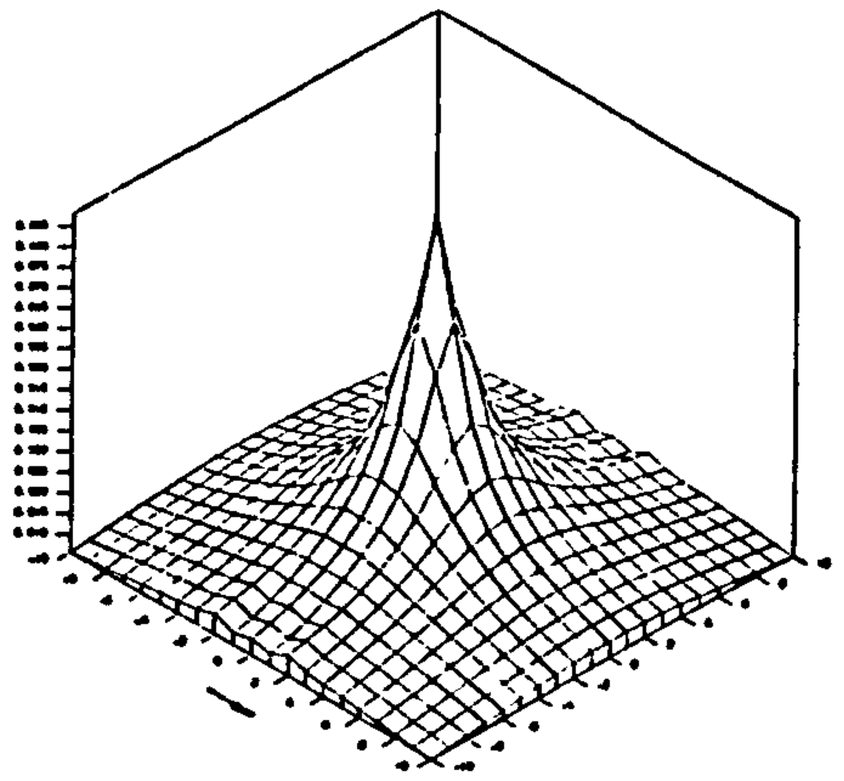

Z-derivative Real Part

FREQ. NO. F=.2 FROUDE NO. FN=0.

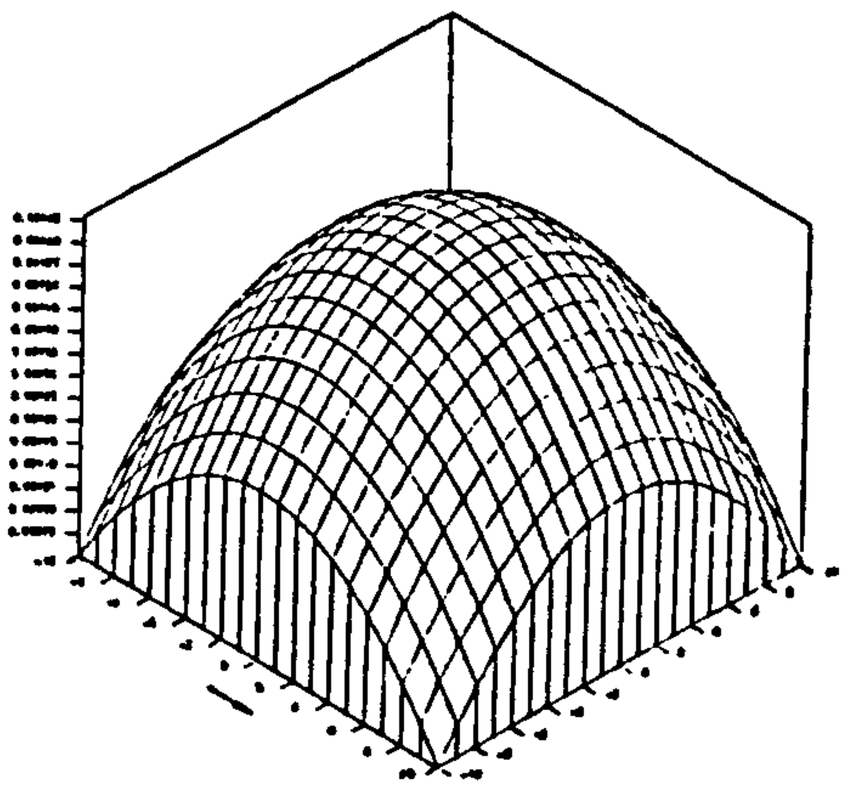

Z-derivative Imaginary Part

FREQ. NO. F=.2 FROUDE NO. FN=0.

Fig.4.6 Three-dimensional isometric view for an oscillating source potential at f=0.2 at infinite water depth

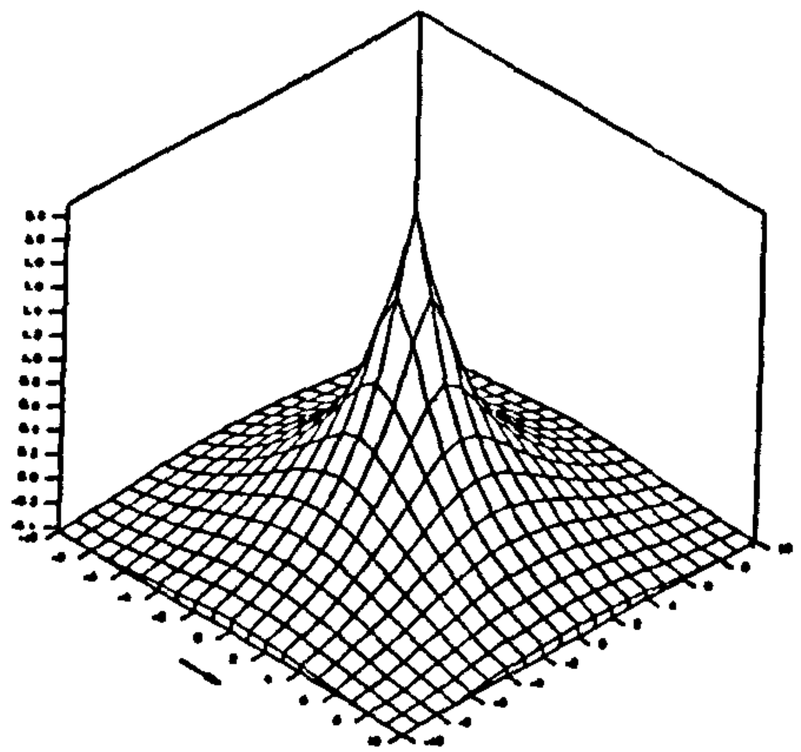

Potential Real Part

FREQ. NO. F=. 4 FROUDE NO. FN=0.

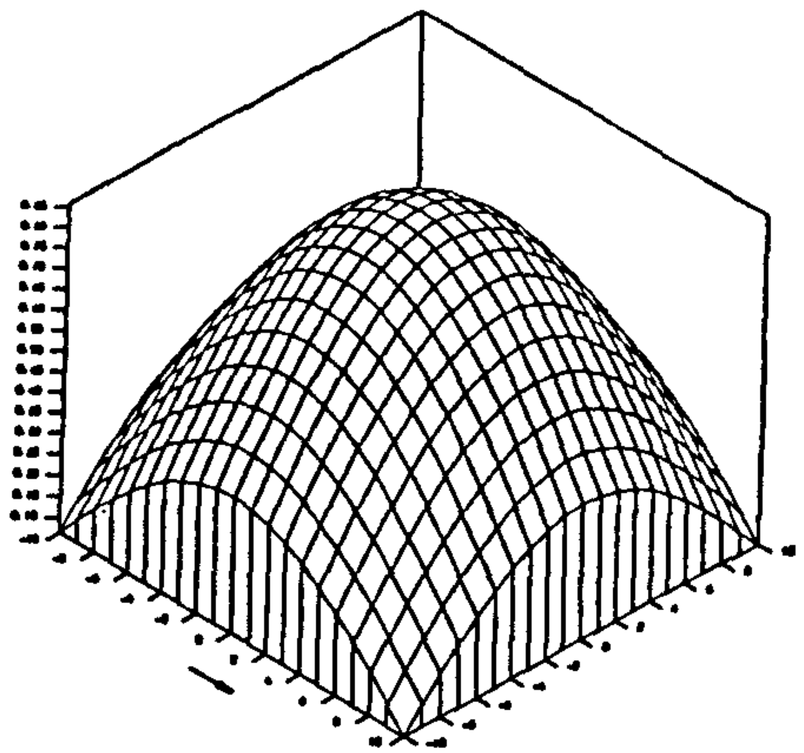

Potential Imaginary Part

FREQ. NO. F=. 4 FROUDE NO. FN=0.

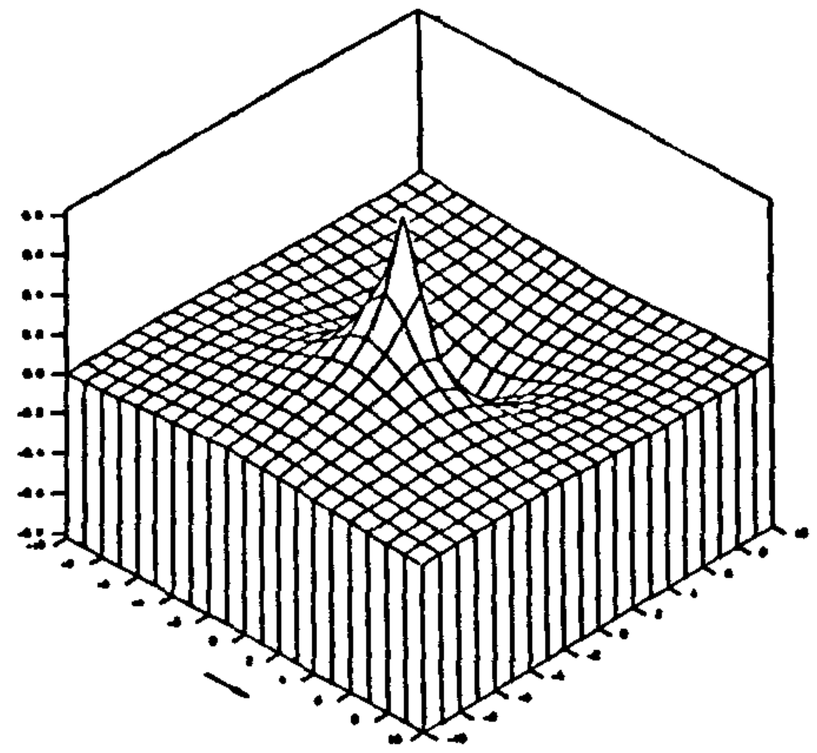

Y-derivative Real Part

FREQ. NO. F=. 4 FROUDE NO. FN=0.

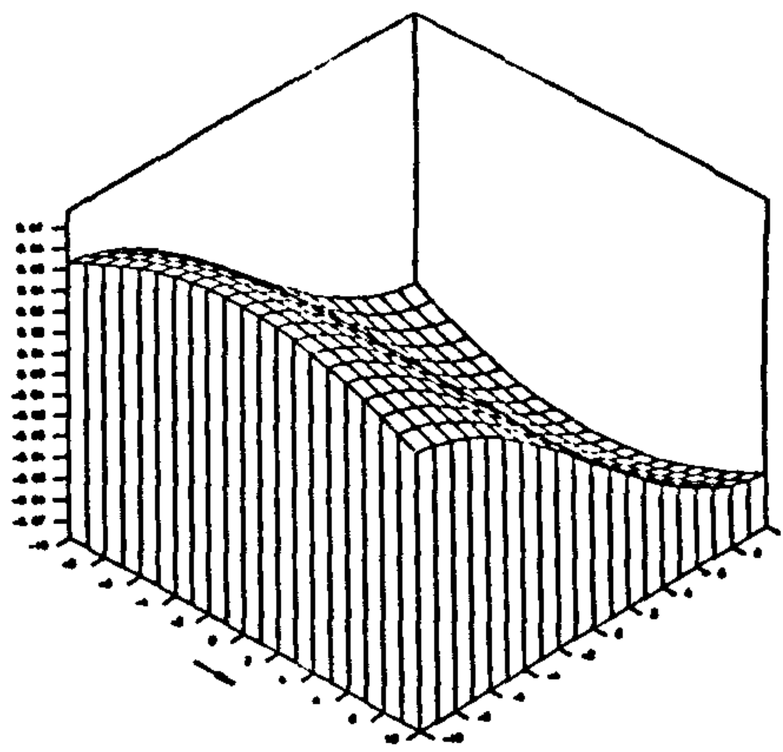

Y-derivative Imaginary Part

FREQ. NO. F=. 4 FROUDE NO. FN=0.

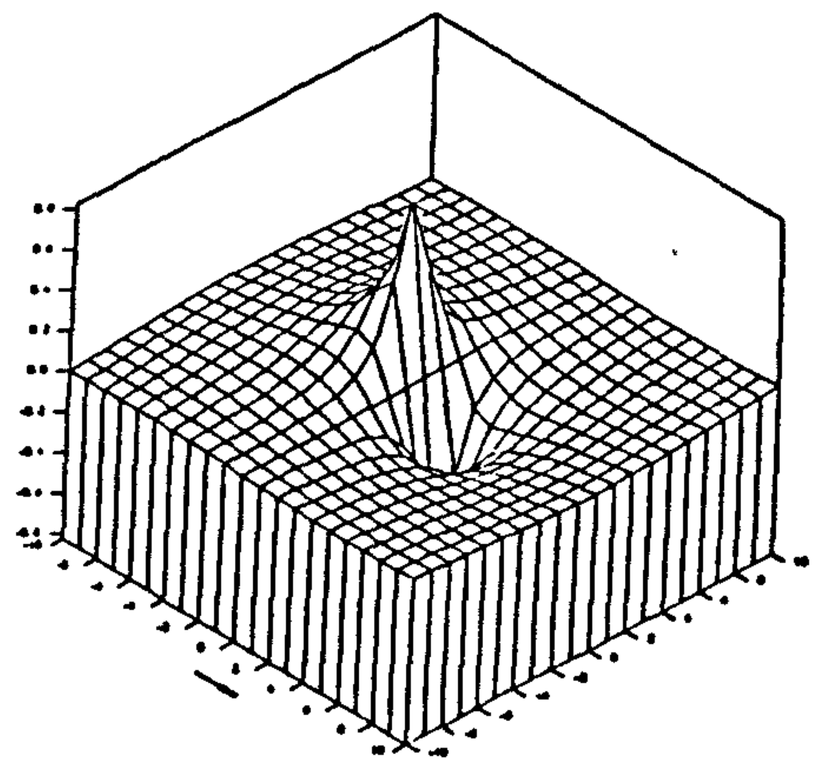

X-derivative Real Part

FREQ. NO. F=. 4 FROUDE NO. FN=0.

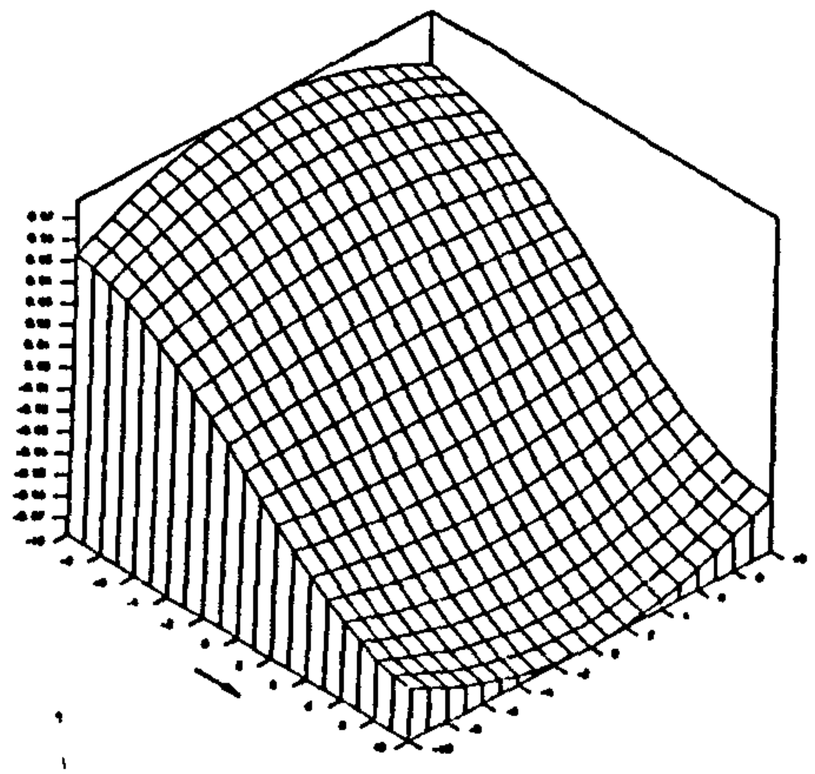

X-derivative Imaginary Part

FREQ. NO. F=. 4 FROUDE NO. FN=0.

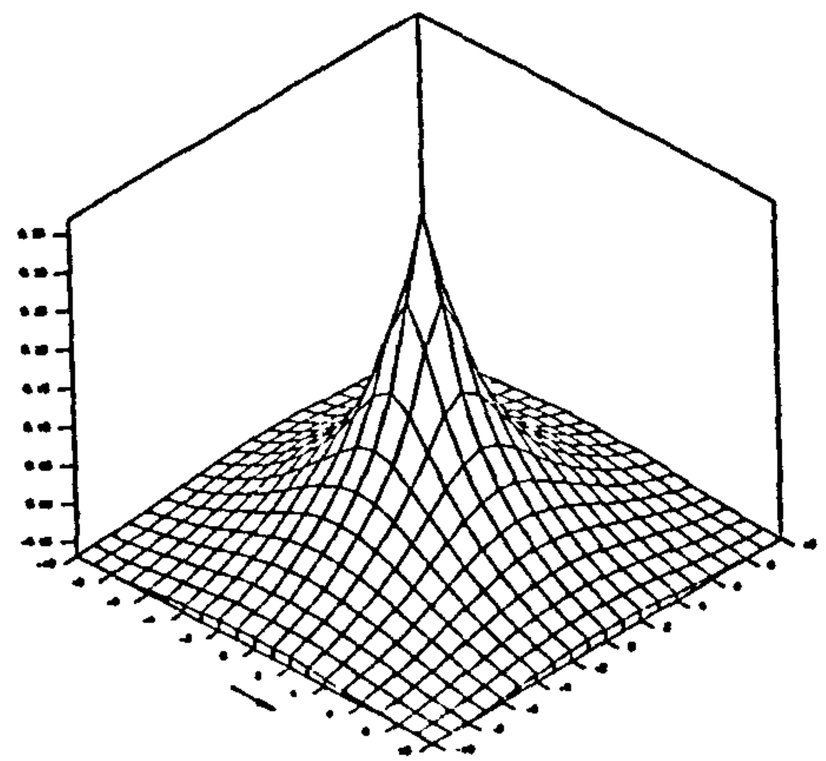

Z-derivative Real Part

FREQ. NO. F=. 4 FROUDE NO. FN=0.

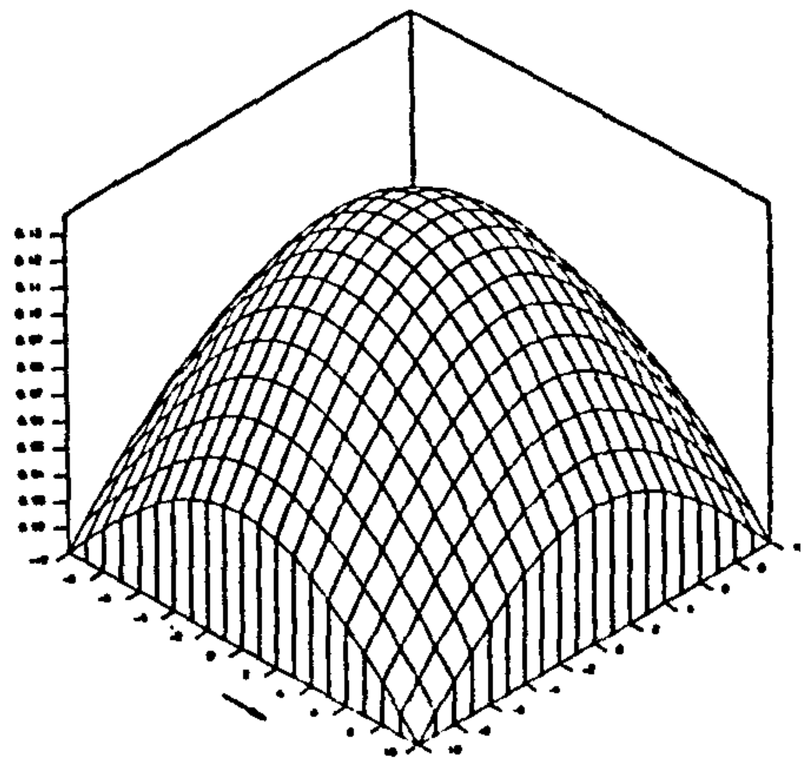

Z-derivative Imaginary Part

FREQ. NO. F=. 4 FROUDE NO. FN=0.

Fig.4.7 Three-dimensional isometric view for an oscillating source potential at f=0.4 at infinite water depth

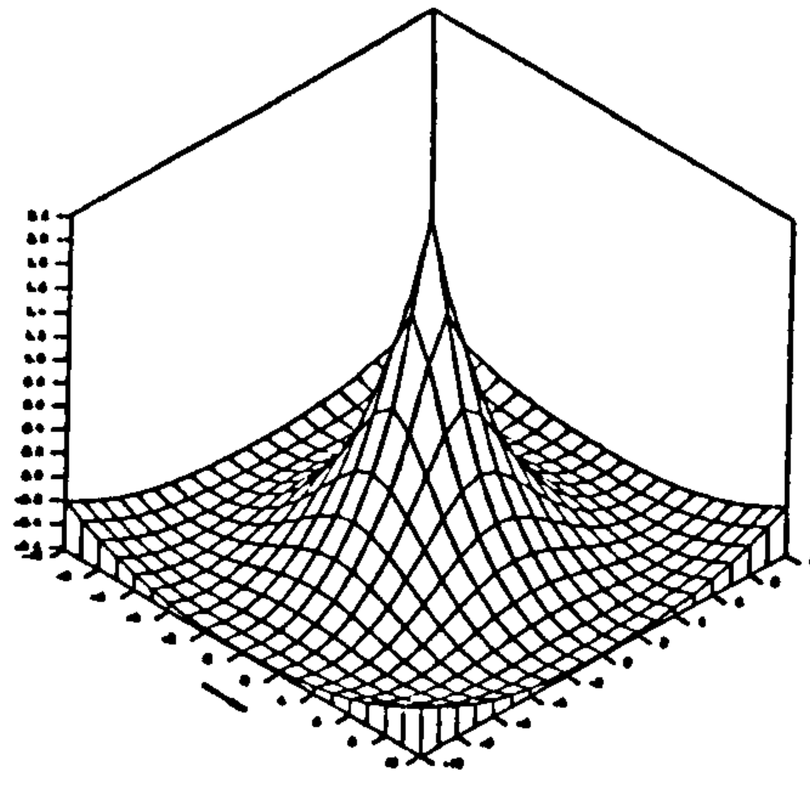

Potential Real Part

FREQ. NO. F=.5 FROUDE NO. FN=0.

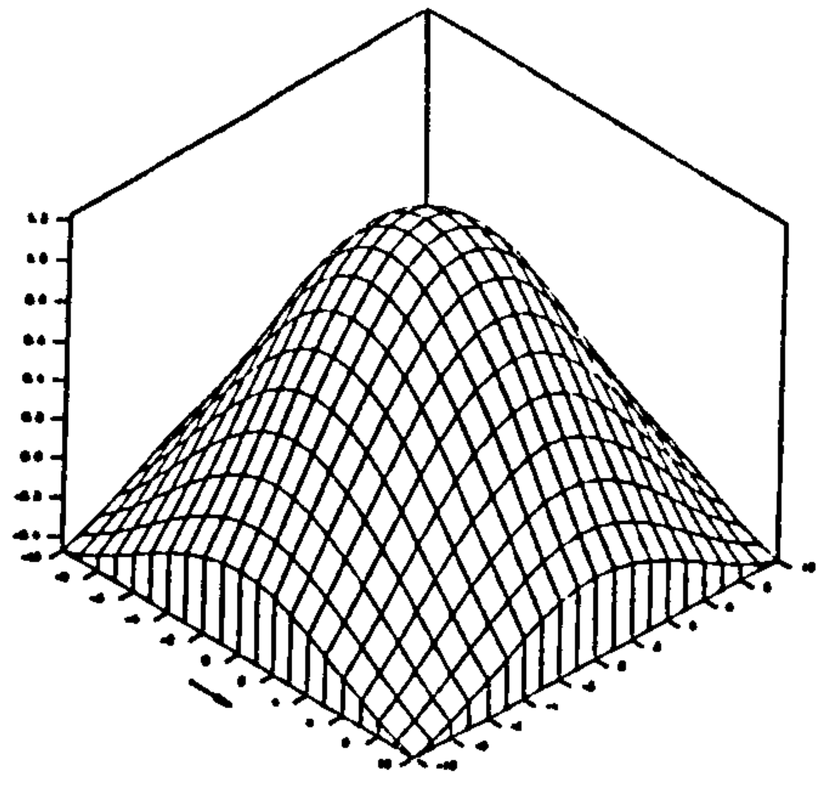

Potential Imaginary Part

FREQ. NO. F=.5 FROUDE NO. FN=0.

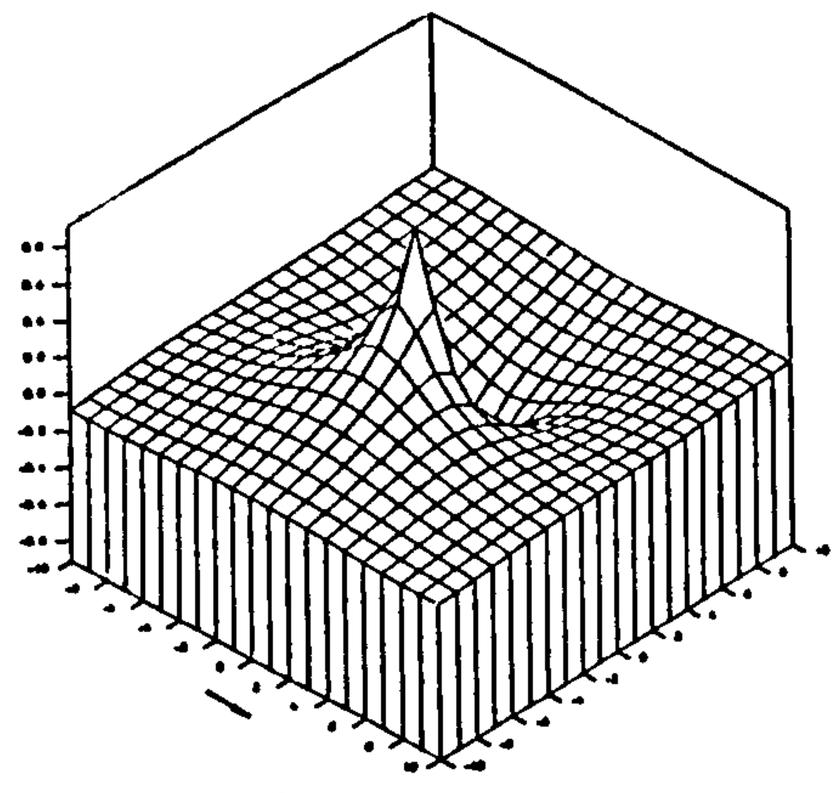

Y-derivative Real Part

FREQ. NO. F=.5 FROUDE NO. FN=0.

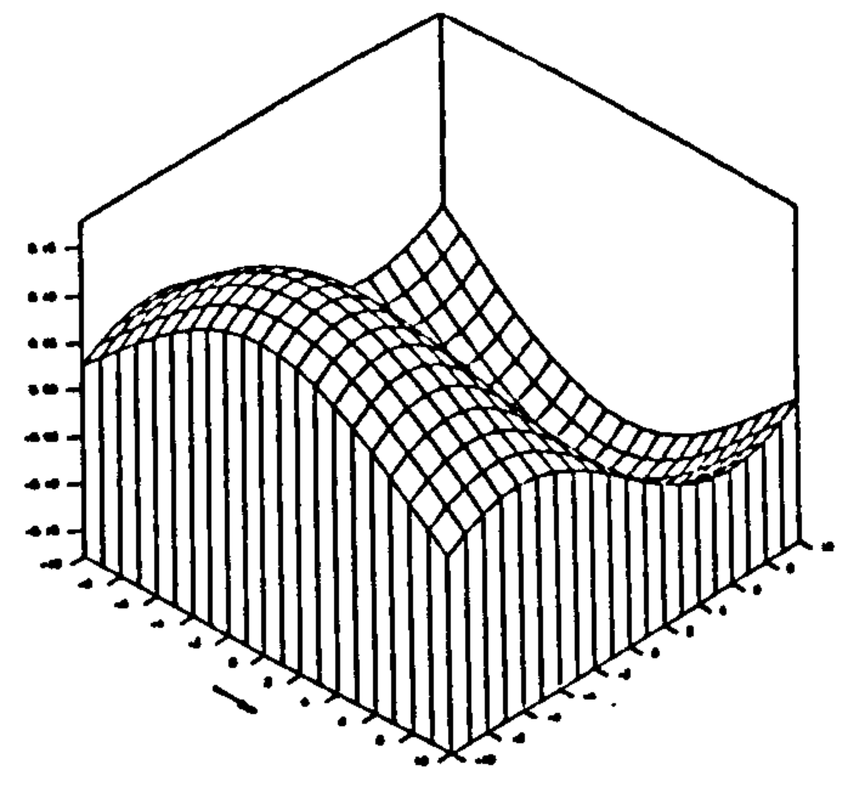

Y-derivative Imaginary Part

FREQ. NO. F=.5 FROUDE NO. FN=0.

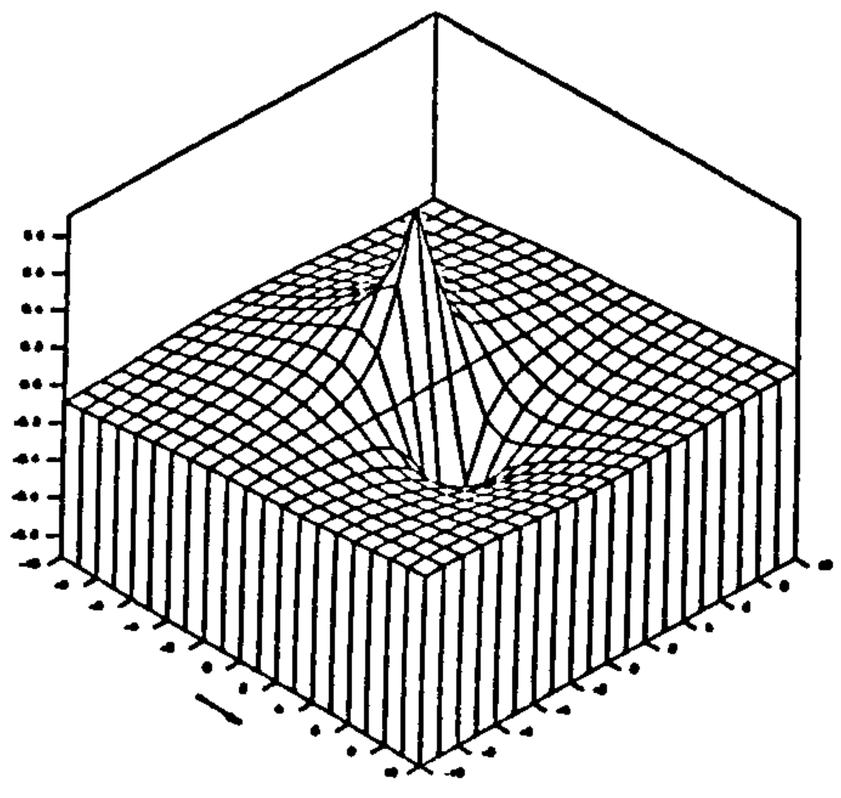

X-derivative Real Part

FREQ. NO. F=.5 FROUDE NO. FN=0.

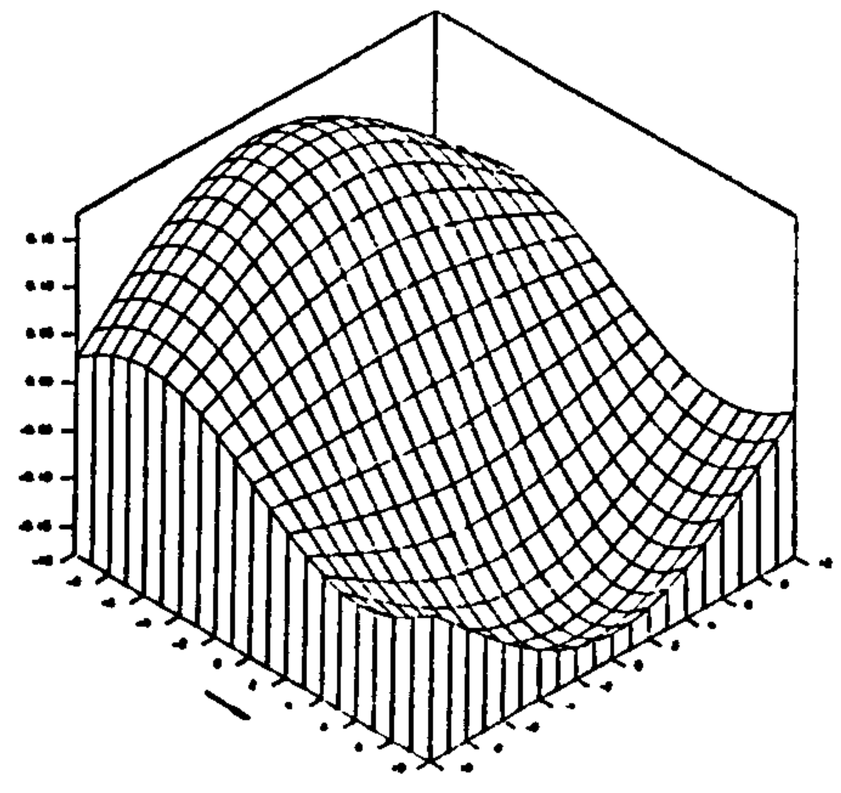

X-derivative Imaginary Part

FREQ. NO. F=.5 FROUDE NO. FN=0.

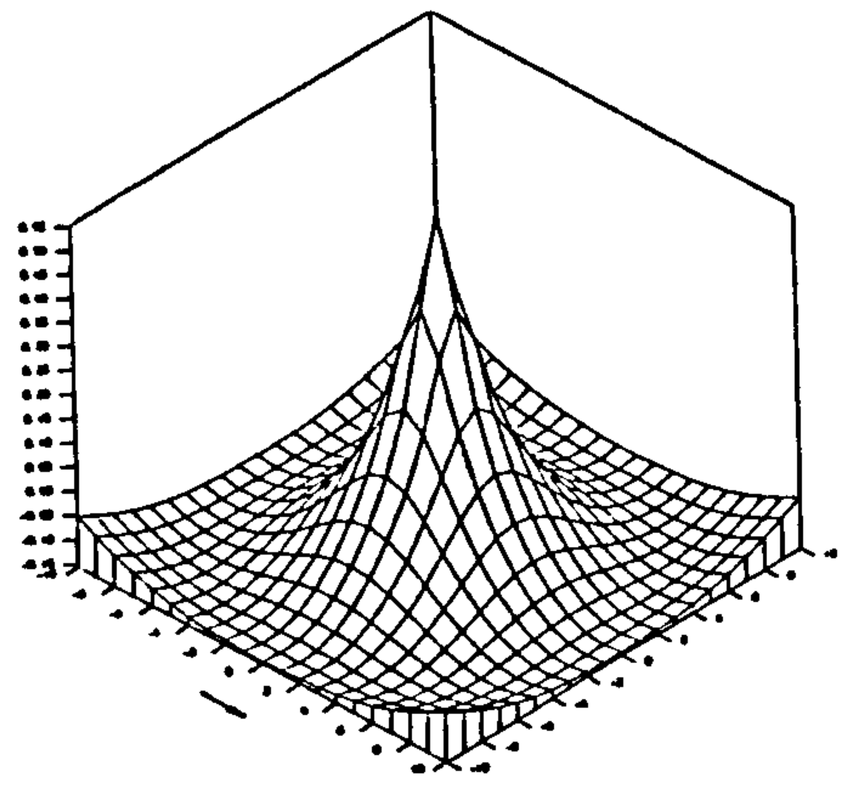

Z-derivative Real Part

FREQ. NO. F=.5 FROUDE NO. FN=0.

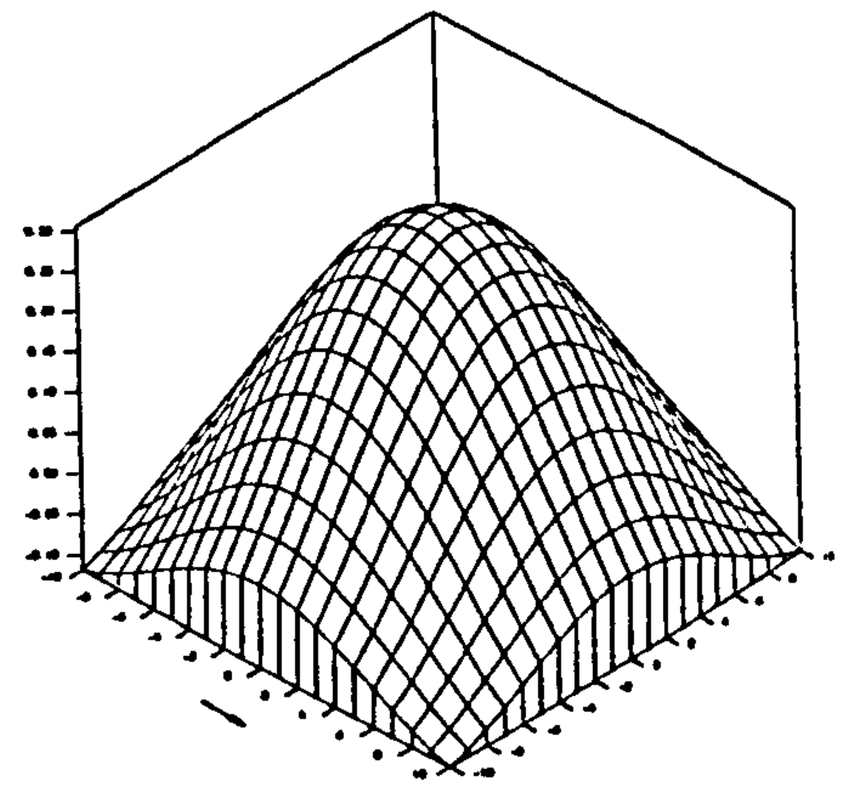

Z-derivative Imaginary Part

FREQ. NO. F=.5 FROUDE NO. FN=0.

Fig.4.8 Three-dimensional isometric view for an oscillating source potential at f=0.5 at infinite water depth

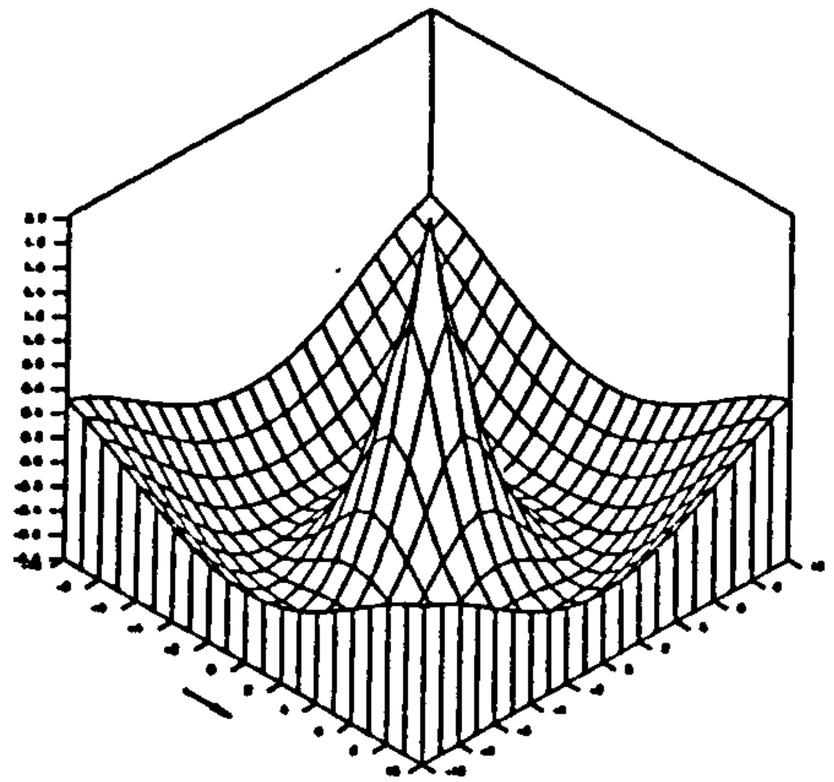

Potential Real Part

FREQ. NO. F=.6 FROUDE NO. FN=0.

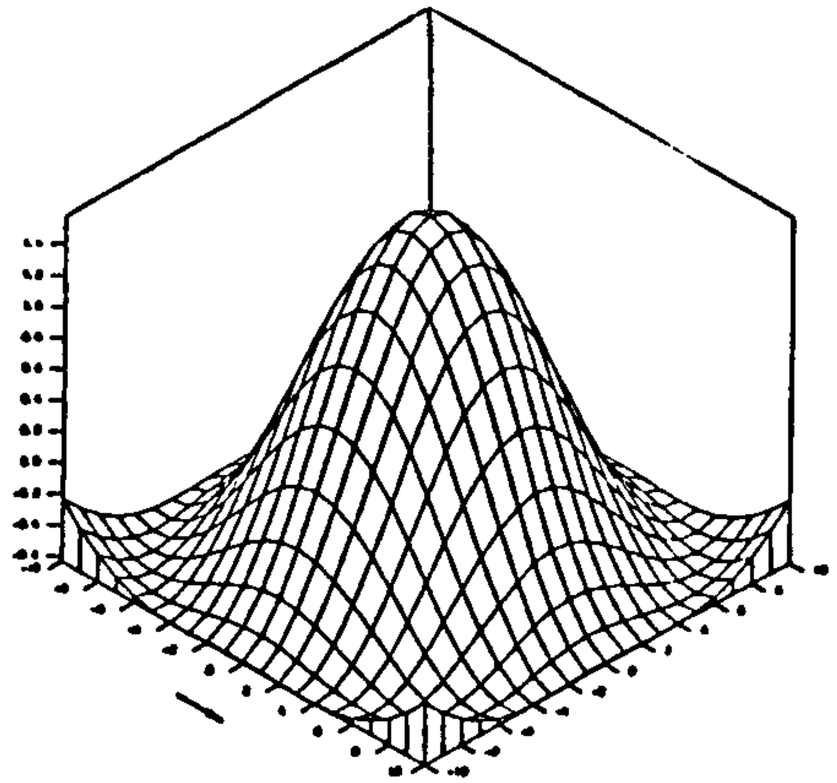

Potential Imaginary Part

FREQ. NO. F=.6 FROUDE NO. FN=0.

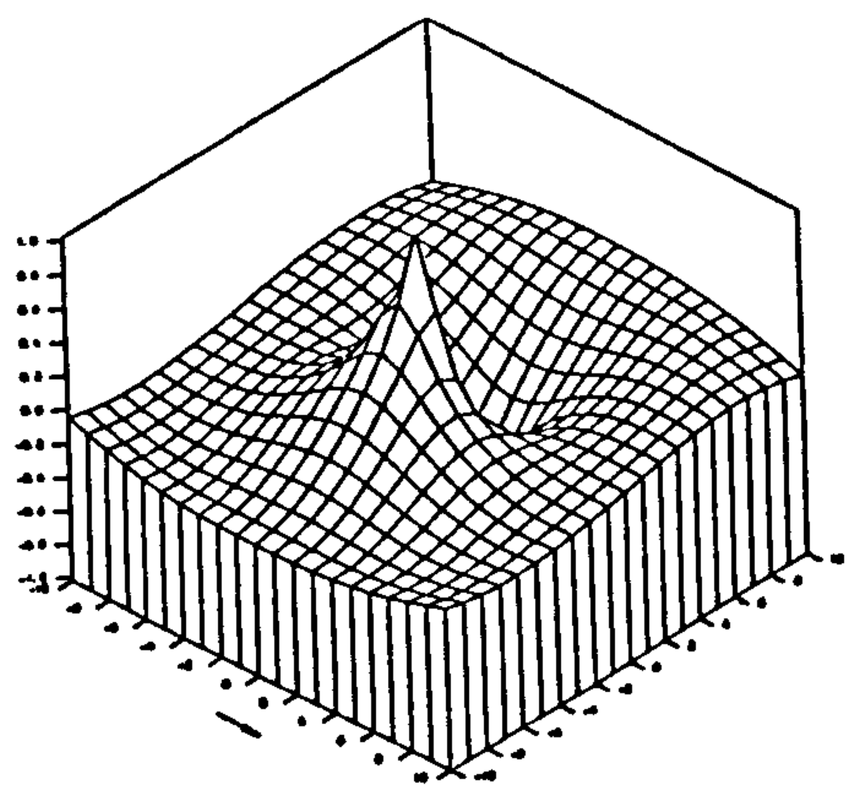

Y-derivative Real Part

FREQ. NO. F=.6 FROUDE NO. FN=0.

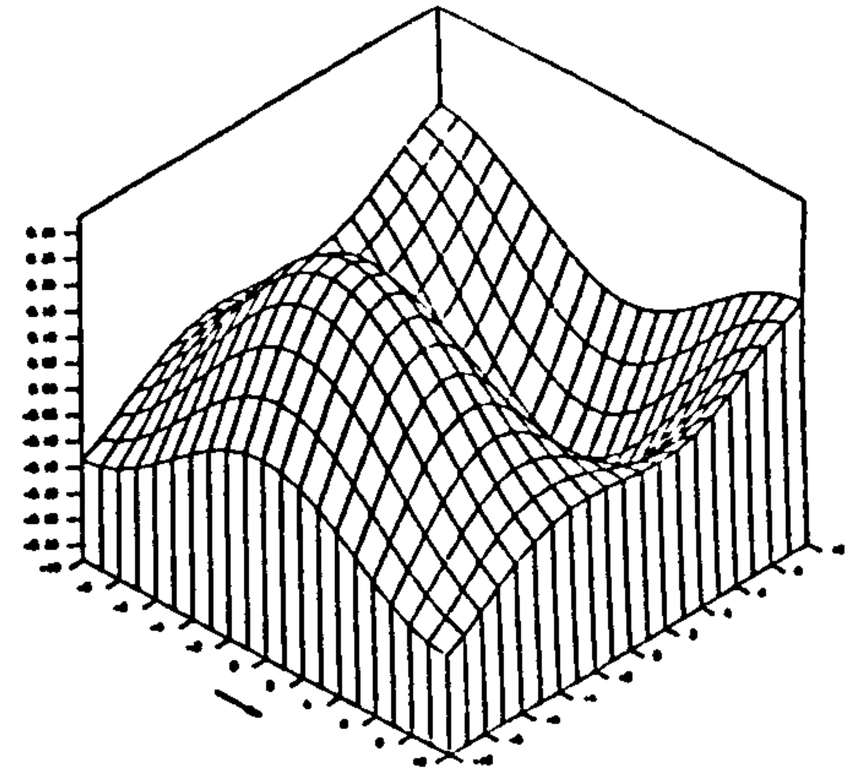

Y-derivative Imaginary Part

FREQ. NO. F=.6 FROUDE NO. FN=0.

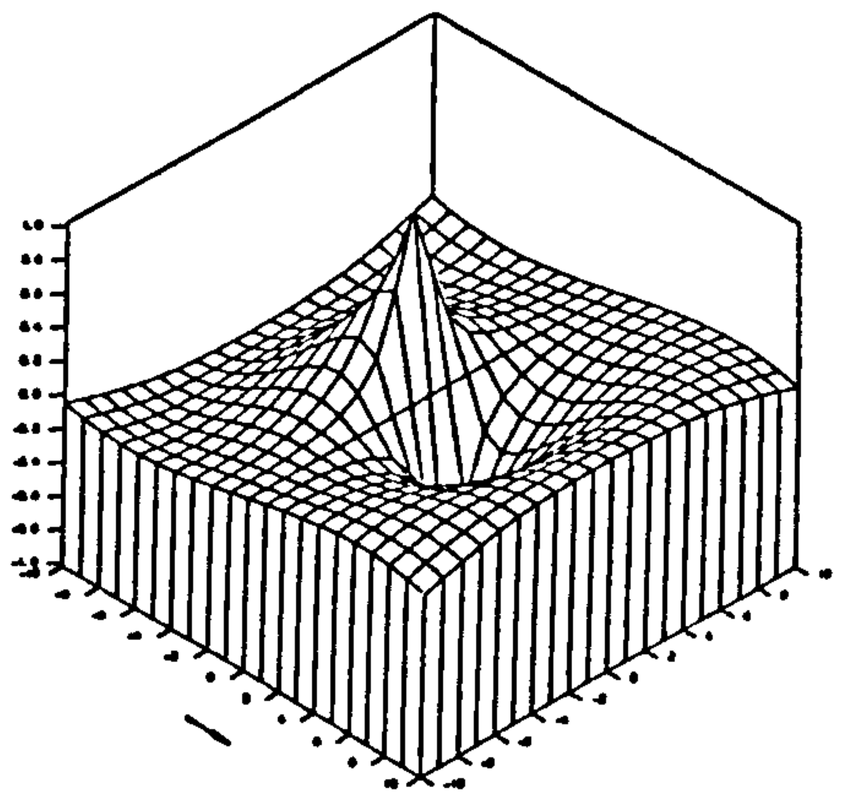

X-derivative Real Part

FREQ. NO. F=.6 FROUDE NO. FN=0.

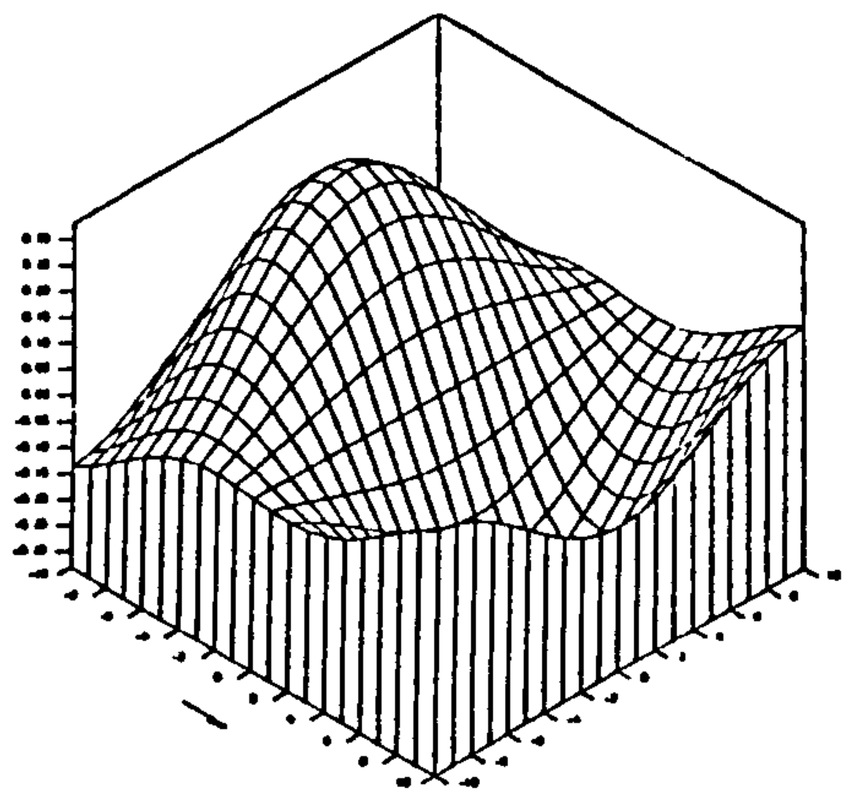

X-derivative Imaginary Part

FREQ. NO. F=.6 FROUDE NO. FN=0.

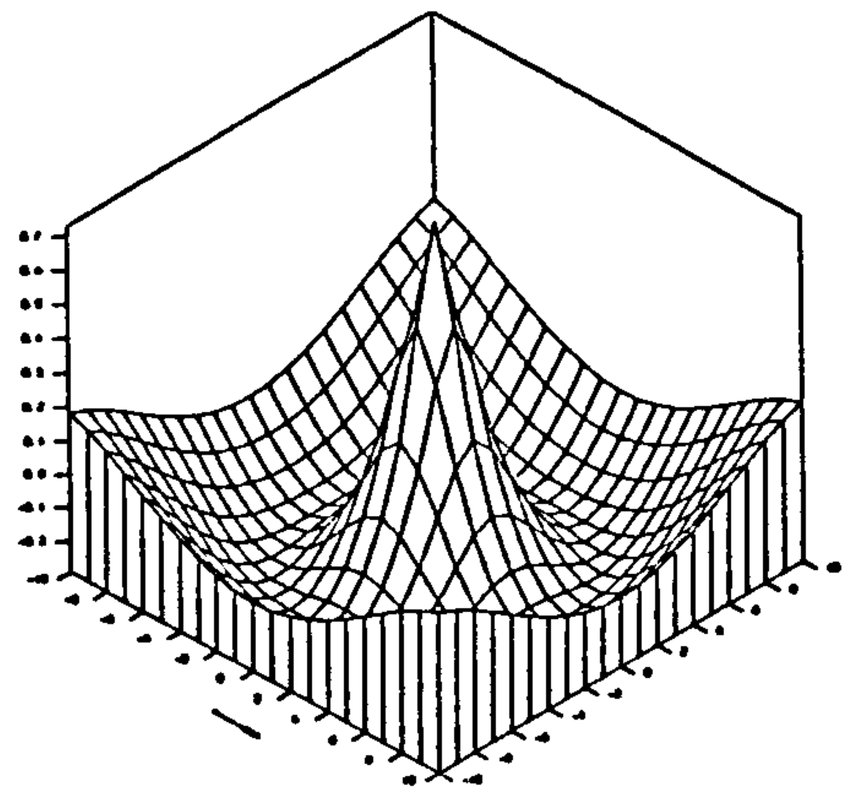

Z-derivative Real Part

FREQ. NO. F=.6 FROUDE NO. FN=0.

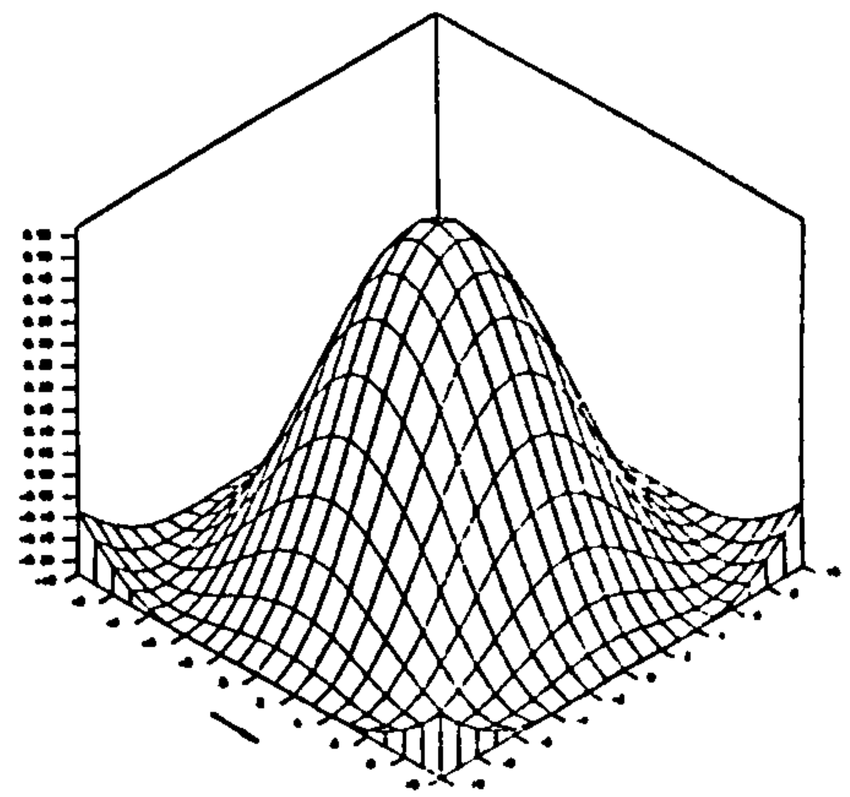

Z-derivative Imaginary Part

FREQ. NO. F=.6 FROUDE NO. FN=0.

Fig.4.9 Three-dimensional isometric view for an oscillating source potential at f=0.6 at infinite water depth

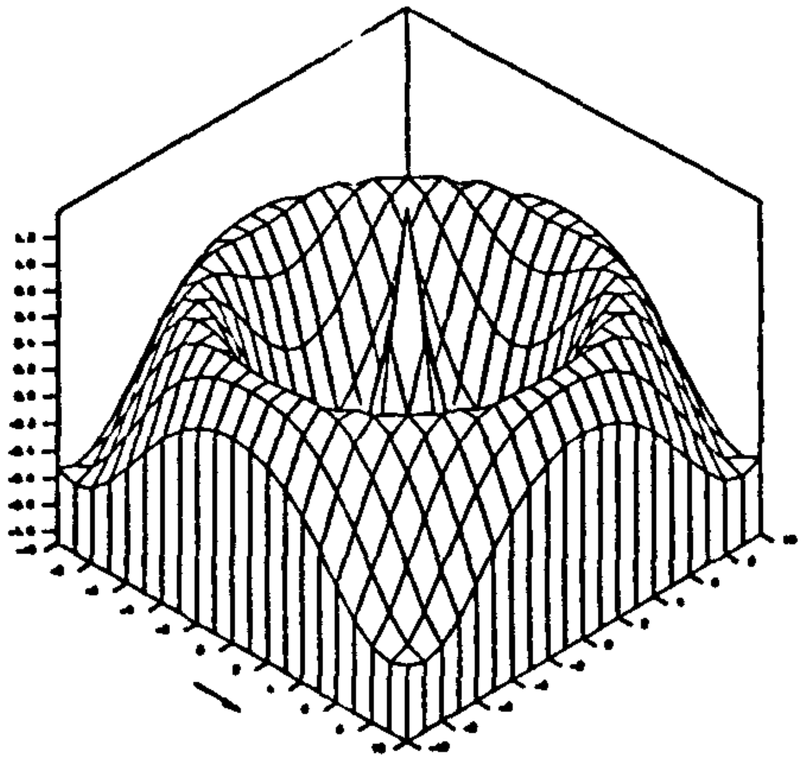

Potential Real Part

FREQ. NO. F=. 8 FROUDE NO. FN=0.

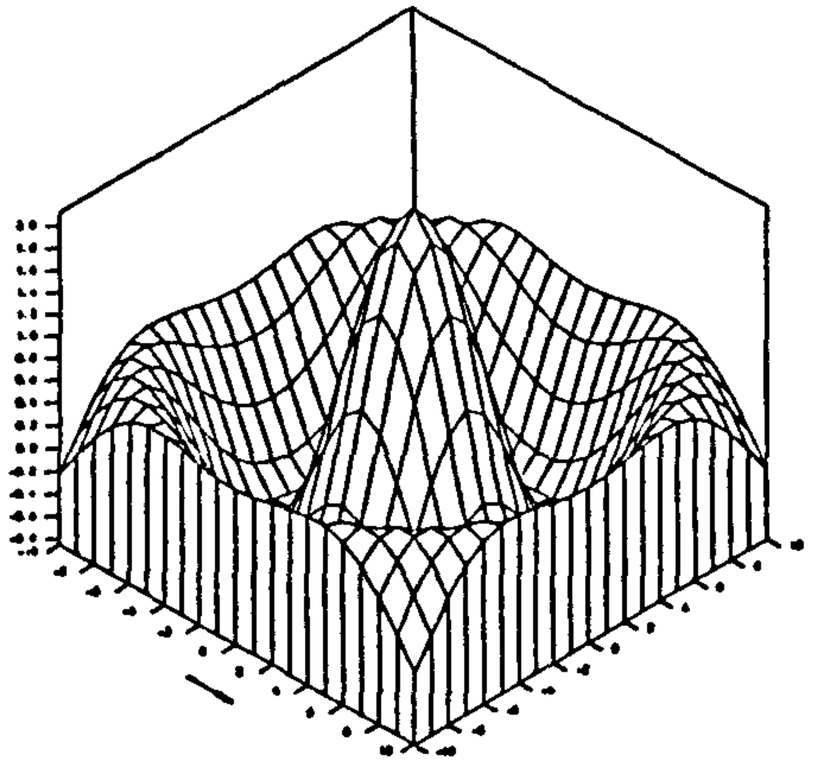

Potential Imaginary Part

FREQ. NO. F=. 8 FROUDE NO. FN=0.

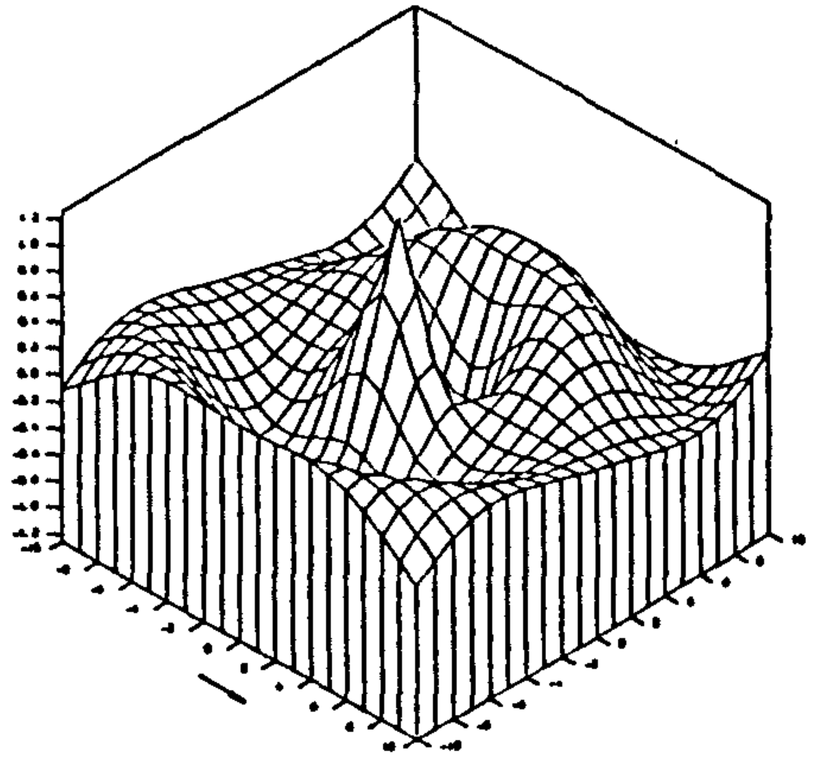

Y-derivative Real Part

FREQ. NO. F=. 8 FROUDE NO. FN=0.

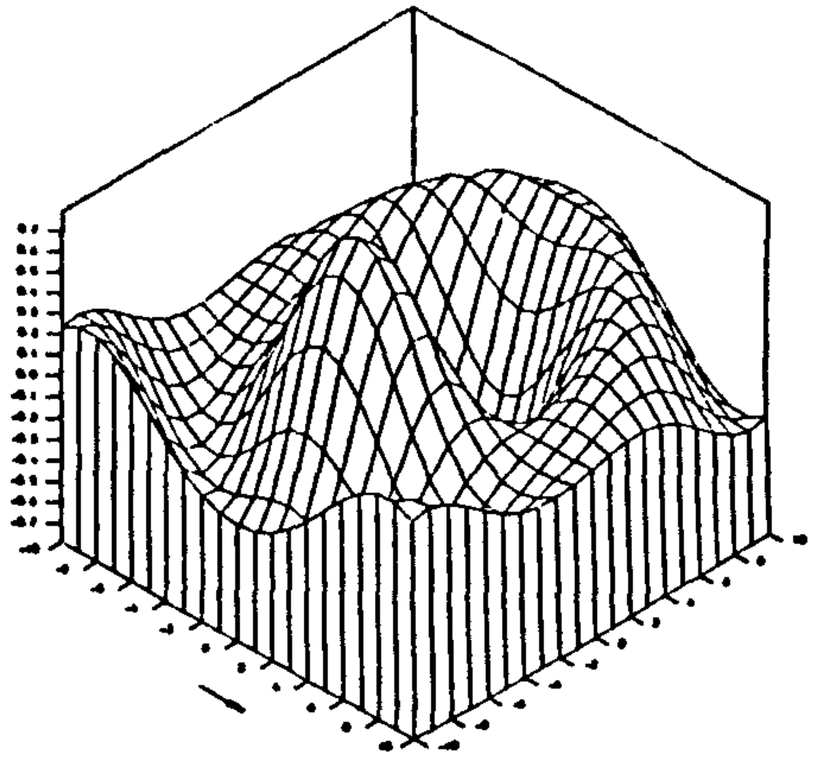

Y-derivative Imaginary Part

FREQ. NO. F=. 8 FROUDE NO. FN=0.

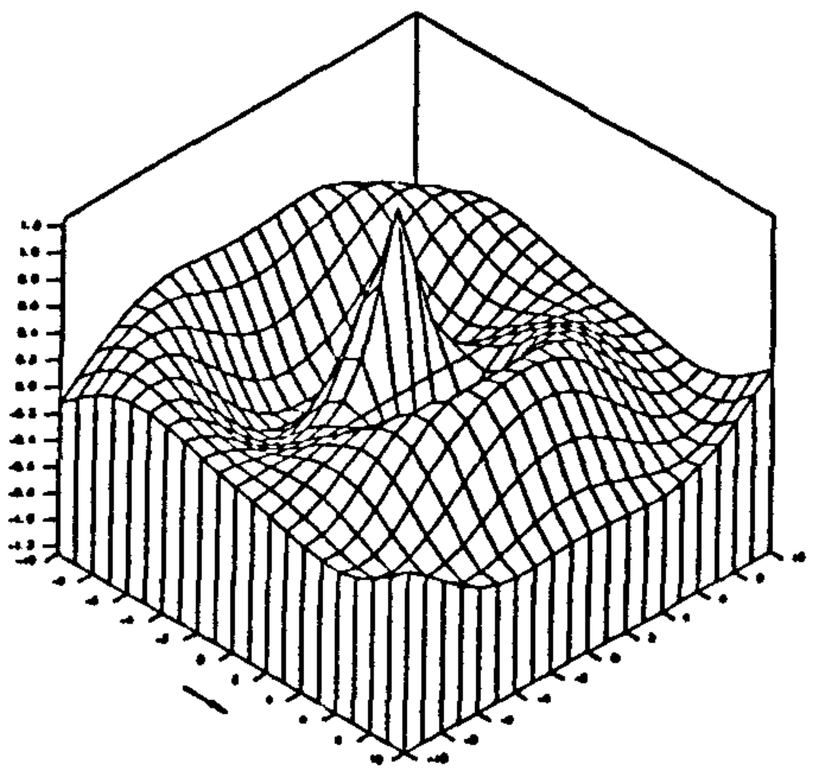

X-derivative Real Part

FREQ. NO. F=. 8 FROUDE NO. FN=0.

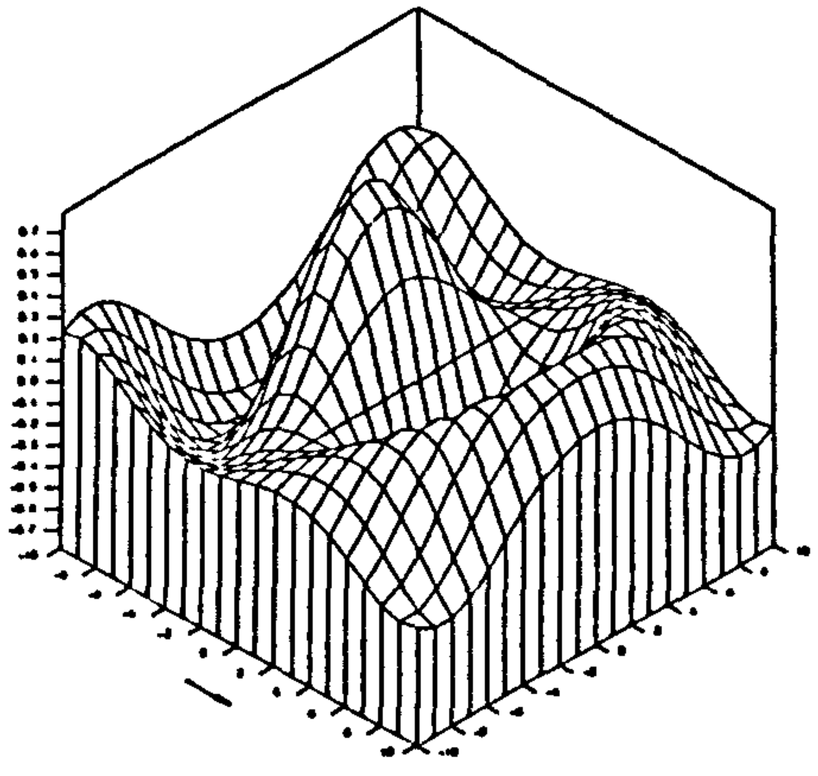

X-derivative Imaginary Part

FREQ. NO. F=. 8 FROUDE NO. FN=0.

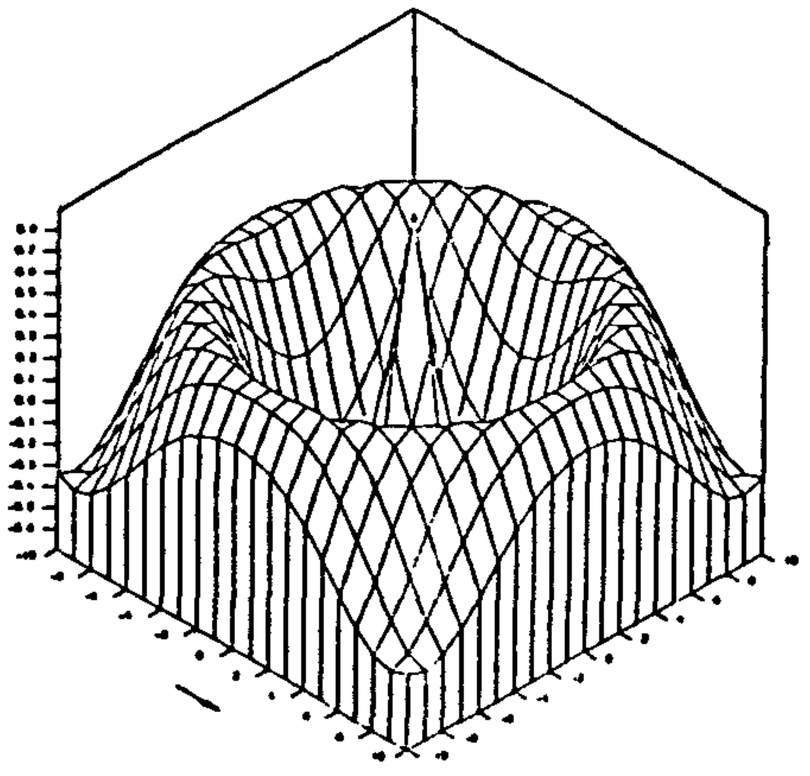

Z-derivative Real Part

FREQ. NO. F=. 8 FROUDE NO. FN=0.

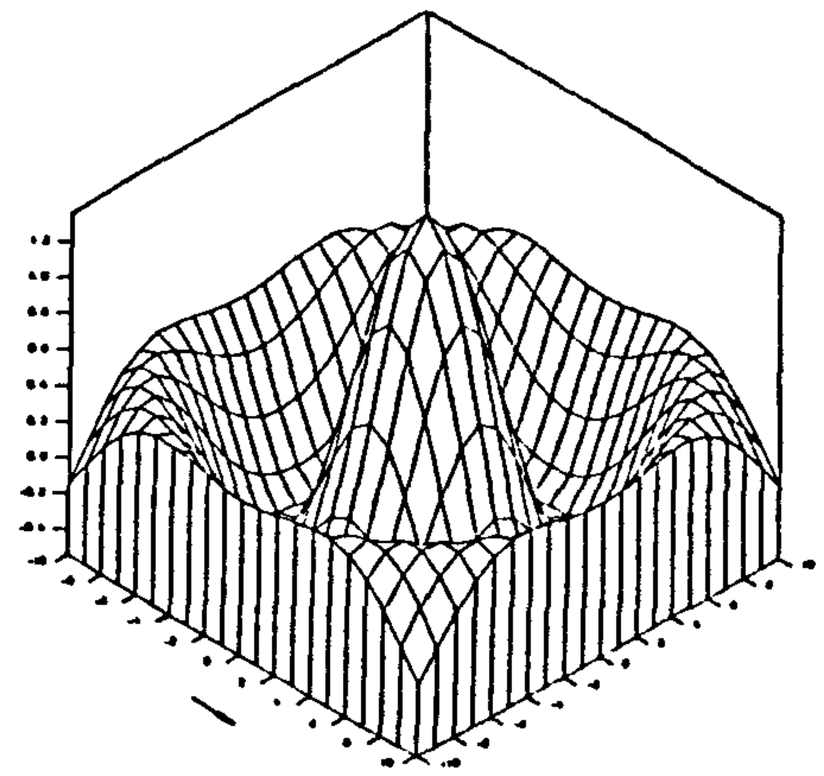

Z-derivative Imaginary Part

FREQ. NO. F=. 8 FROUDE NO. FN=0.

Fig.4.10 Three-dimensional isometric view for an oscillating source potential at f=0.8 at infinite water depth

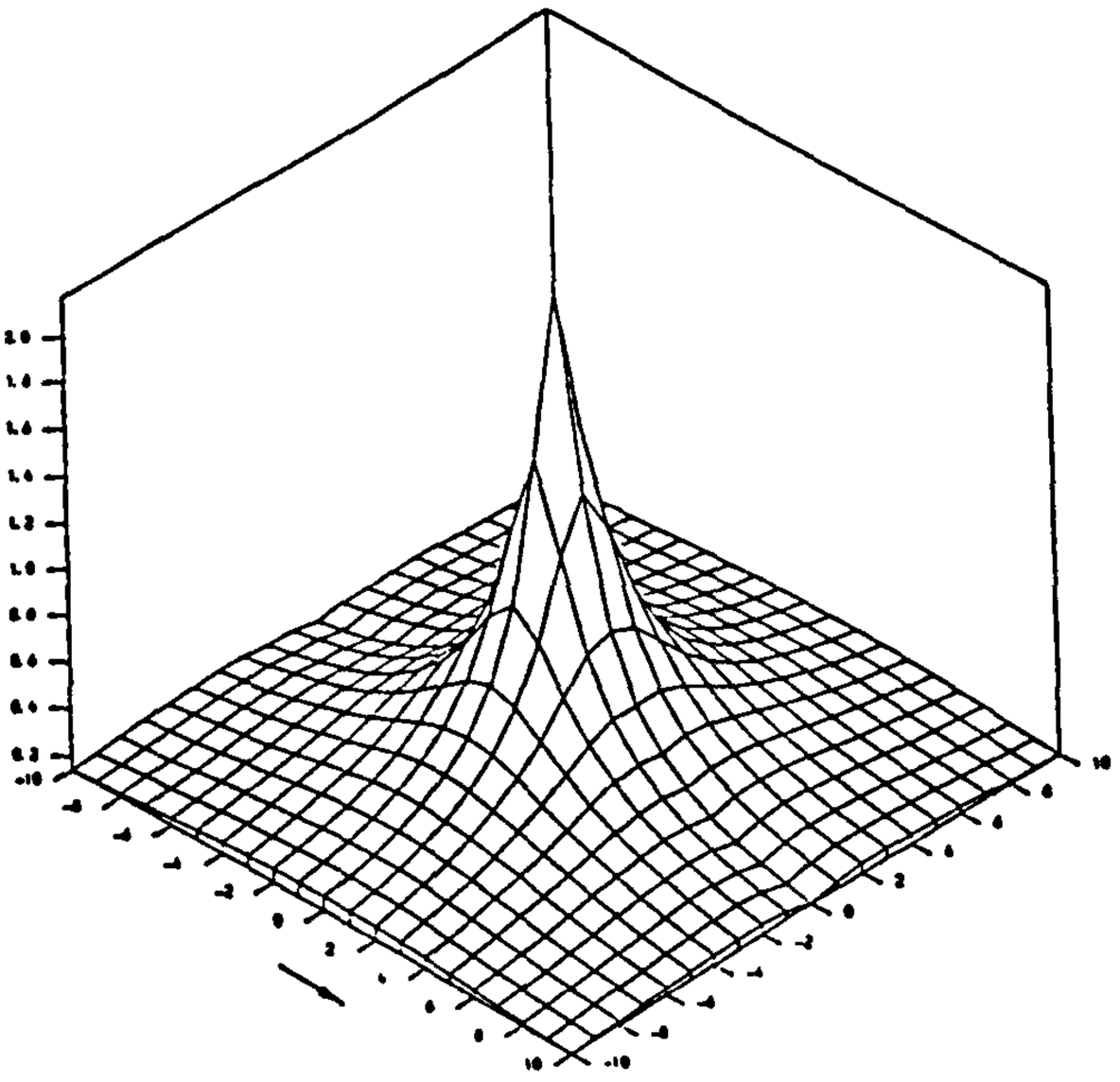

Potential Real Part

FREQ. NO. F=0. FROUDE NO. FN=. 4

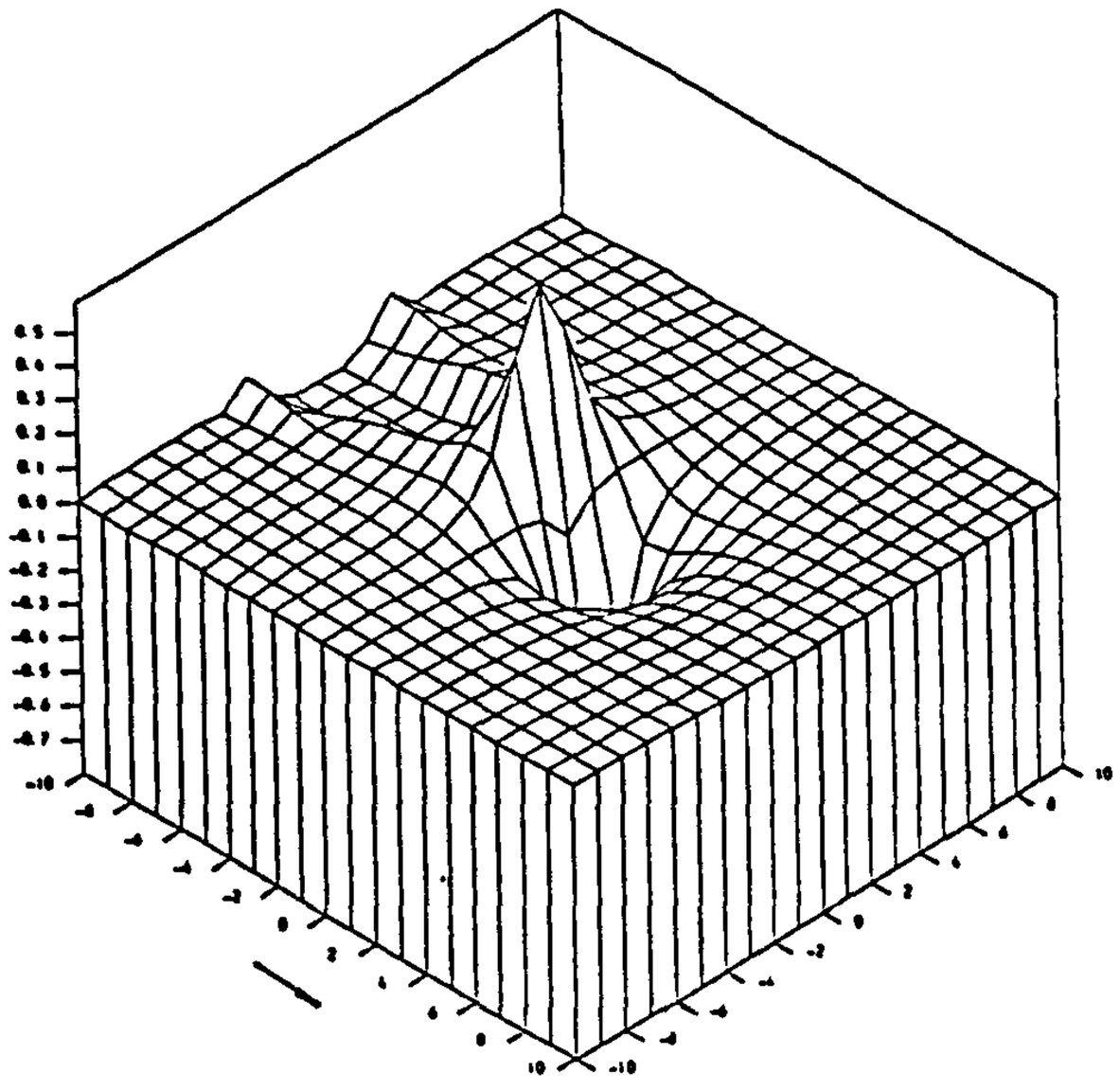

X-derivative Real Part

FREQ. NO. F=0. FROUDE NO. FN=. 4

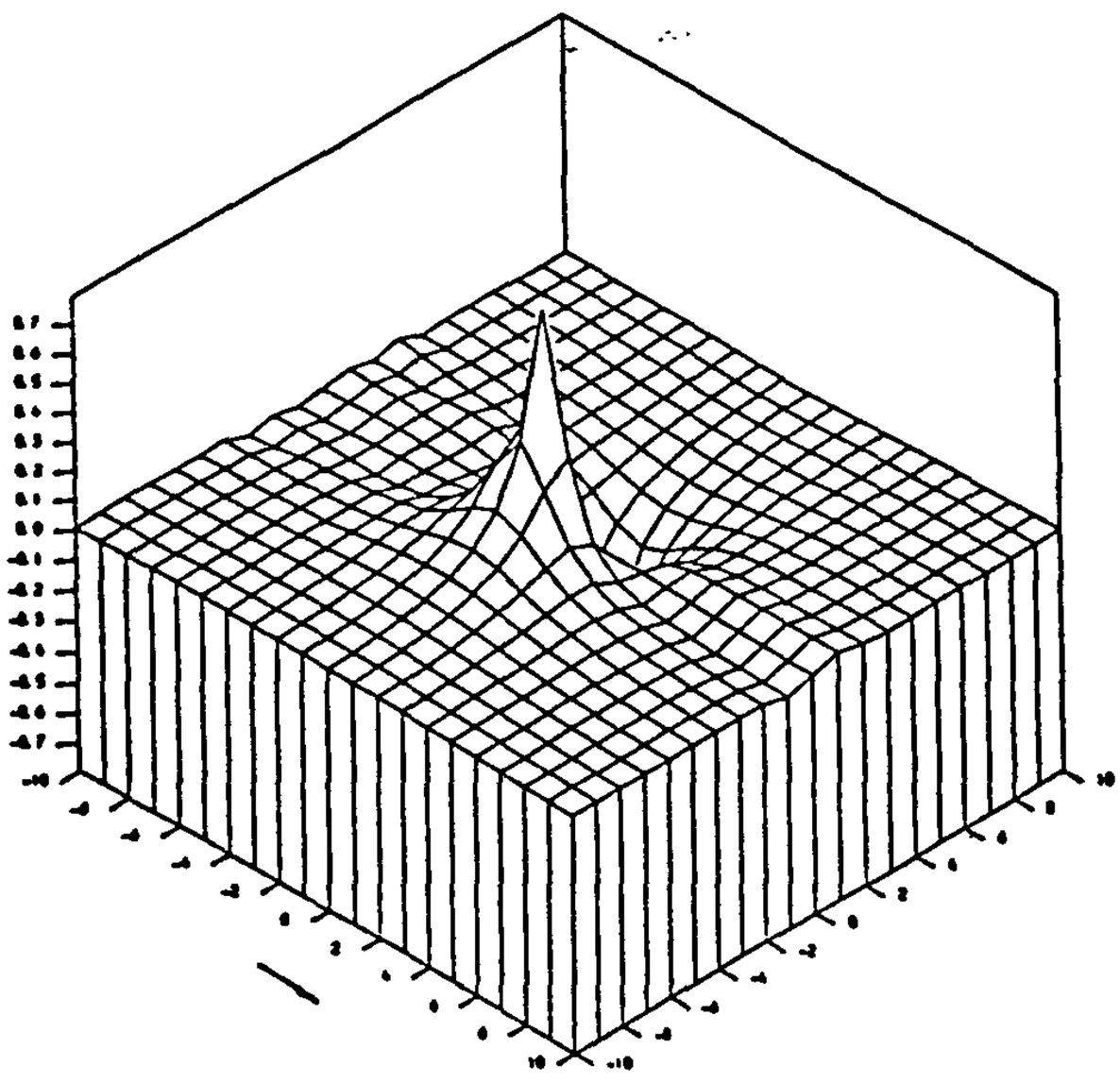

Y-derivative Real Part

FREQ. NO. F=0. FROUDE NO. FN=. 4

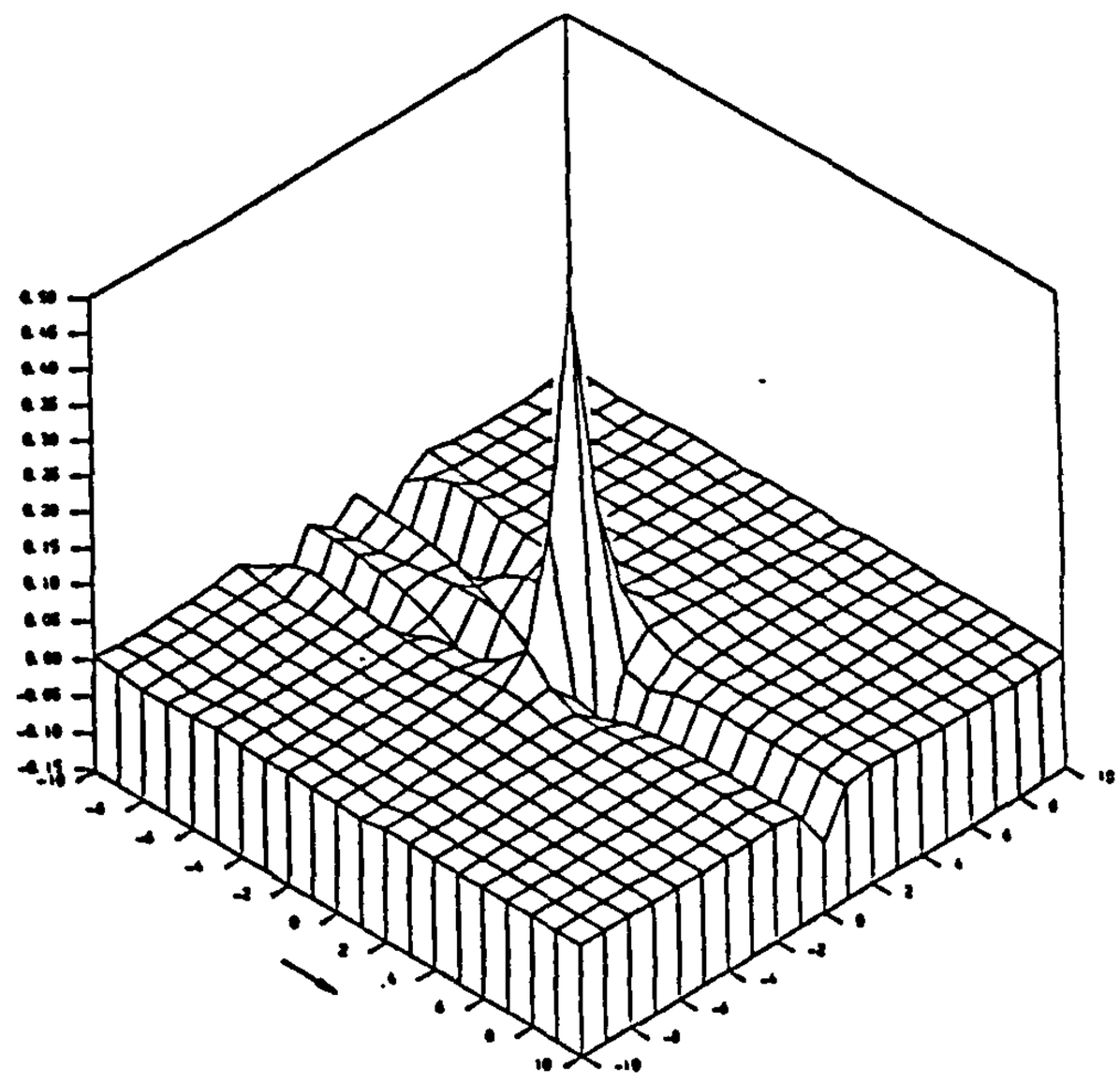

Z-derivative Real Part

FREQ. NO. F=0. FROUDE NO. FN=. 4

Fig.4.11 Three-dimensional isometric view for a translating source potential at F_n=0.4 at infinite water depth

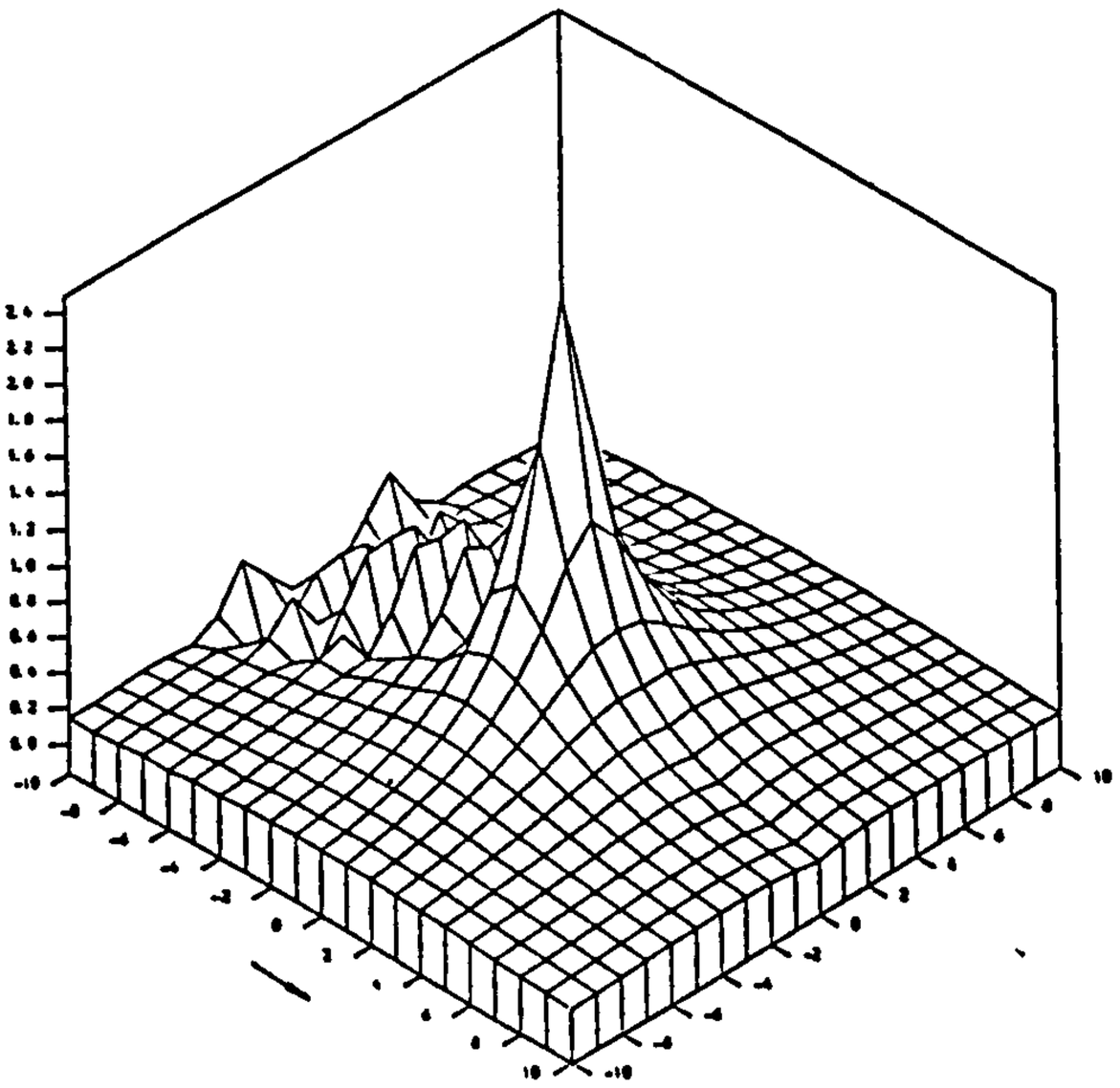

Potential Real Part

FREQ. NO. F=0. FROUDE NO. FN=.6

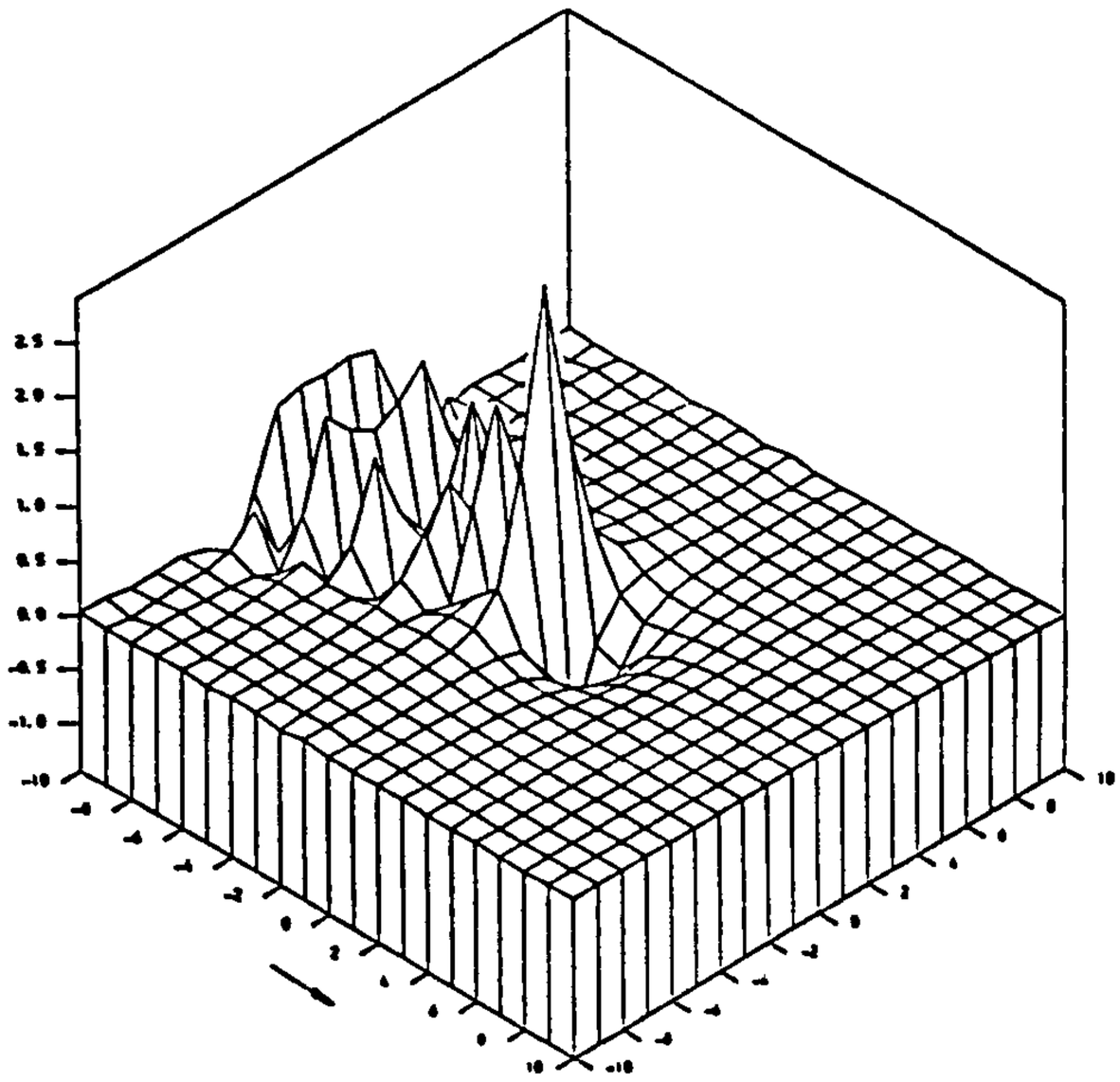

X-derivative Real Part

FREQ. NO. F=0. FROUDE NO. FN=.6

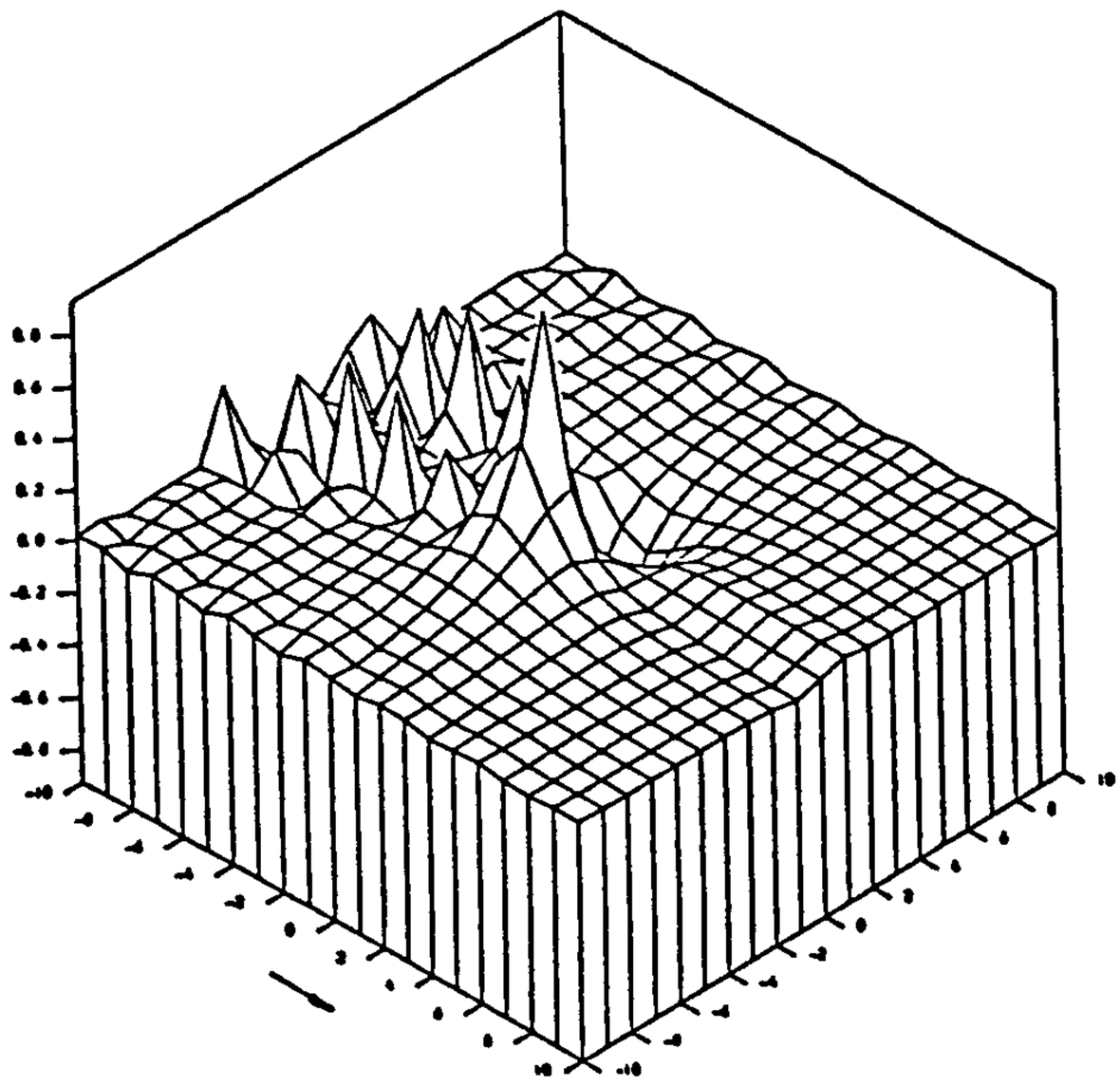

Y-derivative Real Part

FREQ. NO. F=0. FROUDE NO. FN=.6

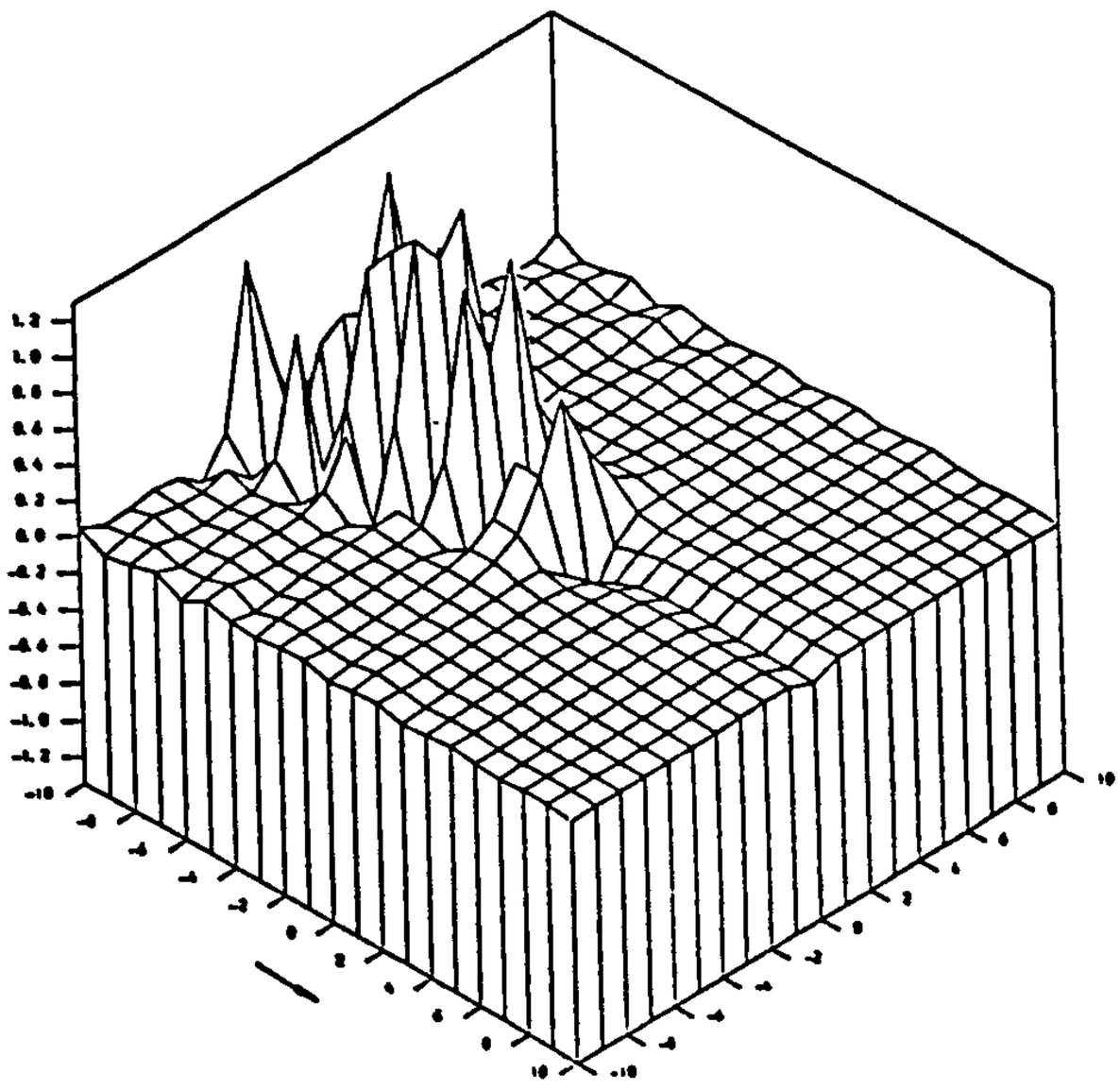

Z-derivative Real Part

FREQ. NO. F=0. FROUDE NO. FN=.6

Fig.4.12 Three-dimensional isometric view for a translating source potential at F_n=0.6 at infinite water depth

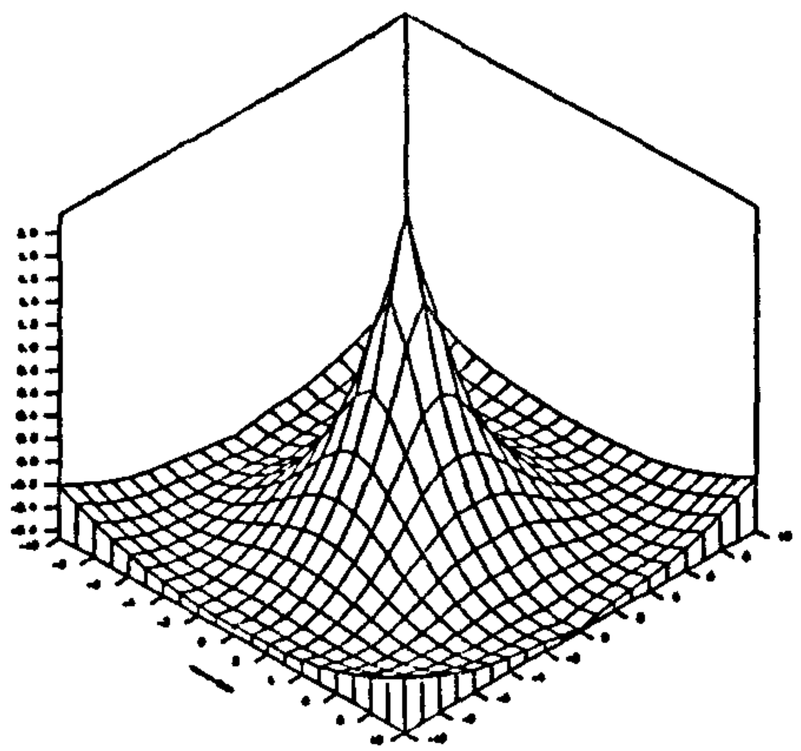

Potential Real Part

FREQ. NO. F=. 5 FROUDE NO. FN=. 05

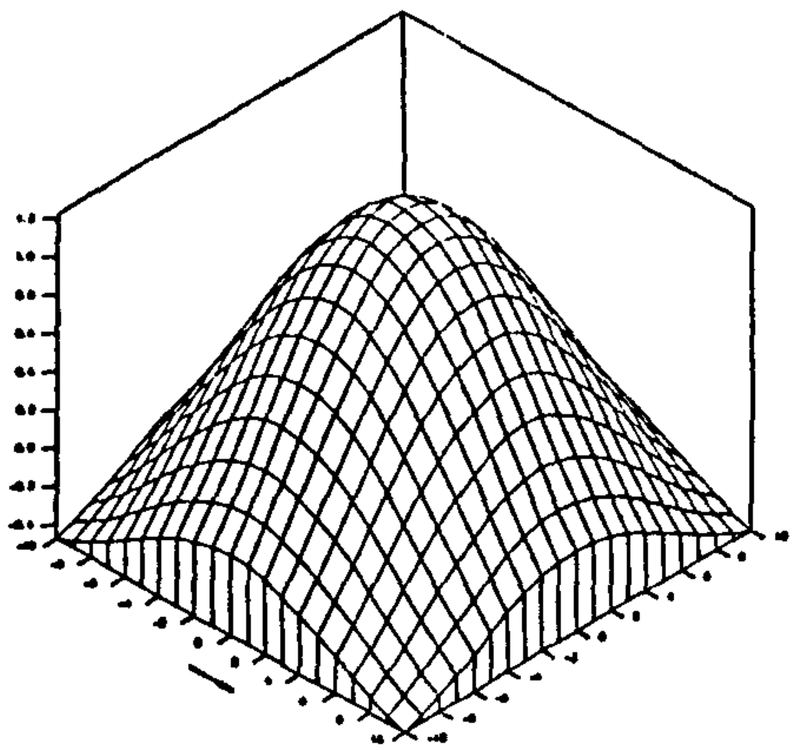

Potential Imaginary Part

FREQ. NO. F=. 5 FROUDE NO. FN=. 05

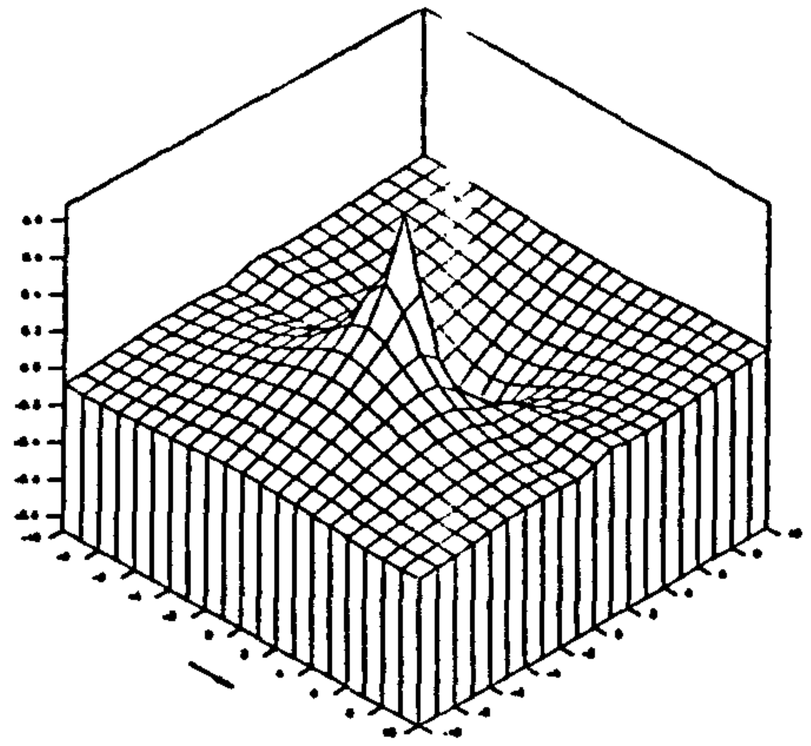

Y-derivative Real Part

FREQ. NO. F=. 5 FROUDE NO. FN=. 05

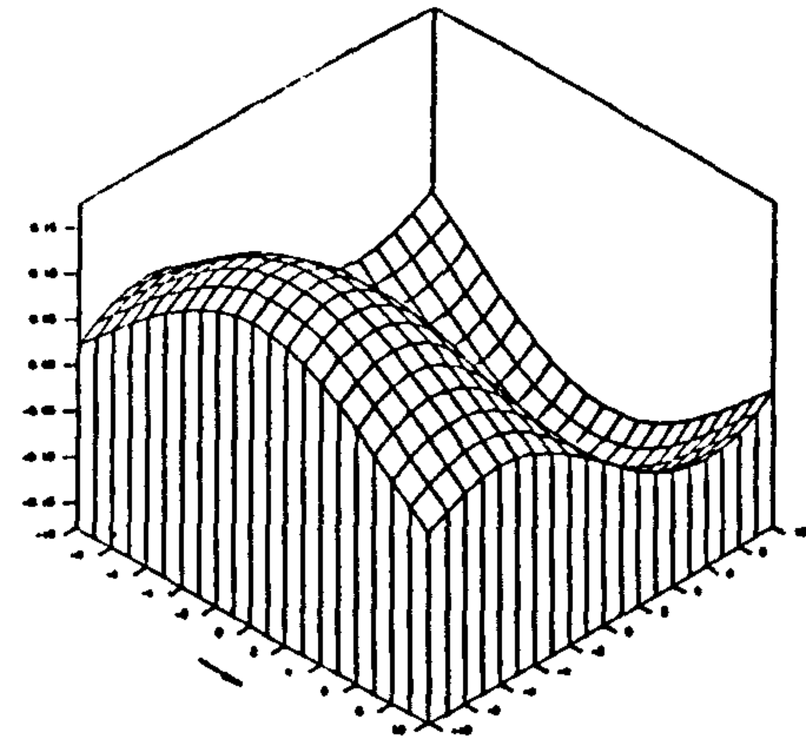

Y-derivative Imaginary Part

FREQ. NO. F=. 5 FROUDE NO. FN=. 05

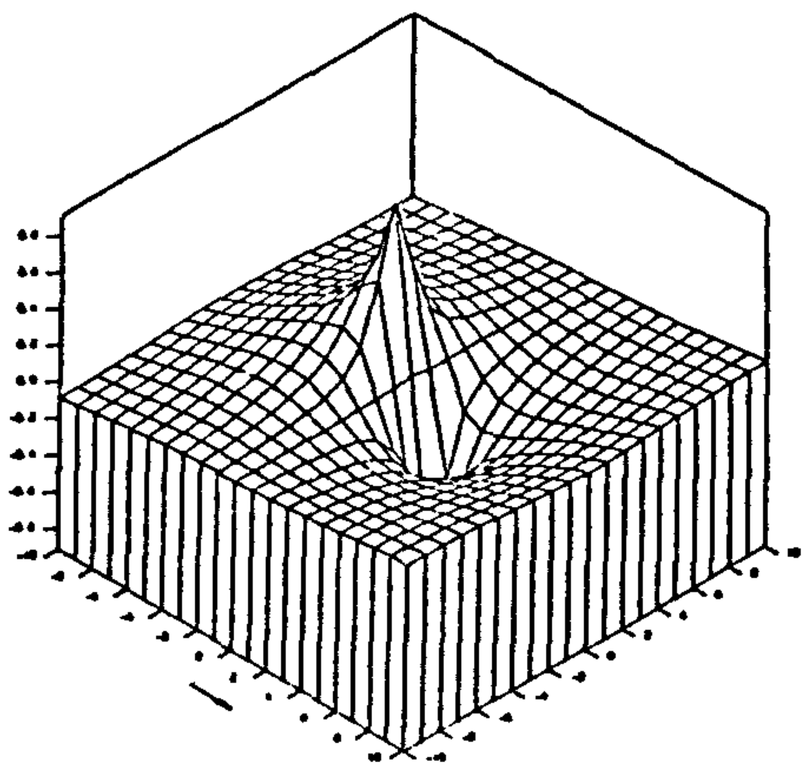

X-derivative Real Part

FREQ. NO. F=. 5 FROUDE NO. FN=. 05

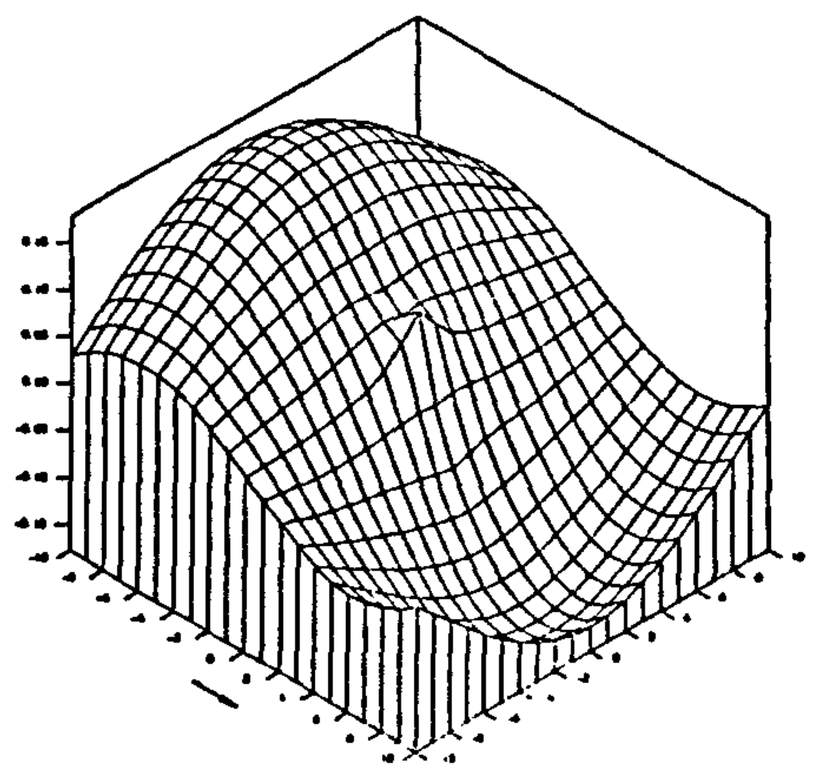

X-derivative Imaginary Part

FREQ. NO. F=. 5 FROUDE NO. FN=. 05

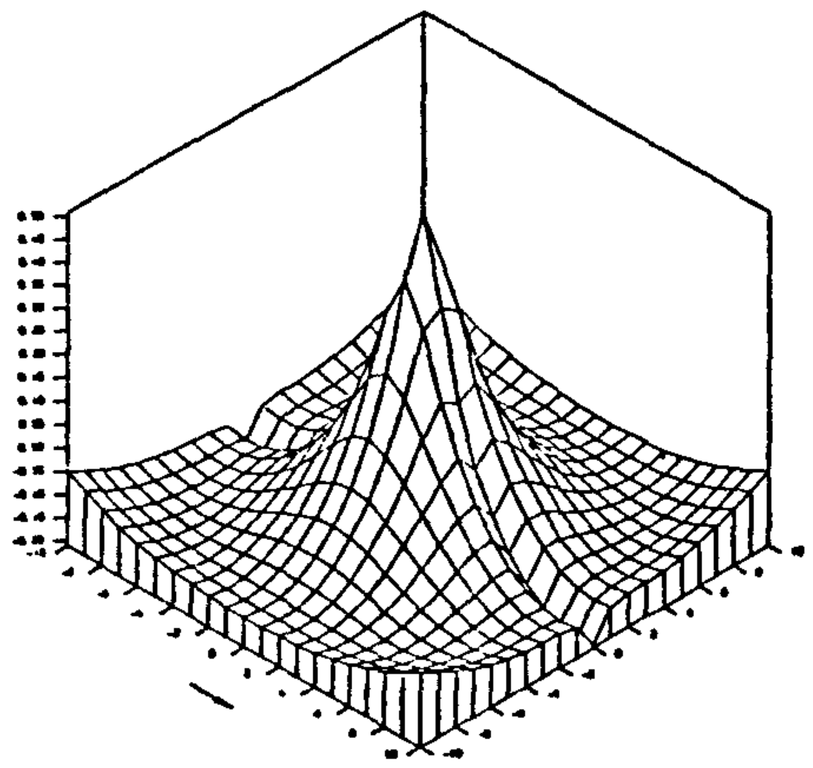

Z-derivative Real Part

FREQ. NO. F=. 5 FROUDE NO. FN=. 05

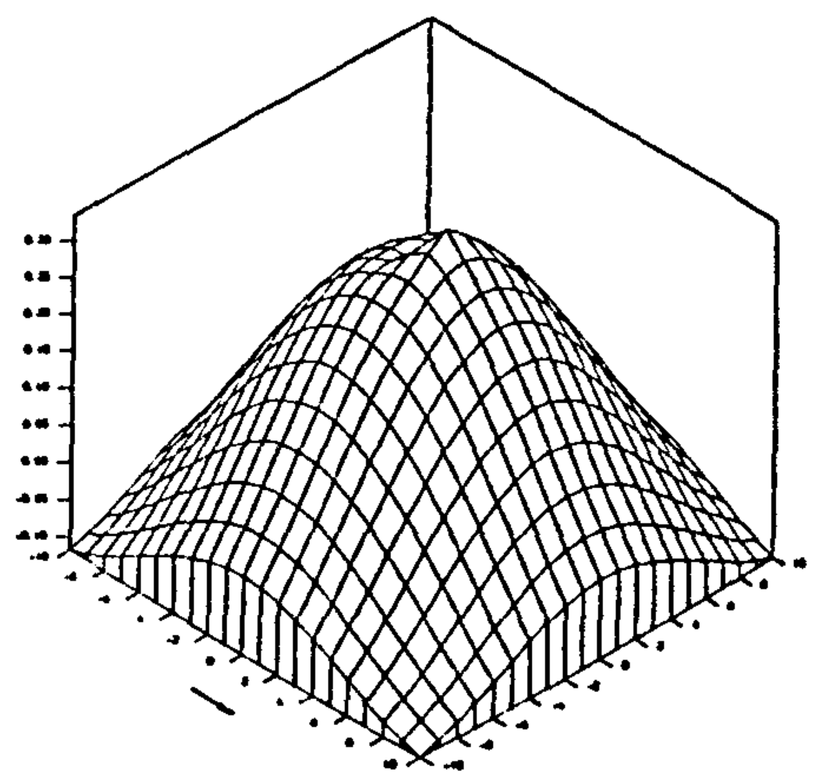

Z-derivative Imaginary Part

FREQ. NO. F=. 5 FROUDE NO. FN=. 05

Fig. 4.13 Three-dimensional isometric view for a translating pulsating source potential at f=0.5 and F_n=0.05 at infinite water depth

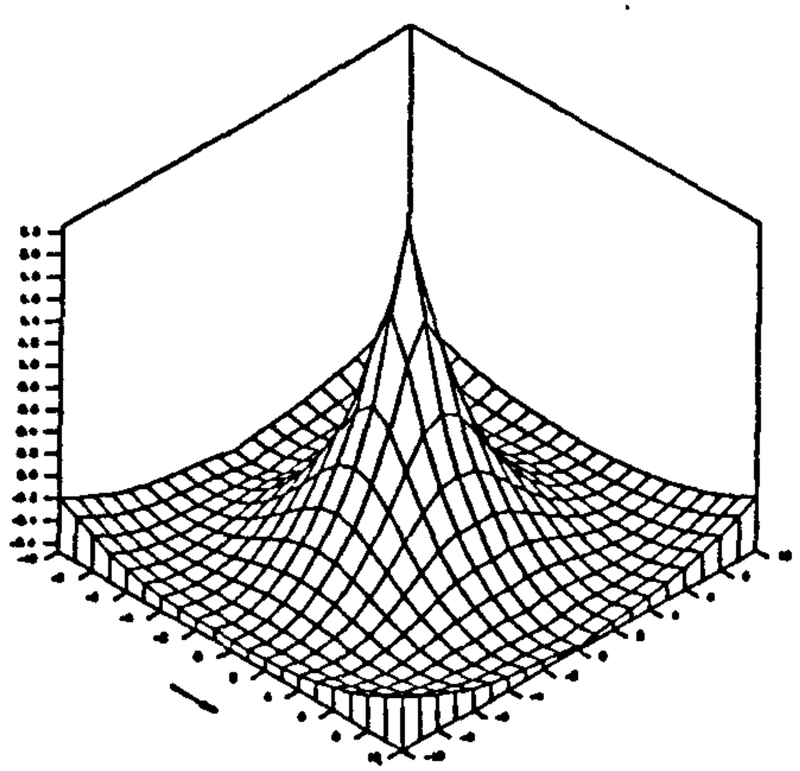

Potential Real Part

FREQ. NO. F=.5 FROUDE NO. FN=.2

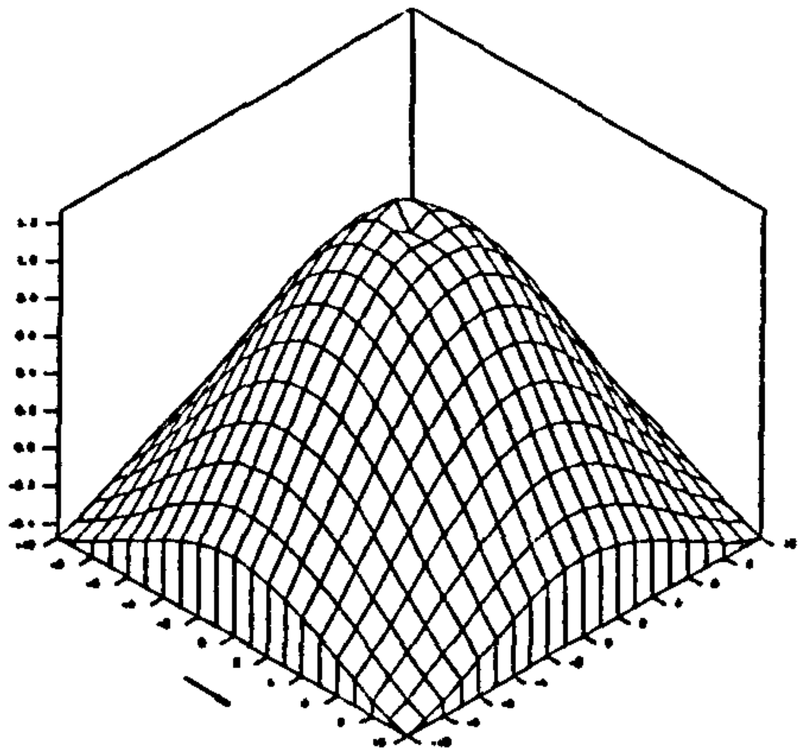

Potential Imaginary Part

FREQ. NO. F=.5 FROUDE NO. FN=.2

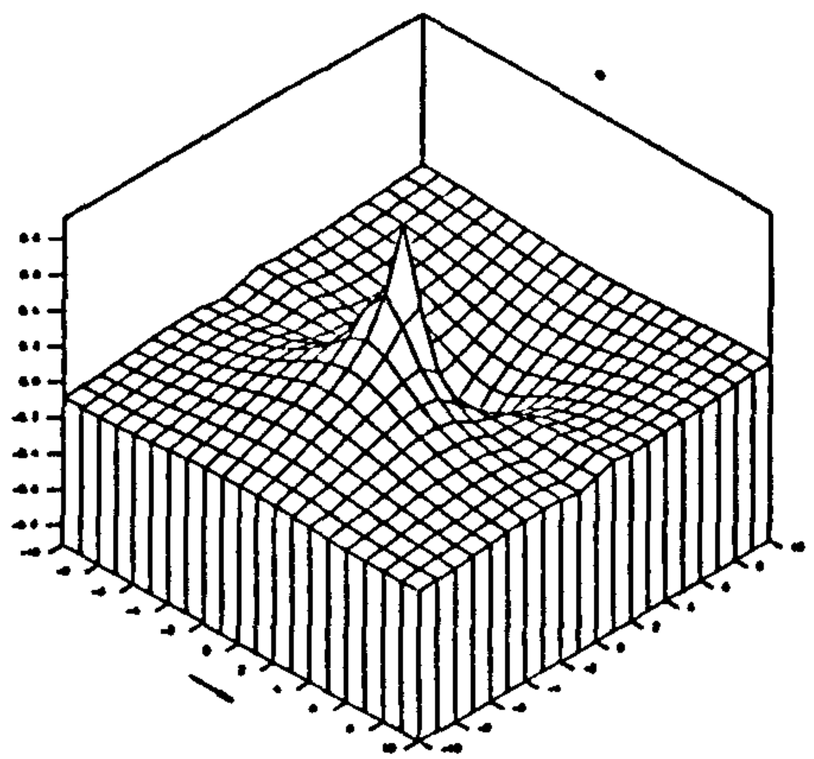

Y-derivative Real Part

FREQ. NO. F=.5 FROUDE NO. FN=.2

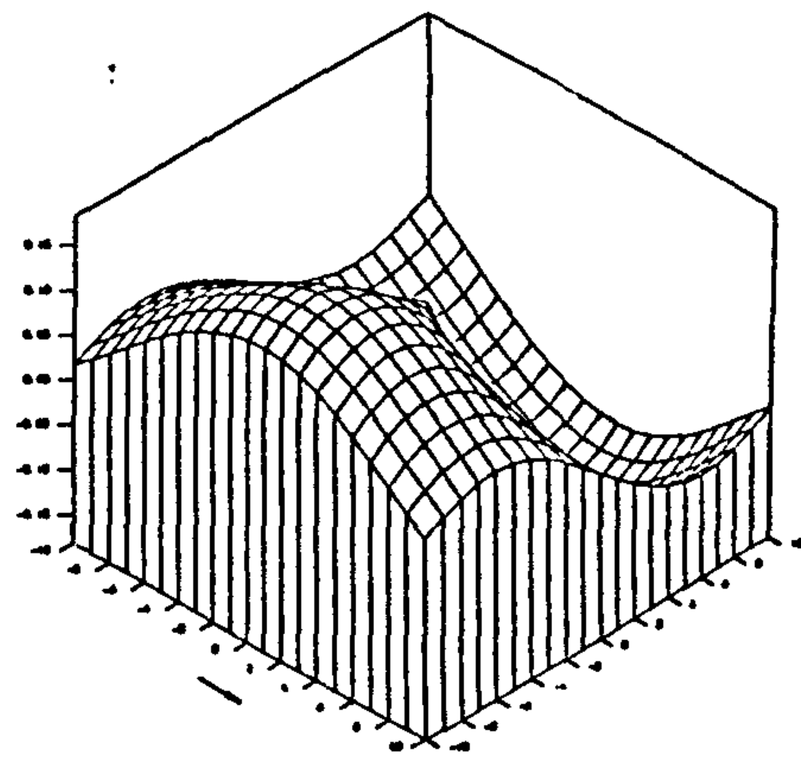

Y-derivative Imaginary Part

FREQ. NO. F=.5 FROUDE NO. FN=.2

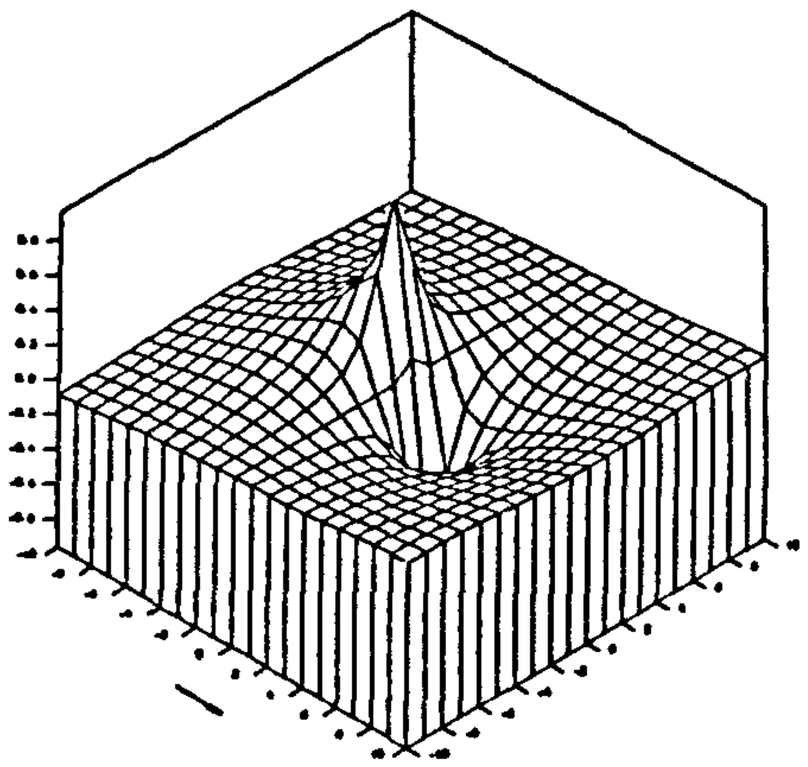

X-derivative Real Part

FREQ. NO. F=.5 FROUDE NO. FN=.2

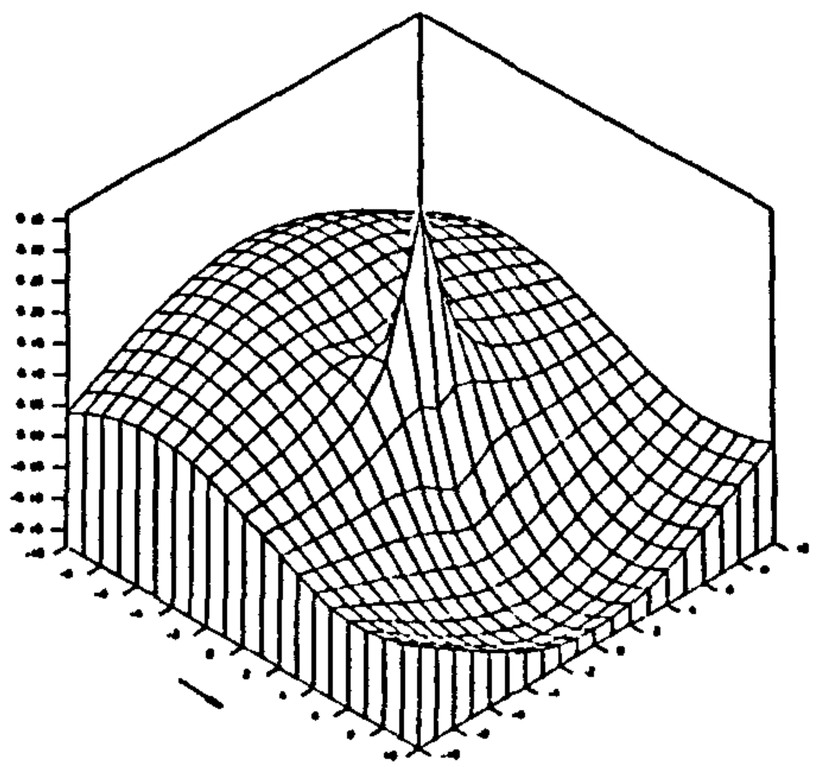

X-derivative Imaginary Part

FREQ. NO. F=.5 FROUDE NO. FN=.2

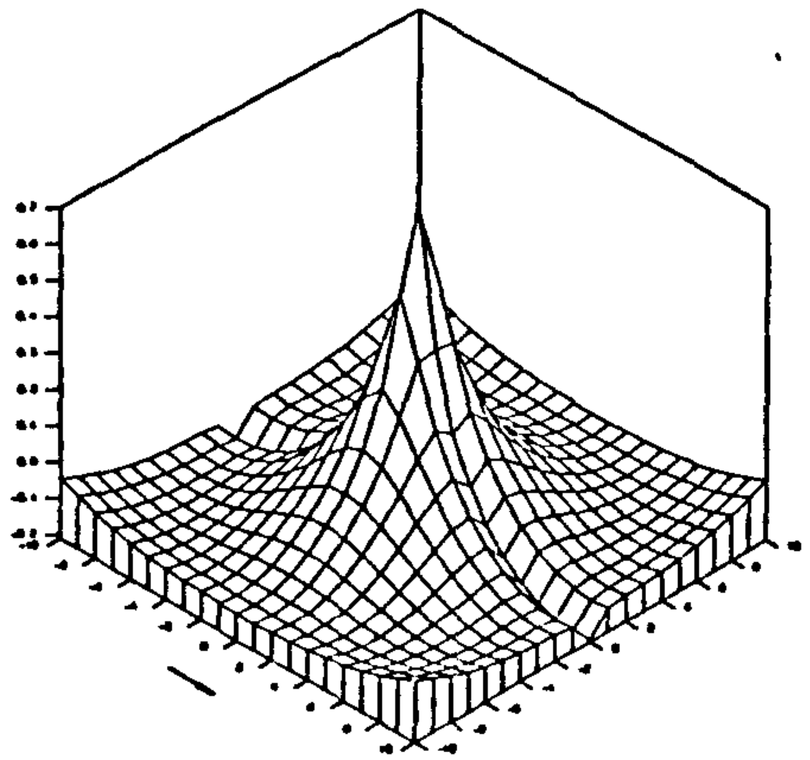

Z-derivative Real Part

FREQ. NO. F=.5 FROUDE NO. FN=.2

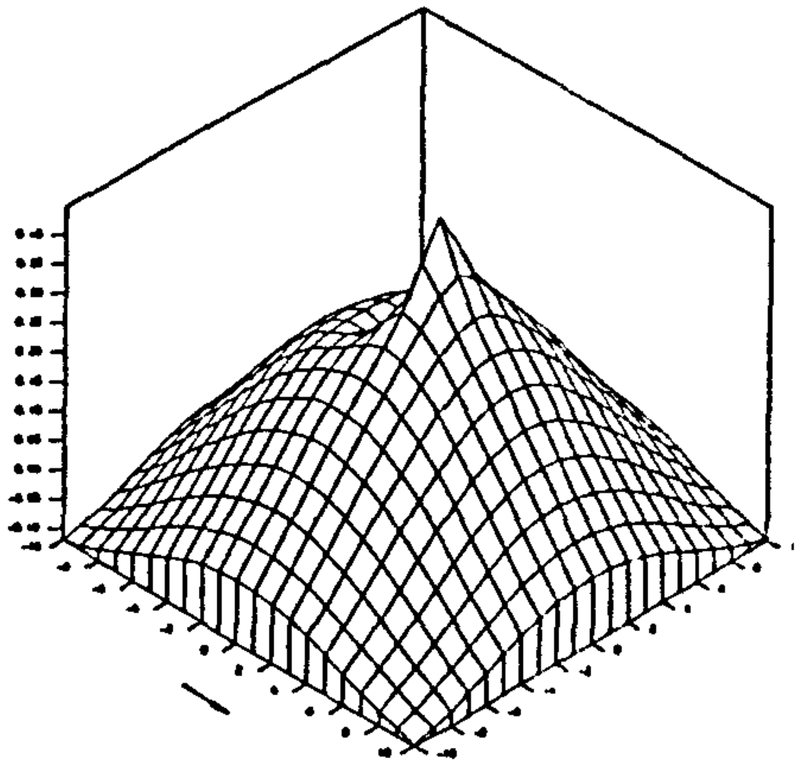

Z-derivative Imaginary Part

FREQ. NO. F=.5 FROUDE NO. FN=.2

Fig.4.14 Three-dimensional isometric view for a translating pulsating source potential at f=0.5 and F_n=0.2 at infinite water depth

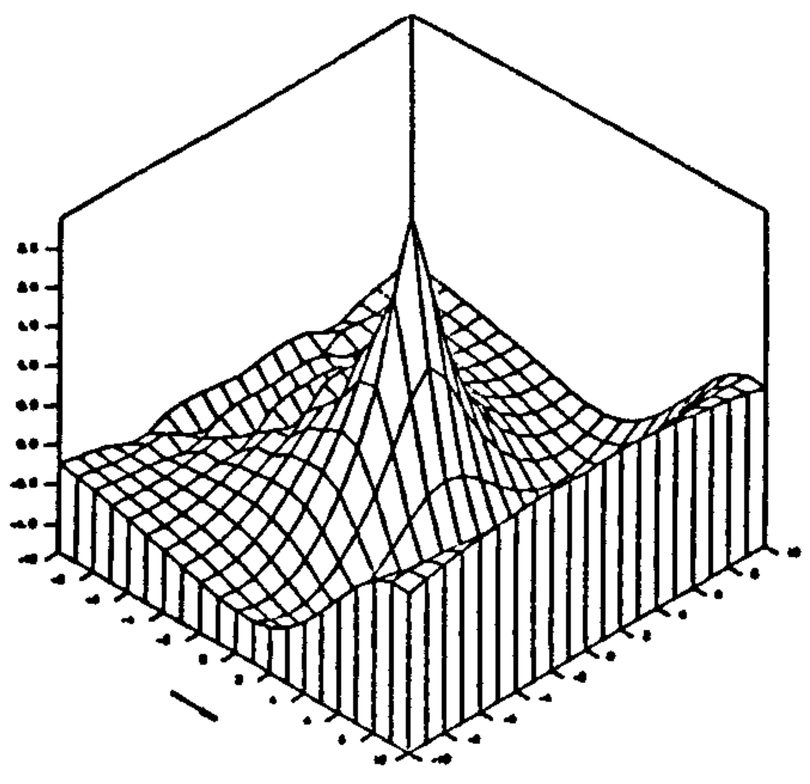

Potential Real Part

FREQ. NO. F=. 5 FROUDE NO. FN=. 4

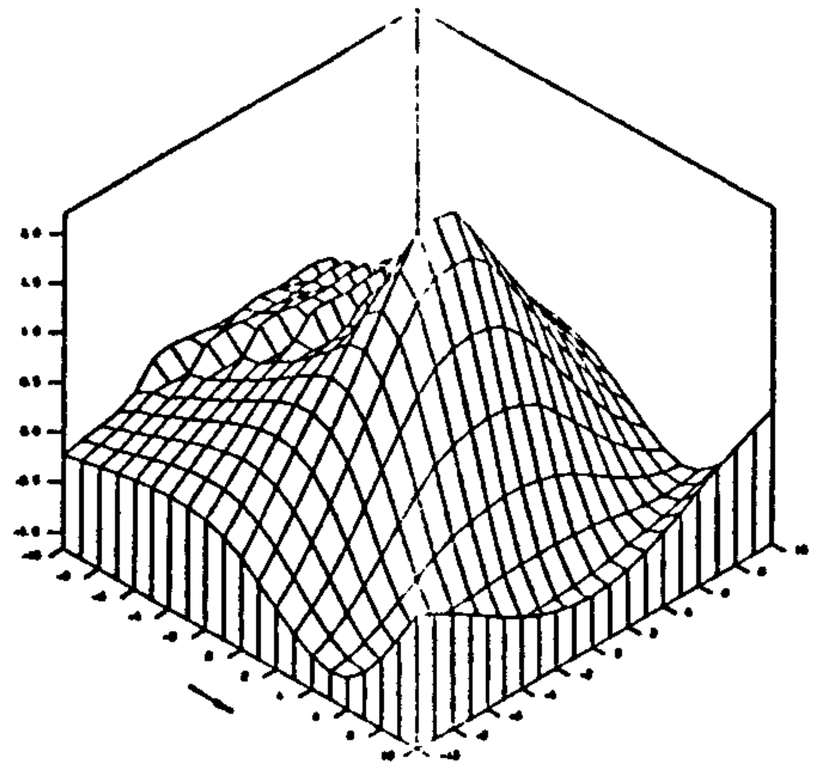

Potential Imaginary Part

FREQ. NO. F=. 5 FROUDE NO. FN=. 4

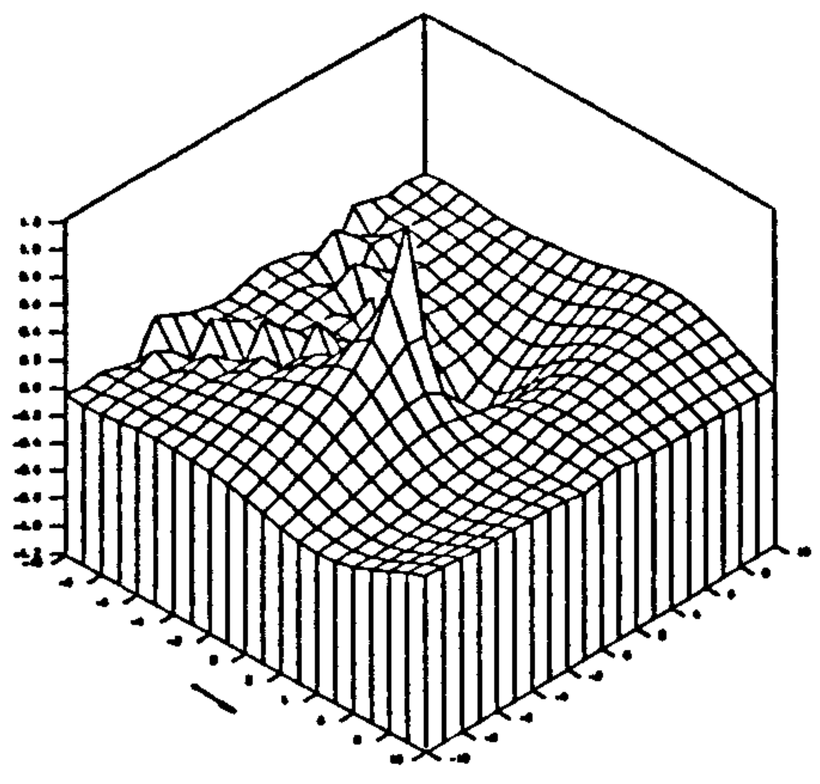

Y-derivative Real Part

FREQ. NO. F=. 5 FROUDE NO. FN=. 4

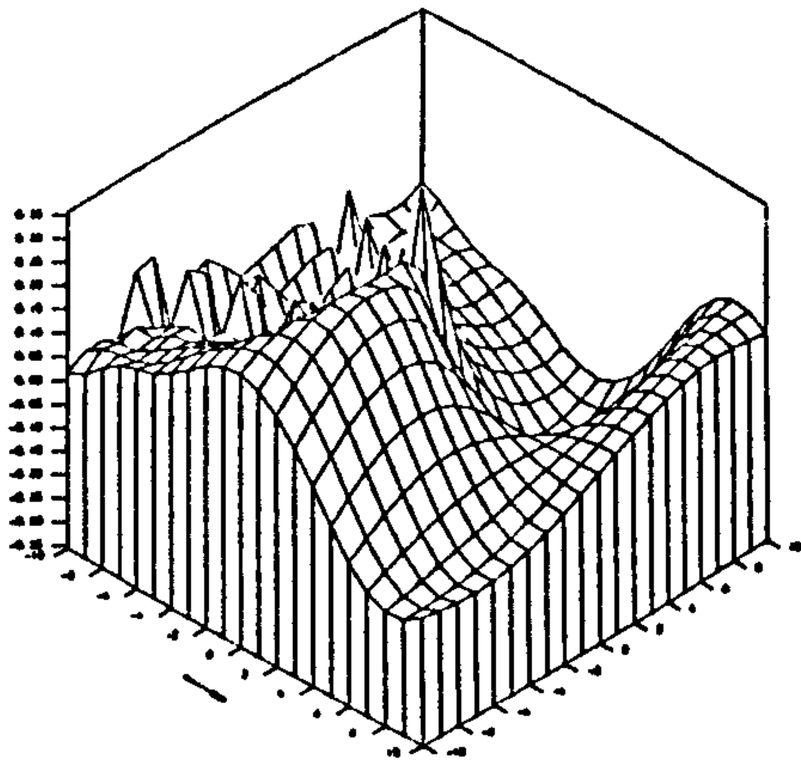

Y-derivative Imaginary Part

FREQ. NO. F=. 5 FROUDE NO. FN=. 4

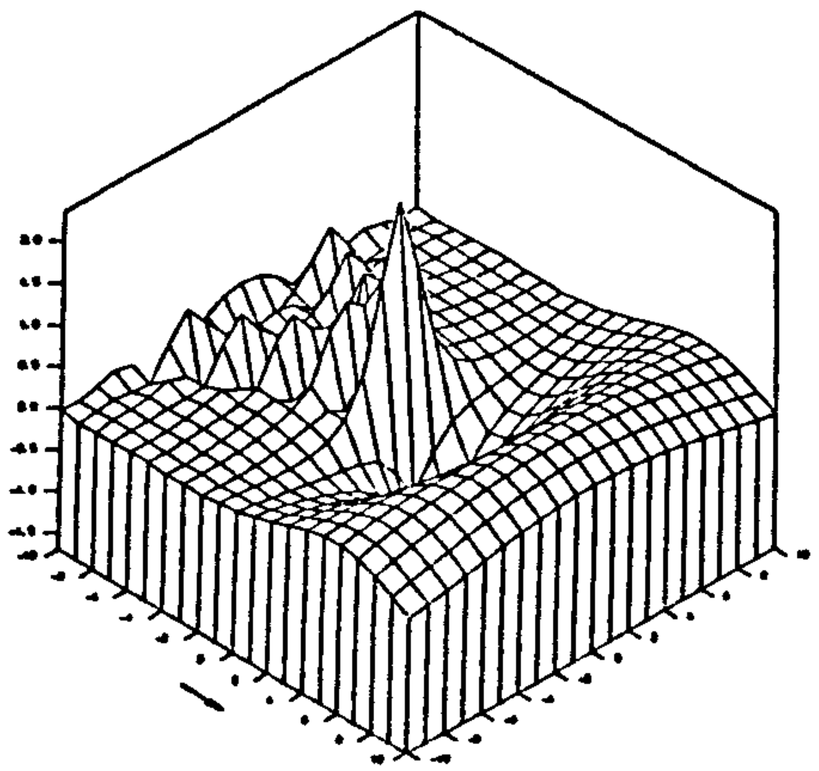

X-derivative Real Part

FREQ. NO. F=. 5 FROUDE NO. FN=. 4

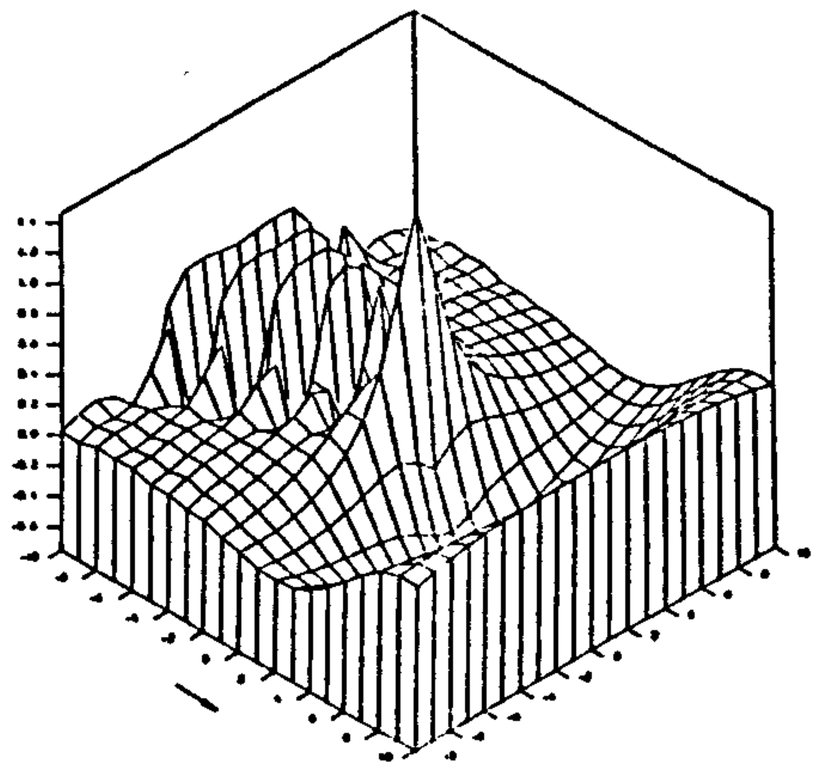

X-derivative Imaginary Part

FREQ. NO. F=. 5 FROUDE NO. FN=. 4

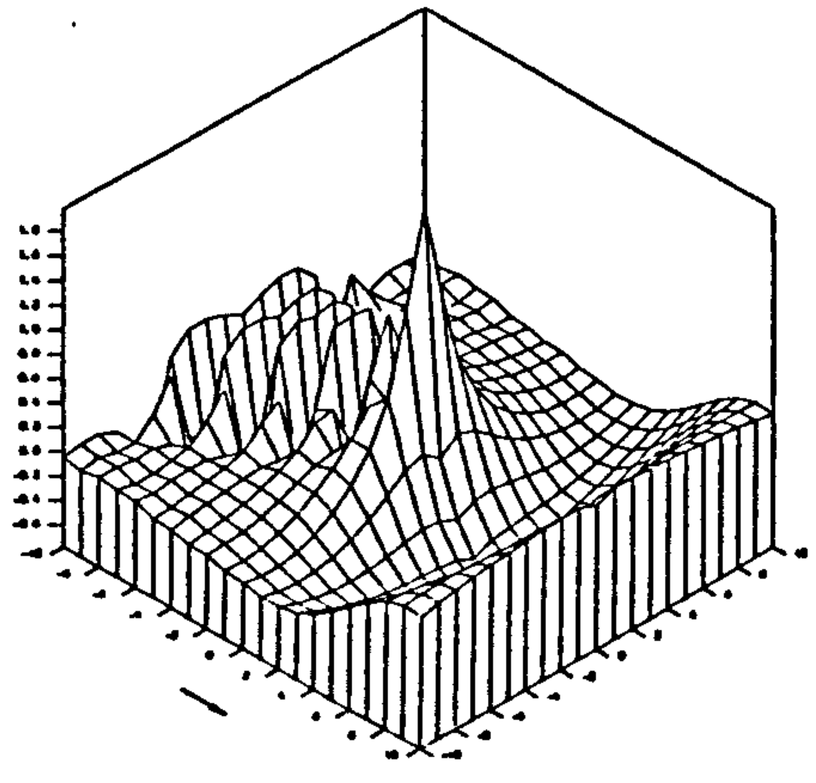

Z-derivative Real Part

FREQ. NO. F=. 5 FROUDE NO. FN=. 4

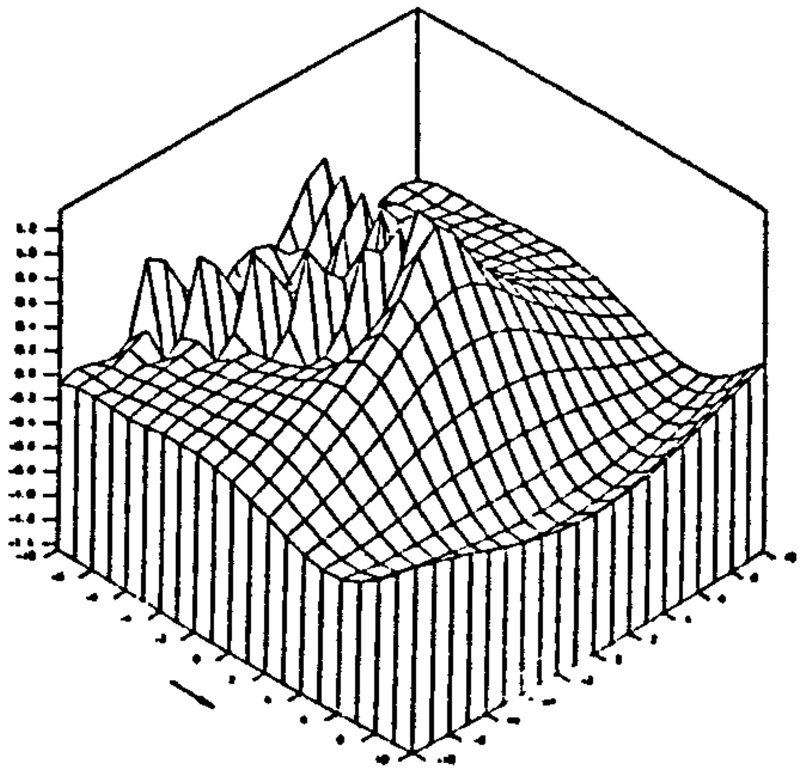

Z-derivative Imaginary Part

FREQ. NO. F=. 5 FROUDE NO. FN=. 4

Fig.4.15 Three-dimensional isometric view for a translating pulsating source potential at f=0.5 and F_n=0.4 at infinite water depth

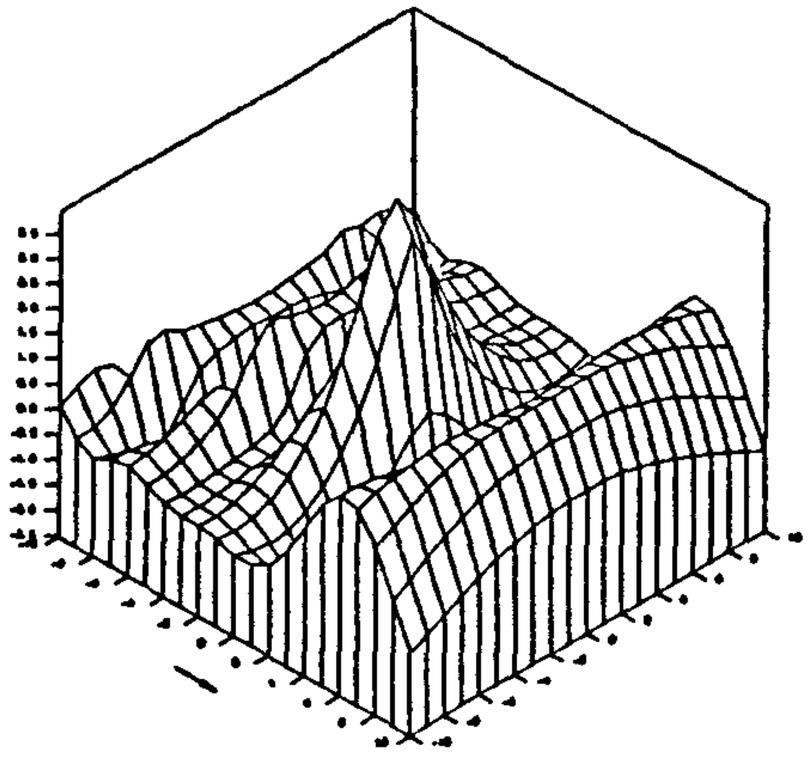

Potential Real Part

FREQ. NO. F=. 5 FROUDE NO. FN=. 48

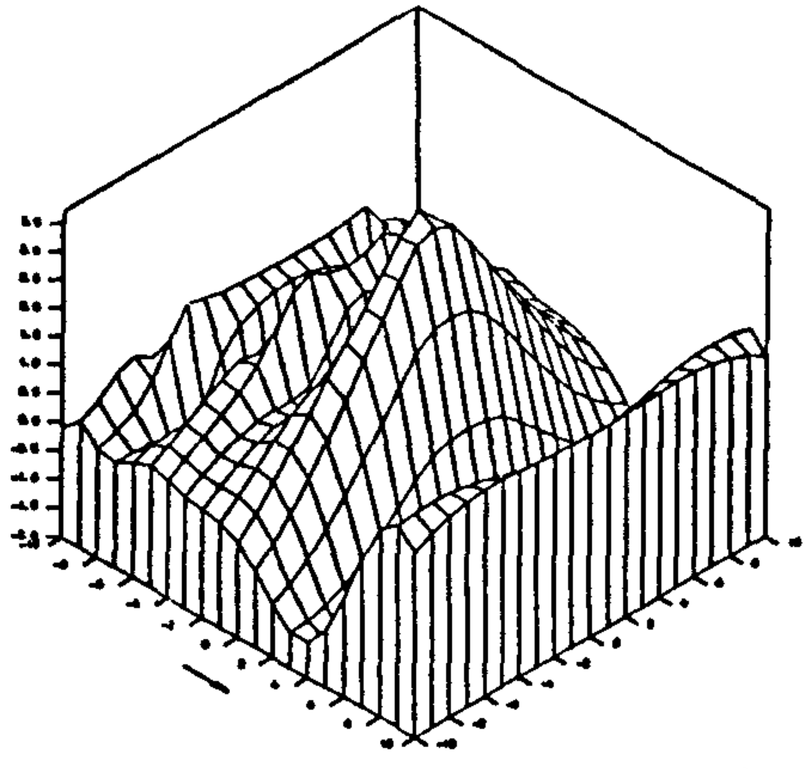

Potential Imaginary Part

FREQ. NO. F=. 5 FROUDE NO. FN=. 48

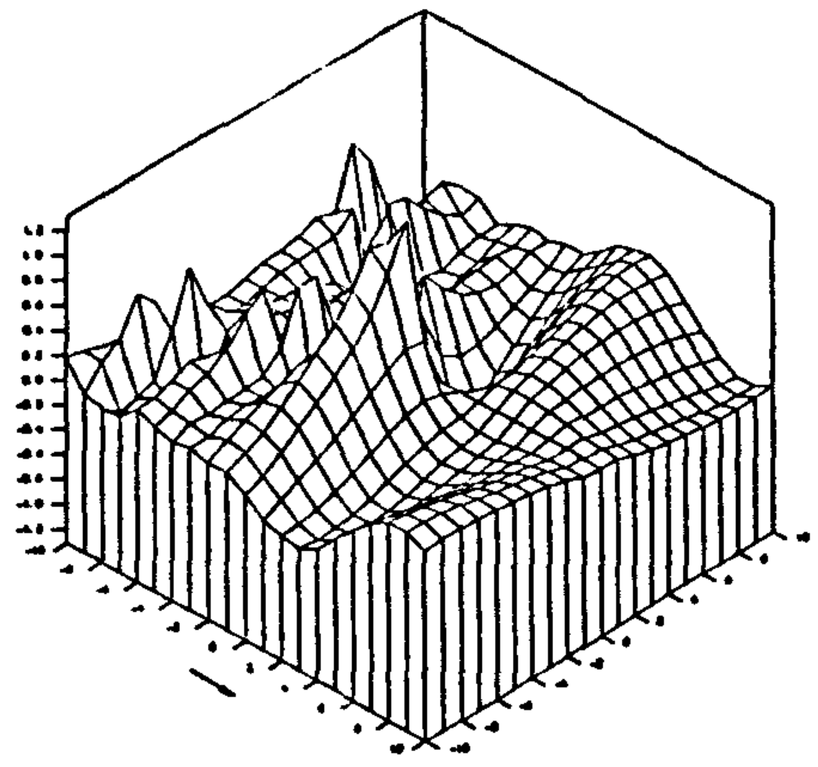

Y-derivative Real Part

FREQ. NO. F=. 5 FROUDE NO. FN=. 48

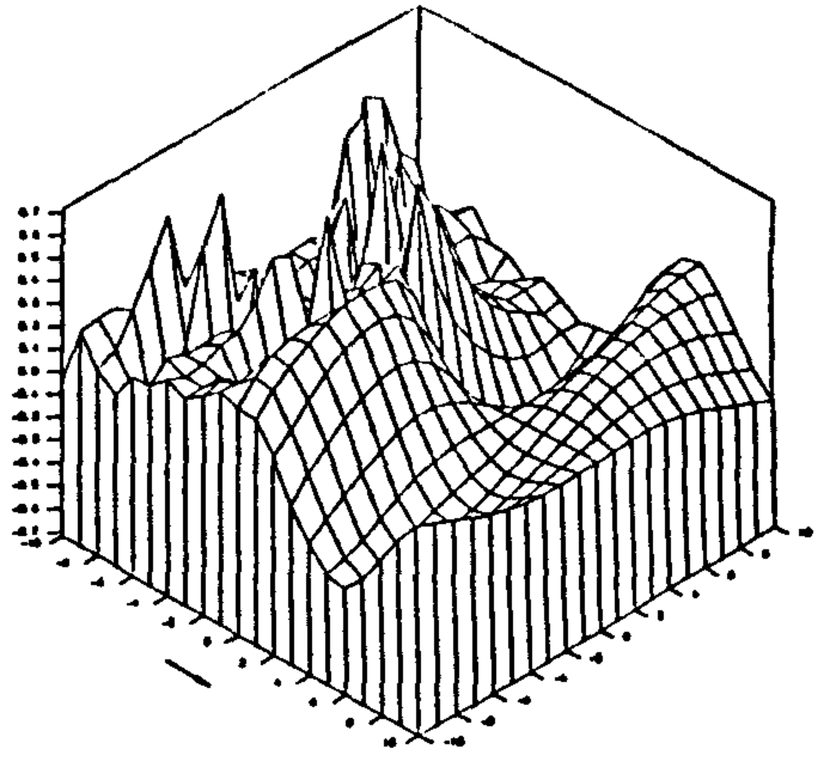

Y-derivative Imaginary Part

FREQ. NO. F=. 5 FROUDE NO. FN=. 48

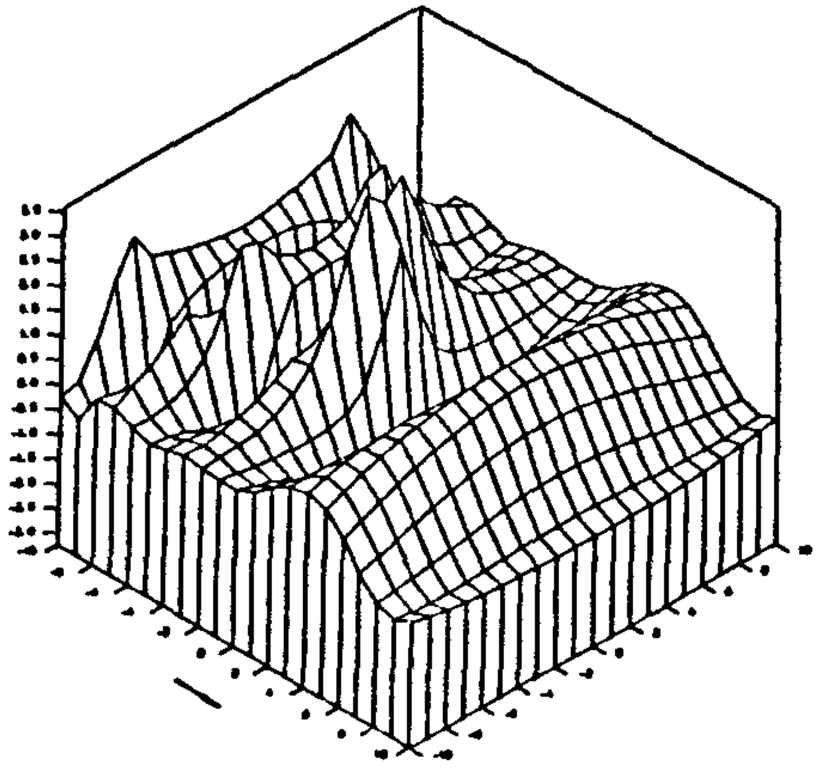

X-derivative Real Part

FREQ. NO. F=. 5 FROUDE NO. FN=. 48

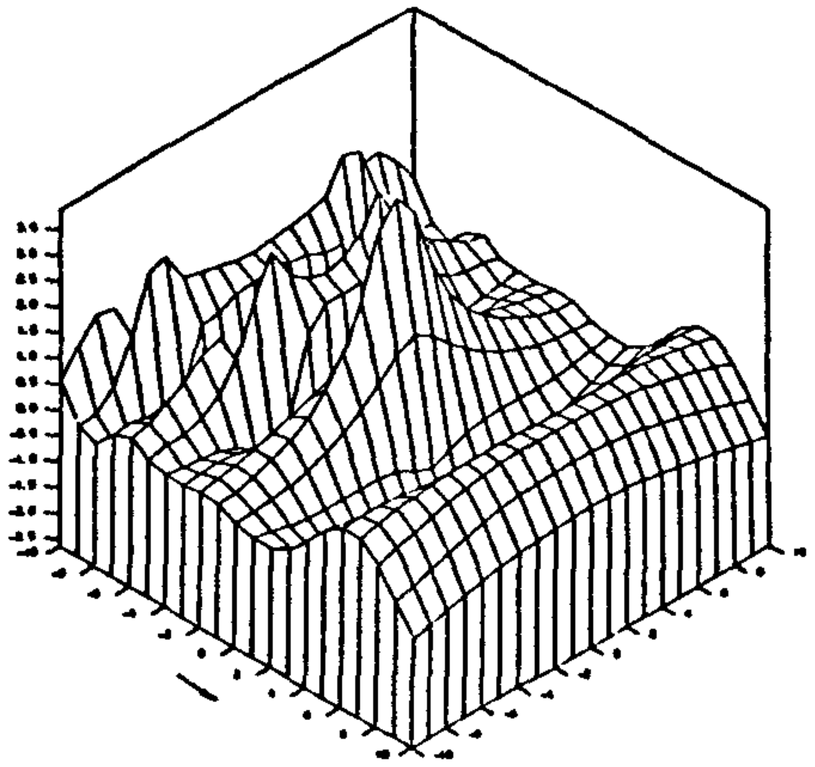

X-derivative Imaginary Part

FREQ. NO. F=. 5 FROUDE NO. FN=. 48

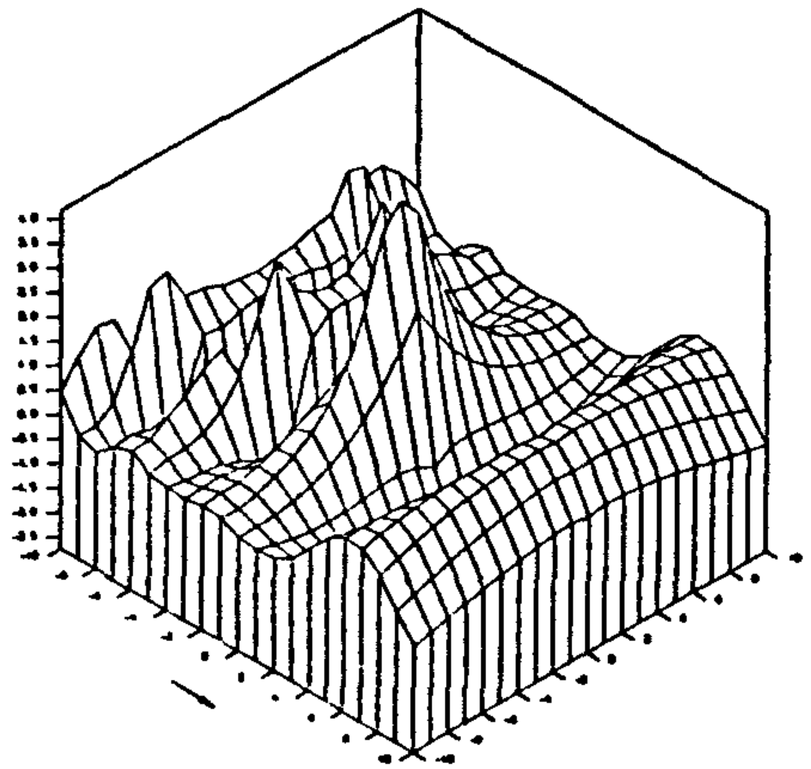

Z-derivative Real Part

FREQ. NO. F=. 5 FROUDE NO. FN=. 48

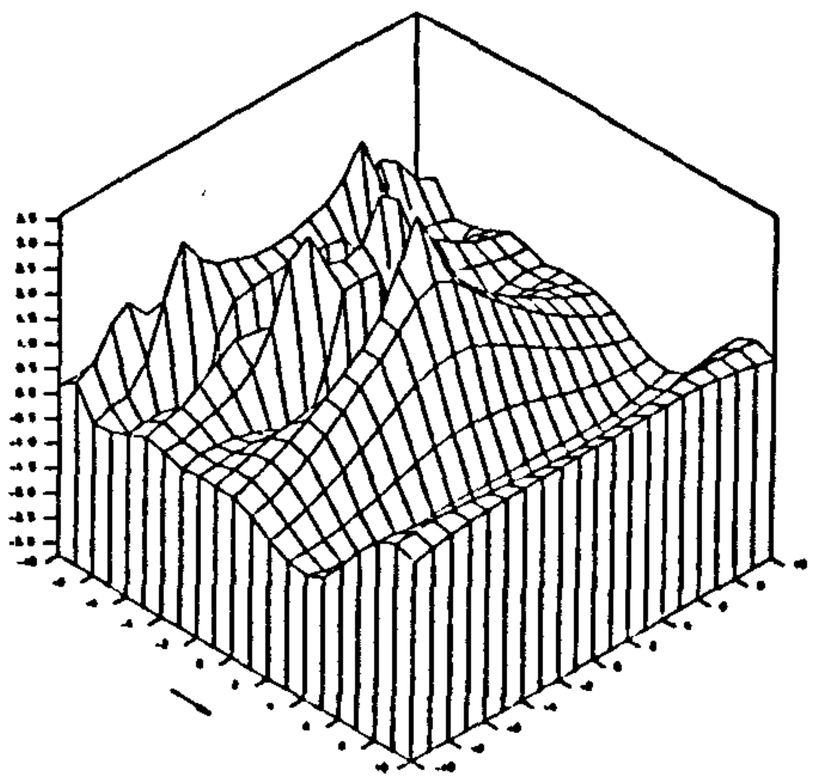

Z-derivative Imaginary Part

FREQ. NO. F=. 5 FROUDE NO. FN=. 48

Fig.4.16 Three-dimensional isometric view for a translating pulsating source potential at f=0.5 and F_n=0.48 at infinite water depth

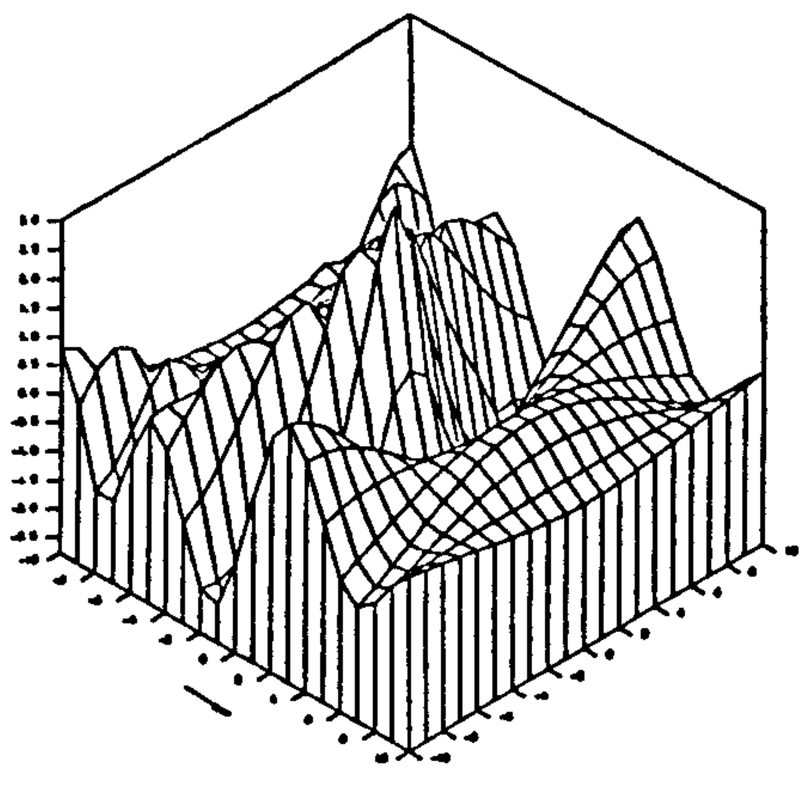

Potential Real Part

FREQ. NO. F=.5 FROUDE NO. FN=.52

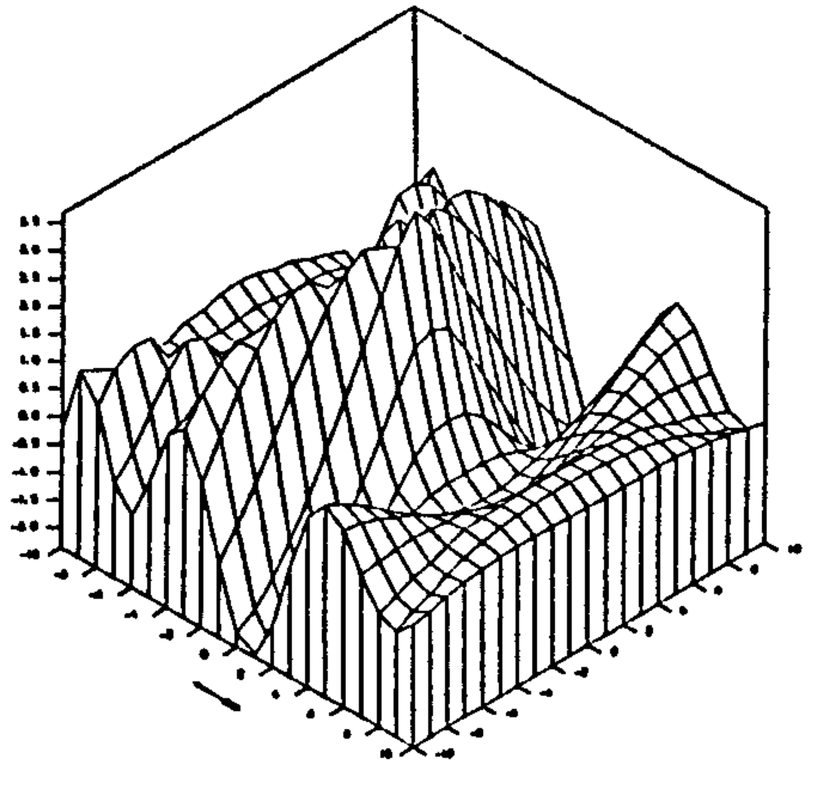

Potential Imaginary Part

FREQ. NO. F=.5 FROUDE NO. FN=.52

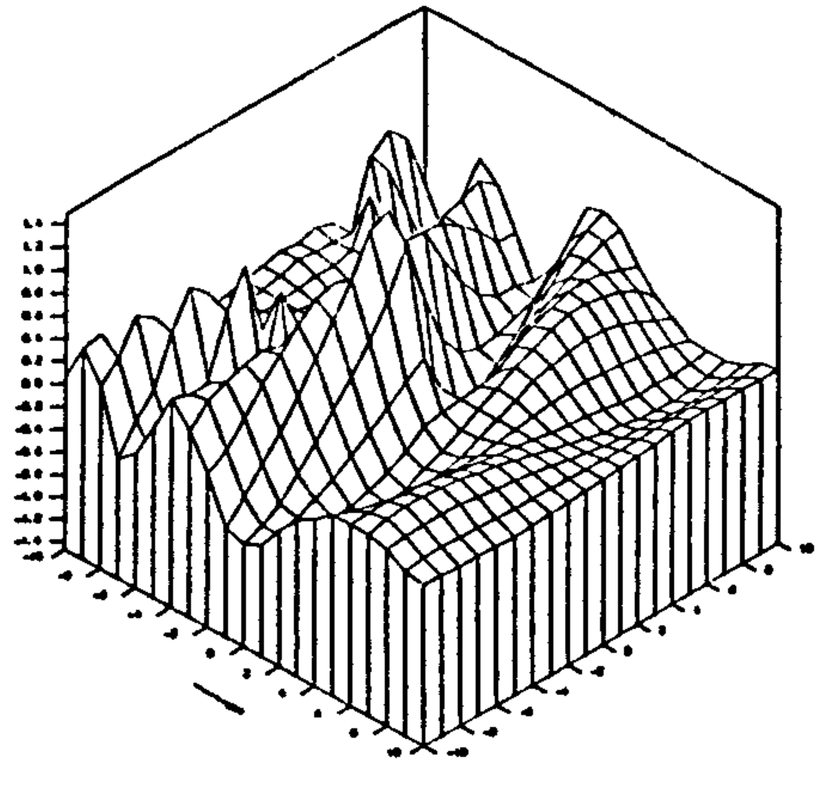

Y-derivative Real Part

FREQ. NO. F=.5 FROUDE NO. FN=.52

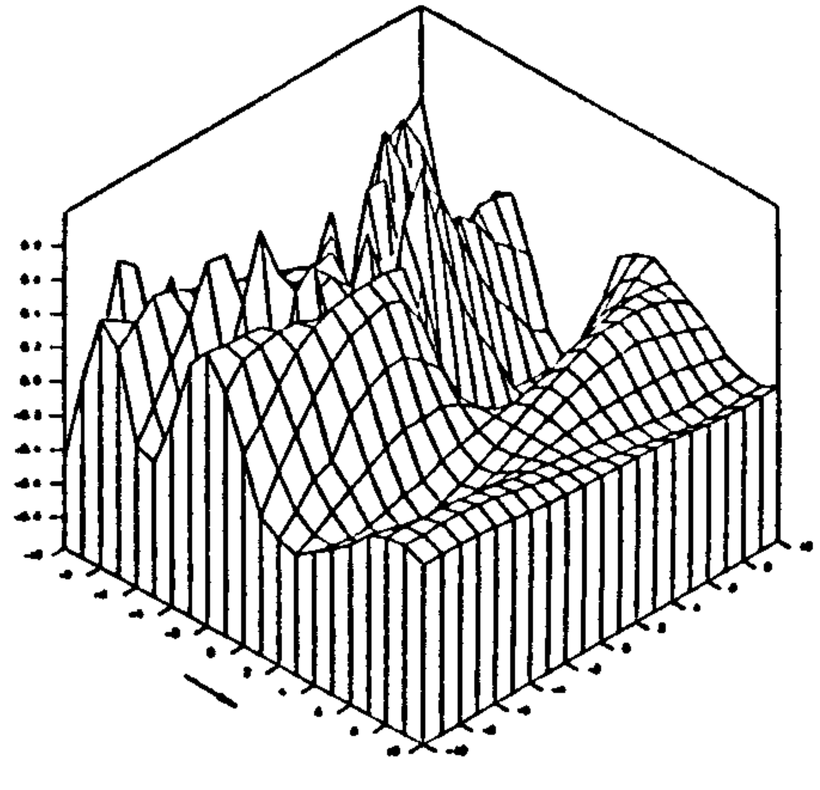

Y-derivative Imaginary Part

FREQ. NO. F=.5 FROUDE NO. FN=.52

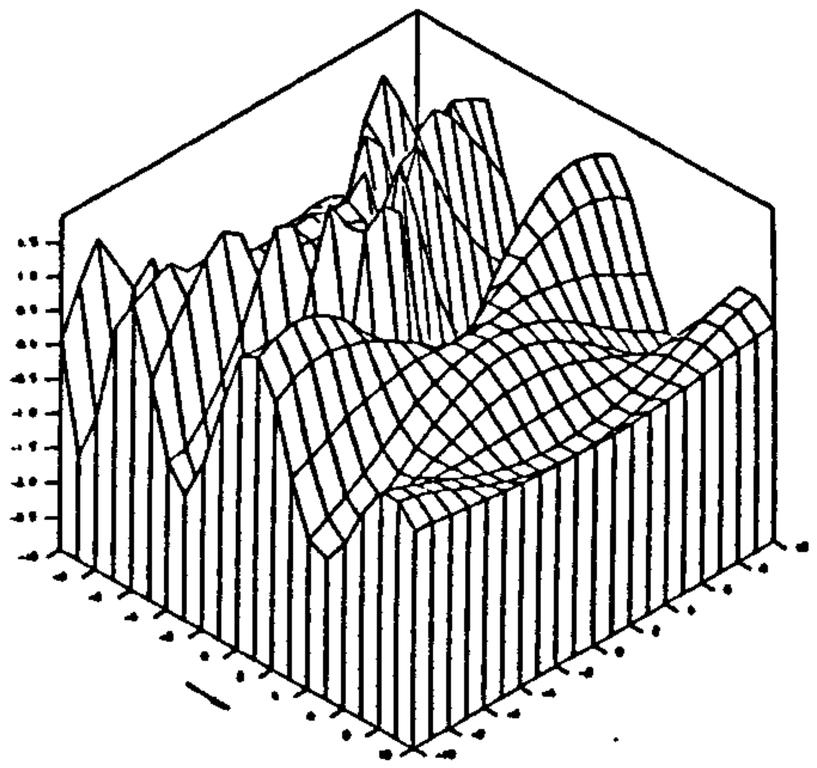

X-derivative Real Part

FREQ. NO. F=.5 FROUDE NO. FN=.52

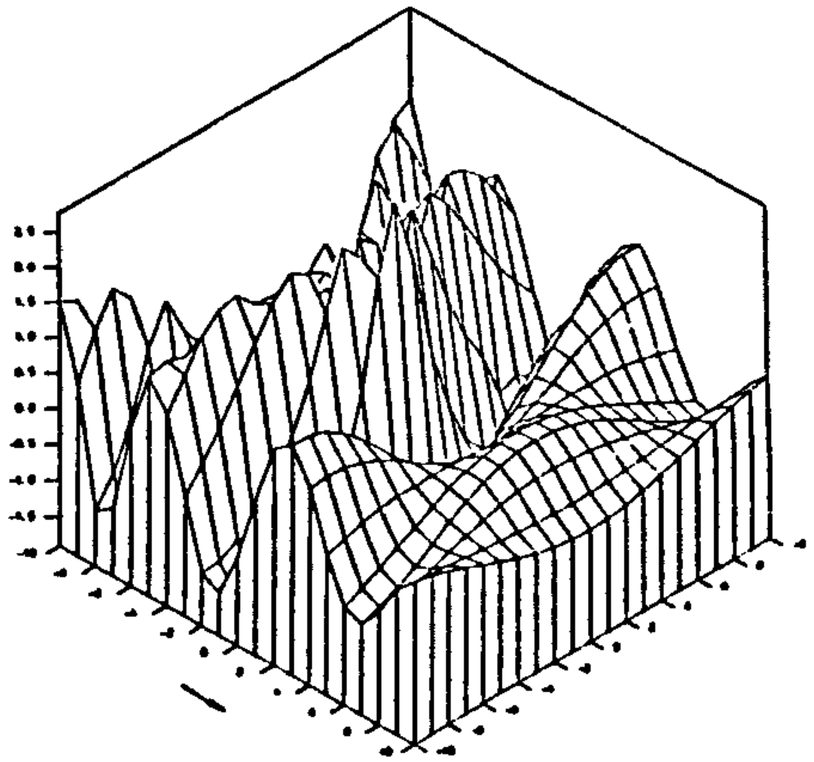

X-derivative Imaginary Part

FREQ. NO. F=.5 FROUDE NO. FN=.52

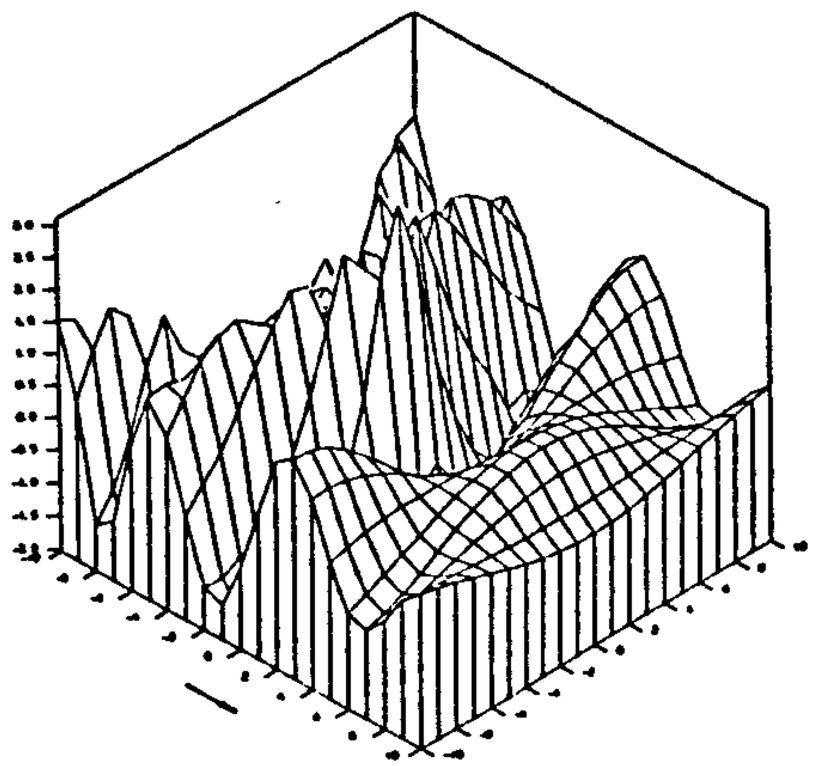

Z-derivative Real Part

FREQ. NO. F=.5 FROUDE NO. FN=.52

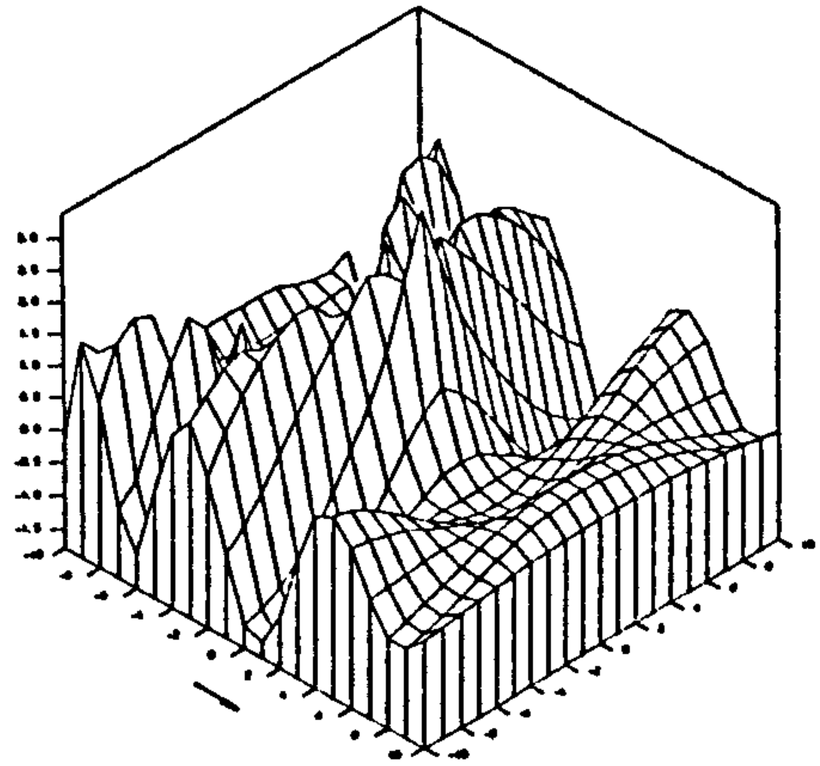

Z-derivative Imaginary Part

FREQ. NO. F=.5 FROUDE NO. FN=.52

Fig.4.17 Three-dimensional isometric view for a translating pulsating source potential at f=0.5 and F_n=0.52 at infinite water depth

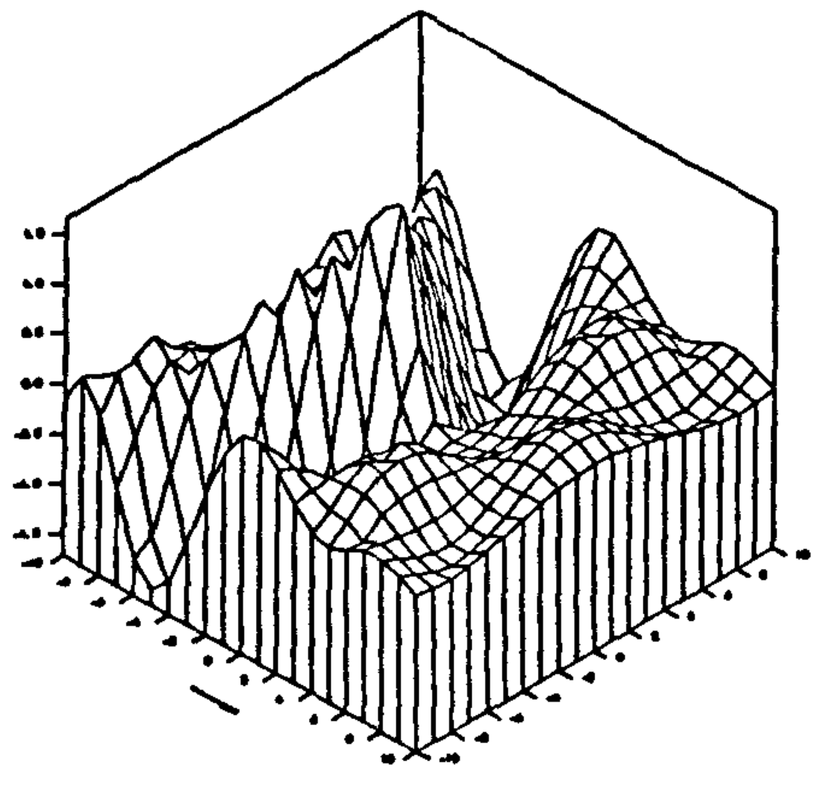

Potential Real Part

FREQ. NO. F=.5 FROUDE NO. FN=.6

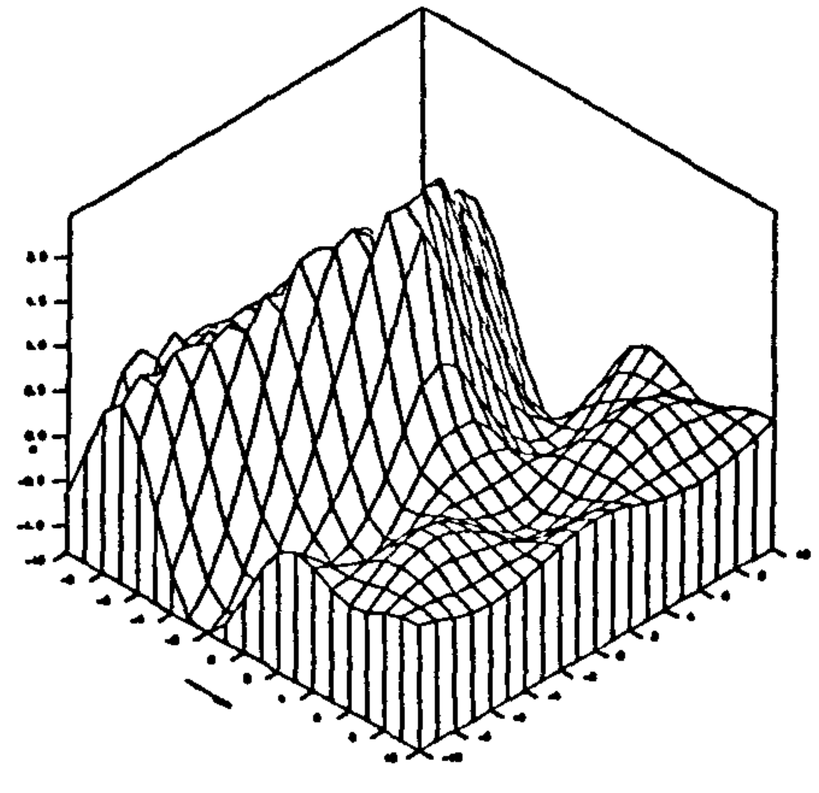

Potential Imaginary Part

FREQ. NO. F=.5 FROUDE NO. FN=.6

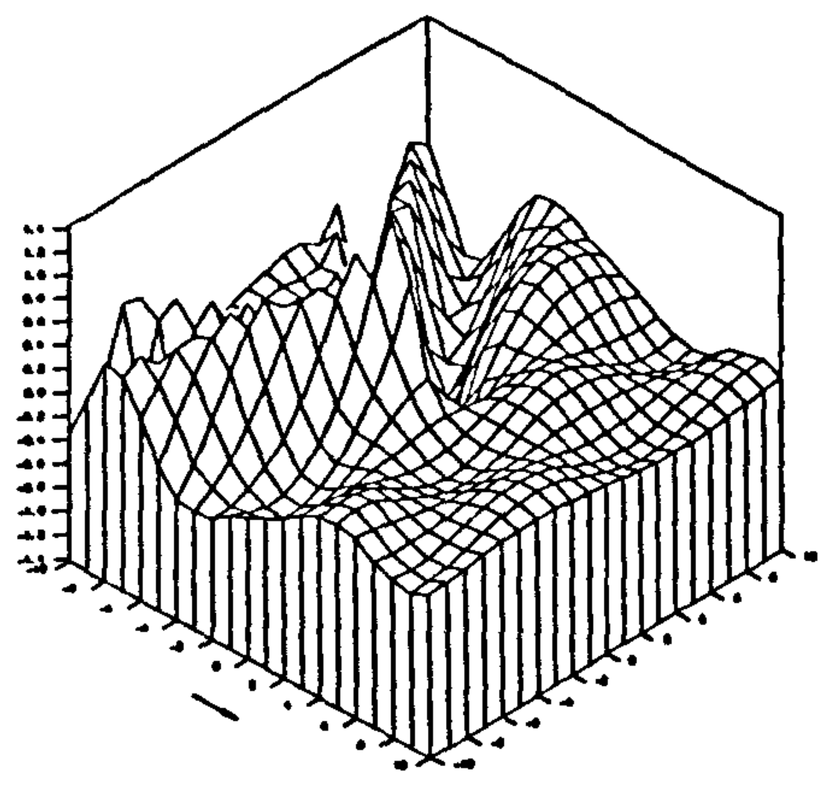

Y-derivative Real Part

FREQ. NO. F=.5 FROUDE NO. FN=.6

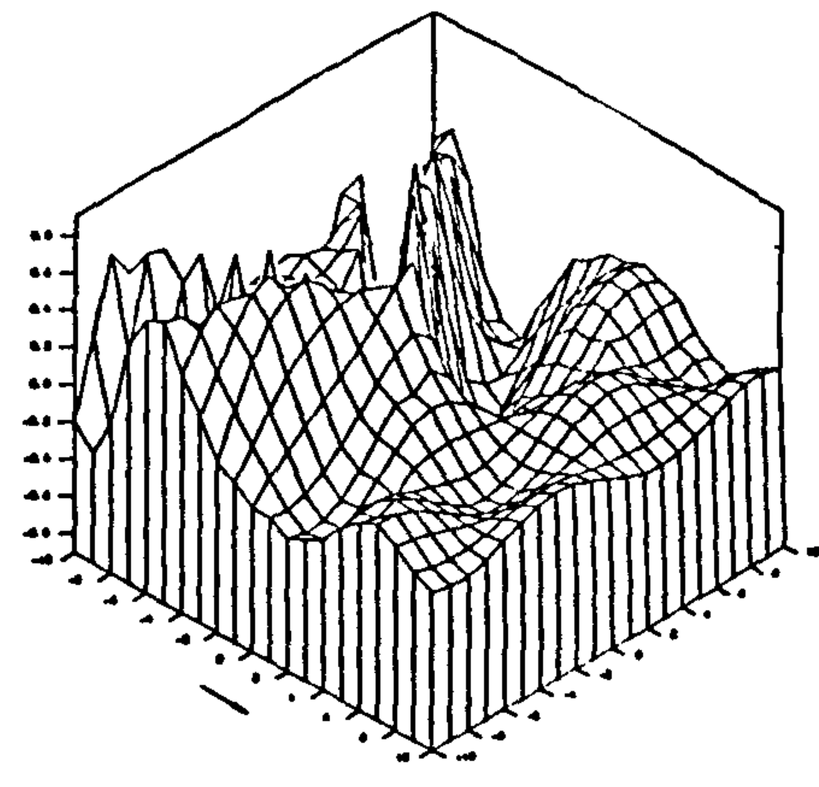

Y-derivative Imaginary Part

FREQ. NO. F=.5 FROUDE NO. FN=.6

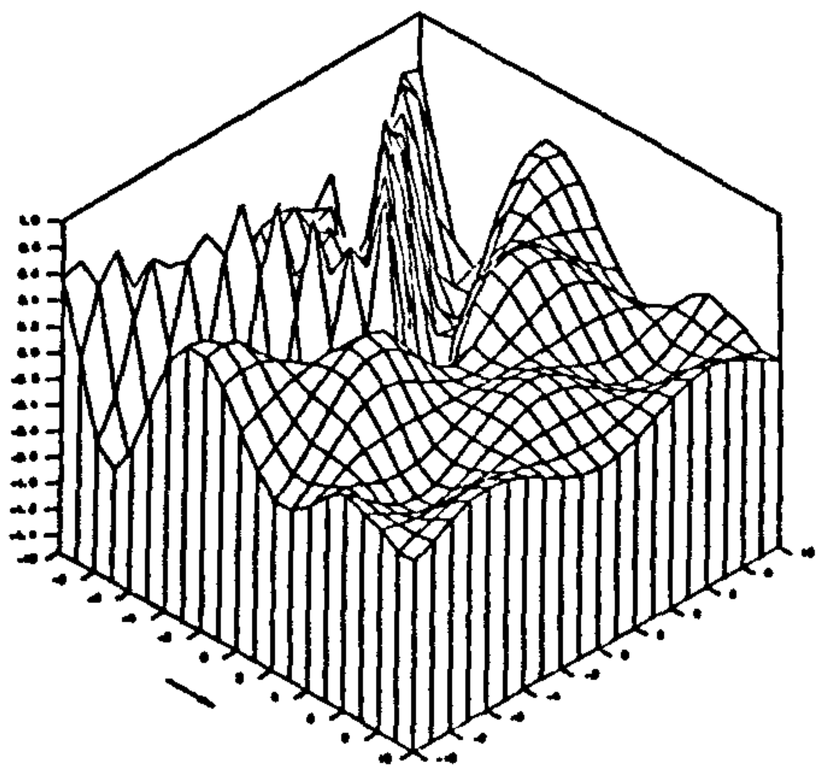

X-derivative Real Part

FREQ. NO. F=.5 FROUDE NO. FN=.6

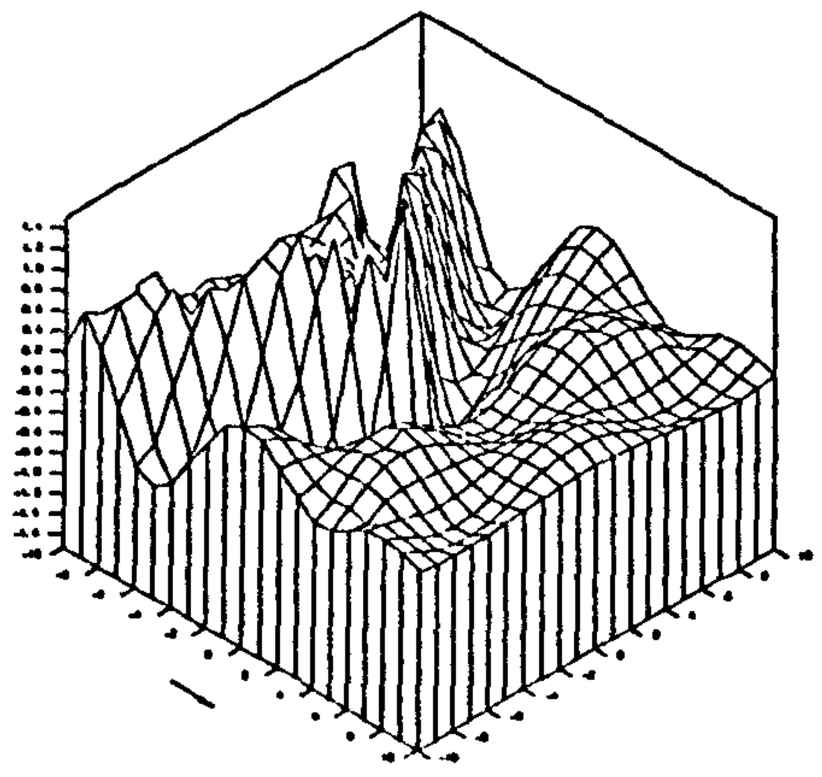

X-derivative Imaginary Part

FREQ. NO. F=.5 FROUDE NO. FN=.6

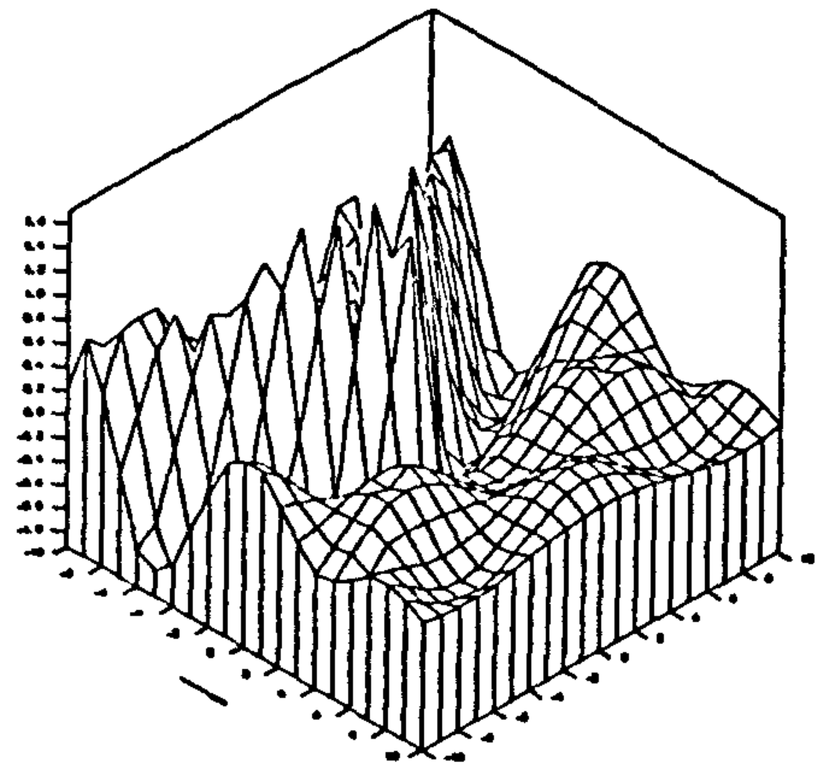

Z-derivative Real Part

FREQ. NO. F=.5 FROUDE NO. FN=.6

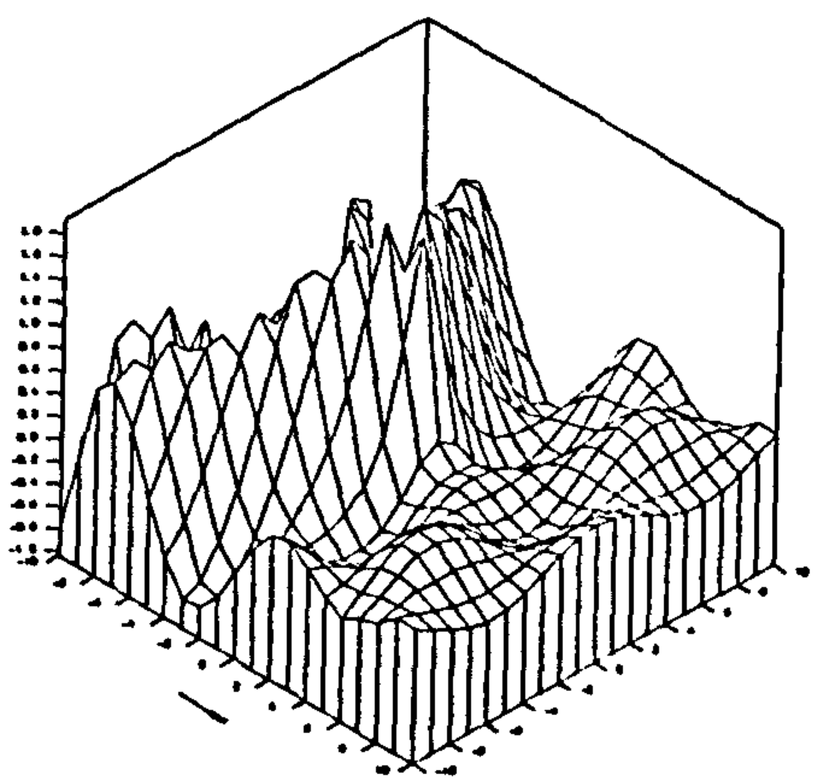

Z-derivative Imaginary Part

FREQ. NO. F=.5 FROUDE NO. FN=.6

Fig.4.18 Three-dimensional isometric view for a translating pulsating source potential at f=0.5 and F_n=0.6 at infinite water depth

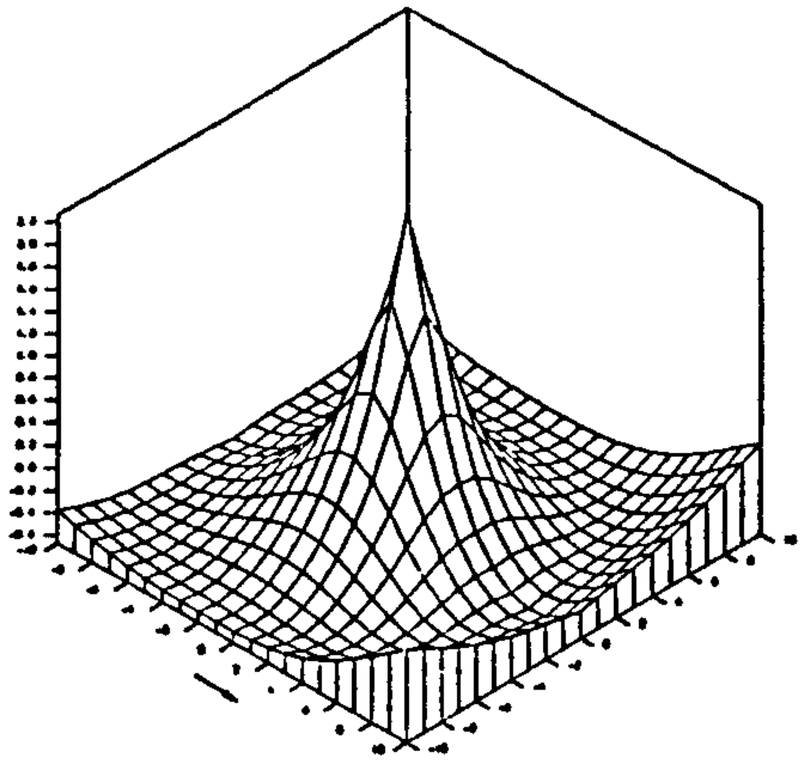

Potential Real Part

FREQ. NO. F=. 5 FROUDE NO. FN=. 2

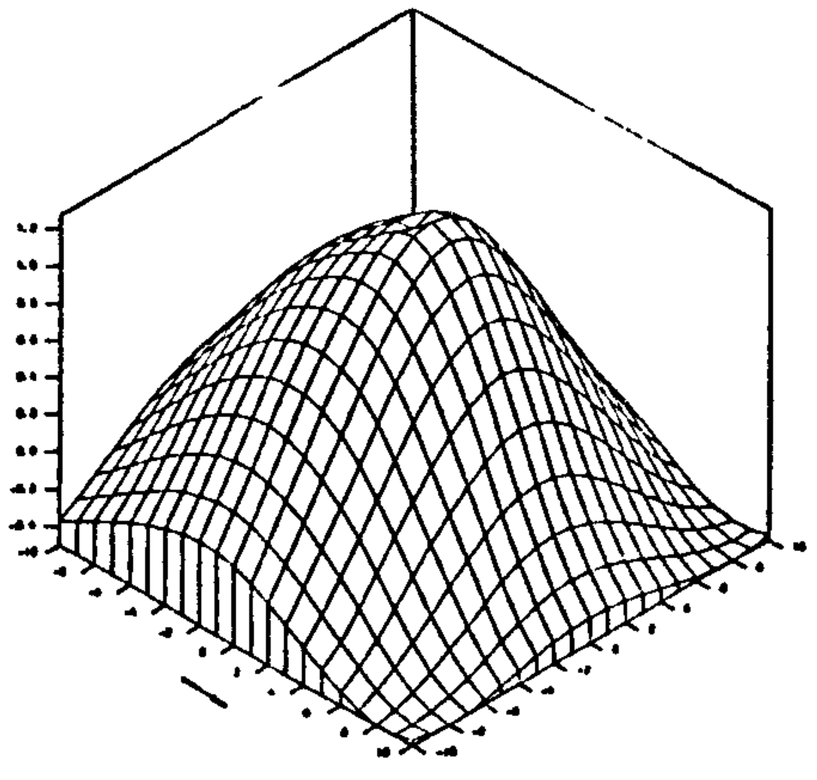

Potential Imaginary Part

FREQ. NO. F=. 5 FROUDE NO. FN=. 2

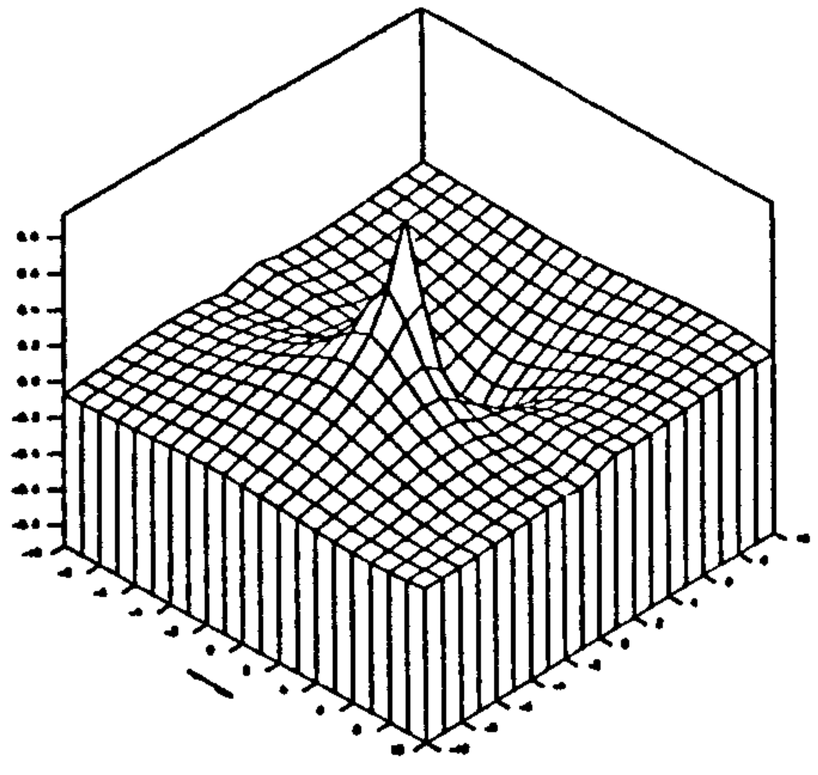

Y-derivative Real Part

FREQ. NO. F=. 5 FROUDE NO. FN=. 2

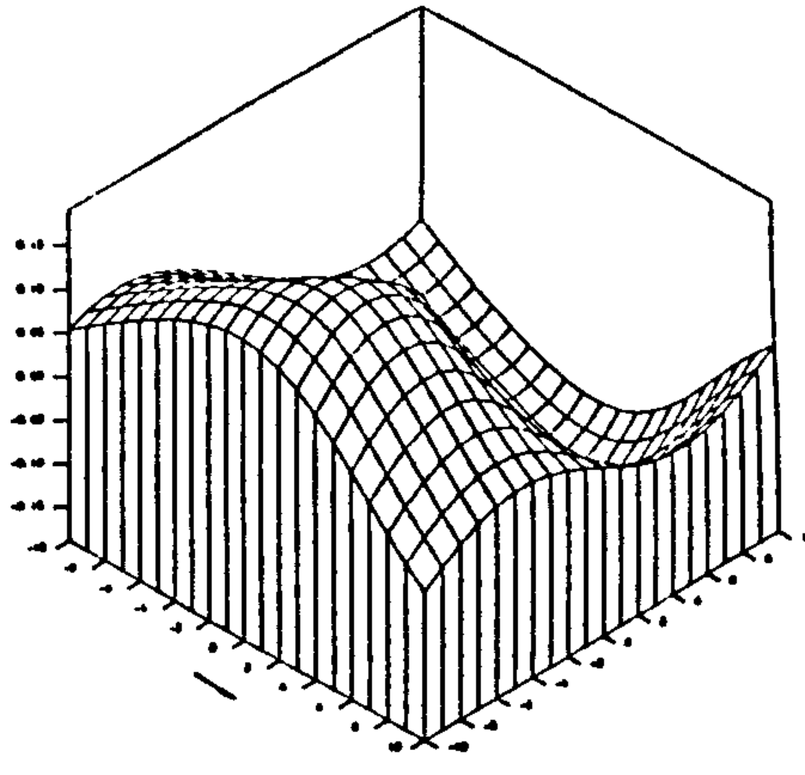

Y-derivative Imaginary Part

FREQ. NO. F=. 5 FROUDE NO. FN=. 2

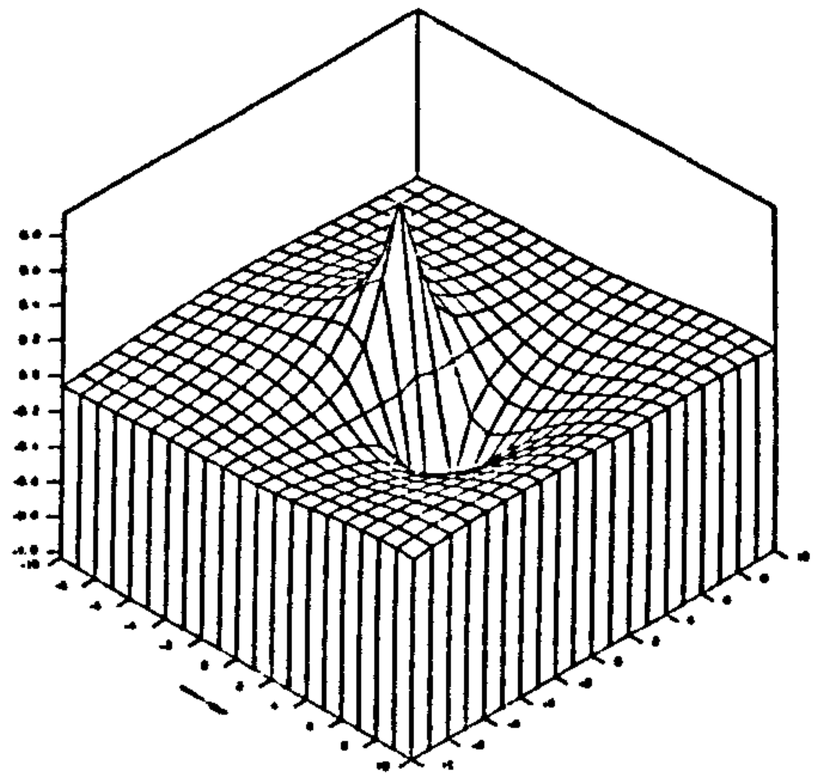

X-derivative Real Part

FREQ. NO. F=. 5 FROUDE NO. FN=. 2

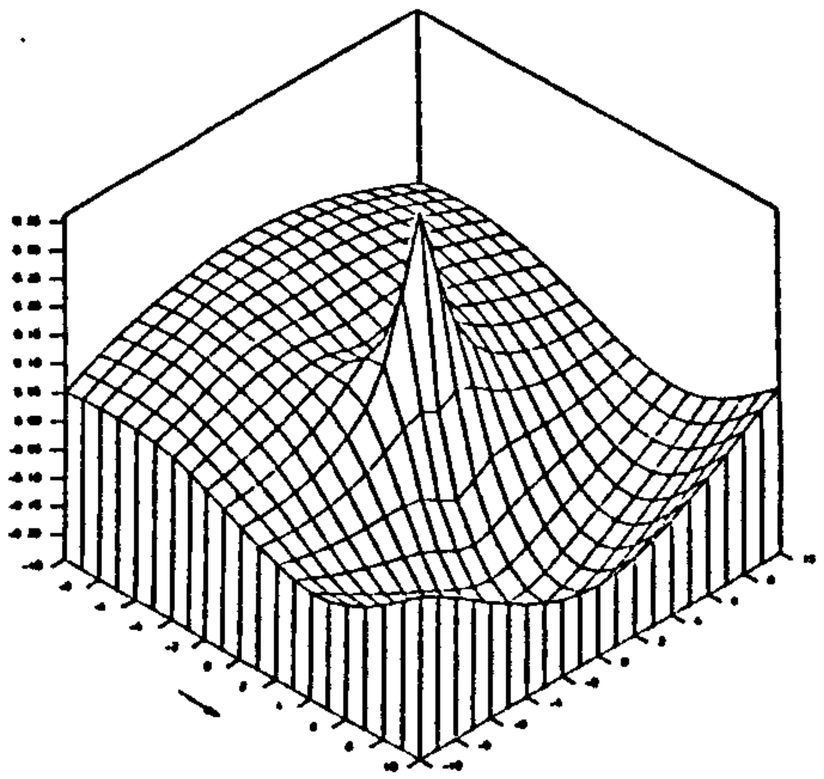

X-derivative Imaginary Part

FREQ. NO. F=. 5 FROUDE NO. FN=. 2

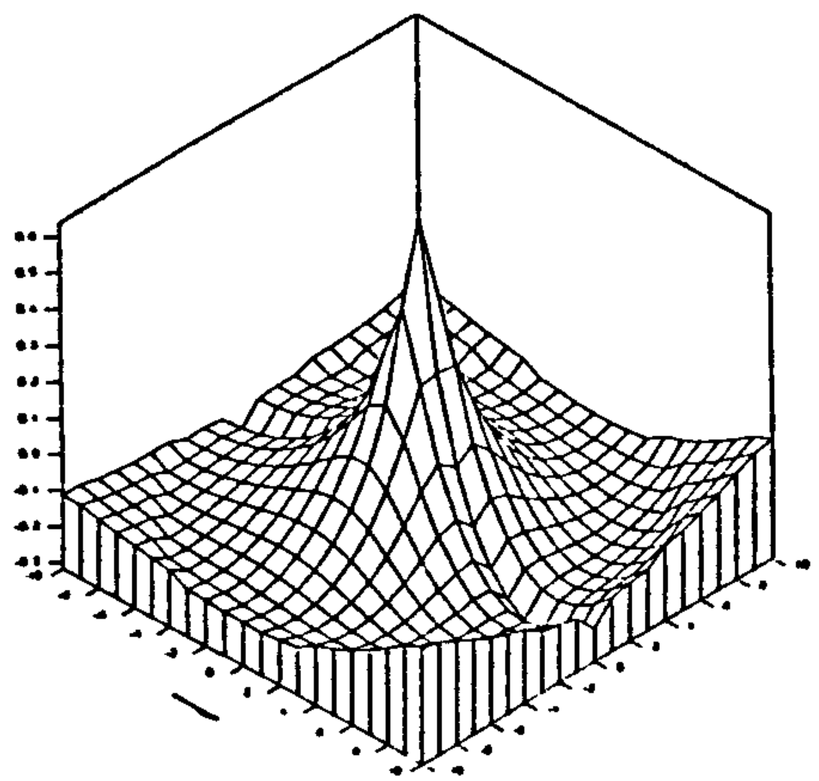

Z-derivative Real Part

FREQ. NO. F=. 5 FROUDE NO. FN=. 2

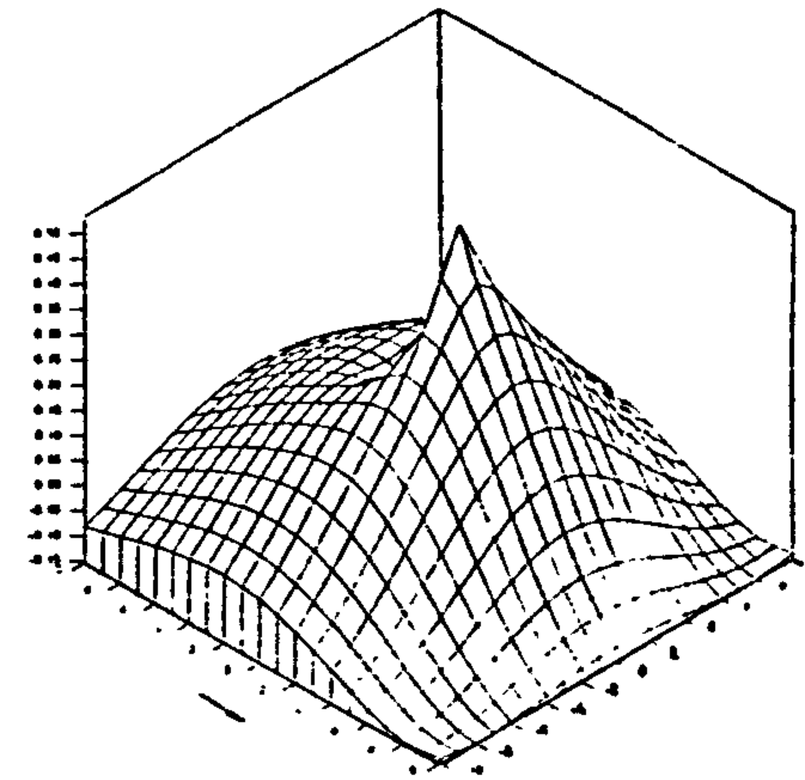

Z-derivative Imaginary Part

FREQ. NO. F=. 5 FROUDE NO. FN=. 2

Fig. 4.19 Three dimensional isometric view for a translating pulsating source potential at f=0.5 and F_n=0.2 and $U/\sqrt{gh}$=0.0365

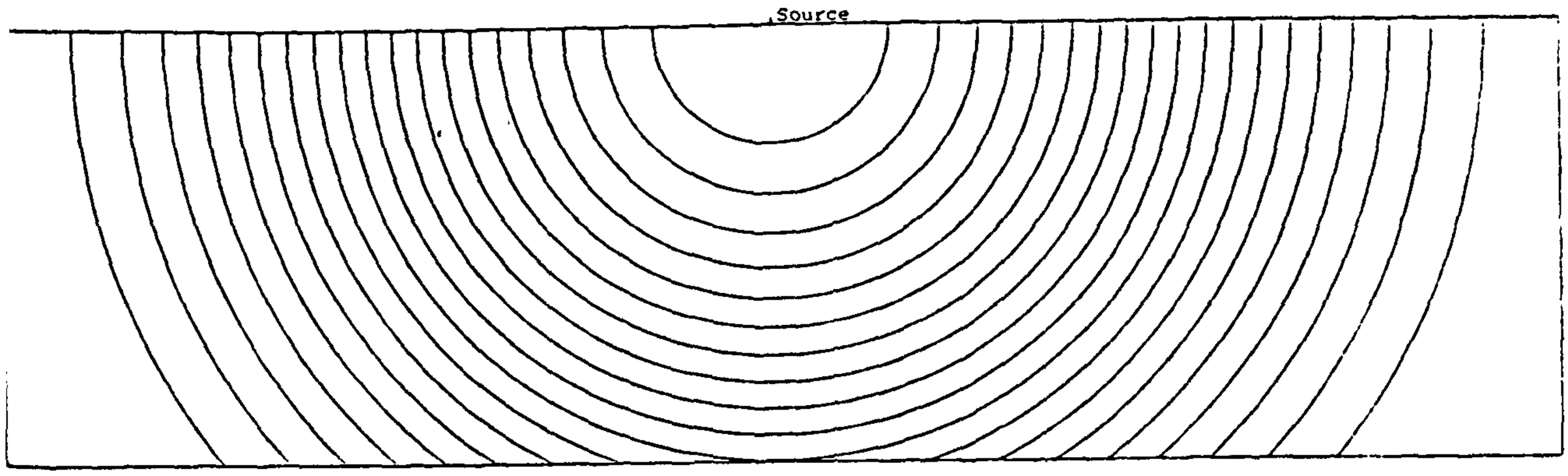

FREQ. NO. F=. 2 FROUDE NO. FN=0.

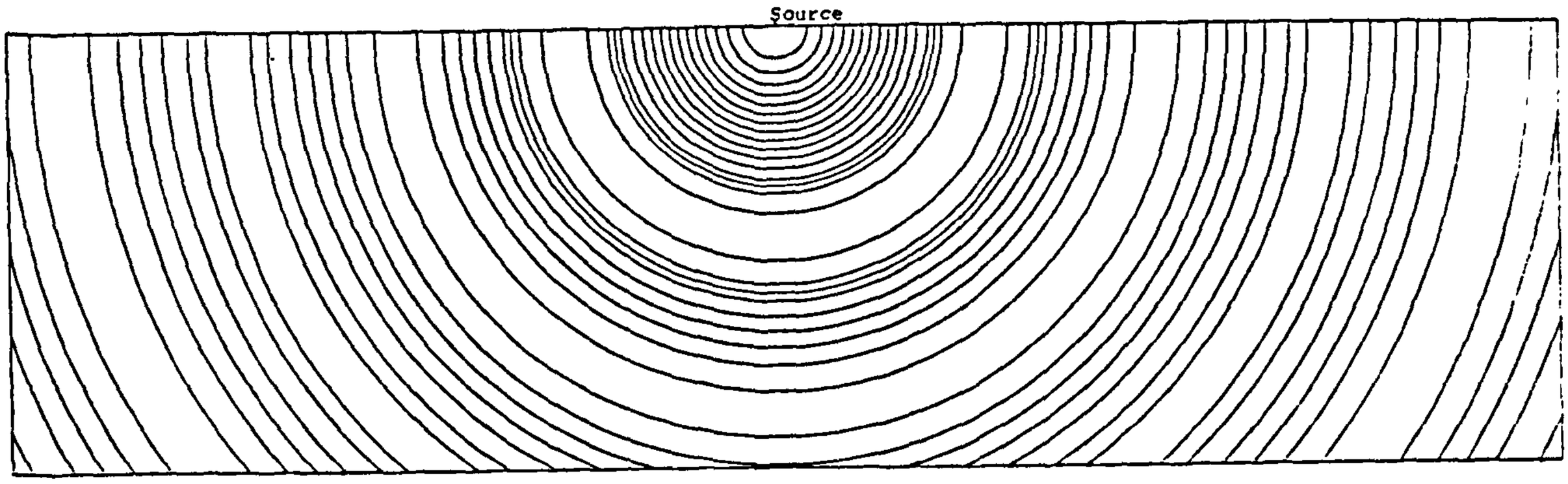

FREQ. NO. F=. 4 FROUDE NO. FN=0.

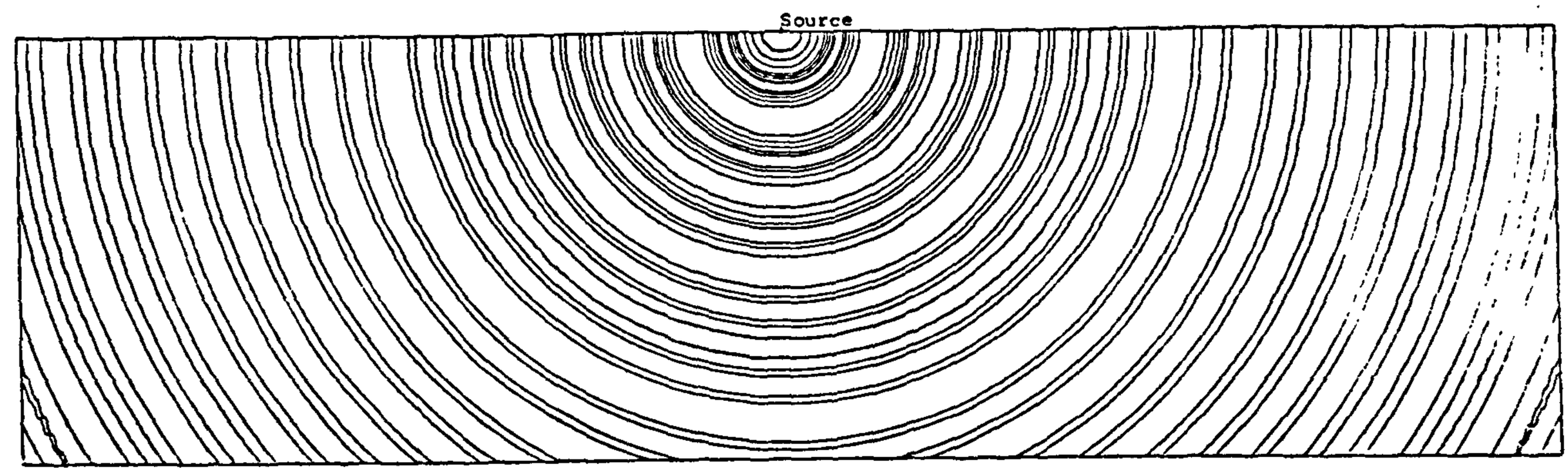

FREQ. NO. F=. 6 FROUDE NO. FN=0.

Fig. 4.20 WAVE CONTOURS DUE TO AN OSCILLATING SOURCE SUBMERGED BELOW THE FREE SURFACE OF INFINITE WATER DEPTH

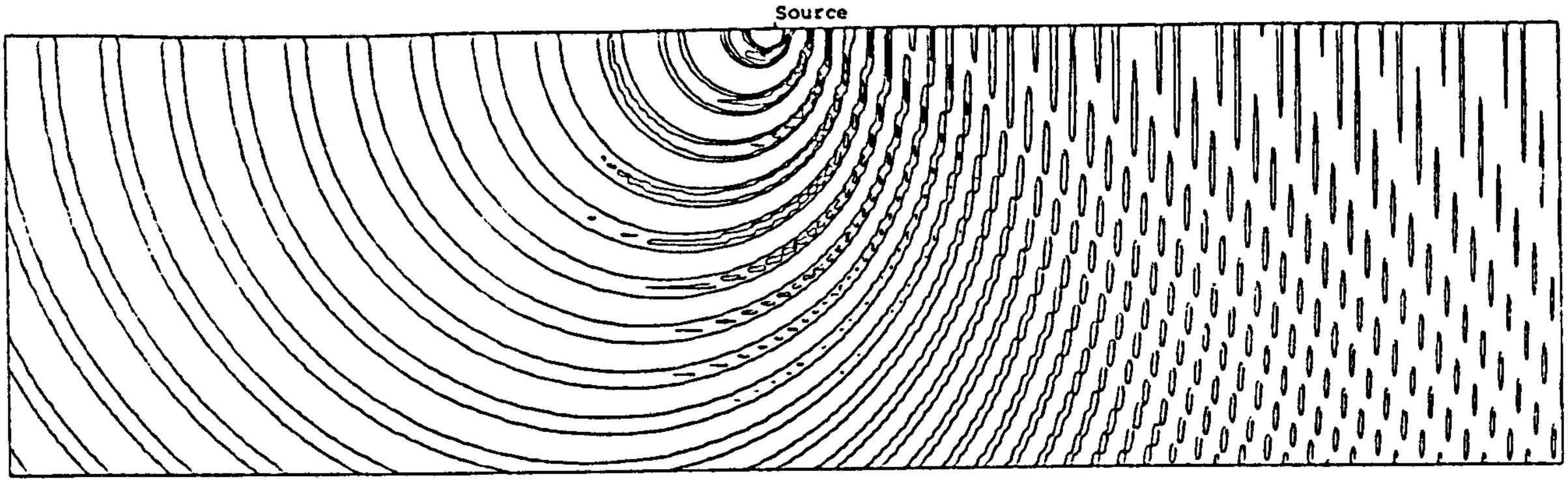

FREQ. NO. F=1. 1 FROUDE NO. FN=. 2

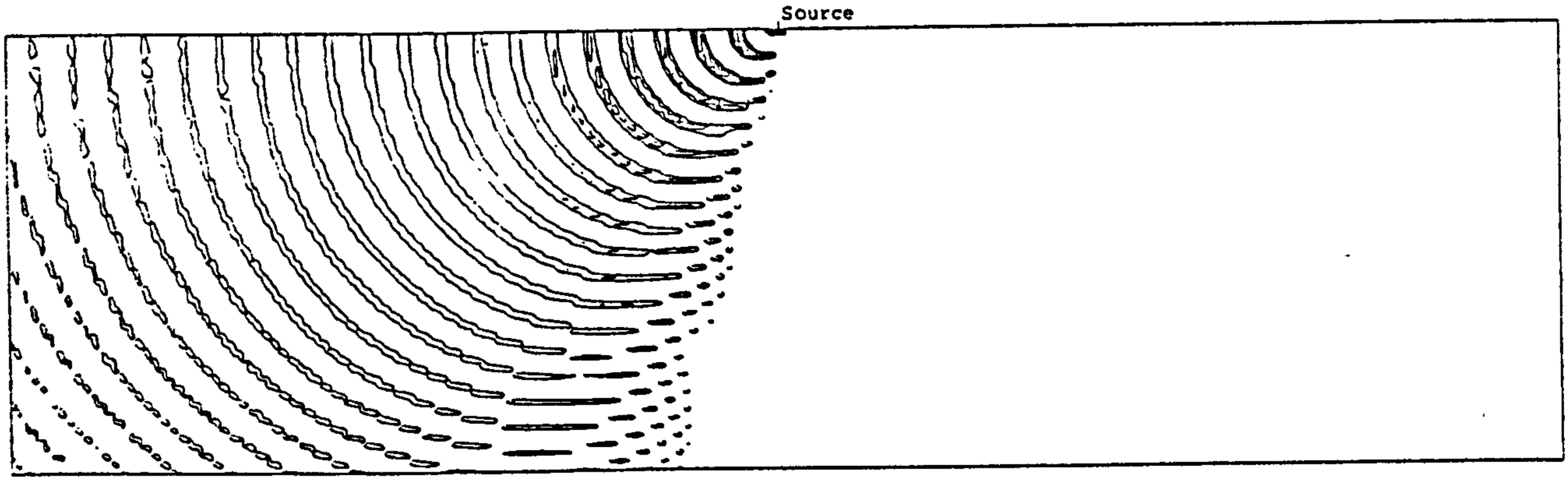

FREQ. NO. F=1. 5 FROUDE NO. FN=. 2

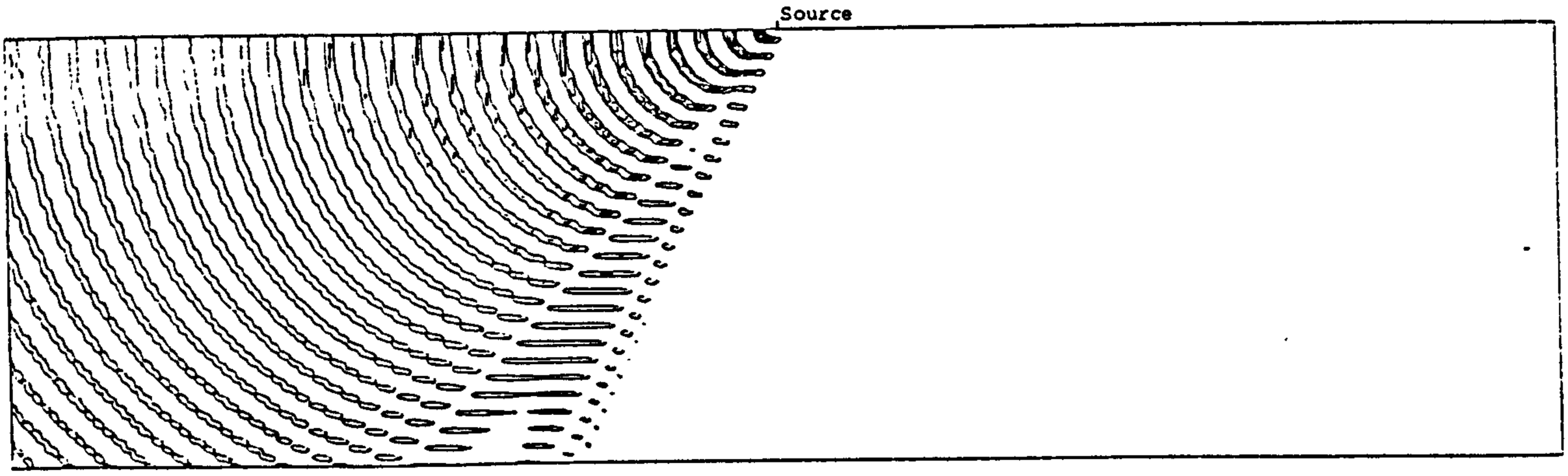

FREQ. NO. F=1. 75 FROUDE NO. FN=. 2

Fig.4.21 WAVE CONTOURS DUE TO A TRANSLATING PULSATING SOURCE SUBMERGED BELOW THE FREE SURFACE OF INFINITE WATER DEPTH AT LOW FROUDE NUMBER F_n=0.2 WITH VARIOUS FREQUENCIES

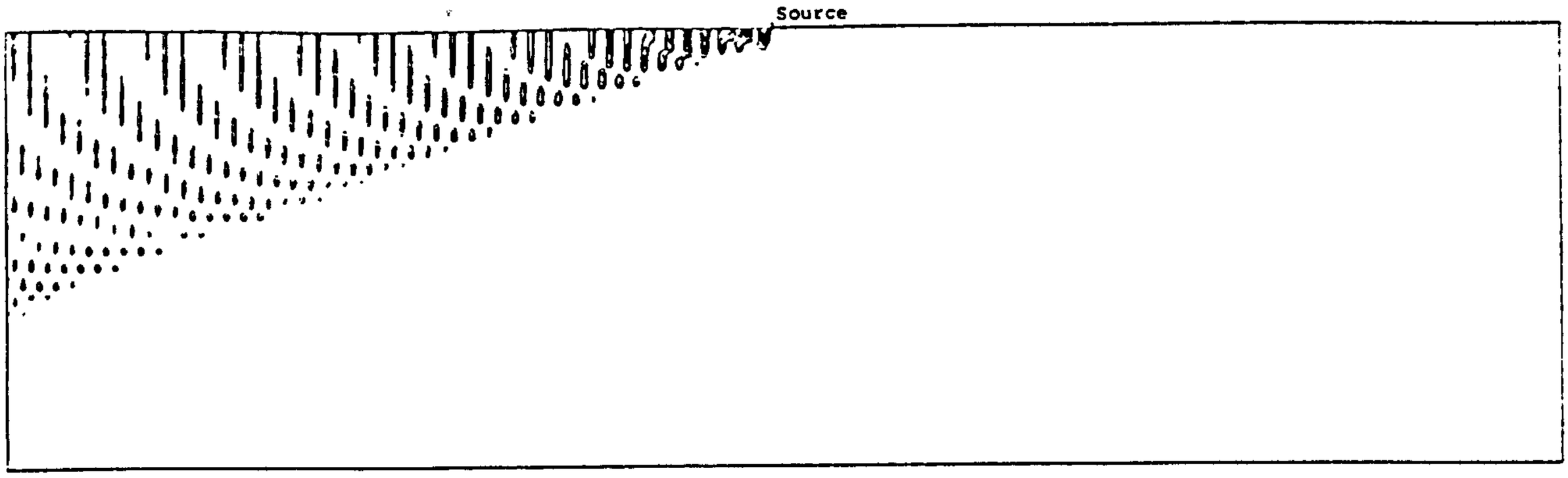

FREQ. NO. F=0. FROUDE NO. FN=. 6

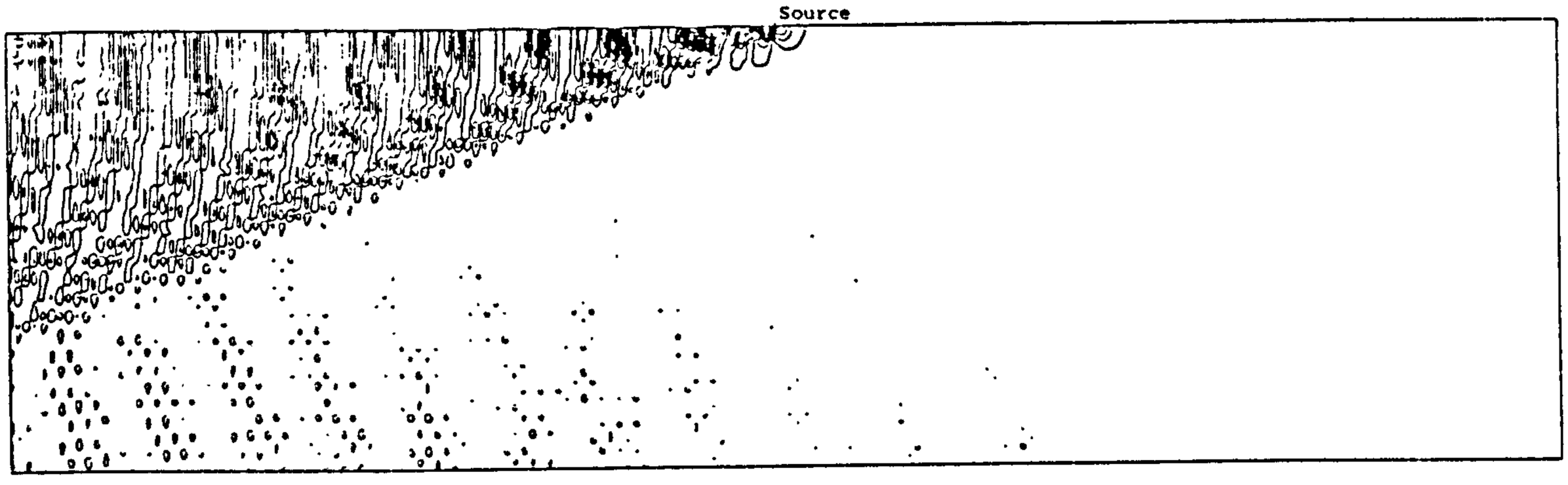

FREQ. NO. F=. 1 FROUDE NO. FN=. 6

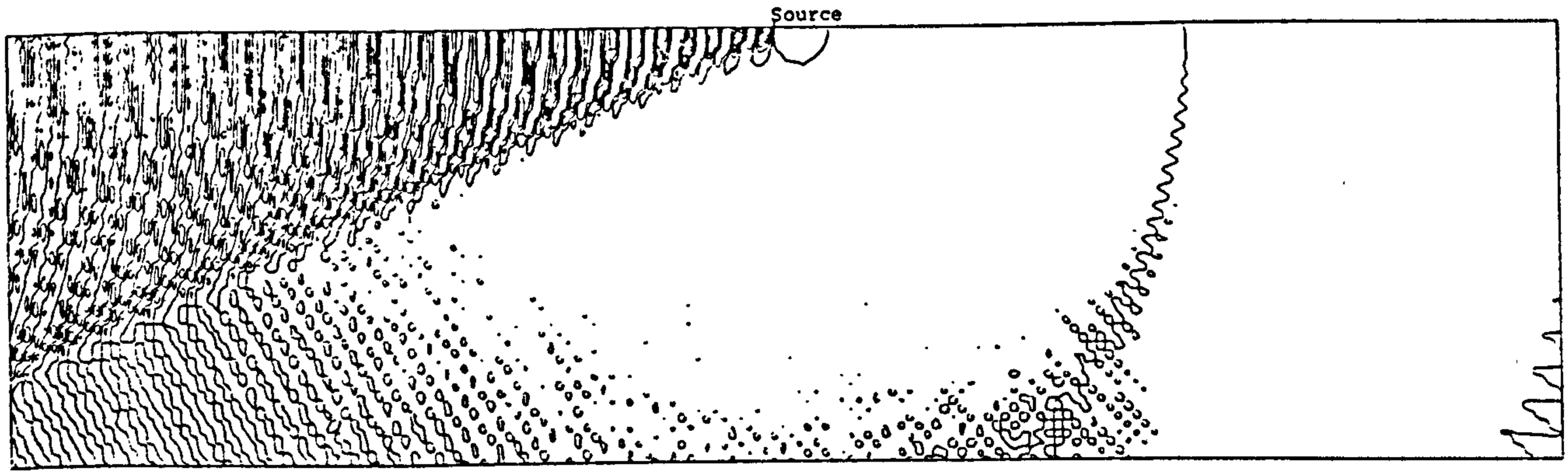

FREQ. NO. F=. 2 FROUDE NO. FN=. 6

Fig.4.22a WAVE CONTOURS DUE TO A TRANSLATING PULSATING SOURCE SUBMERGED BELOW THE FREE SURFACE OF INFINITE WATER DEPTH AT HIGH FROUDE NUMBER F_n=0.6 WITH VARIOUS FREQUENCIES

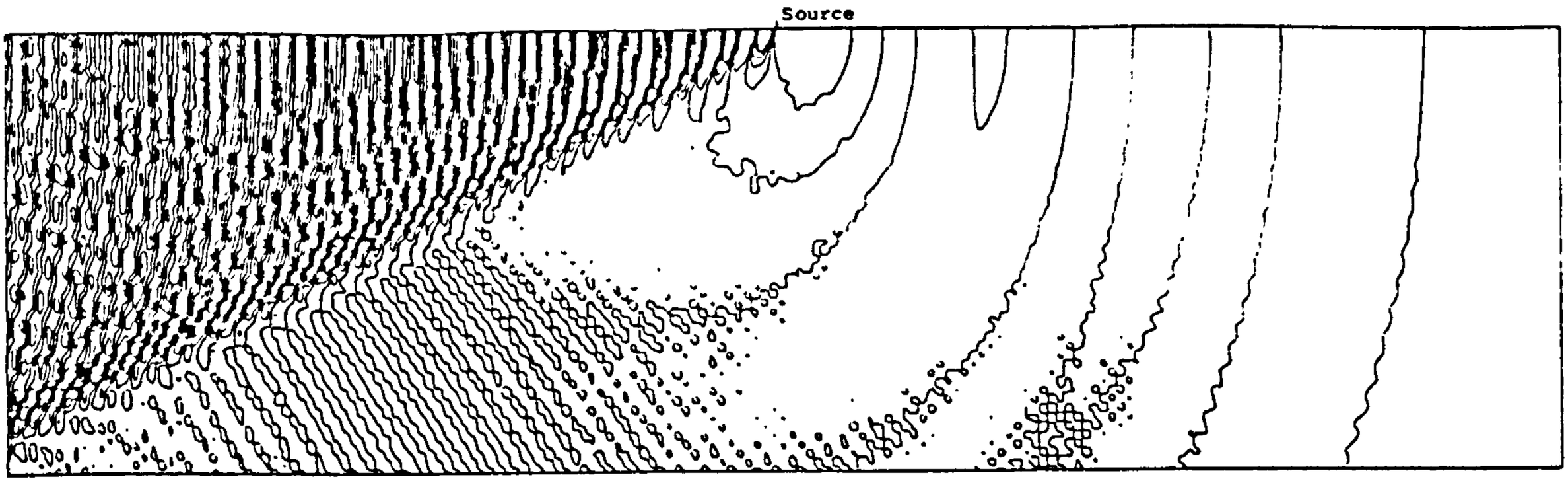

FREQ. NO. F=. 3 FROUDE NO. FN=. 6

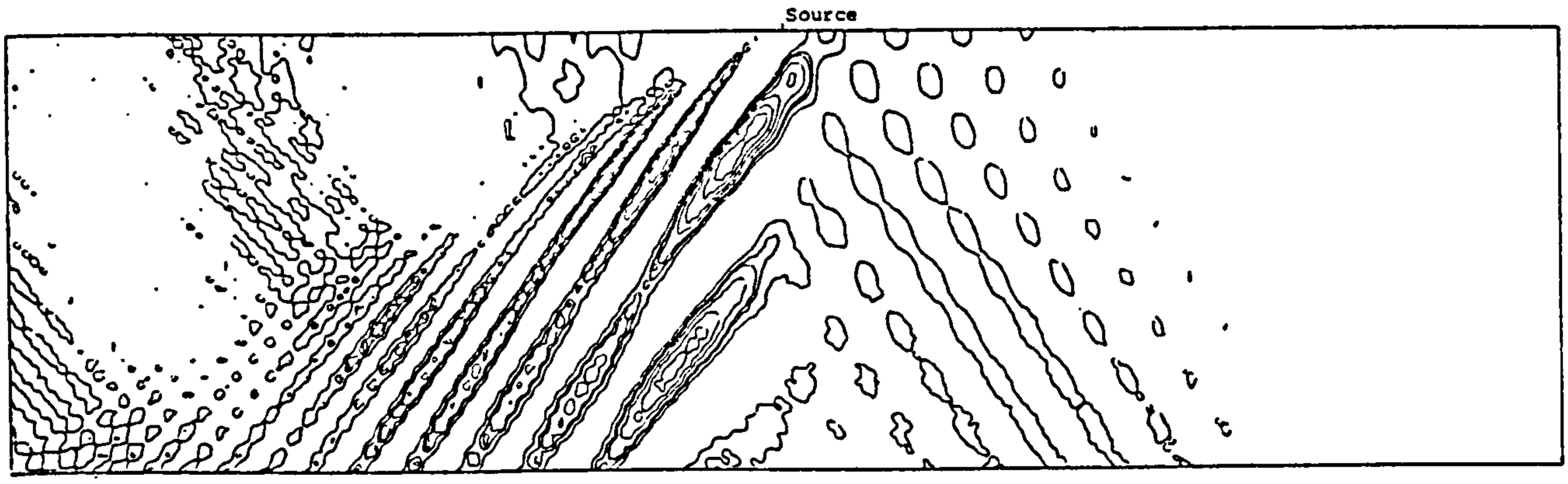

FREQ. NO. F=. 5 FROUDE NO. FN=. 6

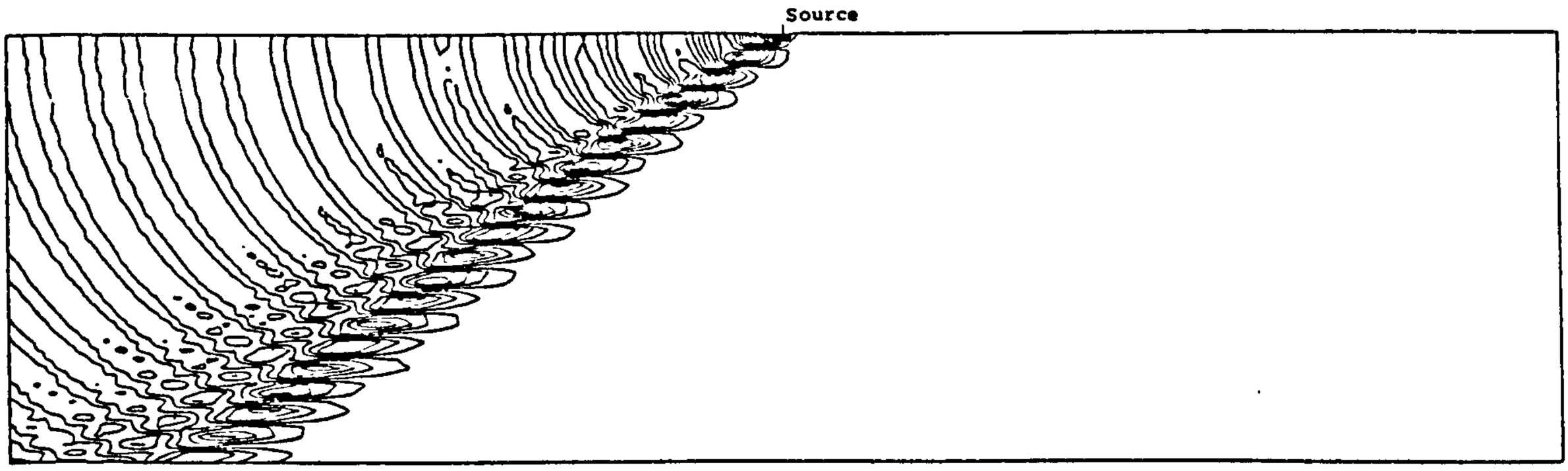

FREQ. NO. F=1. 1 FROUDE NO. FN=. 6

Fig.4.22b WAVE CONTOURS DUE TO A TRANSLATING PULSATING SOURCE SUBMERGED BELOW THE FREE SURFACE OF INFINITE WATER DEPTH AT HIGH FROUDE NUMBER F_n=0.6 WITH VARIOUS FREQUENCIES

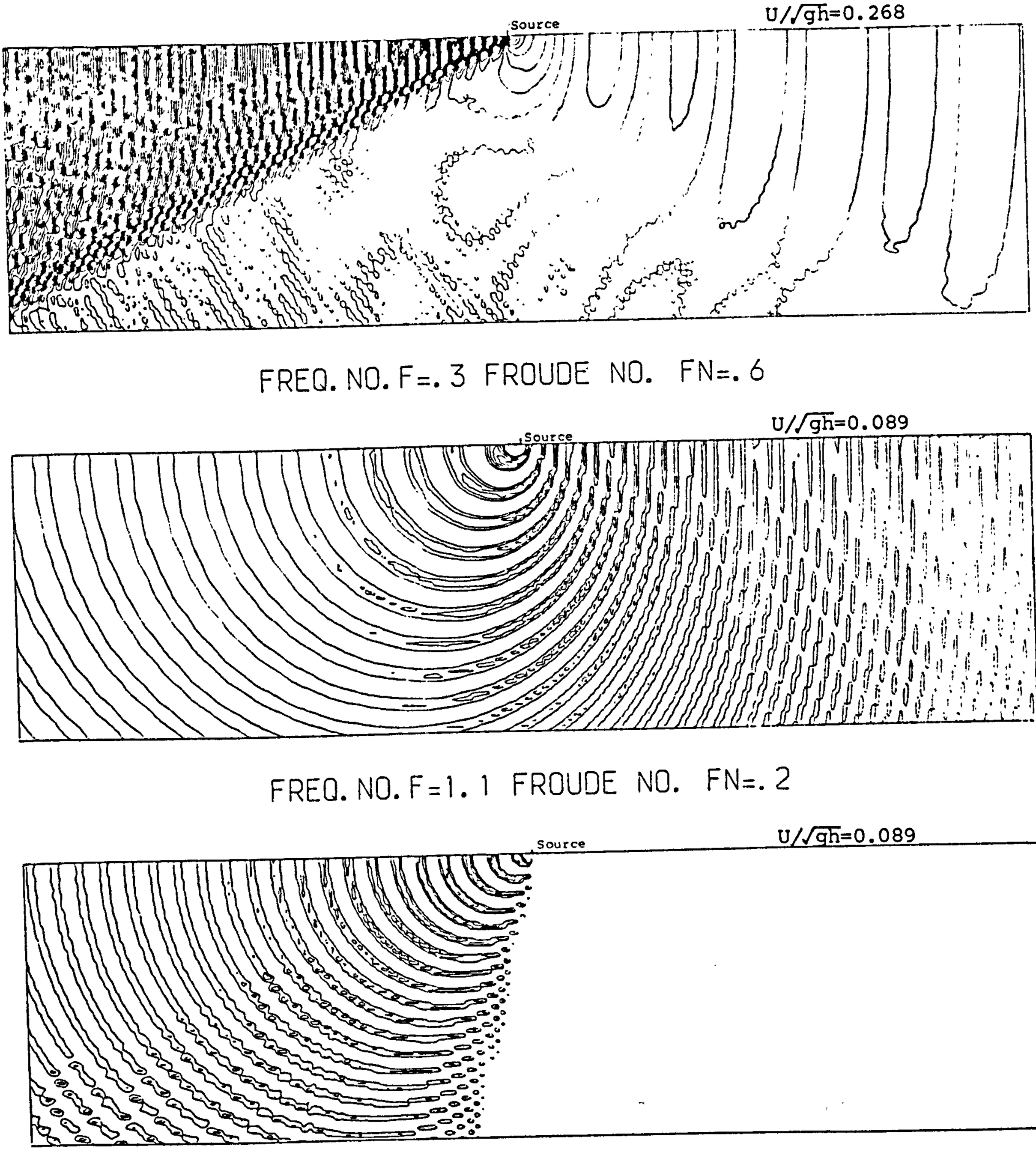

Fig.4.23 WAVE CONTOURS DUE TO A TRANSLATING PULSATING SOURCE SUBMERGED BELOW THE FREE SURFACE OF VARIOUS WATER DEPTHS

CHAPTER 5

NUMERICAL IMPLEMENTATION OF GREEN FUNCTION METHOD

5.1 Introduction

In the fluid-structure interaction analysis, the hydrodynamic forces and the resulting motions of a body moving in a seaway can be found through the knowledge of the velocity potential of the flow field on the mean wetted body surface. As discussed in Chapter 3, the unknown velocity potential can be solved by using a Green function which is the kernel function of an integral equation. For the steady and unsteady forward motion problems, the integral equation is formed by the surface integral over the mean wetted body surface and the free-surface contour integral along the intersection curve between the mean wetted body surface and the undisturbed free-surface. It is impossible to obtain an analytical solution of this integral equation not only because the body surface is arbitrary but also the kernel function of the integral is quite complicated. Therefore, this integral equation must be solved by means of numerical techniques. For numerical approximations, the integral equation which is based on a source singularity distribution on the body surface is approximated by a set of linear algebraic equations. This involves discretisation of the wetted body surface into a finite but large number of surface elements. Sources of initially unknown strength σ are distributed over the surface elements which are constructed by a grid of panels. The application of the integral equation to each of the surface elements leads to a system of simultaneous linear equations whose solution can be obtained by standard numerical techniques.

This Chapter describes the numerical implementation of the Green function method by first introducing the discretisation of the boundary integral equations and wetted body surface. The description of the integration over the surface elements then

follows. In order to reduce computing time in the evaluation of the forward speed Green function, the symmetry properties of the Green function are explored. Finally, the symmetry of the body is utilised to save computing storage and CPU time.

5.2 Discretisation of boundary integral equations

Based on the Green function method, the domain of the flow field exterior to the body is reduced from an infinite fluid domain to the wetted body surface. This results in an integral equation over the mean wetted body surface. The integral equation utilizes a distribution of singularities over the body surface. Various types of singularities may be used, for example, sources, dipole, vortices, etc. As discussed in Chapter 3 the most obvious choice of the singularities is source distributions. The general properties of the source singularities must satisfy the governing equation and all boundary conditions. The unknown source strengths are determined so that the body boundary condition is satisfied. The integral equation for source distributions over the moving body surface is

$$\iint_{S_\bullet} \sigma(q)G(p;q)ds(q) + \frac{U^2}{g}\oint_{L_\bullet} n_1\sigma(q)G(p;q)dy(q) = 4\pi\phi(p) \qquad (5.1)$$

The unknown source strength σ in equation (5.1) can be determined by using the appropriate body boundary conditions. Thus we have

$$2\pi\sigma(p) + \iint_{S_\bullet} \sigma(q)\frac{\partial G(p;q)}{\partial n}ds(q) + \frac{U^2}{g}\oint_{L_\bullet} n_1\sigma(q)\frac{\partial G(p;q)}{\partial n}dy(q) = 4\pi\frac{\partial\phi(p)}{\partial n} \qquad (5.2)$$

The Green function G(p;q) represents the potential at the field point p due to a source of unknown strength σ at the source point q. The first term on the left hand side of equation (5.2) is the contribution due to the source singularity in the immediate neighborhood of the field point p. Due to the arbitrariness of the body surface and the

complexity of the Green function, the integral equation (5.2) may be solved numerically beginning with the discretisation of the mean wetted body surface S_o into N surface elements. In the discretisation process, different procedure can be used to approximate the variation of the source strength σ within the element. The variation could be constant, piecewise linear, quadratic, cubic or higher order polynomial. For simplicity in manipulations, constant source strength approximation is commonly used so that the unknown strength σ can be taken out of the integral. The continuous formulation of the solution indicates that equation (5.2) is to be satisfied at all points on the mean wetted body surface S_o. In order to obtain a discretised numerical solution it is necessary to relax this requirement and apply the body boundary condition at only N control points. On each element a control point is selected at which the normal velocity boundary condition is to be satisfied. The location of the control point may, in principle, be chosen arbitrarily. There are three possibilities for the choice of the control point. They are the centroid of the element, the point whose coordinates are the average of the coordinates of four vertices of a quadrilateral element and the null point at which there is no self induced tangential velocity. Hess & Smith (1962) used the null points as control points but their subsequent results indicated that the centroid of the area of the quadrilateral is an equally good choice. The difference between the null point and the centroid is not significant and it is not necessarily a more correct refinement to use the null point instead of the centroid. For convenience, N control points at the element centroids are used in the present study. Then the discretised boundary integral equation by means of simple point collocation can be written as

$$\frac{1}{2}\sigma_i + \sum_{j=1}^{N} \sigma_j I_{ij} = v_i \qquad i = 1,2,...N \qquad (5.3)$$

where
$$I_{ij} = \frac{1}{4\pi}\left\{ \iint_{\Delta s_j} \frac{\partial G(p_i; q_j)}{\partial n} ds_j + \frac{U^2}{g} \oint_{\Delta L_j} n_1 \frac{\partial G(p_i; q_j)}{\partial n} dy_j \right\} \qquad (5.4)$$

$$v_i = \frac{\partial \phi(p_i)}{\partial n} \qquad (5.5)$$

Δs_j is the area of the j-th surface element and ΔL_j is the length of the j-th line segment of the intersection curve L_o between the wetted body surface S_o and the undisturbed free-surface S_F. n_1 is the x-component of the unit normal vector at the line segment ΔL_j. The normal derivatives $\partial G(p_i;q_j)/\partial n$ and $\partial \phi(p_i)/\partial n$ are with respect to the field point p_i. The calculation of the free-surface line integral is required for those surface elements adjacent to the free-surface. If the j-th element adjacent to the free-surface is parallel to the x-z plane, the y-component of the line segment ΔL_j is equal to zero. The system of the linear algebraic equations in equation (5.3) can be expressed in a matrix form as

$$[A]\{\sigma\} = \{v\} \tag{5.6}$$

The column matrix $\{\sigma\}$ and $\{v\}$ are an unknown source strength vector and the prescribed velocity vector respectively. They are vectors of order N. The matrix [A] of order NxN is called "the influence coefficient matrix". The diagonal entry a_{ii} and the off-diagonal entry a_{ij} of the matrix [A] are respectively

$$a_{ii} = \frac{1}{2} + I_{ii} \tag{5.7}$$

and

$$a_{ij} = I_{ij} \tag{5.8}$$

When i = j, that is, the field point p_i coincides with the source point q_j, the integration of the singular part of the Green function in equation (5.4) is excluded in the influence coefficient I_{ii}, which is taken over by the term 1/2. Once the solution of equation (5.6) is known, the unknown velocity potential ϕ given by equation (5.1) can be solved by discretising the integral equation in the following form

$$\phi(p) = \sum_{j=1}^{N} \sigma_j G_j \tag{5.9}$$

where

$$G_j = \frac{1}{4\pi}\left\{ \iint_{\Delta s_j} G(p; q_j) ds_j + \frac{U^2}{g} \oint_{\Delta L_j} n_1 G(p; q_j) dy_j \right\} \tag{5.10}$$

Equations (5.3) and (5.9) are enforced at a set of collocation points p_i. Alternatively the integral equation can be enforced in an average sense by integrating it over the field element instead of merely satisfying it at a selected point on the element. This technique of solution is called the Galerkin method (Sclavounos & Lee 1985) which is theoretically more accurate than the simple point collocation for the same number of elements. The Galerkin method results in a double integration of the Green function and its derivatives over the field element. Due to the complexity of the forward speed free surface Green function, the Galerkin method is too expensive in terms of computing time and is not recommended. However, the single point collocation method is capable of producing results as good as that of the Galerkin method. Furthermore no special scheme is used to remove irregular frequencies since these frequencies occur in very short waves for a slender body.

5.3 Discretisation of body surface

An approach adopted to solve the integral equation consists of discretising the integral equation into a set of linear algebraic equations. This is accomplished in the discretisation of the mean wetted body surface on which the body boundary condition is satisfied. The body surface is approximated by a finite but large number of surface elements, whose characteristic dimensions are small compared with those of the body. Over each surface element, the source strength σ is assumed to be constant. This reduces the problem of determining the continuous source strength function $\sigma(q)$ to that of determining a finite number of σ, one for each element. Since the source strength is constant over each element, the source distribution is discontinuous and the source strength jumps stepwise at the boundary of two elements. In order to accurately model the variation of the source strength function $\sigma(q)$ over the body surface, it is necessary to use sufficiently large number of elements for constant source strength σ. One might think that the use of variation of source strength function, such as linear variation, would reduce the number of elements but this variation provides no advantages. This is because the discretised body surface of small number of elements becomes coarse and

the computing time is not reduced due to the interlace of the source variable and the Green function.

The secret of a good approximation to the body surface lies in the choice of the surface elements. The simplest representation is flat quadrilateral or triangular elements. Others are also possible using polynomial or spline functions. These types of representations are normally referred to as the higher order boundary element with the flat element being the lowest order. For higher order boundary element, the geometry of the surface element and the source strength distribution are approximated by interpolation of the values at nodes that define this element. The interpolation functions or shape functions are usually polynomials in terms of the nodal coordinates. The order of the polynomial determines the order of the element. Since the shape functions are coupled with the complicated Green function, the evaluation of the influence coefficient becomes cumbersome and time consuming. Therefore the flat panel representation is commonly used in the integral equation method.

5.3.1 Quadrilateral panels

The flat panel representation was first used by Hess & Smith (1962) for the numerical solution of the potential flow around arbitrary three-dimensional bodies where the body surface was represented by quadrilateral elements. The surface of the wetted body is defined by means of the original grid points $\vec{x}(x, y, z)$ in the global co-ordinate system as shown in Fig.5.1. Four grid points which do not in general lie in a plane are grouped to form a quadrilateral element.

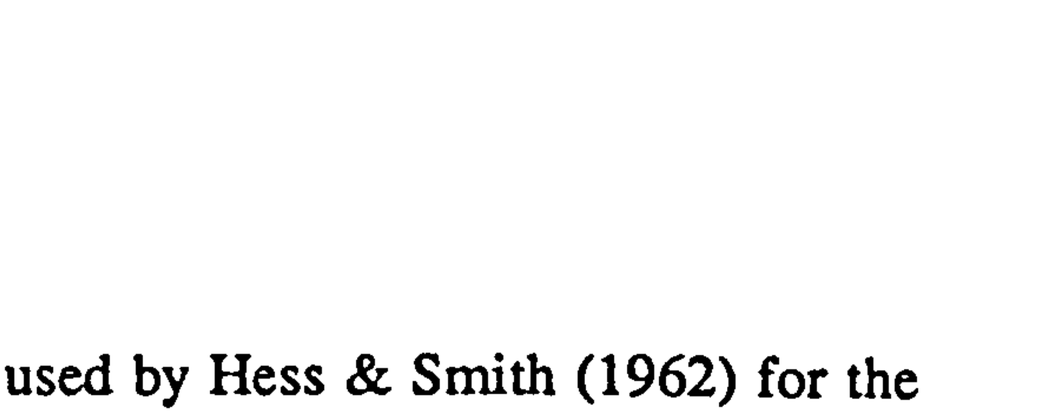

Fig.5.1 Sketch for body discretisation

Let us denote four original grid points as $\vec{x}_1, \vec{x}_2, \vec{x}_3$ and $\vec{x}_4$ in the clockwise sense as seen from the exterior fluid domain. The numbering order of these four points determines which direction is considered the outward normal to the fluid domain. The outward normal vector $\vec{N}$ is found from the cross product of the two diagonal vectors . $(\vec{x}_4 - \vec{x}_2)$ and $(\vec{x}_3 - \vec{x}_1)$ in the form

$$\vec{N} = (\vec{x}_4 - \vec{x}_2) \times (\vec{x}_3 - \vec{x}_1) \tag{5.11}$$

and the unit outward normal vector of the quadrilateral element can be found as

$$\vec{n} = \frac{\vec{N}}{|\vec{N}|} \tag{5.12}$$

The plane of the quadrilateral panel passes through the point $\vec{x}_m$ whose coordinates are the average of the coordinates of the four grid points such that

$$\vec{x}_m = (\vec{x}_1 + \vec{x}_2 + \vec{x}_3 + \vec{x}_4) / 4 \tag{5.13}$$

Afterwards the grid points are projected onto the plane of the panel to obtain the panel's vertices. The vector of the vertex $\vec{a}_k$ corresponding to $\vec{x}_k$ is defined as

$$\vec{a}_k = \vec{x}_k - [(\vec{x}_k - \vec{x}_m) \bullet \vec{n}]\, \vec{n} \qquad k = 1,2,3,4 \tag{5.14}$$

In order to facilitate the mathematical manipulation on panel integration, we have to use a local coordinate system $\bar{o} - \bar{x}\bar{y}\bar{z}$ whose origin is temporarily defined at the average point $\vec{x}_m$ as shown in Fig.5.2. The $\bar{x}$-axis is parallel to the line joining from the vertex $\vec{a}_1$ to $\vec{a}_3$ and the $\bar{z}$-axis is parallel to the unit outward normal vector $\vec{n}$.

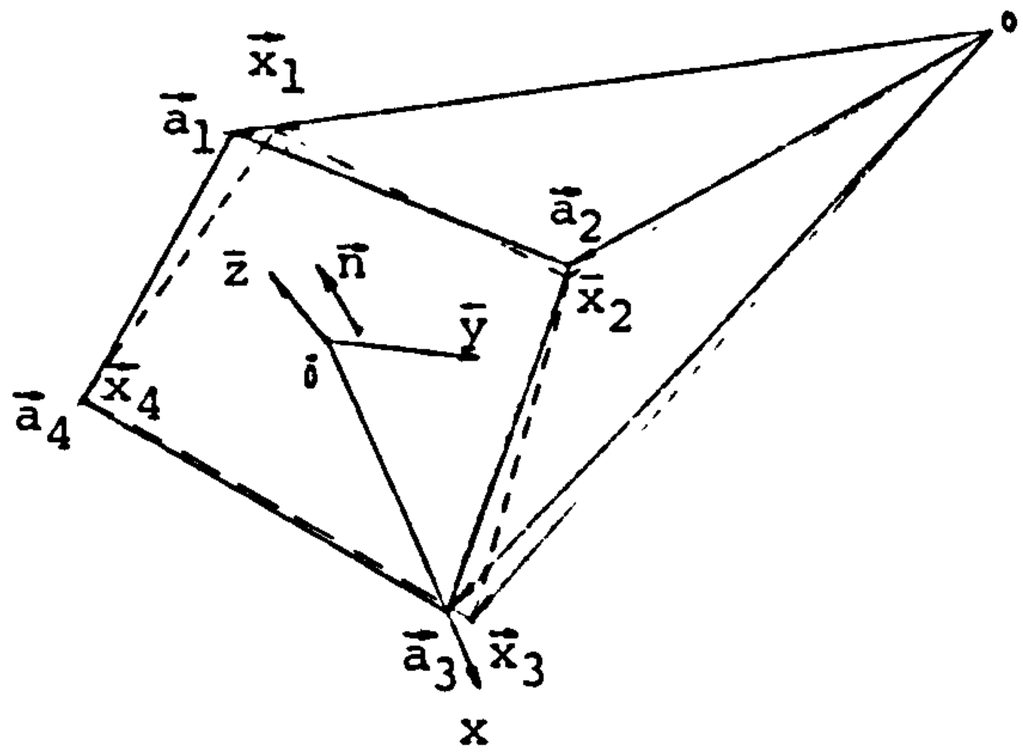

Fig.5.2 Sketch for local coordinate system

If we denote the unit vectors in the $\bar{x}$, $\bar{y}$ and $\bar{z}$ direction by $\vec{e}_1$, $\vec{e}_2$, $\vec{e}_3$ respectively, then we get

$$\vec{e}_1 = \frac{\vec{a}_3 - \vec{a}_1}{|\vec{a}_3 - \vec{a}_1|} = e_{11}\vec{i} + e_{12}\vec{j} + e_{13}\vec{k} \tag{5.15a}$$

$$\vec{e}_2 = \vec{n} \times \vec{e}_1 = e_{21}\vec{i} + e_{22}\vec{j} + e_{23}\vec{k} \tag{5.15b}$$

$$\vec{e}_3 = \vec{n} = e_{31}\vec{i} + e_{32}\vec{j} + e_{33}\vec{k} \tag{5.15c}$$

The transformation from the global system o-xyz to the local system $\bar{o} - \bar{x}\bar{y}\bar{z}$ is obtained through the following matrix

$$(\vec{e}_1, \vec{e}_2, \vec{e}_3) = [e](\vec{i}, \vec{j}, \vec{k}) \tag{5.16}$$

in which the entries of the transformation matrix [e] satisfy equations (15a,b,c). If a given point has the coordinates (x, y, z) in the global system and $(\bar{x}, \bar{y}, \bar{z})$ in the local

system, then

$$(\bar{x}, \bar{y}, \bar{z}) = [\, e \,] \{ (x, y, z) - (x_o, y_o, z_o) \} \tag{5.17}$$

$$(x, y, z) = [\, e \,]^T (\bar{x}, \bar{y}, \bar{z}) + (x_o, y_o, z_o) \tag{5.18}$$

The coordinates (x_o, y_o, z_o) is at the average point $\vec{x}_m$. In the local system $\bar{o} - \bar{x}\bar{y}\bar{z}$, the coordinates of the vertices of the quadrilateral are $(\xi_k, \eta_k, 0)$ where k=1,2,3,4 and the centroid of the area of the quadrilateral is $(\xi^*, \eta^*, 0)$ such that

$$\begin{aligned} \xi^* = \{ & (\eta_2 - \eta_1) [(\xi_2 - \xi_1) (\xi_1 + 2\,\xi_2) + (\xi_3 - \xi_1) (\xi_3 + 2\,\xi_2)] \\ & + (\eta_1 - \eta_4) [(\xi_4 - \xi_1) (\xi_1 + 2\,\xi_4) + (\xi_3 - \xi_4) (\xi_3 + 2\,\xi_4)] \} / (6\,\Delta s) \end{aligned} \tag{5.19a}$$

$$\eta^* = (\eta_1 + \eta_2 + \eta_4) / 3 \tag{5.19b}$$

The area of the quadrilateral is

$$\Delta s = \tfrac{1}{2} (\xi_3 - \xi_1) (\eta_2 - \eta_4) \tag{5.20}$$

After the position of the panel centroid is found, the origin of the local system $\bar{o} - \bar{x}\bar{y}\bar{z}$ is shifted to the centroid. From now on, the coordinates of the vertices of the quadrilateral are with respect to the centroid (x_o, y_o, z_o).

In general, the edges of adjacent panels are not coincident and, as a result, there are small "openings" between the panels. The error due to these openings are of higher order and are negligible since the width of the openings, as measured by the distance between the vertex and original grid point, is small compared to the dimensions of the panel. The plane of the panel is equidistant from the four original grid points to form it. This technique results in minimizing, in a least square sense, the distance between the vertices of the panel and the original grid points. The use of triangular flat panels can

eliminate the openings. In particular, a triangle is a special case of a quadrilateral.

The quality of representation for the body surface depends largely on the distribution of the elements over the surface. Since the control points are taken at the element centroids and a constant source strength over each element is assumed, the aspect ratio of the quadrilateral should be as close to unity as possible to ensure that the mid-point rule is valid in the evaluation of the influence coefficient which will be discussed in the following section. The elements should be concentrated in regions where the body geometry changes rapidly or where the flow properties, particularly the velocities, are expected to vary rapidly. It should be remarked that if several small elements are in the vicinity of a large one, the influence of the large element would swamp the effect of small neighbours. Therefore the size of the elements should change gradually between regions of concentration and the regions where the distribution is sparse. Hess & Smith (1962) suggested that the characteristic dimensions of element should be no more than 50 per cent greater than those of adjacent elements.

The accuracy of computation will increase as the number of elements increase, since smaller elements can model the curved shape better and a finer distribution of sources will approximate the pressure gradient more accurately. Furthermore, for short waves more elements are required than for long waves. Van Oortmerssen (1976) suggested that the characteristic dimension of a element should not exceed one-fifth of the wave length.

5.4 Integration over source elements

Once the wetted body surface has been discretised into panel elements on which the source strength is constant, it is necessary to evaluate the influence coefficients given by equations (5.4) and (5.10) for the integration of the Green function and its derivatives over each panel. It is convenient to consider four terms expressible in the Green function as discussed in Chapter 4 and so we write

$$G(p;q) = -\frac{1}{r} + \frac{1}{r'} - \frac{1}{r_h} + H(p;q) \qquad (5.21)$$

The first term $-1/r$ is the source singularity and the second term $1/r'$ is the image-sink which is the image of the source singularity over the free-surface. The third term $-1/r_h$ is the finite-depth source which is the image of the source singularity over both the free-surface and the sea bottom. The last term H(p;q) is a wave function which consists of the image-sink like function M(p;q), the near-field function N(p;q) and the far-field function W(p;q). The image-sink $1/r'$ has been taken out from the image-sink like function M(p;q). The velocity potential and its derivatives due to the source distribution over a panel are

$$\phi = \psi + \psi' + \psi_h + \psi_H \qquad (5.22)$$

$$\nabla\phi = \nabla\psi + \nabla\psi' + \nabla\psi_h + \nabla\psi_H \qquad (5.23)$$

in which $\phi = \iint_{\Delta s} G\,ds$, $\nabla\phi = \iint_{\Delta s} \nabla G\,ds$, $\psi = \iint_{\Delta s} (-\frac{1}{r})ds$, etc. It should be noted that the normal derivative of the Green function in equation (5.4) is obtained by

$$\frac{\partial G}{\partial n} = n_1\frac{\partial G}{\partial x} + n_2\frac{\partial G}{\partial y} + n_3\frac{\partial G}{\partial z} \qquad (5.24)$$

where n_1, n_2 and n_3 are respectively the x, y and z-components of the unit normal vector $\vec{n}$ at the field point p.

5.4.1 Source term

The contribution of the source singularity and its images for the Green function to the surface integral in equations (5.4) and (5.10) can be calculated analytically over a quadrilateral panel by using the method of Hess & Smith (1967). The influence of the j-th panel on the i-th field point p_i (x,y,z) is obtained by mapping that point into the

local coordinate system $\bar{o} - \bar{x}\bar{y}\bar{z}$ through the transformation equation (5.17). The potential and its derivatives with respect to $\bar{x}$, $\bar{y}$ and $\bar{z}$ at the field point $(\bar{x}, \bar{y}, \bar{z})$ induced by the quadrilateral due to the source $-1/r$ are

$$\psi = \sum_{k=1}^{4} (h_k L_k - |\bar{z}| J_k) + |\bar{z}| \Delta\theta \qquad (5.25)$$

$$\psi_{\bar{x}} = \sum_{k=1}^{4} S_k L_k \qquad (5.26a)$$

$$\psi_{\bar{y}} = - \sum_{k=1}^{4} C_k L_k \qquad (5.26b)$$

$$\psi_{\bar{z}} = \text{sig}(\bar{z}) [\Delta\theta - \sum_{k=1}^{4} J_k] \qquad (5.26c)$$

where

$$L_k = \ln\left(\frac{r_k + r_{k+1} - d_k}{r_k + r_{k+1} + d_k}\right) \qquad r_k = \sqrt{[(\bar{x} - \xi_k)^2 + (\bar{y} - \eta_k)^2 + \bar{z}^2}$$

$$J_k = \tan^{-1}\left[\frac{h_k |\bar{z}| (r_k c_k - r_{k+1} b_k)}{r_k r_{k+1} h_k^2 + \bar{z}^2 b_k c_k}\right] \qquad d_k = \sqrt{[(\xi_{k+1} - \xi_k)^2 + (\eta_{k+1} - \eta_k)^2}$$

$$C_k = (\xi_{k+1} - \xi_k) / d_k \qquad b_k = (\xi_k - \bar{x}) C_k + (\eta_k - \bar{y}) S_k$$

$$S_k = (\eta_{k+1} - \eta_k) / d_k \qquad c_k = (\xi_{k+1} - \bar{x}) C_k + (\eta_{k+1} - \bar{y}) S_k$$

$$h_k = (\bar{x} - \xi_k) S_k - (\bar{y} - \eta_k) C_k \qquad (5.27)$$

It should be noted that the properties of those variables in equations (5.25) through (5.27) at the subscript k=5 are equivalent to those at k=1. No difficulty is

encountered in the evaluation of equations (5.25) and (5.26a,b,c). The quantity L_k would become singular if the field point was on the side of the quadrilateral. This singularity can be avoided since the field points (control points) are located at the element centroids and the flow properties must be evaluated at the control points on the body surface where the body boundary conditions are specified or at points off the body surface. $\Delta\theta$ is easy to evaluate; it is 2π if all the h's are positive and it is zero otherwise. For $\bar{z} = 0$, all the J's vanish and $\psi_{\bar{z}} = \Delta\theta$.

Evaluation of exact solutions for the source term $-1/r$ is quite time-consuming since at least four natural logarithms, four inverse tangents and four square roots are required. The complicated nature of these solutions arises from the effects of all details of the panel geometries. If the field point is sufficiently far from the panel, the details of the geometry become unimportant. Hess & Smith (1962) also gave an approximate solution for the source term $-1/r$ by means of a multipole expansion. The source term $-1/r$ is expanded in a Taylor series in ξ and η about the origin which is the centroid of the area of the quadrilateral. Integration of the series form yields the multipole approximation as

$$\psi = -[w \quad w_{\bar{x}\bar{x}} \quad w_{\bar{x}\bar{y}} \quad w_{\bar{y}\bar{y}}]\,\{Q\} \tag{5.28}$$

$$\bar{\nabla}\psi = -[W]\,\{Q\} \tag{5.29}$$

where

$$[W] = \begin{bmatrix} w_{\bar{x}} & w_{\bar{x}\bar{x}\bar{x}} & w_{\bar{x}\bar{x}\bar{y}} & w_{\bar{x}\bar{y}\bar{y}} \\ w_{\bar{y}} & w_{\bar{x}\bar{x}\bar{y}} & w_{\bar{x}\bar{y}\bar{y}} & w_{\bar{y}\bar{y}\bar{y}} \\ w_{\bar{z}} & w_{\bar{x}\bar{x}\bar{z}} & w_{\bar{x}\bar{y}\bar{z}} & w_{\bar{y}\bar{y}\bar{z}} \end{bmatrix} \tag{5.30}$$

$$\{Q\} = (\Delta s,\ \tfrac{1}{2}I_{\bar{x}\bar{x}},\ I_{\bar{x}\bar{y}},\ \tfrac{1}{2}I_{\bar{y}\bar{y}}) \tag{5.31}$$

The components of $\{Q\}$ are respectively the element area and the three second moments of the element area about the local coordinate system $\bar{o} - \bar{x}\bar{y}\bar{z}$ whose origin is at the

element centroid. The three second moments of the element area are

$$I_{\bar{x}\bar{x}} = \frac{1}{12}(\xi_3 - \xi_1)\,[\,\eta_1\,(\xi_4 - \xi_2)\,(\xi_1 + \xi_2 + \xi_3 + \xi_4) + \xi_2\eta_2\,(\xi_1 + \xi_2 + \xi_3)$$
$$+ (\eta_2 - \eta_4)(\xi_1^2 + \xi_1\xi_3 + \xi_3^2) - \xi_4\eta_4(\xi_1 + \xi_3 + \xi_4)\,]$$

$$I_{\bar{x}\bar{y}} = \frac{1}{24}(\xi_3 - \xi_1)\,[\,2\xi_4(\eta_1^2 - \eta_4^2) - 2\xi_2(\eta_1^2 - \eta_2^2) \qquad (5.32)$$
$$+ (\xi_1 + \xi_3)\,(\eta_2 - \eta_4)\,(2\eta_1 + \eta_2 + \eta_4)\,]$$

$$I_{\bar{y}\bar{y}} = \frac{1}{12}(\xi_3 - \xi_1)\,(\eta_2 - \eta_4)\,[\,(\eta_1 + \eta_2 + \eta_4)^2 - \eta_1\,(\eta_2 + \eta_4) - \eta_2\eta_4\,]$$

The quantity w and its derivatives are

$$w = r_o^{-1} \qquad w_{\bar{x}\bar{x}\bar{x}} = \bar{x}(9r_o^2 - 15\bar{x}^2)r_o^{-7}$$

$$w_{\bar{x}} = -\bar{x}r_o^{-3} \qquad w_{\bar{x}\bar{x}\bar{y}} = \bar{y}(3r_o^2 - 15\bar{x}^2)r_o^{-7}$$

$$w_{\bar{y}} = -\bar{y}r_o^{-3} \qquad w_{\bar{x}\bar{x}\bar{z}} = \bar{z}(3r_o^2 - 15\bar{x}^2)r_o^{-7}$$

$$w_{\bar{z}} = -\bar{z}r_o^{-3} \qquad w_{\bar{x}\bar{y}\bar{y}} = \bar{x}(3r_o^2 - 15\bar{y}^2)r_o^{-7} \qquad (5.33)$$

$$w_{\bar{x}\bar{x}} = -(r_o^2 - 3\bar{x}^2)r_o^{-5} \qquad w_{\bar{x}\bar{y}\bar{z}} = -15\bar{x}\bar{y}\bar{z}r_o^{-7}$$

$$w_{\bar{x}\bar{y}} = 3\bar{x}\bar{y}r_o^{-5} \qquad w_{\bar{y}\bar{y}\bar{y}} = \bar{y}(9r_o^2 - 15\bar{y}^2)r_o^{-7}$$

$$w_{\bar{y}\bar{y}} = -(r_o^2 - 3\bar{y}^2)r_o^{-5} \qquad w_{\bar{y}\bar{y}\bar{z}} = \bar{z}(3r_o^2 - 15\bar{y}^2)r_o^{-7}$$

and $$r_o^2 = \bar{x}^2 + \bar{y}^2 + \bar{z}^2 \qquad (5.34)$$

For the exact formulae (5.26a,b,c) and the multipole approximation in equation (5.29), the velocity components of the source $-1/r$ are calculated in the local coordinate system $\bar{o} - \bar{x}\bar{y}\bar{z}$. These calculated velocity components must be transformed back to the global system o–xyz by means of the following formula

$$\nabla\psi = [e]^T \nabla\psi \tag{5.35}$$

Hess & Smith (1962) suggested that equations (5.28) through (5.34) could be used to replace (5.25) through (5.27) if the distance between the field point and the centroid of the source panel in equation (5.34) is greater than 2.45 times the maximum element diagonal. In the case that this ratio exceeds 4.0, equations (5.28) through (5.34) can be replaced by the even simpler expression

$$\psi = -\frac{1}{r}\Delta s \tag{5.36}$$

$$\nabla\psi = \frac{\vec{x} - \vec{x}_o}{r^3}\Delta s \tag{5.37}$$

It is evident that r is equal to r_o. Equations (5.36) and (5.37) are the point source approximation which is asymptotically valid.

5.4.2 Image-sink term

The potential ψ' and its derivatives $\nabla\psi'$ due to the image-sink 1/r' can be handled in the same way as those of the source term −1/r. The integrations for ψ' and its derivatives $\nabla\psi'$ are carried out on image panels above the undisturbed free-surface. The coordinates of the vertices of a image quadrilateral panel in the global system o–xyz and in the local system $\bar{o} - \bar{x}\bar{y}\bar{z}$ are the same as those of the corresponding source panel except that the signs in the z-direction and $\bar{z}$-direction for the image coordinates are opposite to that for the source coordinates. The matrix of transformation [e] from the global system to the local system is replaced by the following matrix for image panels.

$$[e'] = \begin{bmatrix} e_{11} & e_{12} & -e_{13} \\ e_{21} & e_{22} & -e_{23} \\ -e_{31} & -e_{32} & e_{33} \end{bmatrix} \tag{5.38}$$

in which the magnitudes of the entries are equal to those in equations (5.15a,b,c). Hence equations (5.25) through (5.38) can be applied for ψ' and $\nabla\psi'$ over the image panels. It should be noted the Rankine terms $-1/r+1/r'$ on the free surface cancel each other when the source point or the field point is on the free surface. Therefore they do not contribute to the line integral in the free-surface line integral in equations (5.4) and (5.10).

5.4.3 Finite-depth source term

The finite-depth source $-1/r_h$ is the image of the source $-1/r$ over both the free-surface and the sea bottom. The evaluation of the finite-depth source $-1/r_h$ becomes numerically difficult when the clearance between the bottom of the body and the sea bottom is small and the image source is located just below the field point. This difficulty can be circumvented by analytically integrating the finite-depth source and its derivatives over the image source panels. Equations (5.25) through (5.38) for the image-sink panels are still applicable to the image-source panel which is twice the water depth h below the image-sink panels.

5.4.4 Wave function terms

The complexity of the wave function H(p;q) rules out the possibility of analytically evaluating the wave integral over a surface element. Therefore a method of solution by numerical means must be sought. The wave function H(p;q) is regular throughout the fluid domain except that those field and source points which are

simultaneously located on the free-surface where the wave function H(p;q) becomes unbounded. These difficulties can easily be avoided in practice since the wave integrals over the panels are evaluated by the mid-point rule. By the principle of the mid-point rule, the integral is approximated by evaluating the product of the panel area and the integrand at a selected point. At present, the selected points are the centroids of the areas of the panels, which never lie on the free-surface. The mid-point rule is applicable for the wave function H(p;q) and its derivatives since these functions vary slowly over each panel.

From the theoretical point of view the free-surface contour integral in equations (5.4) and (5.10) should be evaluated along the intersection curve of the wetted body surface and the mean free-surface. This condition is not likely to be satisfied numerically since the source strength σ is assumed constant at the centroid of the panel. Therefore the contour integral is evaluated along a line passing through the centroids of the panels adjacent to the free-surface. The contour integral is then approximated by evaluating the product of the integrand at the centroid of the uppermost panel and the y-component of the line segment ΔL. This approximation could not cause any series errors since the contribution from the line integral is likely to be small.

5.5 Bodies with a symmetry plane

The results of the integrations over the elements are assembled into a set of N equations (the total number of the panels) given by equations (5.4) and (5.10). The total number of the panels N used to represent the mean wetted body surface is only limited by the computer core memory. If the body has one or more symmetry planes, there may also be planes of symmetry or skew-symmetry of the flow field and only the non-redundant portion of the body need be approximated by panel elements. The remainder of the body is taken into account by suitable reflections. The result is a large saving in the body generation for a given accuracy or a large increase in the number of elements and thus a significant improvement in accuracy.

Regardless how many planes of symmetry of the body moving with a constant horizontal velocity at sea, only the symmetry plane parallel to the direction of forward motion can be utilised. This is because the flow disturbances are not symmetrical upstream and downstream. The disturbances are more dominant in the downstream as the upstream effects are being swept downward by the current. Therefore the non-redundant portion representing the moving body surface is the half of the body (N/2 elements) about the longitudinal plane of symmetry. Since a marine vehicle travelling in a seaway possesses at least one plane of symmetry in the direction of forward motion, the computation effort is greatly reduced from the whole body surface to half of the body surface. The solutions on the other half are readily deduced.

Due to the presence of the forward speed, the Green function and its derivatives do not possess any symmetry relationship between the field points and the source points in the direction of forward motion. By symmetry, we mean a reciprocal relationship between G(p;q) and G(q;p). In particular, if the field and the source points lie on the same transverse plane, that is, the relative distance between the field and the source points in the x-direction is zero, the reciprocal relation is valid. In this case, the principle of reflection about the longitudinal plane of symmetry is exploited.

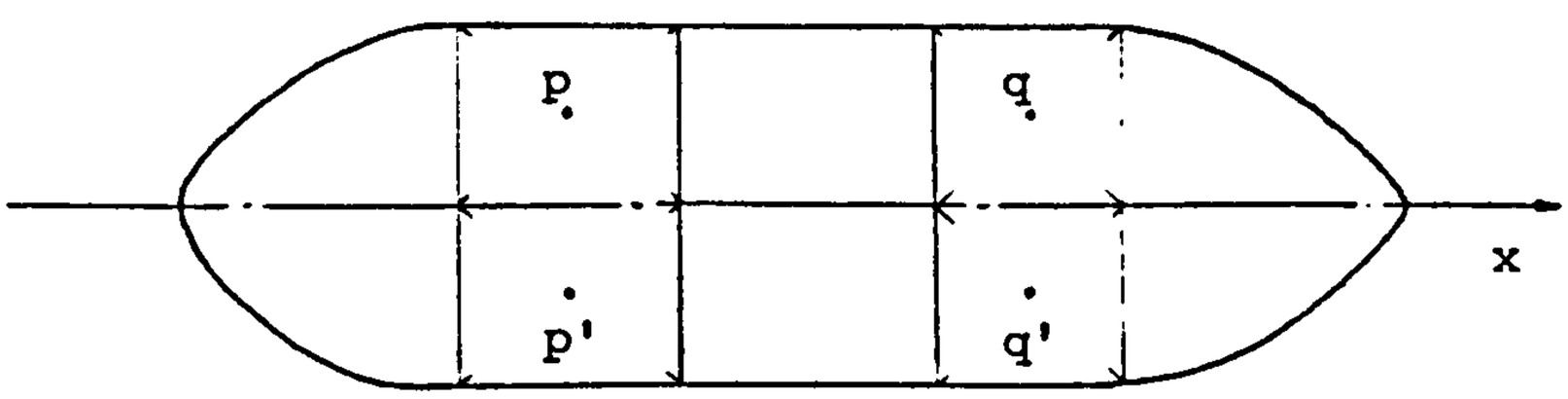

Fig.5.3 Sketch for a body having a longitudinal plane of symmetry

Consider a body with longitudinal plane of symmetry as shown in Fig.5.3. The field point p and the source point q are placed in the non-redundant input portion and the points p' and q' are their images about the longitudinal plane. Since the flow disturbances at upstream and downstream cannot be equal for the forward motion

problem, the Green function $G(p;q) \neq G(q;p)$. However, the reciprocal relations is hold valid if the field point is placed on the non-redundant portion and the source point is on the redundant portion or vice versa. This validates the principle of reflection, that is,

$$G(p;p') = G(p';p) \qquad G(q;q') = G(q';q)$$

$$G(p;q) = G(p';q') \qquad G(p;q') = G(p';q) \tag{5.39}$$

The direct result of the principle of reflection reduces the amount of work for the body generation and computation.

It is apparent that the only contribution to the non-symmetry between G(p;q) and G(q;p) are due to the far-field function W(p;q). The far-field function W(p;q) carries a Heaviside function and determines the direction of wave propagation in the fluid domain. The source singularity $-1/r$, the image-sink $1/r'$, the image-source $-1/r_h$ and the image-sink like function M(p;q) are all symmetrical with respect to the longitudinal plane of symmetry as well as to the transverse plane of symmetry. The near-field function N(p;q) expressed in terms of the exponential integral $E_1(Z)$ possesses a symmetrical relationship between the field and the source points. This relationship exists because of the complex conjugate property of the exponential integral $E_1(Z)$ given by

$$E_1(Z^*) = E_1^*(Z)$$

where the asertisk denotes the complex conjugate of the function. It is easily shown that the near-field function N(p;q) and its derivatives have the following properties :

$$\begin{aligned}
&N(p;\,q) = N^*(q;\,p) && N(p;\,q') = N^*(q;\,p') \\
&N_x(p;\,q) = -N_x^*(q;\,p) && N_x(p;\,q') = -N_x^*(q;\,p') \\
&N_y(p;\,q) = -N_y^*(q;\,p) && N_y(p;\,q') = N_y^*(q;\,p') \\
&N_z(p;\,q) = N_z^*(q;\,p) && N_z(p;\,q') = N_z^*(q;\,p')
\end{aligned} \tag{5.40}$$

The above relationships between N(p;q) and N(q;p) are true irrespective of the body geometry whereas that between N(p;q') and N(q;p') is only valid when the body has a longitudinal plane of symmetry. The numerical work can considerably be reduced by taking into account these properties.

5.6 Body boundary conditions

As discussed in Chapter 2 the body boundary condition for the steady flow problem is

$$\frac{\partial \bar{\Phi}}{\partial n} = U n_1 \tag{5.41}$$

where $\bar{\Phi}$ is the steady perturbation potential, U is the mean forward speed and n_1 is the x-component of the unit outward normal vector at the field point p. If the body has a longitudinal plane of symmetry, the source strength has to be symmetric about this plane. As a result the influence coefficient matrix reduces to the order (N/2)x(N/2).

For the diffraction problem, the body boundary condition is

$$\frac{\partial \phi_7}{\partial n} = - \frac{\partial \phi_0}{\partial n} \tag{5.42}$$

where ϕ_0 and ϕ_7 are the incident wave potential and the diffraction wave potential per unit amplitude respectively. For the longitudinal plane of symmetry, the source strength of the diffraction potential can be split into symmetry and skew-symmetry components.

For the radiation problem, the body boundary condition on the mean wetted body surface is

$$\frac{\partial \phi_j}{\partial n} = -i\omega n_j + U m_j \qquad j = 1,2,...6 \qquad (5.43)$$

where ϕ_j is the radiation wave potential per unit amplitude of motion in the j-th mode of motion. The quantities n_j and m_j are defined in Chapter 2. It is easily proved that if the body has a longitudinal plane of symmetry, the source strength is symmetrical about this plane for surge, heave and pitch, and is skew-symmetrical for sway, roll and yaw. Hence the size of the influence coefficient matrix reduces to the order (N/2)x(N/2) and therefore the computing time is reduced significantly.

By using the above ideas computer programs were written to calculate the velocity potential and the velocity field over the mean wetted body surface. Numerical computations for the first and second-order hydrodynamic forces and moments acting on a marine vehicle will be carried out in Chapters 6 and 7.

CHAPTER 6
HYDRODYNAMIC FORCES AND SHIP MOTIONS IN OBLIQUE WAVES

6.1 Introduction

The problem of a body at sea is that of the dynamic equilibrium of forces and moments in and on an elastic body with or without forward speed on the surface of the sea. In order to predict the resulting motions of the body in waves, the body is considered as a rigid body. As long as no structural and vibrational problems are to be dealt with, the rigid body assumption can be made without hesitation.

The external loads acting on the body arise from the actions of the earth's gravitational field and the fluctuations of the fluid pressure field. If viscous effects are disregarded, the fluid motion can be assumed to be irrotational and the problem can be formulated with the potential flow theory as described in Chapter 2. In potential flow the fluid pressure can be obtained from Bernoulli's equation in terms of the velocity potential and its derivatives. The external fluid loads are then obtained by integrating the pressure over the body surface. When a ship is in dynamic equilibrium state, the external fluid loads are balanced by the gravity and inertia forces on the body.

The ship motion problem is still difficult to solve even though the fluid is assumed to be homogeneous, incompressible and inviscid. The problem must be reduced to manageable proportion through linearisation so that a practical solution can be obtained. As a consequence of linearisation, the linear superposition of hydrodynamic problems is allowed with the aid of perturbation analysis. The principle of superposition plays an important role in efforts towards the solution. The responses of a ship to irregular waves can be considered as the summation of the responses to regular waves of all frequencies (St Denis & Pierson 1953).

With the aid of linear superposition of motions in regular sinusoidal waves, the ship motion problem has been greatly reduced. What remains is the study of the harmonic oscillations of a rigid body in the proximity of the surface of an ideal fluid under the action of gravity waves. In this Chapter we shall develop the expressions for the hydrodynamic forces (moments are understood hereafter) acting on a free floating body with a horizontal constant forward speed. A complete expression for the first-order hydrodynamic forces will be established. It will be noted that there are not only the hydrodynamic forces due to the interactions of the steady flow field with the unsteady flow field but also the additional buoyancy forces due to the unsteady motions in the steady flow. Under the assumptions of small amplitude motions and small steady disturbances, these additional buoyancy forces are small enough to be neglected. If the steady perturbation flow on the wetted body surface is included, the full expression of m_j terms given in the Chapter 2 has to be used and the Neumann-Kelvin problem has to be solved. On the other hand if the body is thin, slender or fully submerged, the steady disturbances in unsteady flow are sufficiently small to be negligible around the wetted body surface. By applying the hypotheses of small steady disturbances on the free surface in the unsteady forward motion problem, the influence of the forward speed on the calculation of unsteady hydrodynamic forces on a ship appears through the modifications to the pressure calculations, the free surface condition and the body boundary condition. The inclusion of the speed effect on the pressure calculation and the body condition is simple since the non-zero m_j terms are m_5 and m_6 which are proportional to the angle of attack due to pitch and yaw motions respectively. The speed effects on the free surface boundary condition lead to the use of the translating pulsating source distribution technique rather than the oscillating source model. Numerical computations have been carried out to predict hydrodynamic loads on a submerged ellipsoid, a floating ellipsoid, a Series-60 ship and a 200,000 dwt tanker. For a symmetrical body such as an ellipsoid the translating pulsating source modelling technique is validated by the well known Timman-Newman relationship (Timman & Newman 1962). Forward speed computations for a Series-60 ship are presented both with and without forward speed modification to the free surface. The shallow water effects on the hydrodynamic loads and the resulting motion responses of three-

dimensional bodies in waves are discussed. Effects of ship heading and forward speed on the hydrodynamic forces and ship motions are investigated. When the experimental data are compared with calculations based on the three-dimensional translating pulsating source model and the three-dimensional oscillating source model with simple speed correction on the linearised body boundary condition, the former gives better agreement than the latter. Both mathematical models give poor correlations in roll and pitch damping predictions. The poor roll damping results are expected due to non-linear effects in large roll motion amplitudes and to viscosity effects. The causes for the discrepancies between the calculated and the experimental pitch damping coefficients are discussed.

6.2 Unsteady hydrodynamic loads

A body moving in an oblique regular wave undergoes oscillatory and lateral drift motions. In order to simplify the analysis we assume that the body maintains its initial course at constant forward speed U and oscillates harmonically in time. Let us define a right handed orthogonal system with o-xy plane on the mean free surface, the x-axis in the direction of the forward motion and the z-axis vertically upward as shown in Fig.6.1. Suppose that the body oscillates as a rigid body in six degrees of freedom with complex amplitudes ξ_j (j=1,2,...6). Here j=1,2,3,4,5,6 refer to surge, sway, heave, roll, pitch and yaw motions respectively.

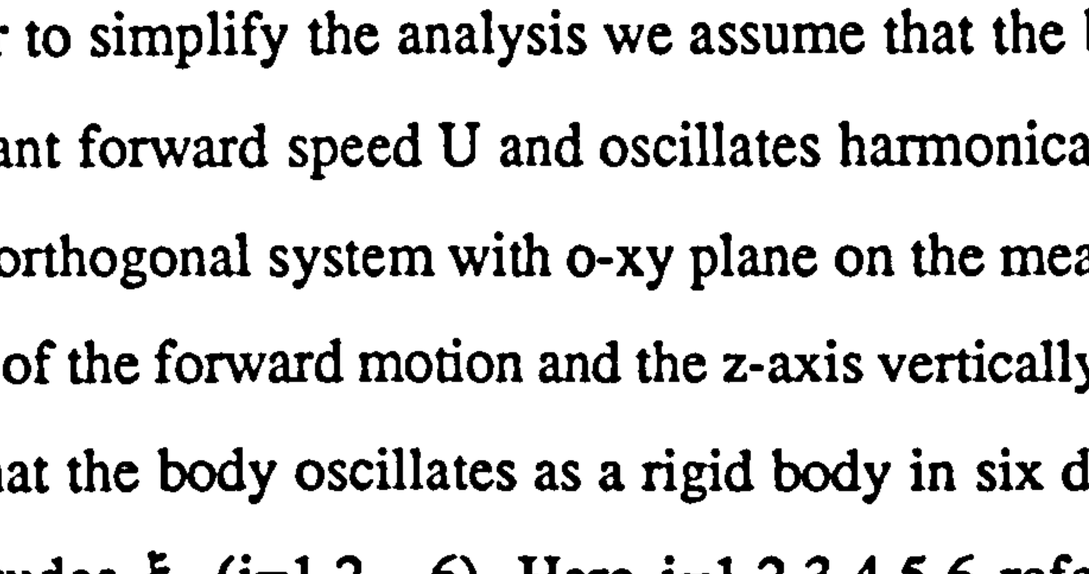

Fig.6.1 Sketch for coordinate system

The oblique regular wave profile is a small amplitude sinusoidal wave of length λ and frequency ω_o as

$$\zeta_i = \zeta_o e^{i[\upsilon(x\cos\beta + y\sin\beta) - \omega t]} \tag{6.1}$$

where ζ_o = incident wave amplitude

υ = wave number

ω = wave encounter frequency

β = angle of incidence with x-axis (180° at head sea).

For a constant depth h, the wave number υ is governed by the dispersion relation

$$\frac{\omega_o}{g} = \upsilon \tanh \upsilon h \tag{6.2}$$

and the wave encounter frequency ω is

$$\omega = |\omega_o - \upsilon U \cos\beta| \tag{6.3}$$

The body moving in waves experiences steady and unsteady external fluid forces. The steady forces arise from the hydrostatic and pressure drag when the body is travelling steadily in calm water. The unsteady forces are contributed mainly from the hydrodynamic pressure as a result of fluid oscillatory motions surrounding the hull. In the study of motion response the unsteady component only is of interest. Other additional unsteady forces caused by the fluid viscosity, the ship's propeller and aerodynamic effects are generally neglected. It has been noted in Chapter 2 that the non-linear effects arising from the interactions of the steady flow field with the unsteady flow field give rise to the inhomogeneous free surface condition for the unsteady forward motion problem. In order to obtain a practical solution, the steady perturbation flow due to the forward speed is assumed to be small and hence neglected if the body is thin, slender or fully submerged.

Through the linearisation process as discussed in Chapter 2, the external unsteady forces associated with the diffraction and the radiation problems can be treated separately. These two problems are more tractable than the complete problem. The diffraction problem deals with the forces produced by waves on the body fixed at its mean advancing position whereas the radiation problem deals with the forces induced by the harmonic oscillations of the rigid body. Both problems are first-order hydrodynamic problems. The interactions between the two first-order problems are of second-order in oscillatory amplitude and therefore are neglected in the first-order theory.

In the diffraction problem, the body is restrained from any oscillatory motion and is subjected to the actions of incident waves of given wavelength, amplitude and heading. Part of the incident waves are diffracted by the body while the remainder passes through unaffected. The resultant forces experienced by the body due to the incident and scattered waves are known as "the hydrodynamic exciting forces" and are directly proportional to the wave amplitude. The hydrodynamic exciting forces are also a function of the wave frequency, the wave heading, the forward speed and the body geometry.

In the radiation problem the radiated waves are generated from the oscillatory motions of the body in calm water. The energy dissipated through the radiated waves can be related to the concept of fluid added mass and damping under the usual assumptions of an inviscid flow. The forces exerted from the fluid on the oscillatory body are known as "the hydrodynamic reactive forces" which can be expressed in terms of added mass and damping coefficients. These coefficients are functions of the forward speed, the body geometry and the frequency of motion but not of the motion amplitude.

The hydrodynamic forces are obtained by integrating the hydrodynamic pressures in terms of the appropriate velocity potential and its derivatives over the mean wetted body surface S_o. The method to find the velocity potential has been fully described in the previous Chapters and is not discussed here.

6.3 Hydrodynamic forces

In the steady translating system o-xyz, the fluid pressure p on the instantaneous wetted body surface S_w is given by Bernoull's equation in term of total velocity potential Φ as

$$p(\vec{x}; t) = -\rho\{\Phi_t + \tfrac{1}{2}\nabla\Phi \bullet \nabla\Phi - \tfrac{1}{2}U^2 + gz\} \quad \text{on } S_w \qquad (6.4)$$

Since the exact wetted body surface S_w is displaced and rotated with respect to the mean wetted surface S_o, we can expand the fluid pressure p on S_o by means of a Taylor series as

$$(p)_{S_w} = (p + \vec{\alpha} \bullet \nabla p + \cdots)_{S_o} \qquad \text{on } S_w, S_o \qquad (6.5)$$

where the vector $\vec{\alpha}$ is the local displacement of a point on S_w due to translational and rotational motions with respect to S_o. Under the usual assumptions on linearisation, the perturbation expansion of the total velocity potential Φ is

$$\Phi(\vec{x}; t) = \bar{\Phi}(\vec{x}) + \varepsilon\tilde{\Phi}^{(1)} + \varepsilon^2\tilde{\Phi}^{(2)} + \cdots \qquad (6.6)$$

The velocity potential $\bar{\Phi}(\vec{x})$ and $\tilde{\Phi}(\vec{x}; t)$ are the steady and unsteady parts respectively. The steady potential $\bar{\Phi}(\vec{x})$ is obtained in the Neumann-Kelvin problem in which the kinematic condition on the body is satisfied exactly.

Substituting equations (6.4) and (6.6) into (6.5) and retaining the expansion up to $O(\varepsilon)$, we have

$$\begin{aligned} p(\vec{x}; t) = -\rho\{ & \tfrac{1}{2}(\vec{W} \bullet \vec{W} - U^2) + (gz + g\vec{\alpha} \bullet \vec{k}) \\ & + \varepsilon[\tilde{\Phi}_t^{(1)} + \vec{W} \bullet \nabla\tilde{\Phi}^{(1)} + \tfrac{1}{2}\vec{\alpha} \bullet \nabla(\vec{W} \bullet \vec{W})]\} \\ & + O(\varepsilon^2) \qquad \text{on } S_w, S_o \end{aligned} \qquad (6.7)$$

The first bracket term on the right hand side of equation (6.7) is the steady pressure on the body due to the steady velocity field $\vec{W}$. The second bracket term is contributed from the hydrostatic pressure and its fluctuation. The last term arises from the action of incident waves and the first-order hydrodynamic pressures on the oscillatory body. It is apparent that the interaction between the steady waves and the unsteady waves appears in the first-order hydrodynamic pressure.

The three components of forces and the three components of moments on the body can be obtained by integrating the fluid pressure over the body surface S_w in the form

$$F_j = -\iint_{S_\bullet} p\, n_j ds$$

$$= -\iint_{S_\bullet} p\, n_j ds - \iint_{\delta S_\bullet} p\, n_j ds \qquad j = 1,2,...6 \qquad (6.8)$$

where n_j is the generalised direction cosine. The integration over the mean wetted body surface S_o is carried out up to z=0 which is equivalent to $z = \vec{\alpha} \bullet \vec{k}$ on the instantaneous surface S_w. The oscillatory part δS_o is the part of the exact surface S_w between $z = \vec{\alpha} \bullet \vec{k}$ and $z=\zeta$. Making use of equations (6.7) and (6.8) and applying the mean-value theorem, we obtain

$$F_j = \tfrac{1}{2}\rho \iint_{S_\bullet} (\vec{W} \bullet \vec{W} - U^2)\, n_j ds + \rho g \iint_{S_\bullet} z\, n_j ds$$

$$+ \varepsilon\rho \Bigg\{ \iint_{S_\bullet} [\Phi_t^{(1)} + \vec{W} \bullet \nabla\Phi^{(1)} + g\vec{\alpha}^{(1)} \bullet \vec{k}]\, n_j ds$$

$$+ \tfrac{1}{2} \iint_{S_\bullet} [\vec{\alpha} \bullet \nabla(\vec{W} \bullet \vec{W})\, n_j + (\vec{W} \bullet \vec{W} - U^2)\, n_j^{(1)}]\, ds$$

$$+ \tfrac{1}{2} \oint_{L_o} (\vec{W} \bullet \vec{W} - U^2)(\zeta^{(1)} - \xi_3^{(1)} - y\xi_4^{(1)} + x\xi_5^{(1)})\, n_j dl' \Bigg\} \qquad (6.9)$$

The first term on the right hand side of equation (6.9) contributes to wave-making drag and dynamic lift. The second term is the hydrostatic force which balances the gravitational force, that is, the weight of the body. These two terms are time

independent and do not enter into the calculation of the unsteady forces. The second last term gives a force proportional to the unsteady displacement of the body and hence an additional buoyancy force to the hydrostatic restoring forces. This additional buoyancy force is due to the unsteady motion of the body within the steady velocity field $\vec{W}$ and is small to be negligible for oscillatory motions in waves. The last term is the first-order relative wave elevation over the steady flow field. This term is also neglected as the steady perturbation potential is small. For notational simplicity, the superscripts for the first-order will be dropped hereafter. Hence the first-order hydrodynamic forces can be written as

$$F_j = \rho g \iint_{S_\bullet} (\vec{\alpha} \bullet \vec{k})\, n_j ds + \rho \iint_{S_\bullet} [\, \Phi_t + \vec{W} \bullet \nabla\Phi \,]\, n_j ds \qquad (6.10)$$

The unsteady velocity potential can be linearly decomposed into potentials due to incident waves, diffraction waves and radiation waves under the linearisation procedure. Afterward, the first-order dynamic forces can be written as the sum of three components in the form

$$F_j = F_j^{\delta} + F_j^{W} + F_j^{R} \qquad j = 1,2,...6 \qquad (6.11)$$

where

$$F_j^{\delta} = \rho g \iint_{S_\bullet} (\vec{\alpha} \bullet \vec{k})\, n_j ds \qquad (6.12)$$

$$F_j^{W} = -\rho \iint_{S_\bullet} (i\omega - \vec{W} \bullet \nabla)(\phi_0 + \phi_7)\, e^{-i\omega t}\, n_j ds \qquad (6.13)$$

$$F_j^{R} = -\rho \sum_{k=1}^{6} \xi_k \iint_{S_\bullet} (i\omega - \vec{W} \bullet \nabla)\phi_k\, e^{-i\omega t}\, n_j ds \qquad (6.14)$$

Equations (6.12), (6.13) and (6.14) are the expressions for the hydrostatic restoring forces, wave exciting forces and hydrodynamic reactive forces respectively. For the

hydrodynamic exciting forces F_j^W and the hydrodynamic reactive forces F_j^R the integral associated with the interaction term $\vec{W}\bullet\nabla\phi$ can be simplified by means of the generalised Stoke's theorem (Brand 1957).

$$\iint_{S_\bullet}\{(\nabla\vec{f})\bullet\vec{n}-(\nabla\bullet\vec{f})\vec{n}\}\,ds=\oint_{L_\bullet}d\vec{r}\times\vec{f}$$

Putting $\vec{f}=\phi\vec{W}$, we get

$$\iint_{S_\bullet}\{(\vec{W}\bullet\vec{n})\nabla\phi+\phi(\nabla\vec{W})\bullet\vec{n}-(\vec{W}\bullet\nabla\phi)\vec{n}-\phi(\nabla\bullet\vec{W})\vec{n}\}\,ds=\oint_{L_\bullet}d\vec{r}\times\phi\vec{W}\quad(6.15)$$

By using the fact that $\vec{W}\bullet\vec{n}=0$ and $\nabla\bullet\vec{W}=0$, the foregoing equation becomes

$$\iint_{S_\bullet}\{\phi(\nabla\vec{W})\bullet\vec{n}-(\vec{W}\bullet\nabla\phi)\vec{n}\}\,ds=\oint_{L_\bullet}d\vec{r}\times\phi\vec{W}\qquad(6.16)$$

Multiplying equation (6.16) by $\vec{r}$, we have

$$\iint_{S_\bullet}\{\phi[(\nabla\vec{W})\bullet\vec{n}]\times\vec{r}-(\vec{W}\bullet\nabla\phi)\vec{n}\times\vec{r}\}\,ds=\oint_{L_\bullet}(d\vec{r}\times\phi\vec{W})\times\vec{r}\qquad(6.17)$$

After some manipulation and using $\nabla\times\vec{W}=0$, equations (6.16) and (6.17) become respectively

$$\iint_{S_\bullet}(\vec{W}\bullet\nabla\phi)\vec{n}\,ds=\iint_{S_\bullet}\phi(\vec{n}\bullet\nabla)\vec{W}ds-\oint_{L_\bullet}d\vec{r}\times\phi\vec{W}\qquad(6.18)$$

and

$$\iint_{S_\bullet}(\vec{W}\bullet\nabla\phi)\vec{r}\times\vec{n}\,ds=\iint_{S_\bullet}\phi(\vec{n}\bullet\nabla)(\vec{r}\times\vec{W})\,ds+\oint_{L_\bullet}(d\vec{r}\times\phi\vec{W})\times\vec{r}\qquad(6.19)$$

Equations (6.18) and (6.19) are identical to the theorem due to Tuck (Ogilvie & Tuck, 1969). The line integral is of higher order for most practical cases and can be ignored.

Making use of the notations n_j and m_j given in Chapter 2, we have

$$\iint_{S_\bullet} (\vec{W} \bullet \nabla\phi)\, n_j ds = -U \iint_{S_\bullet} \phi\, m_j ds \qquad (6.20)$$

6.3.1 Hydrostatic restoring forces

The hydrostatic restoring forces are defined as the fluid forces to restore the body to its static equilibrium state when the body is displaced freely from the rest position. These forces are evaluated by integrating the hydrostatic pressure due to the variation in vertical displacement. By using Gauss's theorem, the surface integral in equation (6.12) can be transformed to the volume integral in the form

$$F_j^{\delta} = \rho g \iiint_{\delta V} n_j dv = -\rho g \iint_A dA \int_0^{\varepsilon(\xi_3 + y\xi_4 - x\xi_5) + \cdots} n_j dz\, e^{-i\omega t}$$

$$= -\sum_{k=1}^{6} C_{jk}\xi_k\, e^{-i\omega t} \qquad j = 1,2,\ldots 6 \qquad (6.21)$$

The quantity C_{jk} is called the hydrostatic restoring coefficient which is a function of the body geometry only and is independent of the motion ξ_k. The indices j and k indicate the mode of the restoring force and the mode of motion respectively. When j=k, the mode of motion is in the same direction as that of the fluid reaction. Since the hydrostatic restoring forces originate from the hydrostatic pressure variation due to vertical movement $\vec{\alpha} \bullet \vec{k}$, they only act vertically. Therefore regardless of the body shape, we have

$$C_{j1} = C_{j2} = C_{j6} = 0 \qquad \text{for all j}$$

$$C_{1k} = C_{2k} = C_{6k} = 0 \qquad \text{for all k} \qquad (6.22a)$$

In the case of a ship hull with one longitudinal plane of symmetry, a motion in the

longitudinal plane cannot produce any force perpendicular to that plane :

$$C_{jk} = 0 \qquad \text{for } j = 2,4,6 \text{ and } k = 1,3,5 \qquad (6.22b)$$

The reverse is also true by the same reason :

$$C_{jk} = 0 \qquad \text{for } j = 1,3,5 \text{ and } k = 2,4,6 \qquad (6.22c)$$

After evaluation of equation (6.21), the non-zero coefficients for C_{jk} are given by

$$\begin{aligned} C_{33} &= \rho g A \\ C_{44} &= \rho g A_{xx} + M g (z_b - z_G) = \rho g V GM_T \\ C_{55} &= \rho g A_{yy} + M g (z_b - z_G) \\ C_{35} &= C_{53} = -\rho g A_y \end{aligned} \qquad (6.23)$$

where A, A_y, A_{xx} and A_{yy} are the area, the first moment and the second moments of the waterplane area at z=0 respectively. M is the mass of the body. z_b and z_G are the vertical coordinates of the centre of buoyancy and centre of gravity of the body respectively. GM_T is the transverse metacentric height and V is the volume of displacement. The last terms in C_{44} and C_{55} are the contributions due to the body weight and are not the restoring moments. For static equilibrium they are incorporated in the restoring coefficient. If the origin o is at the centre of flotation, C_{35} and C_{53} are identical to zero, and C_{55} becomes equal to $\rho g V GM_L$ where GM_L is the longitudinal metacentric height.

6.3.2 Hydrodynamic exciting forces

The evaluation of wave exciting forces can be performed in three different ways : (i) by using the relative motion concept (Korvin-Kroukovsky 1955), (ii) by applying

the Haskind-Newman relationship (Newman 1965) and (iii) by calculating the diffraction potential directly. Through approaches (i) and (ii), the wave exciting forces acting on a captive ship in waves can be expressed in terms of motion induced forces, that is, added mass and damping coefficients, in combination with the incident wave property.

The relative-motion concept was used in the intuitive strip theory initiated by Korvin-Kroukovsky (1955). This concept is based on an assumption that the local exciting force at each section could be expressed in the same form as the pressure force of the radiation problem, but with the ship's velocity and acceleration replaced by the relative motions of the incident wave, at a suitable mean depth. The pressure force under the relative motion assumption is expressed in terms of added mass and damping coefficients, evaluated at the frequency of encounter ω. Due to the assumption being based on two-dimensional theory, the relative motion concept is not adopted in the three-dimensional diffraction problem.

The hydrodynamic exciting forces F_j^W are the result of the pressure associated with the diffraction potential due to the incident waves per unit amplitude and can be expressed in the form

$$F_j^W = -\rho \iint_{S_\bullet} (i\omega n_j + U m_j)(\phi_0 + \phi_7)\, ds\, e^{-i\omega t} \qquad j = 1,2,...6 \qquad (6.24)$$

The expression given by equation (6.24) follows from equations (6.13) and (6.20). Direct use of equation (6.24) requires the solution of the diffraction potential ϕ_7. An alternative expression for the exciting force F_j^W without solving the diffraction problem can be derived by using the body boundary condition of the reverse flow radiation problem with negative forward speed :

$$\frac{\partial \phi_j^-}{\partial n} = -i\omega n_j - U m_j \qquad j = 1,2,...6 \qquad (6.25)$$

where ϕ_j^- is the reverse flow radiation potential. Substituting equation (6.25) into (6.24) yields

$$F_j^W = \rho \iint_{S_\bullet} \frac{\partial \phi_j^-}{\partial n} (\phi_0 + \phi_7)\, ds\, e^{-i\omega t} \qquad (6.26)$$

This reverse flow force expression (6.26) allows the application of Green's second identity for the velocity potential ϕ_j^- and ϕ_7 which satisfy the Laplace's equation and the prescribed boundary conditions. After employing Green's second identity and the diffraction body boundary condition, we have

$$F_j^W = \rho \iint_{S_\bullet} (\phi_0 \frac{\partial \phi_j^-}{\partial n} - \phi_j^- \frac{\partial \phi_0}{\partial n})\, ds\, e^{-i\omega t} \qquad (6.27)$$

Equation (6.27) is known as the Haskind-Newman relationship (Newman 1965). For the zero speed case the superscripts (–) are superfluous and the expression (6.27) reduces to the Haskind identity. By using the Haskind-Newman relationship the total exciting force is expressed in terms of the solution of the reverse-flow radiation problem. Although the representation for F_j^W given by equation (6.27) avoids the solution of the diffraction problem, it involves the evaluation of the velocity potential ϕ_j^- for the reverse-flow problem. If the forward speed is low, the velocity potentials ϕ_j^- are readily obtained from the radiation wave potential ϕ_j. Otherwise the reverse-flow problem must be solved. A drawback to using the Haskind-Newman relationship is that the integral nature of equation (6.27) does not permit the determination of the fluid pressure explicitly.

The exciting force given by equation (6.24) can be decomposed into two components as

$$F_j^W = K_j + D_j \qquad j = 1,2,...6 \qquad (6.28)$$

where $$K_j = -\rho \iint_{S_\bullet} (i\omega n_j + U m_j)\,\phi_0\, ds\, e^{-i\omega t} \qquad (6.29a)$$

$$D_j = -\rho \iint_{S_\bullet} (i\omega n_j + U m_j)\,\phi_7\, ds\, e^{-i\omega t} \qquad (6.29b)$$

The first component K_j is called the incident wave force while the second component D_j is called the diffraction force. Since the steady flow field interacts with the unsteady flow field, the incident wave force is no longer independent of the forward speed. Neglecting the interaction effect and making $\vec{W} = -U\vec{i}$, the only effect of the gradient operator $\vec{W} \bullet \vec{\nabla}$ in equation (6.13) is on the incident wave potential ϕ_0, with the result that $(i\omega - \vec{W} \bullet \nabla) = i\omega_o$ and the incident wave force becomes the Froude-Krylov force in the form

$$K_j = -\rho i\omega_o \iint_{S_\bullet} \phi_0 n_j ds\, e^{-i\omega t} \qquad (6.30)$$

It is noted that neglecting the factors m_j in equation (6.29a) would lead to an incorrect result that differs from equation (6.30) by a factor ω/ω_o. This is a consequence of the slender body assumption that $m_j = 0$ for $j = 1,2,3,4$ and $m_5 = n_3$ and $m_6 = -n_2$.

The Froude-Krylov force given by equation (6.30) involves the incident wave potential only and so it corresponds to the force experienced by the body when the incident wave trains pass through it unaffected. Therefore the Froude-Krylov force is significant in the long wave regime or for a thin body in head waves where scattering waves are little. On the other hand, the diffraction force given by equation (6.29b) becomes important in the short wave regime or for a large body with a large frontal area exposed to the incident waves.

6.3.3 Hydrodynamic reactive forces

The hydrodynamic reactive forces in the j-th direction resulting from the motion ξ_k are obtained by

$$F_{jk}^{R} = -\rho \iint_{S_\bullet} (i\omega n_j + U m_j)\phi_k \, ds \, \xi_k e^{-i\omega t} \qquad j,k = 1,2...6 \qquad (6.31)$$

The indices j and k indicate the direction of the fluid reaction force and the mode of motion respectively. Due to the presence of the free surface a phase difference with respect to the body velocity will develop for the hydrodynamic reactive forces. In consequence, the reactive force can be thought of having one component in phase with the body acceleration and another in phase with the body velocity, that is

$$\begin{aligned} F_{jk}^{R} &= -(A_{jk}\ddot{\xi}_k + B_{jk}\dot{\xi}_k) \\ &= (\omega^2 A_{jk} + i\,\omega\, B_{jk})\,\xi_k\, e^{-i\omega t} \end{aligned} \qquad (6.32)$$

The coefficients A_{jk} and B_{jk} are real quantities. They are functions of the body shape, the forward speed and the frequency of motion. As A_{jk} is associated with the body acceleration, it is normally called "the added mass coefficient". The term added mass stems from the apparent increase in inertia of the body which moves in a fluid and spends some kinetic energy to accelerates the surrounding fluid. The quantity B_{jk} is related to the velocity of the motion in the k-th mode and is called the damping coefficient as it represents a measure of energy dissipation through the radiated waves. Upon equating the real and imaginary parts of equations (6.31) and (6.32), the added mass and damping coefficients are given by

$$A_{jk} = -\frac{\rho}{\omega^2}\,\mathrm{Re} \iint_{S_\bullet} (i\omega n_j + U m_j)\phi_k \, ds \qquad (6.33a)$$

$$B_{jk} = -\frac{\rho}{\omega}\,\mathrm{Im} \iint_{S_\bullet} (i\omega n_j + U m_j)\phi_k \, ds \qquad (6.33b)$$

For a body with one longitudinal plane of symmetry, these two coefficients have the same properties as the hydrostatic restoring coefficients C_{jk} given by equations (6.22a,b) as

$$A_{jk} = B_{jk} = 0 \qquad \text{for } j = 2,4,6 \text{ and } k = 1,3,5 \qquad (6.34a)$$

and

$$A_{jk} = B_{jk} = 0 \qquad \text{for } j = 1,3,5 \text{ and } k = 2,4,6 \qquad (6.34b)$$

For the zero speed case, the speed related factors $m_j = 0$ for all j's and the coupled hydrodynamic coefficients A_{jk} and B_{jk} always satisfy the symmetry relationships

$$A_{jk} = A_{kj} \qquad \text{and} \qquad B_{jk} = B_{kj} \qquad \text{for } U = 0 \qquad (6.35)$$

This symmetry property between the cross-coupling coefficients is known as the Timman-Newman symmetry relationships which can be readily proved using Green's second identity for two velocity potential ϕ_j and ϕ_k, that is,

$$\iint_{S_\bullet} \phi_k \frac{\partial \phi_j}{\partial n} ds = \iint_{S_\bullet} \phi_j \frac{\partial \phi_k}{\partial n} ds$$

Applying the body boundary conditions for the zero speed radiation problem, it follows that

$$i\omega \iint_{S_\bullet} \phi_k n_j ds = i\omega \iint_{S_\bullet} \phi_j n_k ds$$

The foregoing expression proves the symmetry relation that $A_{jk} = A_{kj}$ and $B_{jk} = B_{kj}$ for the zero speed problem.

For the forward speed problem if the body has both longitudinal and transverse symmetry planes, Timman & Newman (1962) used the reverse-flow condition to show that $B_{jk}+B_{kj} = 0$ for all cross-coupling coefficients except $B_{15}+B_{51}$ and $B_{24}+B_{42}$, where $B_{jk}-B_{kj} = 0$.

6.4 Equations of motion

The various components of the hydrodynamic forces have been discussed. In the following the equations of motion for a free oscillating body in waves are derived by equating the external forces to the inertia forces which are associated with the acceleration of the body.

The six components of the inertia force due to the body's acceleration in rigid body motions are

$$F_j = \sum_{k=1}^{6} M_{jk} \ddot{\xi}_k \qquad j = 1,2,...6 \qquad (6.36)$$

where M_{jk} is the body-inertia coefficient for the j-th force induced by the k-th mode of motion. The body-inertia coefficient can be obtained by Newton's second law of motion :

$$\vec{F} = \frac{d}{dt} \iiint_V \rho_B (\vec{v} + \vec{\omega} \times \vec{r})\, dv \qquad (6.37a)$$

and from the conservation of angular momentum :

$$\vec{M} = \frac{d}{dt} \iiint_V \rho_B \vec{r} \times (\vec{v} + \vec{\omega} \times \vec{r})\, dv \qquad (6.37b)$$

The quantity ρ_B is the body density. The velocity vector in equations (6.37a,b) can be expressed in the form

$$\vec{v} + \vec{\omega} \times \vec{r} = \sum_{k=1}^{6} v_k \vec{e}_k \qquad (6.38)$$

where $(\vec{e}_1, \vec{e}_2, \vec{e}_3) = (\vec{i}, \vec{j}, \vec{k})$ (6.38a)

$$(\vec{e}_4, \vec{e}_5, \vec{e}_6) = (\vec{i}, \vec{j}, \vec{k}) \times \vec{r} \qquad (6.38b)$$

Substituting equations (6.38a,b) into (6.37a,b), we have

$$F_j = \sum_{k=1}^{6} \dot{v}_j \iiint_V \rho_B \vec{e}_j \bullet \vec{e}_k dv \qquad j = 1,2,3 \qquad (6.39a)$$

$$F_j = \sum_{k=1}^{6} \dot{v}_j \iiint_V \rho_B \vec{e}_{j-3} \bullet \vec{r} \times \vec{e}_k dv \qquad j = 4,5,6 \qquad (6.39b)$$

Equation (6.39b) is analogous to equation (6.39a) such that

$$F_j = \sum_{k=1}^{6} \dot{v}_j \iiint_V \rho_B \vec{e}_j \bullet \vec{e}_k dv \qquad j = 1,2...6 \qquad (6.39c)$$

By comparison of equations (6.36) and (6.39c) one can deduce that the body-inertia coefficient can be defined as

$$M_{jk} = \iiint_V \rho_B \vec{e}_j \bullet \vec{e}_k dv \qquad (6.40)$$

If the coordinates of the centre of gravity of the body is (x_G, y_G, z_G), the matrix of the body-inertia coefficients given by equation (6.40) can be written as

$$[M] = \begin{bmatrix} M & 0 & 0 & 0 & Mz_G & -My_G \\ 0 & M & 0 & -Mz_G & 0 & Mx_G \\ 0 & 0 & M & My_G & -Mx_G & 0 \\ 0 & -Mz_G & My_G & I_{44} & I_{45} & I_{46} \\ Mz_G & 0 & -Mx_G & I_{54} & I_{55} & I_{56} \\ -My_G & Mx_G & 0 & I_{64} & I_{65} & I_{66} \end{bmatrix} \qquad (6.41)$$

in which the moments of the inertia of the body about the origin are defined by

$$I_{jk} = \iiint_V \rho_B [\, r_j^2 \delta_{jk} - (1 - \delta_{jk}) x_{j-3} x_{k-3} \,] dv \qquad j, k = 4,5,6 \qquad (6.42)$$

where δ_{jk} is the Kronecker delta function such the $\delta_{jk} = 1$ if $j = k$ and $\delta_{jk} = 0$ if $j \neq k$.

r_j is the distance of the mass element to the corresponding axis of rotation about the origin and (x_1, x_2, x_3) is (x, y, z). For the body with one longitudinal plane of symmetry, $y_G = 0$ and $I_{45} = I_{54} = I_{56} = I_{65} = 0$.

Equating the inertia force given by equation (6.36) to the hydrodynamic forces given by equation (6.11), we obtain the equations of six rigid body motions in the frequency domain as

$$\sum_{k=1}^{6} \{ (M_{jk} + A_{jk}) \ddot{\xi}_k + B_{jk} \dot{\xi}_k + C_{jk} \xi_k \} = F_j^W$$

For a regular harmonic wave train the foregoing equation can be written as

$$\sum_{k=1}^{6} [-\omega^2 (M_{jk} + A_{jk}) - i\omega B_{jk} + C_{jk}] \xi_k = F_j^W \qquad j = 1,2...6 \qquad (6.43)$$

These are six simultaneous linear equations, which can be solved for the body motion of amplitude ξ_k by standard numerical techniques. The presence of the free surface renders the amplitude ξ_k a complex quantity that exhibits a phase difference between the incidence wave and the motion. The complex amplitude ξ_k of the body motion is the k-th mode in response to the incident wave of unit amplitude is known as the transfer function or the response amplitude operator.

The motions, because of the longitudinal plane of symmetry of the ship hull and the linearisation of the problem, can generally be partitioned into two groups. One is the

linear coupled surge-heave-pitch equation and the other is the linear coupled sway-roll-yaw. These two groups are entirely independent from each other. Once the added masses A_{jk}, the damping coefficients B_{jk} and the wave exciting forces F_j^W are determined by direct integration of the corresponding radiation potential and the diffraction potential due to the incident wave, the motion response amplitudes in regular waves are readily obtained. Hence the unsteady velocity potential $\tilde{\Phi}(\vec{x}; t)$ is known. This enables us to find any physical quantities derived from the potential $\tilde{\Phi}(\vec{x}; t)$, such as pressure and the free surface elevation at any point in the fluid domain.

6.5 Numerical computations

The formulation of the first-order hydrodynamic forces on a moving ship and the resulting motion responses in regular waves have been described in the previous sections. Under the framework of linearised potential flow theory and the assumption of small steady disturbances on the free surface and around the wetted body surface, we only need to find the radiated wave potentials and the diffracted wave potential. The use of Green functions reduces the determination of the potential to the solution of a surface integral equation which is supplemented by a free surface line integral to account for the speed effects on the free surface. The procedure of solving this integral equation has been described in the previous Chapters. Now we have tools to carry out numerical computations for some ship shaped bodies.

Numerical calculations have been performed to predict the hydrodynamic loads on a fully submerged ellipsoid, a semi-submerged ellipsoid, a Series-60 ship and a 200,000 dwt tanker. Those numerical results are compared with experimental data wherever possible. The presentations for the hydrodynamic coefficients, the wave exciting forces and the response amplitude operators are in the following non-dimensional forms :

Added mass coefficient				
a_{jk}	$A_{jk} / \rho V$	...	$j, k = 1, 2, 3$	
	$A_{jk} / \rho VL$	...	$j = 1, 2, 3$	$k = 4, 5, 6$
		...	$k = 1, 2, 3$	$j = 4, 5, 6$
	$A_{jk} / \rho VL^2$	...	$j, k = 4, 5, 6$	
Damping coefficient				
b_{jk}	$B_{jk} / \rho V\sqrt{(g/L)}$	...	$j, k = 1, 2, 3$	
	$B_{jk} / \rho VL\sqrt{(g/L)}$	...	$j = 1, 2, 3$	$k = 4, 5, 6$
		...	$k = 1, 2, 3$	$j = 4, 5, 6$
	$B_{jk} / \rho VL^2\sqrt{(g/L)}$	...	$j, k = 4, 5, 6$	
Wave exciting forces				
$\lvert F'_j \rvert$	$\lvert F_j \rvert L / \rho g \zeta_o V$	...	$j = 1, 2, 3$	
	$\lvert F_j \rvert / \rho g \zeta_o V$	...	$j = 4, 5, 6$	
Response amplitude operator				
$\lvert \xi'_k \rvert$	$\lvert \xi_k \rvert / \zeta_o$	...	$k = 1, 2, 3$	
	$\lvert \xi_k \rvert / \zeta_o \upsilon$	...	$k = 4, 5, 6$	

Table 6.1 : Non-dimensional forms of hydrodynamic forces and ship responses

A phase angle of the wave exciting force is positive if the force leads the wave elevation at the origin of the coordinates. A positive phase angle of the motion response indicates that a motion reaches its positive maximum value before the crest of the undisturbed incoming regular wave passes the origin.

6.5.1 A fully submerged ellipsoid

In order to provide a validation of the three-dimensional translating pulsating source modelling technique, calculations are made for a fully submerged ellipsoid whose cross coupling hydrodynamic coefficients have to satisfy the well known

Timman-Newman relationships (Timman & Newman 1962). The ellipsoid has a length to beam ratio of 7, and a beam to depth ratio of 2. The centreline of the ellipsoid is twice the body depth below the free surface. The surface of the ellipsoid was represented by a total of 200 panel elements where the half body surface was divided into 20 elements in length wise direction and 5 elements in depth direction as shown in Fig.6.2.

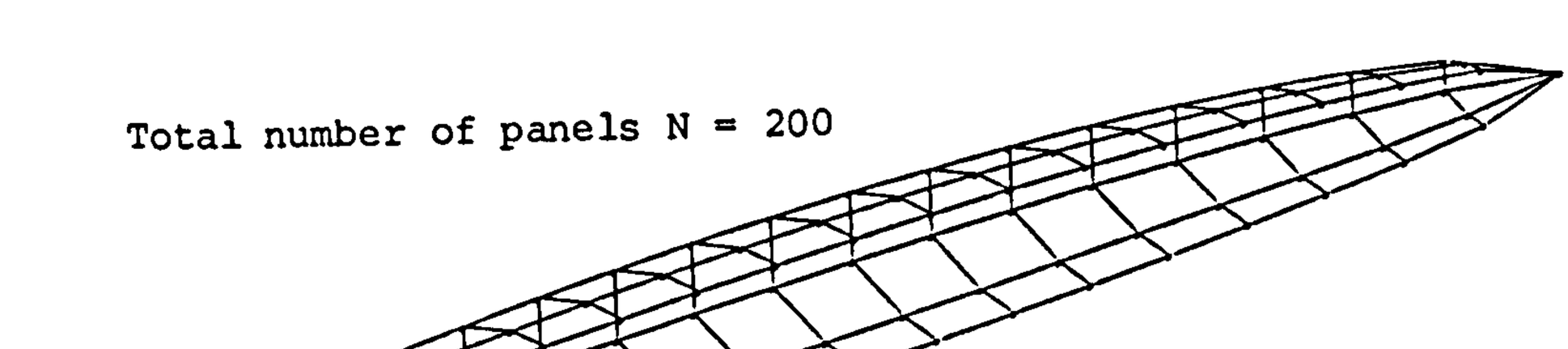

Fig.6.2 Surface Discretisation of a Submerged Ellipsoid
(L/B=7, B/D=2, h/D=2)

6.5.1-1 Hydrodynamic coefficients

Numerical computations have been carried out for four Froude numbers of F_n=0.0, 0.1, 0.2 and 0.3 at infinite water depth with the non-dimensional frequency of encounter $f = \omega\sqrt{(L/g)}$ ranging from 0.0 to 5.5. The dimensionless coefficients for added mass and damping in six rigid modes of motion are illustrated in Fig.6.3 and Fig.6.4 respectively. The coupled added mass and damping coefficients are shown in Fig.6.5 and Fig.6.6 respectively. These coefficients, being function of oscillating frequency, have strong Froude number dependence within the frequency range considered. The calculated coupled hydrodynamic coefficients satisfy the Timman-Newman relationships very well (Timman & Newman 1962). In the translational modes and roll mode and their coupling modes the results obtained from the three-

dimensional translating pulsating source modelling show the coefficients to have a strong speed dependence, especially in surge, which cannot be simulated by strip theory or three-dimensional oscillating source modelling because the linearised free surface condition demonstrates the speed term $U\partial/\partial x$. The hydrodynamic coefficients in pitch and yaw are more speed dependent than the other modes since the non-zero m_5 and m_6 terms in the linearised body boundary condition are proportional to the angle of attack due to pitch and yaw motions respectively. The coupled damping coefficients associated with heave-pitch, sway-yaw and roll-yaw show similar trends in that these coefficients are proportional to the Froude number and slowly vary with the frequency of oscillation.

Generally speaking, speed effects become less significant as the frequency of encounter is progressively increased except the coupling damping coefficients associated with heave-pitch, sway-yaw and roll-yaw. The influence of speed on the calculations of unsteady hydrodynamic forces on a moving body comes from the boundary conditions on the free surface and the wetted body surface. For a thin, slender or fully submerged body the steady disturbance flow is so small that the linearised body boundary condition leads to the terms $m_j=0$ for $j=1,2,3,4$ and $m_5=n_3$ and $m_6=-n_2$. Eventually the linearised body boundary condition becomes frequency dependent in the translational and roll modes of motion. For high frequencies the m_5 and m_6 terms in pitch and yaw modes are less important and thus the body boundary condition in these two modes are frequency dominant in the short wave regime. On the linearised free surface condition the frequency of oscillation ω becomes more dominant than the speed term $U\partial/\partial x$ in the high frequency regime. In fact most strip theory calculations and three-dimensional oscillating source modelling for non-zero speed cases neglect the speed terms in the linearised free surface condition by assuming that the frequency of encounter ω is sufficiently high so that $U\partial/\partial x << \omega$. As illustrated in Fig.6.3 to Fig.6.6, the four curves representing hydrodynamic coefficients for different speeds merge into a single curve at high frequency except the cross coupled damping coefficients for heave-pitch, sway-yaw and roll-yaw where they are slowly varying in the frequency range considered.

It is especially interesting to note that the speed dependent hydrodynamic coefficients in the symmetrical modes of surge, heave, pitch and their coupling motions become infinite at the critical point $\tau=\omega U/g=1/4$ but the coefficients in the anti-symmetrical modes of sway, roll, yaw and their coupling motions are not singular at this point and are bounded for all speeds and frequencies. Similar phenomena were found by Newman (1961), Inglis & Price (1981a) and Lau (1987). The infinity at the critical point is identical to the mathematical singularity in the translating pulsating source function at $\tau=1/4$. The singular behaviour were first recognised by Havelock (1958). The behaviour at the critical point clearly arises from a special case of resonance. Naturally these phenomena were also clearly noticed by the experimental results of Golovato (Havelock 1958) and Tannaka & Kitagawa (1962). The reason for well-behaved hydrodynamic coefficients at the critical point in the anti-symmetrical modes of motion may be due to the cancellation effects in anti-symmetrical flow across the body. Thus there is a fundamental difference between the three modes of oscillation in the vertical x-z plane, which have a singularity at $\tau=1/4$, and the three modes of oscillation perpendicular to this plane, which are well behaved. These characteristics cannot be modelled by strip theory and three-dimensional oscillating source modelling with simple speed correction since they omit the transverse wave field swept downstream. The wave propagation due to a translating pulsating source shows that there are four wave trains, one in advance and three to the rear in the subcritical regime $\tau<1/4$. In the supercritical regime $\tau>1/4$ all waves are swept downstream. At the critical point $\tau=1/4$ one standing wave is formed and moves in the same direction and speed as the source.

6.5.2 A semi-submerged ellipsoid

The numerical study of the fully submerged ellipsoid in the previous section supports the hypotheses that the disturbance of the free surface due to the steady flow is small because the depth of submergence is sufficiently large that the waves are small but not so large that the free surface may be neglected and the fluid considered as infinite.

In order to study to what extent the free surface effects influence the calculations of the hydrodynamic coefficients, numerical computations for the motion coefficients of a semi-submerged ellipsoid have been carried out. The ellipsoid has a length to beam ratio of 8 and semi-circular cross sections. The half submerged surface was modelled by 20 elements in longitudinal direction and 5 elements in the transverse direction making a grand total of 200 elements as shown in Fig.6.7.

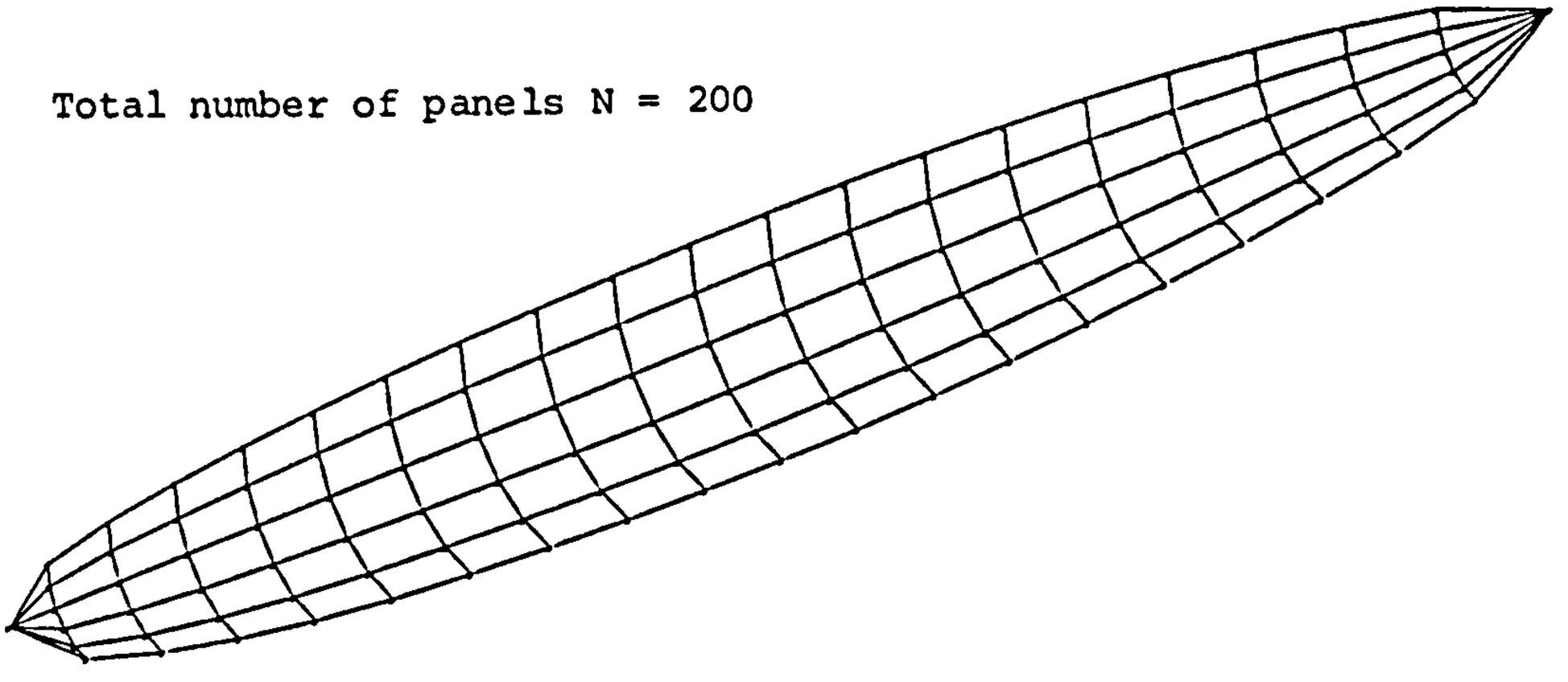

Fig.6.7 Surface Discretisation of a Floating Ellipsoid (L/B=8, B/T=2)

6.5.2-1 Hydrodynamic coefficients

The ellipsoid floating at infinite water depth with forward speeds is investigated for Froude numbers of F_n=0.0 and 0.3 with the non-dimensional frequency f ranging from 0.0 to 5.5. Figs.6.8 and 6.9 illustrate the principal added mass and damping coefficients respectively. The coupled added mass and damping coefficients in sway-yaw mode are also given in Figs.6.8 and 6.9 respectively. The cross coupled added mass and damping coefficients in the vertical symmetrical modes of motion are shown in Fig.6.10. Because of the circular cross sections of the ellipsoid, there are no contributions due to roll mode of motion. Therefore the roll added inertia and the roll damping coefficients as well as the other cross coupled coefficients induced by roll motion are identical to zero no matter what the forward speed is. For the zero speed case the present three-dimensional calculations show good agreement with the numerical results of Kim (1965) who used different numerical procedures to solve the Green function integral equation.

The hydrodynamic coefficients of the free floating ellipsoid demonstrate the strong speed dependence similar to those of the fully submerged ellipsoid. The singular behaviour of the hydrodynamic coefficients of the symmetrical modes of motion at the critical point τ=1/4 is also illustrated by the floating ellipsoid. At the critical point the motion coefficients of the anti-symmetrical modes for the floating ellipsoid are also bounded. When the free floating ellipsoid and the fully submerged ellipsoid geometries investigated in this study are compared, the former is much more slender than the latter. Nevertheless, the hydrodynamic coefficients of the floating ellipsoid at zero speed and for the forward speed cases indicate large humps and hollows compared to those of the fully submerged ellipsoid. This is because of the larger free surface disturbance created by the floating object than by the fully submerged body. As expected the hydrodynamic coefficients of a body would be independent of frequency if the body is deeply submerged. The added mass coefficients of the fully submerged ellipsoid approach asymptotic values which are independent of Froude number at high frequency earlier than those of the floating ellipsoid in the frequency range considered. Meanwhile the damping coefficients of the fully submerged ellipsoid approach small values at high frequencies but those of the floating ellipsoid remain at large values in the high frequency region. These phenomena indicate that more radiated wave energy is dissipated from the floating body over the free surface.

Concerning the cross coupled coefficients the calculations for the floating ellipsoid agree well with the Timman-Newman's symmetry relationships for the zero speed case but they do not agree so well for Froude number of F_n=0.3 especially in the cross coupled surge-heave mode. There are two reasons for this which can be explained by referring to the Timman-Newman relationships for a symmetrical body with forward speed. The hypotheses of Timman and Newman are built on the small disturbances of the free surface so that the Green function is reciprocal if the direction of the streaming flow is reversed. For a deeply submerged symmetrical body, the Timman-Newman relationships are valid and therefore the cross coupled hydrodynamic coefficients of the fully submerged ellipsoid mentioned in section 6.5.1 satisfy these relationships very well. On the other hand the Timman-Newman relationships are questionable for a

floating symmetrical body with forward speed if the body is not thin and slender. However the floating ellipsoid investigated in this study is slender. Therefore the discrepancies may be due to errors in the discretisation of the body surface. Nevertheless, it is noted that the numbers of panel elements used for the floating ellipsoid and the fully submerged ellipsoid are the same but the floating ellipsoid is only half of the whole ellipsoid. Thus the discretisation of the floating ellipsoid is much finer than that of the fully submerged ellipsoid. Hence the discrepancies should be attributed to other sources of error. In fact there are some numerical difficulties in the evaluation of the free surface line integral which exists in the translating pulsating source modelling for a free floating body while these difficulties do not exist for a fully submerged body. The numerical difficulties arise from the weak singularities along the free surface contour. In order to calculate the exact contribution of the free surface line integral the weak singularities must be evaluated on the free surface contour. Unforturnately, the sources are distributed at the centroids of the panel elements. The errors caused by the distribution of the sources can be reduced by using more panels. However an increase in the number of panels causes a significant increase in computing time which is prohibitive in the present study.

6.5.3 A Series-60 ship

In order to evaluate how well the three-dimensional source distribution technique can predict the hydrodynamic coefficients, wave exciting forces and the resulting motion responses of a realistic ship in regular waves, a Series-60 ship of block coefficient C_B=0.7 and length 140 m was used in the investigation for zero speed and Froude number F_n=0.2, for which extensive experimental results are available for comparison. The principal particulars of the Series-60 ship is shown in Table 6.2 and the hull form is discretised into a total of 154 quadrilateral and triangular panels as shown in Fig.6.11.

Total number of panels N = 154

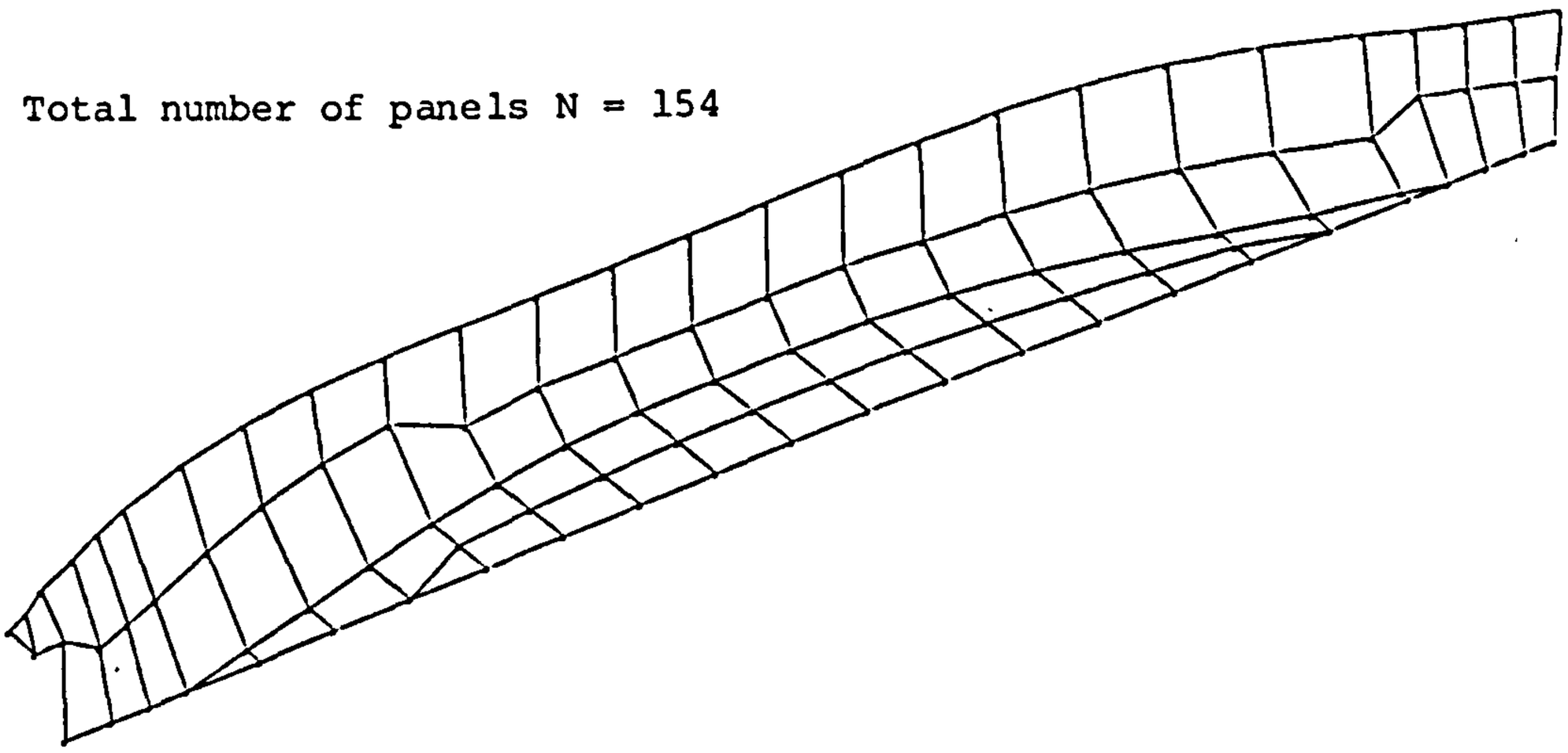

Fig.6.11 Surface Discretisation of a Series-60 Ship C_B=0.7

Model number	4212W
LBP. L (m)	140.00
Breadth B (m)	20.00
Draught D (m)	8.00
Displacement (m^3)	15680.00
C_B	0.7
C_w	0.785
LCB (m)	0.7F
GM_T (m)	1.12
L/B	7.0
B/D	2.5
k_{xx} (m)	8.1
k_{yy} (m)	35.0
k_{zz} (m)	35.0

Table 6.2 : Particulars of a Series 60 Ship (Todd 1953)

The most comprehensive experiments were conducted by Gerritsma & Beukelman (1964) and Vugts (1971) for Series-60 models in deep water. The models used were of a segmented type as well as the whole model. The experimental measurements made by Gerritsma and Beukelman were only for the vertical modes of motion whereas Vugts carried out experiments in both the vertical and horizontal modes. Extensive measurements of the hydrodynamic coefficients associated with lateral motions were performed by Van Leeuwen (1964) for the model with no rudder and with a rudder fixed at zero angle of deflection. For the motion coefficients of the Series-60 model with forward speeds in shallow water vertical heave and pitch motions as well as horizontal sway and yaw motions were conducted by Beukelman & Gerritsma (1982). All experimental data presented are scaled up to the ship size by means of the Froude law of similarity and compared with the present numerical calculations. Forward speed computations for the Series-60 ship in deep water are presented for both three-dimensional translating pulsating source modelling and three-dimensional oscillating source modelling with simple speed correction on body boundary condition. Due to the limitation of computing time in the present study, the Series-60 ship with forward speed of F_n=0.2 at water depth to draught ratio of 1.2 (H/D=1.2) is only modelled by the three-dimensional oscillating source distribution.

6.5.3-1 Zero speed hydrodynamic coefficients

Zero speed added mass and damping coefficients in six rigid body modes of motion are shown in Figs.6.12 and 6.13 respectively. As can be seen from these figures the present calculations of added masses in heave and pitch agree very well with the experimental data over most of the frequency region. There are two peculiar points in the experimental pitch inertia results around the low frequency region presented by Vugts, which deviate from the theoretical results. Their counter parts which are heave and pitch damping coefficients respectively show excellent agreement between the calculated and the measured values. Such good agreement in heave and pitch motion

coefficients were not found by Vugts (1971) who used the strip theory, especially in the low frequency region. This reflects the importance of the three-dimensional effects arising from the fluid interactions between the sections of the ship. These interactions are expected to be most significant at long wavelengths as the relative distance between sections with respect to the wavelength decreases.

The predictions of the principal hydrodynamic coefficients in the symmetrical modes of motion are excellent but for anti-symmetrical modes the predictions are not very good. The predicted added mass coefficients in yaw motions show fairly good agreement with the measurements. The calculated damping coefficients for the sway mode agree fairly well with the measurements and show the same pattern of variation in the frequency domain as the measurements but the magnitudes of the calculated values start to deviate from the measurements when the dimensionless frequencies become higher than 2.5. In this region the predicted values are 25% lower than the measured ones. The agreement between the measured and the calculated roll damping coefficients is worse than that for sway. The calculated roll damping coefficients are much too small. The poor roll damping predictions are expected due to the non-linear effects in large roll motions and viscosity effects. In view of the experimental data for anti-symmetrical modes of motion some information such as sway added mass, roll added mass and yaw damping coefficients were not presented by Vugts (1971). It is suspected that these measurements were not sufficiently reliable and therefore they were not presented. Hence it was not possible to check these coefficients in order to investigate why there was poor agreement in their counter parts. However, the experimental results for a 200,000 dwt tanker to be discussed in the next section do validate the three-dimensional source technique to predict the zero speed hydrodynamic coefficients in six rigid body modes of motion.

Fig.6.14 and Fig.6.15 show the zero speed coupling added mass and damping coefficients respectively. It is evident that the calculated hydrodynamic coupling coefficients agree very well with Timman-Newman's symmetry relationship for the zero speed case. Theoretically the calculated values of coupling coefficients must be

equal so that $a_{jk}=a_{kj}$ and $b_{jk}=b_{kj}$. However errors due to the numerical approximations and body discretisation are inevitable and therefore some discrepancies would be expected in the calculations of the coupling coefficients, which are acceptable. If the number of panel elements is increased, the errors induced in the coupling coefficients will be reduced. In comparison with the experimental results the predicted heave-pitch added mass coefficients show good agreement except in the low frequency region while the calculated damping coefficients in the heave-pitch mode do not correlate well with the measurements. Nevertheless, in examining two independent measurements it is obvious that the measured values obtained from Gerritsma & Beukelman (1964) and Vugts (1971) were also very different and scatter exists in the low frequency range. It seems that the force measurements due to other modes of motion in the oscillation tests are difficult. The same conclusion can be drawn for the discrepancies between the calculated and the measured results in the sway-yaw mode.

6.5.3-2 Zero speed wave exciting forces

The zero speed wave exciting forces and moments acting on the Series-60 ship at infinite water depth in oblique waves with angle of attack $\beta=30^\circ$ and 120° and in head waves ($\beta=180^\circ$) are presented in Fig.6.16 through Fig.6.18. In general, the amplitudes and the phase angles of the predicted heave exciting forces and pitch exciting moments agree very well with the experimental results. Such good correlation between the calculated and the measured values can also be found for sway exciting forces and yaw exciting moments except roll moments. Despite the predicted amplitudes of the roll exciting moments deviate from the measurements considerably their corresponding phase angles are correlated well to each other. The discrepancies may be due to errors in the transformation of the measured roll moments from the centre of gravity to the origin of coordinates for comparison. The calculated and measured values of the phase angles for yaw moments are approximately 180° out of phase against each other. Since the wave reference could not be obtained simultaneously with the yaw moment in Vugts's experiments, all phase relations were measured with respect to the horizontal forces.

Therefore errors in the yaw phase angles might have occurred in the transformation of force reference system to wave reference system.

Fig.6.19a and Fig.6.19b demonstrate the zero speed wave exciting forces and moments acting on the Series-60 ship in deep water for various angles of wave incidence respectively. The wave exciting forces, being functions of wave frequency, are entirely dependent on the wave angles of attack. The sway force, heave force and roll exciting moment in beam waves are larger than those in oblique and head waves. Moreover, the roll moment is always in phase with the sway force in beam waves. This is due to the sway component being dominant in the roll moment in the frequency range considered. Since the Series-60 ship has no fore and aft symmetry, the surge force, pitch moment and yaw moment in beam waves are not equal to zero but are smaller than those at other heading angles. The component of the pitch moment due to heave forces in beam waves is dominant as the phases of the heave force and the pitch moment are coincident. In the low frequency region below f=1.7 the amplitudes of all the wave exciting forces and moments except the pitch moment in the wave angle $\beta=30^{\circ}$ are the same as those in $\beta=150^{\circ}$. This implies that the differences between the fore and aft bodies are hardly distinguishable in the long wave regime. In head waves the sway exciting force, roll and yaw exciting moments are identical to zero because of the longitudinal plane of symmetry. Moreover, the surge exciting force and pitch exciting moment in head waves have larger peak amplitudes than those in oblique and beam waves.

6.5.3-3 Zero speed ship responses

Since the hydrodynamic coefficients and the wave exciting forces were determined, the motion equation can readily be solved. The zero speed motion responses for the Series-60 ship in deep water at various angles of wave heading are illustrated in Fig.6.20a and Fig.6.20b. The sway, heave and roll motion responses of the ship in beam waves are larger than those in oblique and head waves because of

stronger wave forces in beam waves for these modes of motion. In particular, the roll motions in beam and oblique waves exhibit resonance due to weak wave damping. In the roll resonance region the amplitude curves of the sway motions are discontinuous because of coupled motion characteristics in sway-roll-yaw. The amplitudes of sway and roll motions decrease both from beam waves to head waves and from beam waves to following waves. Eventually, there are no responses in sway, roll and yaw motions in head and following waves due to the longitudinal plane of symmetry. The surge, pitch and yaw motion responses in beam waves are smaller than those at other angles of wave incidence. If the Series-60 ship had a transverse plane of symmetry there would be no surge, pitch and yaw motion responses in beam waves. On the other hand, the amplitudes of surge and pitch responses increase at lower frequencies but decrease at higher frequencies, as the wave heading changes from beam waves. Since the amplitudes of the wave exciting forces and moments for a wave angle $\beta=30^{\circ}$ are equal to those at $\beta=150^{\circ}$ in long waves, the amplitudes of the resulting motion responses are the same at these two wave headings. In the long wave regime for all wave angles of attack the phase angle of the sway motion lags 90° behind the incident wave while the heave motion reaches its maximum amplitude at the same time as the incoming wave does. The reason for these phenomena may be that the symmetrical cross flow occurs in heave motion whereas the anti-symmetrical cross flow occurs in sway motion.

6.5.3-4 Forward speed hydrodynamic coefficients

The principal added mass and damping coefficients for the Series-60 ship travelling with the forward speed of $F_n=0.2$ in deep water are presented in Fig.6.21 and Fig.6.22 respectively. The numerical calculations were performed by using three-dimensional translating pulsating source distribution and three-dimensional oscillating source modelling. These mathematical models neglect the steady perturbation flow in the free surface and around the wetted body surface. It is evident that the calculated coefficients in the vertical symmetrical modes of motion have discontinuities near the critical point $\tau=1/4$ for the translating pulsating source modelling. These phenomena

have been discussed in sections 6.5.1 and 6.5.2. which refer to the speed effects on the free surface.

The heave added mass and damping coefficients evaluated by all the mathematical models agree well with the experimental data in the high frequency range but deviate from the measured data at the low frequencies where the measured heave added mass values are significantly reduced and the measured heave damping are increased considerably. The pitch added inertia values predicted by the translating pulsating source modelling agree very well with the measurements, especially in the low frequency region, where the oscillating source modelling cannot give such good correlation. There are significant discrepancies between the calculated and the measured pitch damping coefficients. None of the theoretical methods predict the experimental values of the pitch damping. The oscillating source modelling under-estimates the pitch damping in the low frequency region but over-estimates the values at the high frequencies. Meanwhile the translating pulsating source modelling under-estimates the pitch damping in the frequency region considered. In examining the measured pitch damping coefficients it is evident that these data exhibit a significant peak value at the critical point $\tau=1/4$ where the results obtained from the translating pulsating source modelling also demonstrates this behaviour. It seems that the measured pitch damping coefficients for the Series-60 model may include some physical effects which were not simulated by the present mathematical models, such as the steady perturbation flow, non-linear effects, etc. The omission of these effects in the theory could well be influencing the present results but additional sources of error also exist. For example, the errors may have occurred in the numerical approximation, the body discretisation and the weak singularities along the free surface contour.

The hydrodynamic coefficients of sway and yaw calculated by the translating pulsating source modelling agree generally better with measurements than those obtained by the oscillating source modelling, especially in the low frequency region. This reflects that the high frequency assumption in the linearised free surface conditon for the oscillating source modelling fails at the low frequencies. It is observed in the

measured sway damping coefficients for Froude numbers F_n=0.0 and 0.2 that the speed effects increase the sway damping in the long wave regime and vice versa in the short wave regime. This behaviour is also illustrated by the translating pulsating source modelling. However neither the strip theory nor the three-dimensional oscillating source modelling in which the calculated hydrodynamic coefficients in the translational modes of motion and the roll mode are treated independent of the forward speed show such behaviour. Any theory based on the assumption of an ideal fluid predicts the wavemaking contribution to the fluid damping. In most modes of motion, this is the dominant contribution but in roll motion non-linear effects due to viscosity are significant. The inadequacy of an ideal fluid model is clearly indicated when the calculated and the measured roll damping coefficients are compared. In spite of poor correlations in magnitude between the calculated and measured roll damping values the results obtained from the translating pulsating source modelling demonstrate the same speed effects on the measured roll damping coefficients, namely an increase in the damping coefficients in the low frequency region and a decrease in the high frequency region.

The coupled added mass and damping coefficients for the Series-60 ship in deep water at F_n=0.2 are shown in Fig.6.23 and Fig.6.24 respectively. Since the Series-60 ship does not have fore and aft symmetry, the Timman-Newman relationships are not applicable for verification. The measured heave-pitch cross coupled added mass values are quite small for comparison with the results of mathematical models used in the study. For the heave-pitch cross coupled damping coefficients the results obtained from translating pulsating source technique correlate with the measured values much better than those obtained from the oscillating source technique. Poor agreement is observed between the results obtained from all the mathematical models and the experiments for the sway-yaw cross coupling coefficients However the results obtained from the translating pulsating source technique do show the correct trend and are closest to the measured data.

6.5.3-5 Water depth effects on forward speed hydrodynamic coefficients

Due to limitation in computing time the three-dimensional translating pulsating source technique for finite water depth is still impracticable. Therefore the numerical calculations for the Series-60 ship with forward speed of F_n=0.2 in water depth to draught ratio H/D=1.2 have been performed by the three-dimensional oscillating source modelling only, in order to study some shallow water effects on hydrodynamic coefficients and wave exciting forces. Experimental results carried out by Beukelman & Gerritsma (1982) are available for the hydrodynamic coefficients in sway, heave, pitch and yaw modes of motion for a Series-60 C_B=0.7 model as illustrated in Fig.6.25 for added mass coefficients and Fig.6.26 for damping coefficients.

It seems that the calculated added mass coefficients agree very well with the measured results except the pitch and yaw added inertia values at lower frequencies. This was also noted in the numerical calculations of forward speed motion coefficients for deep water. In contrast the calculated damping coefficients give poor correlations with the experimental values for the rigid modes of motion. Unsatisfactory damping predictions by the three-dimensional oscillating source modelling may be attributed to the omission of the speed effects on the free surface, where wave energy is carried away from the body. These deficiencies may be rectified by using a translating pulsating source modelling. In spite of poor correlation between the calculated and measured damping coefficients at H/D=1.2, the numerical calculations for the principal hydrodynamic coefficients of the Series-60 ship with forward speed of F_n=0.2 at different water depths have been performed as shown in Fig.6.27 and Fig.6.28.

Generally speaking, the effects of water depth on hydrodynamic coefficients become perceptible when the water depth is approximately four times the ship's draught (H/D=4.0) for the non-dimensional frequency ranging from f=0.0 to f=5.0. At the dimensionless frequency lower than f=2.5 the water depth effects are significant as evident in the damping coefficients in the vertical symmetrical modes of motion for H/D=4.0. This is because waves can feel the sea bottom for such low frequency. In the

low frequency range a reduction in water depth produces a large increase in the added mass coefficients. The water depth effects on the added mass coefficients quickly reduce as the frequency of oscillation increases. Increase in added mass implies that more energy is needed to accelerate the fluid around the body. The added mass coefficients in surge, sway and yaw motions increase at lower frequencies but decrease at higher frequencies, as water depth decreases. On the other hand the added mass coefficients in heave, roll and pitch motions increase with decrease in water depth. This explains why an increase in the natural roll period in shallow water is often observed. Similarly an increase in the damping coefficients for six rigid modes of motion can be observed when water depth decreases. It should be noted that the hydrodynamic coefficients in translational modes and roll mode of motion calculated by the oscillating source modelling are independent of forward speed for the slender body assumption.

6.5.3-6 Forward speed wave exciting forces

The only available experimental data on forward speed wave exciting forces are those obtained by Gerritsma & Beukelman (1967) for the Series-60 C_B=0.7 model in head waves. Fig.6.29 illustrates the wave exciting forces and moment acting on the Series-60 ship in deep water at F_n=0.2 in head waves. A good agreement between the results obtained from two mathematical models and the experiments is noticeable in the modulus of the heave exciting forces while the results of pitch exciting moments predicted by two methods are reasonably correlated with the measured data. The translating pulsating source technique gives a better prediction for the phase angle of the heave exciting force at the high frequencies where the oscillating source modelling fails to perform well. Similar observations can be found for the phase angle of the pitch moment. Physically the head waves impinging on the ship bow undergo a gradual deformation as they propagate downstream. As a result, the wave elevation at the ship stern is reduced in amplitude and shifted in phase relative to that of the undisturbed incident wave. For long waves the ship is a weak scatterer, the opposite being true for short waves. Thus the longitudinal flow interactions for head waves become

significant, especially on the free surface, as the wavelength decreases. This may explain why the translating pulsating source modelling gives good prediction for the phase shift relative to the incident wave. In general the oscillating source modelling gives higher amplitude for surge, heave exciting forces and pitch moment than the translating pulsating source technique does in the middle range of the frequency band considered for head seas. It is visible that there are discontinuities on the curves of the surge, heave exciting forces and pitch moments calculated by the translating pulsating source at the critical point τ=1/4.

For a constant forward speed the wave angles of attack produce a Doppler effect so that the frequency of encounter increases from beam waves to head waves but decreases from beam waves to following waves. The curves of wave exciting forces and moments would be oscillating more frequently at the larger wave angles of attack as illustrated in Fig.6.30a and Fig.6.30b respectively for the Series-60 ship at F_n=0.2 in deep water. As in the zero speed case the forward speed sway, heave exciting forces and roll exciting moment in beam waves have larger amplitude than those in other wave directions. Moreover the sway component of the roll exciting moment is dominant in beam waves because they have the same phase angles. For beam waves the longitudinal flow interactions originate from the geometry gradients in the direction of the ship axis, their dependence on the wavelength being similar to that of the radiation problem since no Doppler effect occurs. This phenomena may be confirmed by the similar trends for zero speed and the forward speed F_n=0.2 in the phase angles of the sway, heave exciting forces and roll exciting moment in beam waves. The maximum peaks of the surge exciting forces and the pitch exciting moments occur in head waves. It is interesting to note that the troughs of the curves of the wave exciting forces and moments for zero speed and forward speed cases occur at the transient between the phase lead and the phase lag.

The wave exciting forces and moments for the Series-60 ship in deep water at different forward speeds are plotted on a base of ship length to wavelength ratio L/λ in Fig.6.31 for head waves (β=180°) and Fig.6.32a and Fig.6.32b for the wave angle

120° of attack. Generally speaking, the wave exciting forces and moments at a constant wavelength are strongly speed dependent in the short wave regime. In spite of the Doppler effect the modulus of the heave exciting forces in head waves and the sway exciting forces in oblique waves are not very sensitive to the forward speeds considered at a constant wavelength in the long wave regime. The maximum amplitude of the surge exciting forces decrease as the forward speed increases in head and oblique waves (β=120°). A similar tendency can be found in the roll exciting moment amplitudes at a constant wavelength in the wave direction β=120°. The peak amplitude of the yaw exciting moments in the oblique waves is almost independent of the forward speed.

6.5.3-7 Water depth effects on forward speed wave exciting forces

Since there is no experimental data available for the wave exciting forces acting on the Series-60 ship in shallow water, only numerical calculations carried out by the three-dimensional oscillating source modelling for the wave exciting forces and moments on the Series-60 ship with forward speed of F_n=0.2 at various water depths are presented in Fig.6.33 for head waves and in Fig.6.34a and Fig.6.34b for bow quartering waves. The orbit of a wave fluid particle is strongly dependent on water depth, especially where the flow is constrained by the keel clearance. It is evident in bow quartering waves that the sway exciting forces and yaw moments have stronger water depth dependence than those in surge, heave, roll and pitch. This is because lateral flow is obstructed by the keel clearance and the fluid must pass around the ship ends. For the extreme case where the water depth is equal to the ship's draught, the gap beneath the ship bottom is closed off and the flow must pass entirely around the ends. In general the surge, heave exciting forces and pitch exciting moment increase with decrease in water depth for a given wavelength. Similar trends can be observed in the sway exciting forces and yaw exciting moments except the roll moments.

6.5.3-8 Forward speed ship responses

The theoretical values of the hydrodynamic coefficients and wave exciting forces found previously are used to predict the response of the Series-60 ship in deep water at F_n=0.2 in six degrees of freedom. At forward speed only measurements due to Gerritsma & Beukelman (1967) are available for the heave and pitch responses in head waves. These are illustrated together with the calculated values obtained from three mathematical models for surge, heave and pitch motions in Fig.6.35. These mathematical models are the three-dimensional translating pulsating source distribution technique with higher pitch damping coefficients (method 1), three-dimensional oscillating source technique (method 2) and pure three-dimensional translating pulsating source technique (method 3). Method 1 makes use of higher pitch damping calculated by the three-dimensional oscillating source method in order to show the sensitivity of pitch damping in pitch responses.

In head waves all mathematical models tend to overpredict the amplitude of the heave response but method 1 and method 3 give better correlation with the measured phase angle of the heave response. Near the pitch resonant frequency method 3 overpredicts the pitch responses while method 1 and method 2 underpredict them. This is because none of the methods predict the measured pitch damping; the translating pulsating source technique underpredicts the measured values but the oscillating source technique overpredicts them. At pitch resonance the pitch amplitude response is very sensitive to pitch damping as illustrated by method 1 and method 3. This argument is applicable to other modes of motion resonance such as roll motion. The pitch phase angles for head waves show good agreement between all methods and the measured data at lower frequencies but some differences exist at higher frequencies where method 1 and method 3 give a better prediction. The surge response values in head waves calculated by all methods show very good correlation with each other at all frequencies. However, the amplitudes of surge, heave and pitch responses calculated by the oscillating source technique are higher than those calculated by the translating pulsating source technique at high frequencies. This must be attributed to the wave excitation for

which higher value is obtained by the oscillating source modelling.

The motion response values of the Series-60 ship in deep water at F_n=0.2 in various angles of wave incidence, predicted by the translating pulsating source modelling* (method 1), are shown in Fig.6.36a and Fig.6.36b. Some characteristics, which were observed in the zero speed case, can be found for the forward speed case as well. For example, the amplitudes of the sway and roll responses in beam waves for all wavelengths are larger than those in other wave directions because of stronger wave excitation in beam waves for these two modes of motion. Meanwhile the heave response amplitudes in beam waves are no longer larger than those in oblique waves and head waves except for the short wave regime. The yaw motion response values are more significant in oblique waves than in beam waves. It is interesting to note that the resonant peaks of the heave, roll and pitch responses in oblique waves occur at wavelengths comparable to the ship length. The peak amplitude of the heave response values increases but the peak amplitude of the pitch response values decreases, as the wave angle of attack decreases from 180°. The pitch motions in head waves for a moving ship are more important than in oblique waves because of occurrence of severe wave excitation with lesser wave damping at high frequencies.

A ship spends her life running in the seaway. It is important to know her motion characteristics for different forward speeds so that the severe motions may be avoided by slowing down or speeding up the ship if a localised wave spectrum is known. The motion response values calculated by the translating pulsating source technique* (method 1) for the Series-60 ship with different forward speeds in deep water are illustrated in Fig.6.37 for head waves and in Fig.6.38a and Fig.6.38b for wave direction β=120°. It is observed that the amplitudes of surge and sway responses decrease as forward speed increases for the range of wavelengths considered. Away from the roll resonant period and approximately at the ship length to wavelength ratio L/λ=1/2, the higher the forward speed the resulting roll response values decrease. Similar trends are also visible for the yaw response values. The resonant peaks of heave and pitch response amplitudes occur at wavelengths comparable to the ship length for forward speed cases. An increase in forward speed causes an increase in the resonant

peaks of heave and pitch response curves. This behaviour is vital in the study of the slamming problem in the bow region. Although the forward speed motion response values in beam waves are not illustrated, it is expected that the response values in beam waves are less sensitive to forward speed as there are little difference between the zero speed and forward speed wave excitations in beam waves.

6.5.4 A 200,000 dwt tanker

It has been noted that the three-dimensional oscillating source distribution technique associated with simple speed correction is not adequate to predict the measured hydrodynamic coefficients, especially the damping coefficients, for the Series-60 ship with forward speed in shallow water. The poor agreement may be attributed to the omission of speed effects on the free surface. However the three-dimensional oscillating source distribution method is applicable to calculate the hydrodynamic forces on a stationary body of arbitrary shape in waves under the framework of linear potential theory. In this section numerical calculations for the hydrodynamic forces on a stationary 200,000 dwt tanker in shallow water have been performed by the three-dimensional oscillating source technique. Good agreement is found in comparison with the experimental data published by Van Oortmerssen (1976) and Pinkster (1980). The tanker was modelled by a total of 296 panel elements consisting of combinations of quadrilateral and triangular facets, as shown in Fig.6.39. Principal particulars of the tanker is given in Table 6.3.

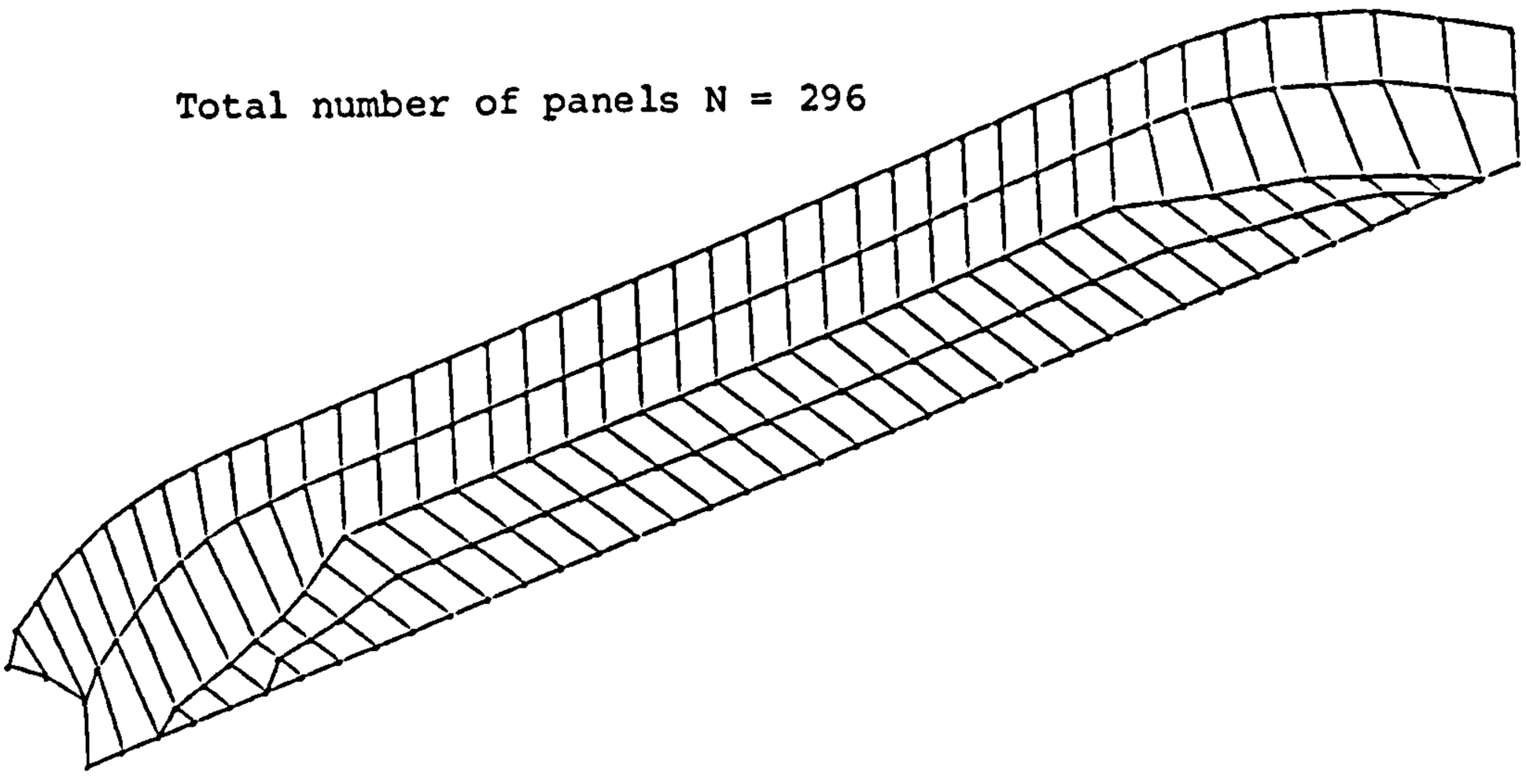

Fig.6.39 Surface Discretisation of a 200,000 dwt Tanker

LBP. L (m)	310.00
Breadth B (m)	47.17
Draught D (m)	18.90
Displacement (m^3)	234994.0
C_B	0.85
LCB (m)	6.6F
GM_T (m)	5.78
L/B	6.57
B/D	2.5
k_{xx} (m)	14.77
k_{yy} (m)	77.47
k_{zz} (m)	79.30

Table 6.3 : Particulars of a 200,000 dwt tanker

6.5.4-1 Zero speed hydrodynamic coefficients

Fig.6.40 and Fig.6.41 demonstrate respectively the principal added mass and damping coefficients for the stationary tanker at shallow water H/D=1.2. The calculated added mass and damping coefficients in sway and heave modes of motion agree very well with the measured results. In contrast, the calculated hydrodynamic coefficients in surge motion give a poor correlation with the experimental data. This unsatisfactory agreement in surge motion may be due to difficulties in measuring the small values of surge motion coefficients. It is known that the measured roll damping coefficients are much higher than the predicted values due to the presence of non-linear viscosity effects. The calculated roll added inertia values are smaller at low frequencies but larger at high frequencies in comparison to the experimental data. For the pitch and yaw modes of motion the agreement between the calculated and the measured damping coefficients are very good but the calculated added inertia values are lower than those obtained by measurements.

The cross coupled added mass and damping coefficients for the tanker at shallow water H/D=1.2 are shown in Fig.6.42 and Fig.6.43 respectively. In spite of the poor agreement between the predicted and the measured cross coupled hydrodynamic coefficients, the calculated coefficients satisfy the Timman-Newman's symmetry relationships very well. Indeed the measured values are so scattered and small that no reliable conclusion can be drawn.

6.5.4-2 Water depth effects on zero speed hydrodynamic coefficients

The principal hydrodynamic added mass and damping coefficients for the stationary tanker at various water depths are illustrated in Fig.6.44 and Fig.6.45 respectively. Generally the most remarkable influence of water depth on the added mass coefficients occurs at low frequencies where the apparent added mass increases considerably with decreasing water depth. This behaviour was also observed in the experiments conducted by Van Oortmerssen (1976). The trends of the added mass coefficients in surge, sway and yaw modes of motion at different water depths can be divided into three parts: first the added mass coefficients increase with decreasing water depth at low frequencies, then decrease for reducing water depth at the middle range of the frequency band considered and finally becomes independent of water depth at high frequencies. For the surge, sway and yaw damping coefficients decrease in water depth results in increase in coefficients at low frequencies but water depth effects become insignificant at high frequencies where the waves never feel the sea bottom for these modes of motion. The hydrodynamic coefficients in heave, roll and pitch modes of motion, except roll damping, increase as water depth decreases with the range of frequencies considered. On the other hand the roll damping coefficients decrease with decreasing water depth at high frequencies. In general, the influence of the water depth on the hydrodynamic coefficients is extremely important since substantial changes in motion characteristics occur, especially in shallow water or at low frequencies if the water depth is finite.

6.5.4-3 Zero speed wave exciting forces

The wave exciting forces and moments acting on the stationary tanker in head waves, bow quartering waves and beam waves are shown in Fig.6.46 through Fig.6.48b. In general the agreement between the calculations and the measurements (Van Oortmerssen 1976) is good. In all cases the trends suggested by the measurements are predicted by the calculations. For head waves the agreement is better than for the other wave directions. However discrepancies between the predictions and the measurements in beam waves are noticeable in surge exciting forces, pitch and yaw exciting moments. This is because these forces are very small and hardly to be detected for the asymmetry of the tanker in beam waves.

The wave exciting moments acting on a stationary body are calculated by taking the moment of exciting forces about a point of rotation. Consequently the roll moment is contributed by the sway and heave exciting forces, the pitch moment by the surge and heave exciting forces and the yaw moment by the surge and sway exciting forces. It is evident in beam waves that the sway exciting forces are dominant in roll moment calculations because of their similar phase angles while the heave exciting forces are dominant in pitch moment calculations for small surge exciting forces.

6.5.4-4 Water depth effects on zero speed wave exciting forces

Wave exciting forces and moments acting on the stationary tanker at various water depths are plotted for different wave frequencies as shown in Fig.6.49 for head waves and in Fig.6.50a and Fig.6.50b for bow quartering waves. It has been noted that the wave exciting forces and moments, except roll moments, for the Series-60 ship with or without forward speed generally increase with decreasing water depth at a given constant wavelength. However this trend may change when the wave exciting forces or moments are plotted on a base of wave frequency since at the same frequency the wavelength becomes shorter with decreasing water depth. Shorter wavelengths produce

a slower phase speed of the incoming wave. This explains why the curve of the phase angle of the wave exciting force or moment shifts in such a way that the phase angle for shallow water leads that for deep water. The trend for the wave exciting force or moment amplitudes is less definite in relation to water depth at a constant wave frequency. Nevertheless the curves of the wave exciting force or moment amplitudes exhibit the shift in humps towards lower frequencies.

6.5.4-5 Zero speed ship responses

Calculations of the motion responses for the stationary tanker in six degrees of freedom have been carried out and the results for head waves, bow quartering waves and beam waves, at shallow water H/D=1.2 (Van Oortmerssen 1976) and deep water H/D = 4.365 (Pinkster 1980) are shown in Fig.6.51 through Fig.6.56b. Again good agreement was found between the calculated and the measured results, except for the roll motion at resonance, where viscous damping plays an important role. Since the roll motion at resonance is overestimated by the potential theory, small humps occur at this frequency in the computed sway and yaw motion response values in beam waves, due to the coupling terms. It should be noted that the calculated and the measured motion amplitudes in surge and sway modes at low frequencies for deep water (H/D=4.365) show a tendency for the curve to be higher. In contrary the surge and sway motion amplitude values for infinite water depth always level off at low frequencies. This is because waves never feel the sea bottom of infinite depth, even at zero frequency.

6.5.4-6 Water depth effects on zero speed ship responses

Fig.6.57 through Fig.6.58b show the motion response values of the stationary tanker in head and bow quartering waves, at various water depths. The curve of phase angles of surge response values illustrates a phase shift towards lower frequencies with decreasing water depth. This trend follows the phase shift in the surge wave exciting

forces. Meanwhile the patterns of phase shift in other modes of motion are more complicated due to strong coupled motions. In general reducing water depth reduces the heave and pitch amplitude response values in head and bow quartering waves at low frequencies but the opposite trend is observed in the high frequency range. On the other hand the surge amplitudes in shallow water are larger than those in deep water at low frequencies. The sway and yaw amplitude values increase but the roll amplitude values decrease, as water depth decreases. Moreover, another effect of shallow water on the roll motion is to alter the frequency of resonance in such a way that the resonant frequency shifts towards lower frequencies as water depth decreases.

6.6 Conclusions

A theoretical formulation of the hydrodynamic forces and moments acting on a ship moving in waves has been presented. Numerical computations of hydrodynamic loads acting on two ellipsoids and two realistic ships have been performed by using the source distribution technique. In these calculations the three-dimensional unsteady forward motion problem has been solved

The calculated hydrodynamic coefficients of the fully submerged ellipsoid and the semi-submerged ellipsoid are strongly speed dependent. The present results for the cross coupled coefficients of the fully submerged ellipsoid satisfy very well the Timman-Newman relationships which are applicable for a moving body having fore and aft symmetry. On the other hand the calculated cross coupled coefficients of the semi-submerged ellipsoid are not in such good agreement with the Timman-Newman relationships. Other than the effects of weak singularities on the free surface contour we cannot single out any particular cause for the noted discrepancy in the translating pulsating source modelling. The forward speed hydrodynamic coefficients in the symmetrical modes of motion are singular at the critical point $\tau=1/4$ but the corresponding coefficients in the anti-symmetrical modes of motion are well-behaved at this point.

Based on the comparisons of the numerical and experimental results for the Series-60 ship in deep water, it may be concluded that the three-dimensional source distribution technique is excellent to predict zero speed wave excitation forces and moments, and the hydrodynamic coefficients except roll damping. The calculated cross coupled hydrodynamic coefficients for the zero speed case agree very well with the Timman-Newman's symmetry relationship.

It has been shown that the simple speed correction normally used in strip theory and three-dimensional oscillating source modelling does not adequately characterise the actual speed effects observed in the measurements. The speed term in the linearised free surface condition leads to the translating pulsating source modelling which has to be used in order to simulate the physical phenomena and obtain reasonable predictions. Singular behaviour at the critical point $\tau=1/4$, which is demonstrated by the translating pulsating source distribution technique, is localised and may be found in experimental measurements. In general the three-dimensional translating pulsating source modelling gives better predictions of hydrodynamic coefficients for the Series-60 ship moving at $F_n=0.2$ in deep water than the three-dimensional oscillating source modelling. However both models do not predict reasonable roll and pitch damping values for the Series-60 ship with forward speed. For the roll case there are some unresolved discrepancies between the potential theory and the experiments. The predictions of forward speed pitch damping coefficients may be improved by the inclusion of the interaction of steady and unsteady flow fields in the calculations of pressure and body boundary condition, which have been neglected in the present study. In the exciting force predictions for head waves both models agree with each other and with the experimental measurements. Nevertheless, the translating pulsating source distribution technique gives better phase predictions.

The heave amplitude values predicted by both the translating pulsating source technique and the oscillating source technique are higher than the measured values for the Series-60 ship at $F_n=0.2$ in head waves. Due to poor correlation in pitch damping coefficients, the translating pulsating source technique overestimates the pitch amplitude

values but the oscillating source technique underpredicts them. However the phase angle results obtained from the translating pulsating source technique are in better correlation with the experimental values than those obtained from the oscillating source modelling.

Numerical calculations for the Series-60 ship moving at F_n=0.2 in shallow water H/D=1.2 has been performed by using the three-dimensional oscillating source technique. It has been found that the results obtained using this technique are in good agreement with the measurements for the predictions of sway and heave added mass coefficients. However the predictions of pitch and yaw added inertia values at low frequencies are in poor agreement with measurements. For damping coefficients the correlation between the calculated and the measured values are poor. The discrepancies may be due to the omission of speed effects on the free surface. However this numerical modelling shows that the water depth effects on the hydrodynamic coefficients for the Series-60 ship at F_n=0.2 become significant at water depth to ship's draught ratio H/D=4.0.

The influence of forward speed and ship heading play an important role in defining the motion response characteristics. This has been demonstrated by the three-dimensional translating pulsating source technique for the Series-60 ship at various forward speed and wave angles of attack in deep water. In general, sway, heave exciting forces and roll exciting moment are larger in beam waves than in other wave directions. The sway and roll amplitude values increase and reach a maximum in beam waves, as the angle of wave incidence decreases from 180°. The peaks of heave and pitch amplitude values increase with increase in forward speeds. This phenomena is vital in the slamming problem.

The wave exciting forces and moments acting on the Series-60 ship at F_n=0.2 at various water depths in head waves and oblique waves have been determined by the three-dimensional oscillating source technique. In general, a reduction in the water depth increases the forward speed wave excitations at a constant wavelength. Since the

lateral flow is obstructed by keel clearance, the sway exciting force and yaw exciting moments have stronger water depth dependence than other wave exciting forces and moments.

The numerical calculations for a stationary tanker at shallow depth H/D=1.2 show that the results of the calculated and measured wave excitation forces and moments, and the principal hydrodynamic coefficients except the roll damping coefficient were in good agreement with each other. Similar good correlations between the predicted and the measured motion response values in head waves, bow quartering waves and beam waves were found. Moreover, it has been found that the calculated cross coupled hydrodynamic coefficients agree very well with the Timman-Newman's symmetry relationship for the zero speed case. Water depth effects on the hydrodynamic coefficients, wave excitation forces and moments, and the resulting motion response values for the tanker at zero speed have been illustrated. At high frequencies the zero speed hydrodynamic coefficients were found to be less sensitive to water depth. On the other hand the hydrodynamic coefficients have strong water depth dependence at low frequencies. At a constant wave frequency the phase angle of wave excitation force or moment for shallow water leads that for deep water. The sway and yaw amplitude values increase but the roll response values decrease, as water depth decreases.

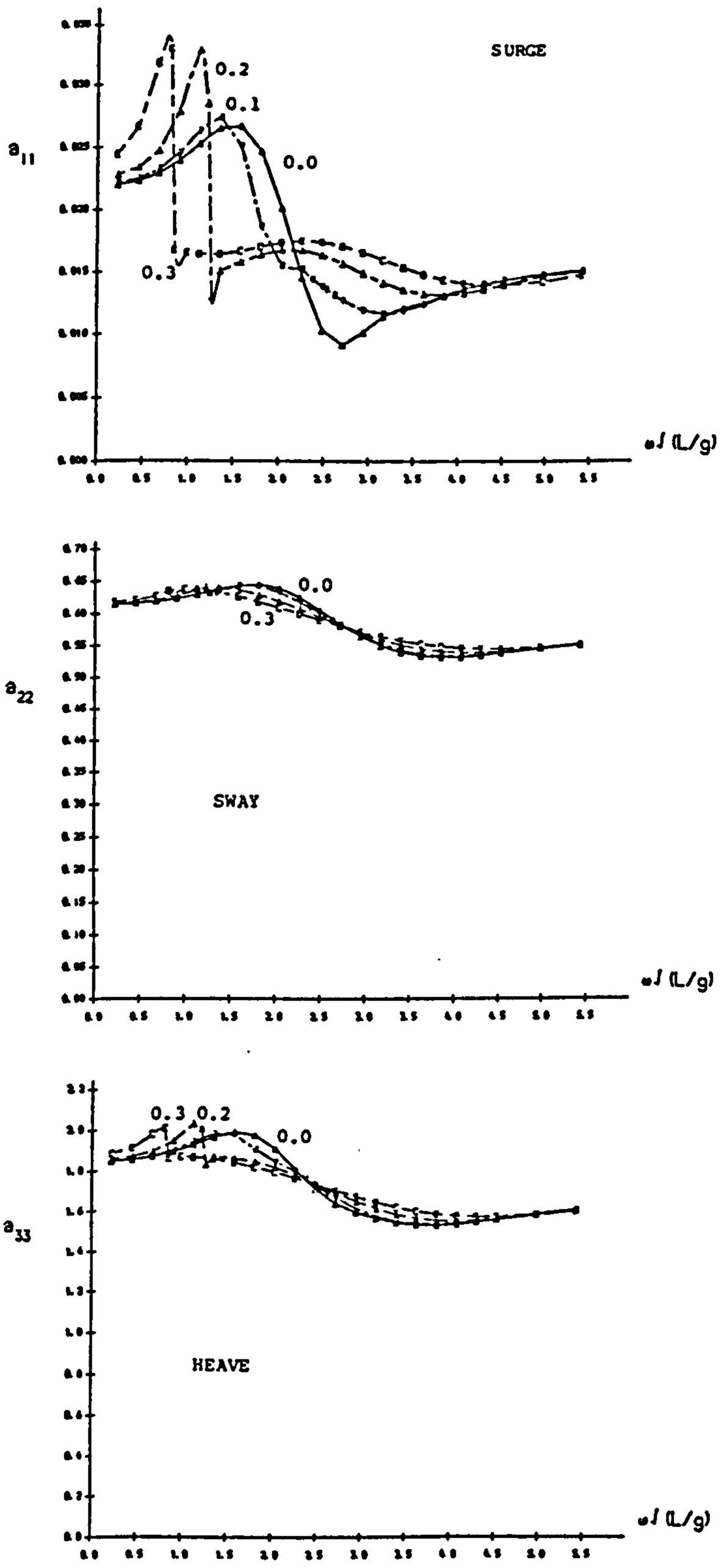

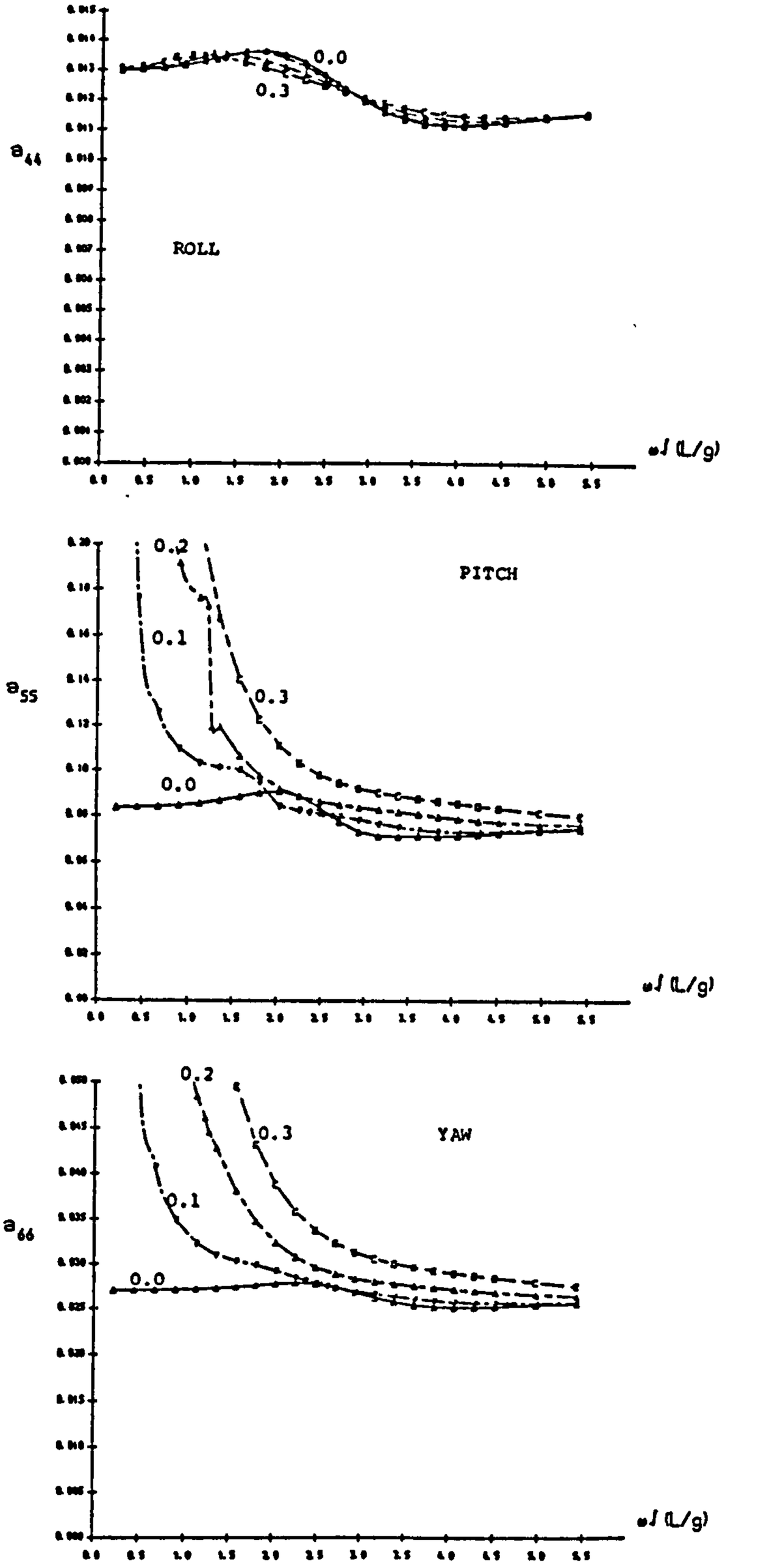

Fig.6.3 NON-DIMENSIONAL ADDED MASS COEFFICIENTS OF A SUBMERGED ELLIPSOID (L/B=7,B/D=2,h/D=2) FOR SIX RIGID MODES OF MOTION AT INFINITE WATER DEPTH AT VARIOUS FROUDE NUMBERS

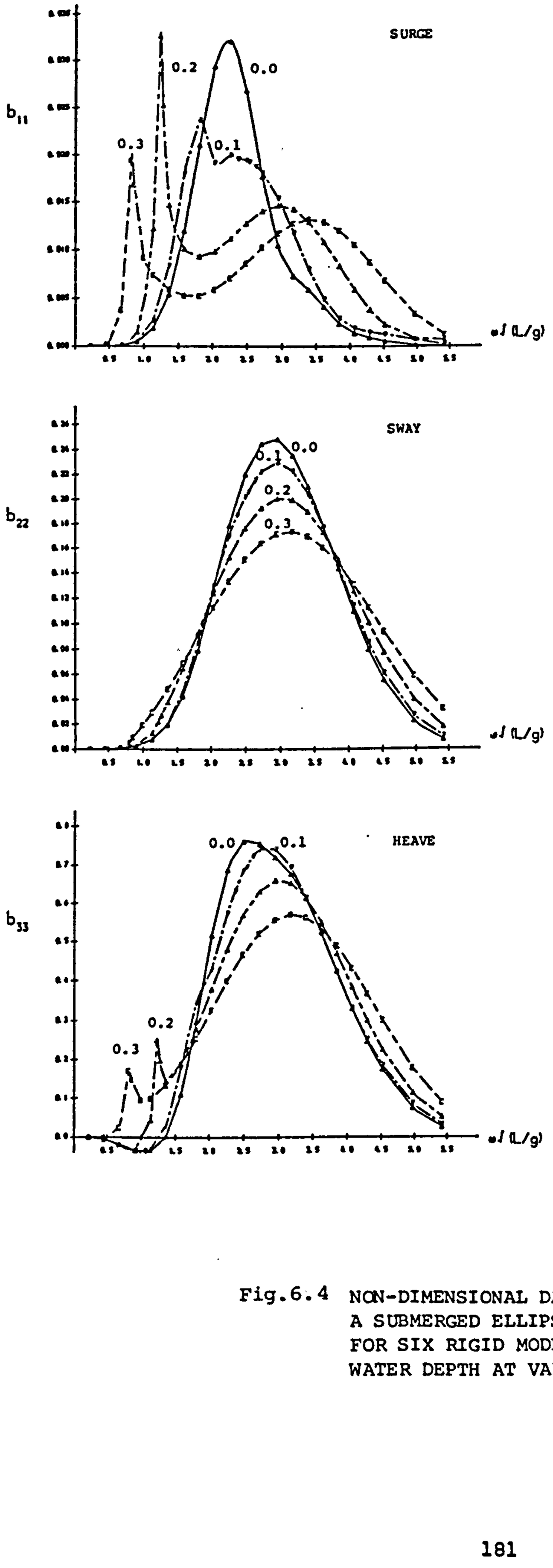

Fig.6.4 NON-DIMENSIONAL DAMPING COEFFICIENTS OF A SUBMERGED ELLIPSOID (L/B=7,B/D=2,h/D=2) FOR SIX RIGID MODES OF MOTION AT INFINITE WATER DEPTH AT VARIOUS FROUDE NUMBERS

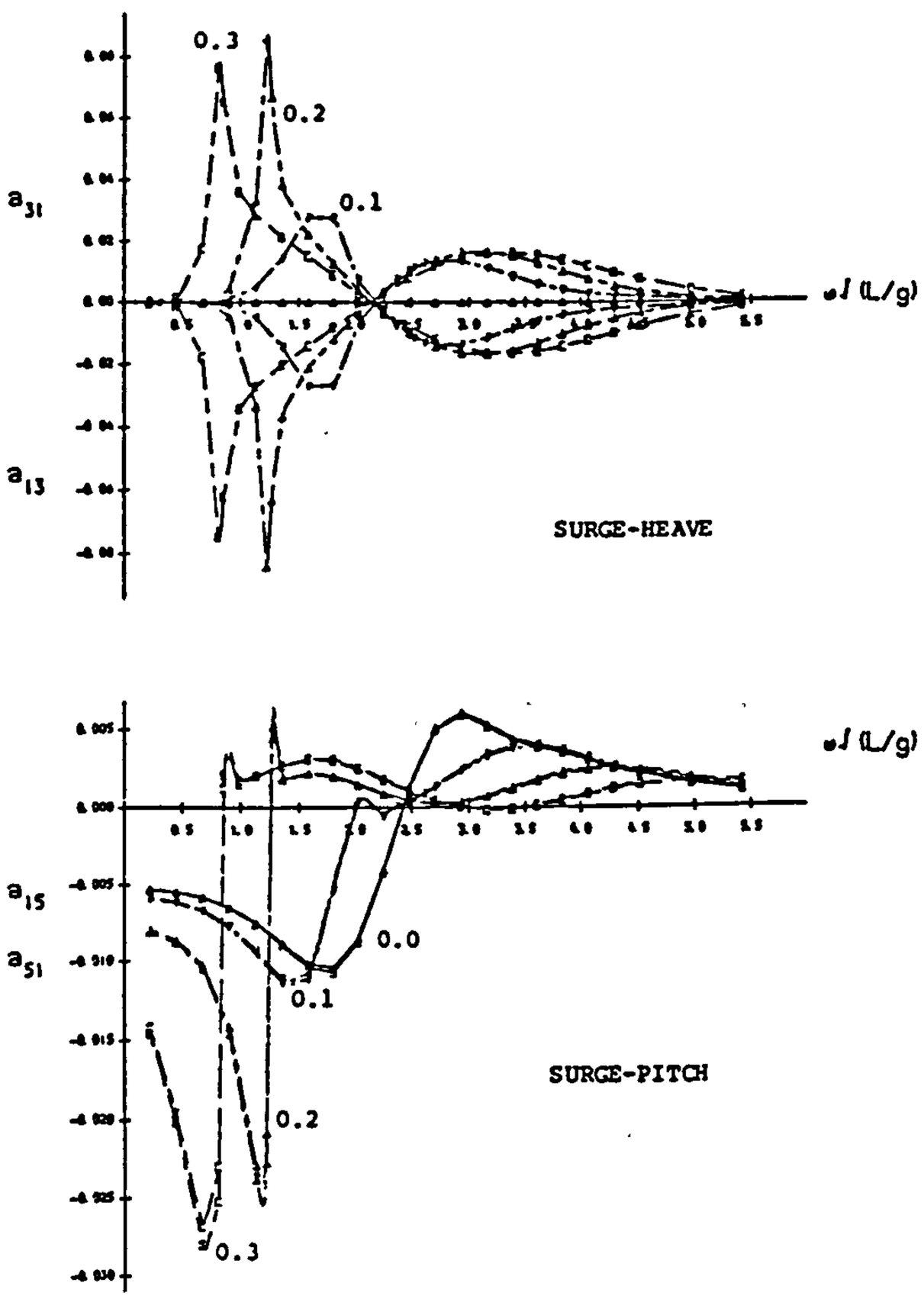

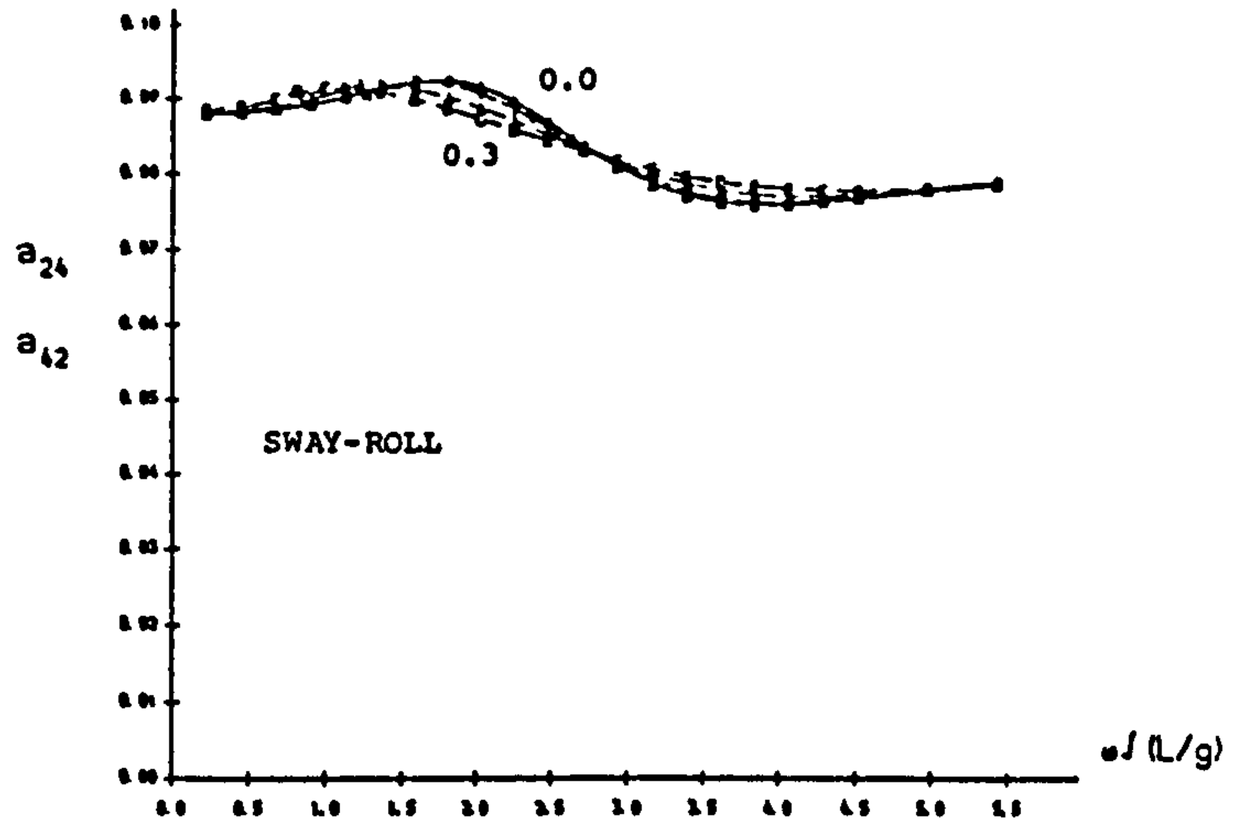

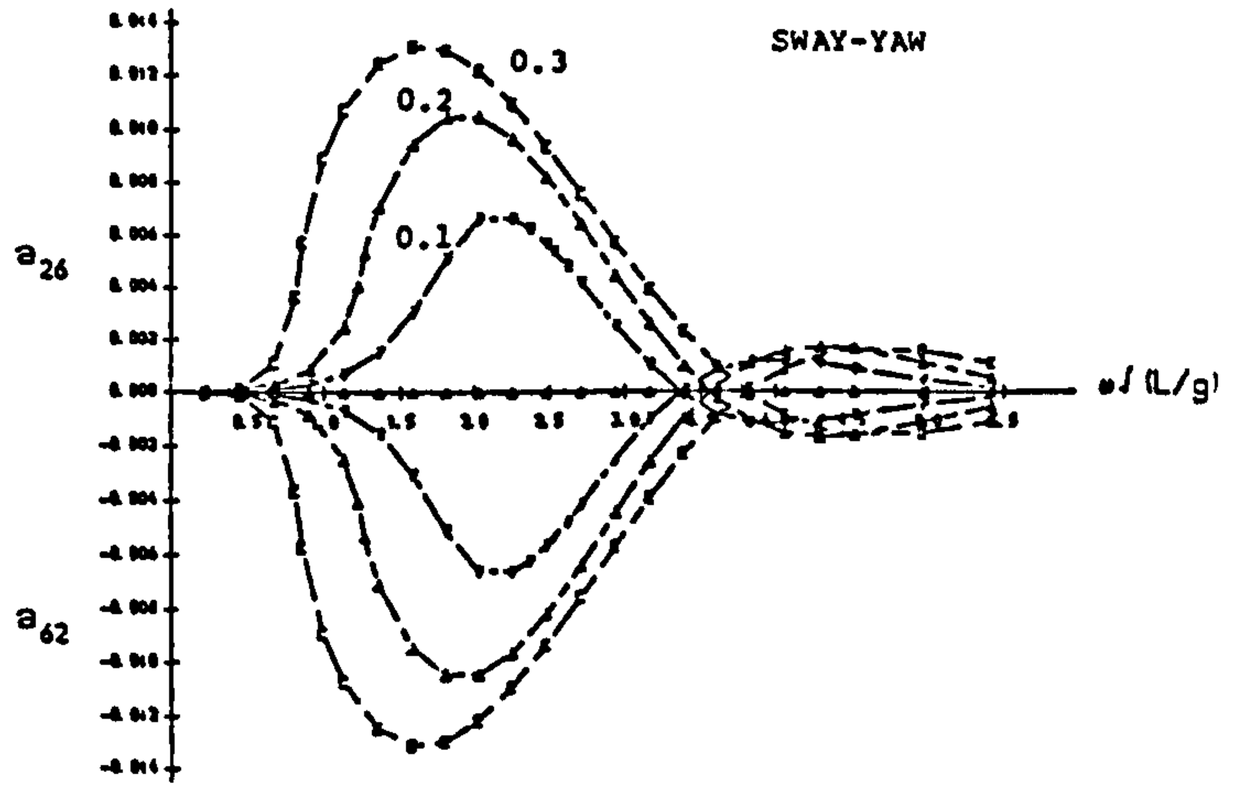

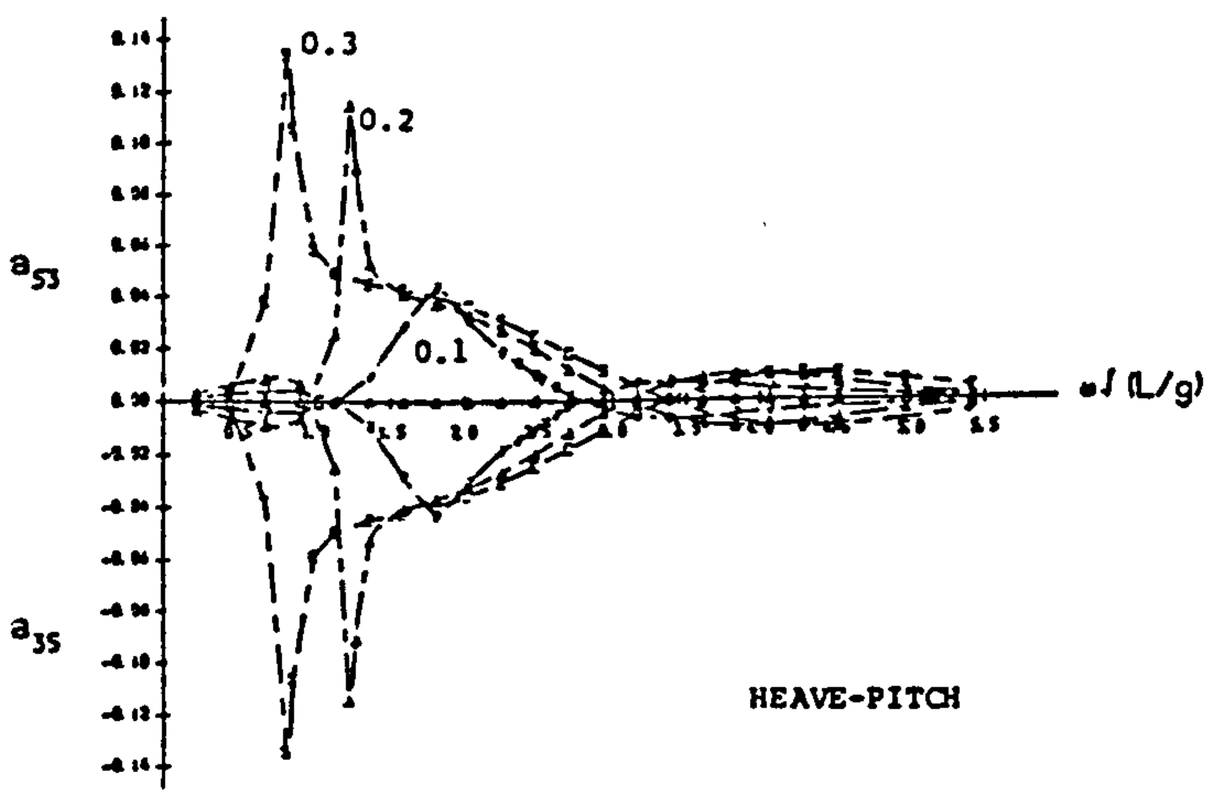

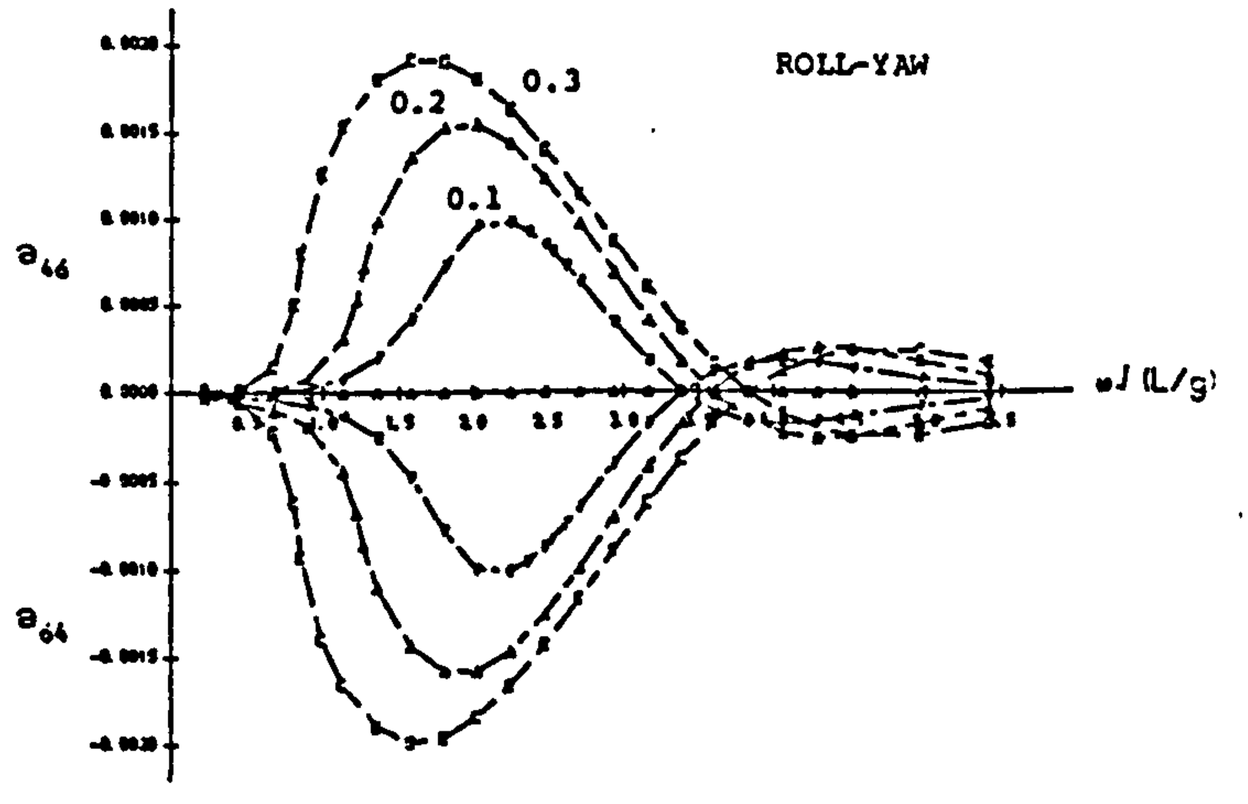

Fig.6.5 NON-DIMENSIONAL COUPLED ADDED MASS COEFFICIENTS OF A SUBMERGED ELLIPSOID (L/B=7,B/D=2,h/D=2) AT INFINITE WATER DEPTH AT VARIOUS FROUDE NUMBERS

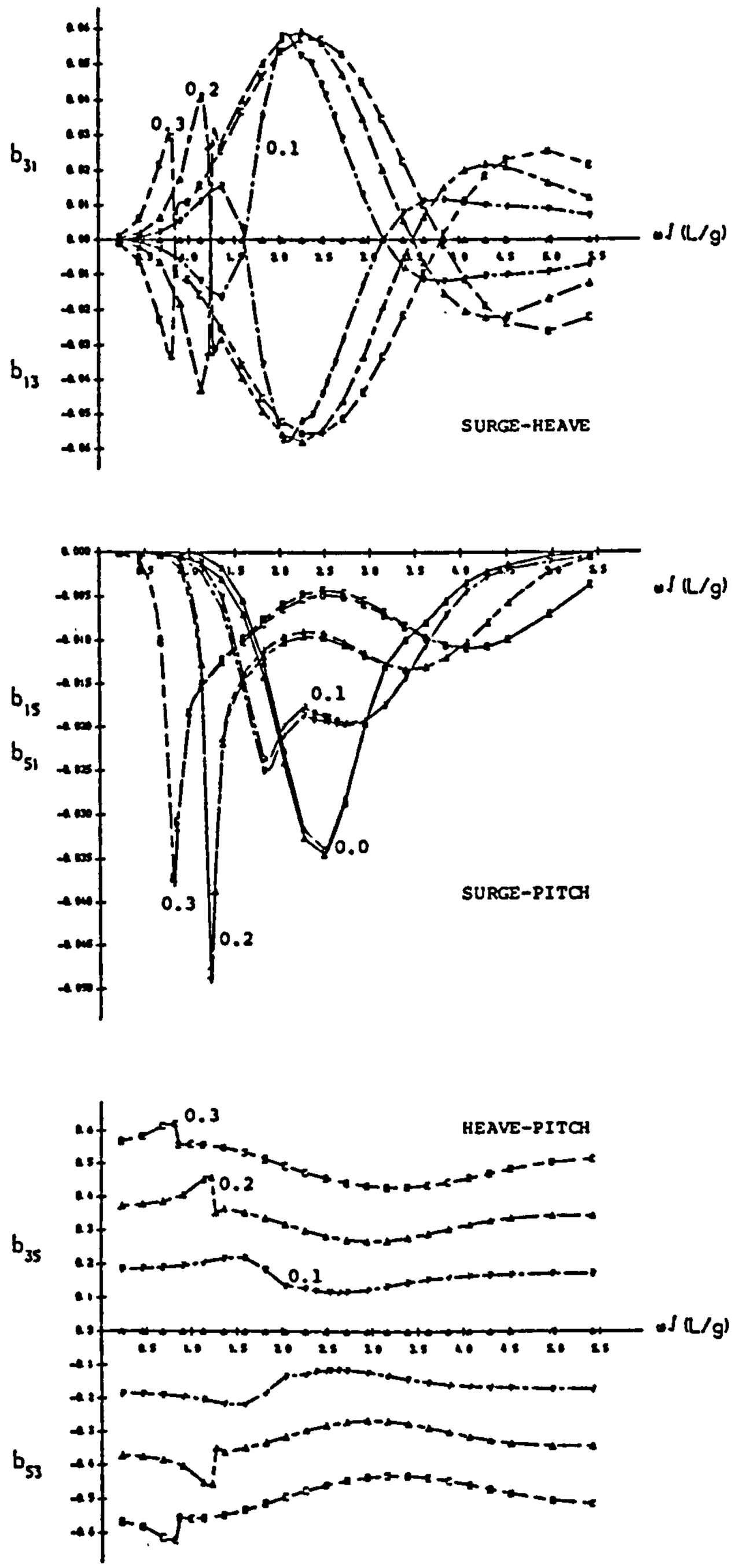

Fig.6.6 NON-DIMENSIONAL COUPLED DAMPING COEFFICIENTS OF A SUBMERGED ELLIPSOID (L/B=7,B/D=2,h/D=2) AT INFINITE WATER DEPTH AT VARIOUS FROUDE NUMBERS

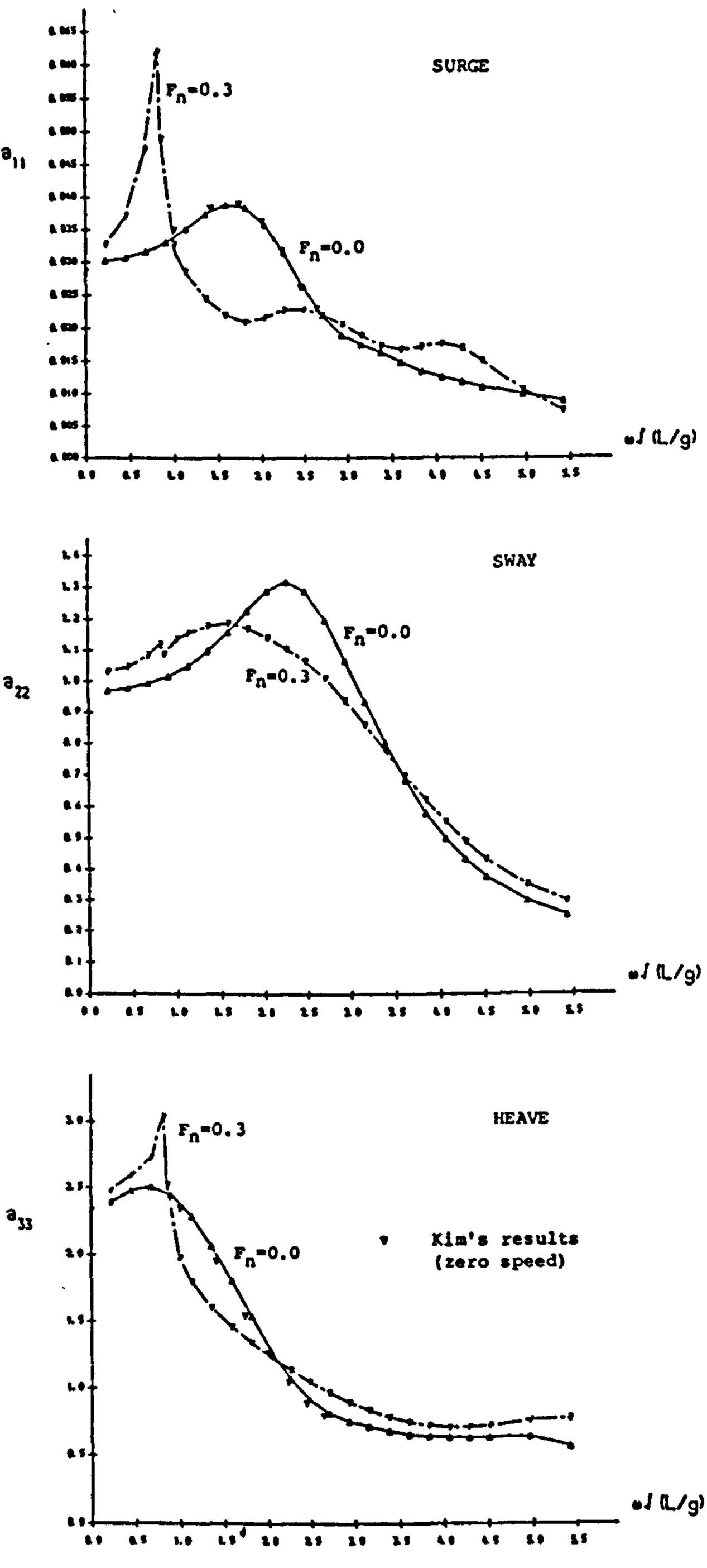

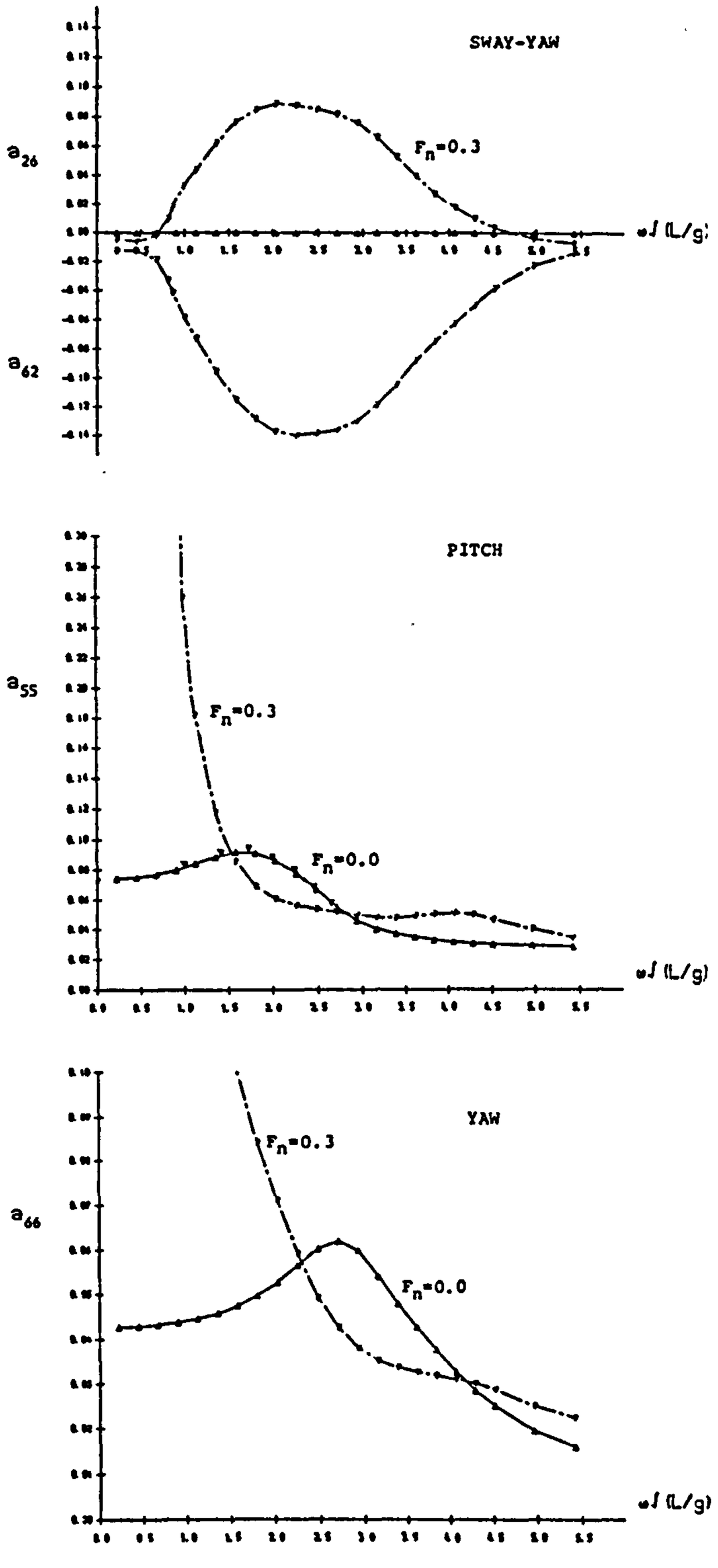

Fig.6.8 NON-DIMENSIONAL ADDED MASS COEFFICIENTS OF A FLOATING ELLIPSOID (L/B=8,B/T=2) AT INFINITE WATER DEPTH AT FROUDE NUMBER 0.0 AND 0.3

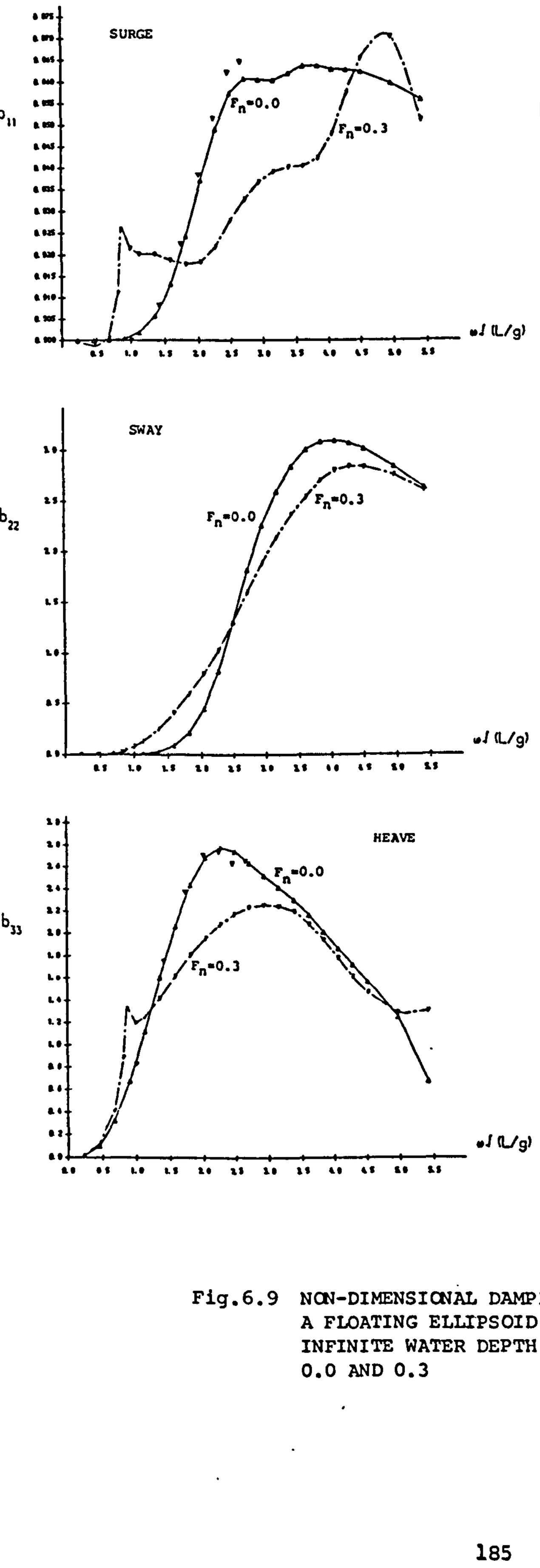

Fig.6.9 NON-DIMENSIONAL DAMPING COEFFICIENTS OF A FLOATING ELLIPSOID (L/B=8,B/T=2) AT INFINITE WATER DEPTH AT FROUDE NUMBER 0.0 AND 0.3

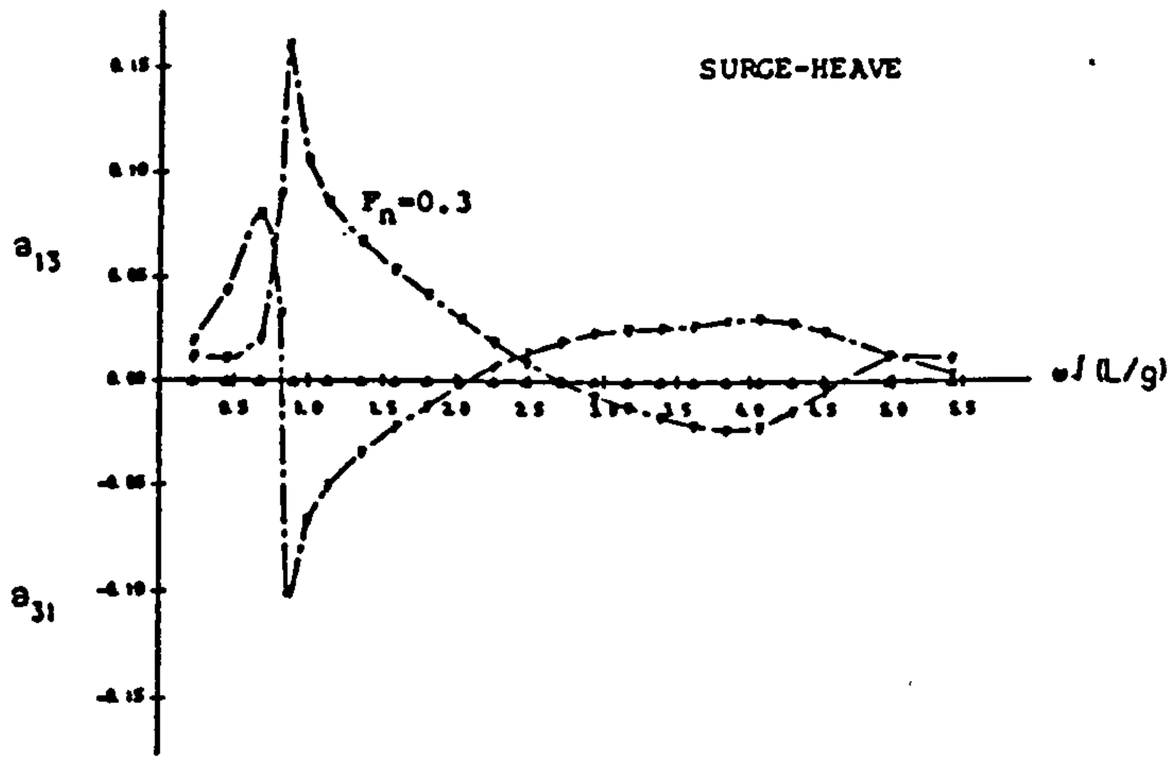

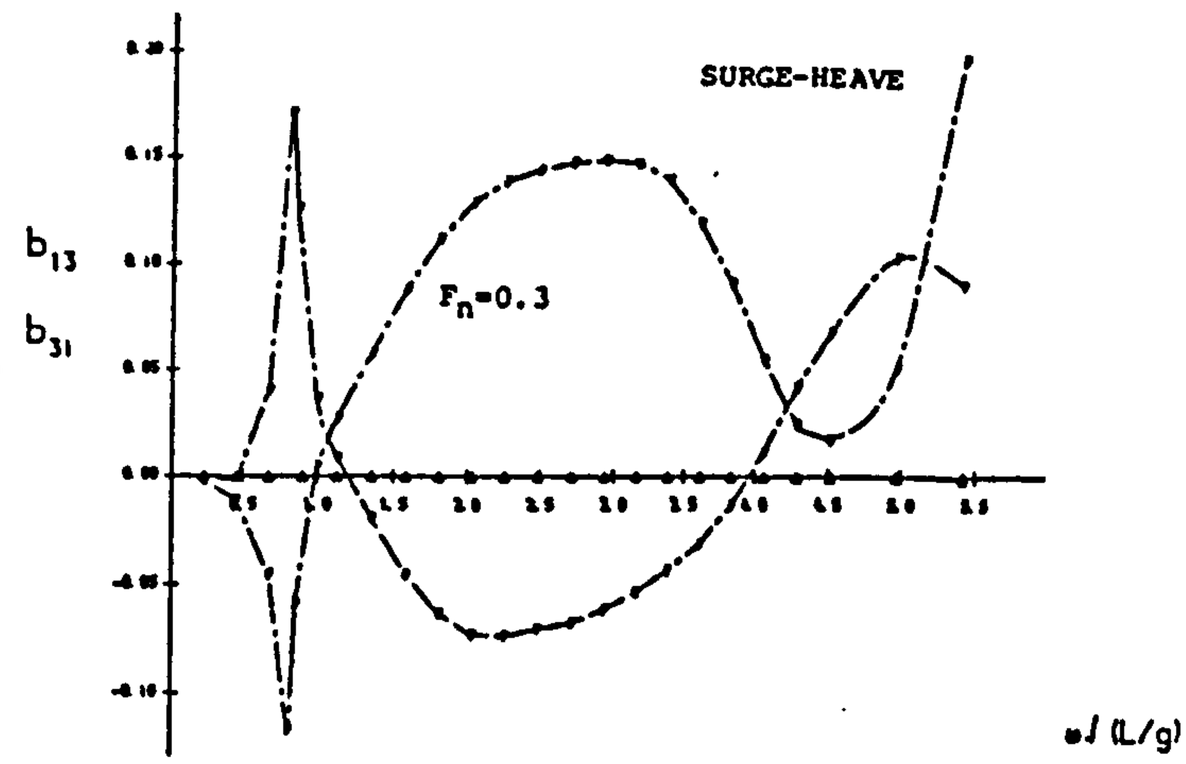

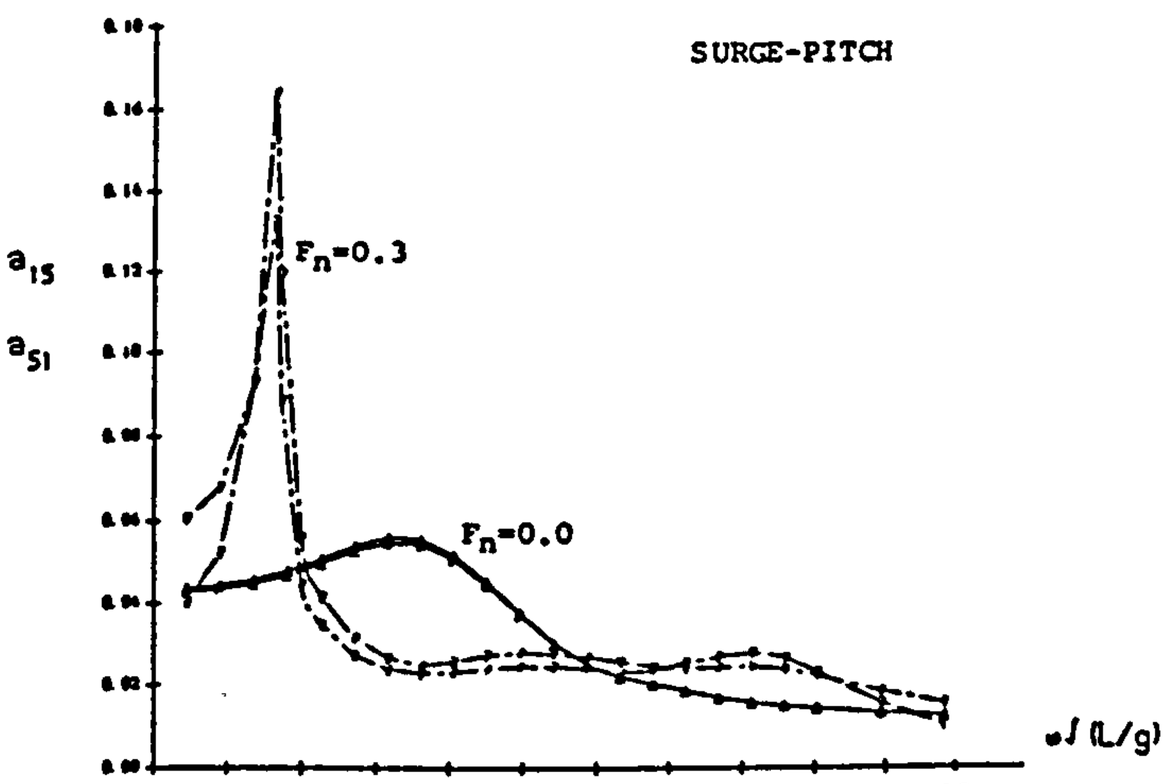

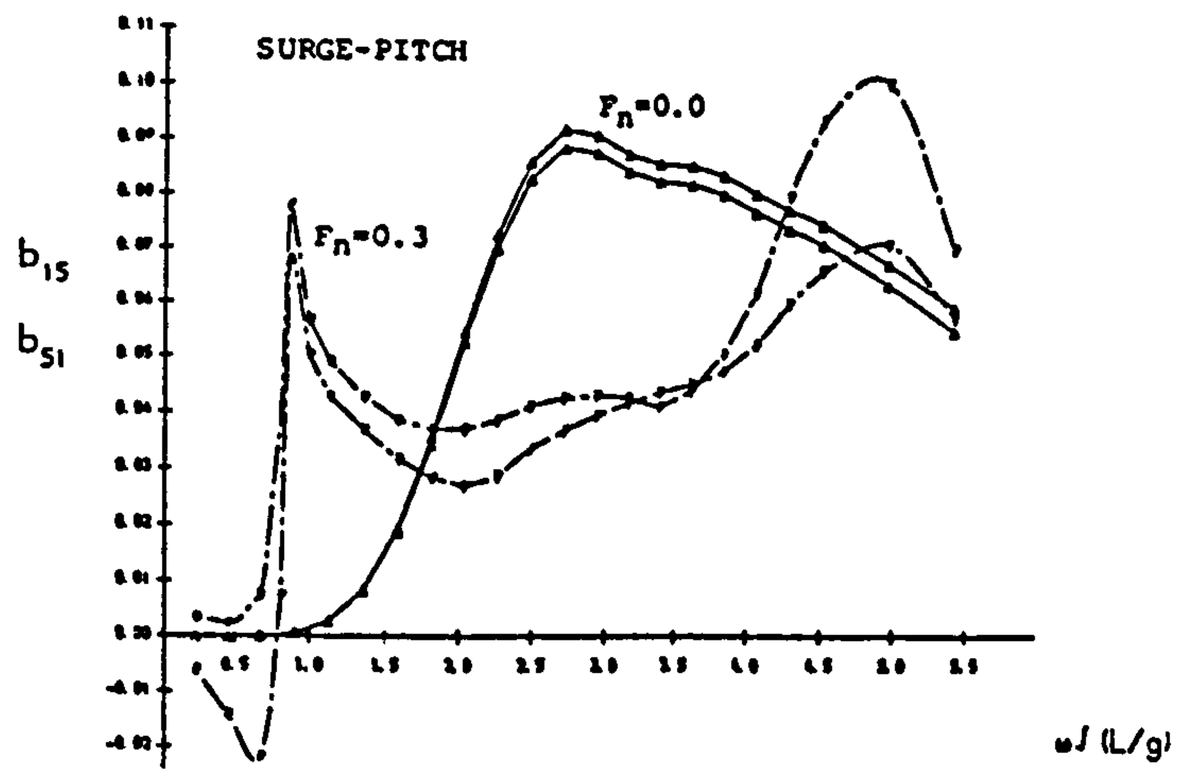

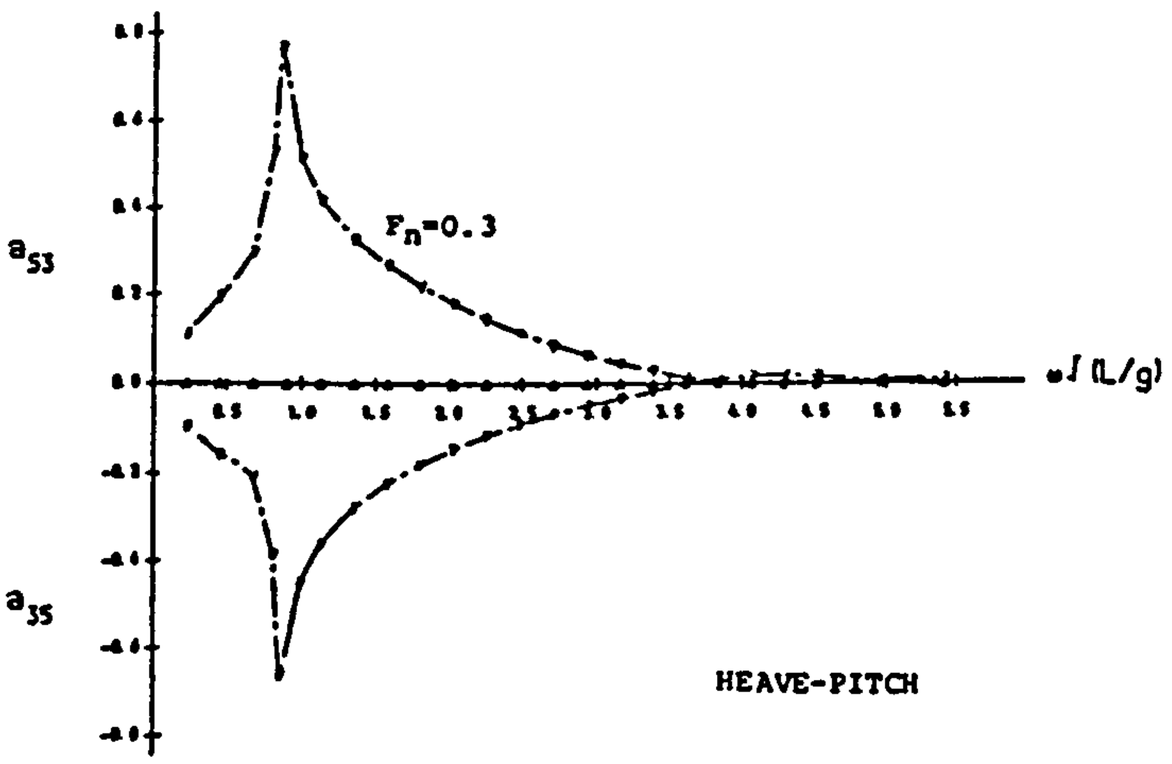

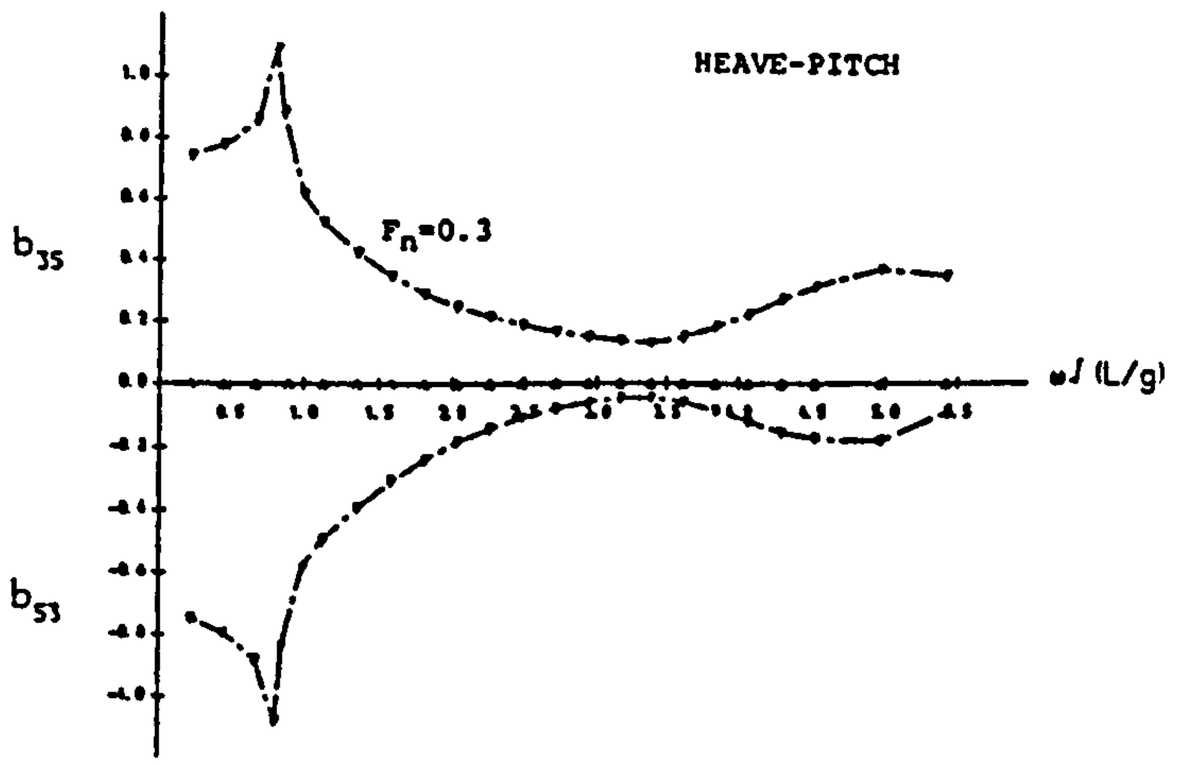

Fig.6.10 NON-DIMENSIONAL COUPLED ADDED MASS AND DAMPING COEFFICIENTS OF A FLOATING ELLIPSOID (L/B=8, B/T=2) AT INFINITE WATER DEPTH AT FROUDE NUMBER 0.0 AND 0.3

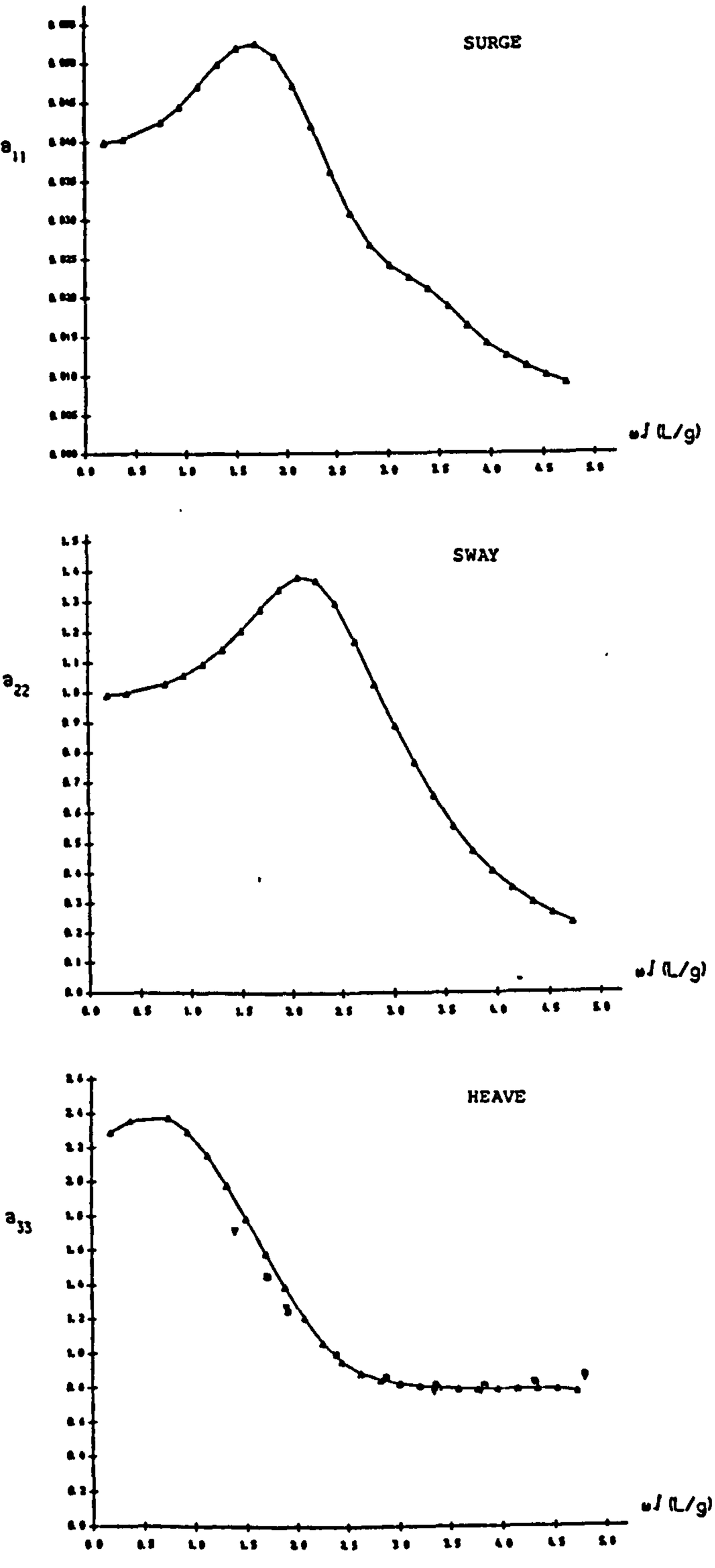

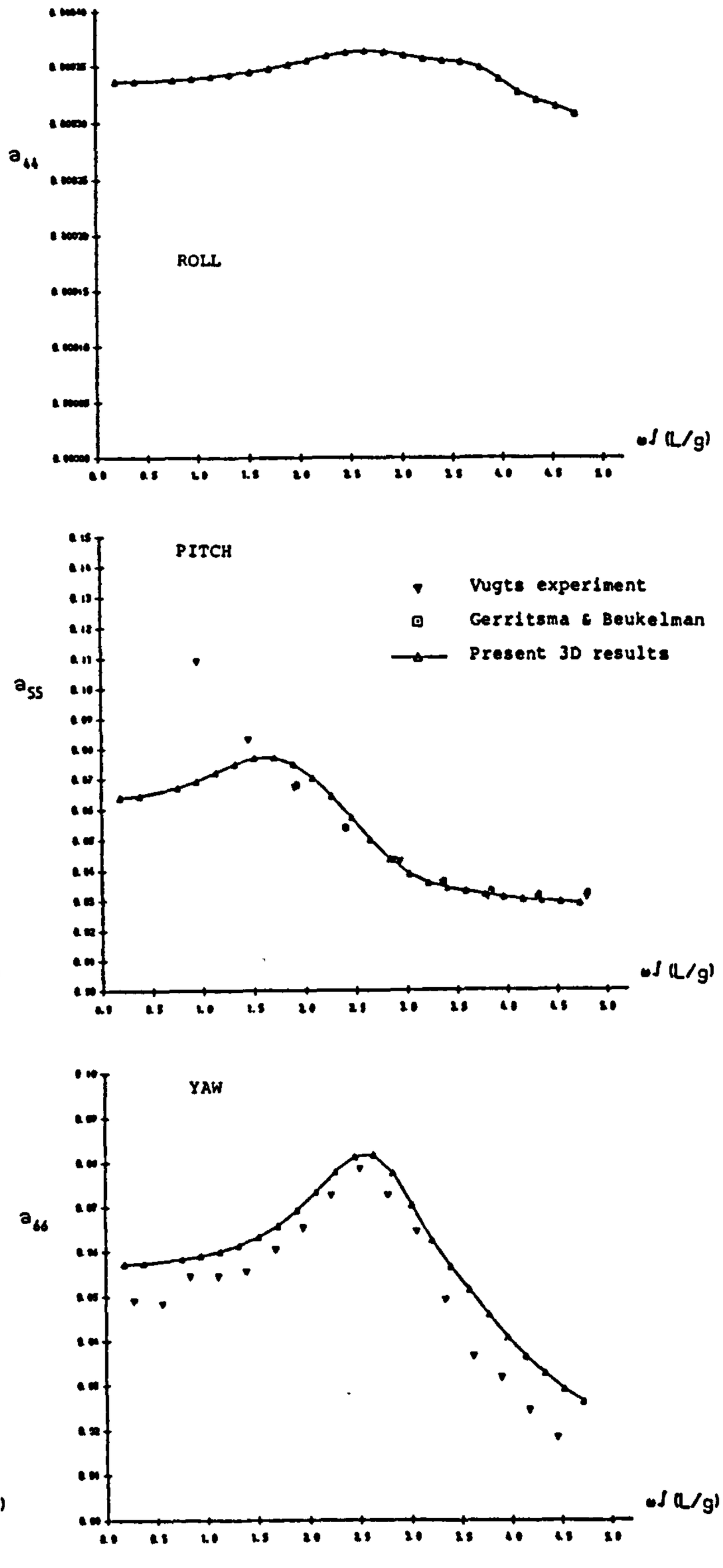

Fig.6.12 NON-DIMENSIONAL ADDED MASS COEFFICIENTS OF A SERIES-60 SHIP OF C_B=0.7 FOR SIX RIGID MODES OF MOTION AT INFINITE WATER DEPTH AT ZERO FROUDE NUMBER

Fig.6.13 NON-DIMENSIONAL DAMPING COEFFICIENTS OF A SERIES-60 SHIP OF C_B=0.7 FOR SIX RIGID MODES OF MOTION AT INFINITE WATER DEPTH AT ZERO FROUDE NUMBER

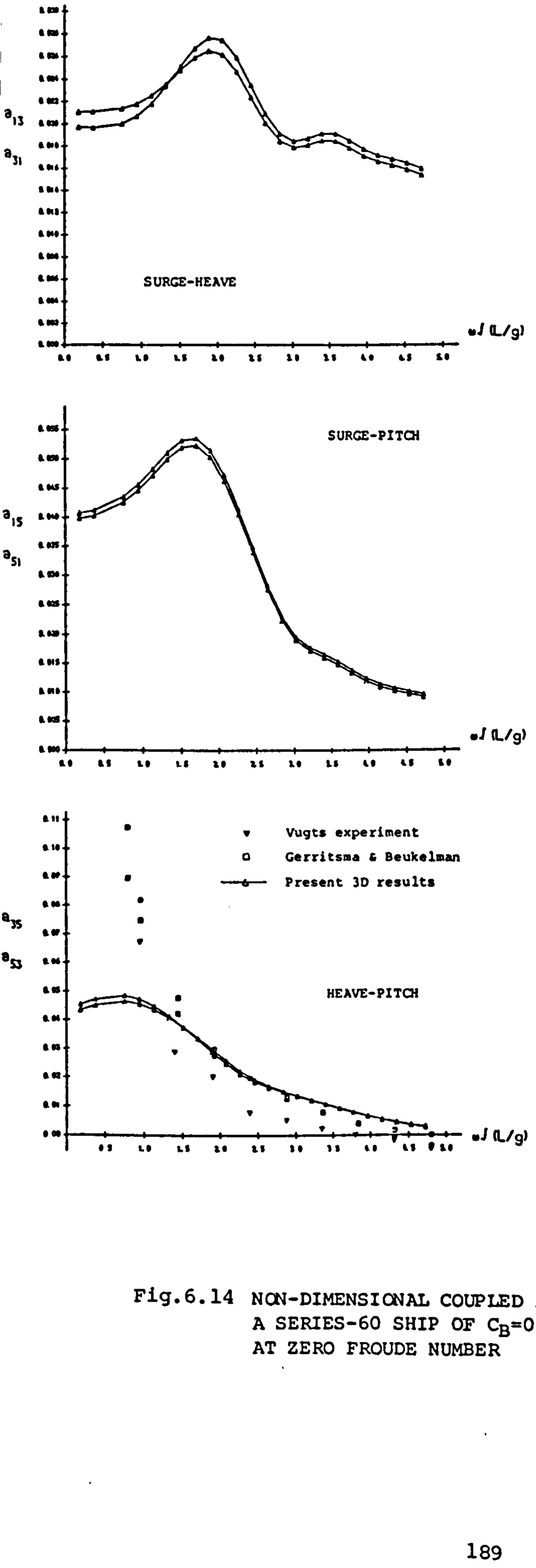

Fig.6.14 NON-DIMENSIONAL COUPLED ADDED MASS COEFFICIENTS OF A SERIES-60 SHIP OF C_B=0.7 AT INFINITE WATER DEPTH AT ZERO FROUDE NUMBER

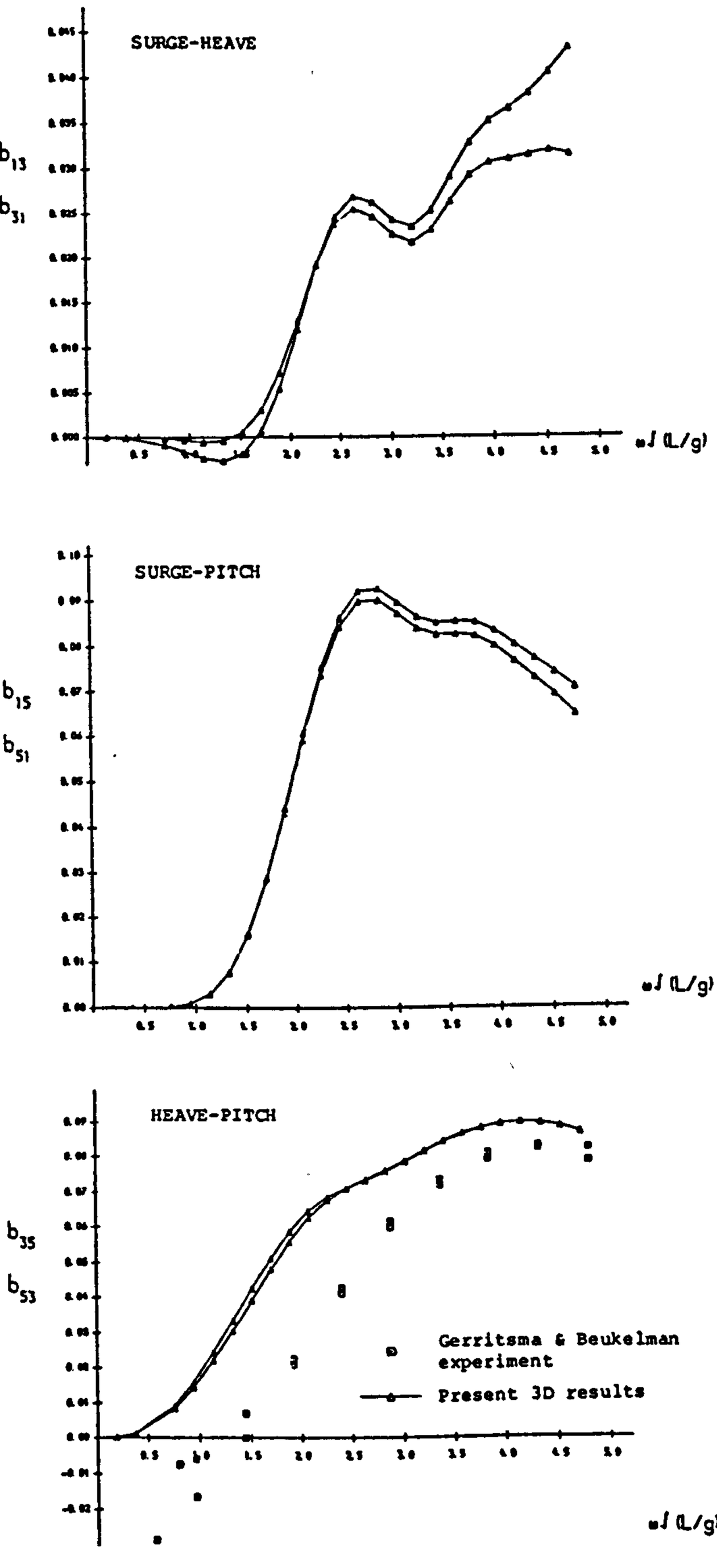

Fig.6.15 NON-DIMENSIONAL COUPLED DAMPING COEFFICIENTS OF A SERIES-60 SHIP OF C_B=0.7 AT INFINITE WATER DEPTH AT ZERO FROUDE NUMBER

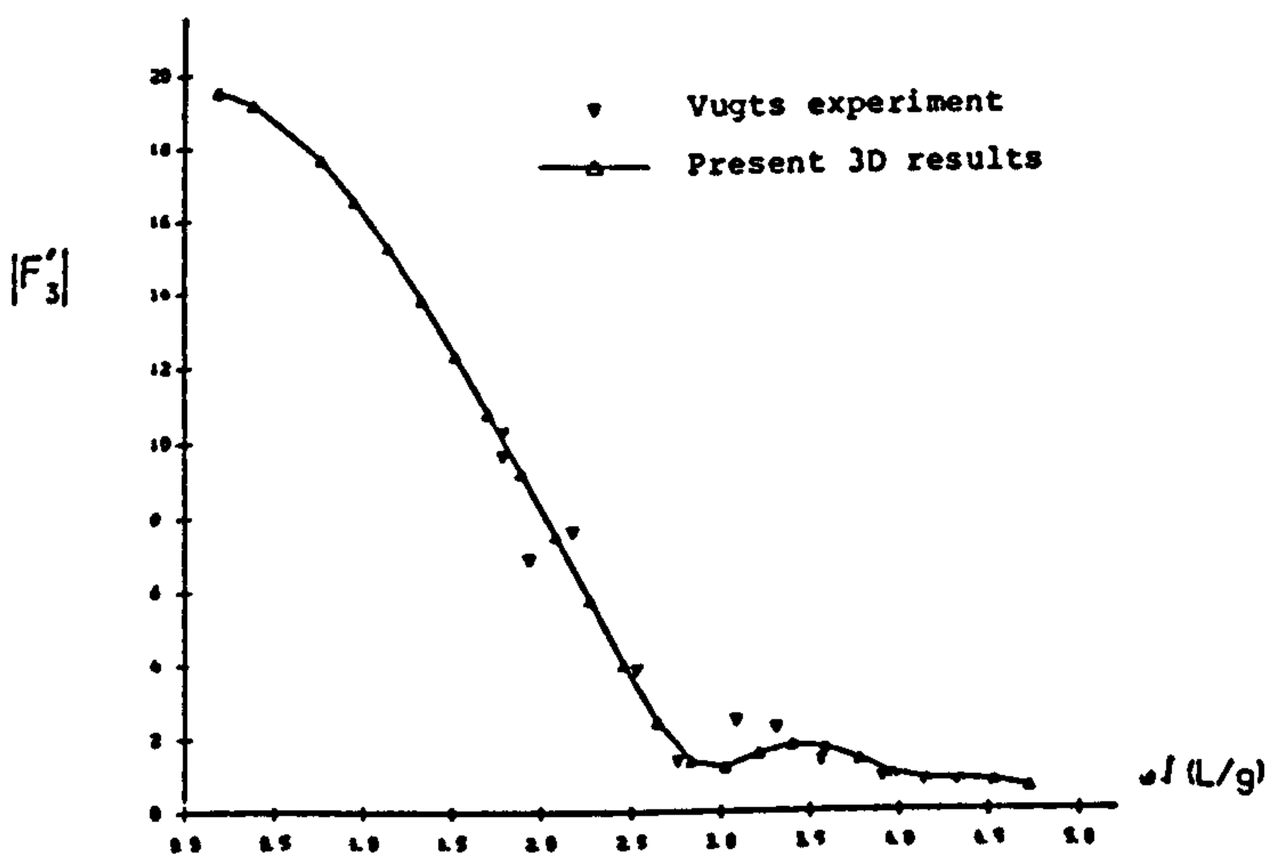

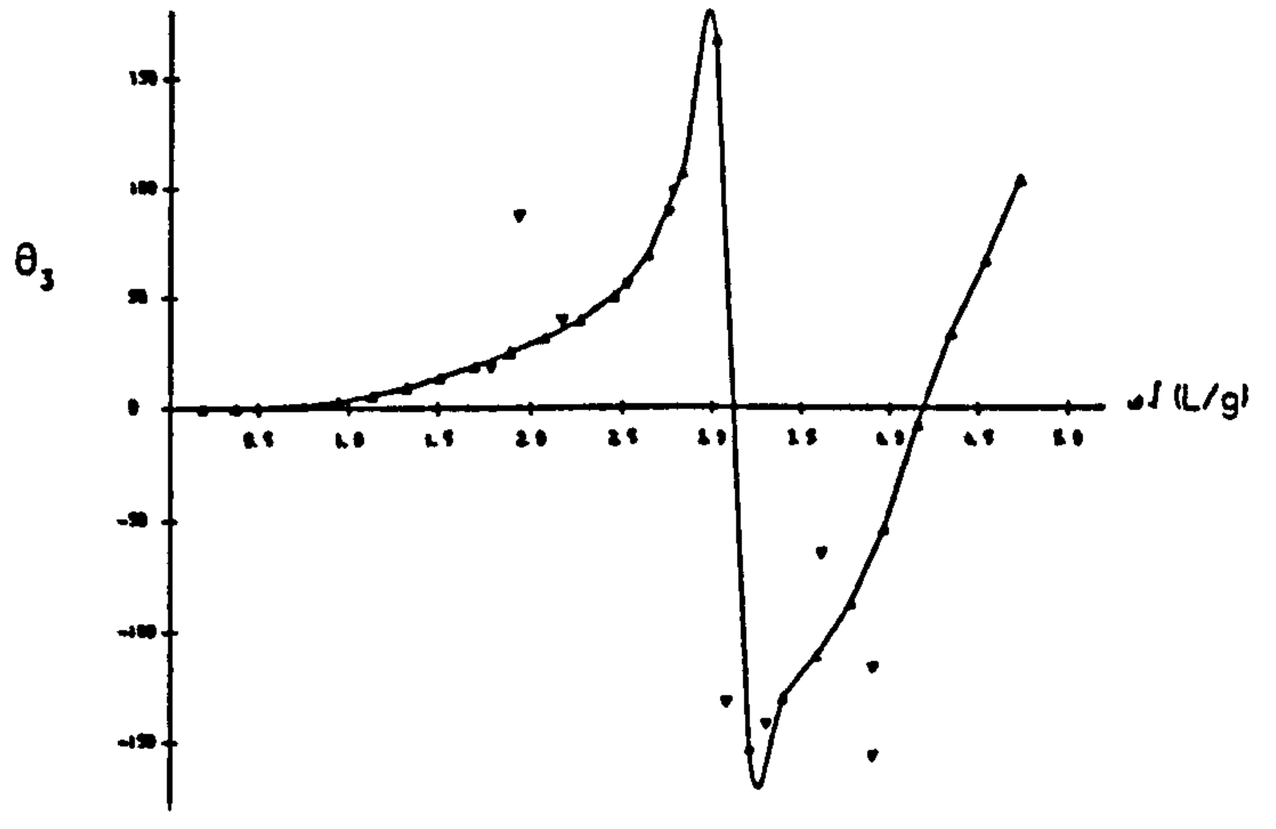

Fig.6.16a ZERO SPEED WAVE EXCITING FORCES (AMPLITUDE AND PHASE) FOR A SERIES-60 SHIP OF C_B=0.7 AT β = 30° AT INFINITE WATER DEPTH.

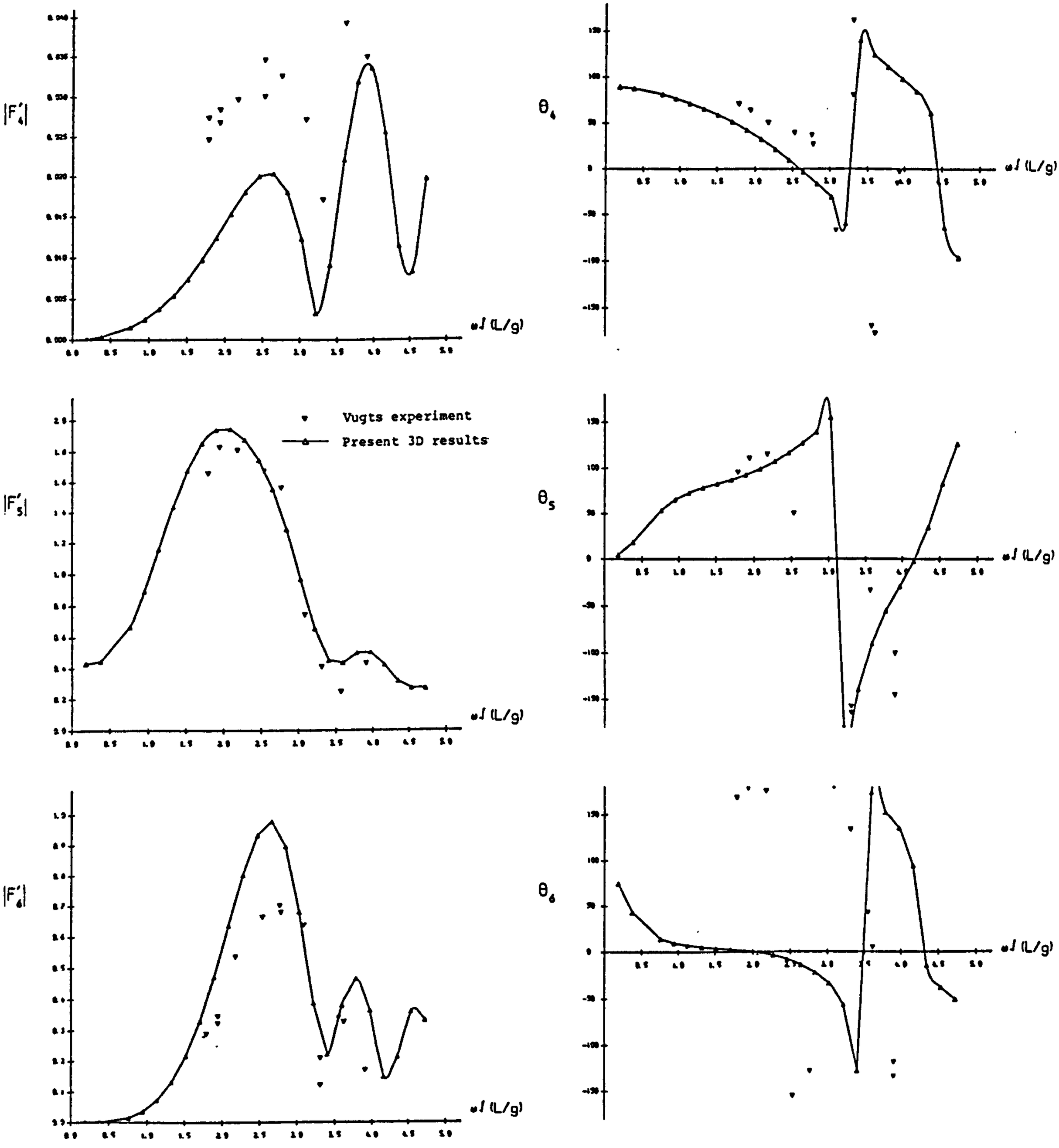

Fig.6.16b ZERO SPEED WAVE EXCITING MOMENTS (AMPLITUDE AND PHASE) FOR A SERIES-60 SHIP OF C_B=0.7 AT β= 30° AT INFINITE WATER DEPTH.

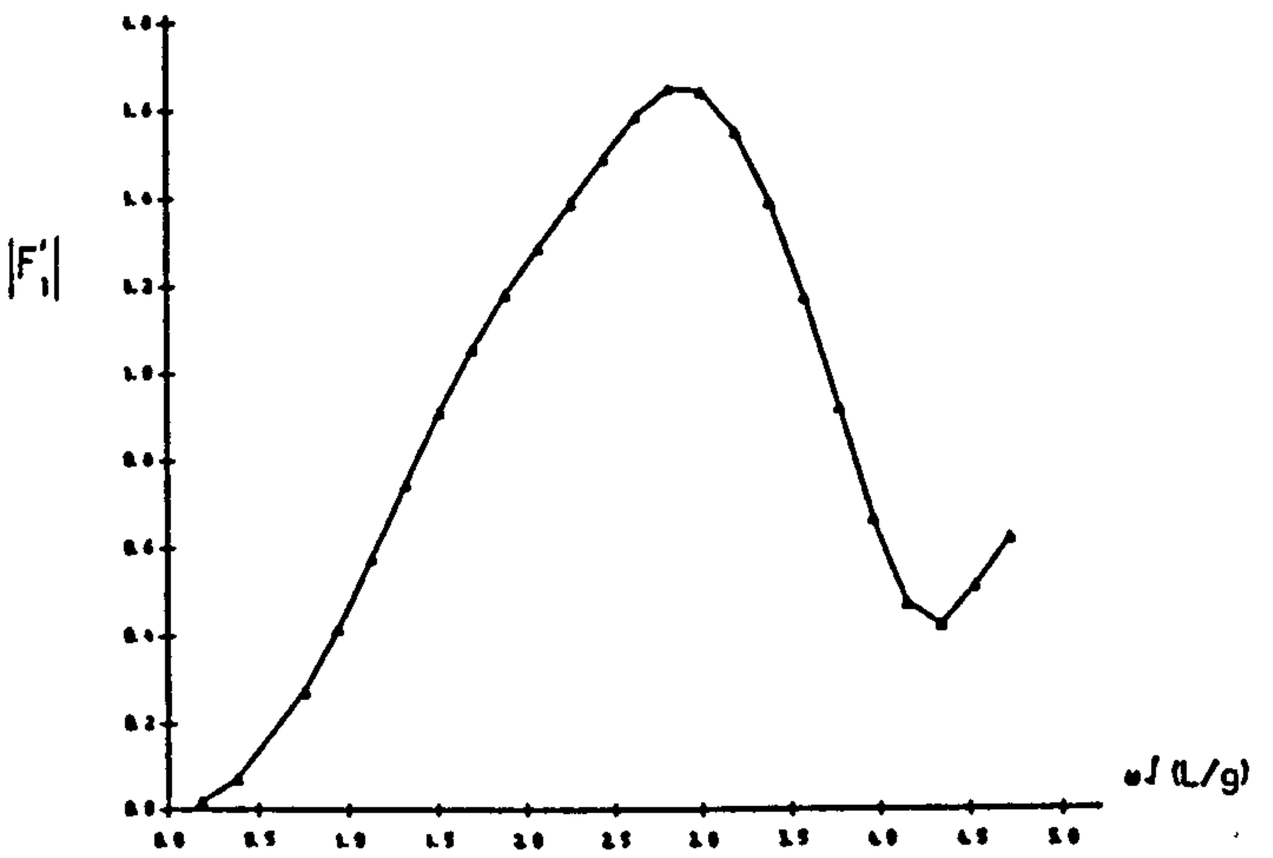

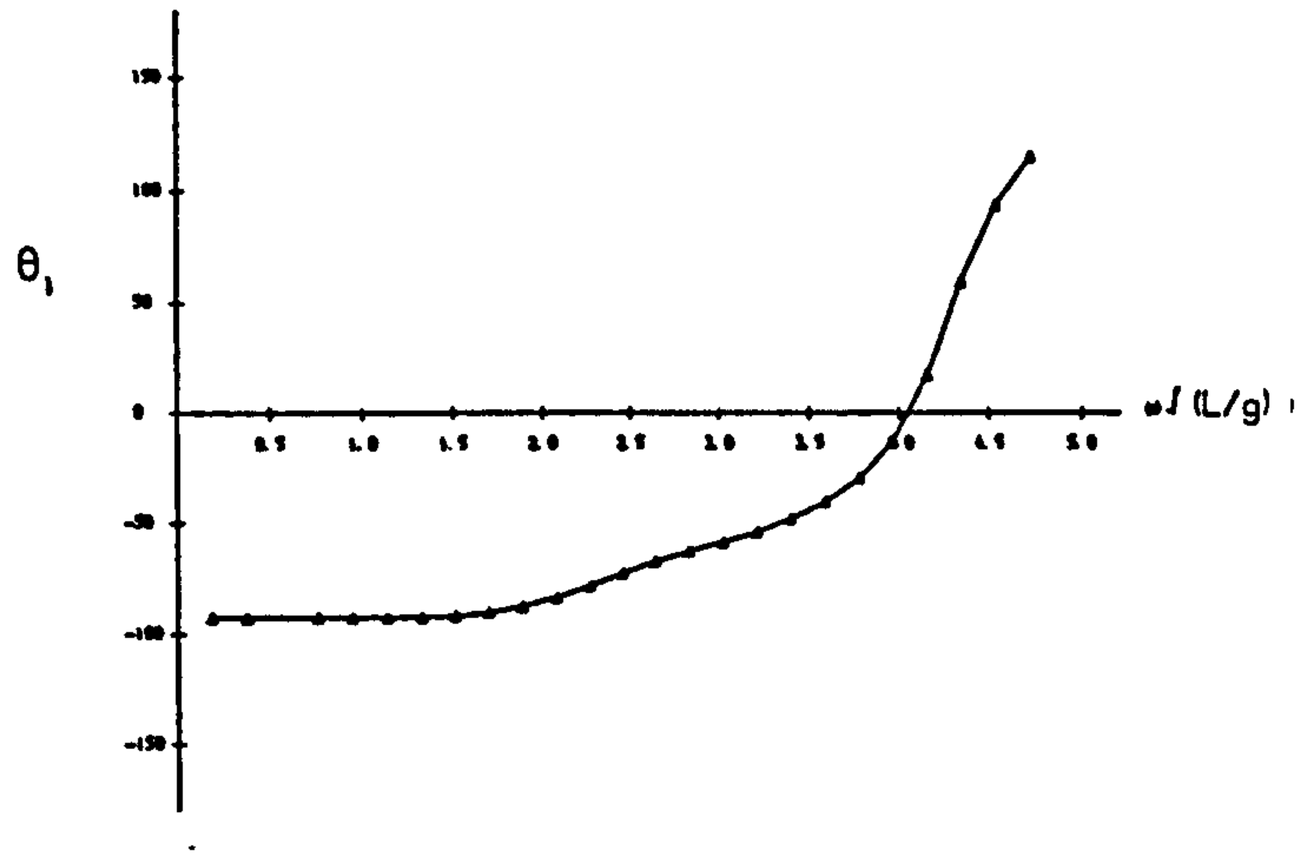

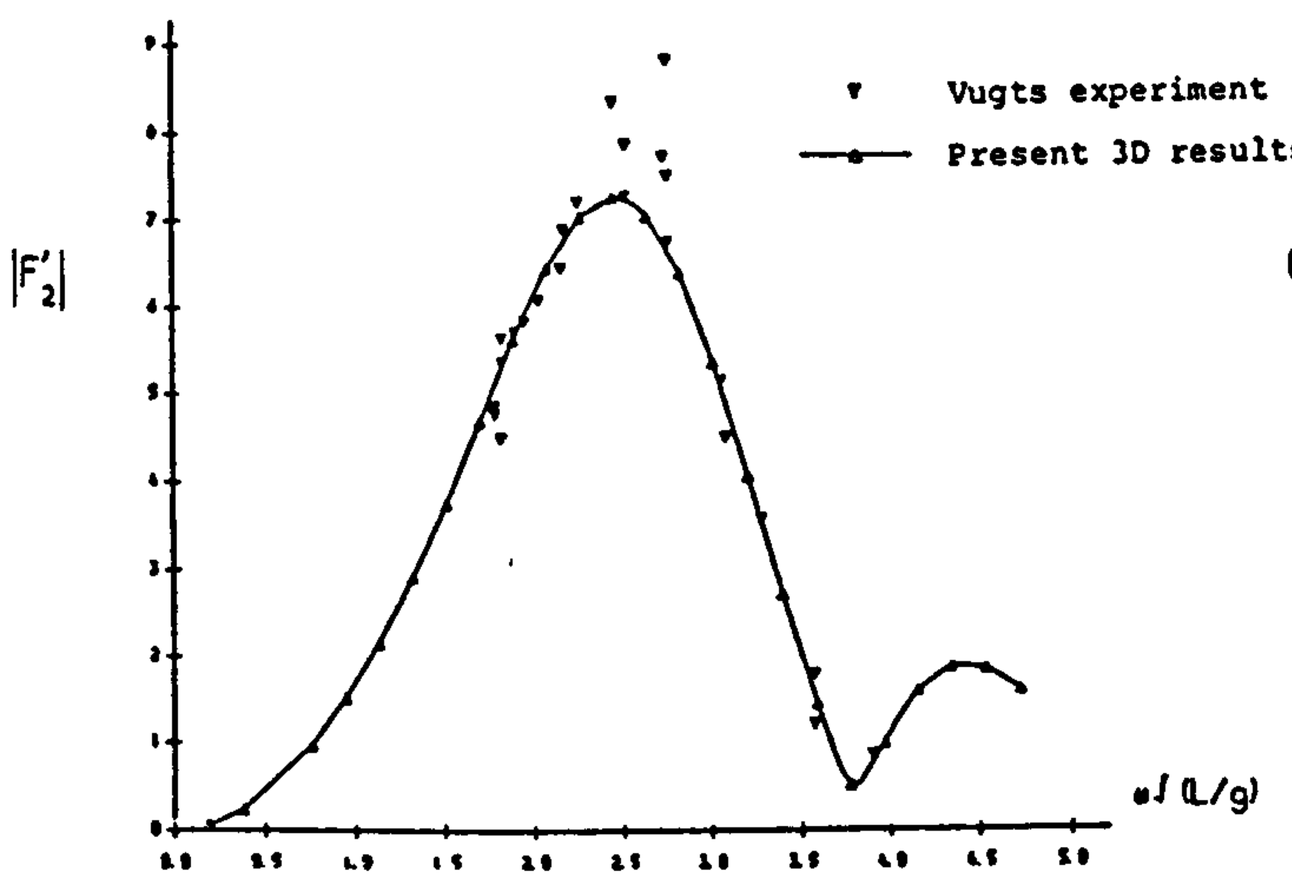

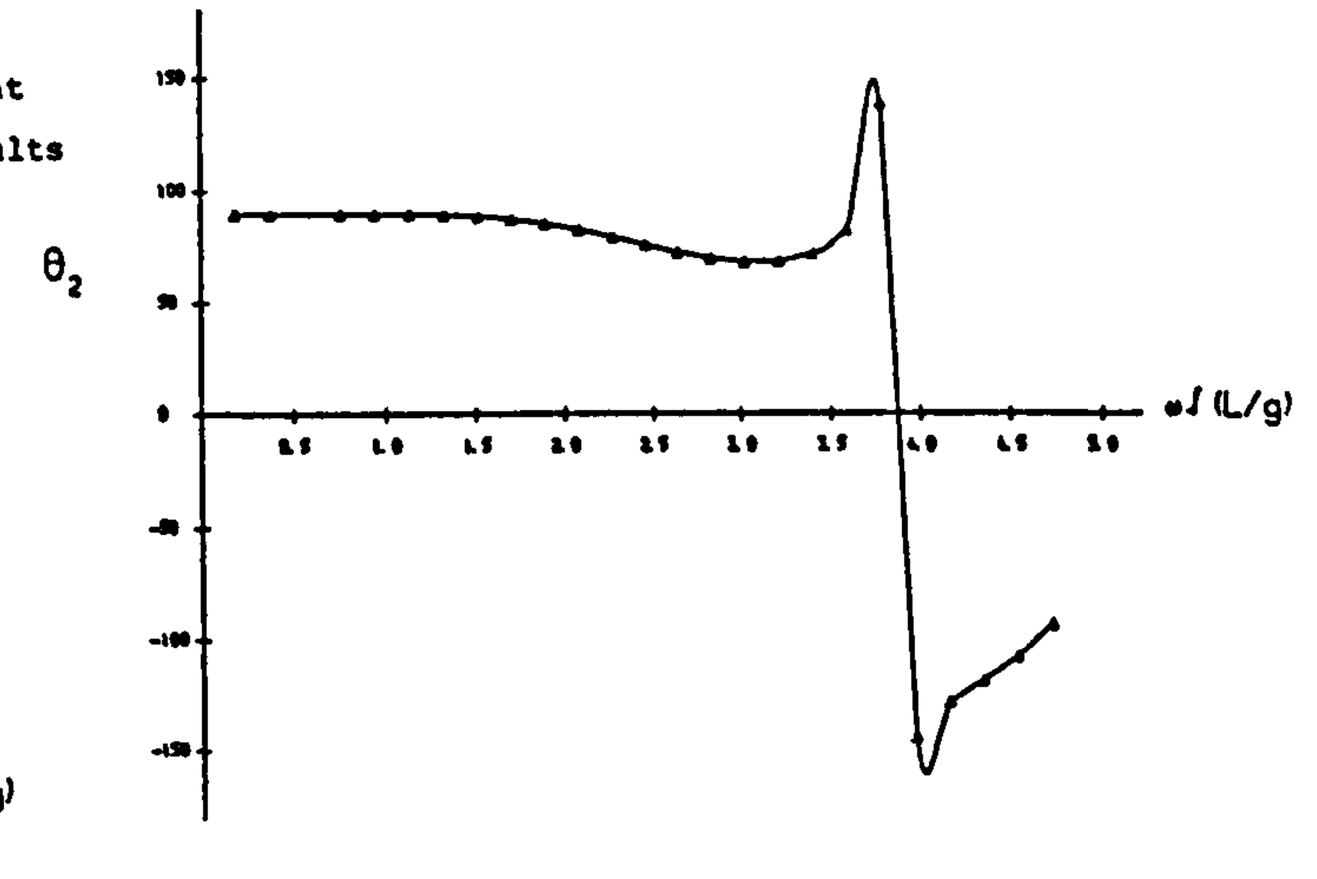

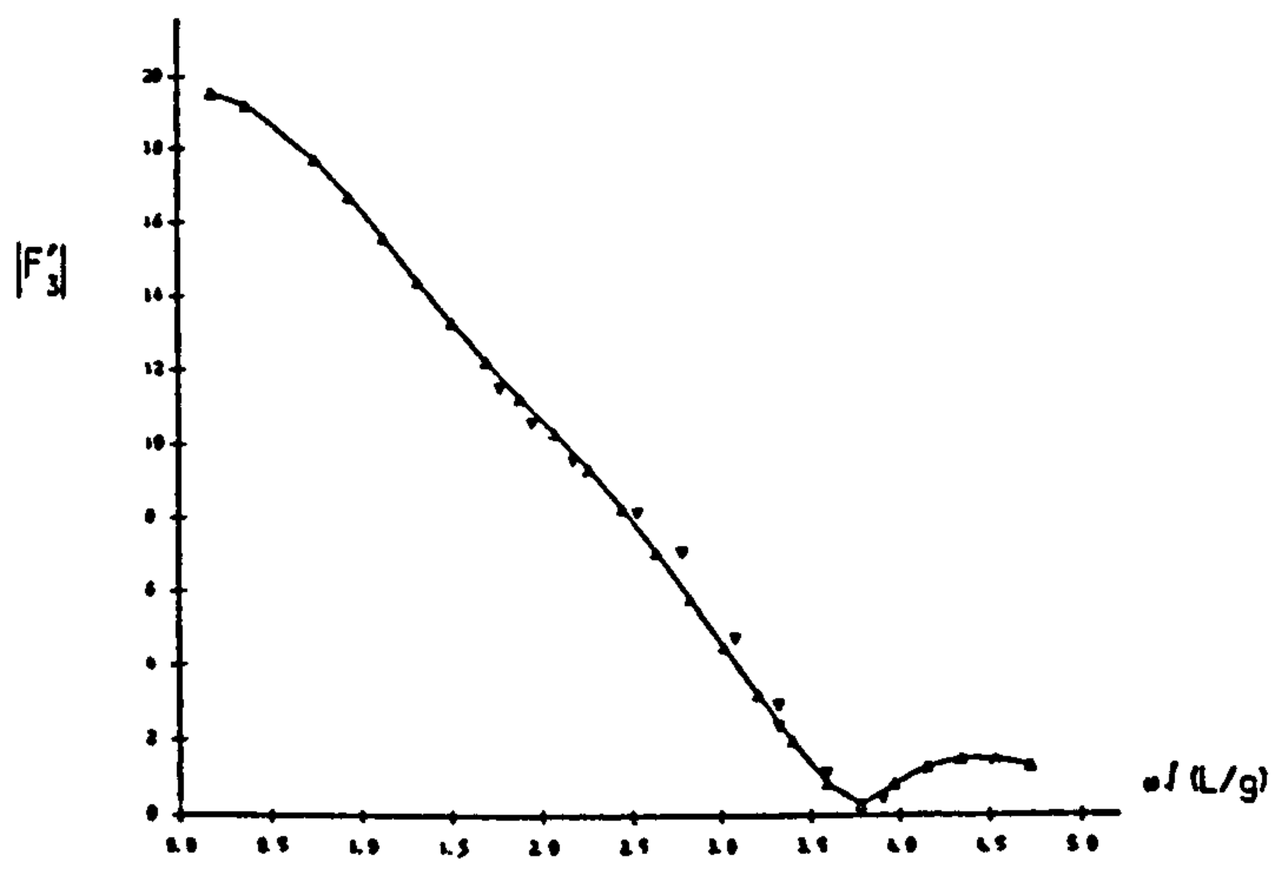

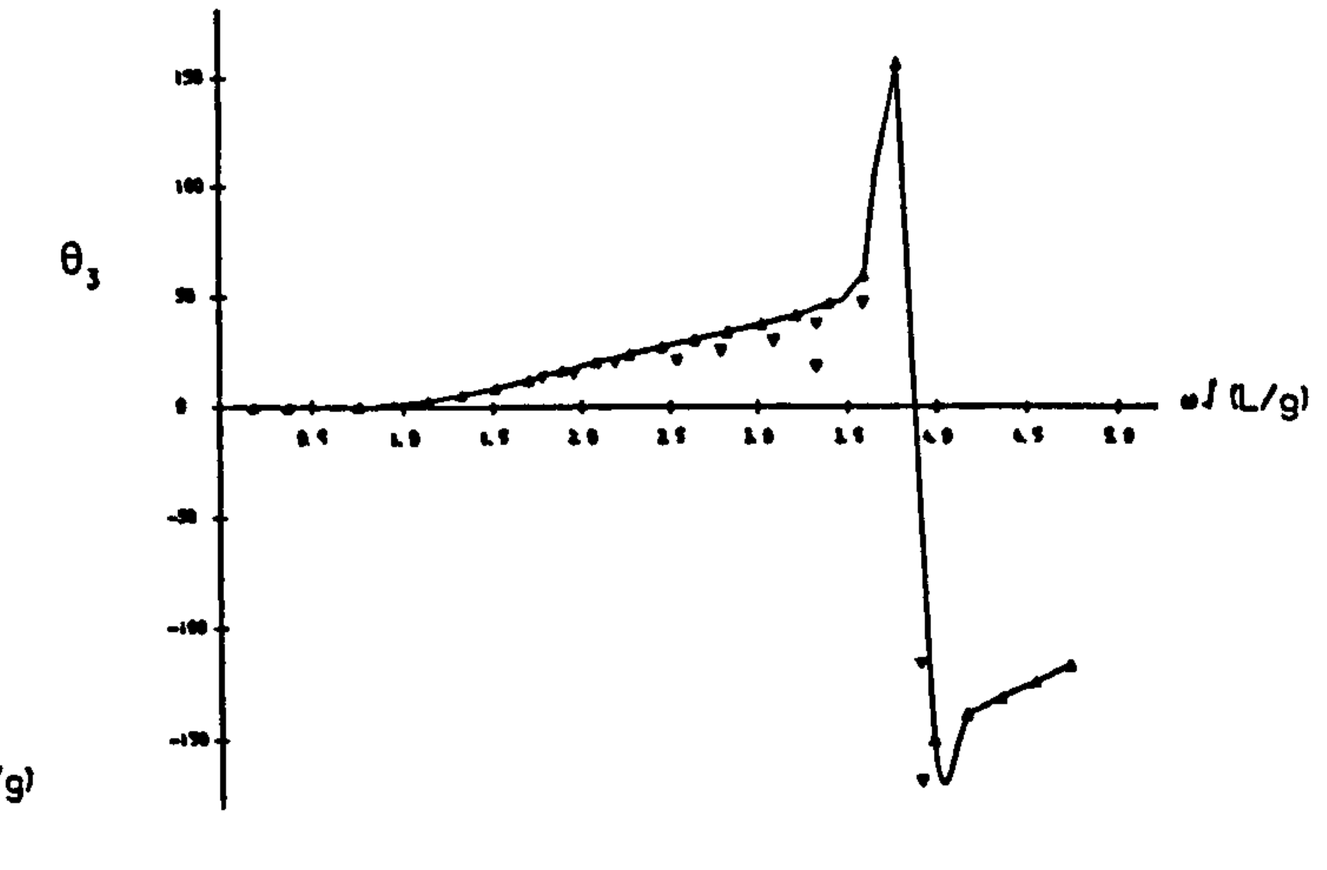

Fig.6.17a ZERO SPEED WAVE EXCITING FORCES (AMPLITUDE AND PHASE) FOR A SERIES-60 SHIP OF C_B=0.7 AT β=120° AT INFINITE WATER DEPTH.

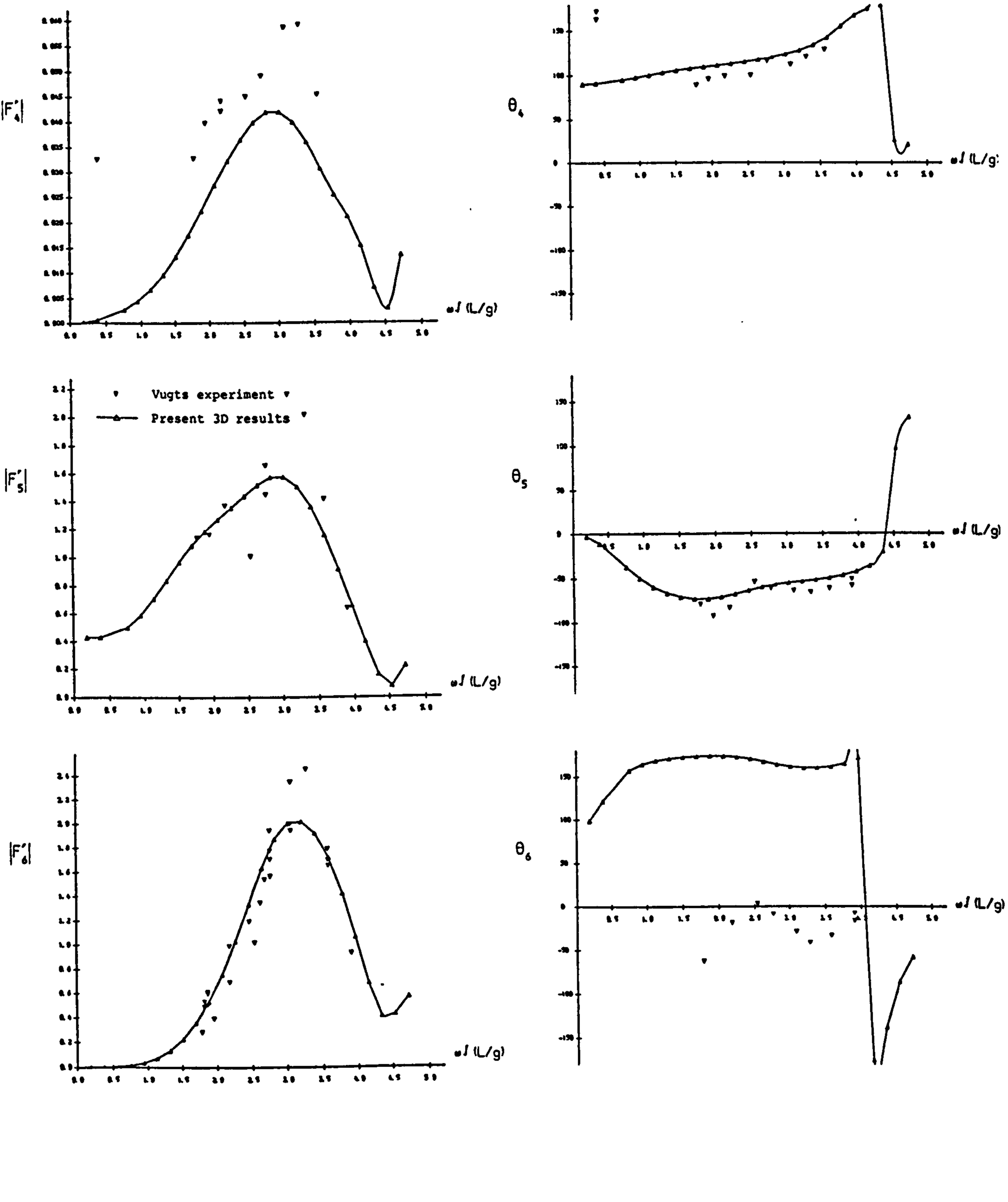

Fig.6.17b ZERO SPEED WAVE EXCITING MOMENTS (AMPLITUDE AND PHASE) FOR A SERIES-60 SHIP OF C_B=0.7 AT β=120° AT INFINITE WATER DEPTH.

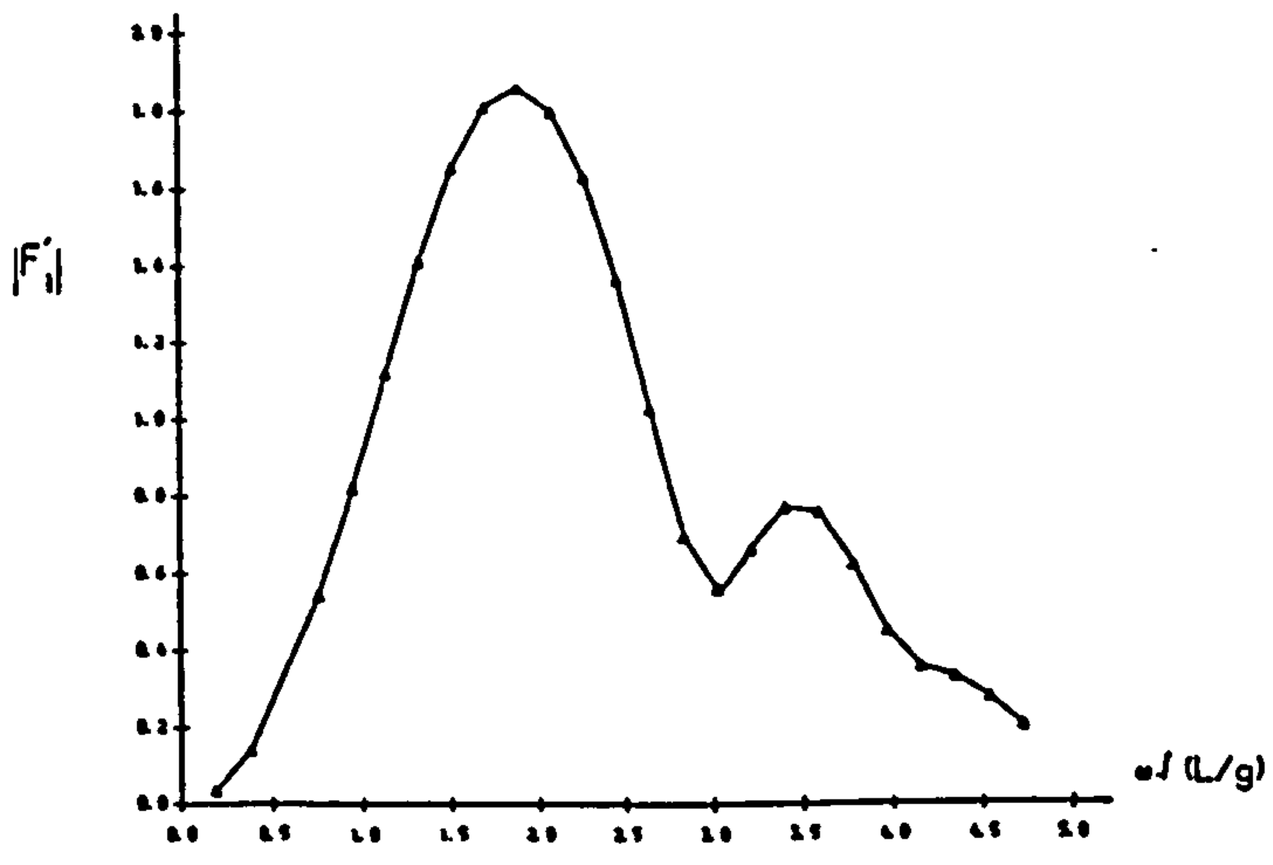

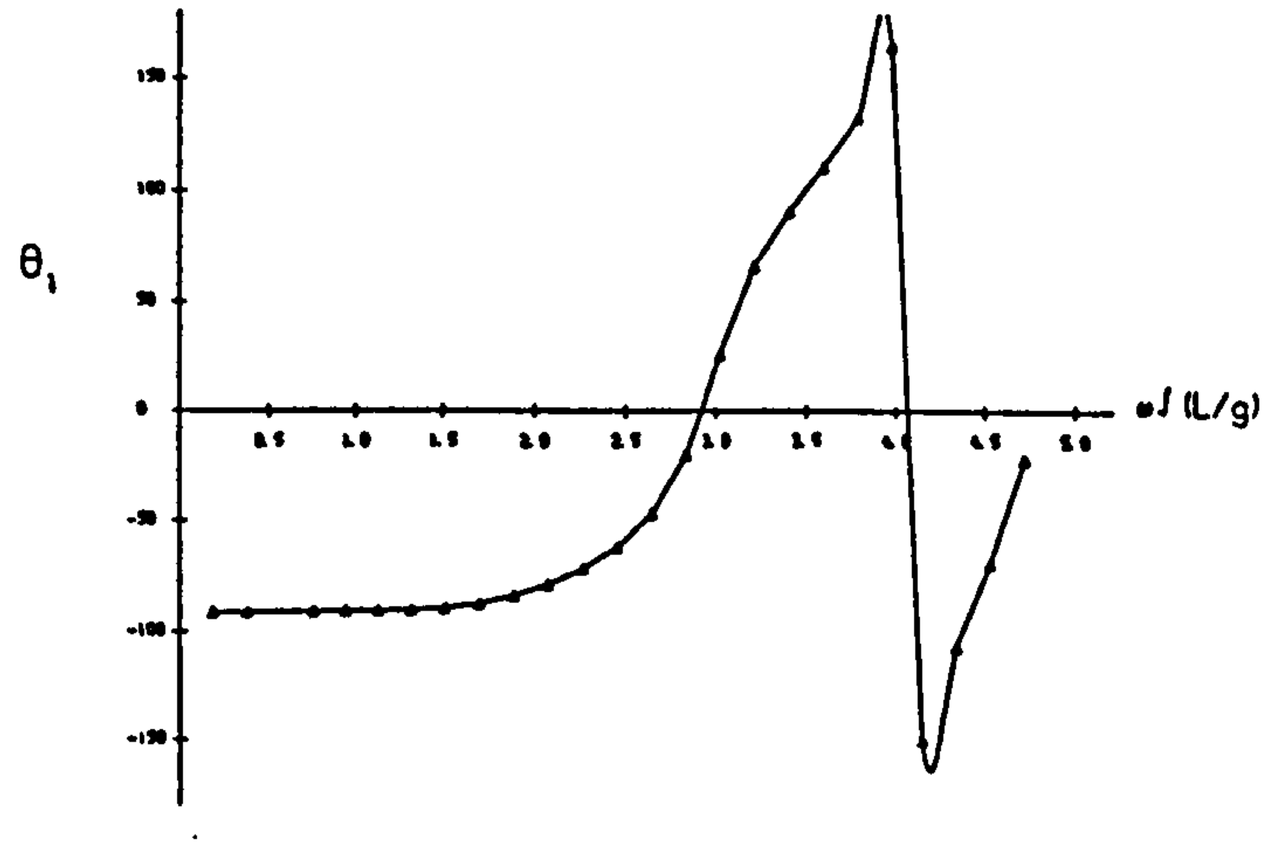

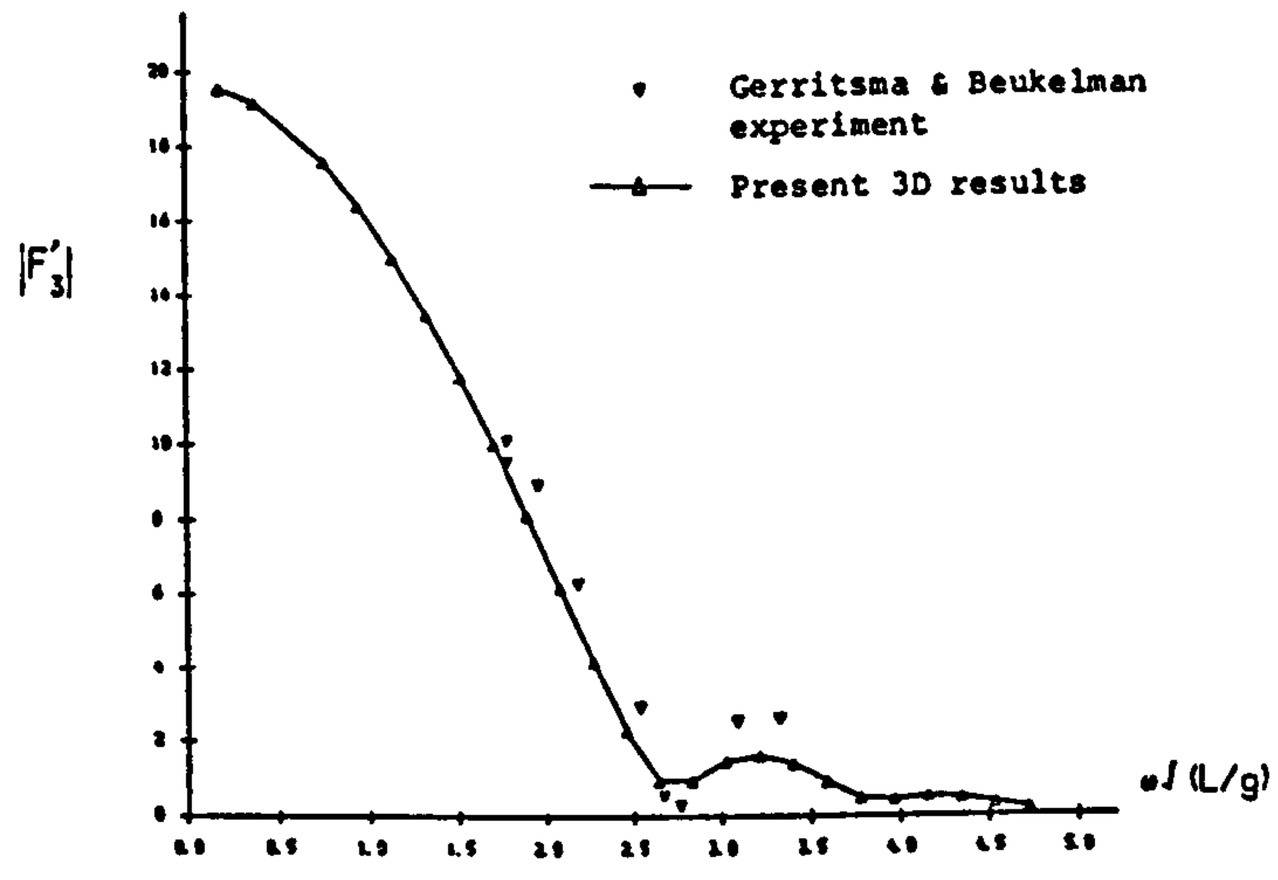

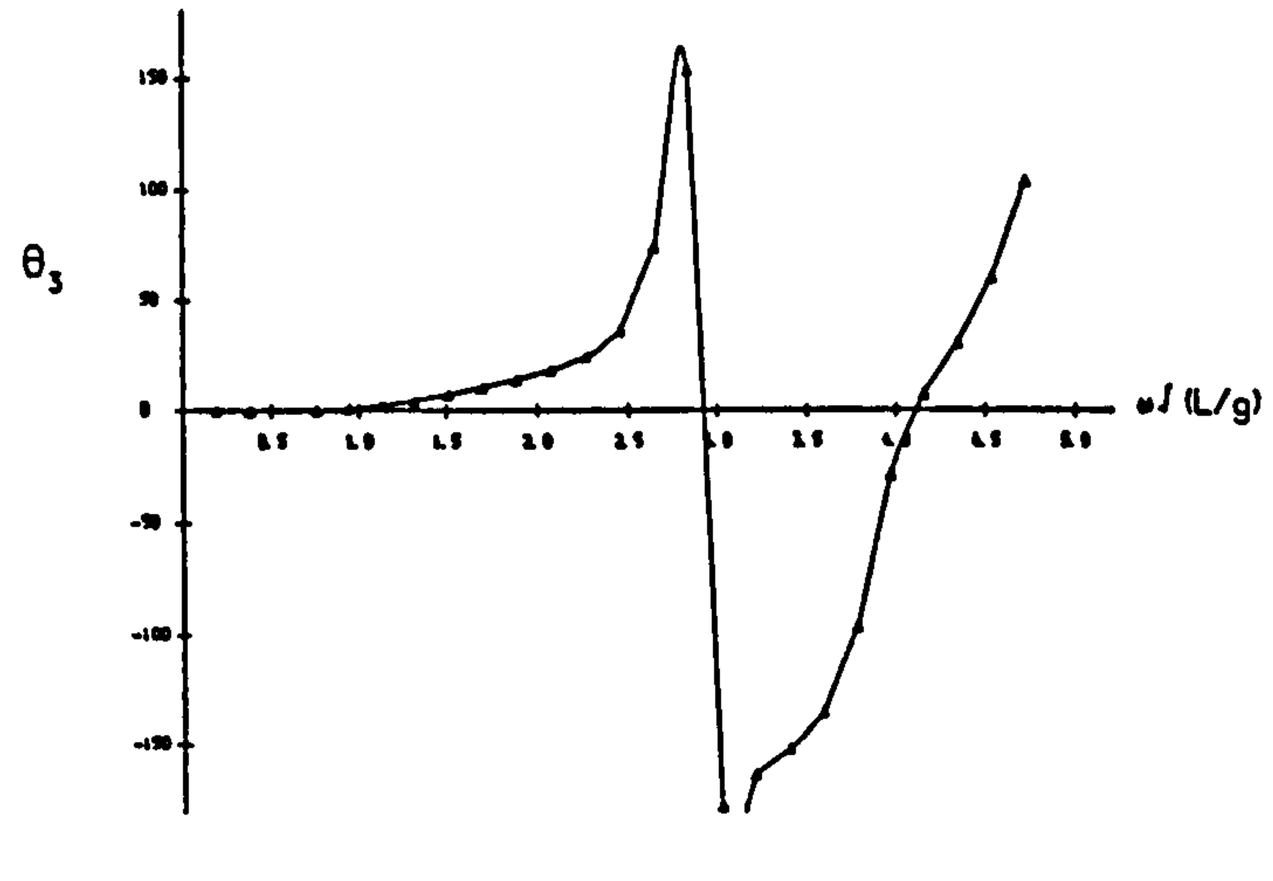

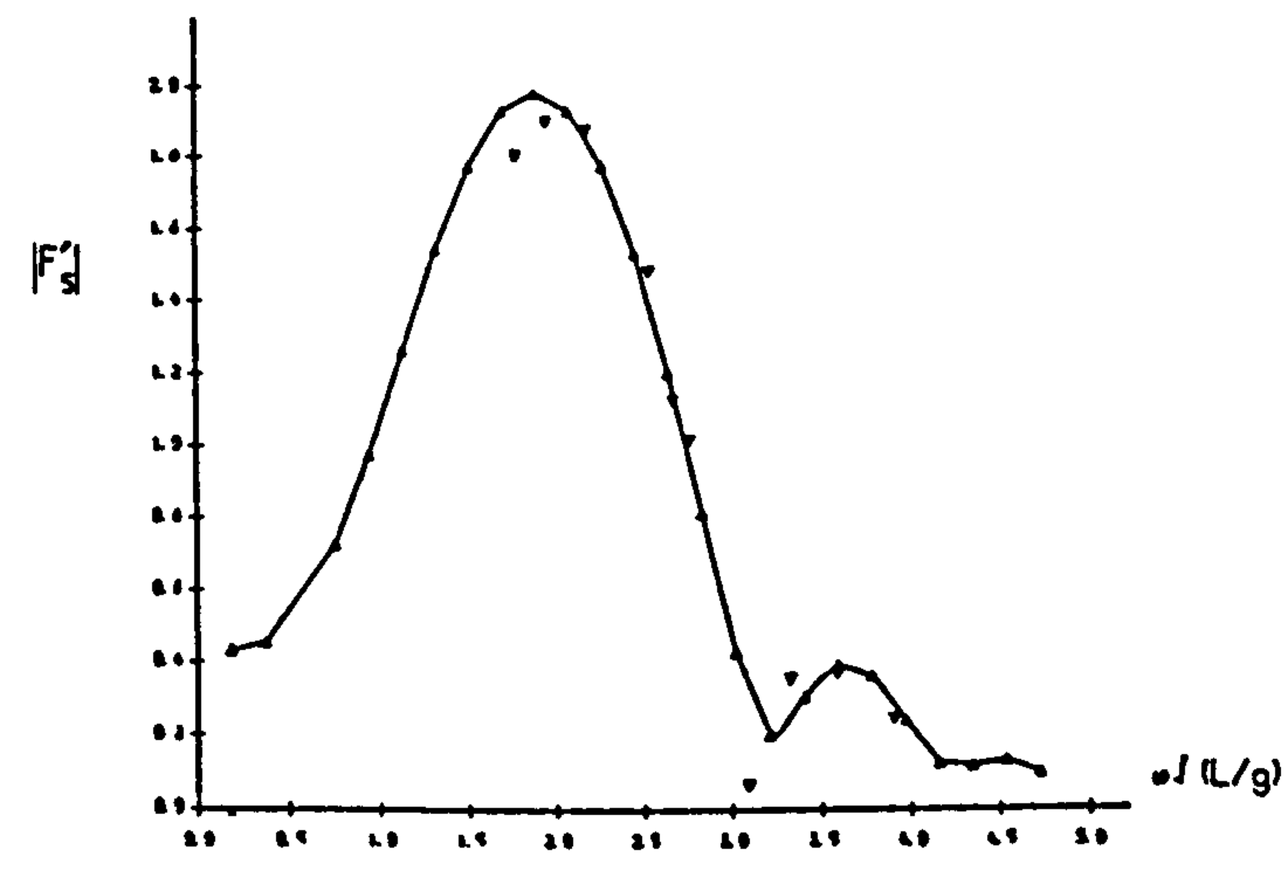

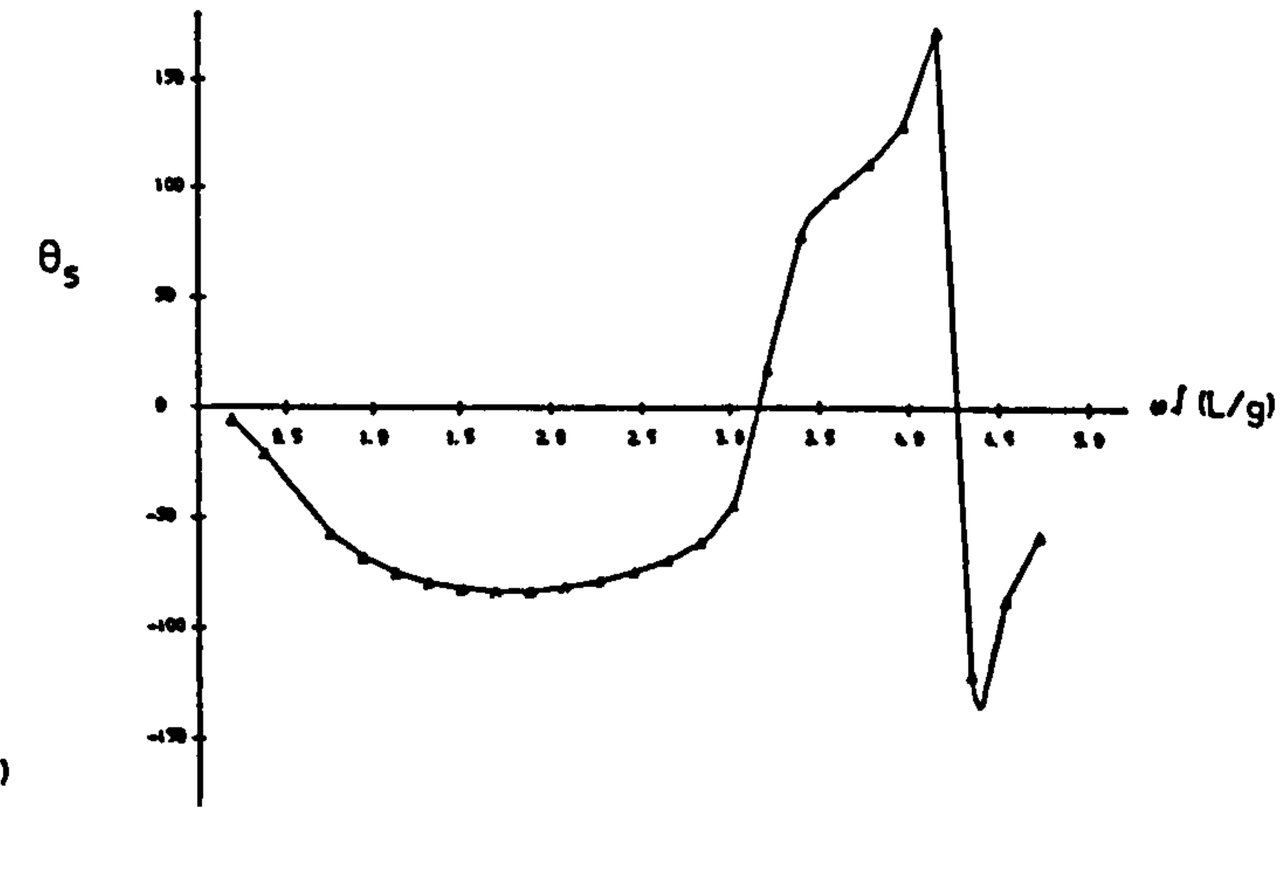

Fig.6.18 ZERO SPEED WAVE EXCITING FORCES AND MOMENT (AMPLITUDE AND PHASE) FOR A SERIES-60 SHIP OF C_B=0.7 AT INFINITE WATER DEPTH IN HEAD WAVES.

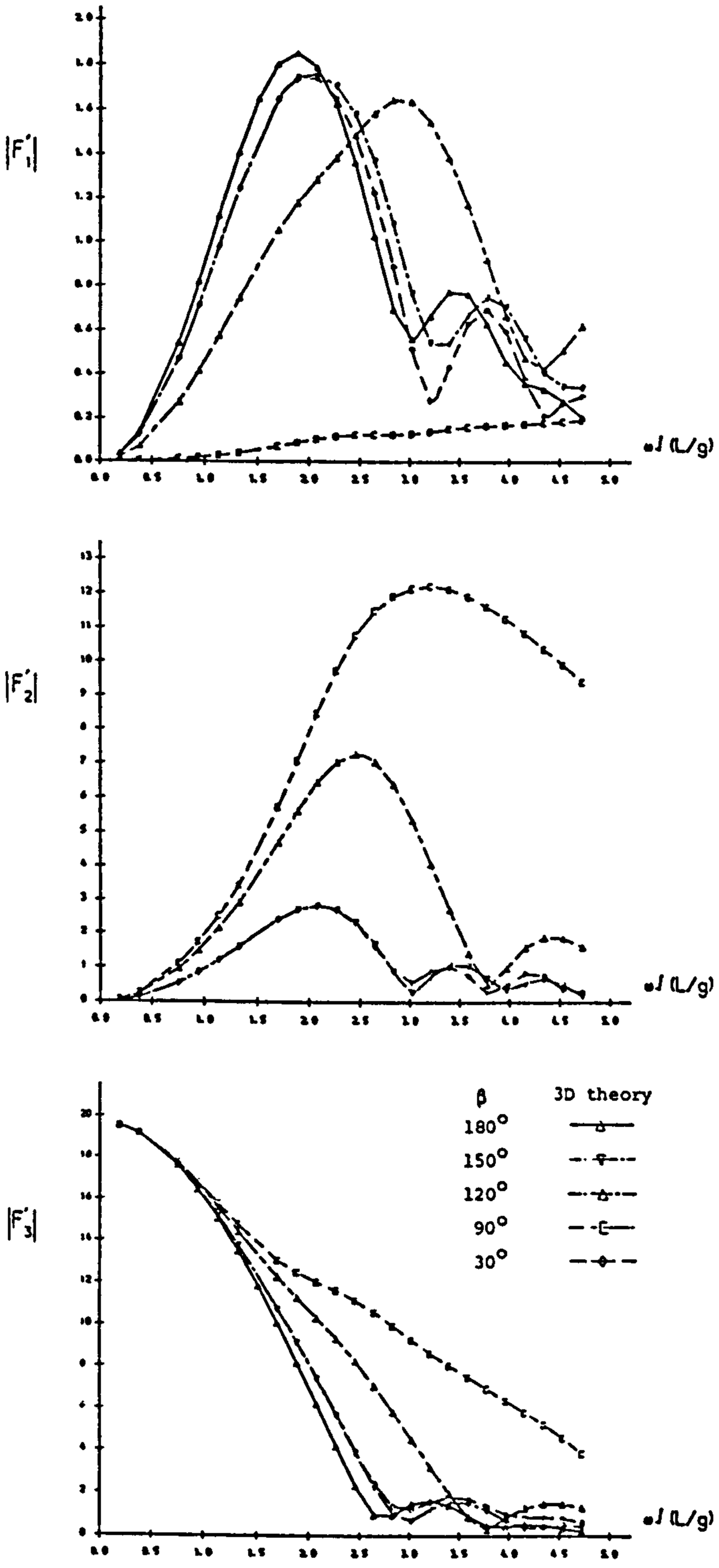

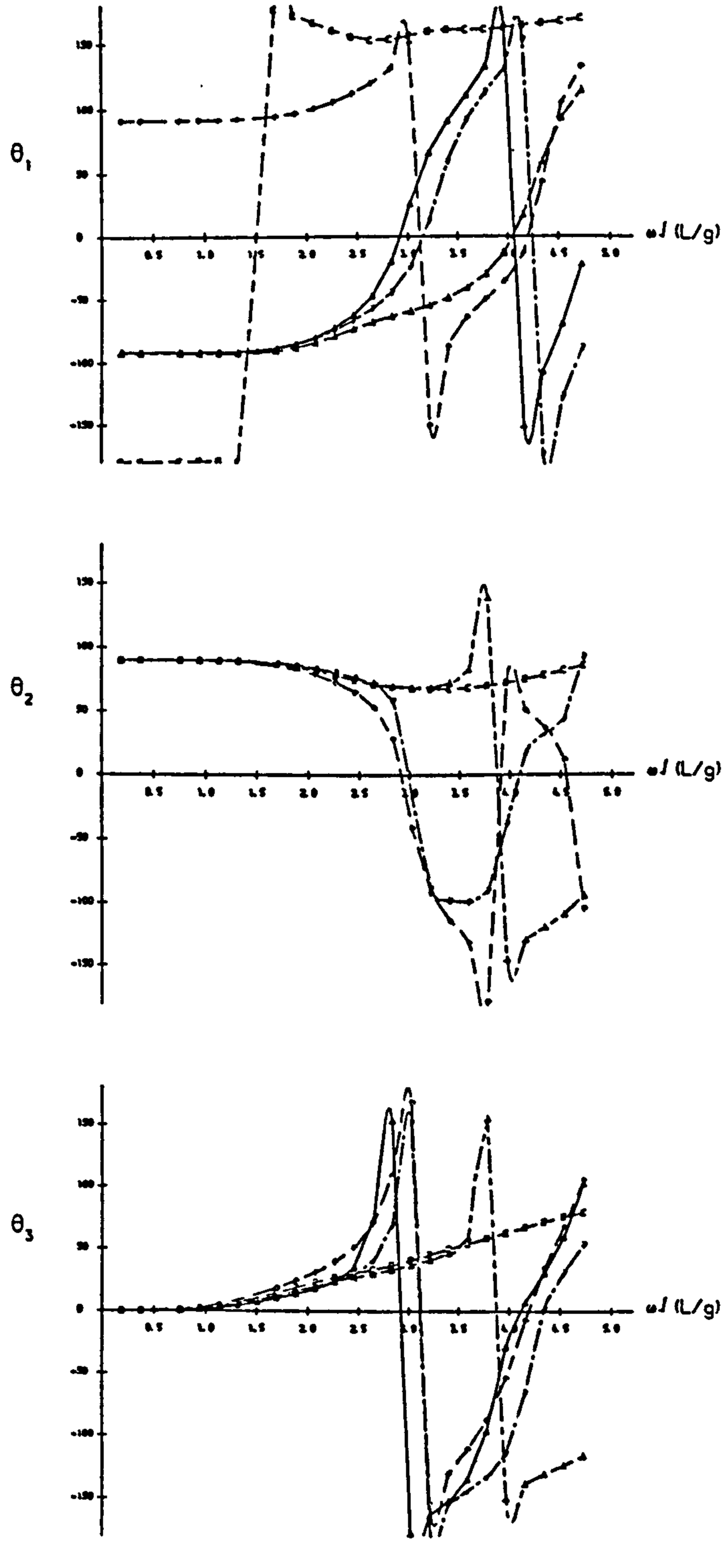

Fig.6.19a ZERO SPEED WAVE EXCITING FORCES (AMPLITUDE AND PHASE) FOR A SERIES-60 SHIP OF C_B=0.7 AT INFINITE WATER DEPTH AT VARIOUS ANGLES OF WAVE INCIDENCE

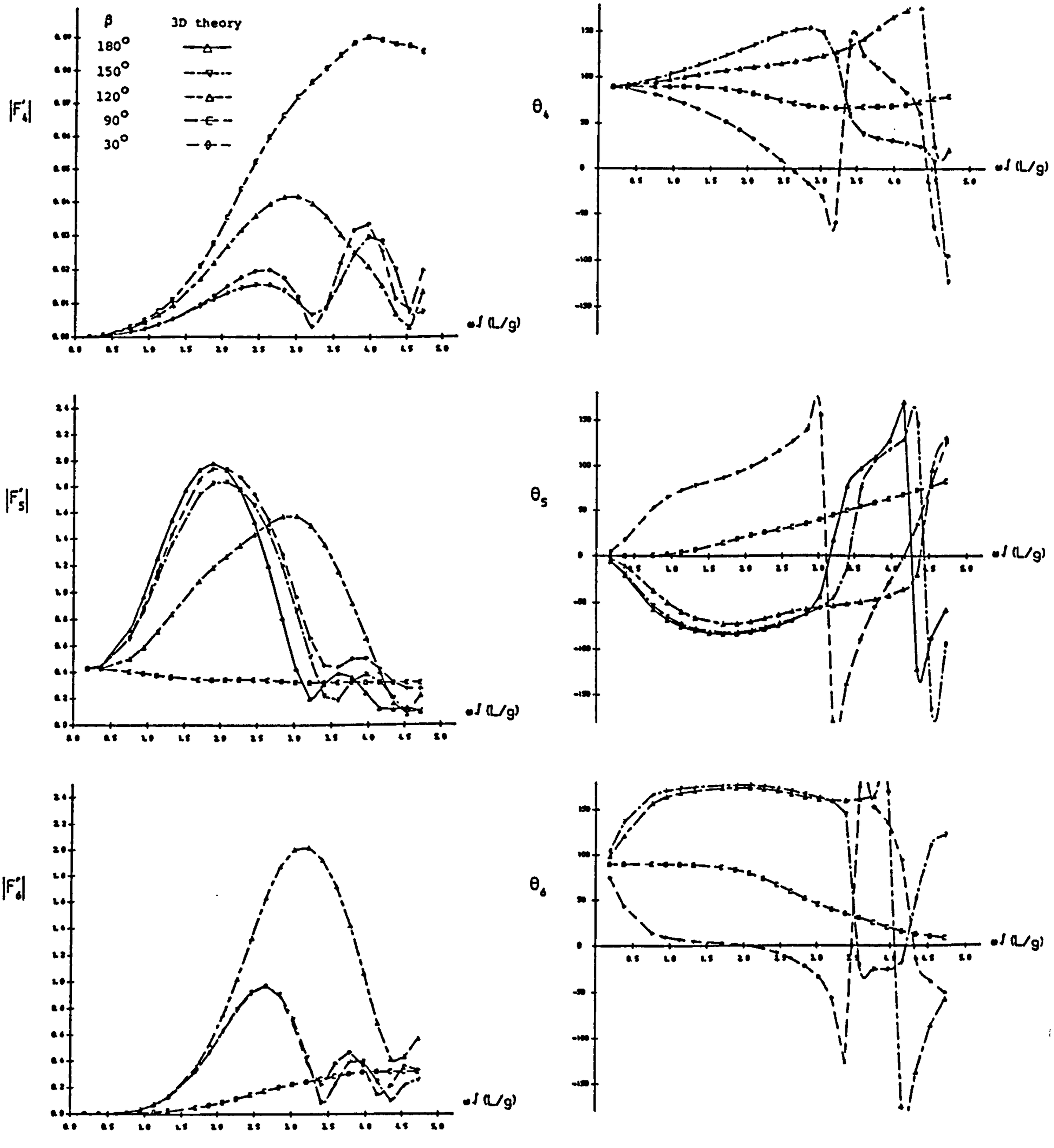

Fig.6.19b ZERO SPEED WAVE EXCITING MOMENTS (AMPLITUDE AND PHASE) FOR A SERIES-60 SHIP OF C_B=0.7 AT INFINITE WATER DEPTH AT VARIOUS ANGLES OF WAVE INCIDENCE

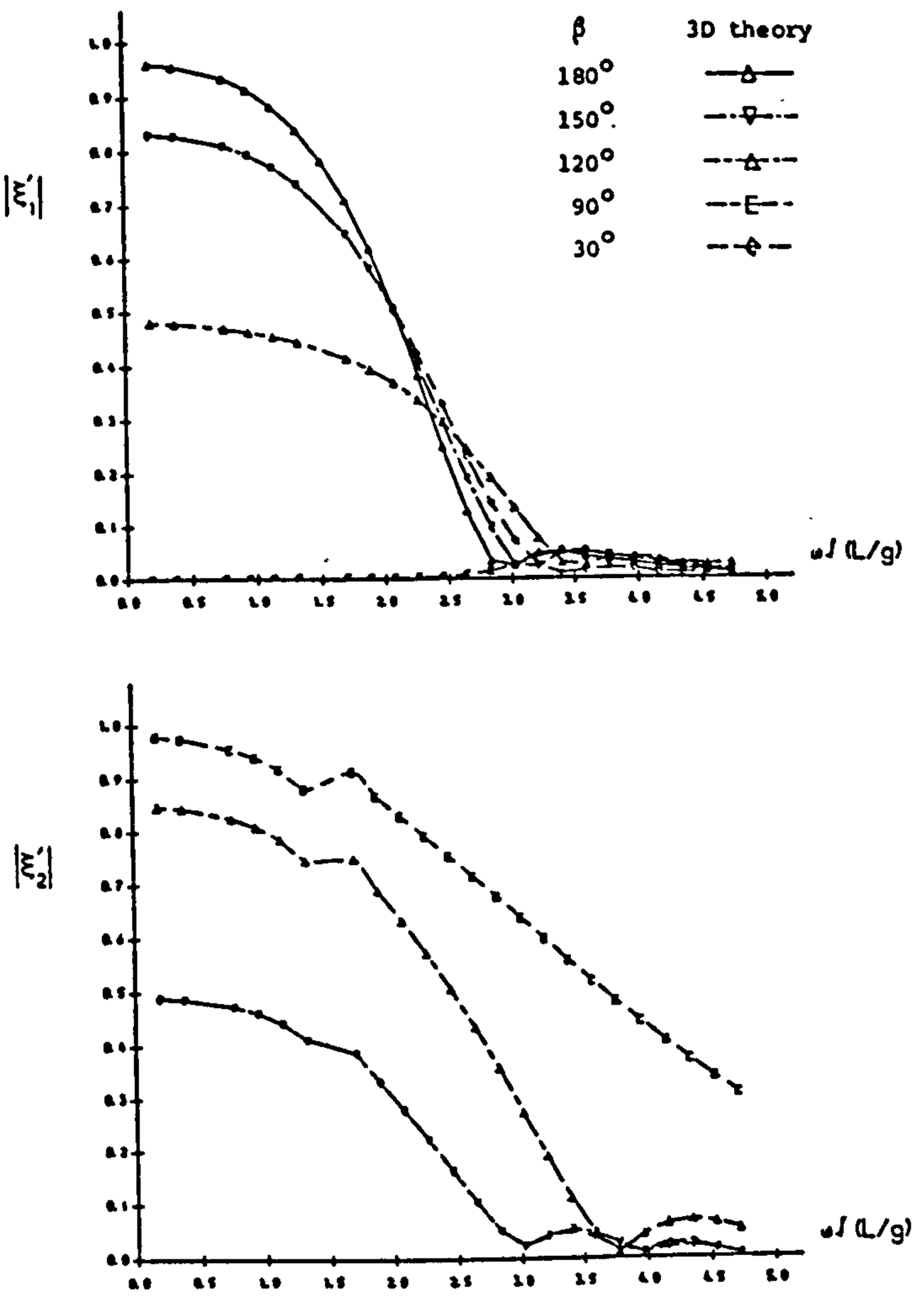

Fig.6.20a ZERO SPEED MOTION RESPONSES (AMPLITUDE AND PHASE) FOR A SERIES-60 SHIP OF C_B=0.7 AT INFINITE WATER DEPTH AT VARIOUS ANGLES OF WAVE INCIDENCE

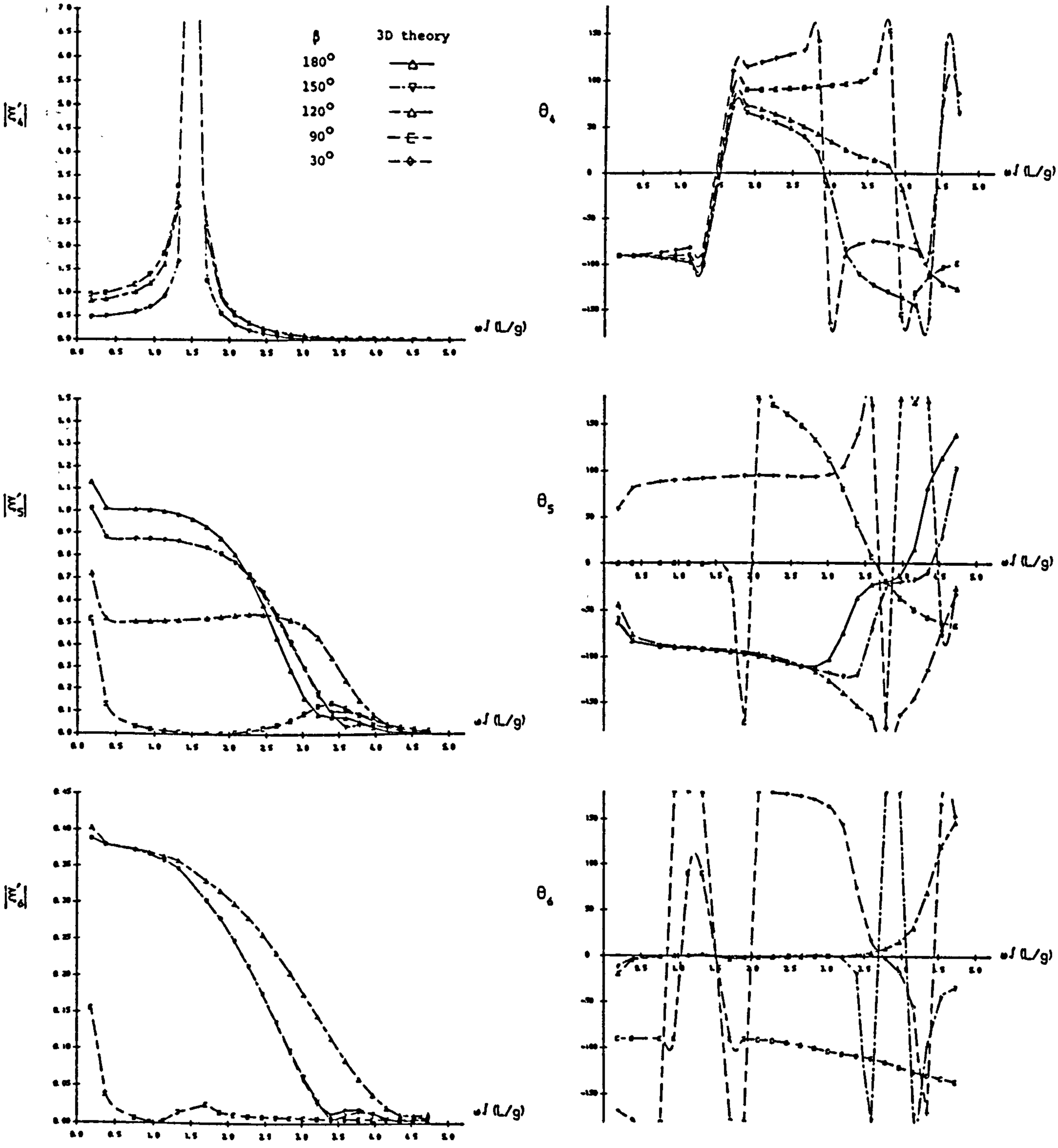

Fig.6.20b ZERO SPEED MOTION RESPONSES (AMPLITUDE AND PHASE) FOR A SERIES-60 SHIP OF C_B=0.7 AT INFINITE WATER DEPTH AT VARIOUS ANGLES OF WAVE INCIDENCE

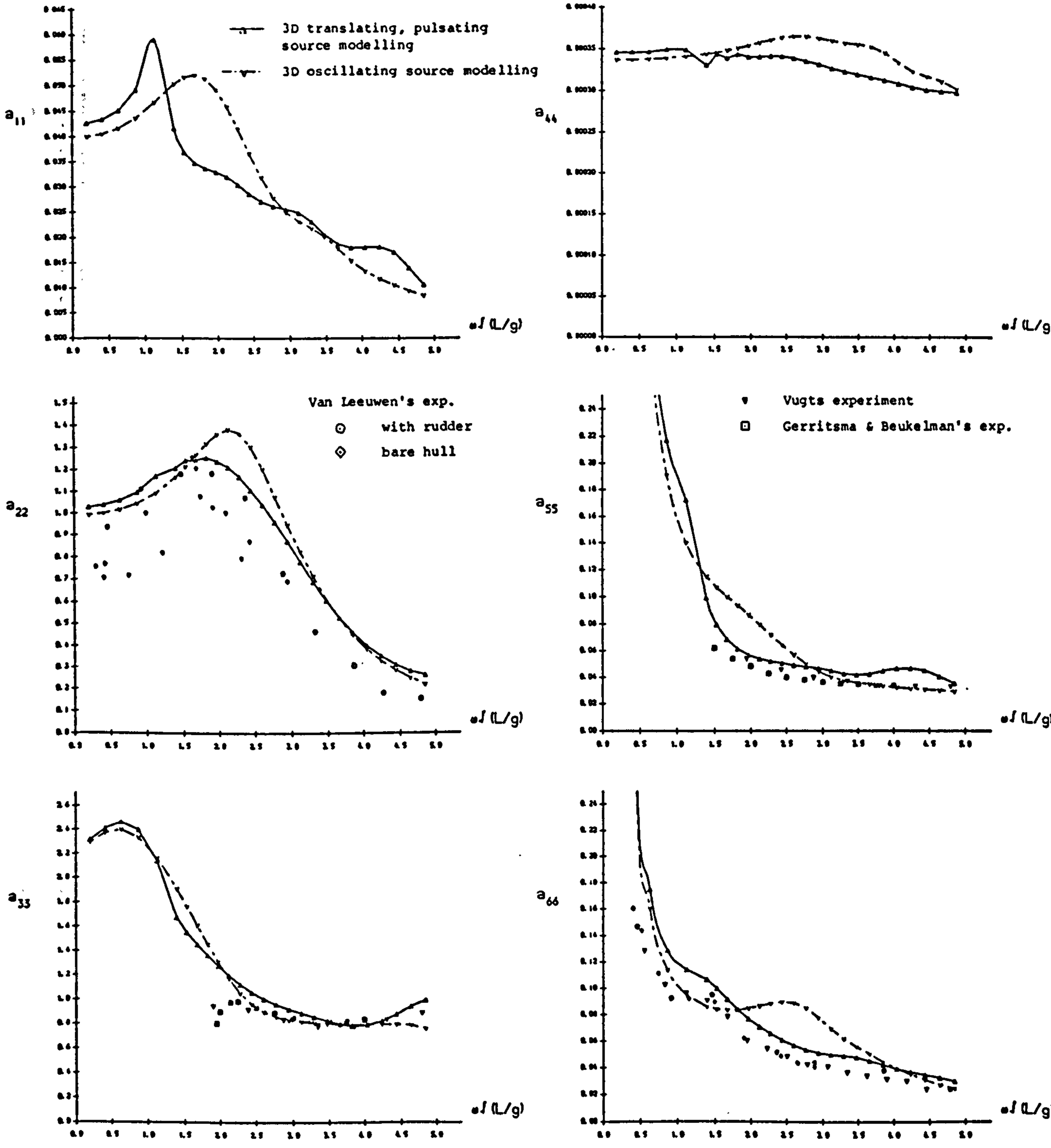

Fig.6.21 NON-DIMENSIONAL ADDED MASS COEFFICIENTS OF A SERIES-60 SHIP OF C_B=0.7 AT INFINITE WATER DEPTH AT F_n=0.2 FOR SIX RIGID MODES OF MOTION.

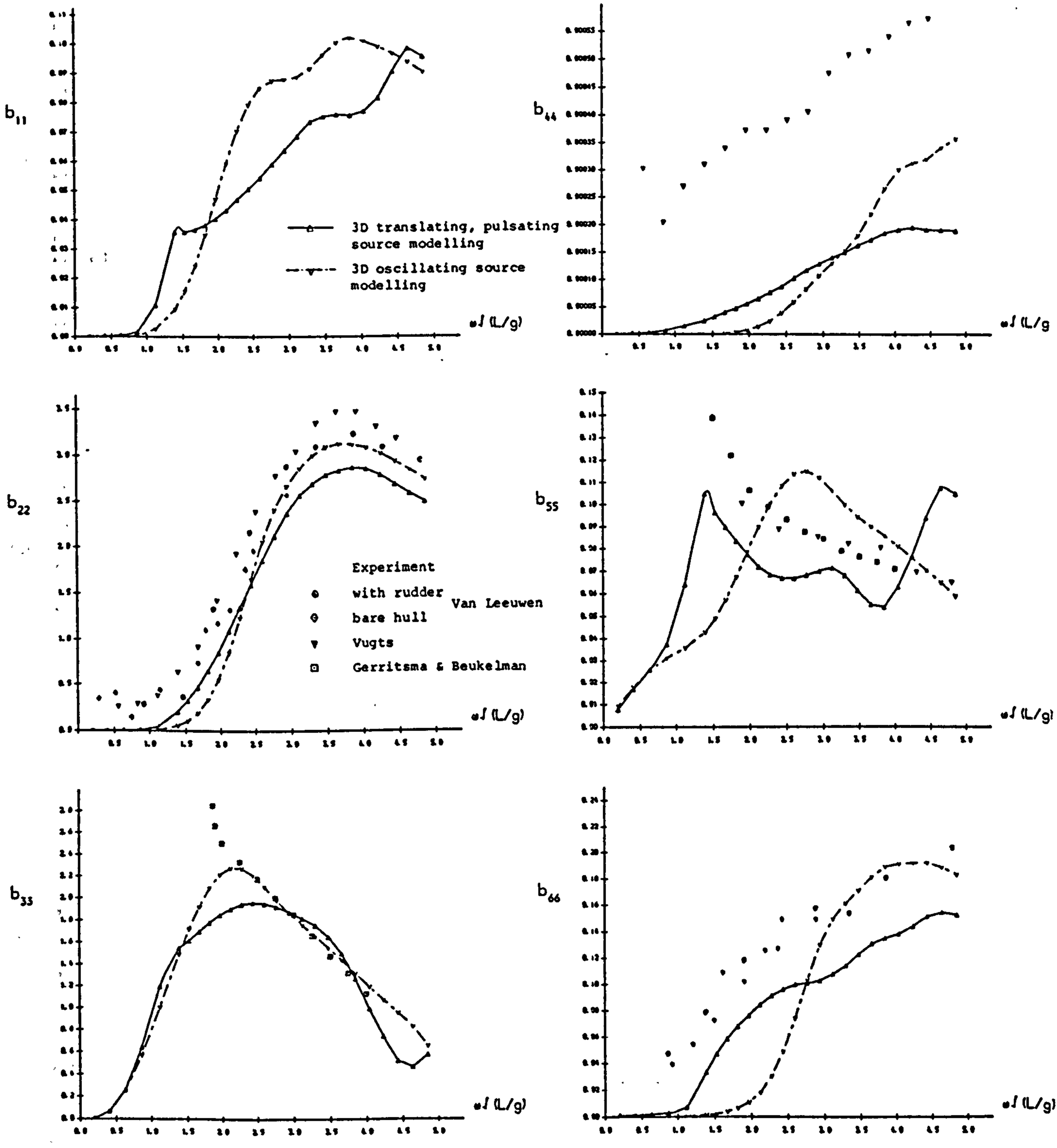

Fig.6.22 NON-DIMENSIONAL DAMPING COEFFICIENTS OF A SERIES-60 SHIP OF C_B=0.7 AT INFINITE WATER DEPTH AT F_n=0.2 FOR SIX RIGID MODES OF MOTION.

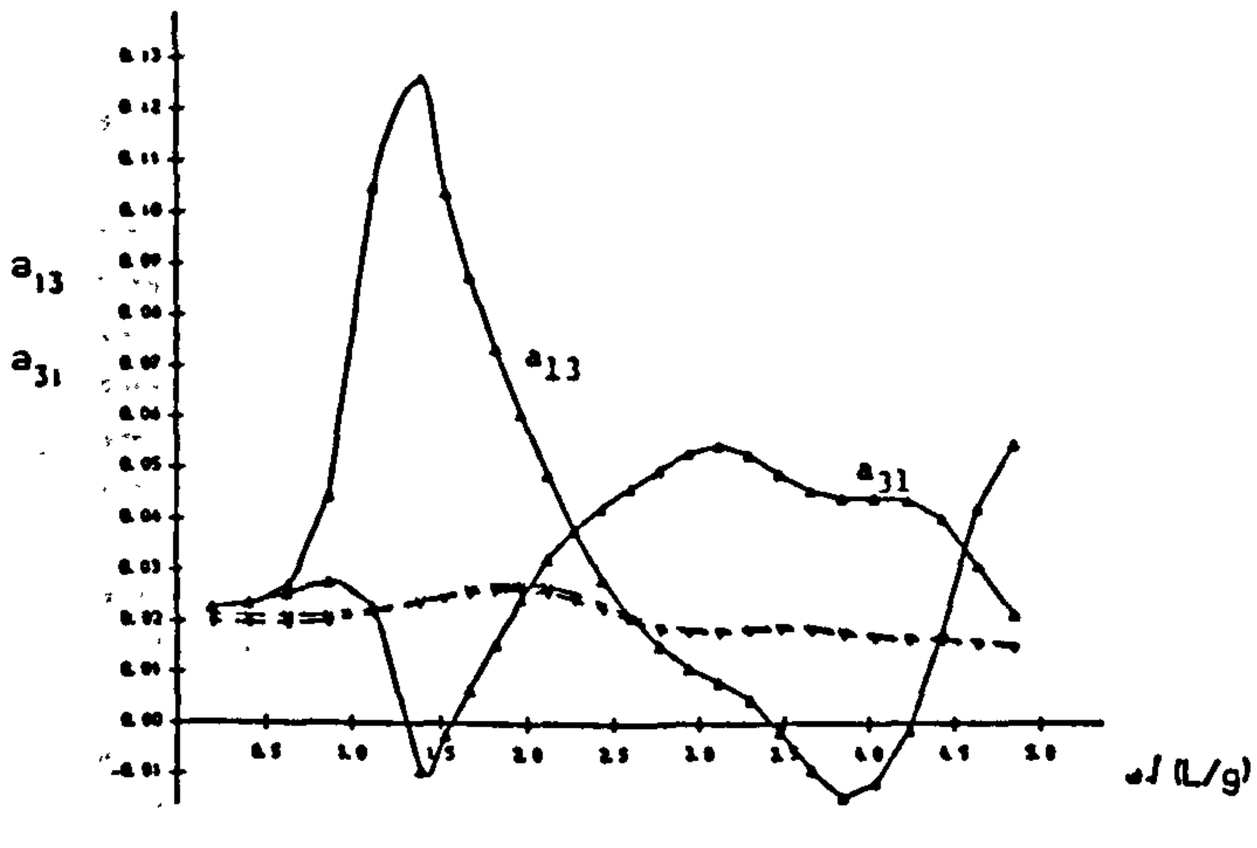

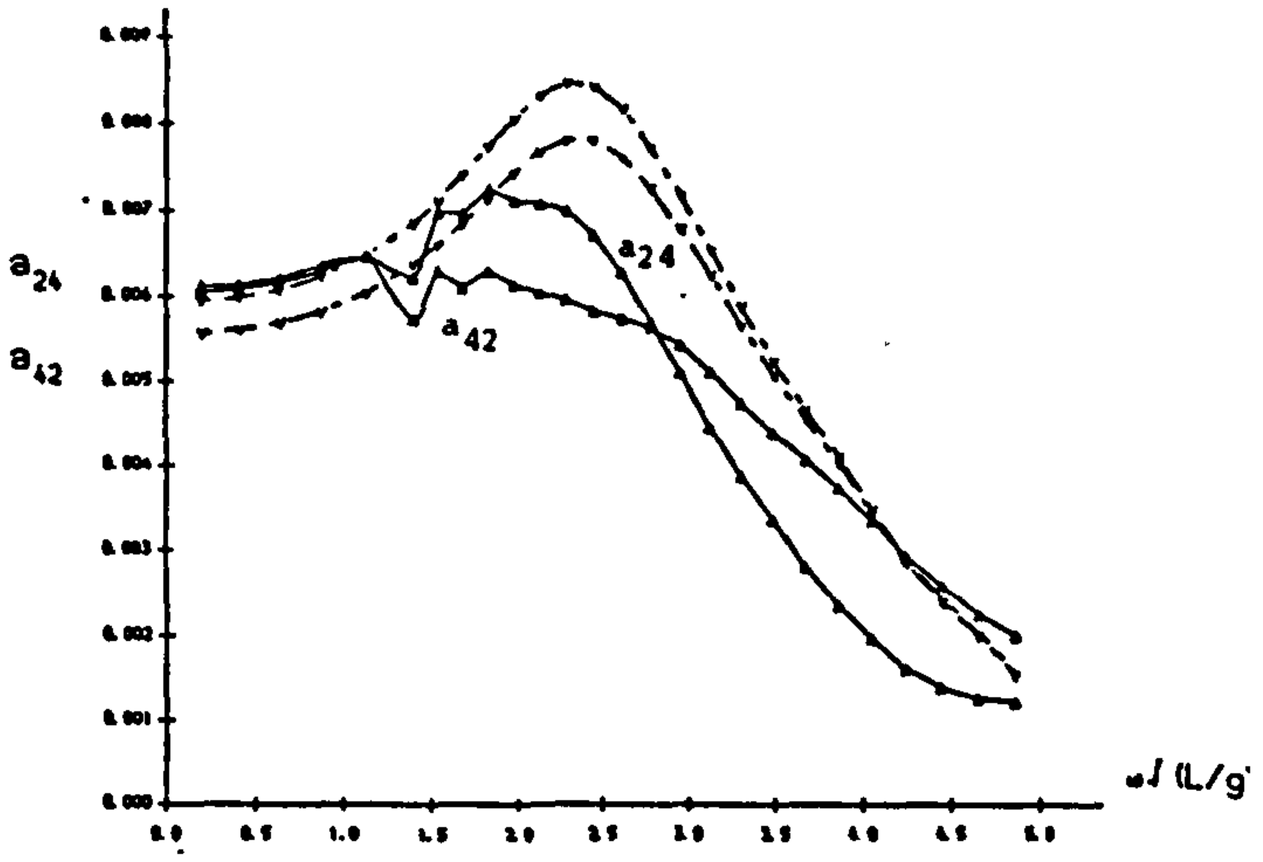

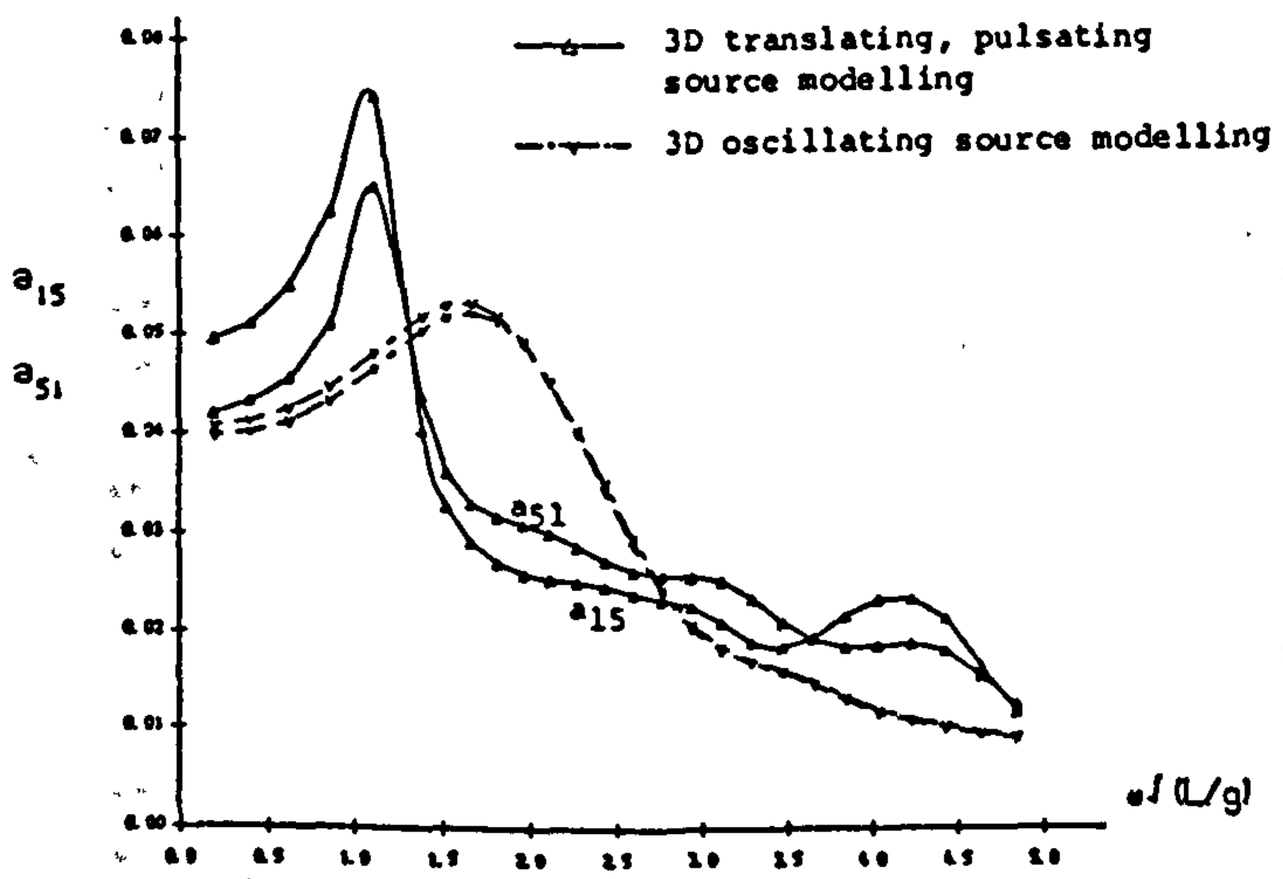

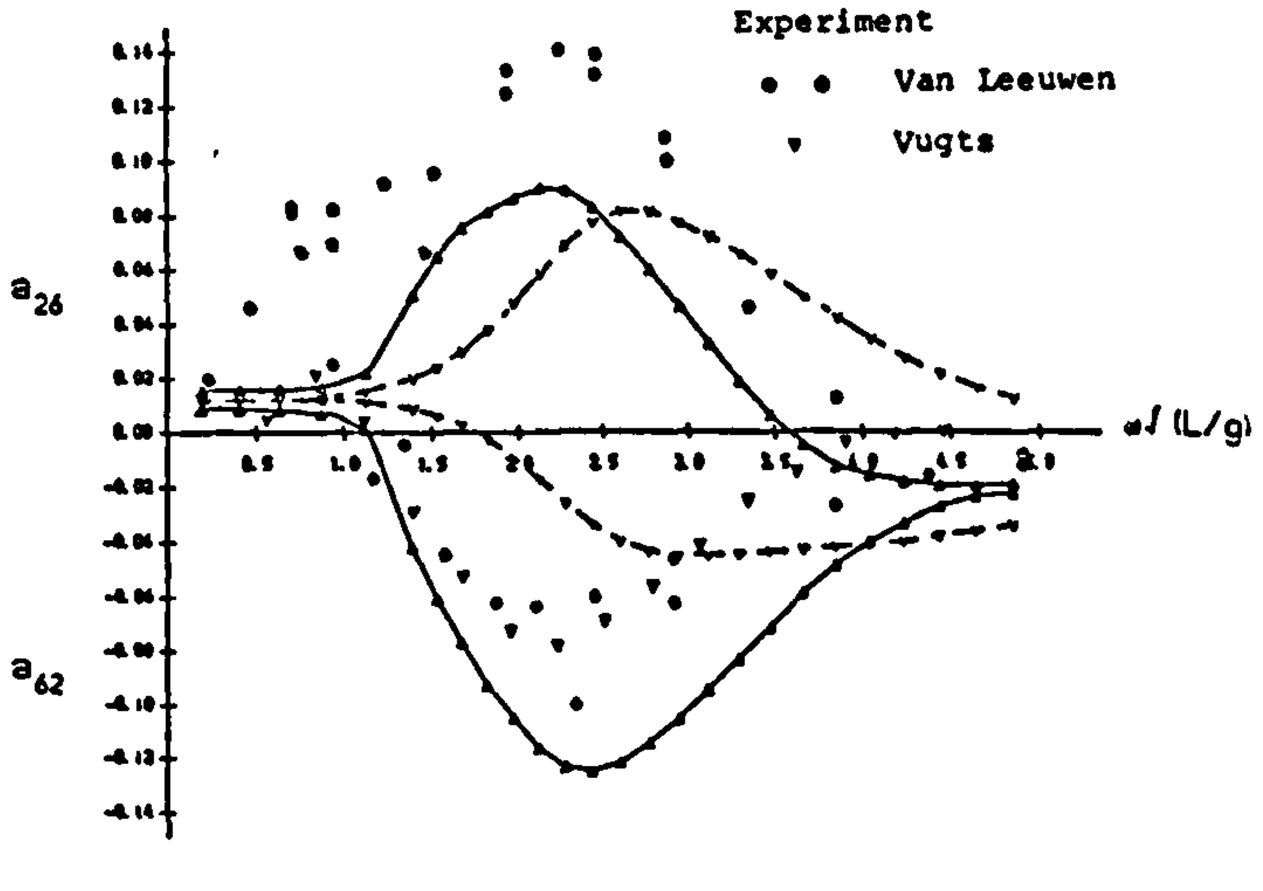

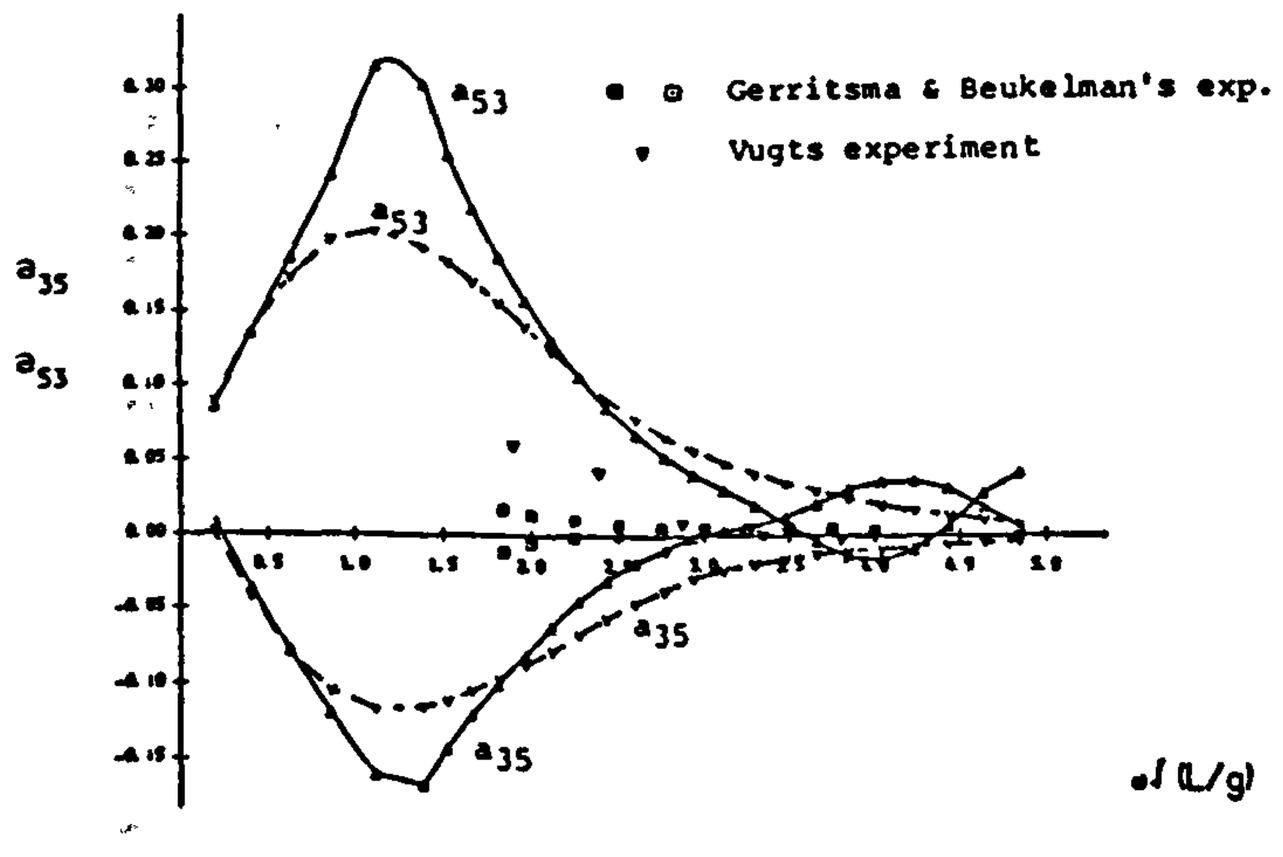

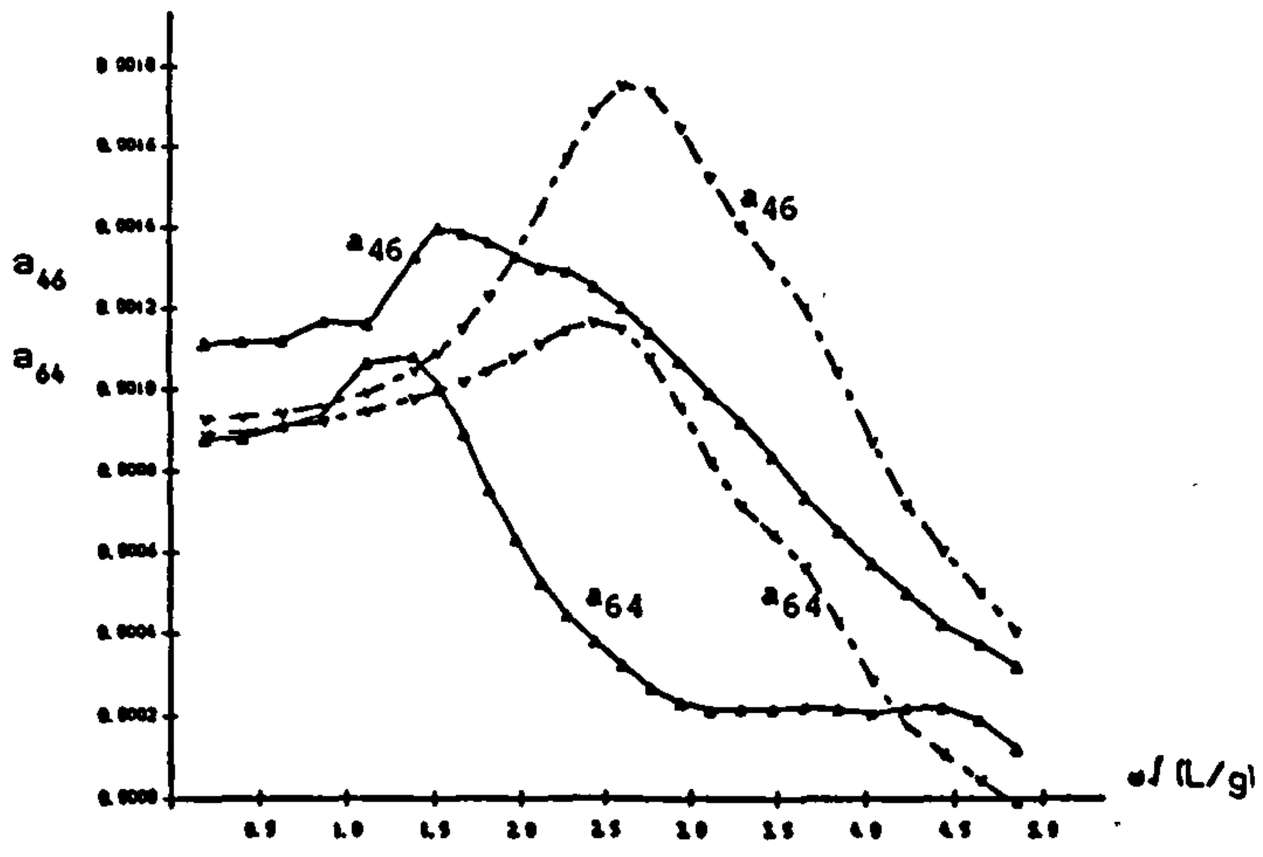

Fig.6.23 NON-DIMENSIONAL COUPLED ADDED MASS COEFFICIENTS OF A SERIES-60 SHIP OF C_B=0.7 AT INFINITE WATER DEPTH AT F_n=0.2

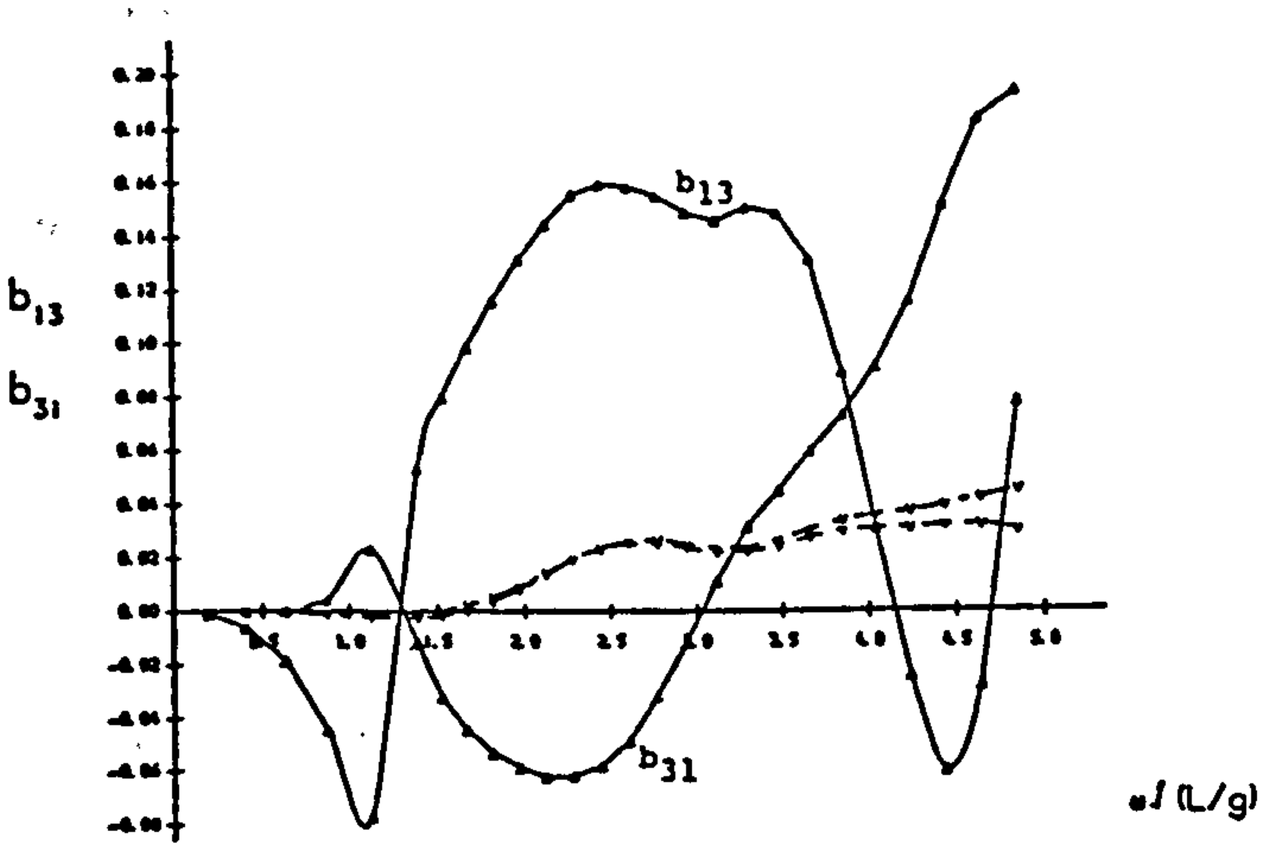

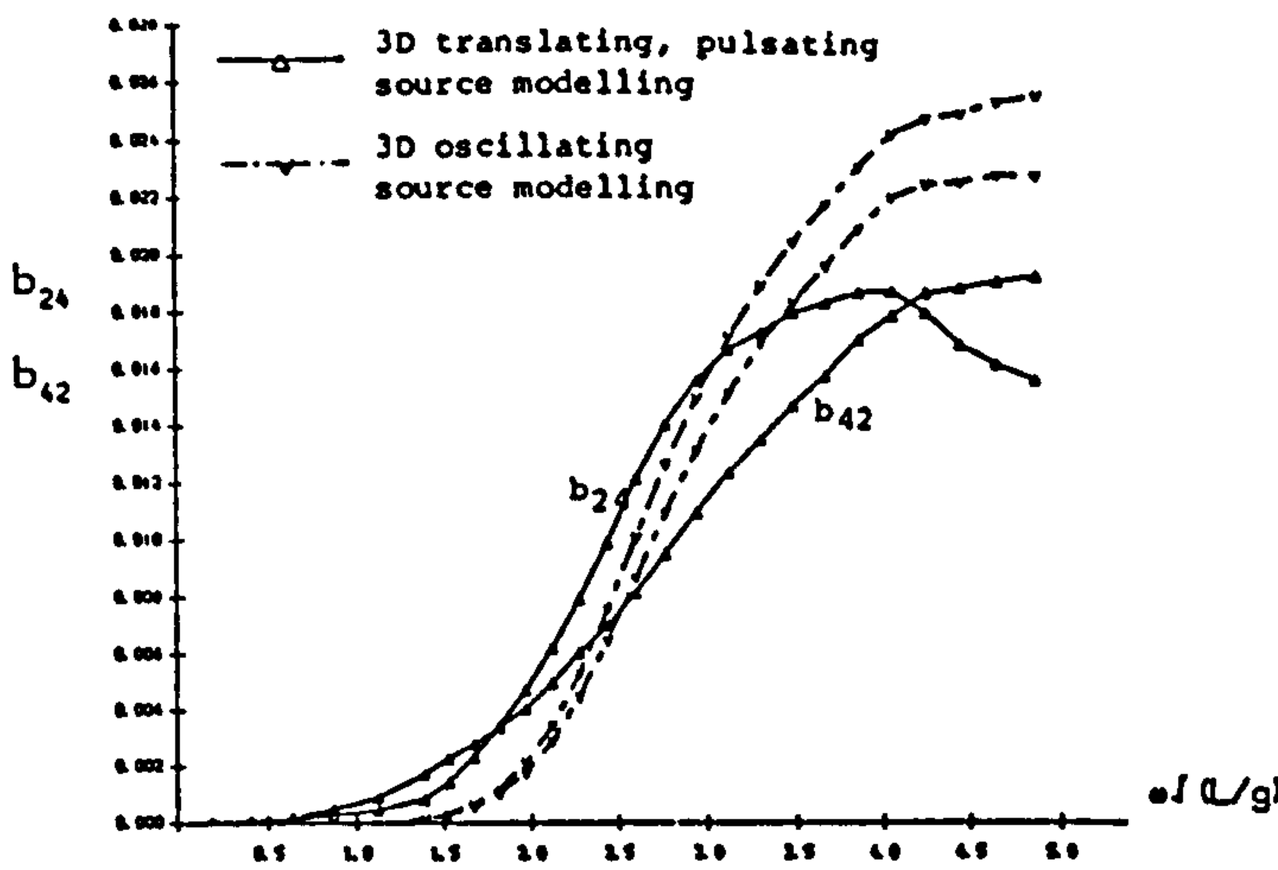

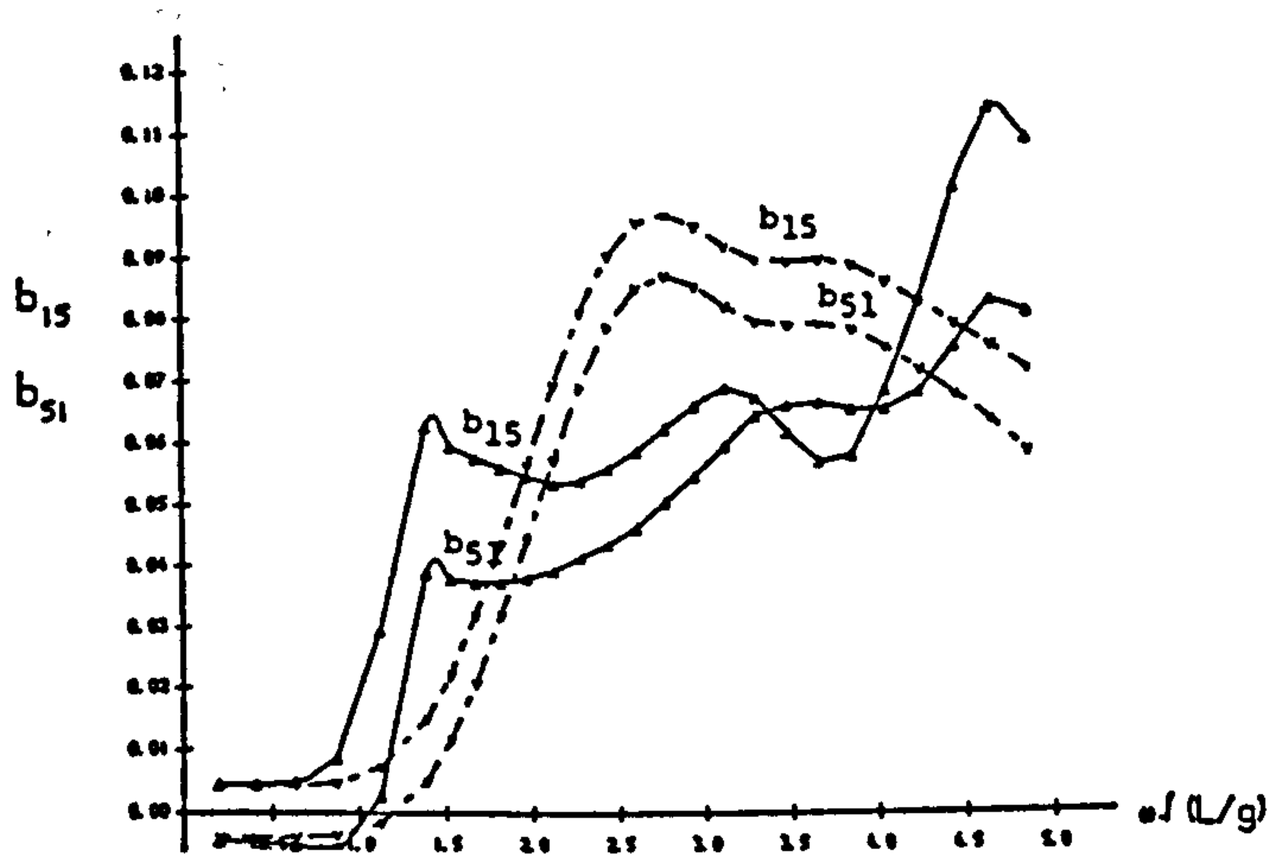

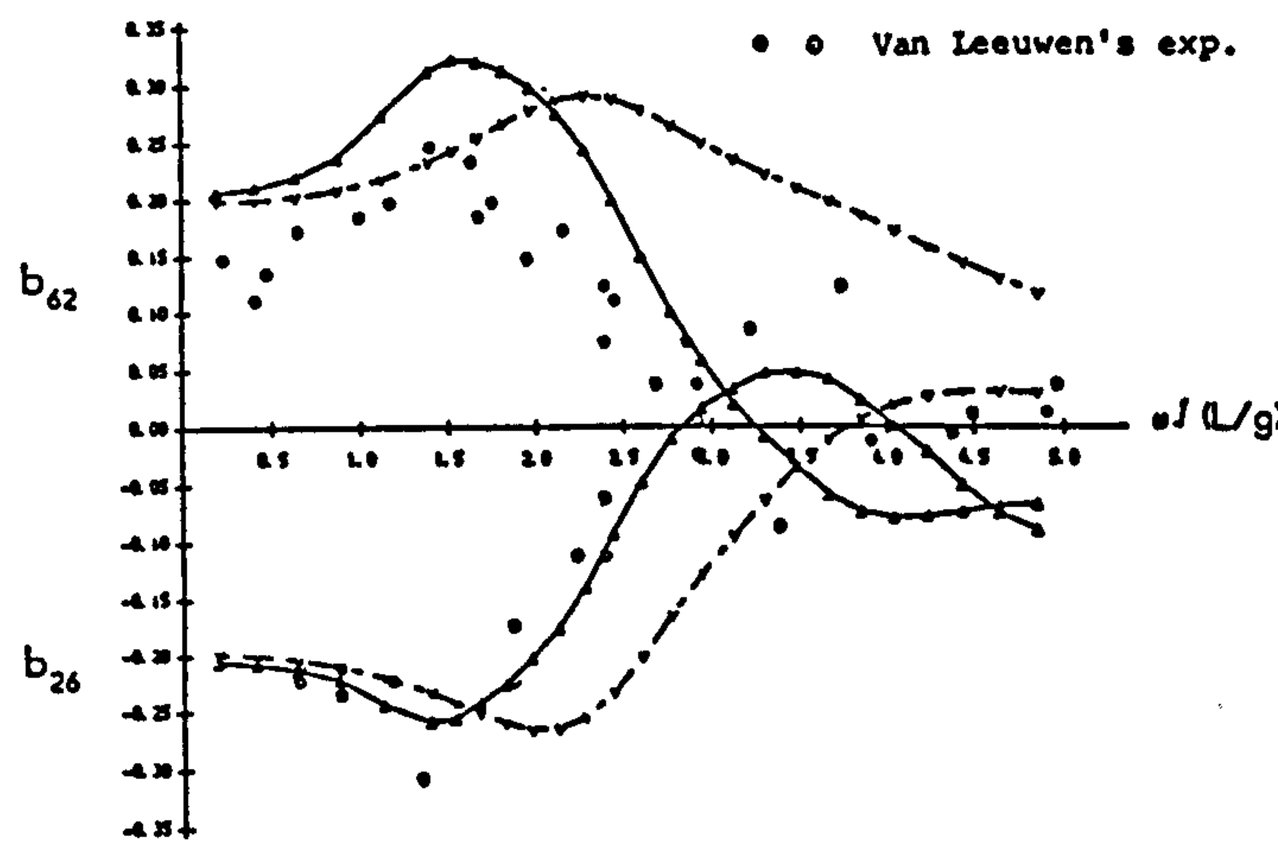

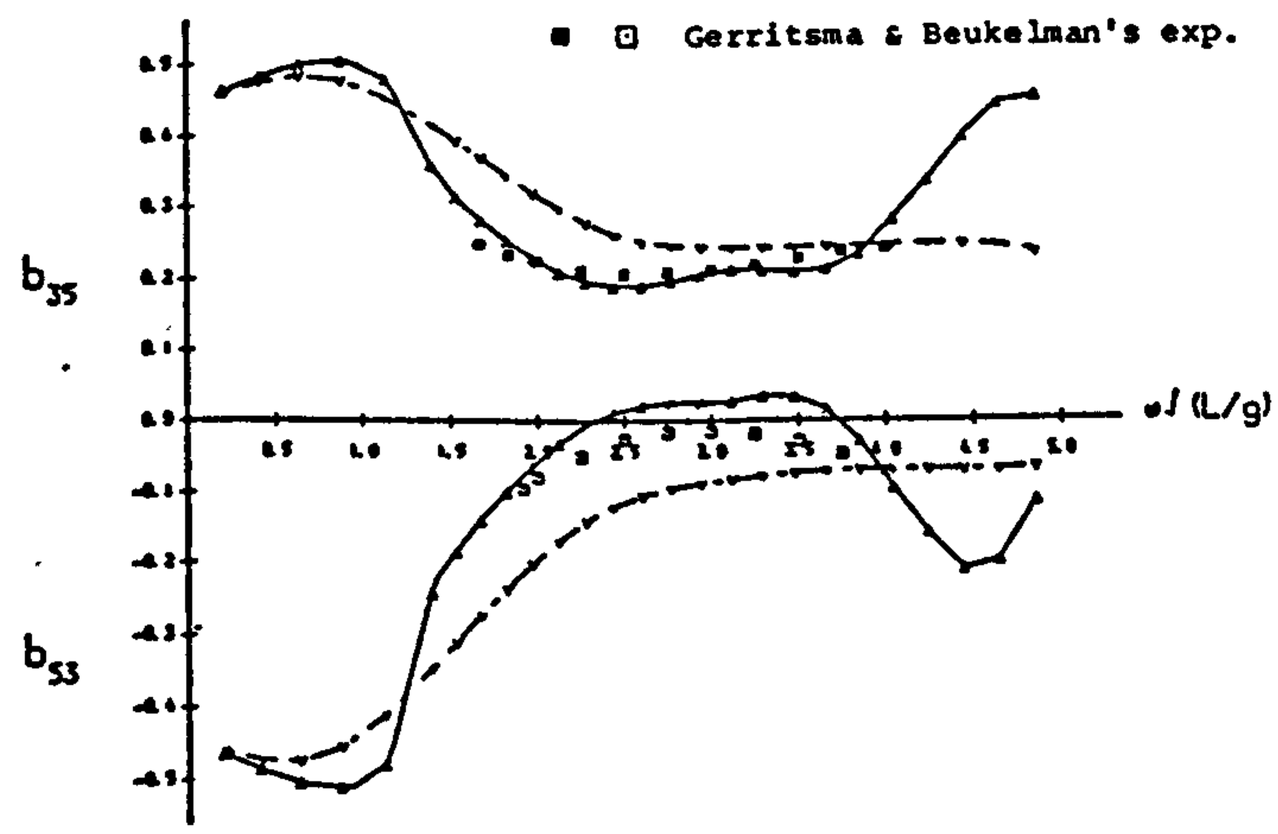

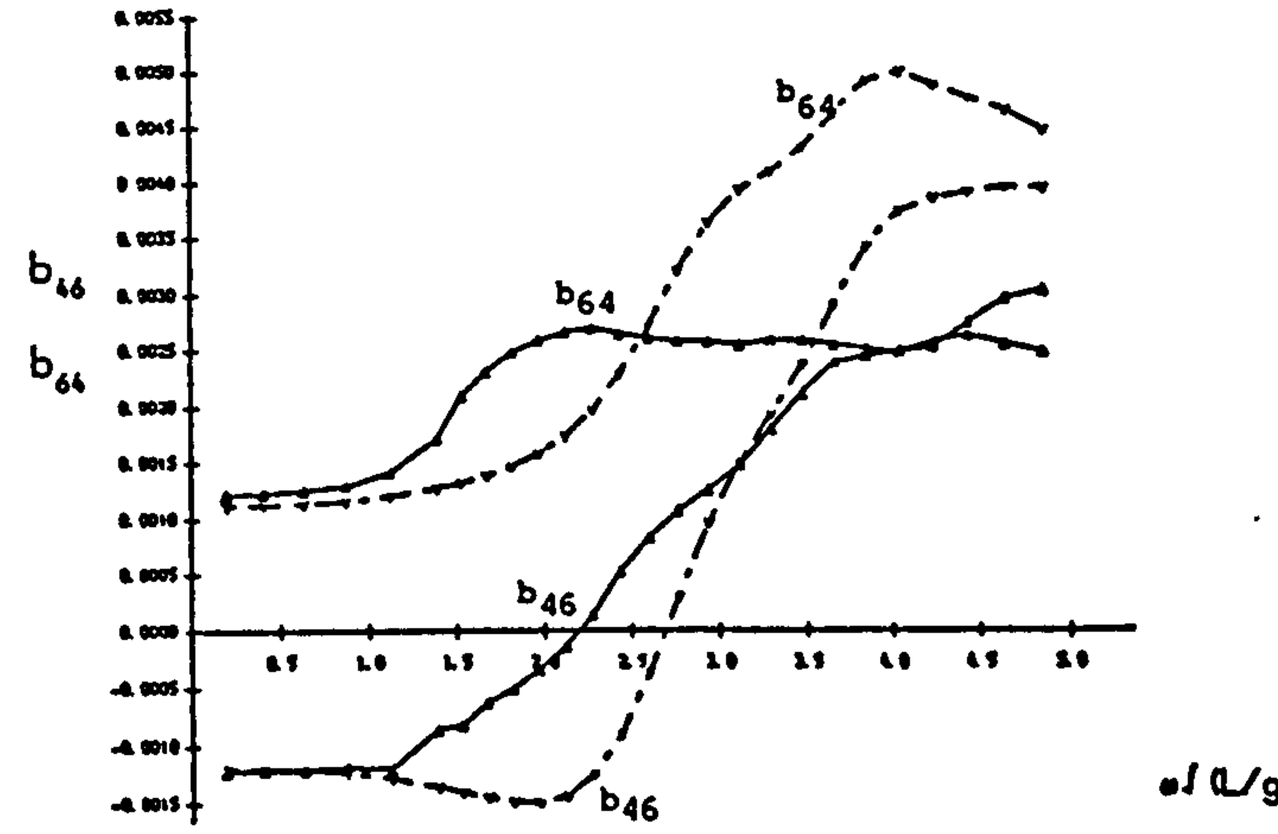

Fig.6.24 NON-DIMENSIONAL COUPLED DAMPING COEFFICIENTS OF A SERIES-60 SHIP OF C_B=0.7 AT INFINITE WATER DEPTH AT F_n=0.2

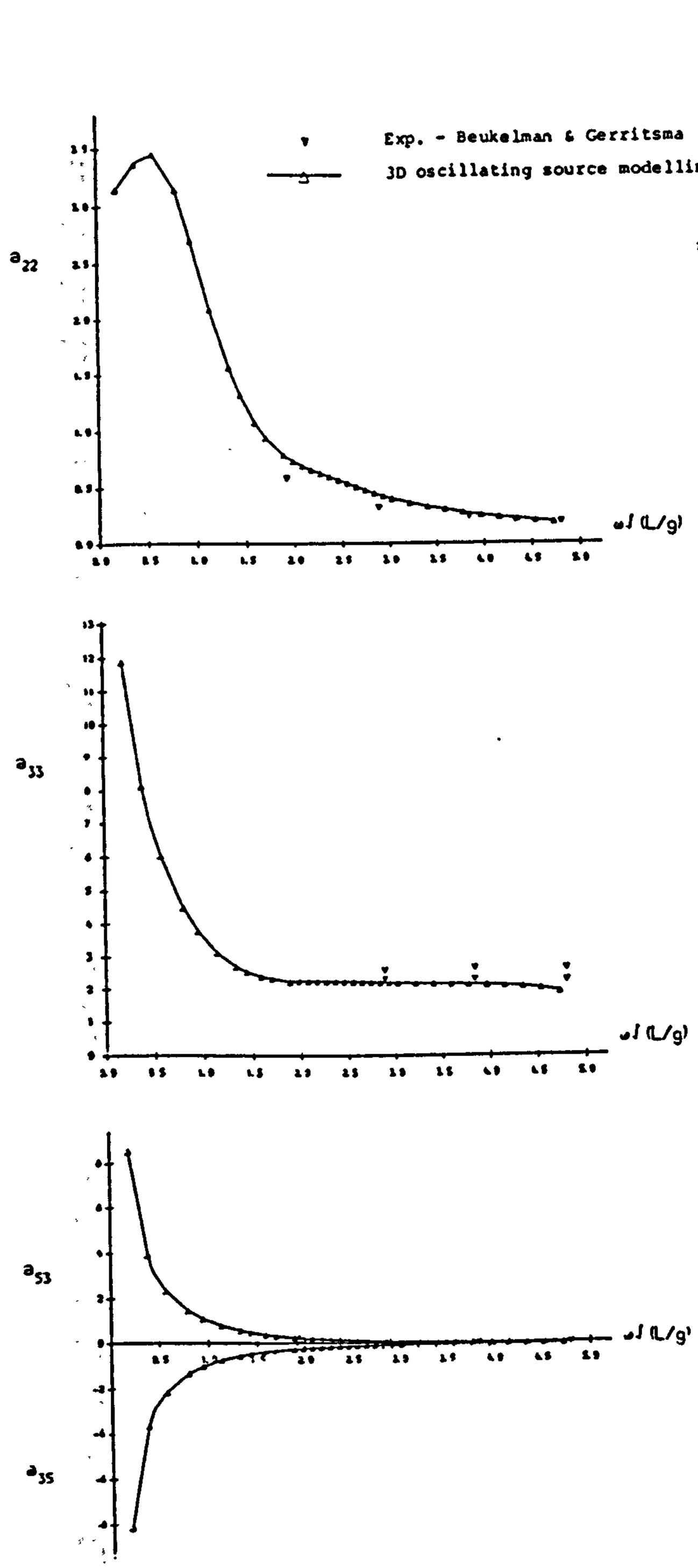

Fig.6.25 NON-DIMENSIONAL ADDED MASS COEFFICIENTS FOR A SERIES-60 SHIP OF C_B=0.7 AT F_n=0.2 IN SHALLOW WATER H/D=1.2

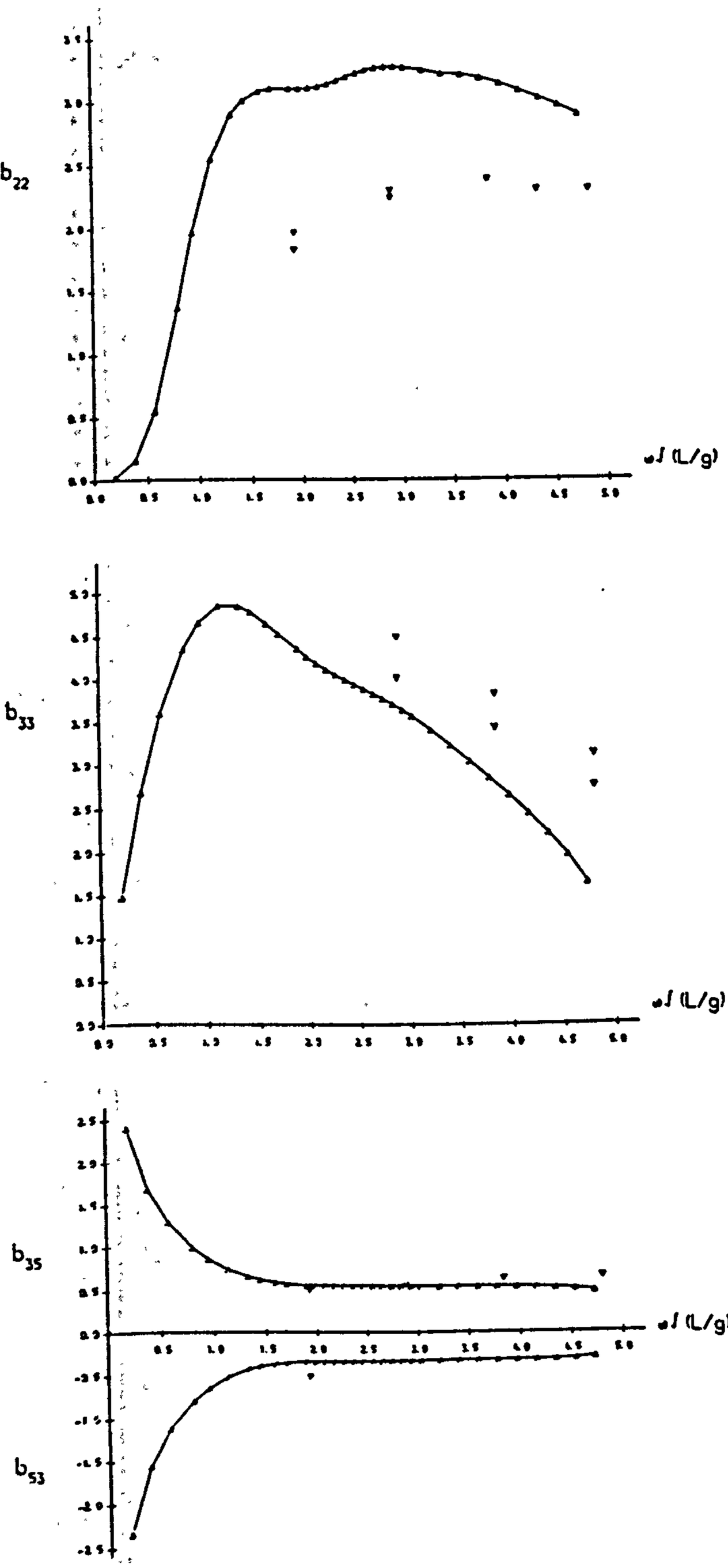

Fig.6.26 NON-DIMENSIONAL DAMPING COEFFICIENTS FOR A SERIES-60 SHIP OF C_B=0.7 AT F_n=0.2 IN SHALLOW WATER H/D=1.2

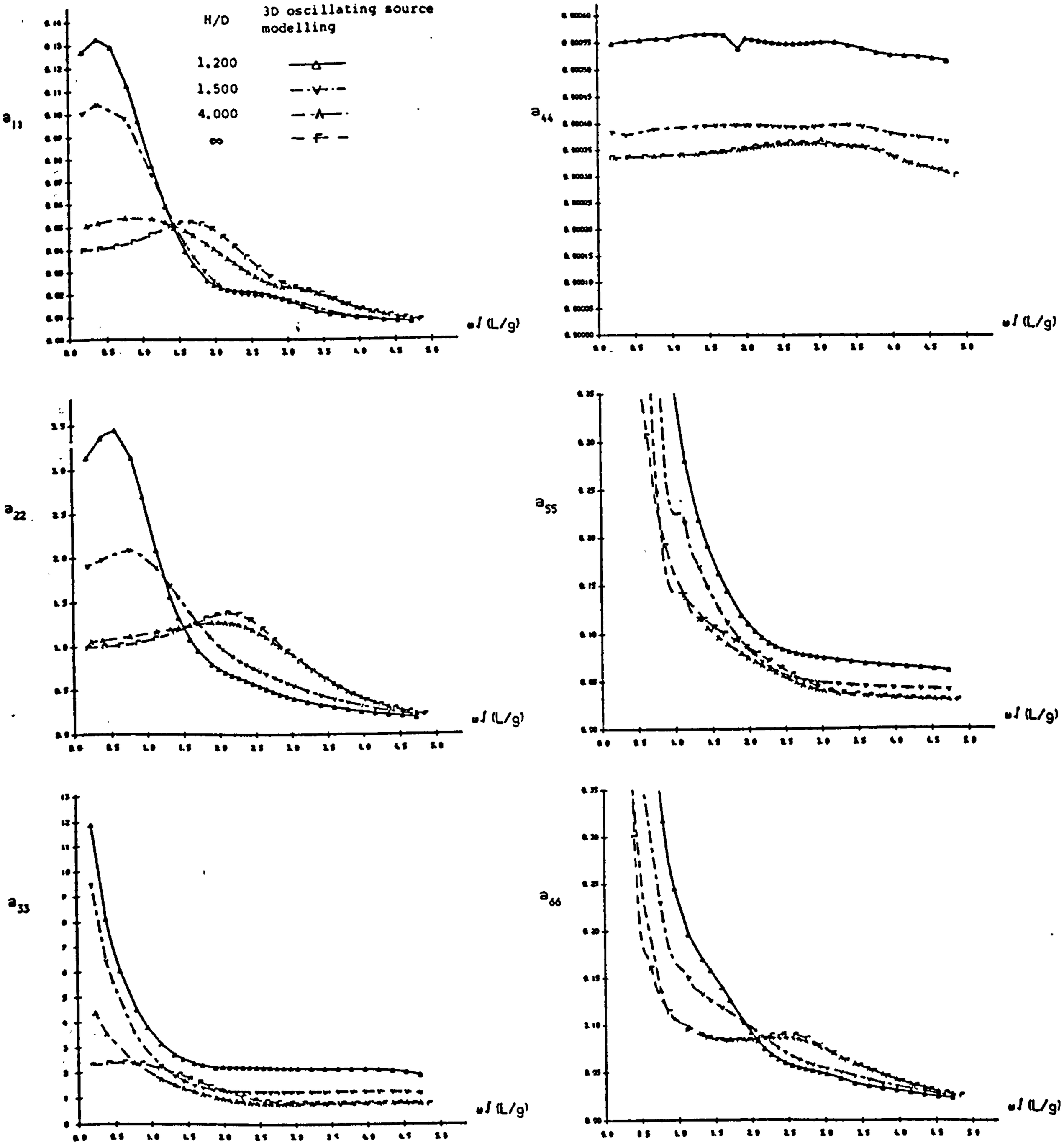

Fig.6.27 NON-DIMENSIONAL ADDED MASS COEFFICIENTS OF A SERIES-60 SHIP OF C_B=0.7 AT F_n=0.2 AT VARIOUS WATER DEPTHS FOR SIX RIGID MODES OF MOTION.

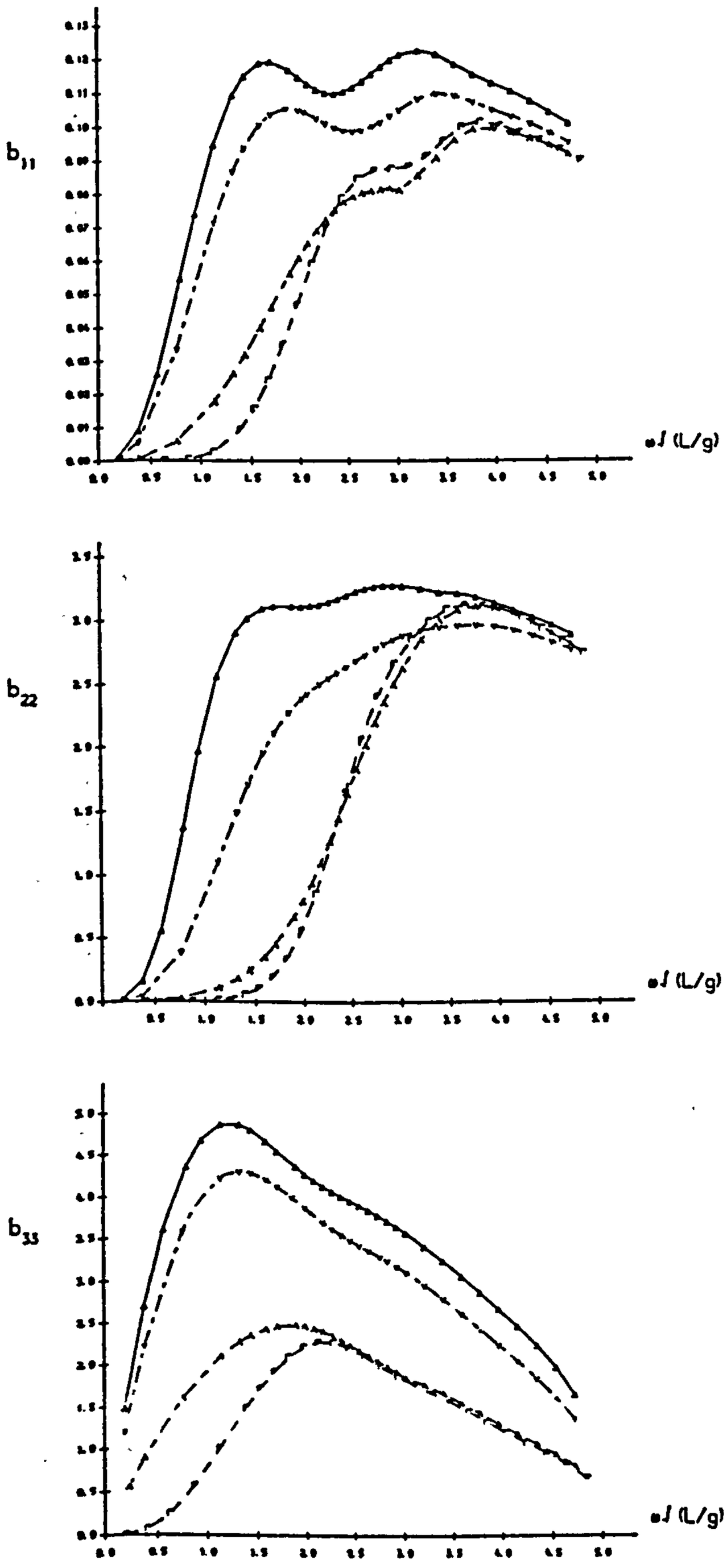

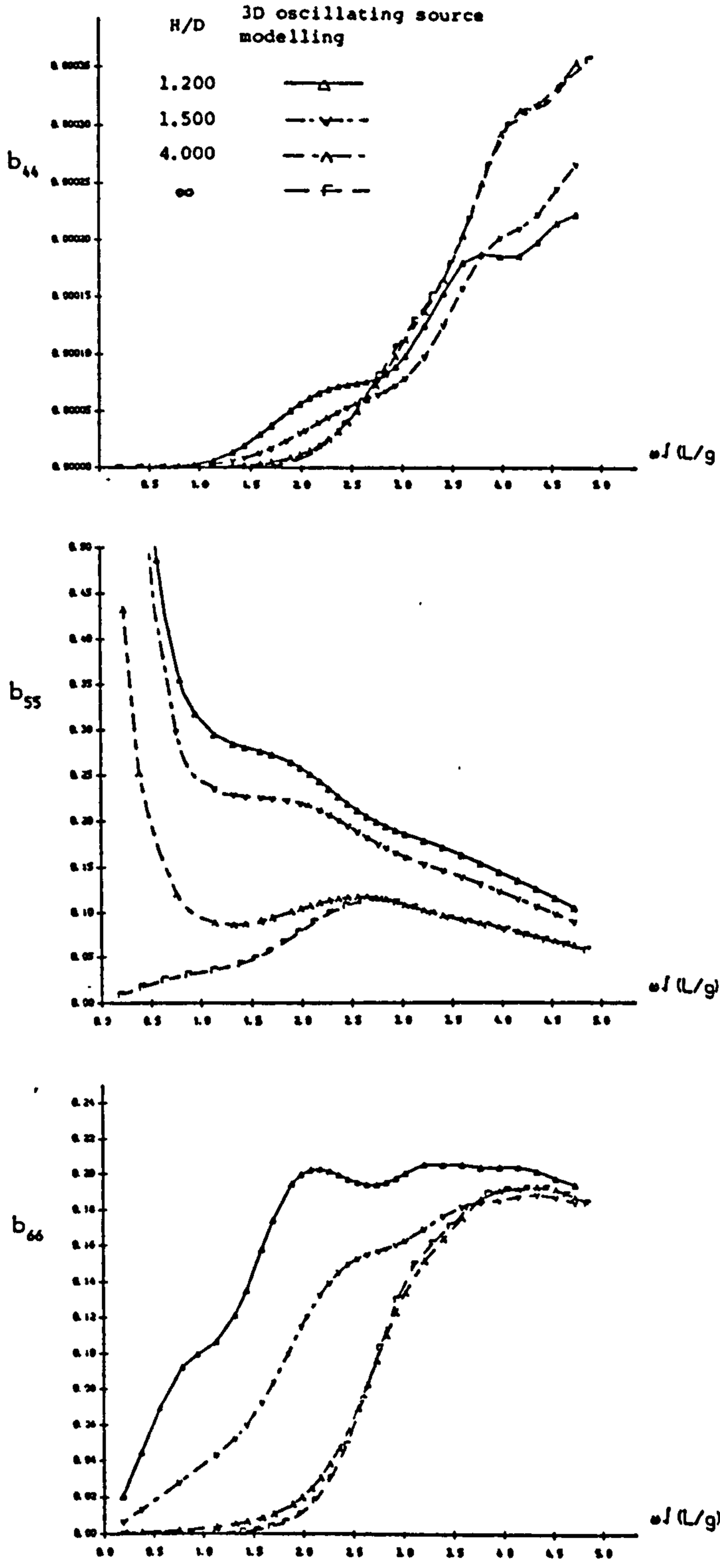

Fig.6.28 NON-DIMENSIONAL DAMPING COEFFICIENTS OF A SERIES-60 SHIP OF C_B=0.7 AT F_n=0.2 AT VARIOUS WATER DEPTHS FOR SIX RIGID MODES OF MOTION.

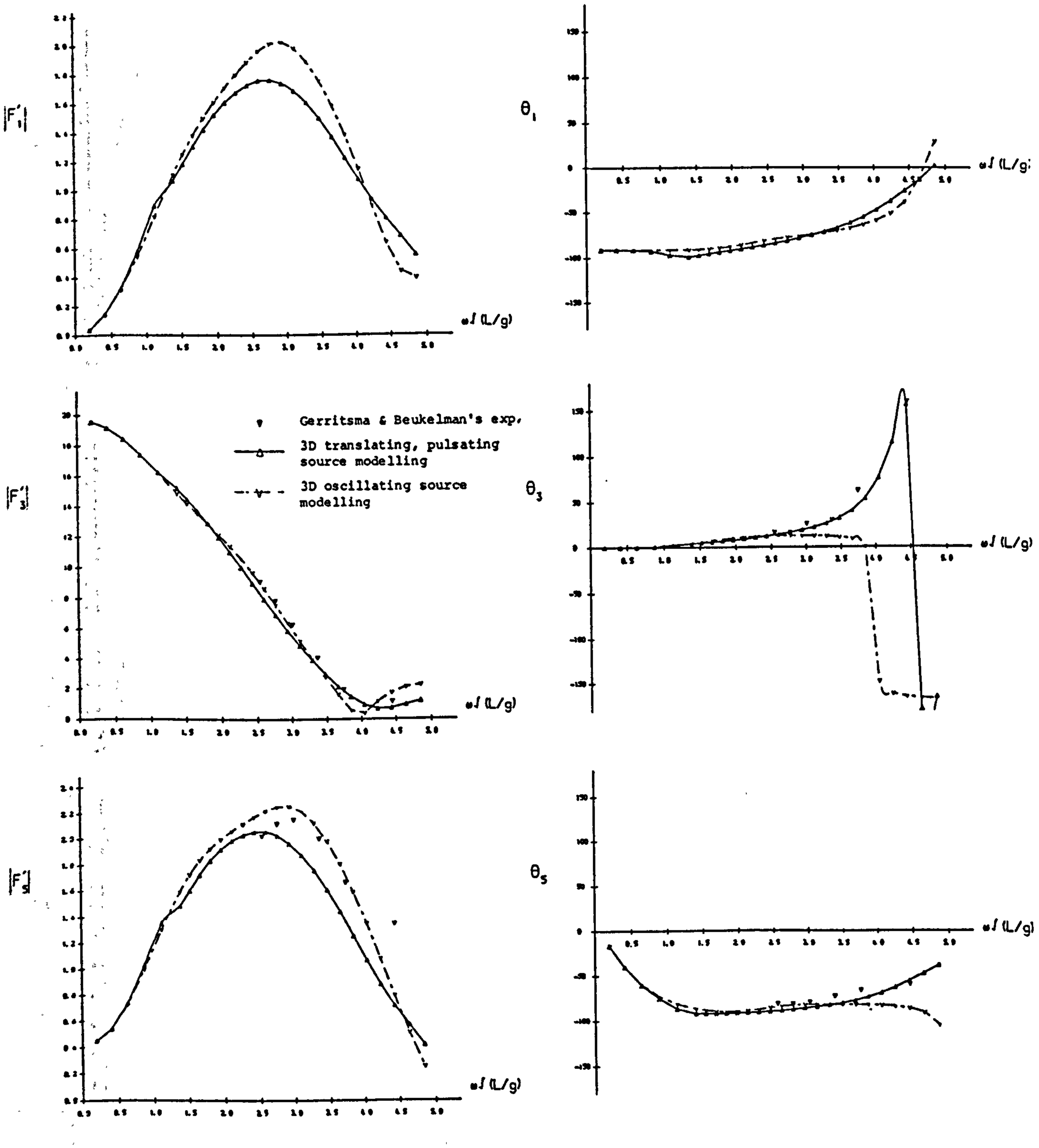

Fig.6.29 WAVE EXCITING FORCES AND MOMENT (AMPLITUDE AND PHASE) OF A SERIES-60 SHIP OF C_B=0.7 AT INFINITE WATER DEPTH AT F_n=0.2 IN HEAD WAVES.

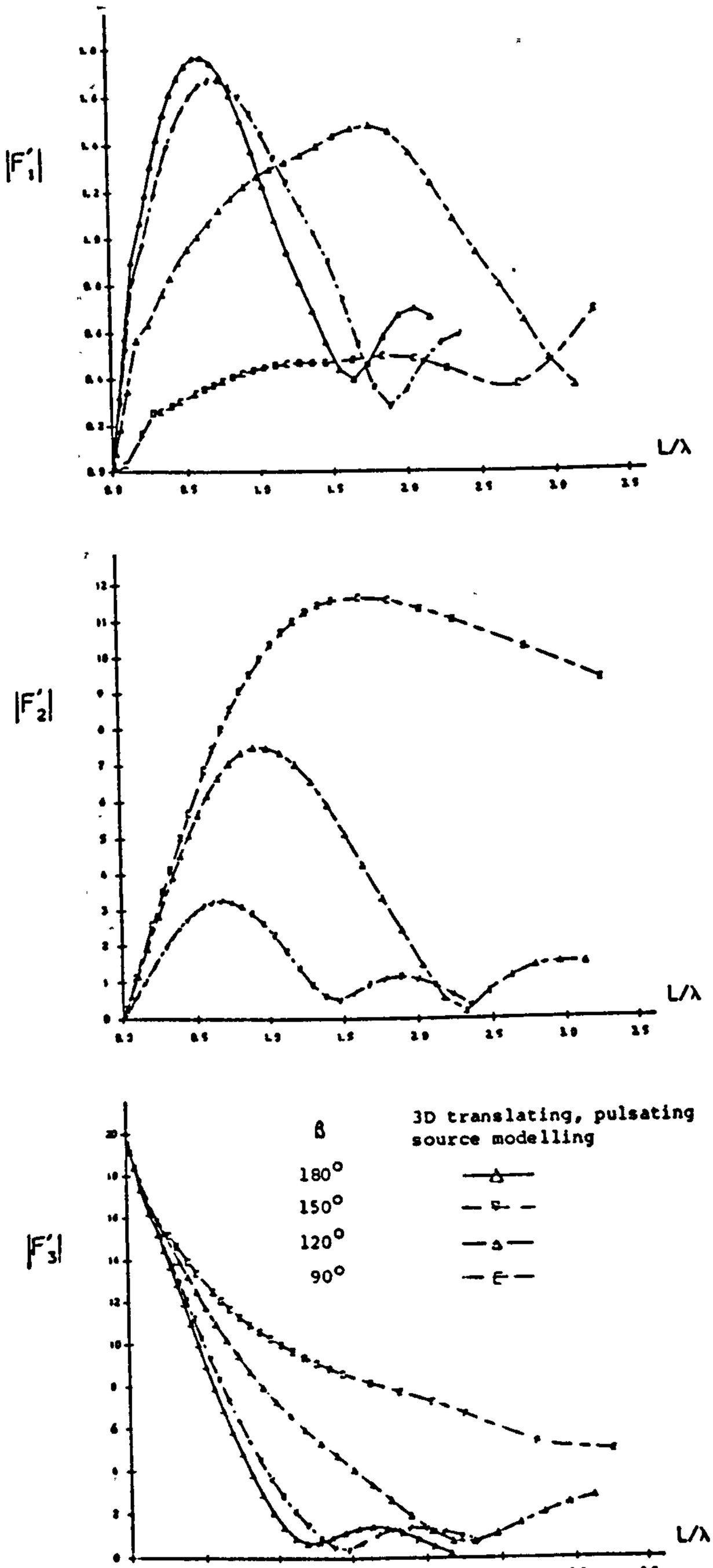

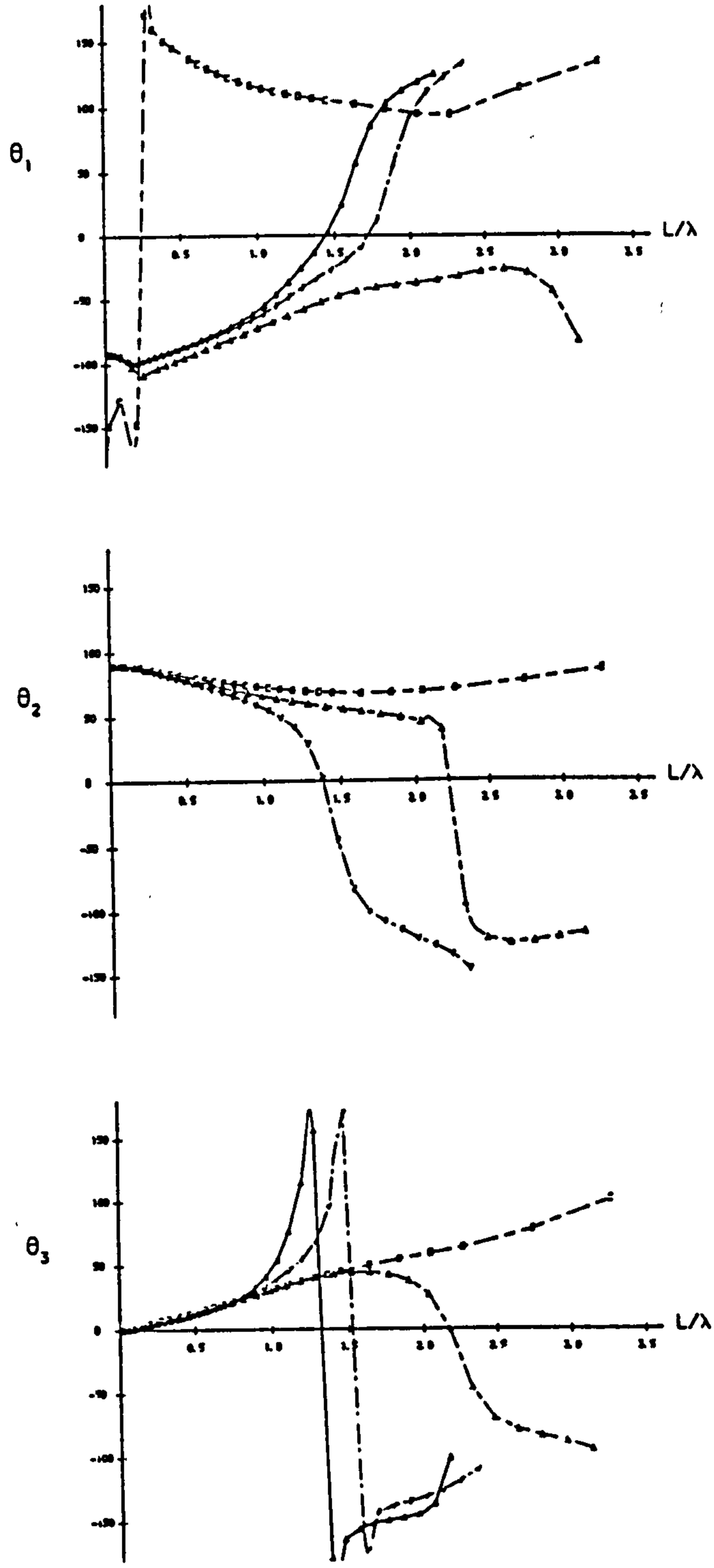

Fig.6.30a WAVE EXCITING FORCES (AMPLITUDE AND PHASE) FOR A SERIES-60 SHIP OF C_B=0.7 AT INFINITE WATER DEPTH AT F_n=0.2 IN VARIOUS ANGLES OF WAVE INCIDENCE.

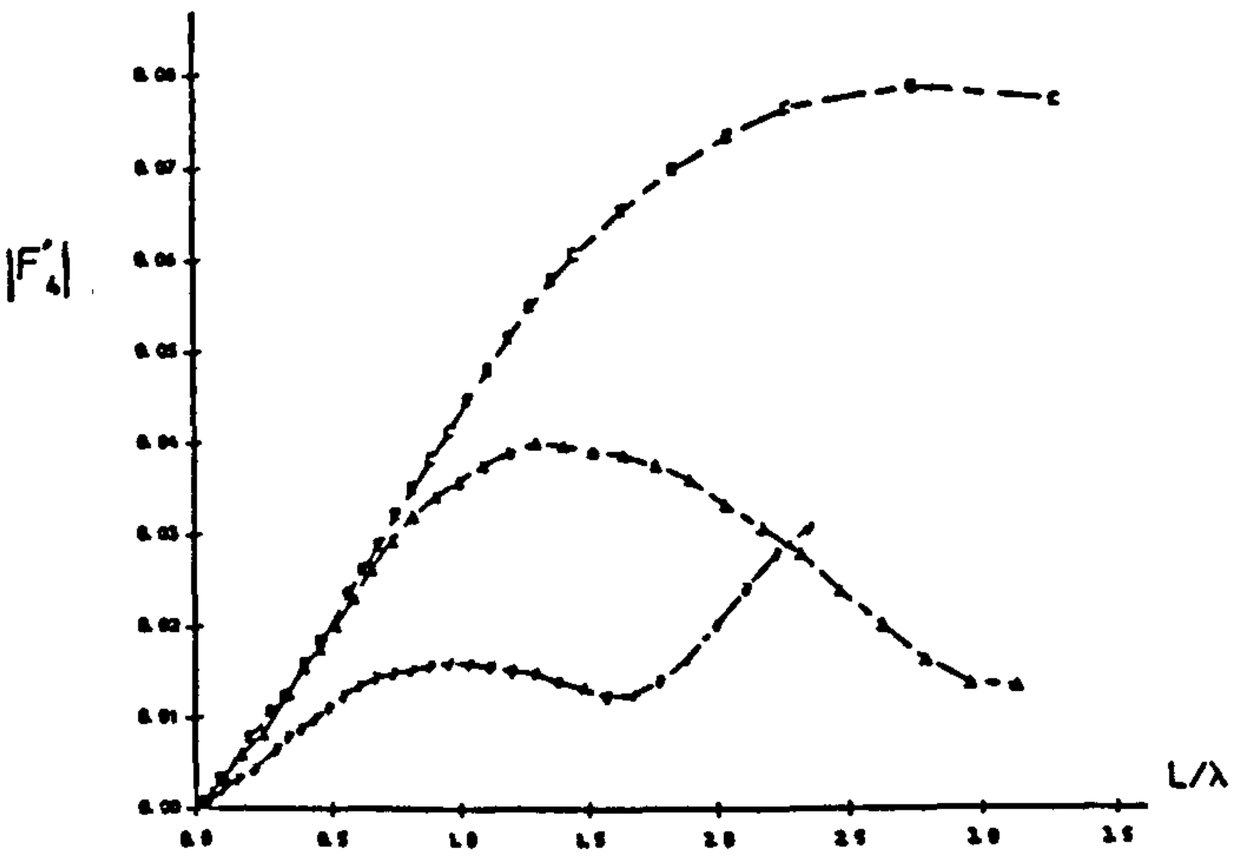

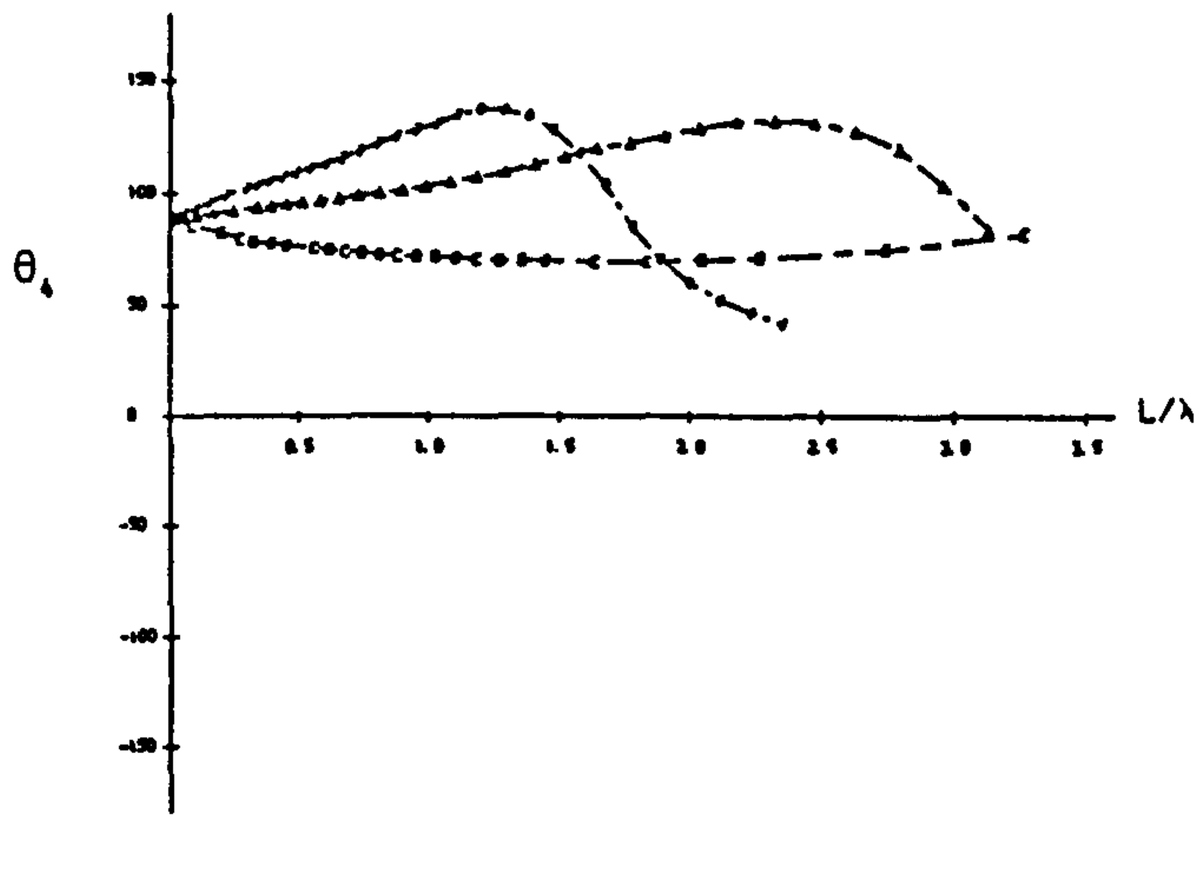

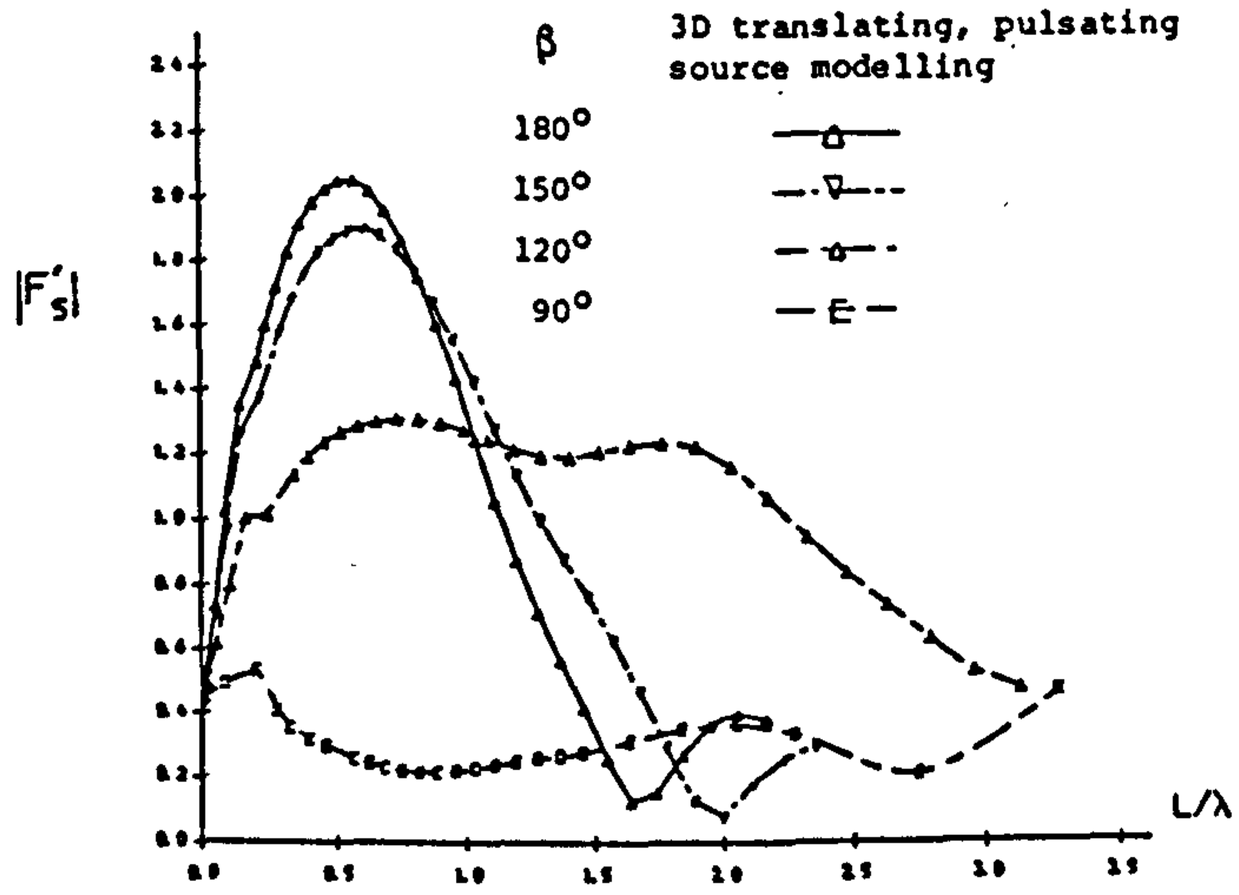

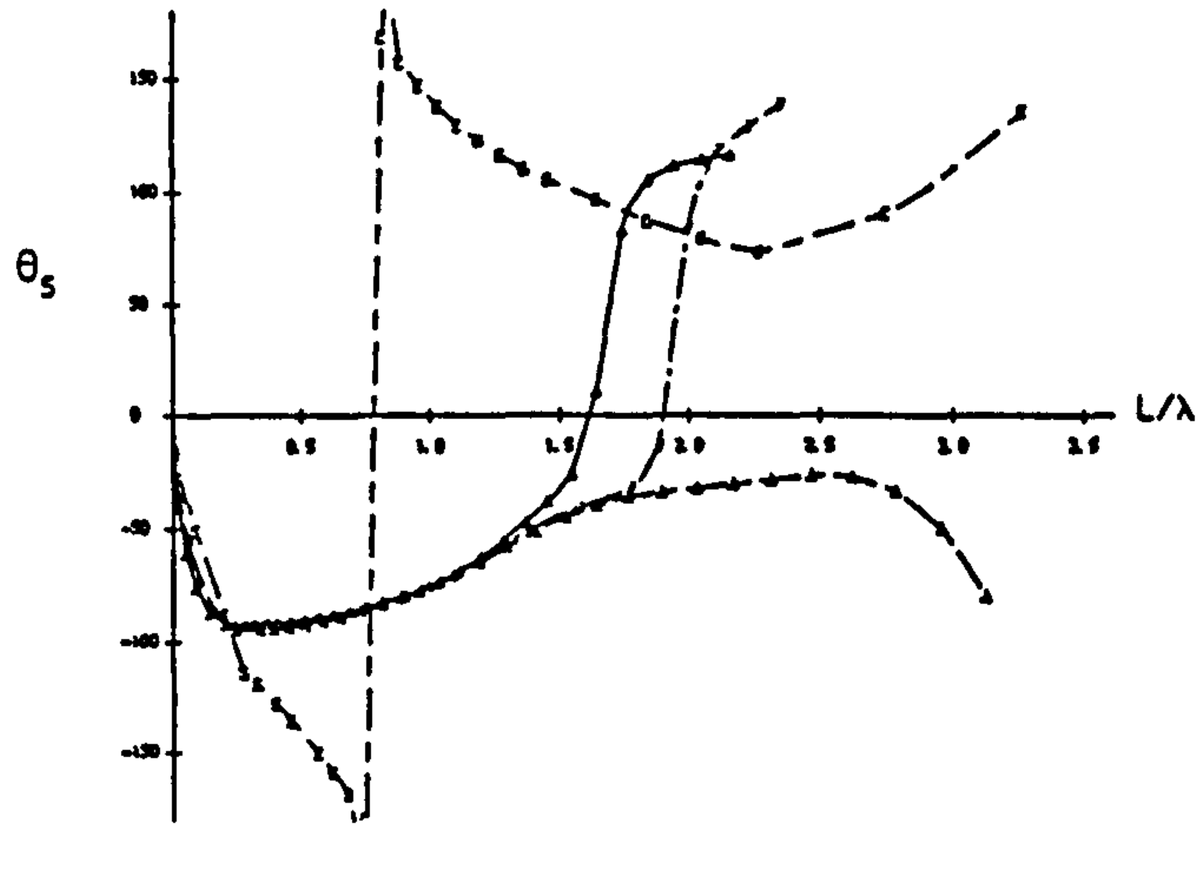

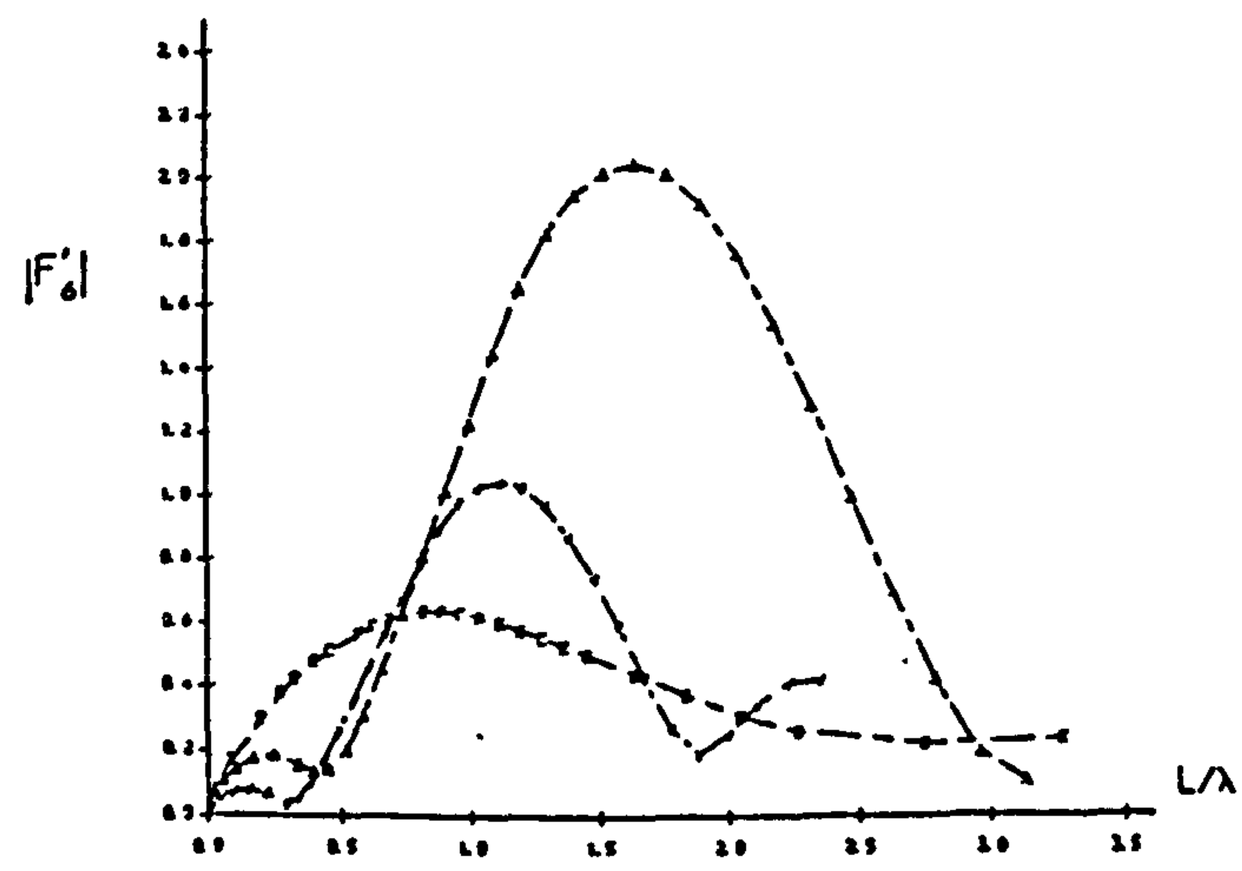

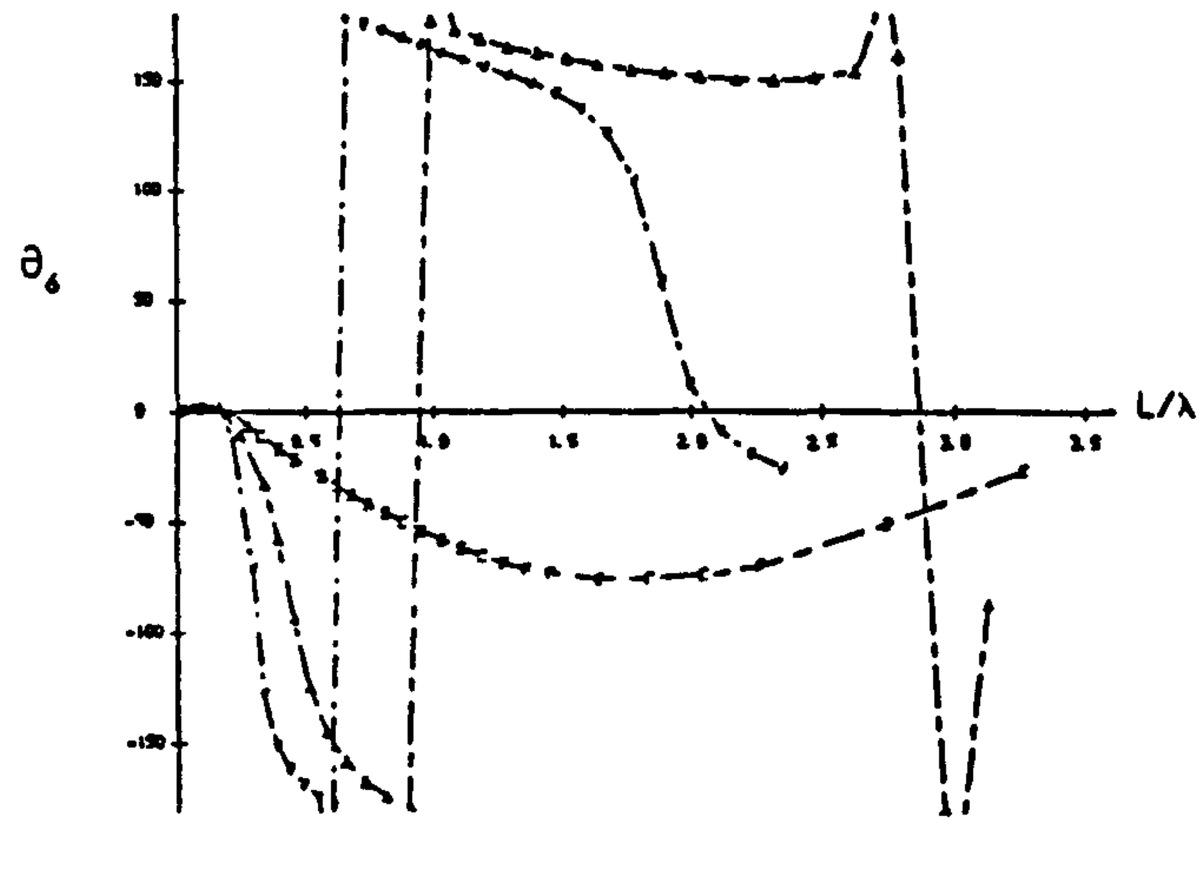

Fig.6.30b WAVE EXCITING MOMENTS (AMPLITUDE AND PHASE) FOR A SERIES-60 SHIP OF C_B=0.7 AT INFINITE WATER DEPTH AT F_n=0.2 IN VARIOUS ANGLES OF WAVE INCIDENCE.

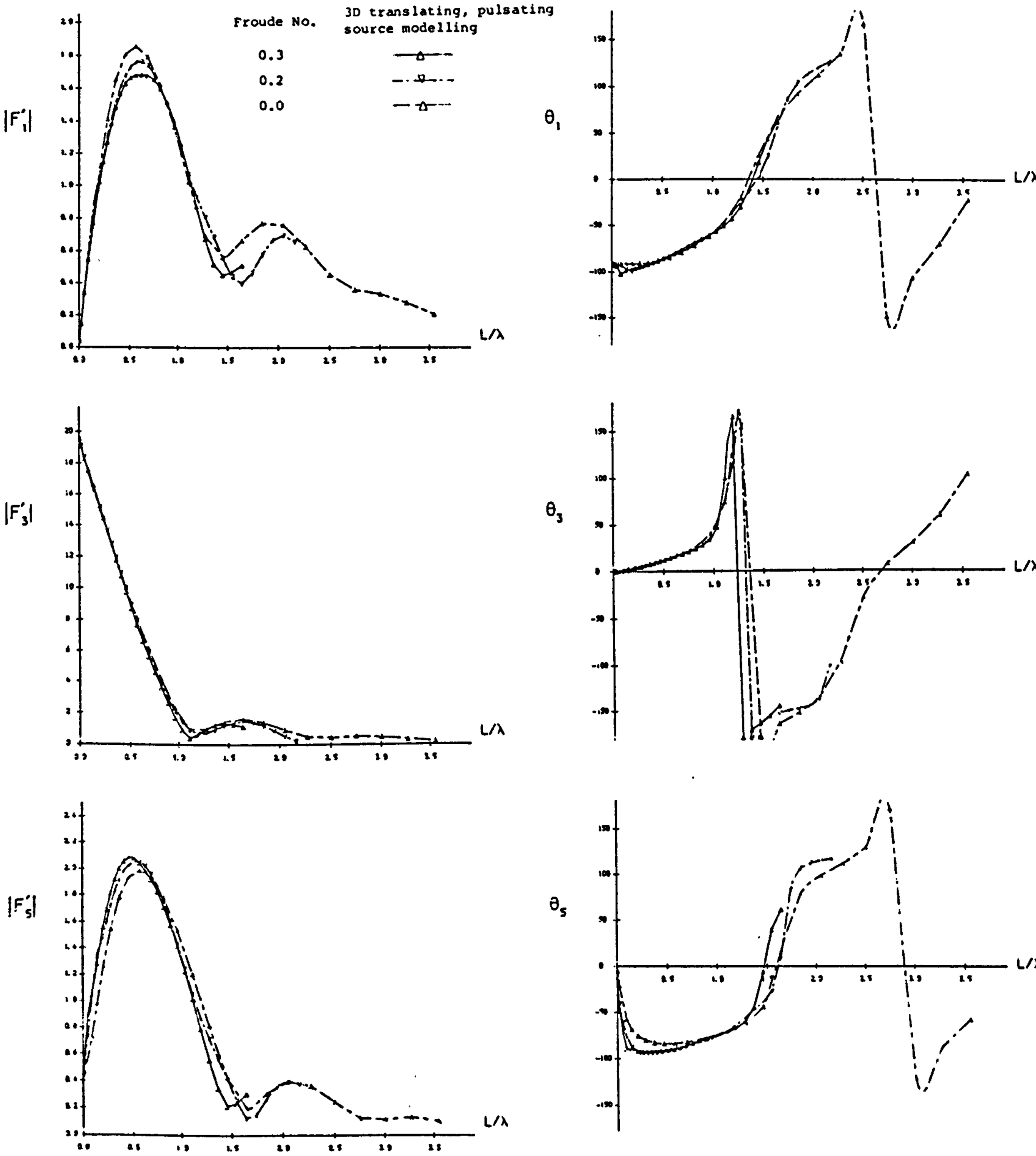

Fig.6.31 WAVE EXCITING FORCES AND MOMENT (AMPLITUDE AND PHASE) FOR A SERIES-60 SHIP OF C_B=0.7 AT INFINITE WATER DEPTH AT VARIOUS FROUDE NUMBERS IN HEAD WAVES.

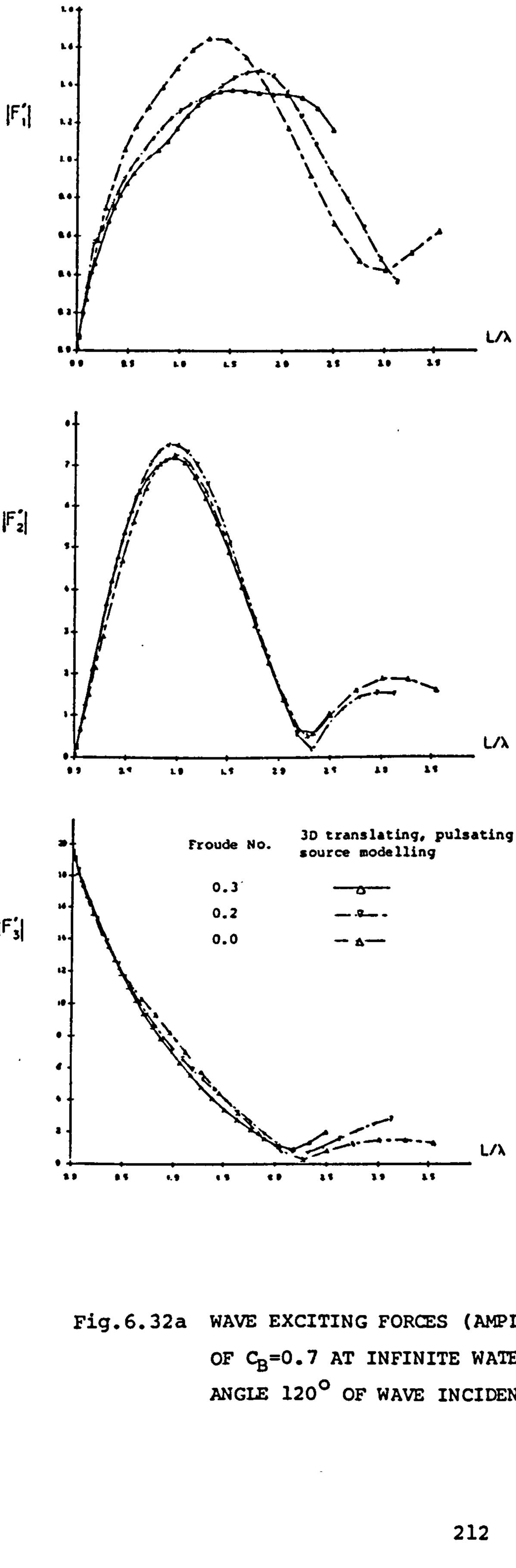

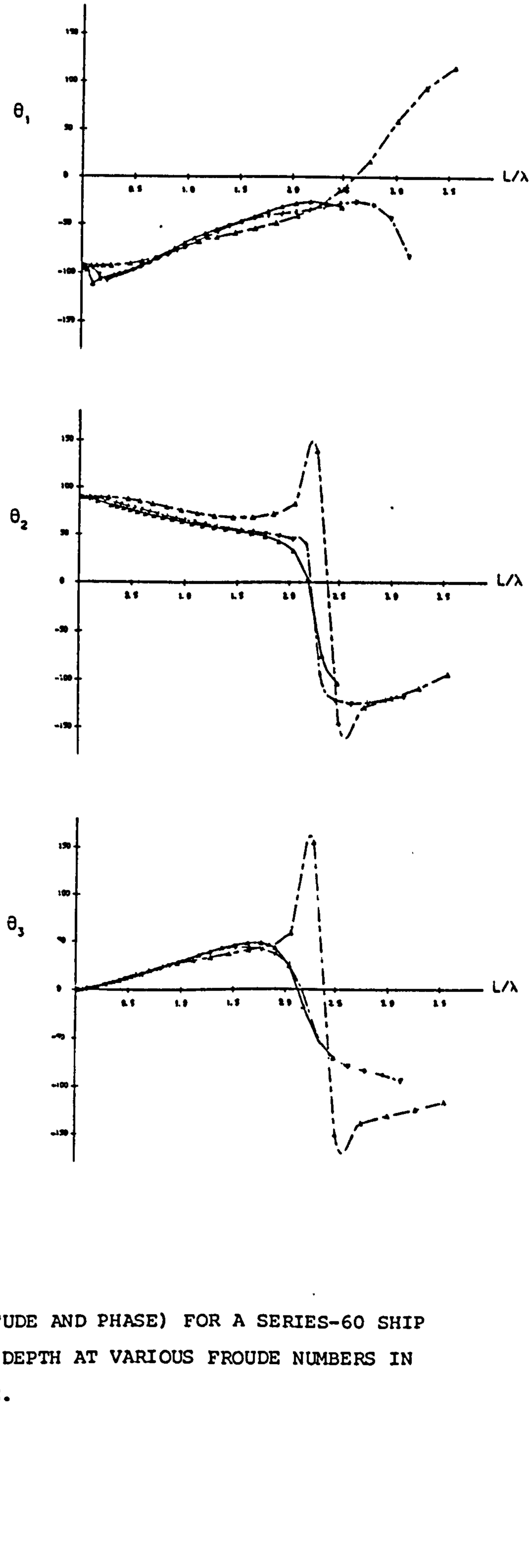

Fig.6.32a WAVE EXCITING FORCES (AMPLITUDE AND PHASE) FOR A SERIES-60 SHIP OF C_B=0.7 AT INFINITE WATER DEPTH AT VARIOUS FROUDE NUMBERS IN ANGLE 120° OF WAVE INCIDENCE.

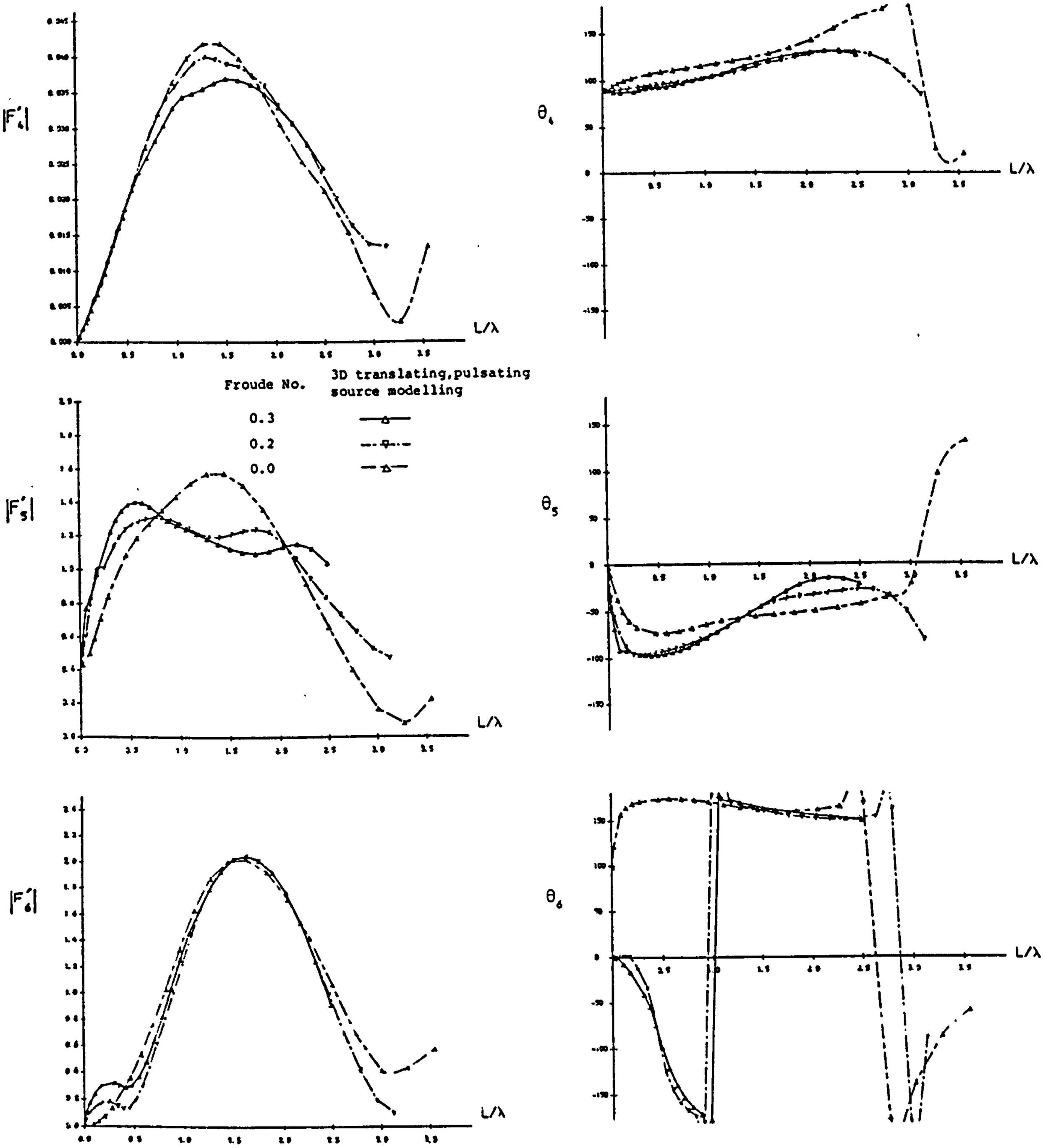

Fig.6.32b WAVE EXCITING MOMENTS (AMPLITUDE AND PHASE) FOR A SERIES-60 SHIP OF C_B=0.7 AT INFINITE WATER DEPTH AT VARIOUS FROUDE NUMBERS IN ANGLE 120° OF WAVE INCIDENCE.

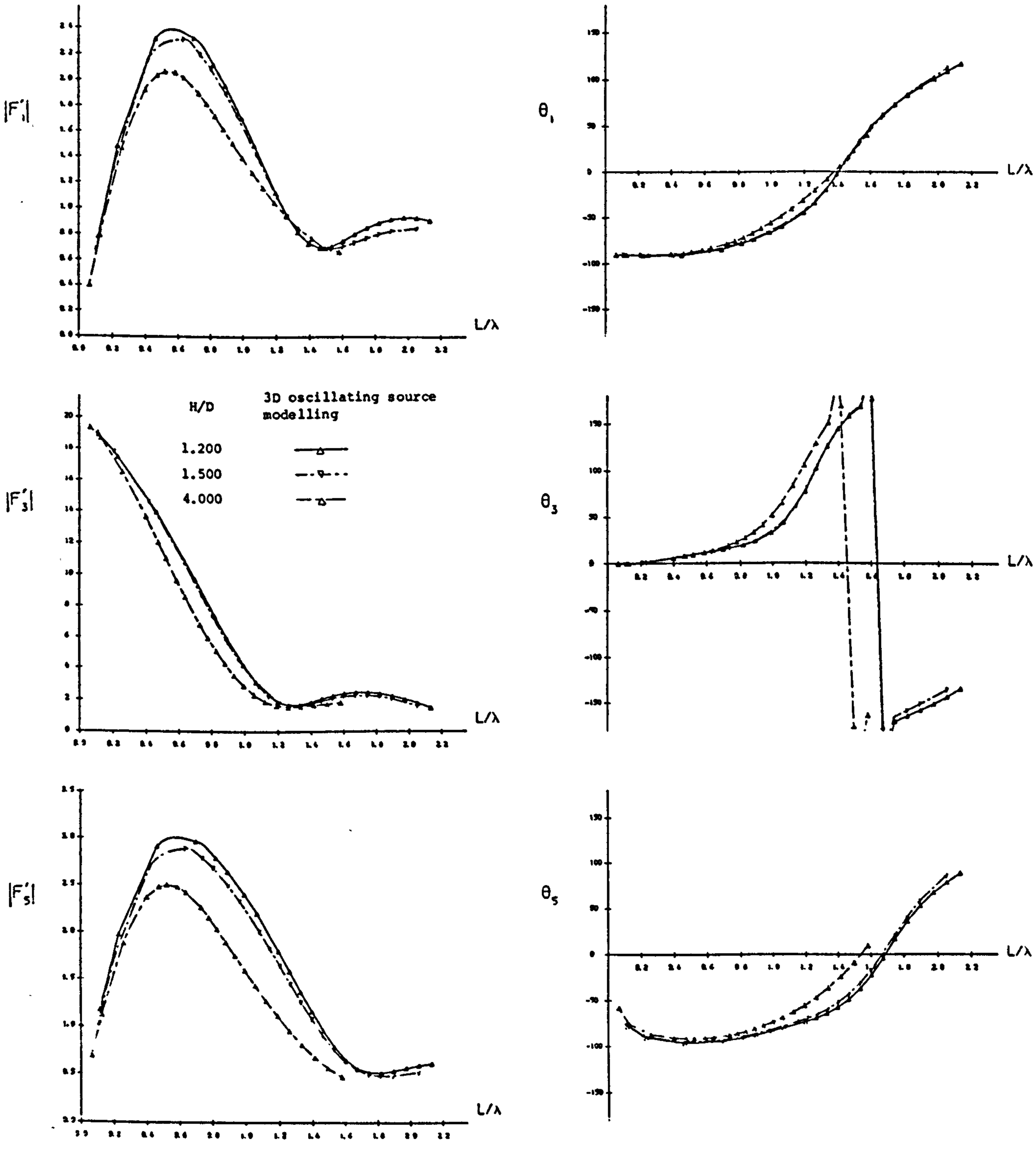

Fig.6.33 WAVE EXCITING FORCES AND MOMENT (AMPLITUDE AND PHASE) FOR A SERIES-60 SHIP OF C_B=0.7 AT F_n=0.2 AT VARIOUS WATER DEPTHS IN HEAD WAVES.

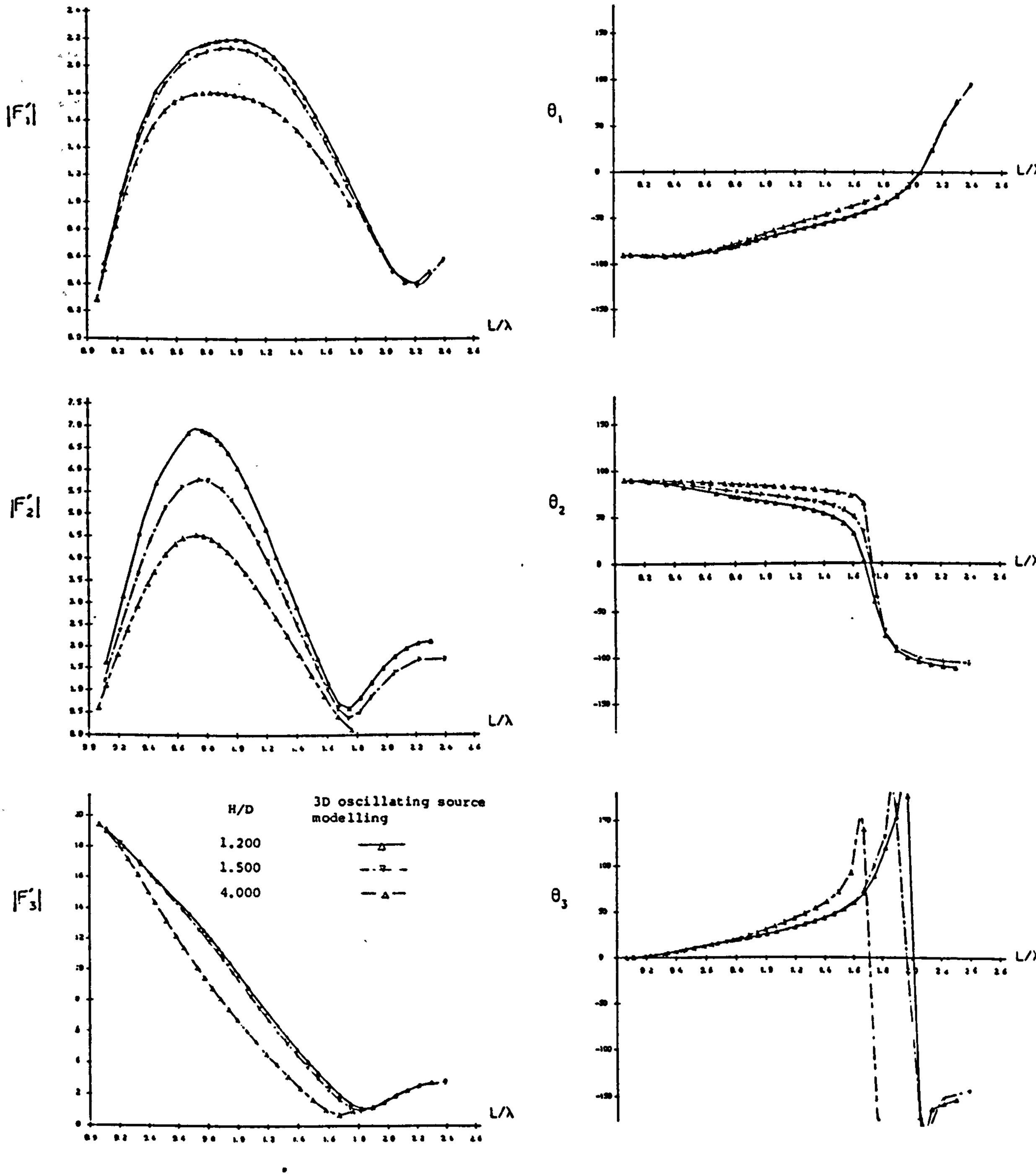

Fig.6.34a WAVE EXCITING FORCES (AMPLITUDE AND PHASE) FOR A SERIES-60 SHIP OF C_B=0.7 AT F_n=0.2 AT VARIOUS WATER DEPTHS IN BOW QUARTERING WAVES.

Fig.6.34b WAVE EXCITING MOMENTS (AMPLITUDE AND PHASE) FOR A SERIES-60 SHIP OF C_B=0.7 AT F_n=0.2 AT VARIOUS WATER DEPTHS IN BOW QUARTERING WAVES.

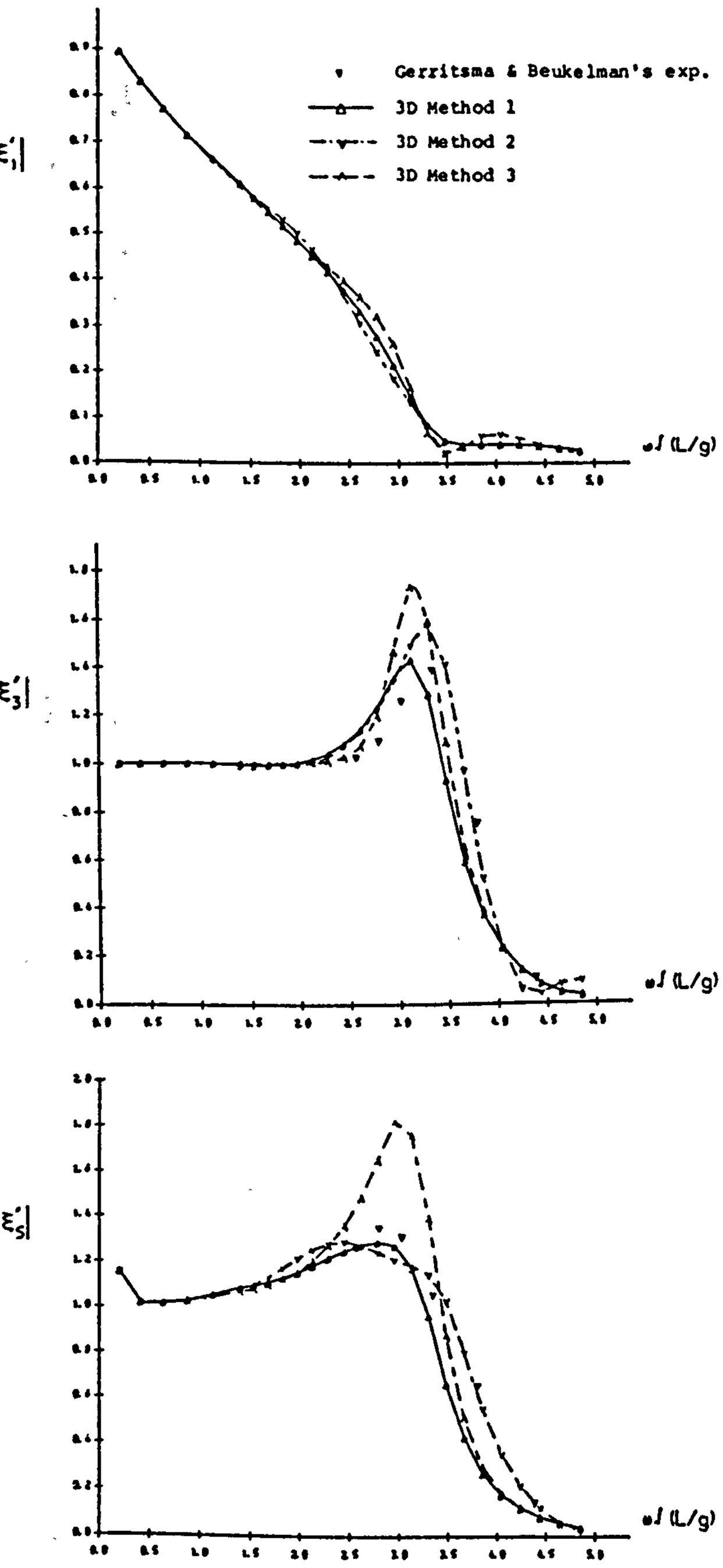

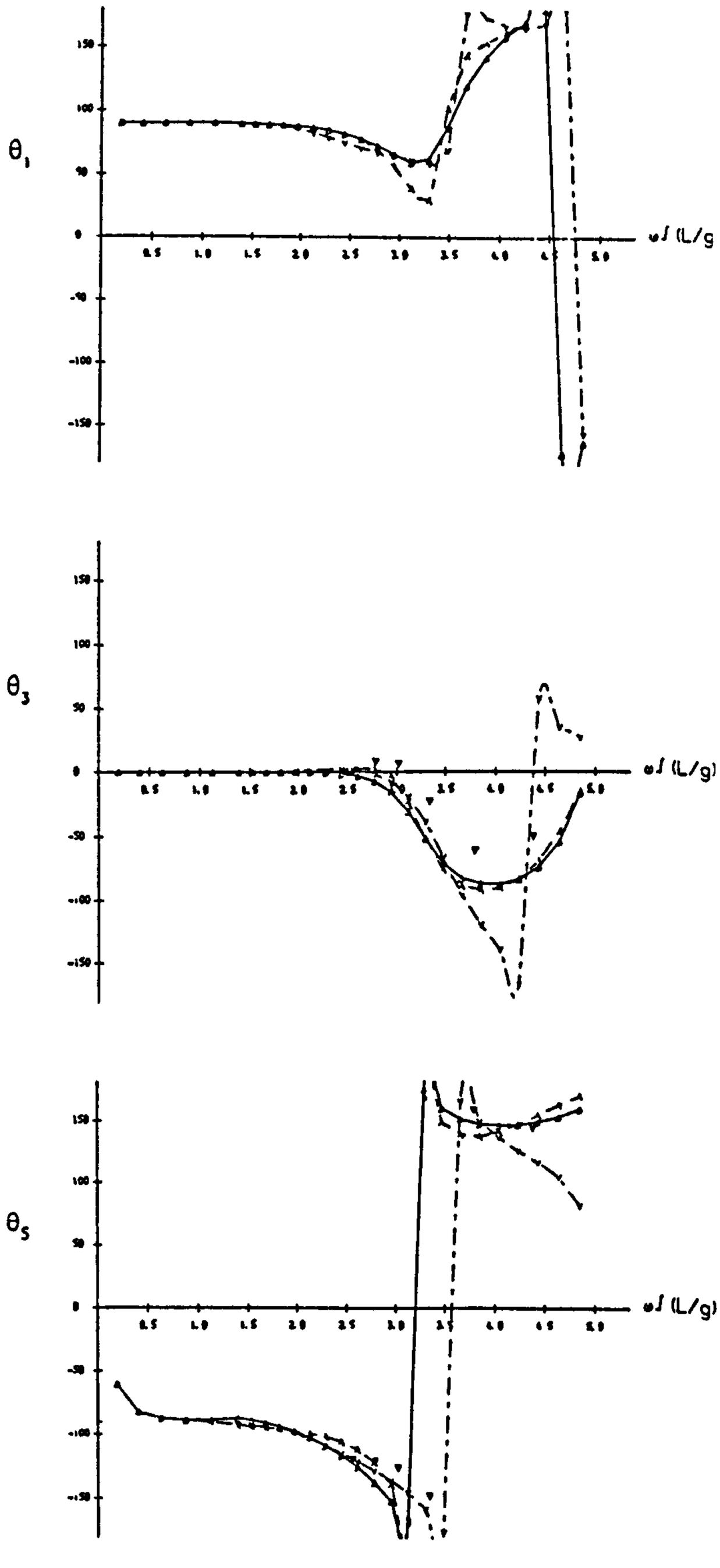

Fig.6.35 MOTION RESPONSES (AMPLITUDE AND PHASE) FOR A SERIES-60 SHIP OF C_B=0.7 AT INFINITE WATER DEPTH AT F_n=0.2 IN HEAD WAVES.

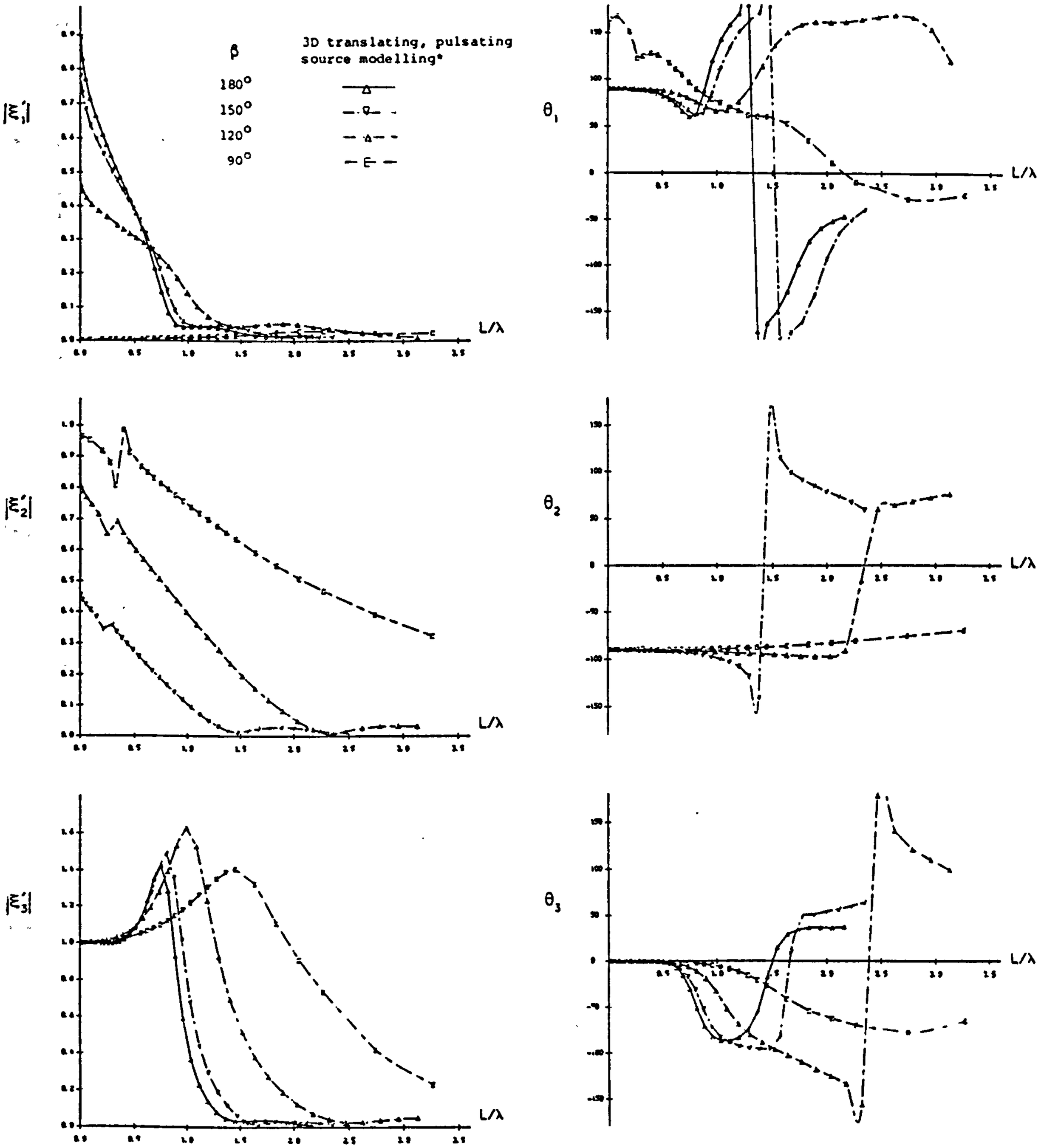

Fig.6.36a TRANSLATIONAL MOTION RESPONSES (AMPLITUDE AND PHASE) FOR A SERIES-60 SHIP OF C_B=0.7 AT INFINITE WATER DEPTH AT F_n=0.2 IN VARIOUS ANGLES OF WAVE INCIDENCE.

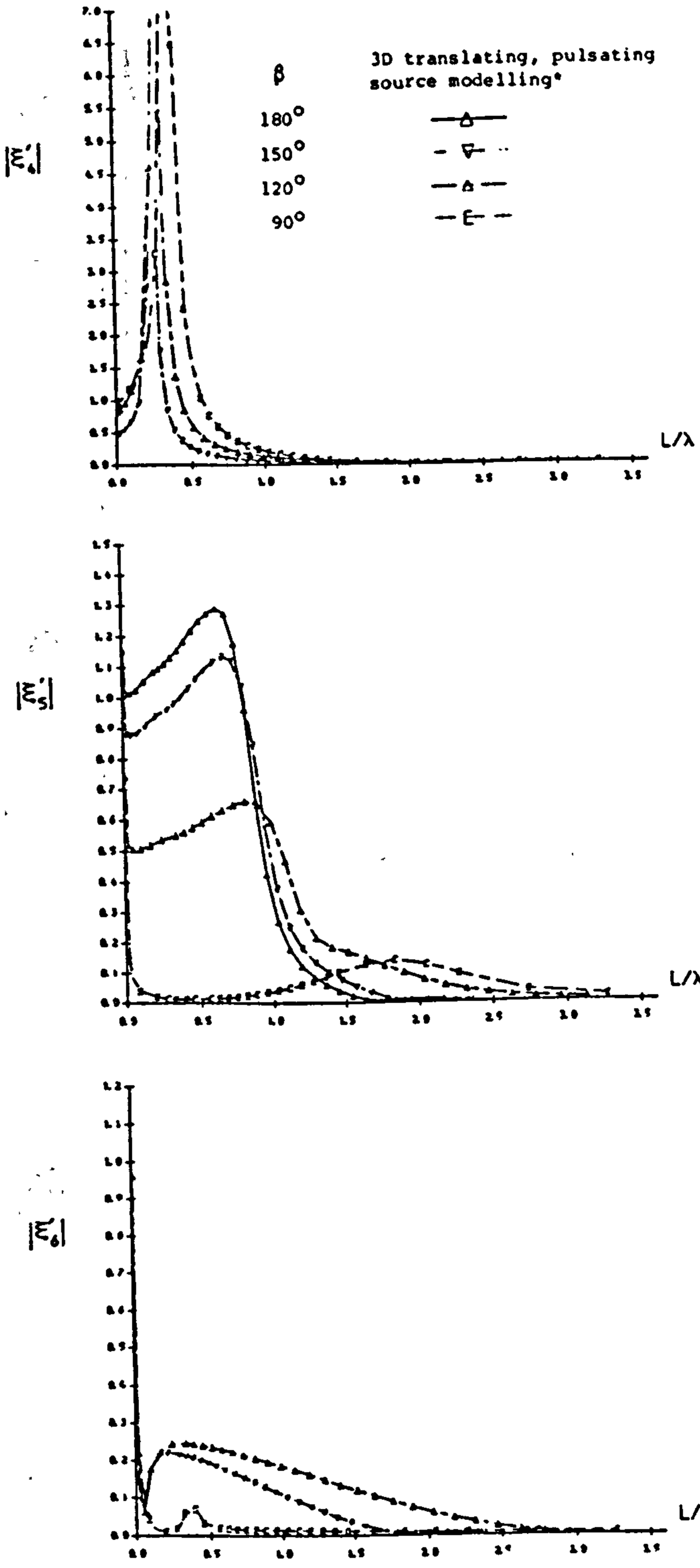

Fig.6.36b ANGULAR MOTION RESPONSES (AMPLITUDE AND PHASE) FOR A SERIES-60 SHIP OF C_B=0.7 AT INFINITE WATER DEPTH AT F_n=0.2 IN VARIOUS ANGLES OF WAVE INCIDENCE.

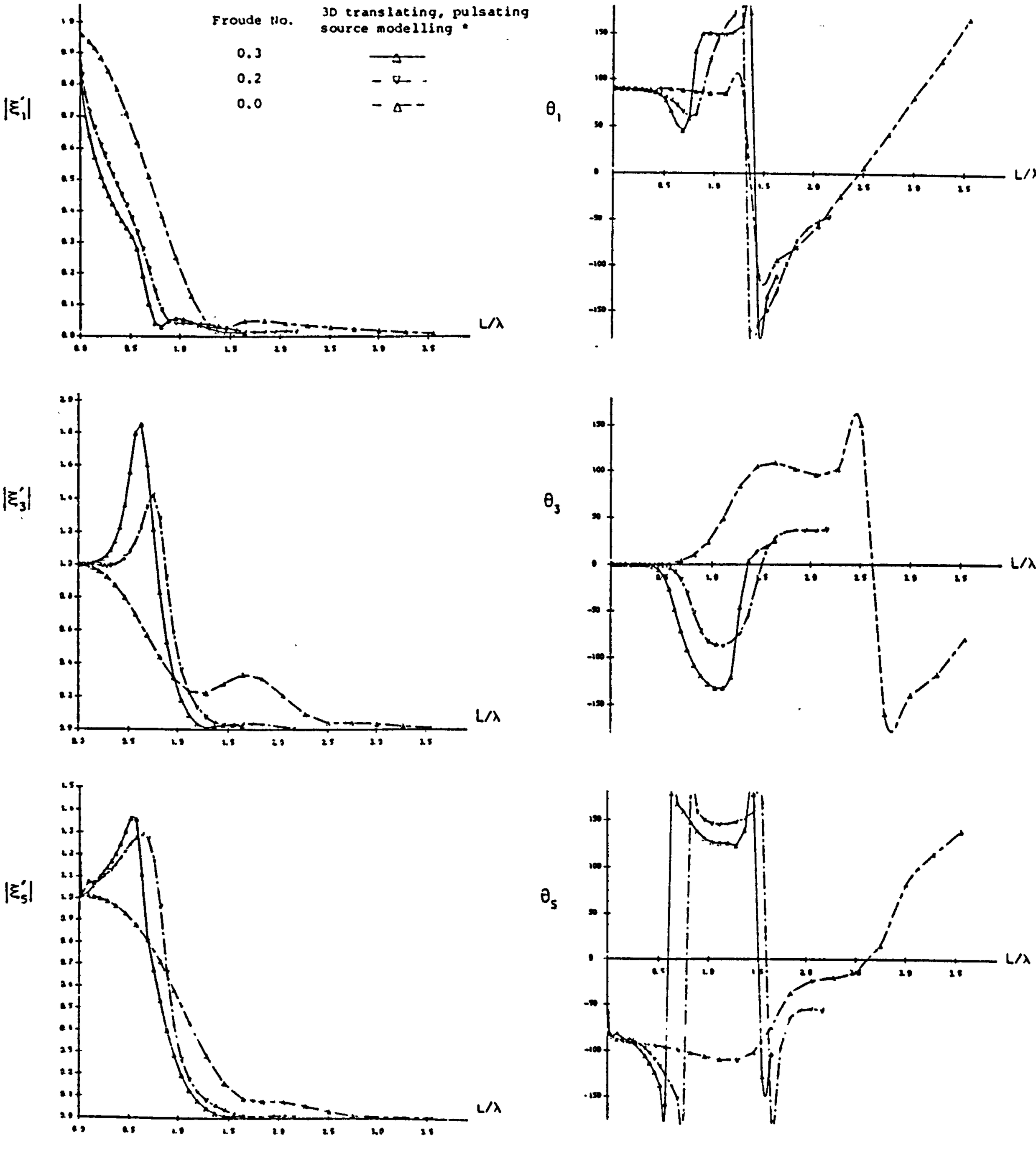

Fig.6.37 MOTION RESPONSES (AMPLITUDE AND PHASE) FOR A SERIES-60 SHIP OF C_B=0.7 AT INFINITE WATER DEPTH AT VARIOUS FROUDE NUMBERS IN HEAD WAVES.

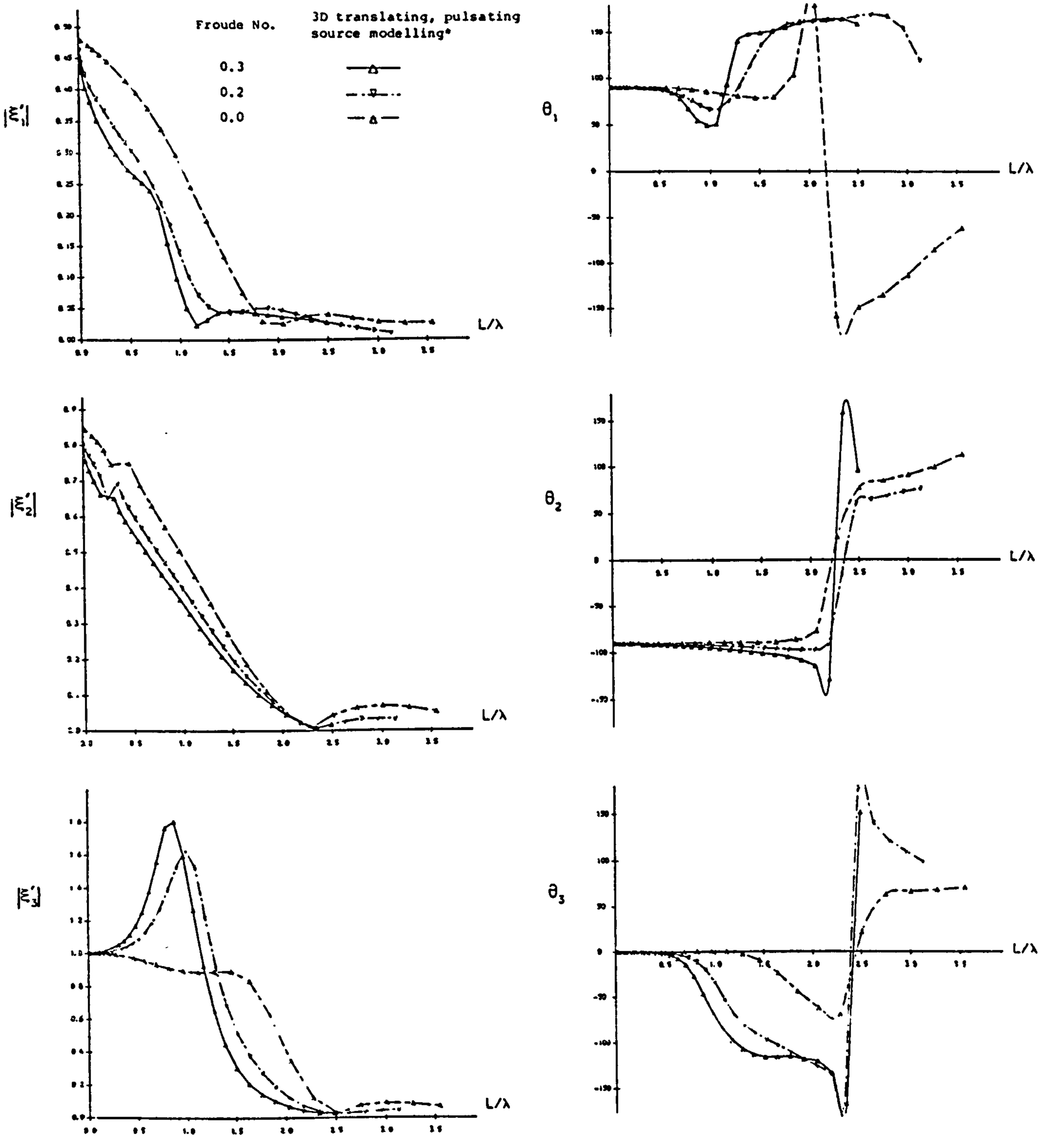

Fig.6.38a TRANSLATIONAL MOTION RESPONSES (AMPLITUDE AND PHASE) FOR A SERIES-60 SHIP OF C_B=0.7 AT INFINITE WATER DEPTH AT VARIOUS FROUDE NUMBERS IN ANGLE 120° OF WAVE INCIDENCE.

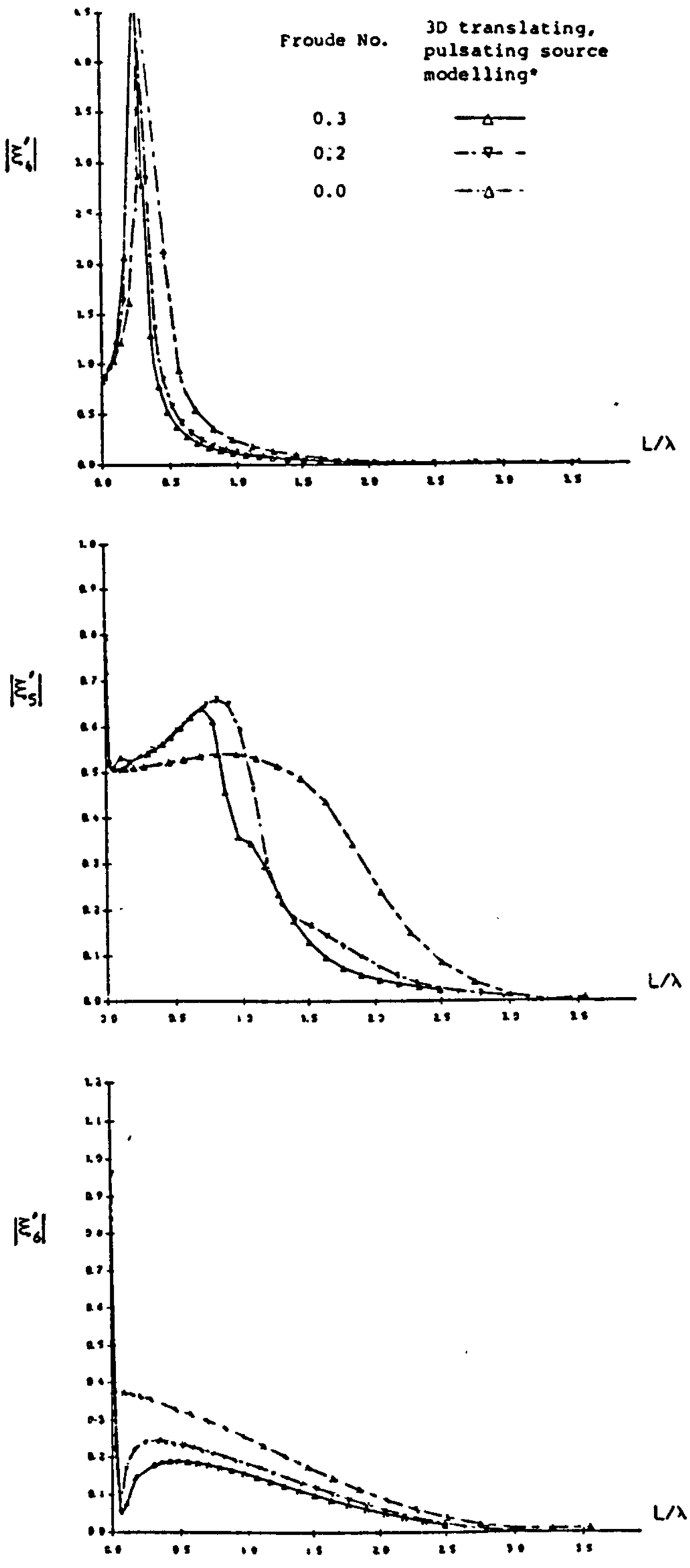

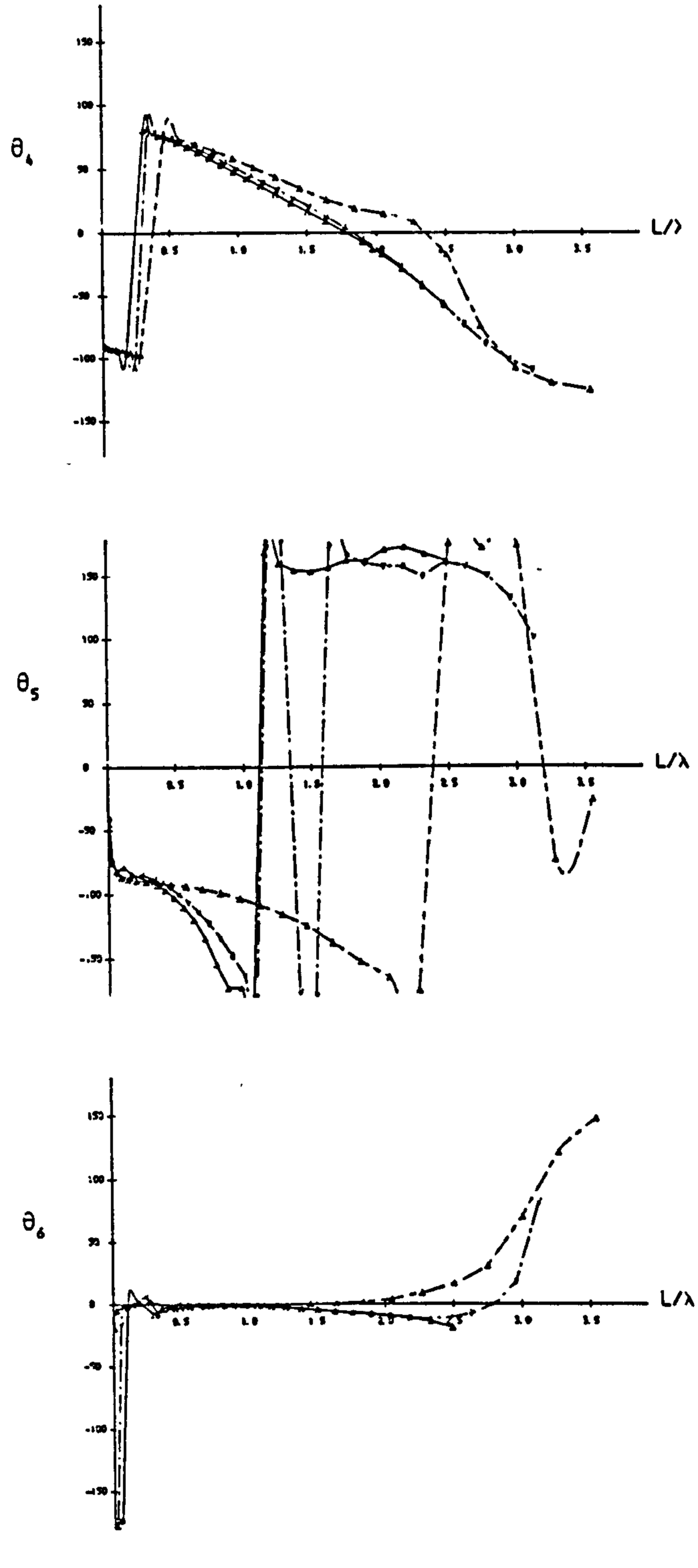

Fig.6.38b ANGULAR MOTION RESPONSES (AMPLITUDE AND PHASE) FOR A SERIES-60 SHIP OF C_B=0.7 AT INFINITE WATER DEPTH AT VARIOUS FROUDE NUMBERS IN ANGLE 120° OF WAVE INCIDENCE.

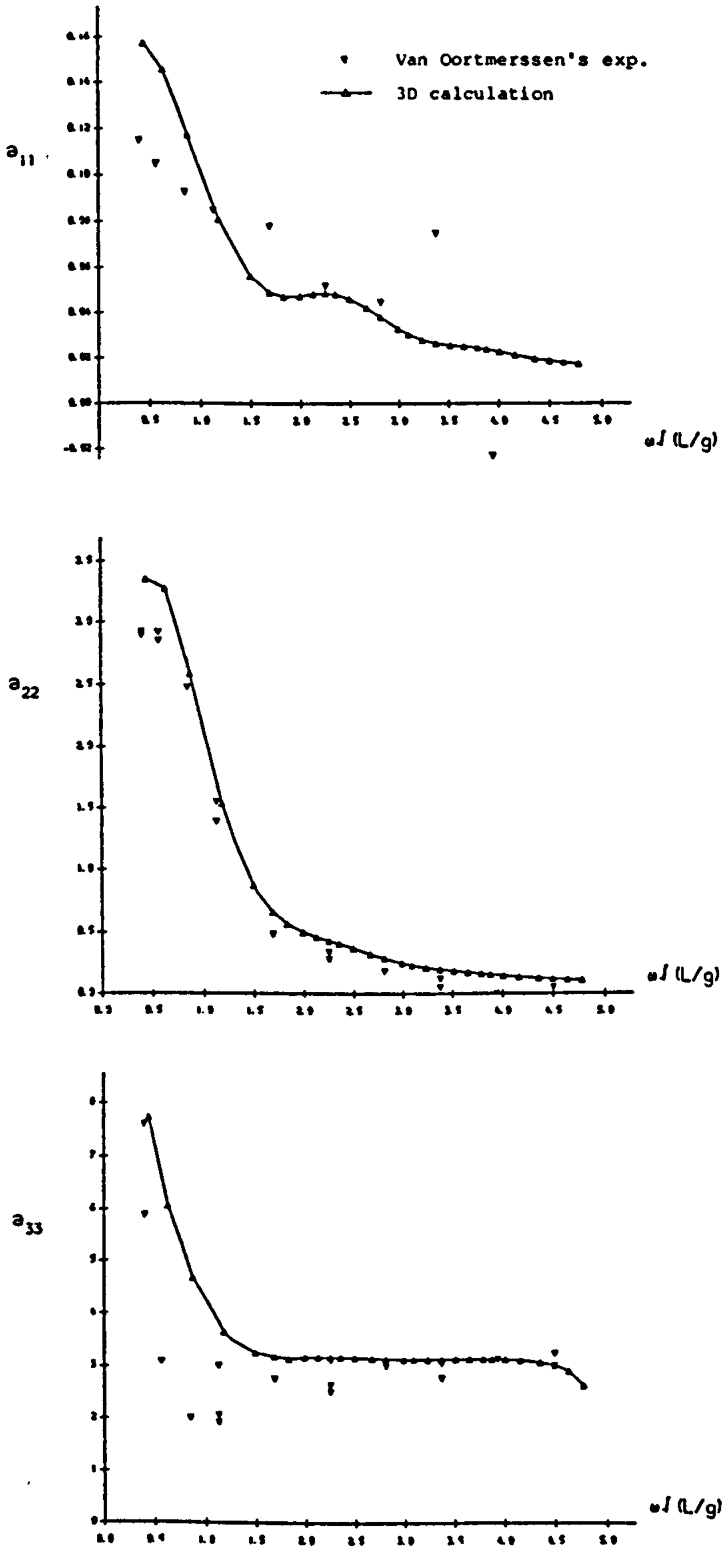

Fig.6.40 ZERO SPEED NON-DIMENSIONAL ADDED MASS COEFFICIENTS OF 200,000 DWT TANKER AT WATER DEPTH OF 22.68M (H/D=1.2) FOR SIX RIGID MODES OF MOTION.

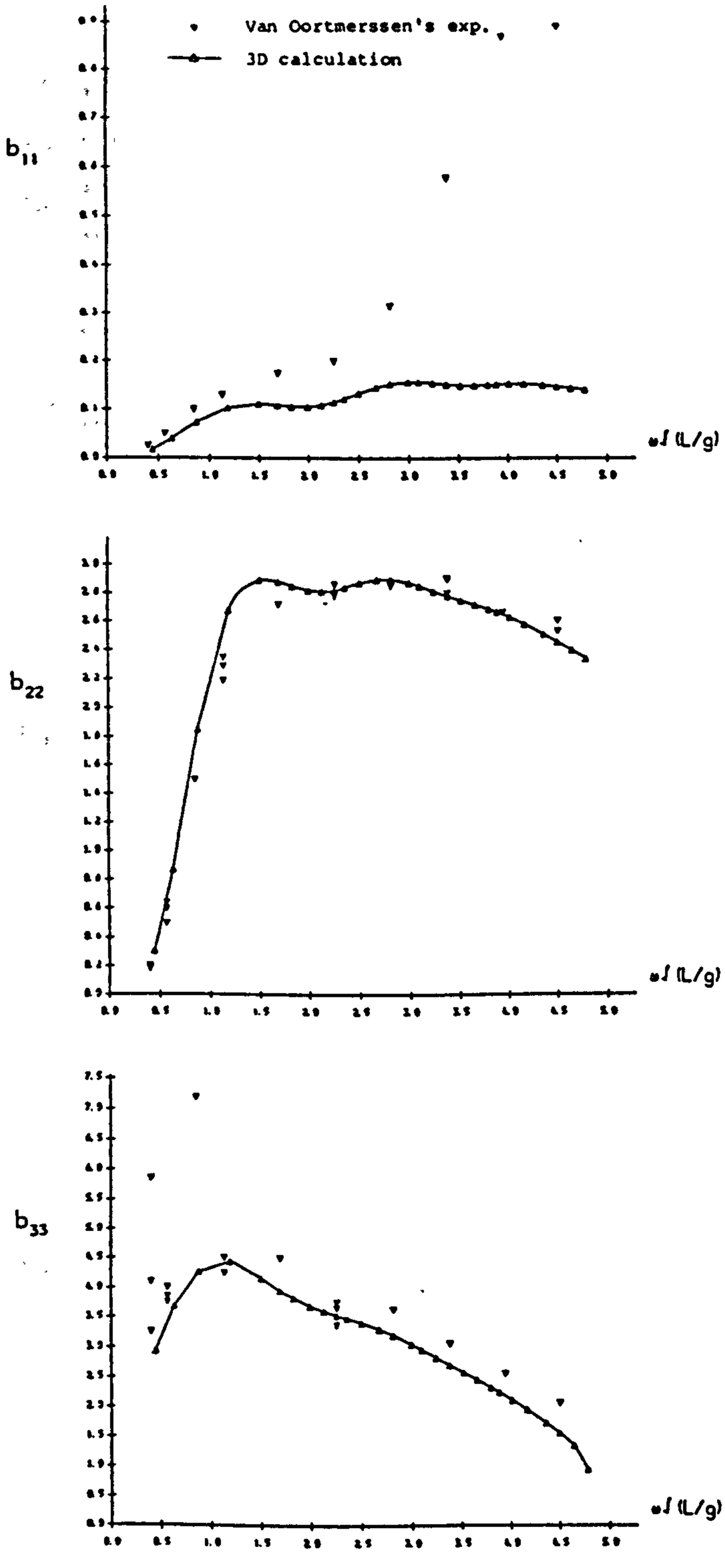

Fig.6.41 ZERO SPEED NON-DIMENSIONAL DAMPING COEFFICIENTS OF 200,000 DWT TANKER AT WATER DEPTH OF 22.68M (H/D=1.2) FOR SIX RIGID MODES OF MOTION.

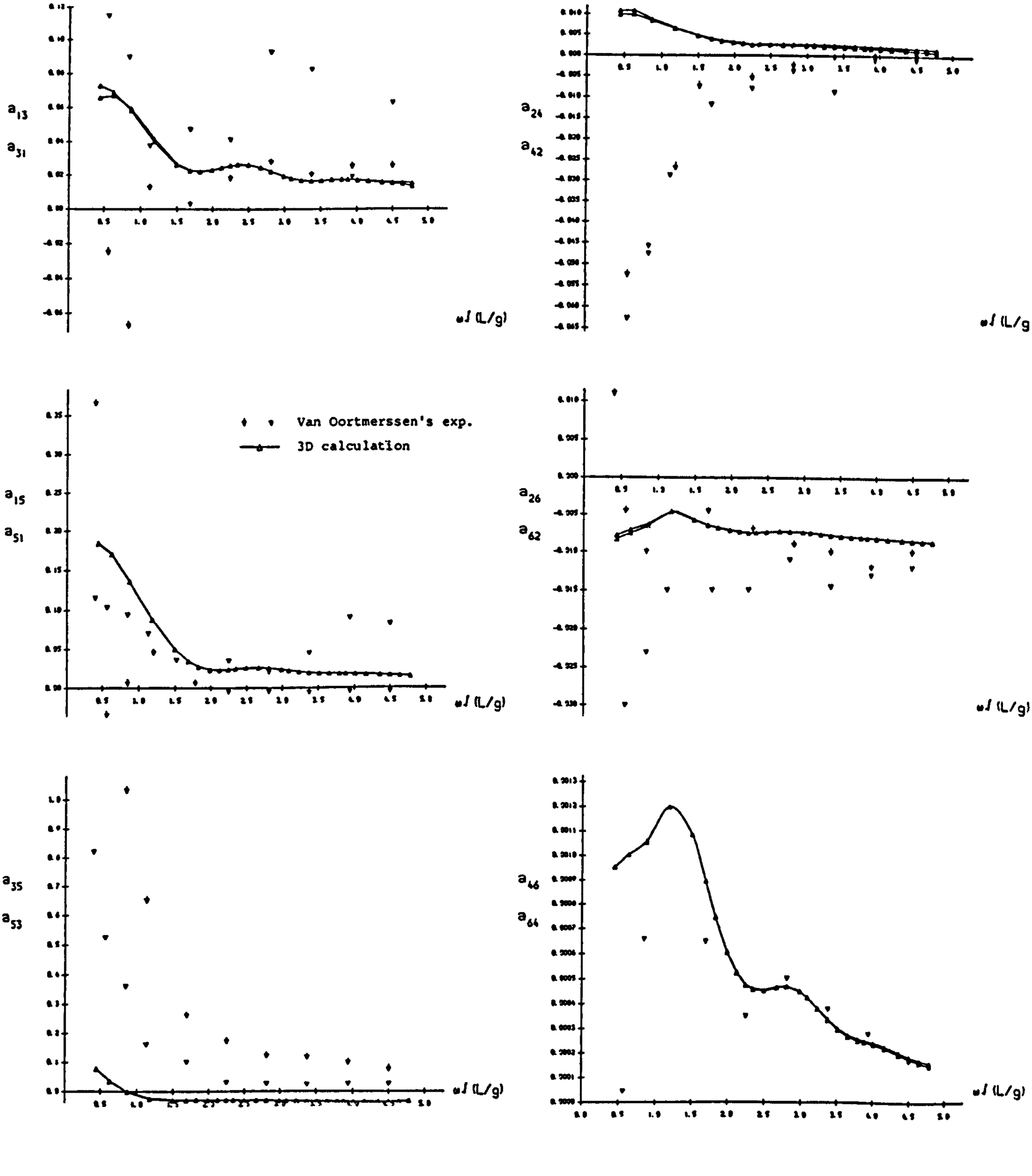

Fig.6.42 ZERO SPEED NON-DIMENSIONAL COUPLED ADDED MASS COEFFICIENTS OF 200,000 DWT TANKER AT WATER DEPTH OF 22.68M (H/D=1.2)

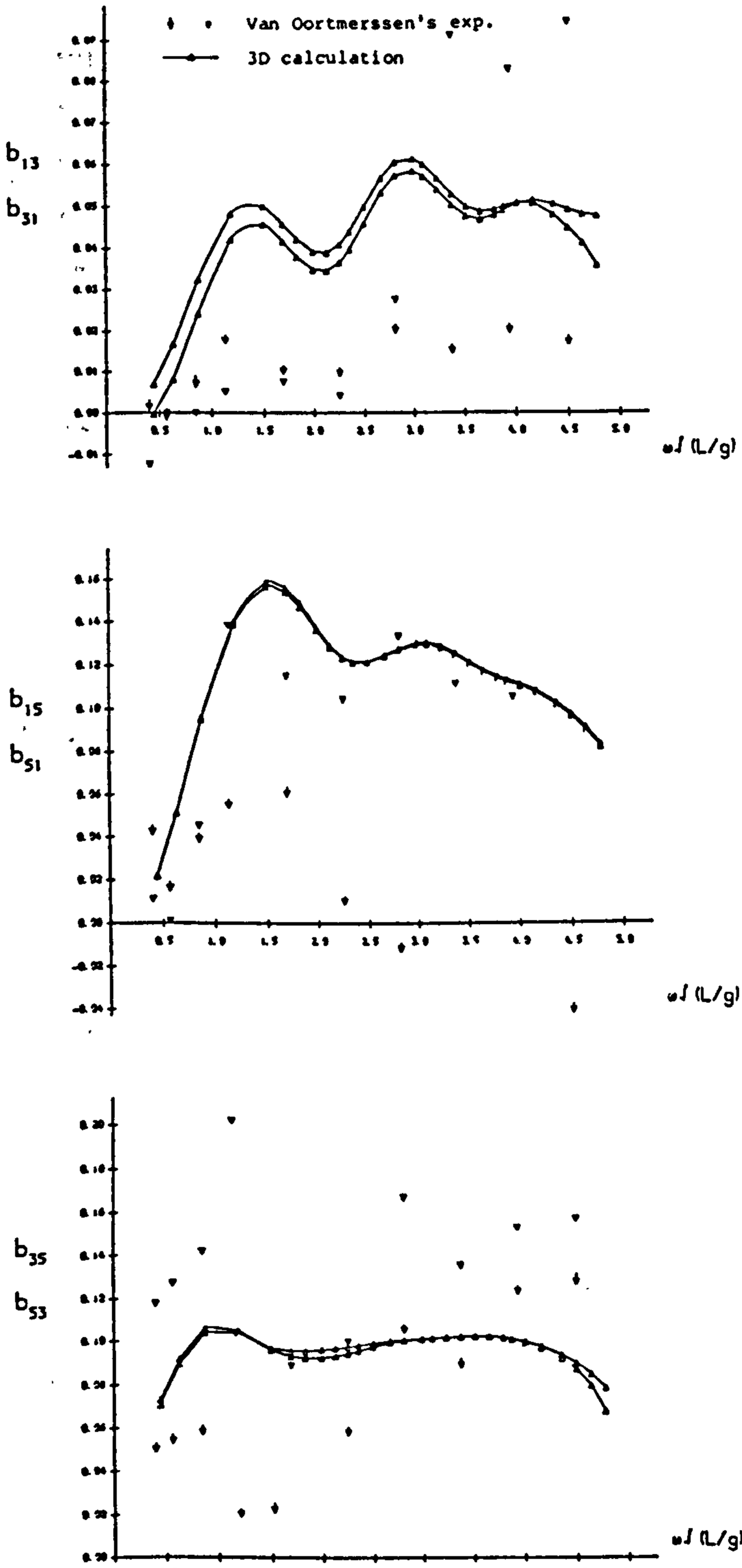

Fig.6.43 ZERO SPEED NON-DIMENSIONAL COUPLED DAMPING COEFFICIENTS OF 200,000 DWT TANKER AT WATER DEPTH OF 22.68M (H/D=1.2)

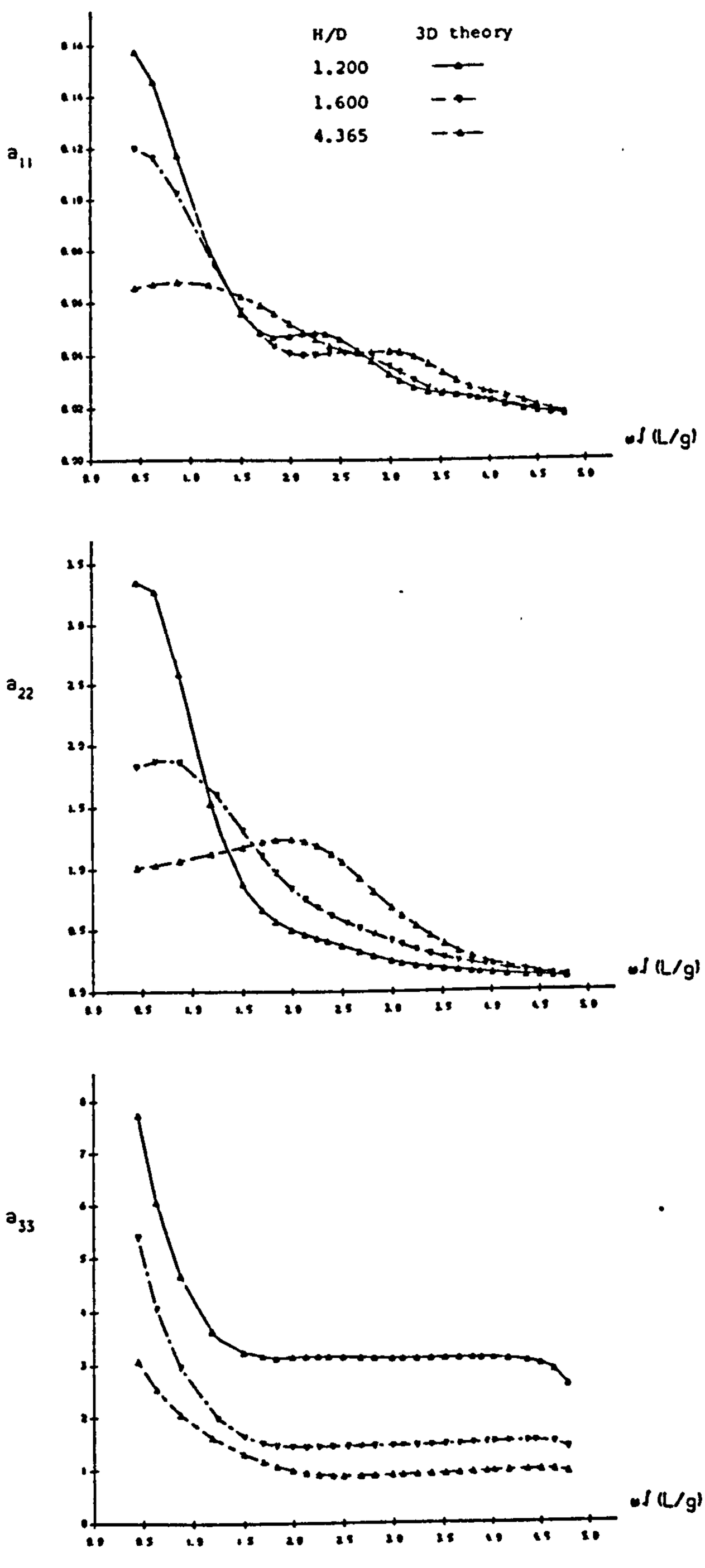

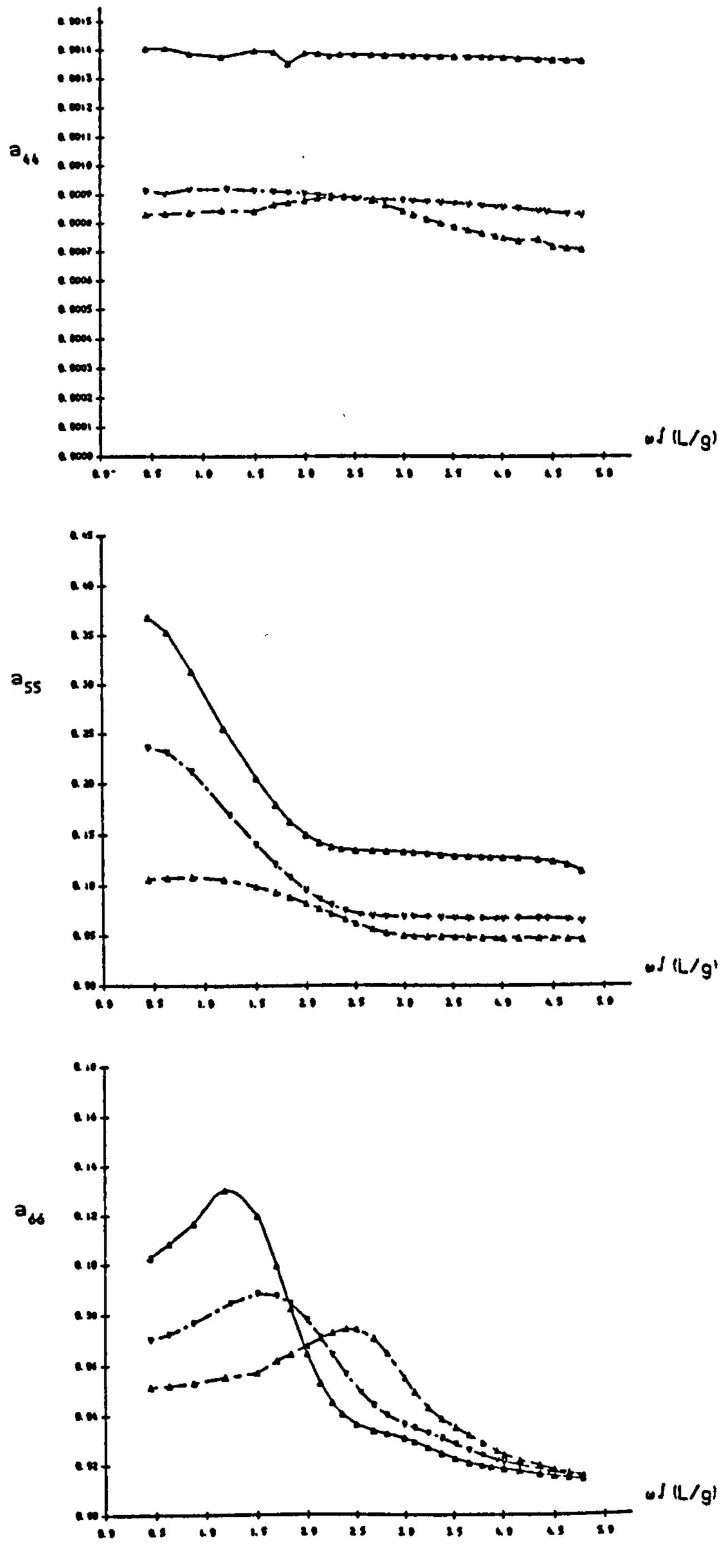

Fig.6.44 ZERO SPEED NON-DIMENSIONAL ADDED MASS COEFFICIENTS OF 200,000 DWT TANKER AT VARIOUS WATER DEPTHS FOR SIX RIGID MODES OF MOTION.

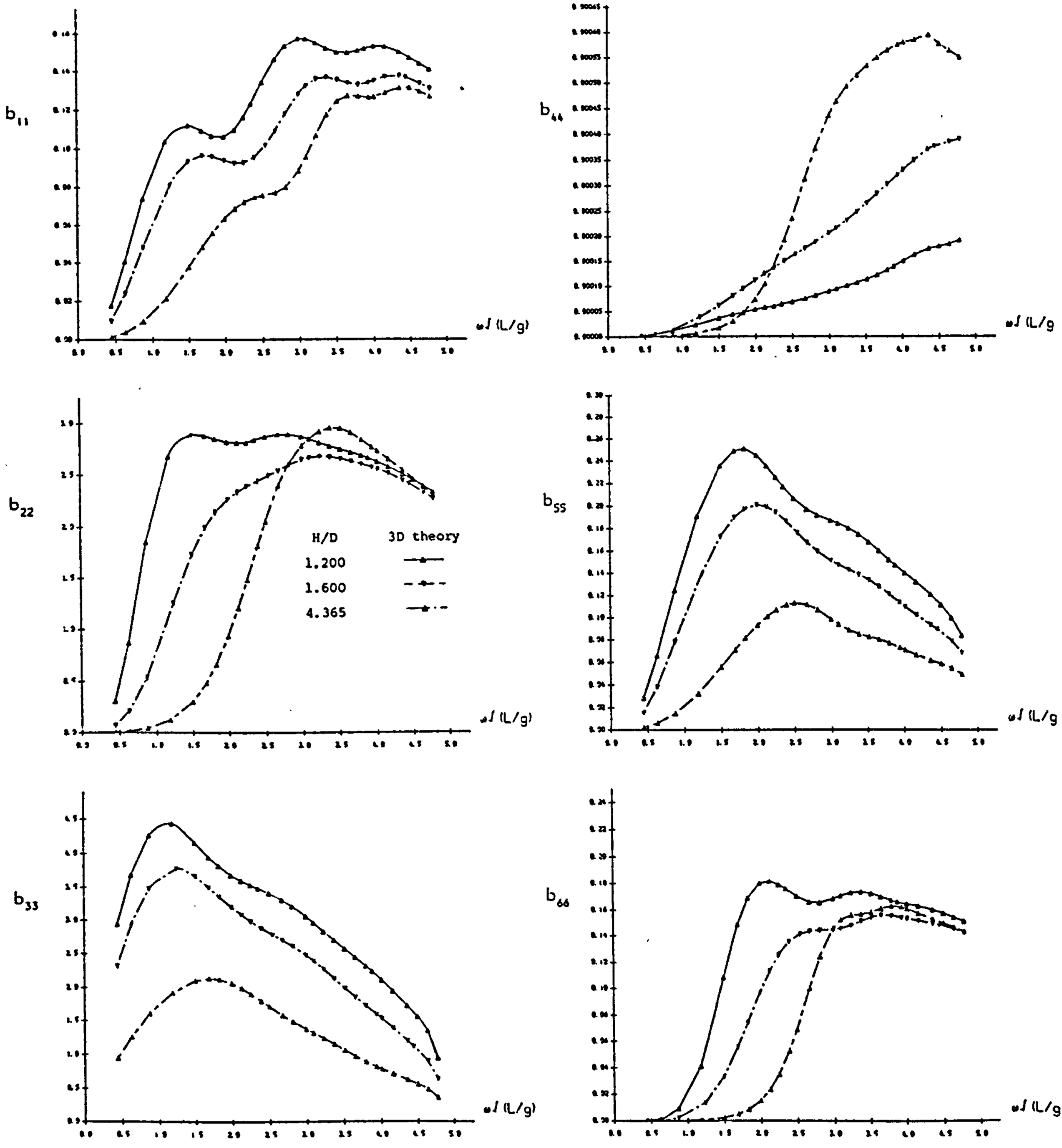

Fig.6.45 ZERO SPEED NON-DIMENSIONAL DAMPING COEFFICIENTS OF 200,000 DWT TANKER AT VARIOUS WATER DEPTHS FOR SIX RIGID MODES OF MOTION.

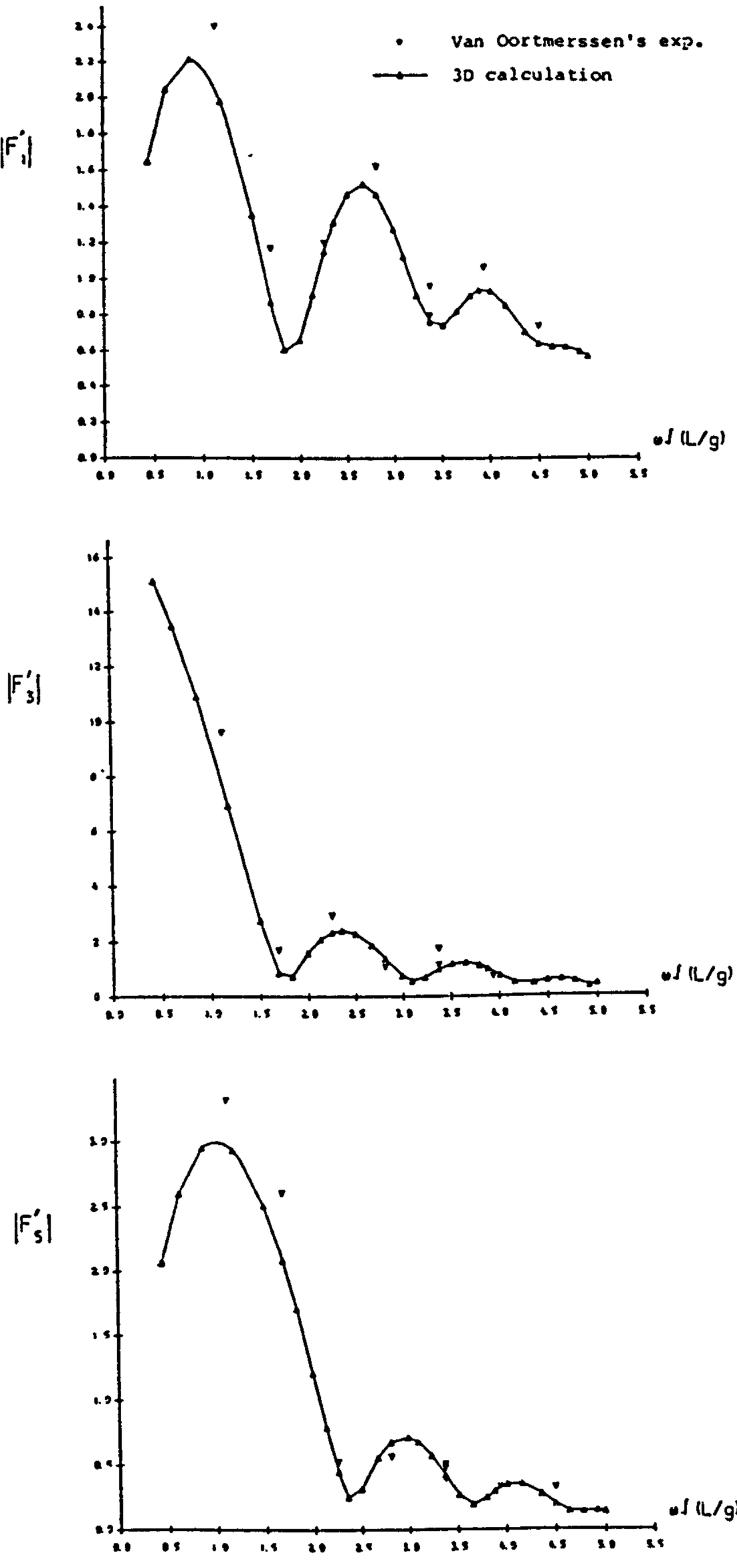

Fig.6.46 ZERO SPEED WAVE EXCITING FORCES (AMPLITUDE AND PHASE) OF 200,000 DWT TANKER AT WATER DEPTH OF 22.68M (H/D=1.2) IN HEAD WAVES.

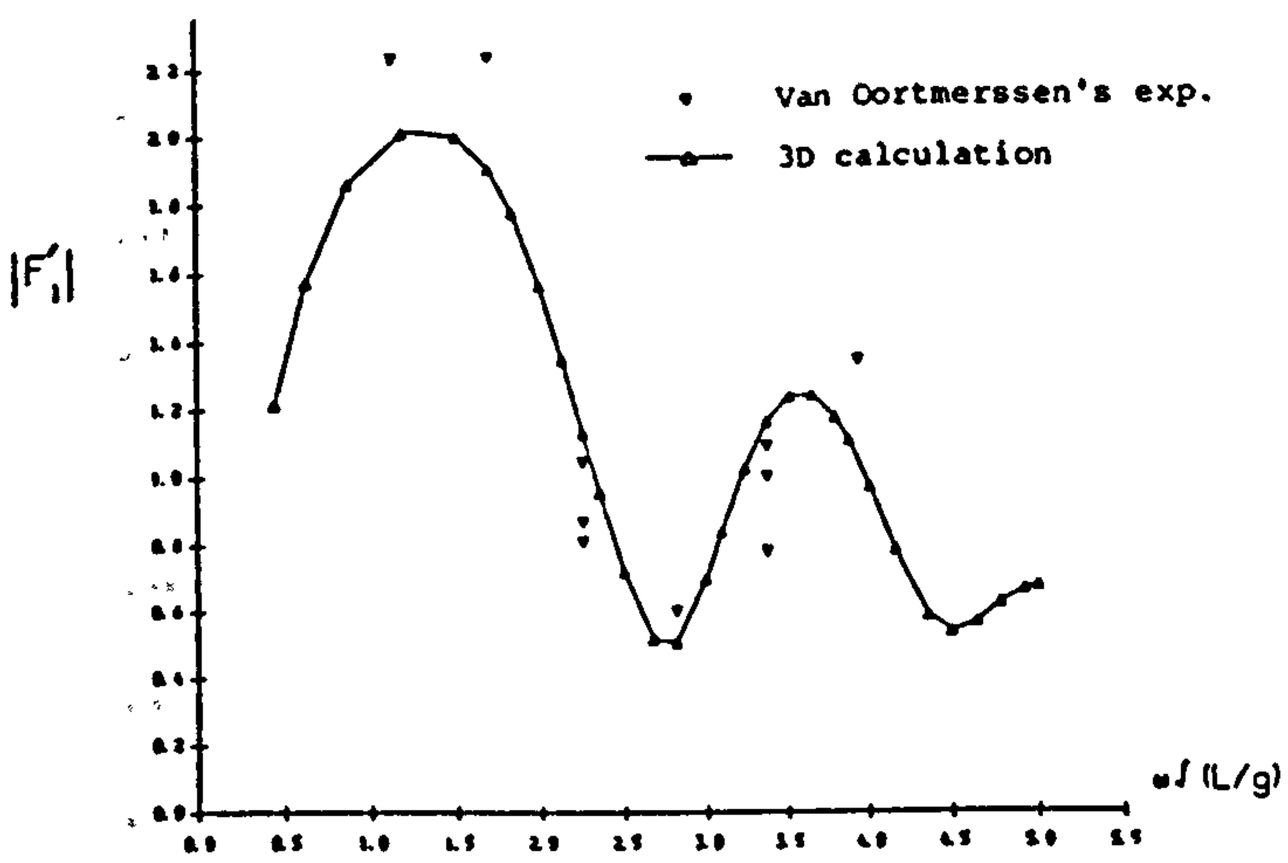

Fig.6.47a ZERO SPEED WAVE EXCITING FORCES (AMPLITUDE AND PHASE) OF 200,000 DWT TANKER AT WATER DEPTH OF 22.68M (H/D=1.2) IN BOW QUARTERING WAVES.

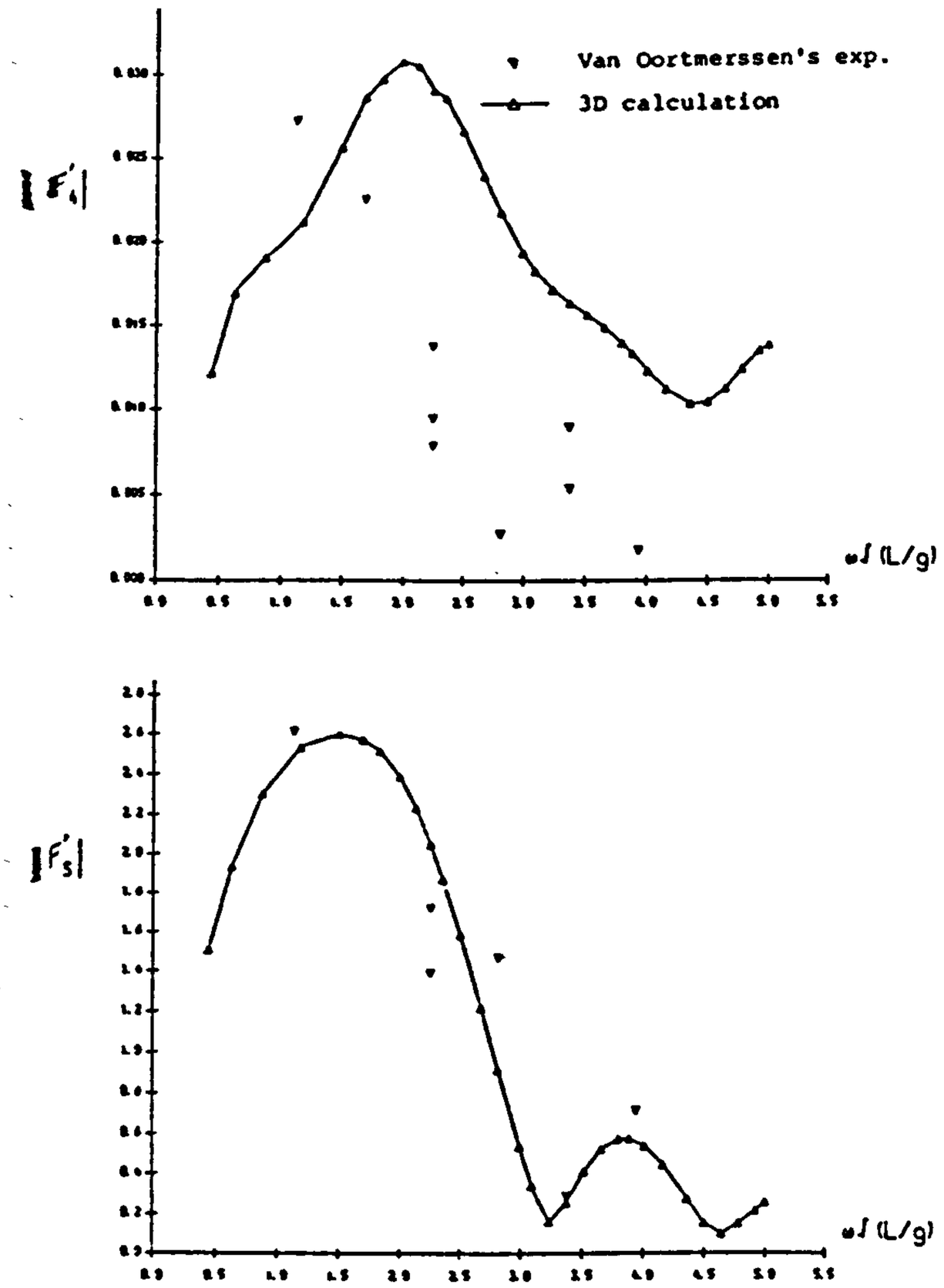

Fig.6.47b ZERO SPEED WAVE EXCITING MOMENTS (AMPLITUDE AND PHASE) OF 200,000 DWT TANKER AT WATER DEPTH OF 22.68M (H/D=1.2) IN BOW QUARTERING WAVES.

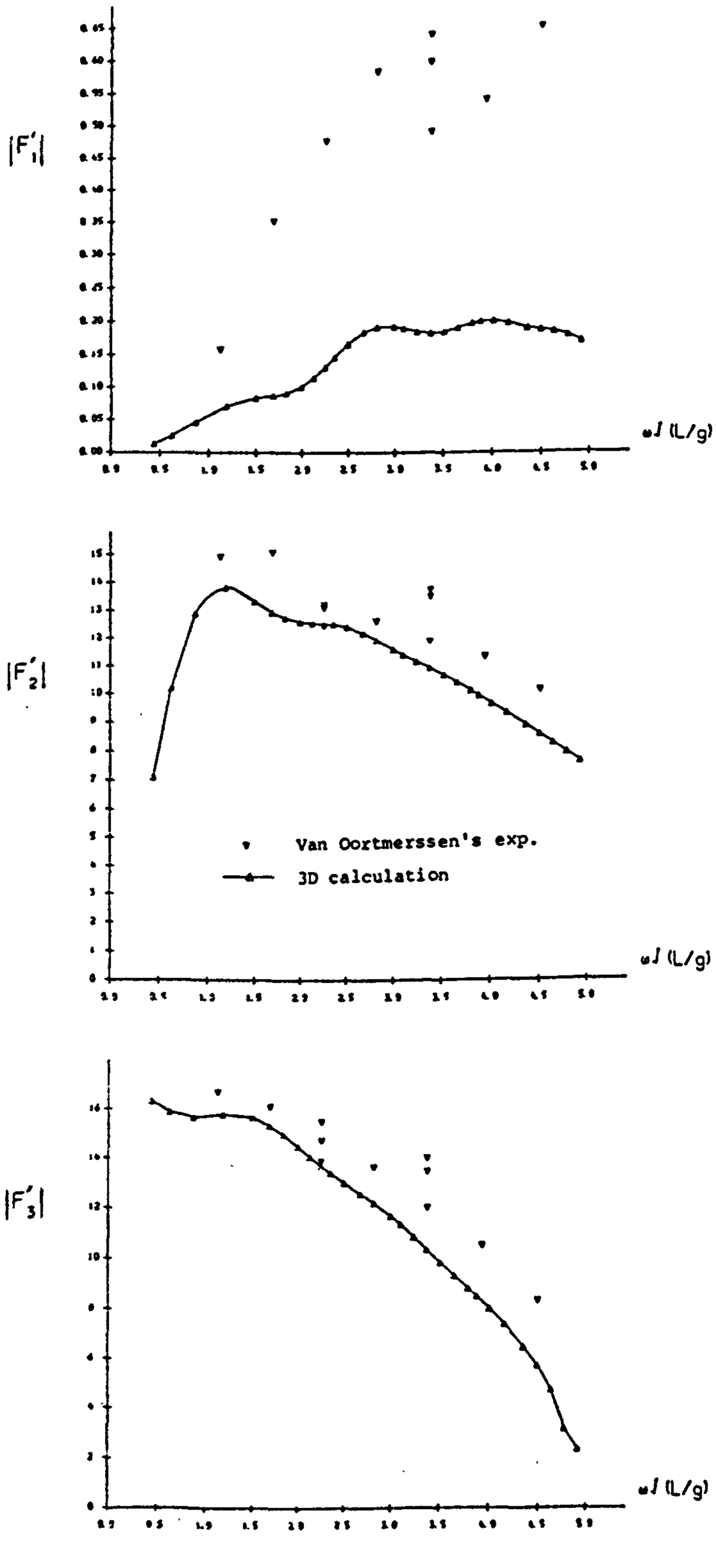

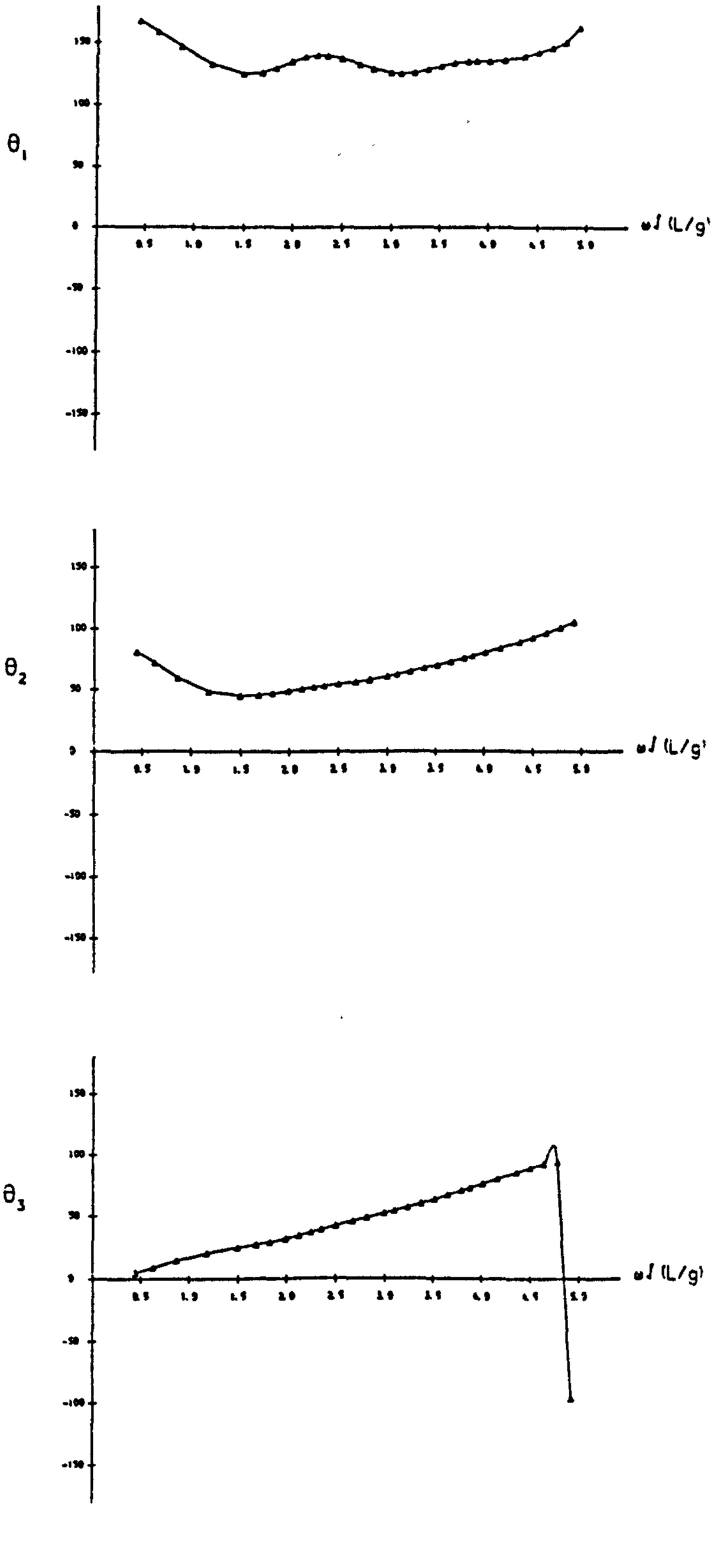

Fig.6.48a ZERO SPEED WAVE EXCITING FORCES (AMPLITUDE AND PHASE) OF 200,000 DWT TANKER AT WATER DEPTH OF 22.68M (H/D=1.2) IN BEAM WAVES.

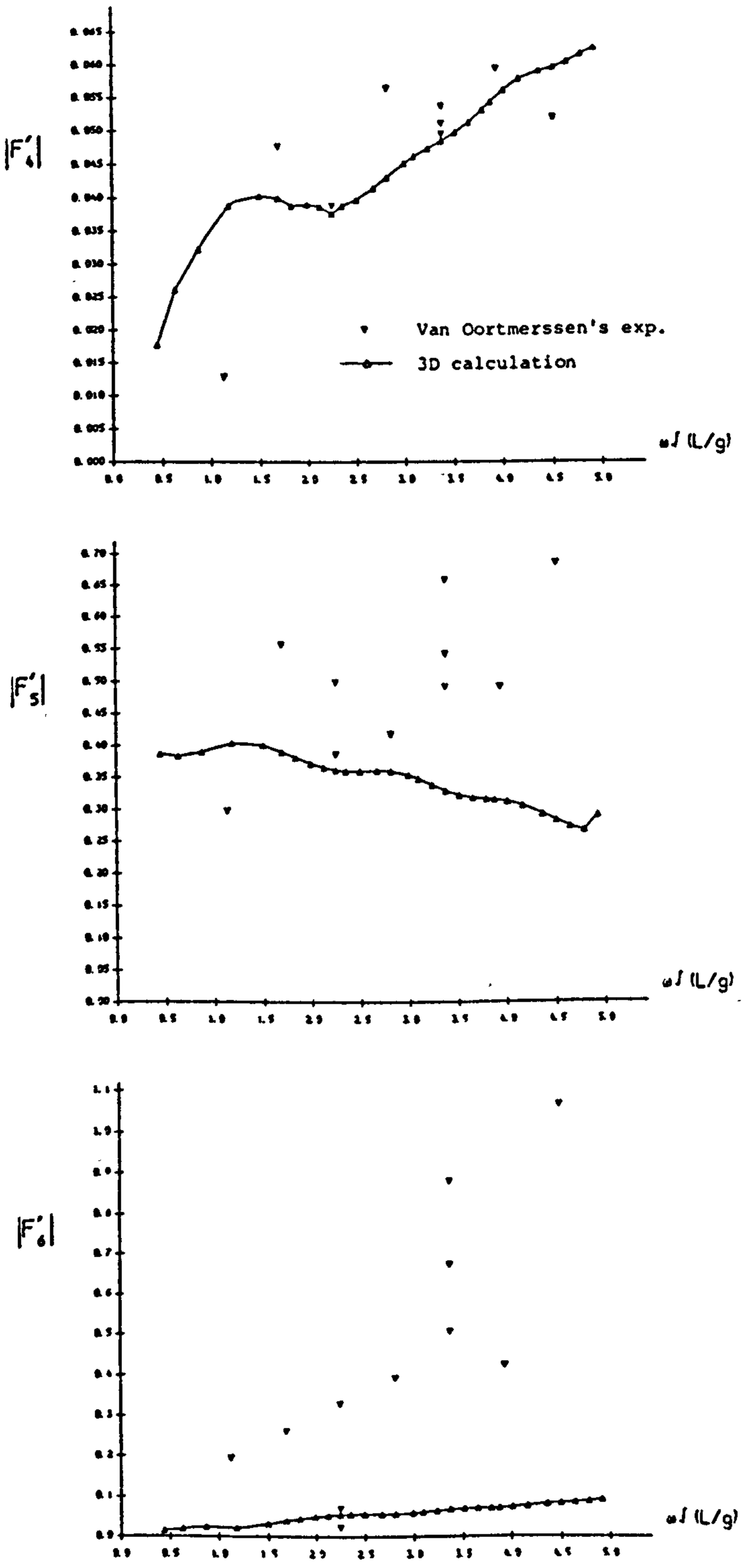

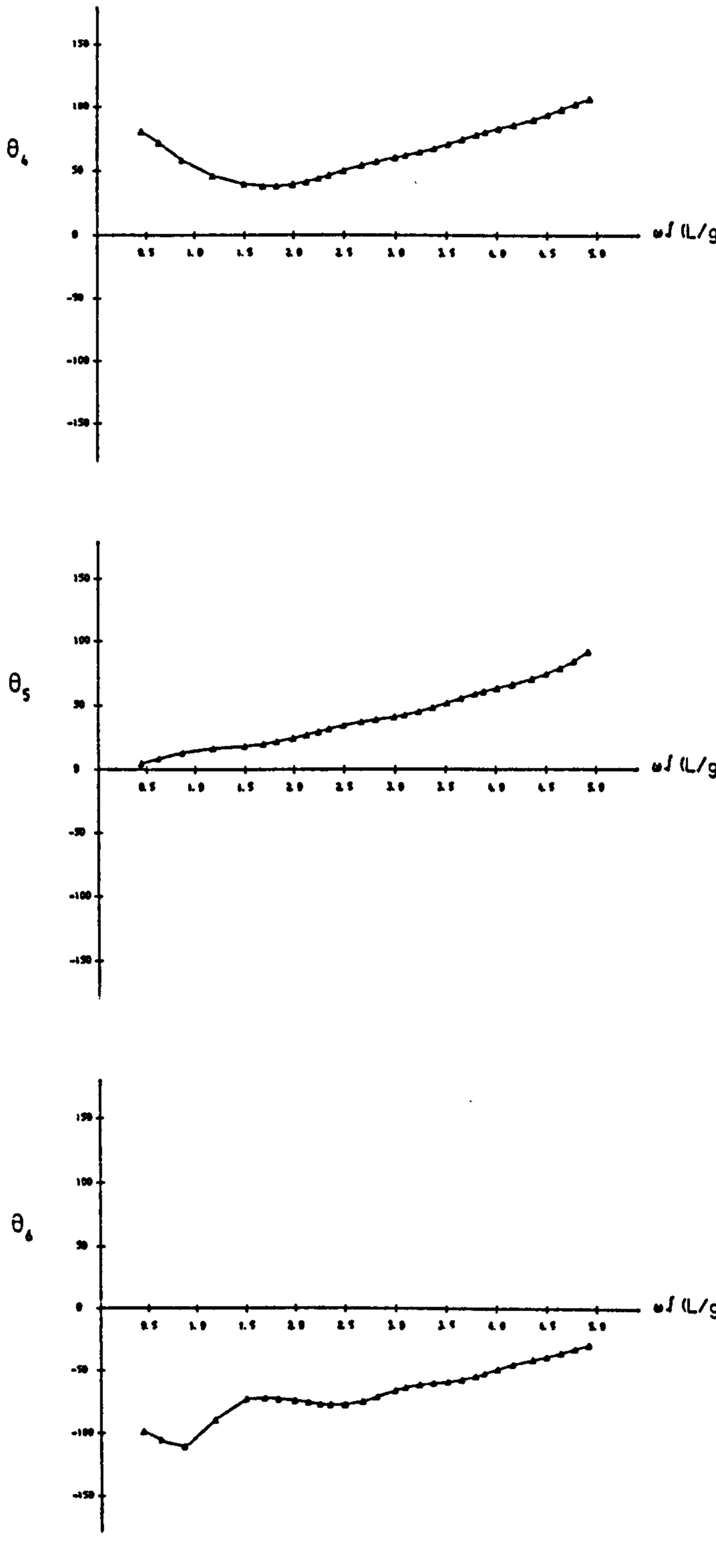

Fig.6.48b ZERO SPEED WAVE EXCITING MOMENTS (AMPLITUDE AND PHASE) OF 200,000 DWT TANKER AT WATER DEPTH OF 22.68M (H/D=1.2) IN BEAM WAVES.

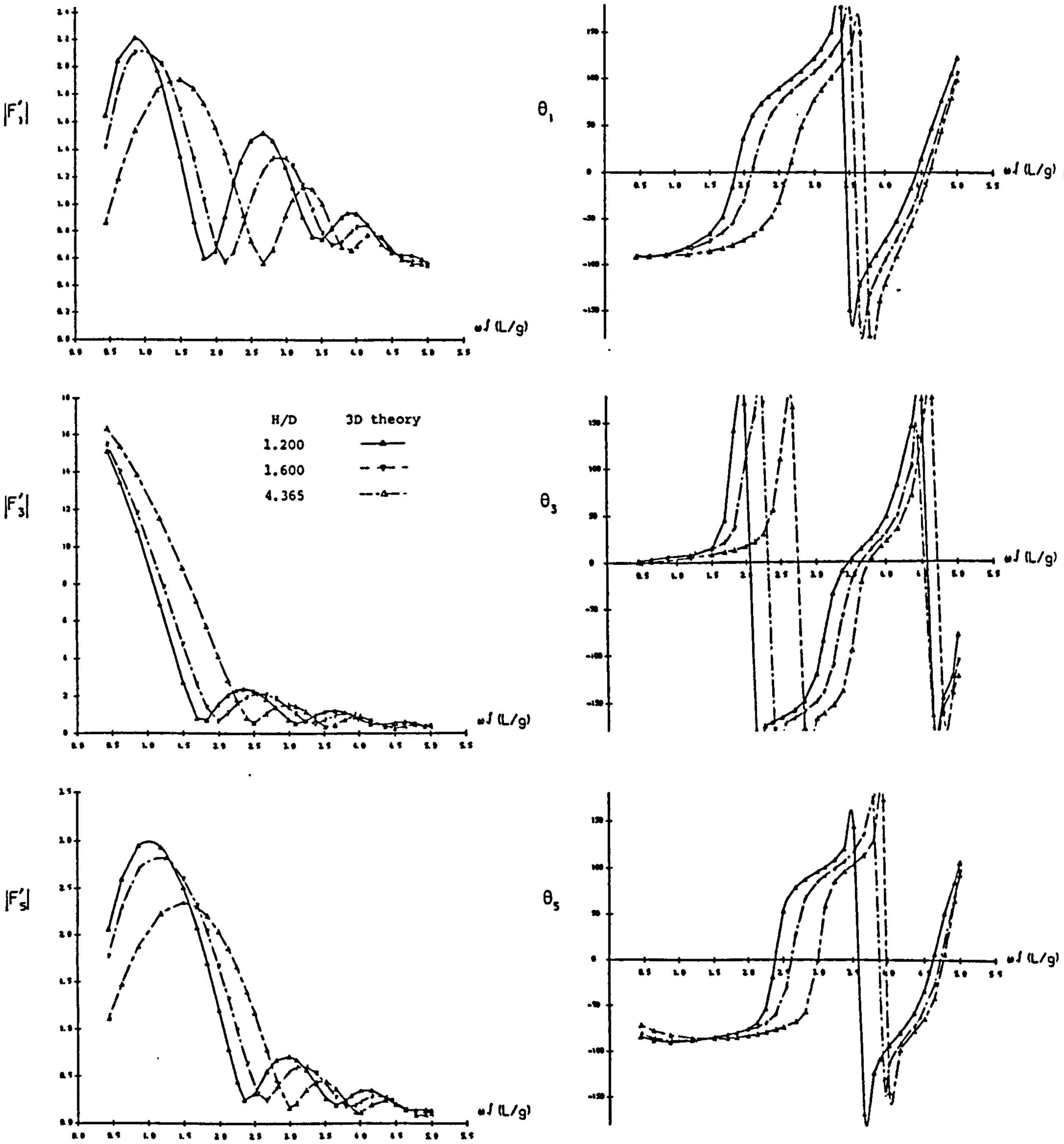

Fig.6.49 ZERO SPEED WAVE EXCITING FORCES (AMPLITUDE AND PHASE) OF 200,000 DWT TANKER AT VARIOUS WATER DEPTHS IN HEAD WAVES.

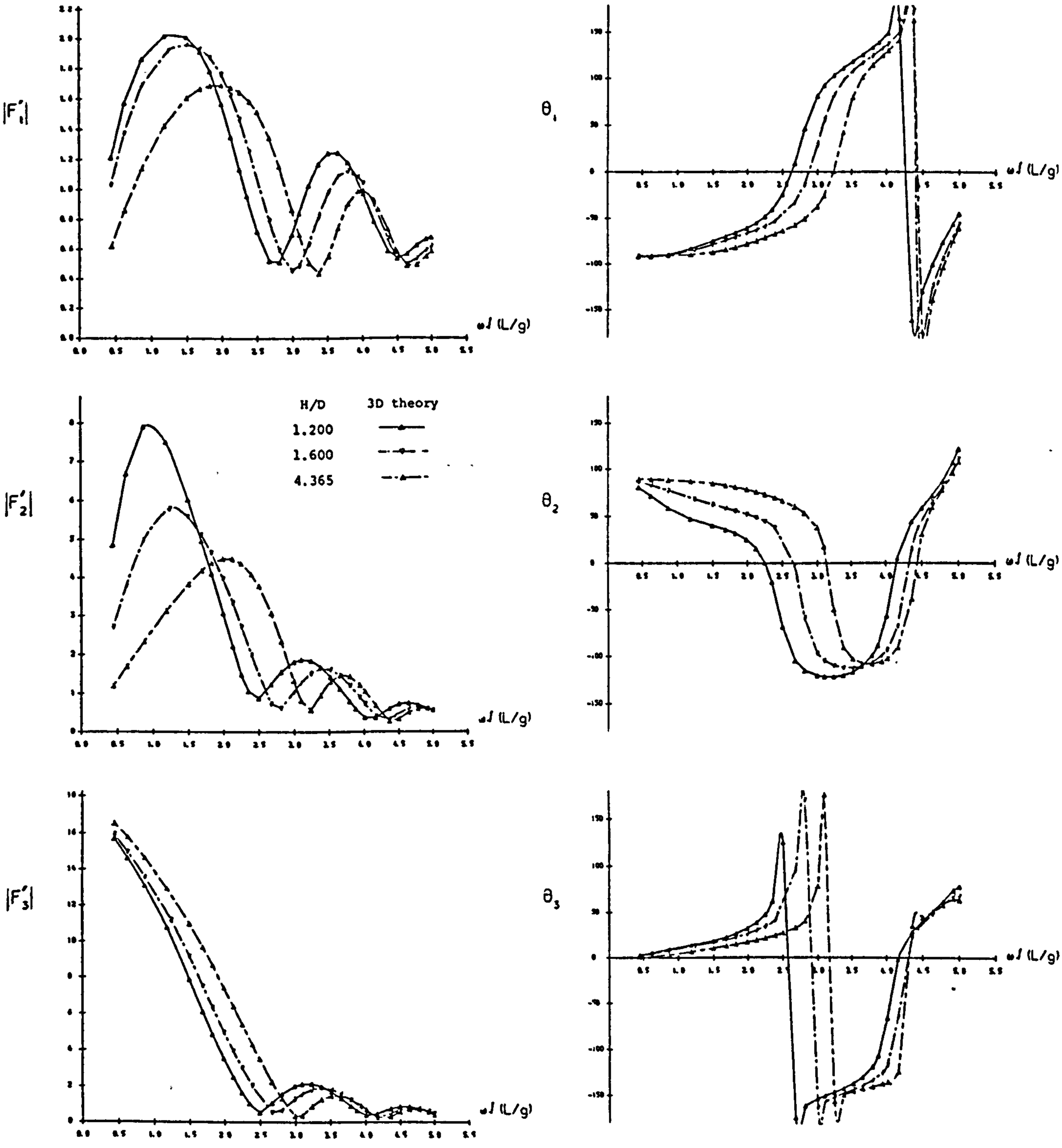

Fig.6.50a ZERO SPEED WAVE EXCITING FORCES (AMPLITUDE AND PHASE) OF 200,000 DWT TANKER AT VARIOUS WATER DEPTHS IN BOW QUARTERING WAVES.

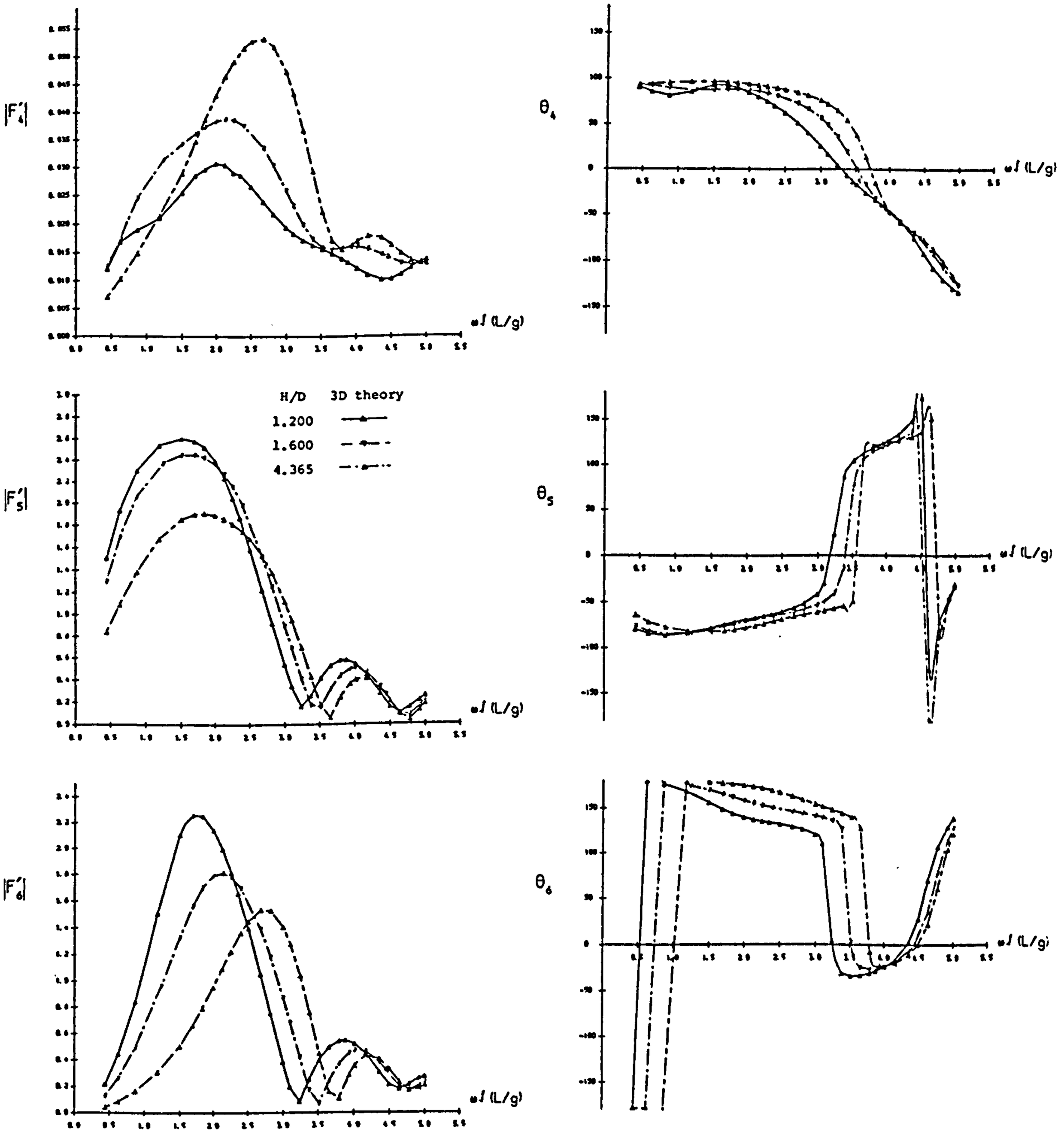

Fig.6.50b ZERO SPEED WAVE EXCITING MOMENTS (AMPLITUDE AND PHASE) OF 200,000 DWT TANKER AT VARIOUS WATER DEPTHS IN BOW QUARTERING WAVES.

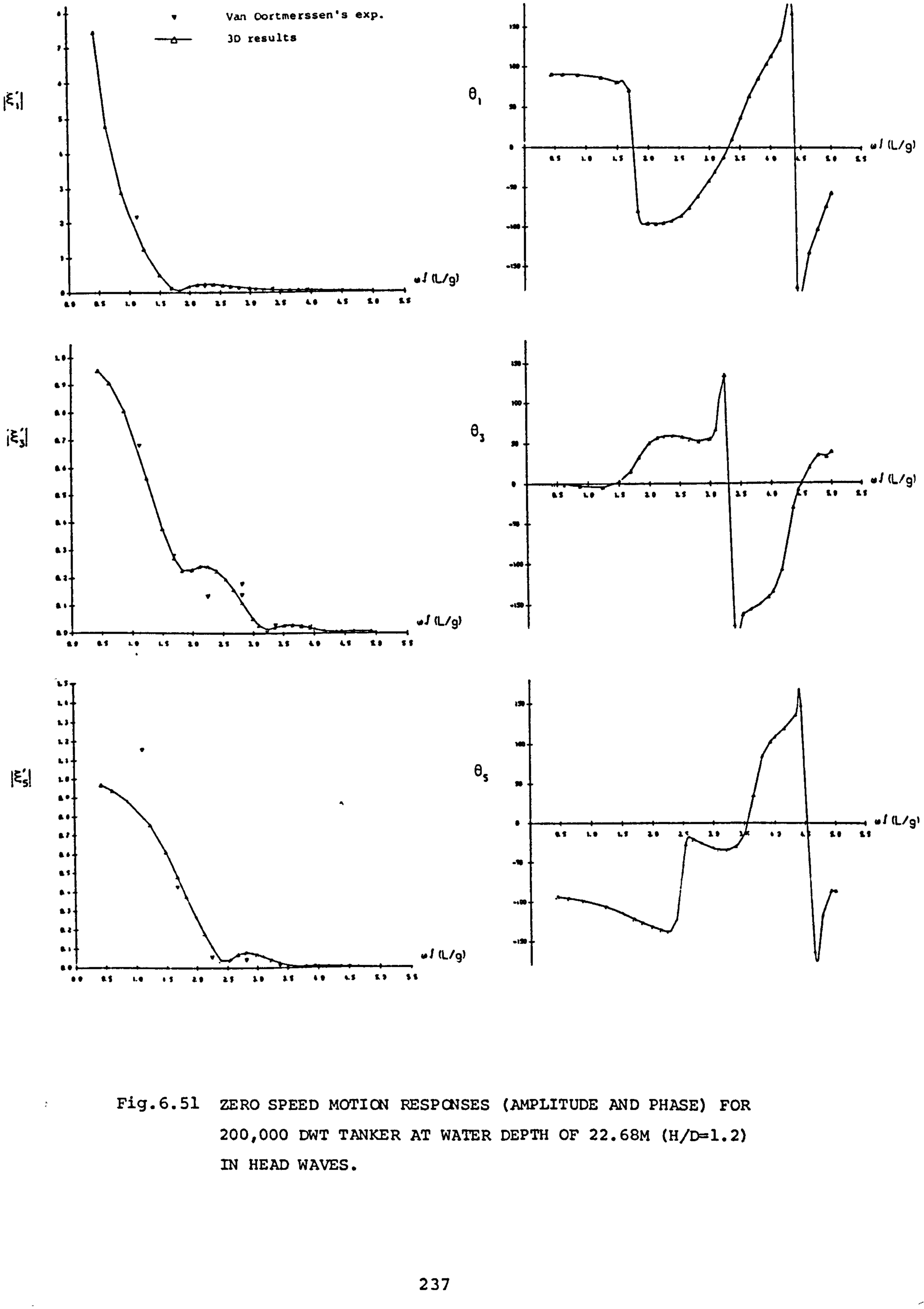

Fig.6.51 ZERO SPEED MOTION RESPONSES (AMPLITUDE AND PHASE) FOR 200,000 DWT TANKER AT WATER DEPTH OF 22.68M (H/D=1.2) IN HEAD WAVES.

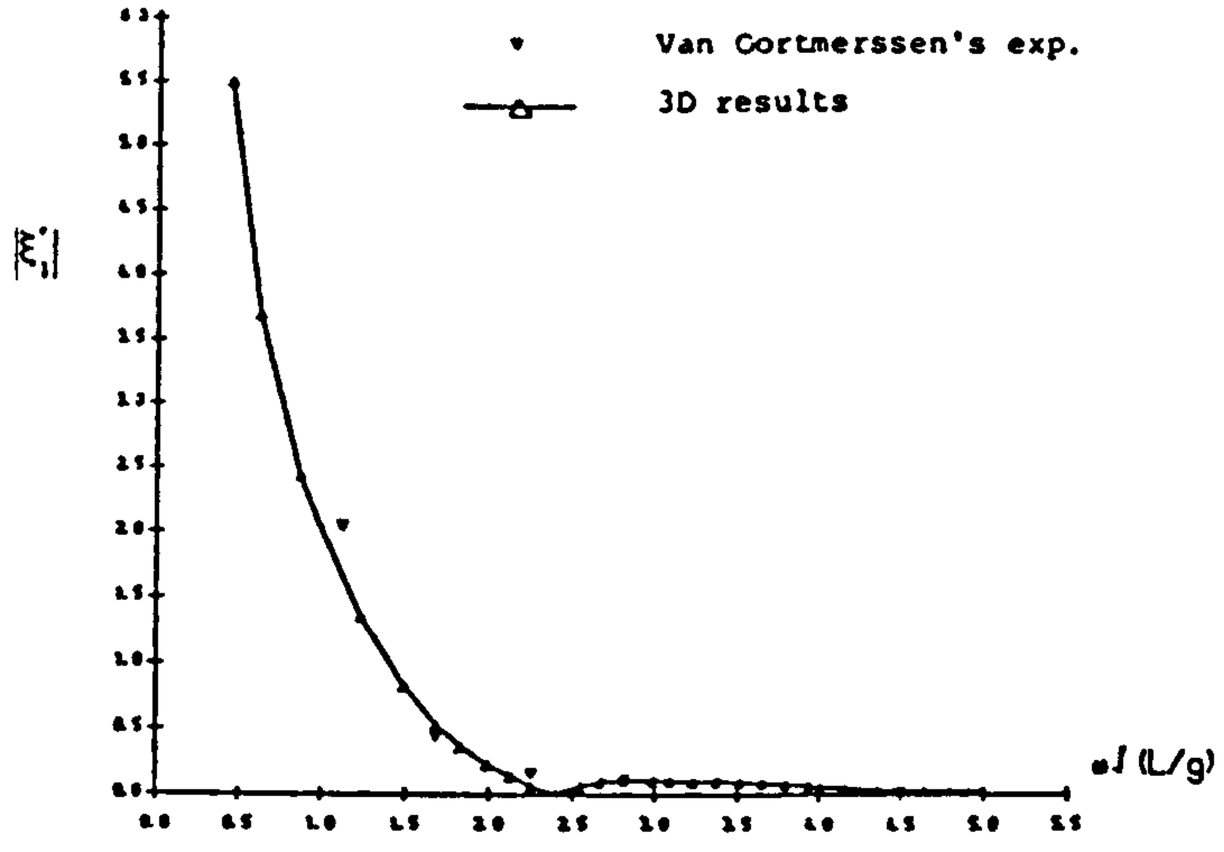

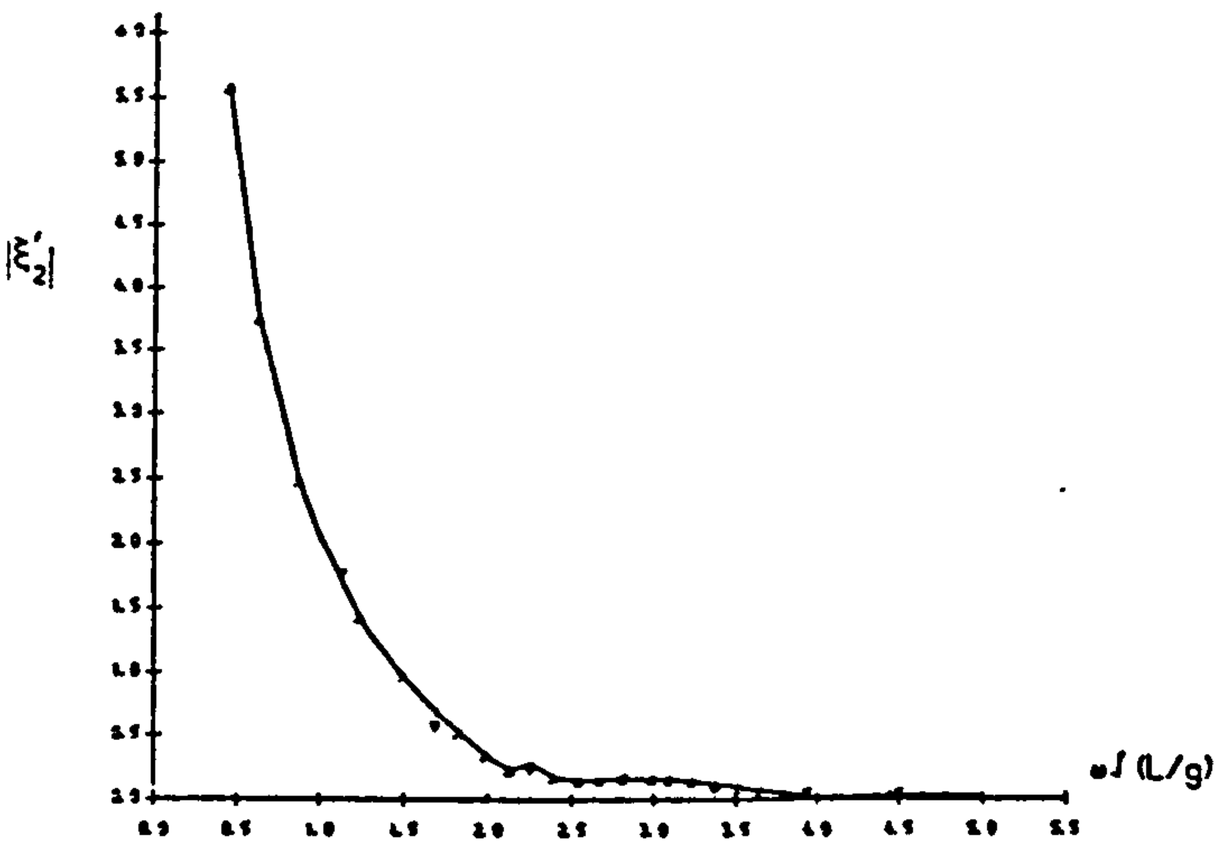

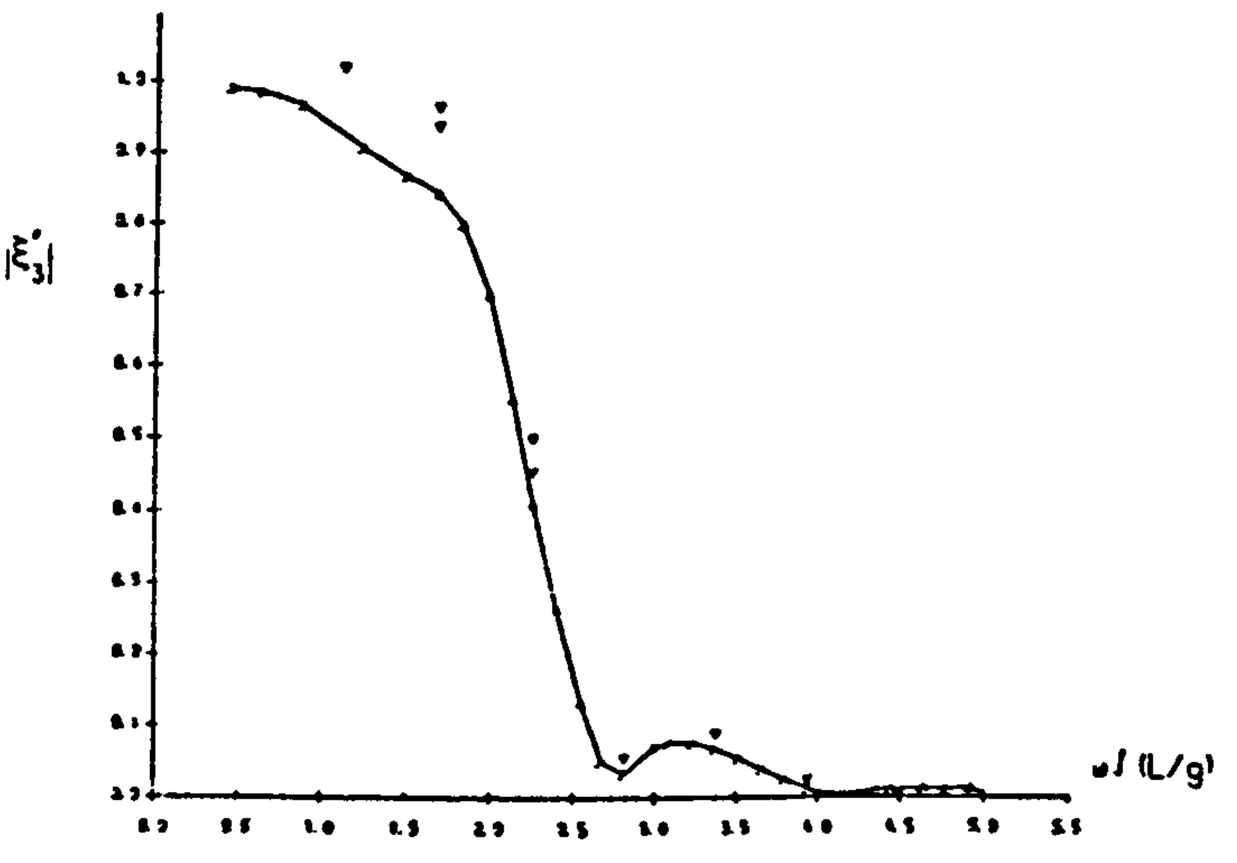

Fig.6.52a ZERO SPEED TRANSLATIONAL MOTION RESPONSES (AMPLITUDE AND PHASE) FOR 200,000 DWT TANKER AT WATER DEPTH OF 22.68M (H/D=1.2) IN BOW QUARTERING WAVES.

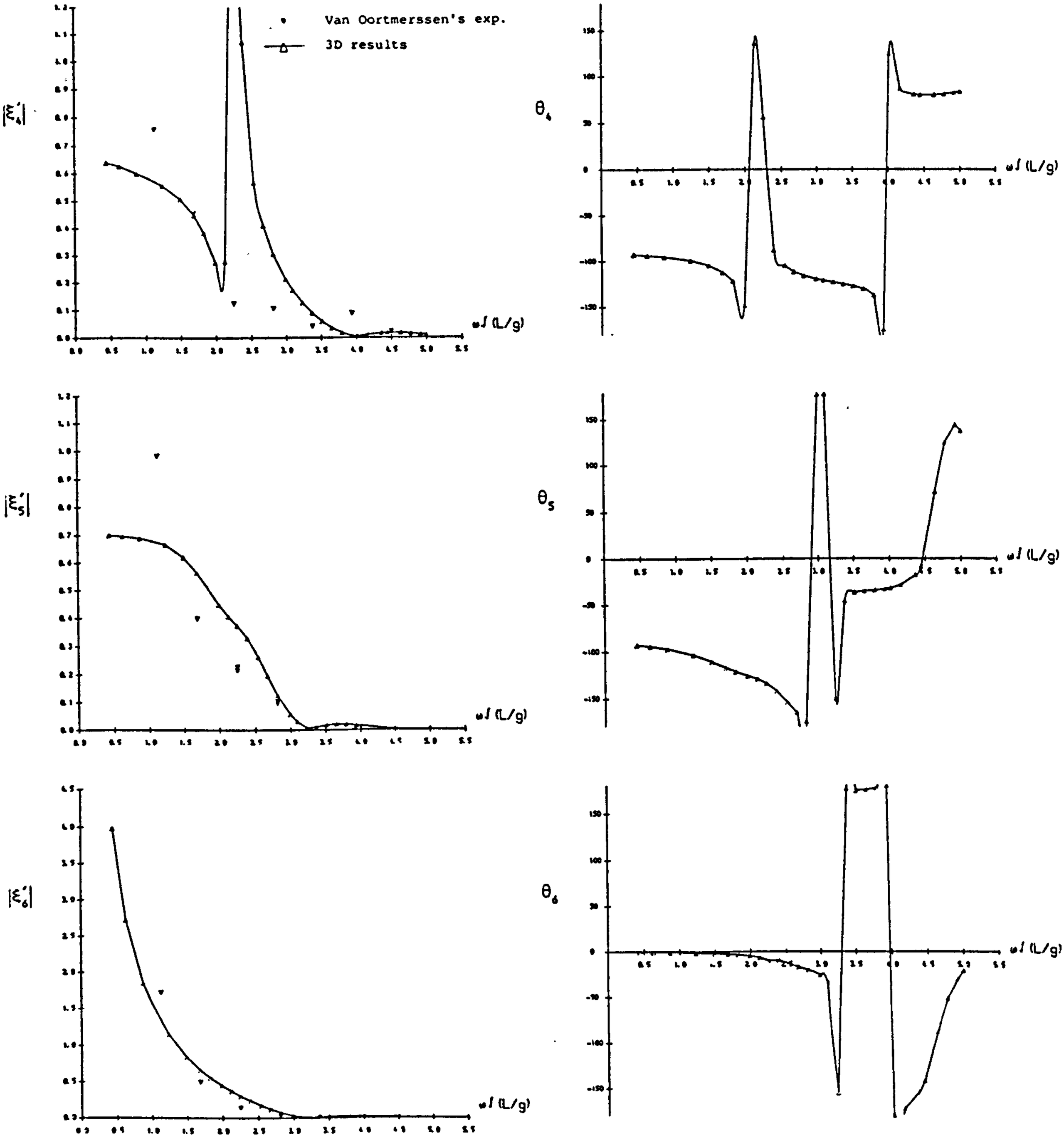

Fig.6.52b ZERO SPEED ANGULAR MOTION RESPONSES (AMPLITUDE AND PHASE) FOR 200,000 DWT TANKER AT WATER DEPTH OF 22.68M (H/D=1.2) IN BOW QUARTERING WAVES.

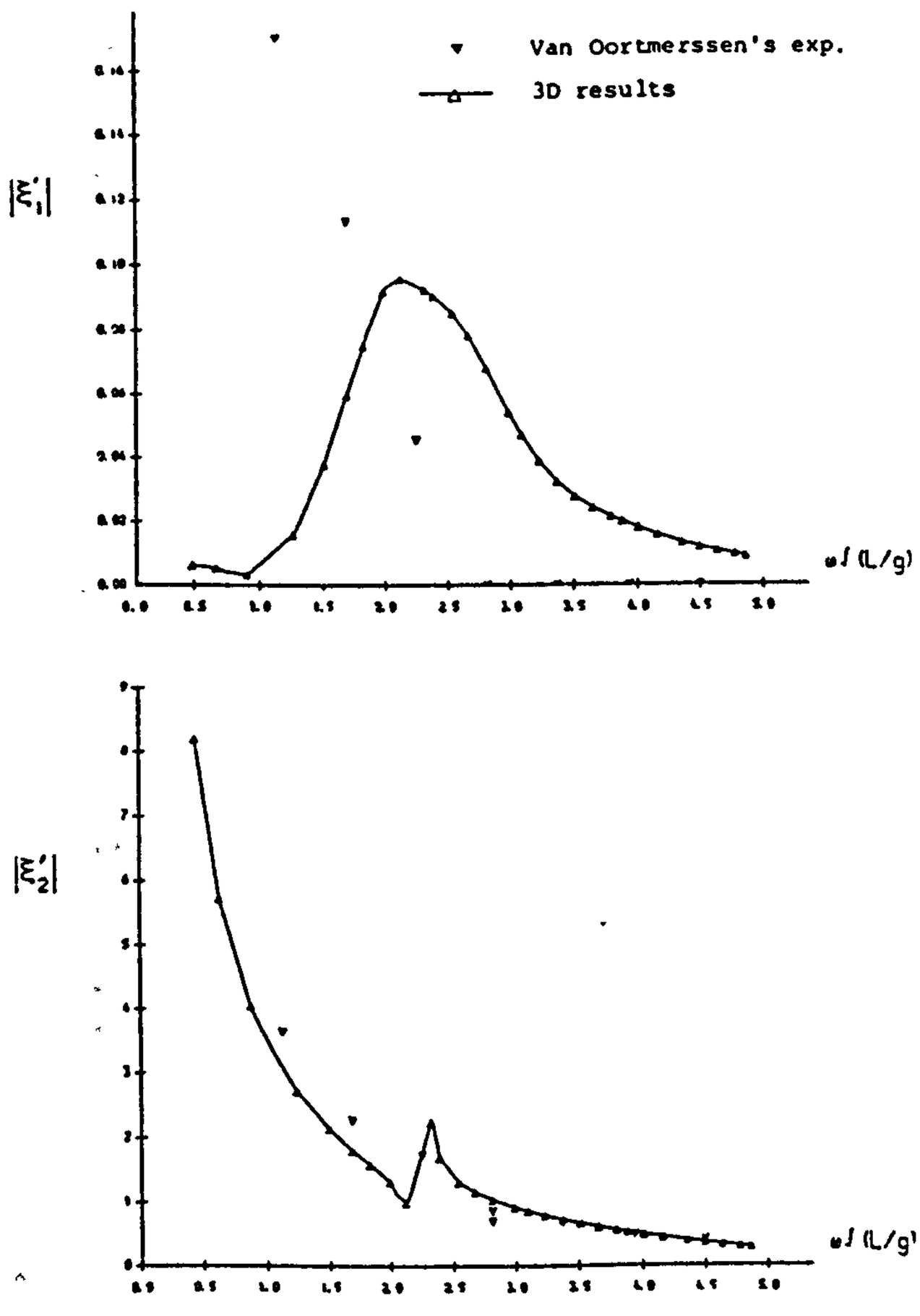

Fig.6.53a ZERO SPEED TRANSLATIONAL MOTION RESPONSES (AMPLITUDE AND PHASE) FOR 200,000 DWT TANKER AT WATER DEPTH OF 22.68M (H/D=1.2) IN BEAM WAVES.

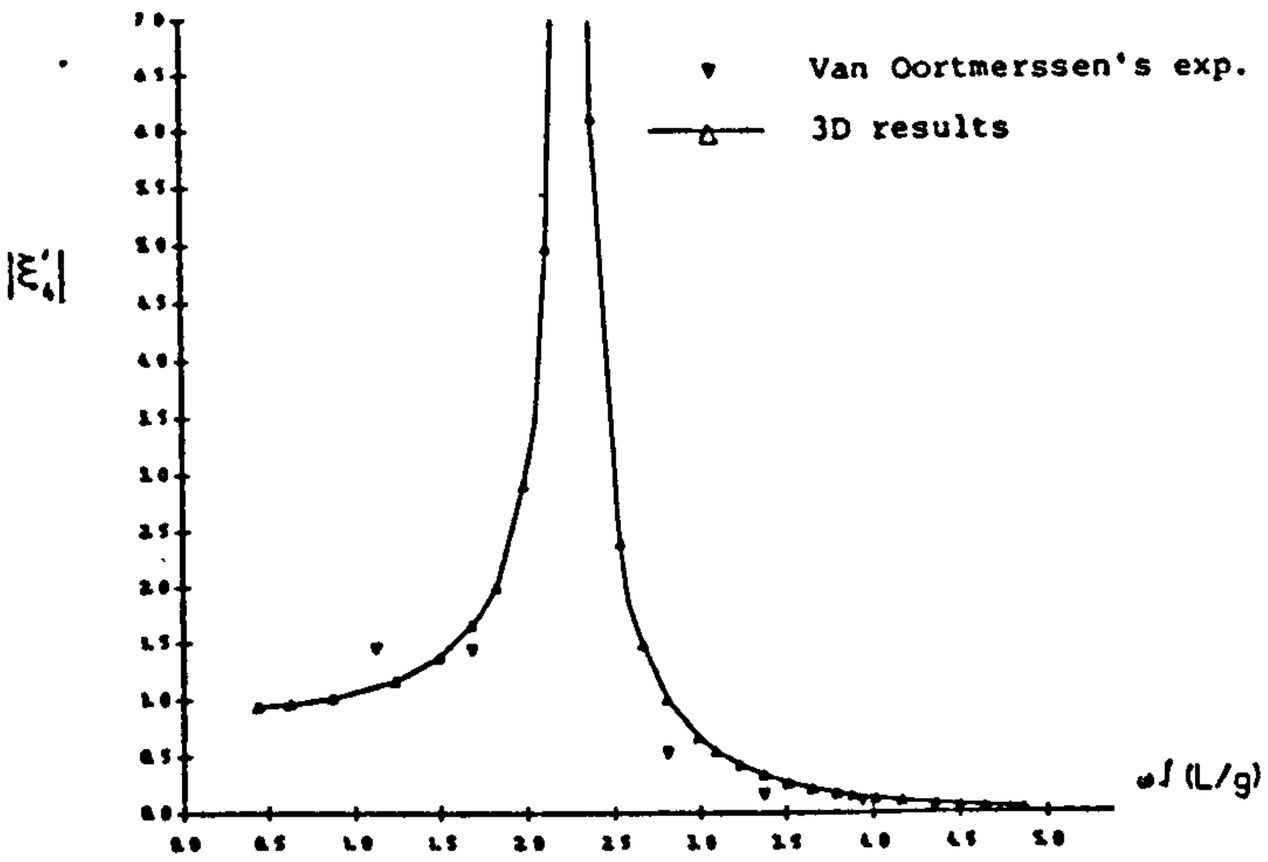

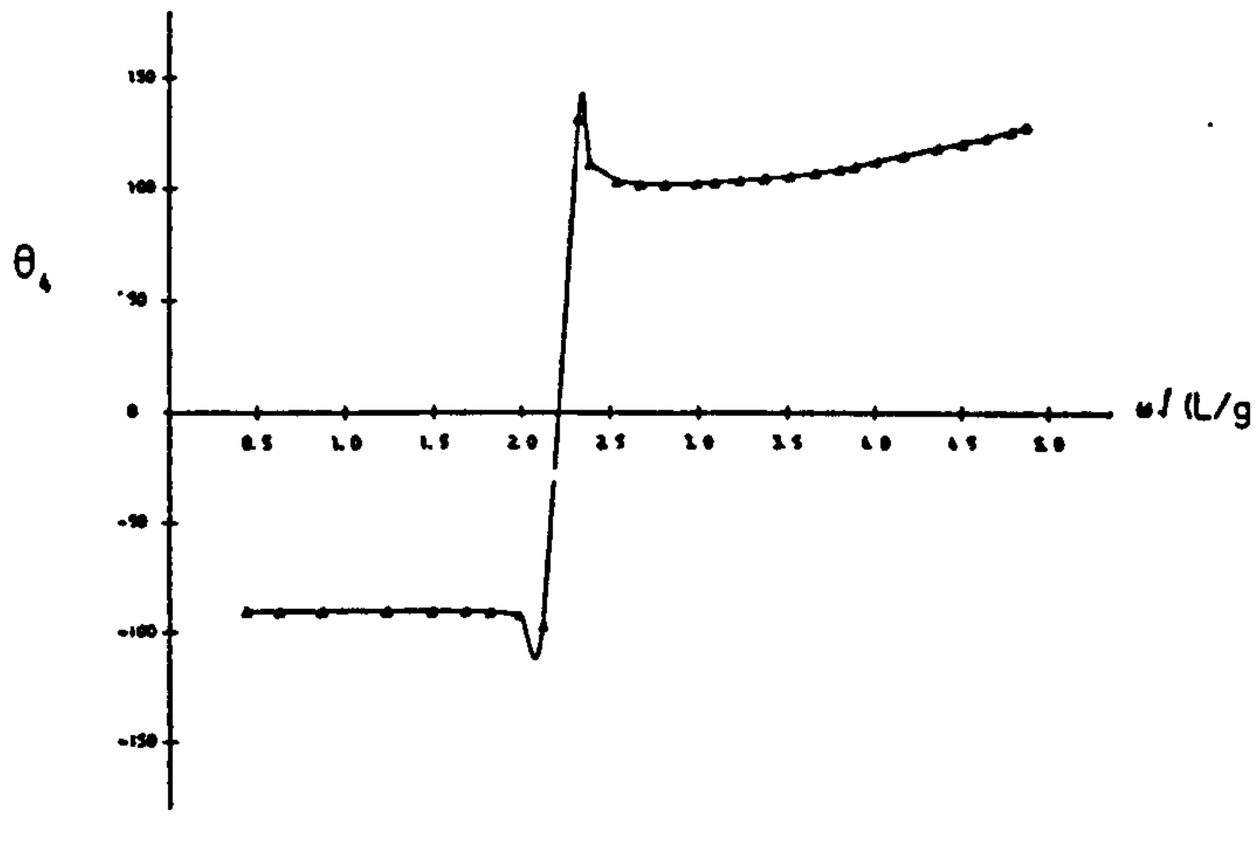

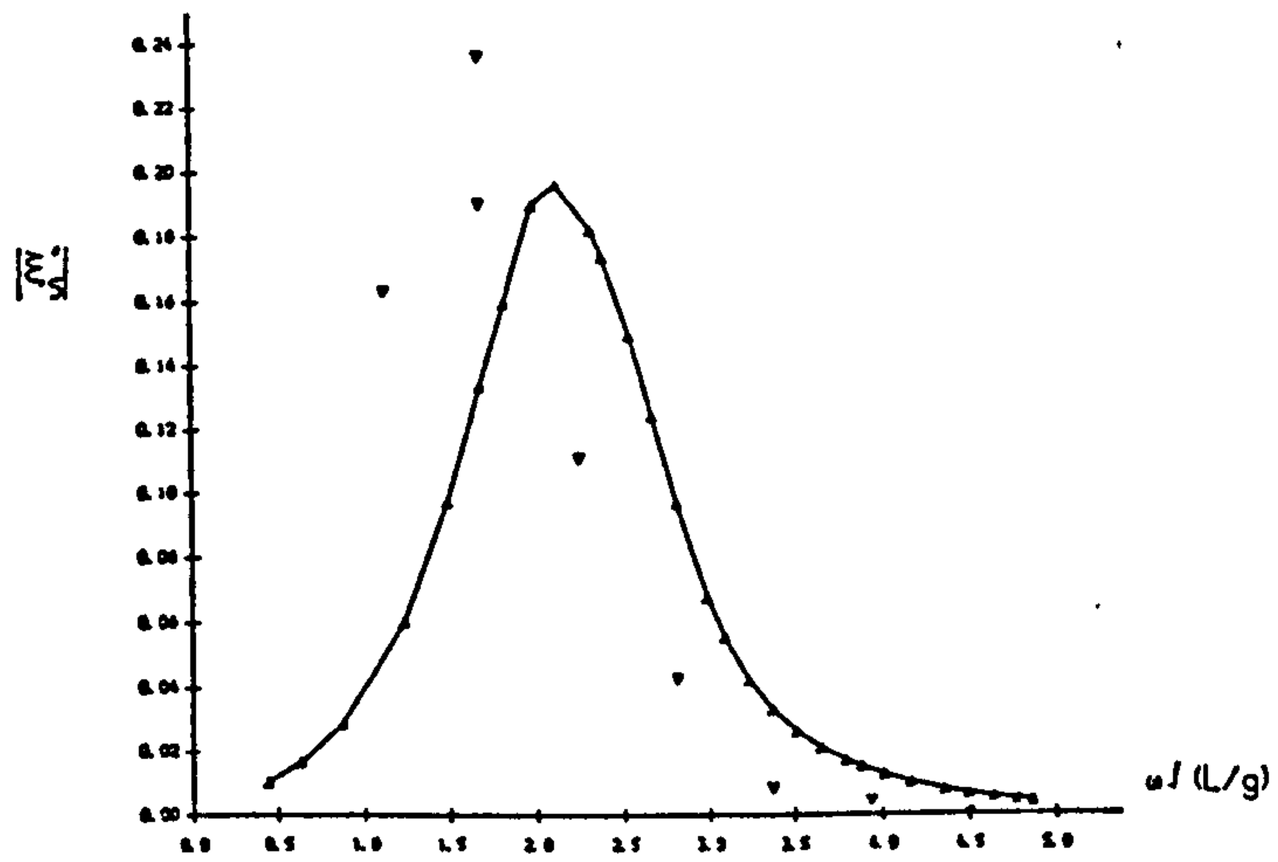

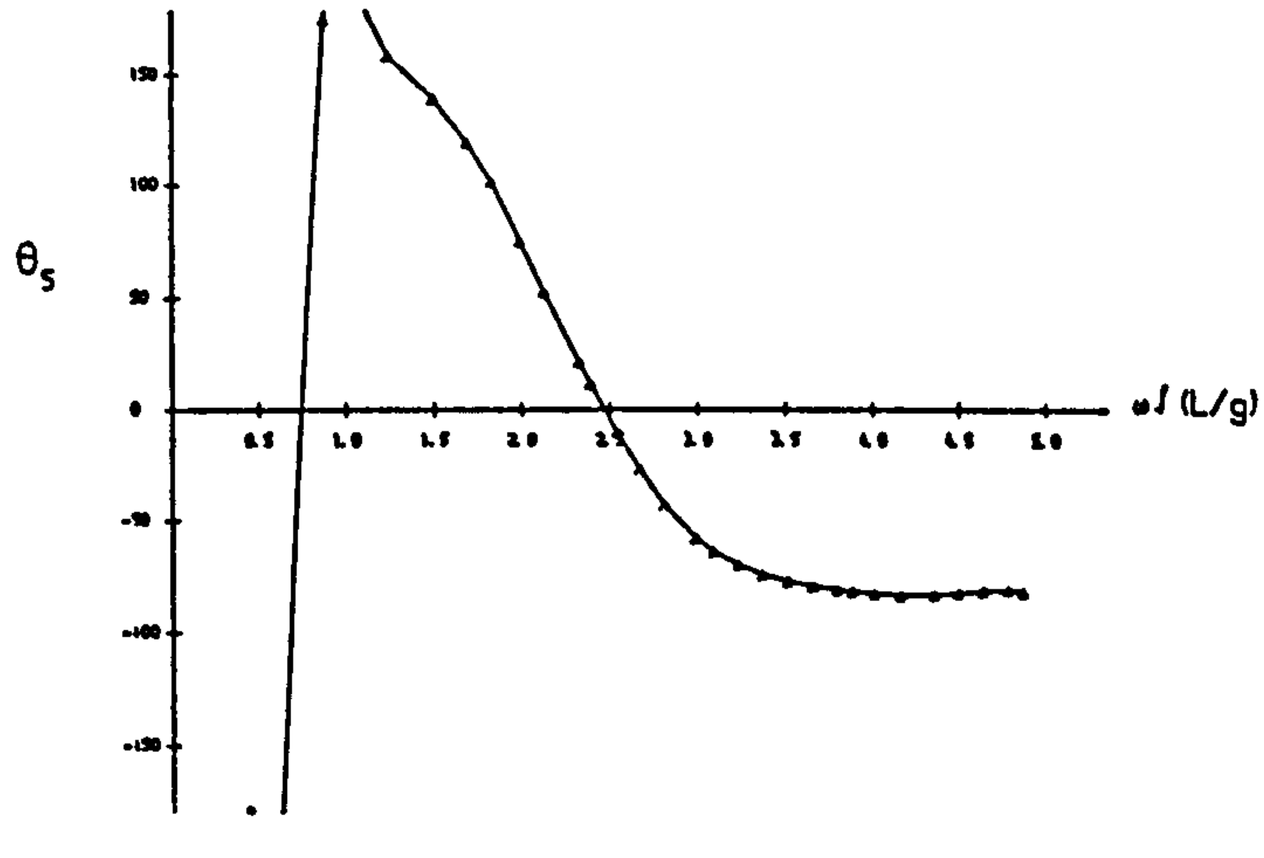

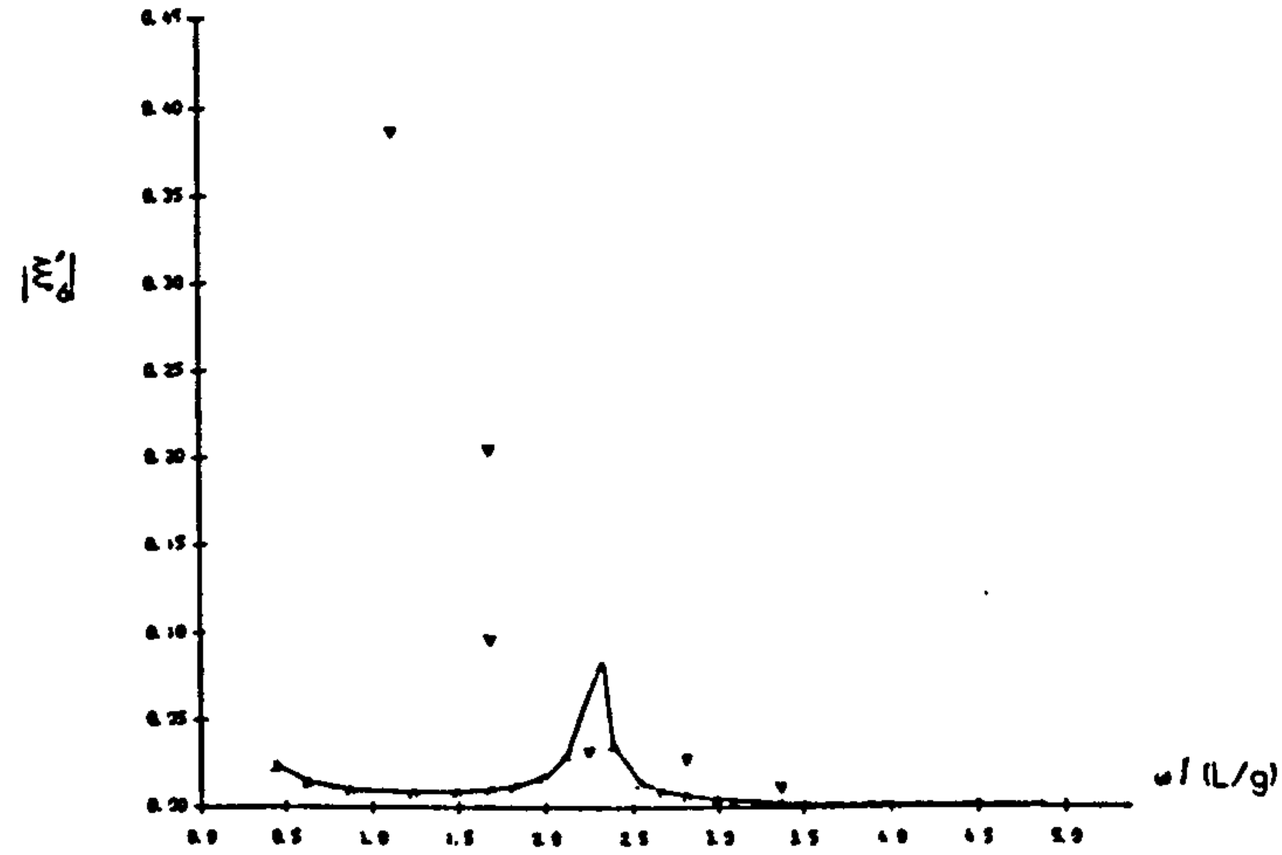

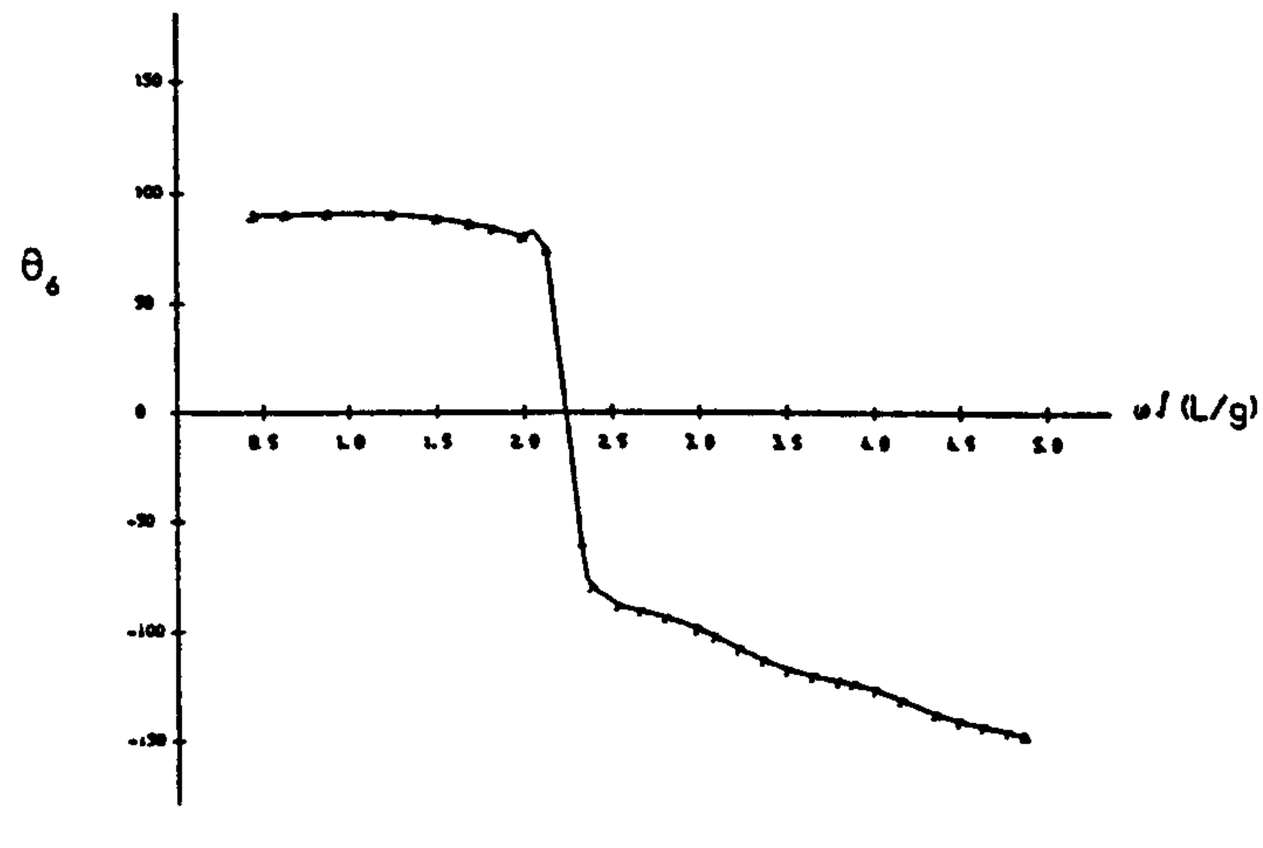

Fig.6.53b ZERO SPEED ANGULAR MOTION RESPONSES (AMPLITUDE AND PHASE) FOR 200,000 DWT TANKER AT WATER DEPTH OF 22.68M (H/D=1.2) IN BEAM WAVES.

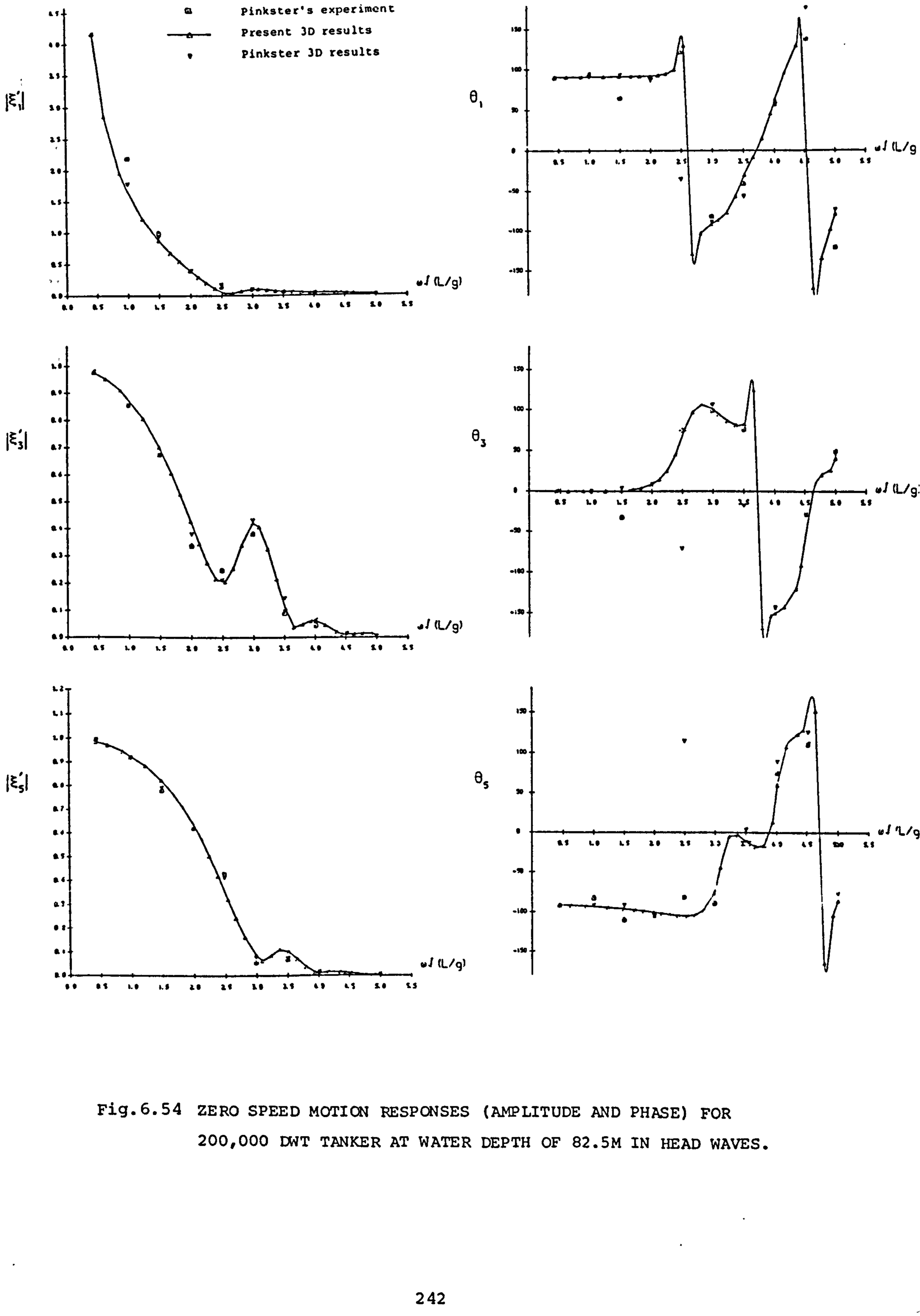

Fig.6.54 ZERO SPEED MOTION RESPONSES (AMPLITUDE AND PHASE) FOR 200,000 DWT TANKER AT WATER DEPTH OF 82.5M IN HEAD WAVES.

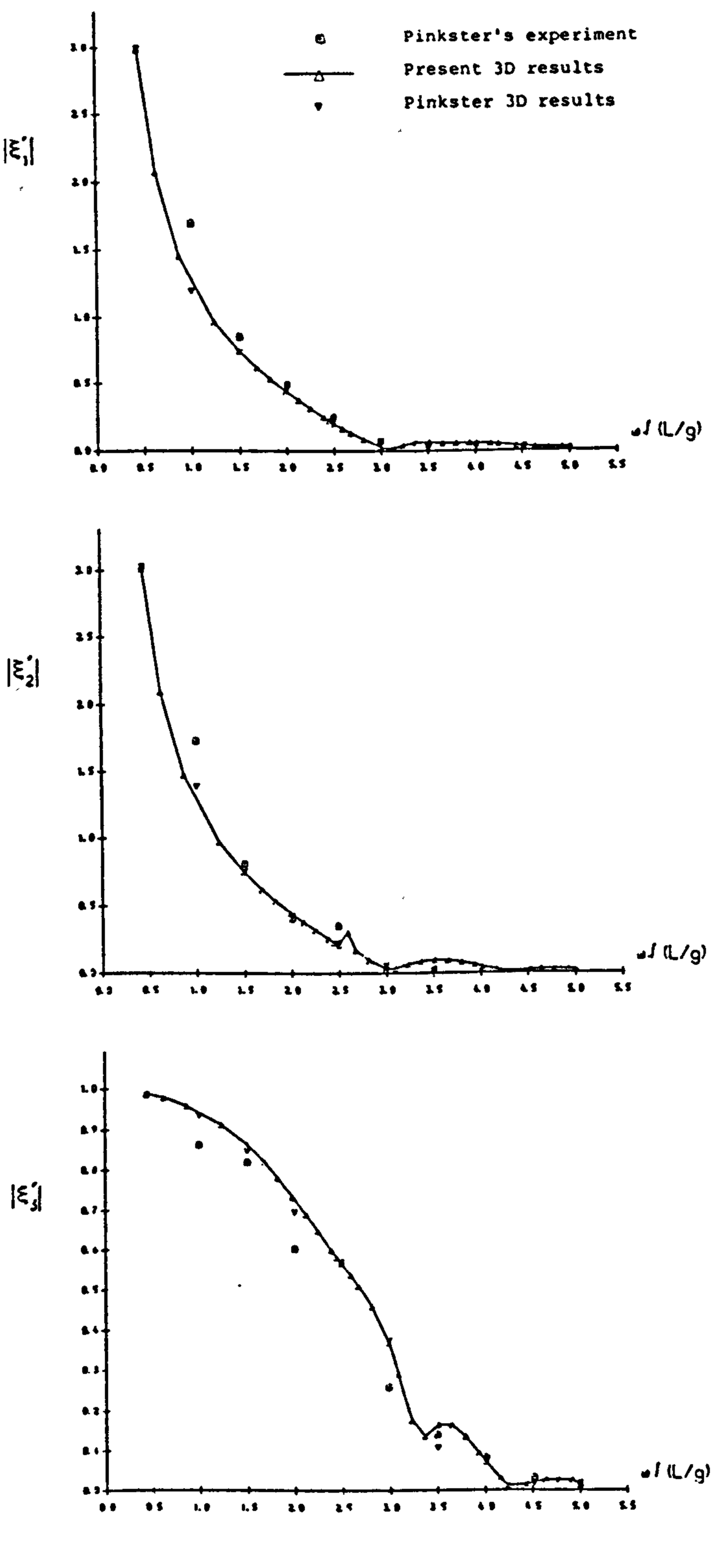

Fig.6.55a ZERO SPEED TRANSLATIONAL MOTION RESPONSES (AMPLITUDE AND PHASE) FOR 200,000 DWT TANKER AT WATER DEPTH OF 82.5M IN BOW QUARTERING WAVES.

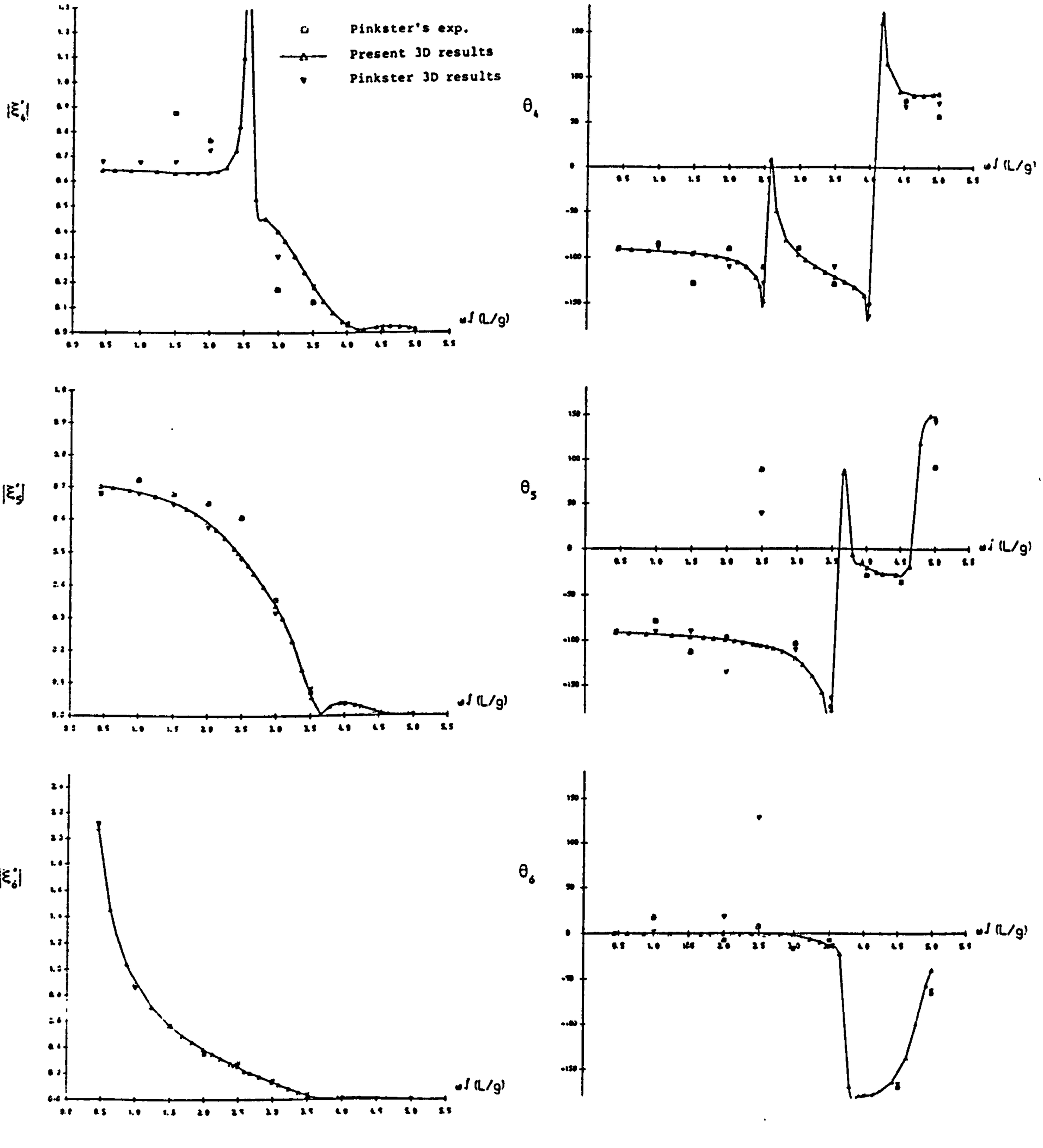

Fig.6.55b ZERO SPEED ANGULAR MOTION RESPONSES (AMPLITUDE AND PHASE) FOR 200,000 DWT TANKER AT WATER DEPTH OF 82.5M IN BOW QUARTERING WAVES.

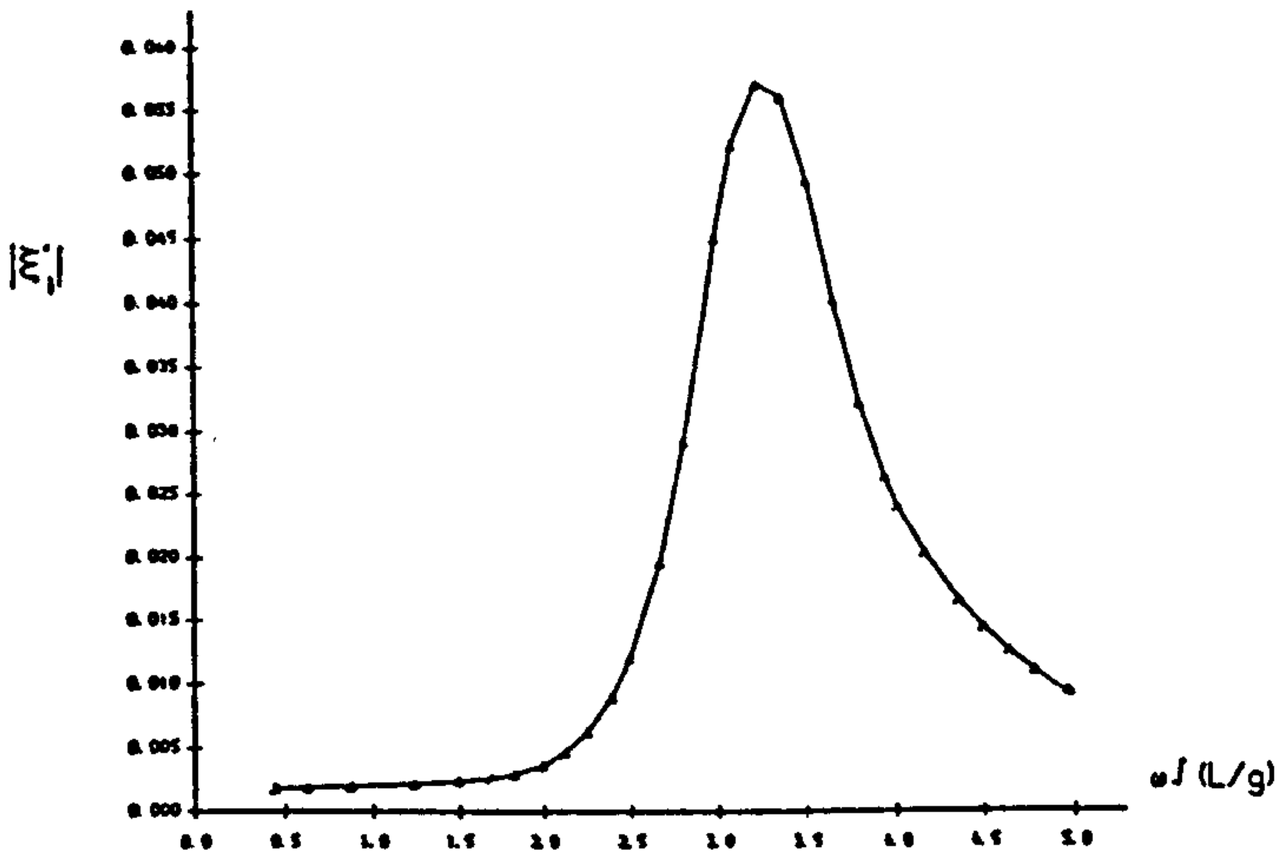

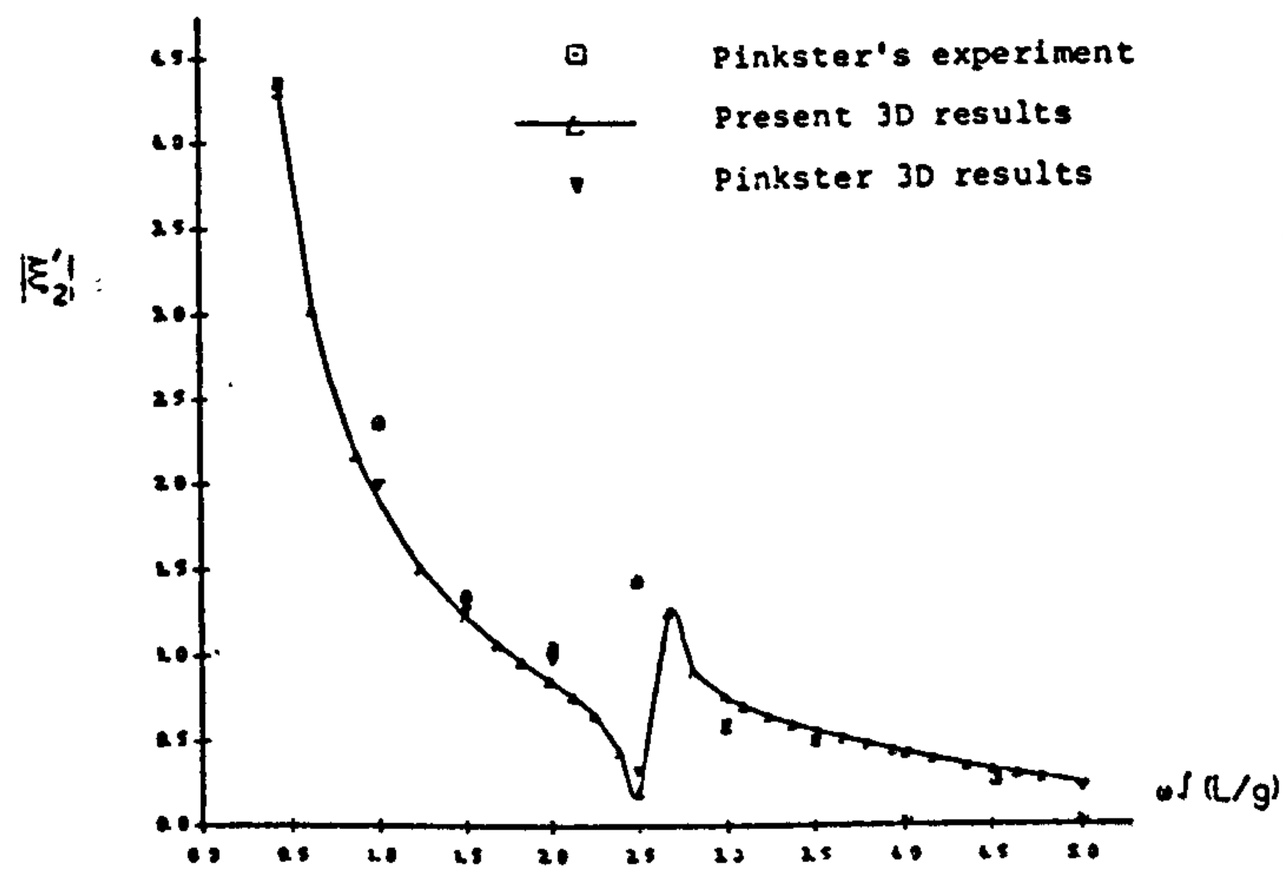

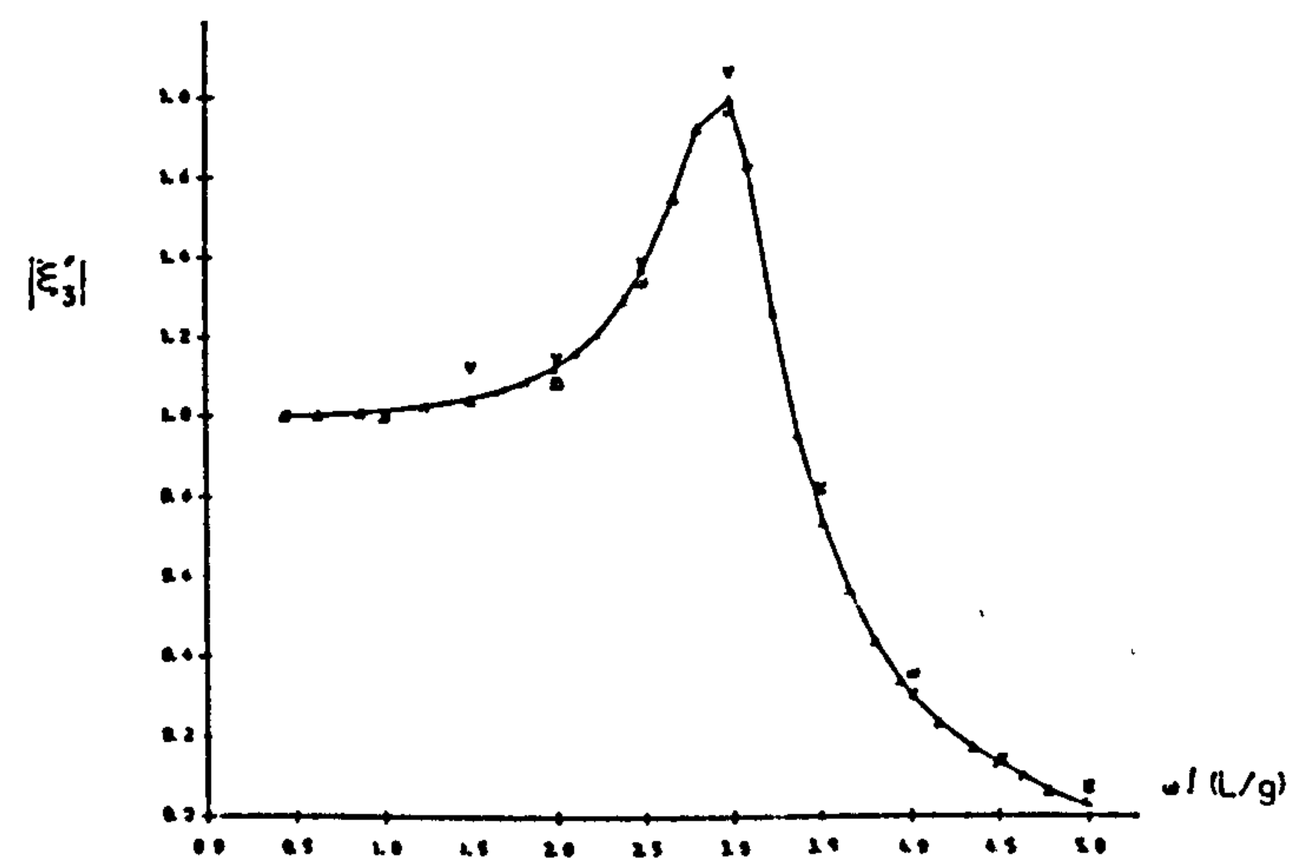

Fig.6.56a ZERO SPEED TRANSLATIONAL MOTION RESPONSES (AMPLITUDE AND PHASE) FOR 200,000 DWT TANKER AT WATER DEPTH OF 82.5M IN BEAM WAVES.

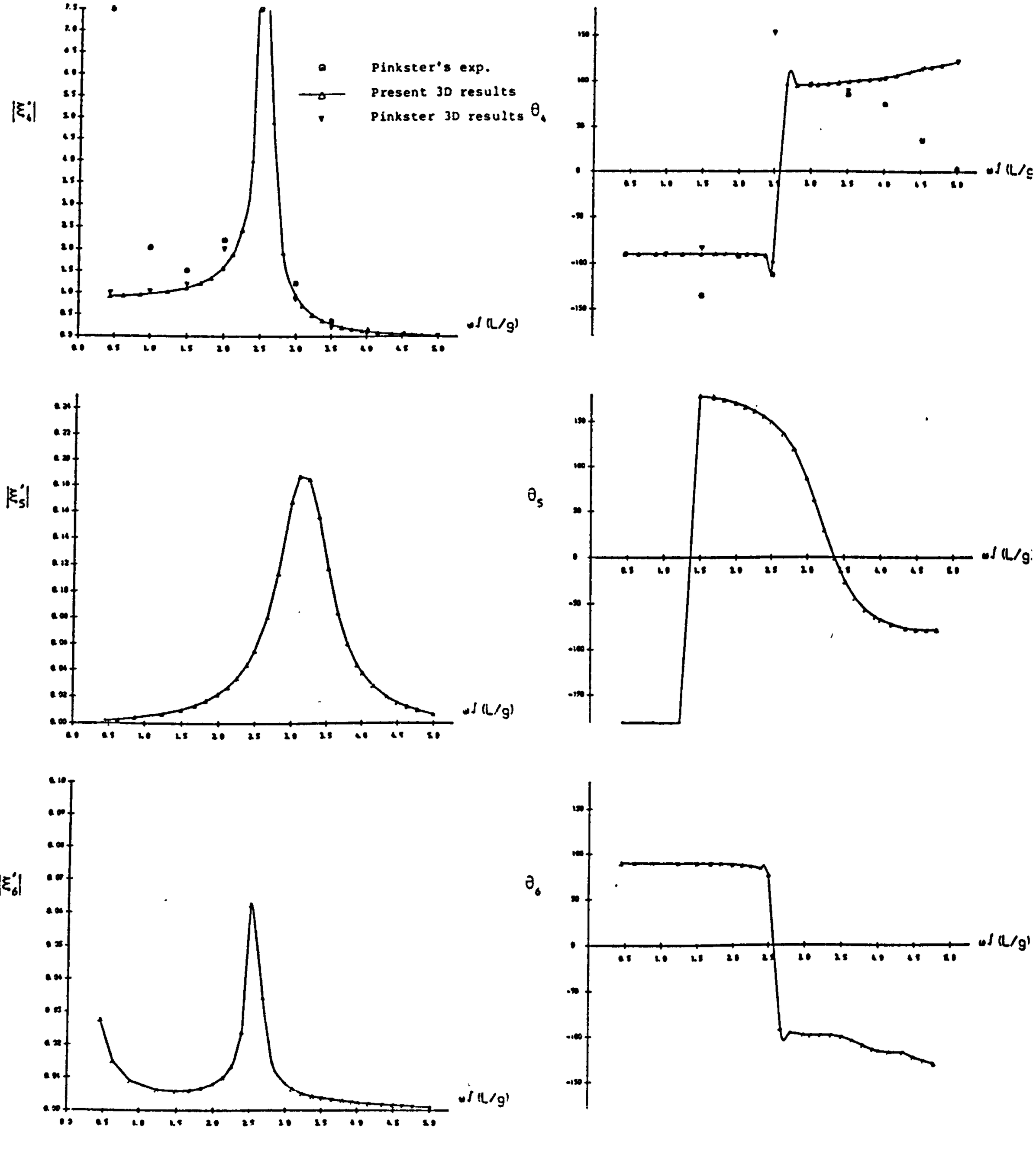

Fig.6.56b ZERO SPEED ANGULAR MOTION RESPONSES (AMPLITUDE AND PHASE) FOR 200,000 DWT TANKER AT WATER DEPTH OF 82.5M IN BEAM WAVES.

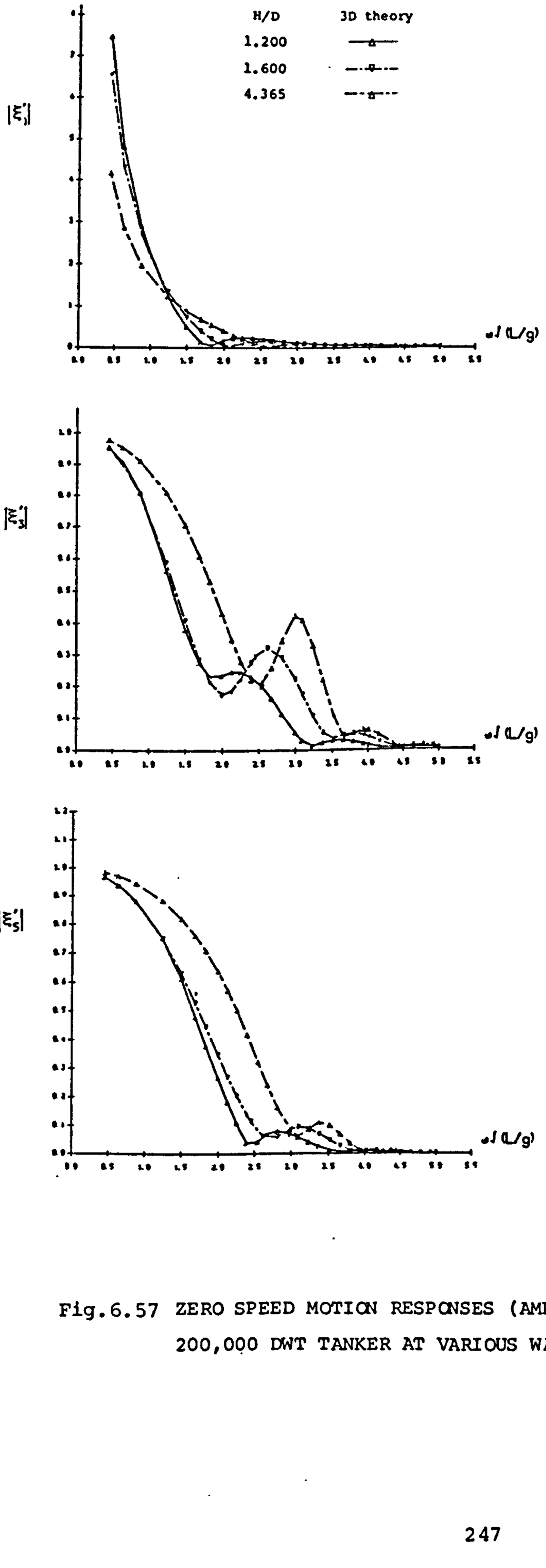

Fig.6.57 ZERO SPEED MOTION RESPONSES (AMPLITUDE AND PHASE) FOR 200,000 DWT TANKER AT VARIOUS WATER DEPTHS IN HEAD WAVES.

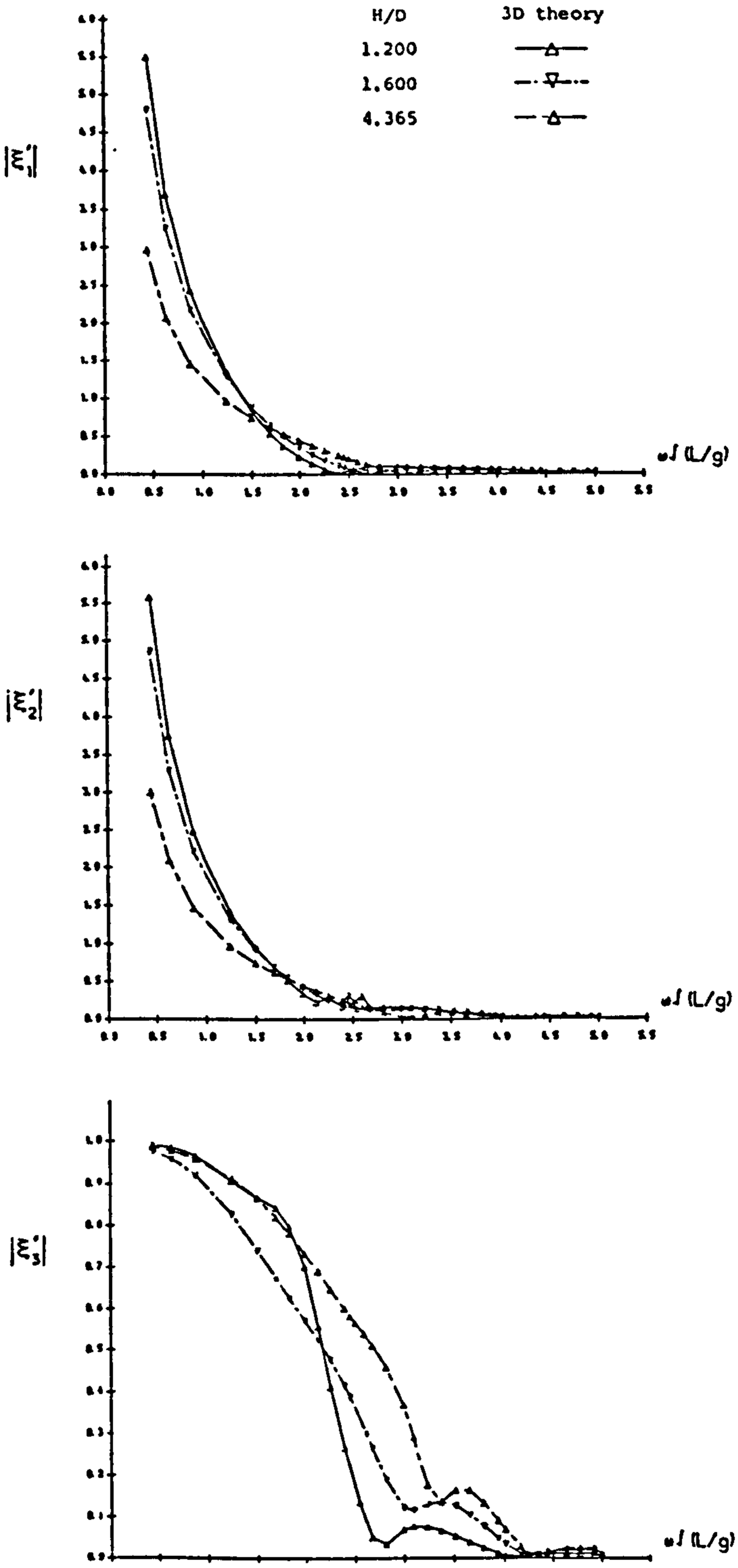

Fig.6.58a ZERO SPEED TRANSLATIONAL MOTION RESPONSES (AMPLITUDE AND PHASE) OF 200,000 DWT TANKER AT VARIOUS WATER DEPTHS IN BOW QUARTERING WAVES.

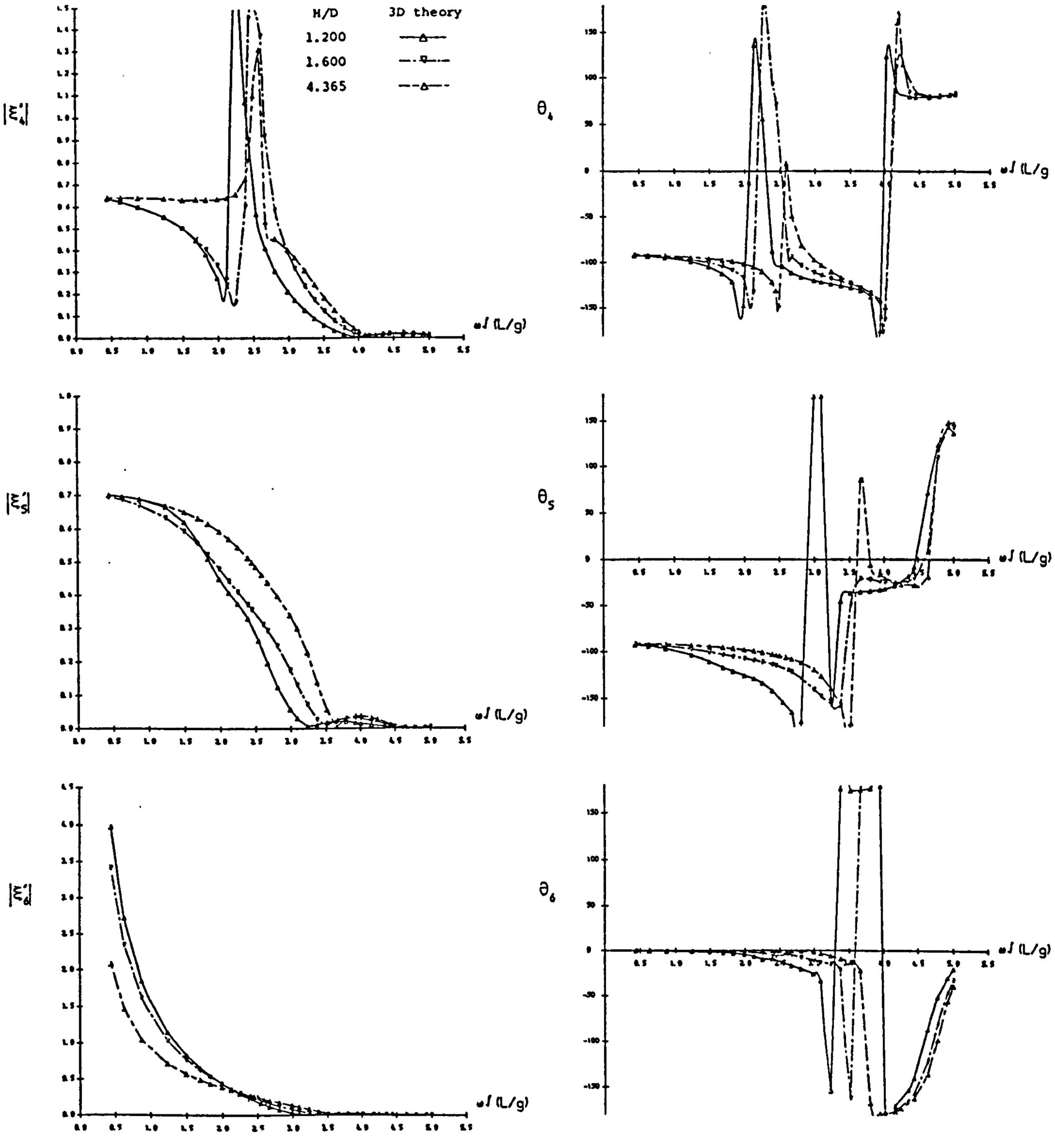

Fig.6.58b ZERO SPEED ANGULAR MOTION RESPONSES (AMPLITUDE AND PHASE) OF 200,000 DWT TANKER AT VARIOUS WATER DEPTHS IN BOW QUARTERING WAVES.

CHAPTER 7

MEAN SECOND-ORDER WAVE FORCES AND MOMENTS ON A SHIP ADVANCING IN OBLIQUE WAVES

7.1 Introduction

When a body is exposed to the action of incident waves, hydrodynamic forces and moments are exerted on the body by the surrounding fluid. These forces and moments can be separated into two components; namely oscillatory and non-oscillatory. The oscillatory forces and moments which are proportional to the wave amplitude cause the well known first order motions of the body. The non-oscillatory components, due to various non-linear effects, are of second-order with respect to the wave amplitude. The first-order components possess zero mean values over a period while the second-order components exhibit non-zero time averages and are constant in time when the wave system is regular harmonic, or slowly-varying when the body is subjected to the action of random waves. These second-order forces and moments are generally too small to influence the oscillatory motions of the body but they cannot be neglected in certain circumstances. For instance, the steady slow drift motion of a floating vessel is considered as a result of mean (time average) second-order forces.

The mean second-order forces and moments are known as drift forces and moments in the orizontal plane of motion. The prediction of the drift forces and moments is of importance in the design of mooring or dynamic positioning systems if it is desired to maintain the mean position or heading of a floating structure in waves. The calculation of the longitudinal drift force acting on a vessel advancing in waves is applicable to the prediction of the added resistance which is additional to wave making resistance in calm water while the calculation of the lateral drift force and yawing moment may be applied to the prediction of steering and control characteristics of the vessel.

The vertical components of the mean second-order forces and moments exhibit a vertical drifting force and moment. For a submerged body such as a submarine vehicle the steady vertical force and pitching moment can cause the vehicle to rise and broach when the vehicle is travelling near the free-surface. These vertical excursions may be more important than the first-order oscillatory motions.

Apart from the mean second-order components, the second-order wave excitation forces consist of the difference-frequency components and the sum-frequency components in irregular waves. The difference-frequency components are well-known as the low frequency or slowly-varying second-order wave forces which can cause large amplitude motions of moored structure at low frequency due to the resonant response of the mooring system. On the other hand, the sum-frequency components are expected to be of importance at high frequency. For example, the resonant response and the resulting tension-leg loads of a deep water tension leg platform are the result of the high-frequency excitations since the natural periods of the vertical plane motions are typically about 1 ~ 4 seconds for such platforms. The source of the high-frequency excitations may come from the second-order sum-frequency exciting forces, often called "springing forces". A similar high frequency phenomena known as "springing" may be experienced by a ship which resonates as a vibrating beam in response to periodic wave excitation. Since the lowest mode of the frequency of a hull girder generally corresponds to ambient waves of very short wave length, which can hardly be expected to excite overall hull vibration, springing may very well be a response to the harmonics and sum-frequency components which appears in the second-order analysis.

From the foregoing it can be seen that, depending on the kind of structure or vessel considered, one or more of the six components of the second-order wave forces and moments can be of importance. In order to evaluate the influence of such force and moment on the performance or behaviour of a structure, simulation techniques based on numerical computation must be sought. In the present study, such a technique is developed based on the potential theory. The final expressions are valid for all six degrees of freedom and are obtained through direct integration of the fluid pressures on the mean wetted body surface.

7.2 Mean second-order force and moment

In the past two decades a significant amount of attention has been given to the subject of mean second-order forces and moments experienced by ships or floating platforms. Various analytical methods with increasing sophistication have been developed over the years by different research workers. Since the second-order steady forces and moments depend only on the first-order velocity potential and arise through non-linearities in the mechanism by which the first-order waves act on the body, analytical methods inevitably involve the solution of the first-order boundary-value problems. Within the first-order problems, the fluid-structure interactions can be modelled in a number of different ways and so can the second-order problem. Two principal different approaches have been presented in the literature dealing with the determination of the mean second-order forces and moments. One is the far-field method and the other is the near-field method. Both methods are constructed under the usual assumptions that the fluid flow is homogeneous, incompressible and irrotational. Moreover, the surface tension is negligible and perturbation theory can be applied. Before we derive a general expression to predict the second-order forces and moments, a short review is given to indicate the developments in the far-field and the near-field methods in the past.

7.2.1 Far-field method

The far-field method, introduced by Maruo (1961), starts from consideration on the change of momentum of the fluid within a control surface surrounding the body. The control surface is normally taken to be a cylindrical surface of a large radius extending vertically from the free-surface to the sea bottom. By considering the rate of change of the linear momentum or angular momentum within the fluid domain, the forces and moments acting on the wetted body surface can be related to the fluid flow characteristics in other boundary surface. When the control surface is taken to infinity,

the horizontal components of the mean second-order forces and moments may easily be obtained from the asymptotic form of the velocity potential. The far-field method is a very significant simplification in practical problems. Nevertheless, this method appears less attractive when one is dealing with the vertical components since one has to calculate supplementary integrals over the free-surface and sea bottom.

Maruo (1961) first derived expressions for the horizontal surge and sway drift forces on a stationary body in deep water using the far-field momentum approach. Newman (1967) extended Maruo's expressions to include the yaw drift moment and carried out numerical calculations for a Series-60 ship using the slender body assumptions. Maruo and Newman did not give satisfactory verification of the applicability of the theory due to lack or absence of experimental data.

Both Maruo's and Newman's expressions are given in terms of Kochin functions. Faltinsen & Michelsen (1974) modified Newman's formulation in connection with the three-dimensional pulsating source distribution technique and showed that their expressions were valid for infinite and finite water depth. The results of computations compared with the experimental data for the mean horizontal force on a box shaped floating body showed good agreement but no drift moment results were produced. Hong (1983) applied Newman's formulation and used the three-dimensional pulsating source technique to calculate the Kochin function. His numerical results for a SWATH ship and stretched SSP ship could not validate the theory since experimental data were insufficient.

The application of the momentum approach for predicting the vertical mean force and pitch moment leads to expressions, which involve integrals in the far-field surface supplemented by the free-surface and the sea bottom. For a fully submerged body in deep water, Lee & Newman (1971) gave free surface integral expressions in terms of Kochin functions.

For a body moving in waves Maruo (1963) gave a far-field expression in terms

of Kochin functions for added resistance of ships in regular waves in deep water. Later Hosoda (1973) used Maruo's formula associated with a line source distribution to calculate the added resistance of a container ship in oblique waves. Poor agreement with the experimental results was noticed, especially in the short wave regime. Maruo & Iwase (1980) applied slender body theory and high frequency assumptions to modify Maruo's original added resistance formula. Their numerical results showed poor agreement with the results of measurements obtained for a Series-60 model in stern quartering waves.

Lin & Reed (1976) presented the most complete derivation of the far-field expression for the mean second-order forces and moment on a ship advancing in oblique waves at infinite water depth. In their results the second-order steady forces are expressed in terms of Kochin functions but they were not able to express the second-order steady moment in a form suitable for numerical calculations. No results of computations were given. Lau (1987) made use of their formula and obtained some added resistance results for Series-60 models and a container ship. His results were found in reasonable agreement with experimental data (Strom-Tejsen et al 1973) for the range below and above the resonant frequency.

Ankudinov (1969),(1972) and Salvensen (1974) used direct integration over the mean wetted body surface but they transformed the surface integral to the far-field surface integral by means of Gauss's theorem. Aukudinow expressed the mean second-order forces in terms of Kochin functions. In order to carry out numerical computations, he employed the thin ship assumption while Salvensen assumed the body to be a weak scatterer and obtained results from the two-dimensional pulsating source technique. Numerical results presented by both authors provided reasonable correlation with experimental measurements of added resistance in head waves. However, the thin ship and weak scatterer assumptions cannot be justified in quartering and beam seas.

Although the far-field method needs lesser computational effort in the evaluation of the horizontal mean second-order forces, it presents other difficulties in predicting the vertical mean second-order forces and moments.

7.2.2 Near-field method

When the simple procedure in the far-field method is not valid, one must in general find the second-order forces and moments by the direct integration of fluid pressure over the mean wetted body surface. The fluid pressure is determined from Bernoulli's equation. Because integration of the fluid pressure requires a detailed knowledge of the flow field on the body surface, the name "near-field" is used to describe this approach. This method provides a great deal of physical insight into the mechanism of second-order forces and moments, such as the effects of wave elevation, velocities and pressure. The advantages of the near-field method are that six components of the mean second-order forces and moments can be obtained and the slowly-varying and sum-frequency excitations may be predicted. On the other hand, the near-field approach is cumbersome to programme and computationally more demanding in terms of CPU time and core storage.

The study of Watanabe (1938) is the earliest known attempts to use the near-field approach to predict the mean sway force. He derived a drift force expression from a kinematic theory by which the hydrostatic pressure in the undisturbed wave and a phase difference between the roll oscillation and exciting moment were taken into account. The results of Watanabe's calculations accounted for about half of the values measured by Suyehiro (1924). Havelock (1942) used a similar approach to that of Watanabe to calculate the added resistance of a ship by employing the Froude-Krylov parts of the heave force and pitching moment and the resulting motion response values. His results generally overestimated the added resistance at pitch resonance and underestimated it in the range of short wave lengths. Watanabe's and Havelock's expressions neglected diffraction effects.

Since the near-field procedures need more computing power, much effort has been devoted to using the far-field approach to accomplish simplifications. These efforts have been partially successful but not entirely. After the pioneering work of Hess & Smith (1962) demonstrated the three-dimensional source distribution technique,

the application of the three-dimensional source technique in solving first-order boundary-value problem can be found elsewhere. Pinkster & Van Oortmersen (1977) computed the horizontal mean second-order forces and moments on a stationary free floating barge using the complete near-field expressions in connection with the three-dimensional source technique. The results were found to be in good agreement with experimental data.

Huijsmans & Dalling (1983) made use of Pinkster's expression to calculate the vertical drift force on a stationary LNG carrier and found reasonable agreement with experimental results. Molin (1983) used the momentum approach for the evaluation of the vertical components of the mean second-order force and moment on free floating axi-symmetric bodies. He employed the mean wetted body surface as the control surface and applied a numerical fluid finite element method to compute the velocity potential. His results showed good correlations with the experimental data.

In the case of the forward speed problem Faltinsen et al (1980) employed the two-dimensional pulsating source technique associated with the near-field method to calculate the added resistance of a ship in oblique waves. Their results showed good agreement with the measured results for three Series-60 ships and a container ship in head waves but underestimated that of the container ship in bow oblique waves. Hearn, Tong and Lau (1987) used different procedures to calculate the added resistance of a Series-60 ship and a 200,000 dwt tanker in deep water. These procedures included two-dimensional and three-dimensional oscillating source techniques coupled with the near-field approach and the three-dimensional translating pulsating source technique combined with the far-field approach. They found reasonable agreement with the experimental results given by Strom-Tejsen et al (1973).

It has been noted that the application of the near-field approach is often found in the zero speed problem but lesser in the forward speed problem. This is because direct integration of the pressure for the forward speed problem leads to the evaluation of second derivatives of the velocity potential. In order to remove the high frequency

assumption in the forward speed problem, a three-dimensional linearised formulation which is applicable to any angles of wave attack is required. Since the far-field approach has its limited applicability, the near-field approach is the only way to find all components of second-order forces and moments. In the following section, the near-field expressions will be derived for the second-order forces and moments acting on a body advancing in regular waves. The zero speed case can be obtained by removing all the speed dependent term.

7.2.3 Expressions for second-order force and moment calculation

We consider a body travelling with a mean forward horizontal speed U on the free surface of an ideal incompressible fluid and oscillating in response to the excitation of an incoming regular wave system. Let o-xyz be a right-handed system of coordinates translating in the same direction and speed as the moving body. The x-axis is parallel to the longitudinal plane of the body, that is, pointing upstream. The z-axis is taken as vertical, point upward with the undisturbed free surface on the plane z=0.

The total velocity potential $\Phi(\vec{x}; t)$, due to the incident wave system and the forward and oscillatory motion of the body, may be expressed as

$$\Phi(\vec{x}; t) = \bar{\Phi}(\vec{x}) + \tilde{\Phi}(\vec{x}; t) \tag{7.1}$$

The potentials $\bar{\Phi}(\vec{x})$ and $\tilde{\Phi}(\vec{x}; t)$ are the steady and unsteady parts respectively. The steady potential $\bar{\Phi}(\vec{x})$ due to the forward motion of the body in calm water is the resultant of the uniform stream potential –Ux and a steady perturbation potential $\bar{\phi}$. On the other hand, the unsteady potential $\tilde{\Phi}(\vec{x}; t)$ consists of the incoming wave potential ϕ_o and the body potential ϕ_B. The fluid motion is assumed to be harmonic in time with the frequency of encounter ω.

The steady perturbation potential $\bar{\Phi}$ and the body potential ϕ_B may be determined in relation to the Green function which satisfies the linearised free surface condition, the sea bottom condition and the far-field radiation condition. The particular solution of $\bar{\Phi}$ and ϕ_B are obtained through the application of the body boundary condition.

In order to linearise the boundary-value problem for the unsteady forward motion, a perturbation analysis is employed. Then the unsteady velocity potential $\tilde{\Phi}(\vec{x}; t)$ and the free surface elevation $\zeta(\vec{x}; t)$ can be written as

$$\tilde{\Phi}(\vec{x}; t) = \varepsilon \tilde{\Phi}^{(1)} + \varepsilon^2 \tilde{\Phi}^{(2)} + \cdots \tag{7.2}$$

$$\zeta(\vec{x}; t) = \bar{\zeta}(\vec{x}) + \varepsilon \zeta^{(1)} + \varepsilon^2 \zeta^{(1)} + \cdots \tag{7.3}$$

The steady perturbation potential $\bar{\Phi}$ and the free surface elevation $\bar{\zeta}$ for the steady forward motion problem can also be expressed as a perturbation series. Since the steady perturbation potential $\bar{\Phi}$ is assumed to be small, it is negligible in the linearised free surface condition and the linearised body boundary condition for the unsteady forward motion problem. Therefore irrespective of the order of magnitude associated with the steady perturbation potential $\bar{\Phi}$ and the steady free surface elevation $\bar{\zeta}$, no expansions are offered for these quantities. On the other hand the body potential ϕ_B can be decomposed into six radiation potentials ϕ_j (j=1,2,...6) and diffraction potential ϕ_7 for the first-order theory.

In the steady translating system o-xyz, the fluid pressure on the instantaneous wetted body surface S_w is given by Bernoulli's equation in terms of the unsteady velocity potential $\tilde{\Phi}(\vec{x}; t)$ as

$$p(\vec{x}; t) = -\rho \{ \tilde{\Phi}_t + \tfrac{1}{2} \nabla\tilde{\Phi} \bullet \nabla\tilde{\Phi} + \vec{W} \bullet \nabla\tilde{\Phi} + \tfrac{1}{2}(\vec{W} \bullet \vec{W} - U^2) + gz \}$$

$$\text{on } S_w \tag{7.4}$$

where $\vec{W}(\vec{x})$ is the steady velocity field.

The forces and moments acting on the body can be obtained by direct integration of pressure over the exact wetted body surface S_w.

$$\vec{F} = -\iint_{S_w} p\,\vec{n}\,ds \tag{7.5}$$

$$\vec{M} = -\iint_{S_w} p\,(\vec{r} \times \vec{n})\,ds \tag{7.6}$$

The unit normal vector $\vec{n}$ in equations (7.5) and (7.6) must be evaluated instantaneously as a function of time since the exact wetted surfaceS_w is varying with time. In order to proceed further analytically, we transform the integral over S_w into an integral over S_o, the mean wetted surface of the body in its equilibrium position in calm water. The position vector $\vec{r}$, the unit normal vector $\vec{n}$ and their vector product are expanded from the exact wetted surface S_w to the mean wetted surface S_o through perturbation expansions :

$$\vec{r} = \vec{r}^{(0)} + \varepsilon\vec{r}^{(1)} + \varepsilon^2\vec{r}^{(2)} + \cdots \tag{7.7}$$

$$\vec{n} = \vec{n}^{(0)} + \varepsilon\vec{n}^{(1)} + \varepsilon^2\vec{n}^{(2)} + \cdots \tag{7.8}$$

$$\vec{r} \times \vec{n} = \vec{\Gamma} = \vec{\Gamma}^{(0)} + \varepsilon\vec{\Gamma}^{(1)} + \varepsilon^2\vec{\Gamma}^{(2)} + \cdots \tag{7.9}$$

where

$$\vec{r}^{(0)} = \vec{r}, \qquad \vec{r}^{(1)} = \vec{\delta}^{(1)} + \vec{\Omega}^{(1)} \times \vec{r}, \qquad \vec{r}^{(2)} = [H]\vec{r} + \vec{\delta}^{(2)} + \vec{\Omega}^{(2)} \times \vec{r} \tag{7.10}$$

$$\vec{n}^{(0)} = \vec{n}, \qquad \vec{n}^{(1)} = \vec{\Omega}^{(1)} \times \vec{n}, \qquad \vec{n}^{(2)} = [H]\vec{n} \tag{7.11}$$

$$\vec{\Gamma}^{(0)} = \vec{r} \times \vec{n}, \qquad \vec{\Gamma}^{(1)} = \vec{\delta}^{(1)} \times \vec{n} + \vec{\Omega}^{(1)} \times (\vec{r} \times \vec{n})$$

$$\vec{\Gamma}^{(2)} = \vec{\delta}^{(1)} \times (\vec{\Omega}^{(1)} \times \vec{n}) + [H]\vec{r} \times \vec{n} + \vec{\delta}^{(2)} \times \vec{n} + \vec{\Omega}^{(2)} \times (\vec{r} \times \vec{n}) \tag{7.12}$$

The vectors $\vec{\delta} = (\xi_1, \xi_2, \xi_3)$ and $\vec{\Omega} = (\xi_4, \xi_5, \xi_6)$ are translational and rotational displacement vectors respectively. The matrix [H] is defined by (Ogilvie 1983)

$$[H] = -\frac{1}{2}\begin{bmatrix} (\xi_5^{(1)2} + \xi_6^{(1)2}) & 0 & 0 \\ -2\xi_4^{(1)}\xi_5^{(1)} & (\xi_4^{(1)2} + \xi_6^{(1)2}) & 0 \\ -2\xi_4^{(1)}\xi_6^{(1)} & -2\xi_5^{(1)}\xi_6^{(1)} & (\xi_4^{(1)2} + \xi_5^{(1)2}) \end{bmatrix} \tag{7.13}$$

The fluid pressure p given by equation (7.4) can be expanded from the instantaneous wetted surface S_w to the mean wetted surface S_o by means of a Taylor series expansion. Then the integration on S_w can be divided into two parts : (i) the mean wetted surface S_o of the body in its equilibrium condition, which extends up to z=0 and (ii) the time-dependent part ΔS_o between z=0 and $z = \varepsilon(\zeta^{(1)} - \vec{\alpha}^{(1)} \bullet \vec{k})$. Hence we get

$$\vec{F} = -\left(\iint_{S_\bullet} + \iint_{\Delta S_\bullet}\right)(p + \vec{\alpha} \bullet \nabla p + \cdots)\,\vec{n}\,ds \tag{7.14}$$

$$\vec{M} = -\left(\iint_{S_\bullet} + \iint_{\Delta S_\bullet}\right)(p + \vec{\alpha} \bullet \nabla p + \cdots)\,\vec{r} \times \vec{n}\,ds \tag{7.15}$$

where the vector $\vec{\alpha}$ is the local displacement of a point on S_w due to translational and rotational motions with respect to S_o. Substituting equations (7.4) and (7.7) through (7.13) into equations (7.14) and (7.15) and making use of Gauss's theorem to

transform the surface integral of the hydrostatic term ρgz to the volume integral, we have

$$\vec{F} = \rho g V \vec{k} + \frac{1}{2}\rho \iint_{S_\bullet} (\vec{W} \bullet \vec{W} - U^2)\,\vec{n}\,ds$$

$$+ \varepsilon\rho\left\{ \iint_{S_\bullet} [\Phi_t^{(1)} + \vec{W} \bullet \nabla\Phi^{(1)}]\,\vec{n}\,ds - g(\xi_3^{(1)} S_{00} + \xi_4^{(1)} S_{01} - \xi_5^{(1)} S_{10})\vec{k} \right.$$

$$\left. + \frac{1}{2}\iint_{S_\circ} [\vec{\alpha}^{(1)} \bullet \nabla(\vec{W} \bullet \vec{W})]\,\vec{n} + (\vec{W} \bullet \vec{W} - U^2)\vec{\Omega}^{(1)} \times \vec{n}\,ds - g \oint_{L_\circ} \zeta\zeta_r^{(1)}\,\vec{n}\,dl' \right\}$$

$$+ \varepsilon^2\rho\left\{ \iint_{S_\bullet} [\Phi_t^{(2)} + \frac{1}{2}\nabla\Phi^{(1)} \bullet \nabla\Phi^{(1)} + \vec{W} \bullet \nabla\Phi^{(2)} + \vec{\alpha}^{(1)} \bullet \nabla\Phi_t^{(1)} + \vec{\alpha}^{(1)} \bullet \nabla(\vec{W} \bullet \nabla\Phi^{(1)})]\,\vec{n}\,ds \right.$$

$$+ \iint_{S_\circ} [\Phi_t^{(1)} + \vec{W} \bullet \nabla\Phi^{(1)} + g\vec{\alpha}^{(1)} \bullet \vec{k}]\vec{\Omega}^{(1)} \times \vec{n}\,ds$$

$$+ \frac{1}{2}\iint_{S_\bullet} [\vec{\alpha}^{(2)} \bullet \nabla(\vec{W} \bullet \vec{W})]\,\vec{n} + (\vec{W} \bullet \vec{W} - U^2)[H]\,\vec{n} + [\vec{\alpha}^{(1)} \bullet \nabla(\vec{W} \bullet \vec{W})]\,\vec{\Omega}^{(1)} \times \vec{n}\,ds$$

$$+ \frac{1}{2}\oint_{L_\circ} \zeta_r^{(1)2} \frac{\partial}{\partial z}(\vec{W} \bullet \vec{W})\,\vec{n}\,dl' - g \oint_{L_\circ} \zeta\zeta_r^{(1)}\vec{\Omega}^{(1)} \times \vec{n}\,dl'$$

$$\left. - \frac{1}{2}g\oint_{L_\circ} \zeta_r^{(1)2}\,\vec{n}\,dl' - g[\xi_3^{(2)} S_{00} + \xi_4^{(2)} S_{01} - \xi_5^{(2)} S_{10} + \xi_6^{(1)}(\xi_4^{(1)} S_{10} + \xi_5^{(1)} S_{01})]\vec{k} \right\}$$

(7.16)

$$\vec{M} = \rho g V(y_b\vec{i} - x_b\vec{j}) + \frac{1}{2}\rho \iint_{S_\bullet} (\vec{W} \bullet \vec{W} - U^2)\,\vec{r} \times \vec{n}\,ds$$

$$- \varepsilon\rho g \begin{pmatrix} -V\xi_2^{(1)} + \xi_3^{(1)} S_{01} + \xi_4^{(1)}(S_{02} + Vz_b) - \xi_5^{(1)} S_{11} - Vx_b\xi_6^{(1)} \\ V\xi_1^{(1)} - \xi_3^{(1)} S_{10} - \xi_4^{(1)} S_{11} + \xi_5^{(1)}(S_{20} + Vz_b) - Vy_b\xi_6^{(1)} \\ 0 \end{pmatrix}$$

$$+ \varepsilon\rho\left\{ \iint_{S_\bullet} [\Phi_t^{(1)} + \vec{W} \bullet \nabla\Phi^{(1)}]\,\vec{r} \times \vec{n}\,ds - g \oint_{L_\circ} \zeta\zeta_r^{(1)}\,\vec{r} \times \vec{n}\,dl' \right.$$

$$\left. + \frac{1}{2}\iint_{S_\bullet} [\vec{\alpha}^{(1)} \bullet \nabla(\vec{W} \bullet \vec{W})]\,\vec{r} \times \vec{n} + (\vec{W} \bullet \vec{W} - U^2)\vec{r}^{(1)}\,ds \right\}$$

$$+\varepsilon^2\rho\Bigg\{\iint_{S_o}[\Phi_t^{(2)}+\tfrac{1}{2}\nabla\Phi^{(1)}\bullet\nabla\Phi^{(1)}+\vec{W}\bullet\nabla\Phi^{(2)}+\vec{\alpha}^{(1)}\bullet\nabla\Phi_t^{(1)}+\vec{\alpha}^{(1)}\bullet\nabla(\vec{W}\bullet\nabla\Phi^{(1)})]\,\vec{r}\times\vec{n}\,ds$$

$$+\iint_{S_o}[\Phi_t^{(1)}+\vec{W}\bullet\nabla\Phi^{(1)}+g\vec{\alpha}^{(1)}\bullet\vec{k}]\vec{\Gamma}^{(1)}\,ds-\tfrac{1}{2}g\oint_{L_o}\zeta_r^{(1)2}\vec{r}\times\vec{n}\,dl'$$

$$+\tfrac{1}{2}\iint_{S_o}[\vec{\alpha}^{(2)}\bullet\nabla(\vec{W}\bullet\vec{W})]\vec{r}\times\vec{n}+(\vec{W}\bullet\vec{W}-U^2)\vec{\Gamma}^{(2)}+[\vec{\alpha}^{(1)}\bullet\nabla(\vec{W}\bullet\vec{W})]\vec{\Gamma}^{(1)}\,ds$$

$$+\tfrac{1}{2}\oint_{L_o}\zeta_r^{(1)2}\frac{\partial}{\partial z}(\vec{W}\bullet\vec{W})\,\vec{r}\times\vec{n}\,dl'-g\oint_{L_o}\zeta\,\zeta_r^{(1)}\vec{\Gamma}^{(1)}\,dl'\Bigg\}$$

+ other second-order terms with $\vec{i}$ and $\vec{j}$ components due to hydrostatic variation

(7.17)

where V and (x_b, y_b, z_b) are respectively the volume and the centre of buoyancy of the body in its equilibrium position. and S_{ij} is the properties of the waterplane at z=0 such that

$$S_{ij}=\iint_A x^i y^j dxdy\Big|_{z=0} \qquad (7.18)$$

The first-order relative wave elevation $\zeta_r^{(1)}$ and the steady wave elevation ζ in equations (7.16) and (7.17) are defined by

$$\zeta_r^{(1)}=\zeta^{(1)}-\xi_3^{(1)}-y\,\xi_4^{(1)}+x\,\xi_5^{(1)} \qquad \text{on } z=0 \qquad (7.19)$$

$$\zeta=-\frac{1}{2g}(\vec{W}\bullet\vec{W}-U^2) \qquad \text{on } z=0 \qquad (7.20)$$

The mechanism of the second-order forces and moments on a ship moving in waves is complicated in nature as the formulations given by equations (7.16) and (7.17) stand. The forward motion and oscillatory motions of the ship induce steady flow and unsteady flow respectively. These flows interact with each other on the instantaneous wetted surface. Through the perturbation analysis the interaction between the steady and unsteady flows is transformed from that on the instantaneous wetted surface to that on

the mean wetted surface. Due to oscillatory motions there are different convective flows in the steady velocity field and unsteady velocity field. On the free surface the interaction between the steady and unsteady waves are revealed on the waterline integral. In the present state of the art the full second-order boundary-value problem is still unsolvable analytically because of the non-homogeneous free surface condition. Therefore we should seek a solution of the second-order problem without solving the second-order velocity potential.

If we assume the first-order waves and motions are purely sinusoidal in time, the time average of all the first-order terms is zero. The second-order potential and motions are also sinusoidal and so their mean values over one period are also zero. Hence the mean second-order force and moment are expressed in the form

$$\begin{aligned}\langle \vec{F}^{(2)} \rangle = \langle & -\frac{1}{2}\rho g \oint_{L_o} \zeta_r^{(1)2} \vec{n}\, dl' + \frac{1}{2}\rho \iint_{S_o} (\nabla\Phi^{(1)} \bullet \nabla\Phi^{(1)})\vec{n}\, ds + \rho \iint_{S_o} (\vec{\alpha}^{(1)} \bullet \nabla\Phi_t^{(1)})\vec{n}\, ds \\ & + \vec{\Omega}^{(1)} \times \vec{F}^{(1)} - \rho U \iint_{S_\bullet} (\vec{\alpha}^{(1)} \bullet \nabla\Phi_x^{(1)})\vec{n}\, ds - \rho g \xi_4^{(1)} \xi_6^{(1)} S_{10} \vec{k} \rangle \end{aligned} \tag{7.21}$$

$$\begin{aligned}\langle \vec{M}^{(2)} \rangle = \langle & -\frac{1}{2}\rho g \oint_{L_o} \zeta_r^{(1)2} \vec{r} \times \vec{n}\, dl' + \frac{1}{2}\rho \iint_{S_o} (\nabla\Phi^{(1)} \bullet \nabla\Phi^{(1)})\vec{r} \times \vec{n}\, ds \\ & + \rho \iint_{S_\bullet} (\vec{\alpha}^{(1)} \bullet \nabla\Phi_t^{(1)})\vec{r} \times \vec{n}\, ds + \vec{\delta}^{(1)} \times \vec{F}^{(1)} + \vec{\Omega}^{(1)} \times \vec{M}^{(1)} \\ & - \rho U \iint_{S_\bullet} (\vec{\alpha}^{(1)} \bullet \nabla\Phi_x^{(1)})\vec{r} \times \vec{n}\, ds \\ & - \rho g \begin{pmatrix} \xi_2^{(1)}(\xi_3^{(1)} S_{00} - \xi_5^{(1)} S_{10}) + \xi_3^{(1)} \xi_6^{(1)} S_{10} + \xi_5^{(1)} \xi_6^{(1)} (S_{02} - S_{20}) \\ -\xi_1^{(1)}(\xi_3^{(1)} S_{00} - \xi_5^{(1)} S_{10}) + \xi_4^{(1)} \xi_6^{(1)} (S_{02} - S_{20}) \\ 0 \end{pmatrix} \rangle \end{aligned} \tag{7.22}$$

where the brackets $\langle\ \rangle$ denote the time averaged value over one wave period. In deriving

equations (7.21) and (7.22), we have assumed the body has one longitudinal plane of symmetry and the centre of buoyancy is $(0, 0, z_b)$ on the same vertical line through the centre of gravity of the body. Moreover the steady perturbation potential $\bar{\Phi}$ is small enough to be negligible. Expressions (7.21) and (7.22) for the mean second-order forces and moments are grouped from six components. They are :

(I) Relative wave elevation

This represents the first-order pressure field acting between the mean waterline and instantaneous free surface. Since the square of the relative wave elevation is always positive, the pressure due to the relative wave elevation is acting inward on the wetted surface.

(II) Pressure drop due to first-order velocity field

This is a quadratic term in Bernoulli's equation and is evaluated over the mean wetted surface. This pressure is acting outward on the wetted surface.

(III) Product of first-order motion and gradient of first-order pressure field

In response to wave excitation, the body oscillates from its mean position. The oscillatory motions change the wetted surface on the first-order pressure field. Term III corrects the first-order pressure on the mean surface to that on instantaneous surface.

(IV) Cross product of first-order motion and first-order force

This term makes a correction to the direction of the first-order force in oscillatory motion. The first-order force is the direct integration of the first-order pressure normal to the mean wetted surface, so that the force vector rotates as the body oscillates.

(V) Contribution due to forward speed

This is the product of forward speed, first-order motion and the x-component of the gradient of unsteady velocity field. Term V corrects the convective effect of

the unsteady velocity field due to forward speed on the mean surface to that on instantaneous surface.

(VI) Contribution due to second-order motions

This term represents changes in the buoyancy force due to second-order motions. For the mean second-order forces and moments, the second-order motions are second-order effects of the first-order motion responses.

The first-order forces and moments, which include both hydrodynamic and hydrostatic components, are expressed as

$$\begin{bmatrix} \vec{F}^{(1)} \\ \vec{M}^{(1)} \end{bmatrix} = [M]\{\ddot{\xi}\} \tag{7.23}$$

[M] is the body-inertia matrix and $\{\ddot{\xi}\}$ is the rigid-body acceleration vector. In order to account for the slope of the wetted surface at the free surface, the line segment dl' along the free surface line integral in equations (7.21) and (7.22) is written as

$$dl' = dl \,/\, (n_1^2 + n_2^2)^{1/2} \tag{7.24}$$

It is plausible to assume that the numerical solution would not undergo singular behaviour for an inclined side wall in the first-order problem as well as in second-order problem although the existence of a solution requires that the body intersects the free surface perpendicularly in first-order theory (John 1950).

7.3 Numerical computations

The near-field expressions given by equations (7.21) and (7.22) for the mean second-order forces and moments involve the first-order unsteady velocity potential and its derivatives. Evaluation of these two equations depends critically upon the solutions of the radiation and diffraction problems and motion responses. In the present study the three-dimensional source distribution technique coupled with the near-field method was applied to carry out numerical calculations. The present three-dimensional method was first validated by comparing predictions with available experimental results of the zero speed drifting forces and mean yaw moment for an ocean-going barge and a 200,000 dwt tanker (Pinkster 1980) in head waves, bow quartering waves and beam waves. Water depth effects on the mean second-order forces and moments for the tanker are discussed. For forward speed cases numerical calculations for added resistances of three Series-60 ships with different block coefficients were performed by using three-dimensional translating pulsating source modelling and three-dimensional oscillating source modelling associated with simple speed correction on body boundary condition. Theoretical predictions were compared with the experimental data of Strom-Tejsen et al (1973) for the three Series-60 ships in head waves. Scaling from model experiment to full scale was carried out by Froude's law of similarity. The influence of forward speed and ship heading on the mean second-order forces and moments are demonstrated.

For notational simplicity in presentation the mean second-order forces and moments are designated by $\bar{F}_j^{(2)}$ for j=1,2,3,4,5,6 refer to surge, sway, heave, roll, pitch and yaw respectively. The principal particulars of the ocean-going barge, a 200,000 dwt tanker and three Series-60 ships are shown in Table 7.1.

Ship type	Barge	Tanker	Series-60 ships		
Source	NSMB	NSMB		NSRDC	
LBP. L(m)	150.0	310.00	140.00	140.0	140.00
Breadth B(m)	50.0	47.17	18.67	20.0	21.54
Draught D(m)	10.0	18.90	7.47	8.0	8.62
C_B	0.98	0.85	0.6	0.7	0.8
C_w	1.0	0.91	0.71	0.79	0.87
LCB (m)	0.0	6.6F	2.1A	0.7F	3.5F
GM_T (m)	16.23	5.78	1.12	1.12	1.12
L/B	3.0	6.57	7.5	7.0	6.5
B/D	5.0	2.5	2.5	2.5	2.5
k_{xx} (m)	20.0	14.77	7.5	8.1	8.6
k_{yy} (m)	39.0	77.47	35.0	35.0	35.0
k_{zz} (m)	39.0	79.30	35.0	35.0	35.0

Table 7.1 : Particulars of Barge, tanker and Series-60 ships

7.3.1 An ocean-going barge

An ocean-going barge is a rectangular hull whose body can be exactly modelled by flat panels. The hull was modelled by a total of 164 flat panels where the half of the hull was discretised by 12 elements in the longitudinal direction and 5 elements in the transverse direction as shown in Fig.7.1.

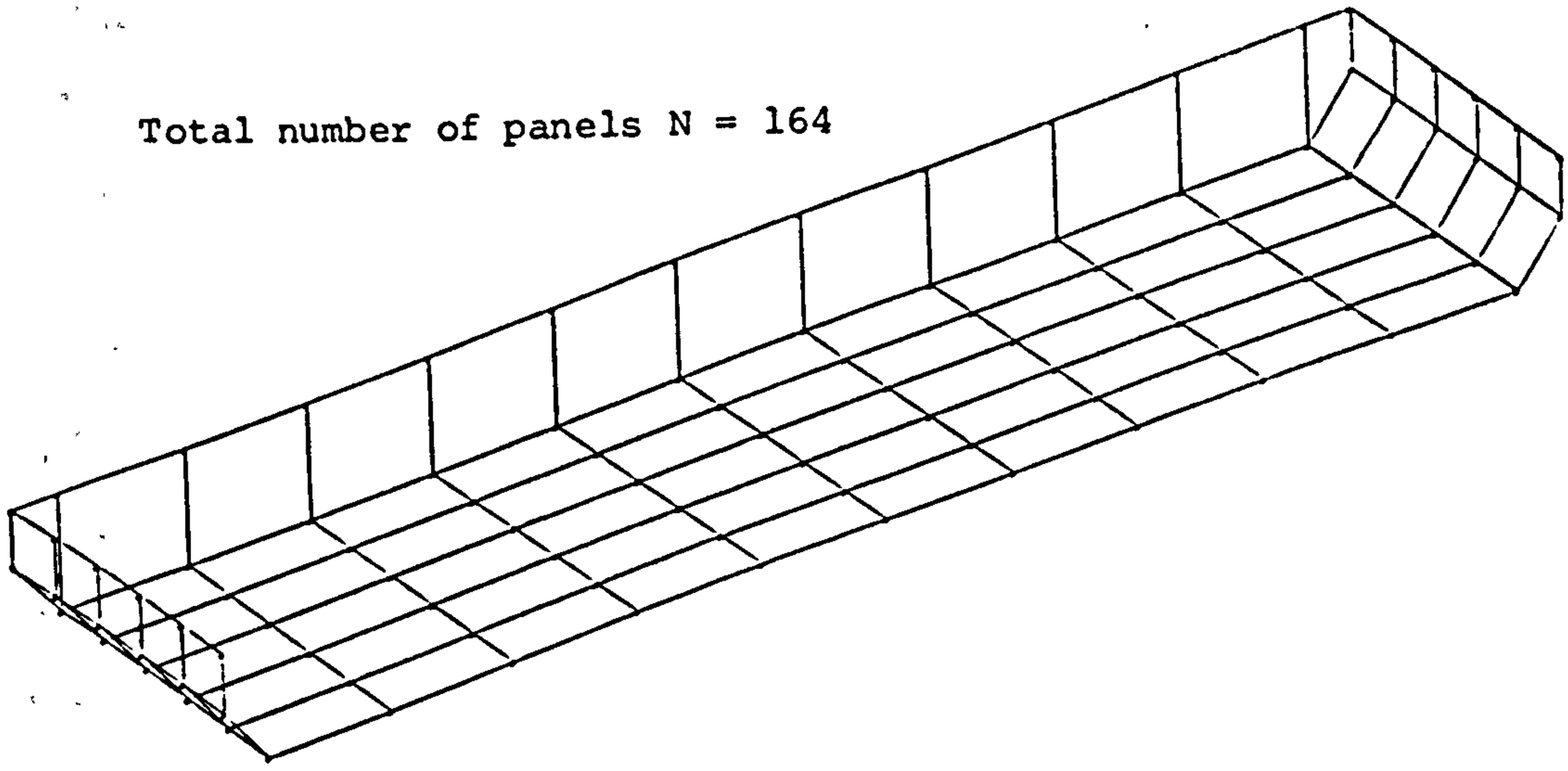

Fig.7.1 Surface Discretisation of an Ocean-going Barge

7.3.1-1 Horizontal drifting forces and mean yaw moment

Numerical calculations for the drifting forces and mean yaw moment on the stationary barge in head waves, bow quartering waves and beam waves, at a water depth of 50m, were carried out. Fig.7.2 through Fig.7.4 illustrate the present numerical results together with Pinkster's three-dimensional numerical results and experimental data. It was found that the present calculations and Pinkster's results agree very well with each other and with the measured data. However discrepancies between the theoretical and measured results are noticeable at high frequencies where the measured results are scattered due to difficulties in measurement in the short wave regime. It seems that the agreement in head waves is better than that in other wave directions considered. This may be due to the absence of roll motion, in head waves, which causes non-linear effects due to viscosity. In bow quartering waves the calculated longitudinal drifting force predicts two peak values; one is at the natural roll period 12.1sec. and the other near the natural period of pitch 9.4 sec. These were confirmed by experiment. Meanwhile there is no evidence in the experimental data for the peak value of the calculated lateral drifting force at roll resonance in beam waves and bow

quartering waves. An abrupt change in sign of the predicted mean yaw moment at roll resonance was found. It is felt that, as in the case of the first-order motions, these discrepancies may be due to the omission of viscous damping in the prediction of roll motion.

It is seen that the horizontal drifting forces are vanishingly small below non-dimensional frequency f=2.0 which corresponds to wavelength to ship's length ratio λ/L=1.57. In the long wave regime the barge oscillates at its mean position without any noticeable horizontal drift in the wave headings considered. However there is a mean yaw moment turning the barge to starboard in bow quartering waves at low frequencies. It seems that the horizontal drifting forces tend to asymptotic values at high frequencies where an asymptotic form of the horizontal drifting force as given by Havelock (1942) is only applicable for short waves.

The calculated components I through IV of the horizontal drifting forces and mean yaw moment for the stationary barge in head waves, bow quartering waves and beam waves are also illustrated in Fig.7.2 through Fig.7.4. For the free floating barge without forward speed the component V due to convective effects of forward speed is equal to zero. Moreover the component VI due to second-order motions does not contribute to the horizontal drifting forces and mean yaw moment. The component I represents the inward pressure between the mean waterline and instantaneous waterline. The sign of this force contribution I is generally in the direction of propagation of the incoming waves. This reveals that the relative wave elevation on the incoming wave side is larger than on the shadow side of the barge.

In general the component I is dominant while the other three components tend to reduce the effect of contribution I. The component II represents the outward pressure due to first-order velocity field on the mean wetted surface. The first-order velocity field tends to be largest on the incoming wave side so that the direction of the force component II is opposite to that of incoming wave. The components III and IV are strongly motion dependent because they correct the first-order pressure field and the

first-order forces respectively on the mean wetted surface to those on the instantaneous wetted surface due to oscillatory motions. The sign of the component III depends on the phase angles of the first-order motions and the first-order pressure gradient while the sign of the component IV depends on the phase angles of the first-order motions and the first-order forces. In the case of the barge the direction of the force component III is opposite to that of the incoming waves. Meanwhile the force component IV has the same direction as the component III in head waves and beam waves. The contributions III and IV have their largest values when there is a considerable amount of rigid-body oscillations. At high frequencies the motions and hence these two components tend to zero. In the short wave regime only the relative wave elevation and the second-order pressure due to the fluid velocity exist.

7.3.2 A 200,000 dwt tanker

A 200,000 dwt tanker was modelled by a total of 296 flat panels which included quadrilateral and triangular elements as shown in Fig.6.39. Fig.7.5 shows the present three-dimensional numerical results for the horizontal drifting forces and mean yaw moment on the stationary tanker at a water depth of 82.5m in head waves, beam waves and bow quartering waves. The calculated and measured results conducted by Pinkster (1980) are also presented in Fig.7.5.

7.3.2-1 Horizontal drifting forces and mean yaw moment

The present calculated results and Pinkster's calculations show good agreement with each other and with the measured data. However there are some discrepancies between the present results and Pinkster calculated results for longitudinal drifting forces. In the long wave regime the present results give small positive longitudinal drifting forces which are not presented in Pinkster's results. This small positive surge drifting force which causes the tanker drift in the direction opposite to that of wave

propagation is abnormal since a particle always drifts in the direction of free wave propagation (Ursell 1953). However the direction of the drifting force is governed by the resultant of the components I through IV. When the component I due to relative wave elevation is overwhelmed by other components, especially the components III and IV, the direction of the drifting force will be opposite to that of wave propagation. The present calculated positive surge drifting force occurs near the maximum pitch response which has about 100° phase lag behind the incident wave.

In the short wave regime the present results give better predictions than Pinkster's predictions. The reason for these differences may be that Pinkster (1980) did not account for the slope of panels adjacent to the free surface. For the mean yaw moment at the natural roll period 14.2 sec. Pinkster's result shows the opposite sign to the experimental result but the present result does not show this discrepancy.

It is clear that the drift velocity of a body is governed by the magnitude and direction of the drifting force while the heading angle of the body with respect to the waves is governed by mean yaw moment. For example the free floating 200,000 dwt tanker in bow quartering waves of height 1.0 m and period 7 sec. undergoes a longitudinal drifting force of 18 kN, a lateral drifting force of 225 kN and mean yaw moment of 7352 kN-m. Assuming that the drag coefficient (Stuntz & Taylor 1964) is 0.75, then the tanker will drift with a longitudinal velocity of 0.2 m/sec., a lateral velocity of 0.27 m/sec. and angular velocity 0.06 deg/sec to port side. In this situation an appropriate mooring system has to be used to maintain the position of the tanker in exposed seas for loading or anchoring.

7.3.2-2 Water depth effects on drifting forces and moments

Water depth effects on drifting forces and moments for the stationary tanker are illustrated in Fig.7.6 for head waves and in Fig.7.7 for bow quartering waves. In general the lateral drifting force at a given wave frequency increases with decreasing

water depth in the frequency range considered. A similar trend is observed for the longitudinal drifting force at dimensionless frequency lower than 3.0 or higher than 3.75. The mean yaw moments for the tanker at different water depths demonstrate a similar increase at dimensionless frequency lower than 2.5 or higher than 3.5. Larger horizontal drifting forces in shallow water than those in deep water may be due to more waves scattered in shallow water since the wavelength becomes shorter in reducing water depth at a constant wave frequency. It is evident that the curves of longitudinal drifting forces exhibit a similar phase shift as those of surge excitation and surge phase angles discussed in Chapter 6. This phenomenon demonstrates that the phase difference between the oscillation of the body and the wave excitation (Maruo 1960) is a factor causing the drifting force. In shallow water the mean second-order forces and moments are very sensitive to change in water depth at low frequencies but they are independent of water depth in very short waves. This is because motion responses vanish and diffraction is the only component of the drifting forces at high frequencies where waves never feel the sea bottom.

The vertical drifting force on the tanker in deep water (H/D=4.365) is acting upward in the long wave regime but downward in the short wave regime. In shallow water the vertical drifting force is nearly always acting downward in the frequency range considered. Moreover the vertical drifting force is very sensitive to small changes of water depth in shallow water in the long wave regime. The peak of the mean pitch moment increases with decreasing water depth and shifts toward lower frequency. In shallow water the sign of the mean roll moment below roll resonant frequency is opposite to that above the resonant frequency. Although the vertical drifting force, mean roll and pitch moments are not important for a ship having large waterplane area, it may be significant for a small waterplane area vessel such as semi-submersible and SWATH, where tilting effects are of importance in assessing the minimum static stability.

7.3.3 Series-60 ships

The Series-60 ships of length 140 m with block coefficients of C_B=0.6, 0.7 and 0.8 were considered. The choice of these ships was partly governed by the availability of the experimental data and partly the need to cover as wide a range of hull fullness as possible to confirm the applicability of three-dimensional source distribution technique for the calculations of mean second-order forces on a ship moving in waves. Because of the lack of experimental data, the comparison of mean second-order forces on the Series-60 ships with the measurements is restricted to added resistance values (surge drifting forces) in head waves. Two types of source distributions were used to calculate the added resistances of Series-60 ships at infinite water depth in head waves. They are the three-dimensional translating pulsating source modelling and the three-dimensional oscillating source modelling with simple speed correction on the linearised body boundary condition. The hulls were modelled by total 144, 154 and 166 flat panels for the Series-60 ships of C_B=0.6, 0.7 and 0.8 respectively as shown in Fig.7.8.

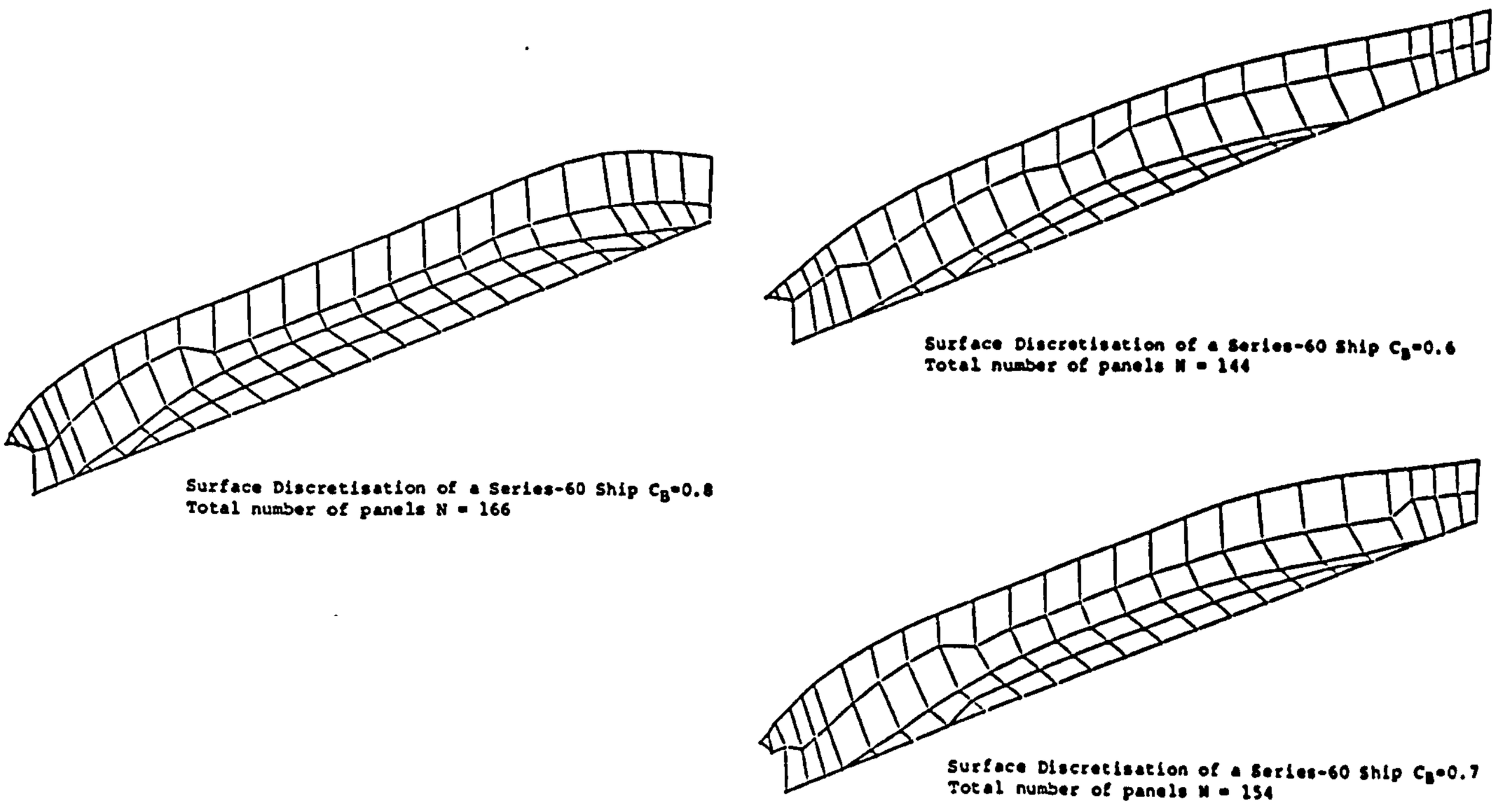

Fig.7.8 Surface Discretisation of three Series-60 Ships

7.3.3-1 Added resistance

It has been noted, in Chapter 6, that the present translating pulsating source modelling underpredicts the pitch damping near pitch resonance where the pitch response amplitude is very sensitive to the pitch damping. In order to investigate how the pitch response influences the prediction of added resistance, the translating pulsating source modelling* with higher pitch damping (method 1) was employed to predict the added resistance of a Series-60 ship C_B=0.7 travelling at F_n=0.2 in head waves as shown in Fig.7.9. Method 1 makes use of higher pitch damping coefficients calculated by the oscillating source distribution. Moreover the theoretical added resistances for this ship predicted by the oscillating source modelling (method 2) and the translating pulsating source distribution (method 3) are also illustrated in Fig.7.9. The theoretical results calculated by these three methods show very good agreement with each other and with the measured data at frequencies below the measured peak of added resistance. Although method 2 predicts lower pitch response amplitudes in the region of pitch resonance, it predicts a higher peak of added resistance than method 1 or method 3. Meanwhile method 1 gives a lower peak than method 3 because of the high pitch damping used in method 1 which results in better agreement between the calculated motion response amplitudes and the measured data. Based on the analysis of the translating pulsating source modelling, the prediction of added resistance in head waves is very sensitive to the heave and pitch motion responses in the region of resonances. Because of this motion sensitivity those hulls with poor motion responses, particularly in pitch, will produce large added resistance. This is because the added resistance is partly related to the rate of energy supplied from the ship to the fluid. The major portion of the energy is transmitted to the waves radiating from the hull. The oscillating source distribution produces waves radiating in all horizontal directions and so overestimates the measured added resistance values where the contribution of motion responses is dominant. On the other hand the translating pulsating source distribution simulating transverse waves swept downstream gives a better peak prediction of added resistances. Similar arguments hold for using method 1 and method 2 in the prediction of added

resistances of two Series-60 ships C_B=0.6 at F_n=0.283 and C_B=0.8 at F_n=0.165 in head waves also shown in Fig.7.9. In view of the prediction of added resistances for these three ships in head waves, the oscillating source modelling (method 2) well predicts the peak of added resistance for the Series-60 ship C_B=0.8 at F_n=0.165 but predicts 65% higher than the measured peak for the Series-60 ship C_B=0.6 at F_n=0.283. The translating pulsating source modelling predicts well the peaks for these three ships with various fullness. No convergence test for the numerical results is given, since it is believed that doubling the number of hull surface panels for ship form body may improve the prediction by about 9% at the peak value of the added resistance (Hearn et al 1987).

At high frequencies away from resonance the added resistance calculated by method 2 is progressively decreasing and fluctuates in very short waves as demonstrated in Fig.7.9. This fluctuation is due to the appearance of irregular frequencies present in the oscillating source distribution. Nevertheless method 2 predicts an added resistance smaller than the measured data in the short wave regime. It is often observed that added resistance predicted by the two-dimensional source distribution method combined with near-field method (Faltinsen et al 1980) or combined with the radiation energy approach (Gerristma & Beukelman 1972) is substantially smaller than the measured values in short waves. One obvious reason for this discrepancy is that the strip theory is not applicable in the fluid domain close to the ship's bow where three-dimensional flow is important. Furthermore the radiation energy approach does not account for diffraction which is dominant in the short wave regime. As the frequency of encounter increases away from resonance, motion responses become smaller and hence diffraction progressively increases. In very short waves diffraction is only a component contributed to the added resistance. However the added resistance calculated by the present three-dimensional oscillating source modelling (method 2) is still smaller than the measured data in the high frequency regime. At high frequencies the sensitivity of added resistances to motion responses is insignificant. This is confirmed by a single curve merged from the mean added resistance response curves of method 1 and method 3 as shown in Fig.7.9. It is surprising that the results obtained from the translating pulsating source distribution

technique show a similar asymptotic trend as the measurements in the short wave regime.

The mechanism which gives rise to the added resistance of a ship in regular waves can be explained by five components of the surge drifting force acting on the ship. These five components I through V are constituted from the asymmetry flow field around the hull and the energy carried away from the radiated and diffracted waves. The top of Fig.10 shows the components of the added resistance calculated by the translating pulsating source modelling* (method 1) while the bottom illustrates those components calculated by the oscillating source modelling (method 2) for the Series-60 ship C_B=0.7 at F_n=0.2 in head waves. Apart from different magnitudes in the components for method 1 and method 2, both method 1 and method 2 give similar trends. As in the case of zero forward speed the component I of the added resistance due to relative wave elevation is dominant and other components reduce the effect of contribution I. The component II due to the first-order velocity field around the hull is small in comparison with the components III and IV in the region of resonance. Components III and IV due to the oscillatory motions interact with the gradients of the first-order pressures and with the first-order forces respectively, and have their largest magnitudes near the heave and pitch resonances. Since these two components are motion related, they become very small at high frequencies where the motion response amplitudes are small. The component V due to the convective effect of the first-order velocity field due to forward speed is small in the frequency range considered. At high frequencies only the components I and II remain. Therefore the cancellation between component I and II yields an asymptotic value of added resistance in the short wave regime. If the irregular trend of the component I calculated by method 2 is faired, this trend shows an asymptotic value which is the same order but opposite to component II in short waves. As a result method 2 cannot predict a reasonable asymptotic value of added resistance at high frequencies. On the other hand the component I calculated by method 1 shows an asymptotic trend which is higher than that by method 2. It seems that the asymptotic value of added resistance is mainly contributed from the asymmetry flow around the waterline. This may be due to the small wave length and the rapid

exponential decay of the waves down in the fluid.

In examining the literature on added resistance theory, one finds that various authors made attempts to develop new short wave asymptotic theories to circumvent the inadequacy of simple formulation such as Gerristma and Beukelman's formula. Among them the most notable ones are Fujii & Takahashi (1975) and Faltinsen et al (1980). Because of the short wavelength nature inherent in the problem, all theories reduce the diffraction problem to one involving a vertical wall of infinite depth. Fujii and Takahashi used Havelock's wave reflection formula with modification for a wave reflection coefficient and the effect of forward speed. Their numerical results showed reasonable agreement with the measurements for a blunt ship form. On the other hand Faltinsen et al adopted a more analytical approach by allowing the local steady velocity to interact with the reflected waves. Based on the low speed assumption the local steady velocity is restricted to a local horizontal uniform stream tangential to the bow. The local force is obtained by far-field momentum analysis. As a result the asymptotic expression for the mean drifting forces and yaw moment is the integration of the local forces along the waterline. Faltinsen's formula produced some promising numerical results for ships with blunt ends, as illustrated by Fujii (Faltinsen et al 1980). However, when the formula is applied to a fine form ship travelling at high speeds, large discrepancies occur between the calculated and measured added resistance values.

7.3.3-2 Effects of ship heading

The zero speed second-order forces and moments are the results of the interference between incident waves, radiation waves and diffraction waves. Waves radiating from the body are extremely dependent on motion responses which are caused by wave excitations. Meanwhile the diffracted waves are due to the obstruction of incident waves on the body. Both radiated and diffracted wave systems change in different ship headings and hence the free floating body will experience different second-order forces and moments. Fig.7.11 shows the zero speed horizontal drifting

forces and mean yaw moment calculated by the three-dimensional source distribution technique for a Series-60 ship C_B=0.7 at various wave angles of attack in deep water. The vertical drifting force, mean roll and pitch moments are also presented in Fig.7.11 for completeness. We are not going to discuss these mean heave force, roll and pitch moments since strong hydrostatic restoring force and moments make them insignificant.

It is seen in Fig.7.11 that the ship will oscillate itself with no noticeable linear or angular drift displacements for all heading angles in the long wave regime. The lateral drifting force, mean roll and yaw moments vanish for head waves and following waves as no waves are radiated or diffracted transversely. When the ship's heading changes towards beam waves, the lateral drifting force increases and reaches its maximum in beam waves. These numerical results justify that the slender body theory associated with the far-field method used by Newman (1967) is not applicable to predict the mean second-order forces, especially in short waves. Newman's method yields lateral drifting forces identical to zero in beam waves. The deficiency of Newman's method is due to the result of the assumption that the ship will follow the orbital motion of the incident beam waves in the slender body theory. The lateral drifting forces on the stationary Series-60 ship at β=150° and β=30° are slightly different in magnitude while their corresponding yaw moments and longitudinal drifting forces are opposite in sign and unequal in magnitude. This leads to the conclusion that the symmetry properties of the horizontal drifting forces and mean yaw moment for an arbitrary slender ship with zero forward speed, with respect to heading angle, given by Newman (1967) are approximate.

The trends of the longitudinal drifting forces and mean yaw moments are less definite in Fig.7.11. However their strengths are governed by the motion responses in the frequency range considered. The longitudinal drifting force is no longer larger in head waves than in other wave directions at high frequencies where the surge and pitch responses are largest at the heading β=120°. Moreover, the longitudinal drifting forces and mean yaw moments in beam waves are comparable to those at other wave angles of attack at high frequencies since the motion responses in beam waves are not equal to

zero. It is evident that the longitudinal drifting forces are always negative in the quadrant $180^\circ \geq \beta \geq 90^\circ$ for the Series-60 ship C_B=0.7, and the opposite is the case in the quadrant $90^\circ > \beta \geq 0^\circ$. This means that the ship drifts in the direction of wave propagation. In beam waves the Series-60 ship C_B=0.7 drifts astern, which may be due to more waves radiated and diffracted on the fore body as the volume of fore body is large than that of aft body. This phenomenon cannot be simulated by Newman's method which simplifies the problem significantly.

The forward speed horizontal drifting forces and mean yaw moments calculated by the three-dimensional translating pulsating source modelling* (method 1) are presented in Fig.7.12 for a Series-60 ship C_B=0.7 at F_n=0.2 in various wave angles of attack in deep water. For the sake of completeness, the mean heave forces, roll and pitch moments are also presented in Fig.7.12, although their effects on a ship having large waterplane area will not be discussed here.

The peak of added resistance (surge drifting force) on the Series-60 ship C_B=0.7 in head waves is higher than those in oblique waves and occurs at longer wavelength where the pitch motion response is dominant. As the wavelength becomes shorter the added resistance values in oblique waves become comparable to those in head waves. This may have been caused by disturbance due to the sway-roll-yaw motions in oblique waves. It seems that the added resistance increases with increasing wave angle of attack in short waves where ship motions are less important. When diffraction is the only contribution to the added resistance in very short waves, the longitudinal flow becomes stronger at large wave angles of attack. Therefore the added resistance in head waves of very short wavelength is larger than that in oblique waves with the same wavelength. As in the case of zero forward speed, the added resistance in beam waves has small values in the short wave regime.

The Series-60 ship C_B=0.7 is able to travel at F_n=0.2 on a straight course with a slight drift angle against the incoming waves of very long wavelength about one and a half times the ship length as shown in Fig.7.12. Since the incoming waves associated

with uniform stream attacks the moving ship, the wave disturbances are much complicated than those in the zero speed case. Apart from incident waves, radiation and diffraction waves, the moving ship will create transverse and divergent waves which are swept downstream. The interference of these wave systems causes an asymmetrical flow field around the hull. This asymmetrical flow field appears significantly at wavelength shorter than one and a half ship length in oblique waves and at ship length to wavelength ratio $L/\lambda=1.2$ in beam waves as evident in the lateral drifting forces on the Series-60 ship. The lateral drifting forces in oblique waves are larger than those in beam waves for the range of wavelengths considered. This phenomenon is opposite to that in the zero speed case. The reason for this behaviour is due to the presence of transverse and divergent wave systems in the forward speed case. The mean yaw moments at the ship headings considered cause the ship to have a drift angle against the incoming waves in the long wave regime, the opposite being the case in the short wave regime.

7.3.3-3 Effects of forward speed

It has been noted, in Chapter 6, that the peaks of heave and pitch amplitude responses increase with increasing forward speed and their peaks occur for longer waves at higher speeds in head waves. As a consequence of the mean second-order forces and moments related to motion responses, the added resistance of the Series-60 ship $C_B=0.7$, predicted by the three-dimensional translating pulsating source modelling* (method 1), increases considerably with increasing forward speed and its maximum value also occurs for longer waves at higher speeds in head waves as shown in Fig.7.13. On the other hand the peaks of the calculated added resistance values for the Froude numbers $F_n=0.3$, 0.2 and 0.0 are of the same order in wave angle of attack $\beta=120°$ as shown in Fig.7.14. This is because their corresponding pitch response amplitudes have the same order. The corresponding vertical drifting forces, mean roll and pitch moments are also illustrated in these two figures for completeness but they will not be discussed for the Series-60 ship having large waterplane area.

The added resistance values calculated by the present method have small negative value in very long waves and are magnified with increasing forward speed as shown in Figs.7.13 and 7.14 for head waves and wave angle of attack $\beta=120^{\circ}$ respectively. The appearance of negative added resistance is unusual for a mono hull form. However, there is not any proof that the drifting force must always be in the direction of propagation of the incident waves. In view of the components I through V of the added resistance, the added resistance is positive if the component I due to the relative wave elevation is dominant. In the region of pitch resonance, if the resultant of all components except the component I is larger than the component I, a negative added resistance arises. It is interesting to note that the negative added resistance was predicted at frequencies, below pitch resonant frequency, where the pitch responses took place about 100° to 180° phase lag behind the incident wave. The predicted negative added resistance for the Series-60 ship was, indeed, very small and it may not be possible to measure during experiments because other physical effects being present in experiments were not included in the present mathematical model..

The calculated lateral drifting forces and mean yaw moments for the Series-60 ship with various Froude numbers in wave angle of attack $\beta=120^{\circ}$ are illustrated in Fig.7.14. It is shown that the lateral drifting force increases with increasing forward speed in the range of wavelengths considered. Meanwhile the mean yaw moments for the Series-60 ship with forward speed are positive in the long wave regime but negative in short waves. On the other hand the mean yaw moments for the Series-60 ship with zero forward speed are always positive and significant in the short wave regime. The stationary ship has a tendency towards head waves where the mean yaw moment is eliminated, which is often observed in a free floating body.

Increases in lateral drifting forces for higher forward speed cannot be explained by the corresponding motion responses in sway, roll and yaw modes, since it has been found, in Chapter 6, that the corresponding response amplitudes decrease with increasing forward speed. The reason for this increment may be due to the strong interference of transverse and divergent waves swept downstream. Hence a strong asymmetrical flow field around the hull is created at higher forward speeds.

7.4 Conclusions

A theoretical formulation of the second-order forces and moments acting on a ship with a forward speed in waves has been presented. Without solving the second-order potential, numerical calculations for the mean second-order forces and moments on an ocean-going barge, a 200,000 dwt tanker and three Series-60 ships with different block coefficients were performed by using the three-dimensional source distribution technique coupled with the near-field method. For the forward speed case two techniques are used for the prediction of the added resistances on the Series-60 ships in head waves. These two techniques are the three-dimensional translating pulsating source modelling and the three-dimensional oscillating source modelling with simple speed correction on the linearised body boundary condition.

The present calculations for the zero speed horizontal drifting forces and mean yaw moments acting on the barge and the tanker agree very well with Pinkster's three-dimensional numerical calculations and experimental results. The horizontal drifting forces on the stationary tanker increase with decreasing water depth at a constant wave frequency. In shallow water the mean second-order forces and moments are very sensitive to change in water depth at low frequencies but they are independent of water depth in very short waves.

The theoretical added resistance values of the three Series-60 ships in head waves, calculated by the three-dimensional translating pulsating source technique and the three-dimensional oscillating source technique, agree well with each other and with the measured data at frequencies below the peak of the added resistance. The peaks of the added resistance values for the three Series-60 ships are well predicted by the three-dimensional translating pulsating source technique. On the other hand the three-dimensional oscillating source technique predicts the peak of the added resistance values about 65% higher than the measured peak of the added resistance for the Series-60 ship C_B=0.6 at F_n=0.283. The results obtained from the three-dimensional translating pulsating source technique demonstrate a similar asymptotic trend as the measurements

in short waves but the three-dimensional oscillating source technique underpredicts the measured added resistance at high frequencies.

The effects of ship heading and forward speed on the mean second-order forces and moments for the Series-60 ship C_B=0.7 have been demonstrated by using the three-dimensional translating pulsating source distribution technique. In the short wave regime the longitudinal drifting forces on the Series-60 ship with or without a forward speed in oblique waves are comparable to that in head waves. The peak of added resistance values in head waves increases with increasing forward speed. However the peaks of added resistance values in oblique waves for different forward speeds may have the same order in magnitude. For zero speed the lateral drifting forces on the Series-60 ship in beam waves have larger values than those in other wave directions. However this may not be the case for a ship with forward speed at a given wavelength.

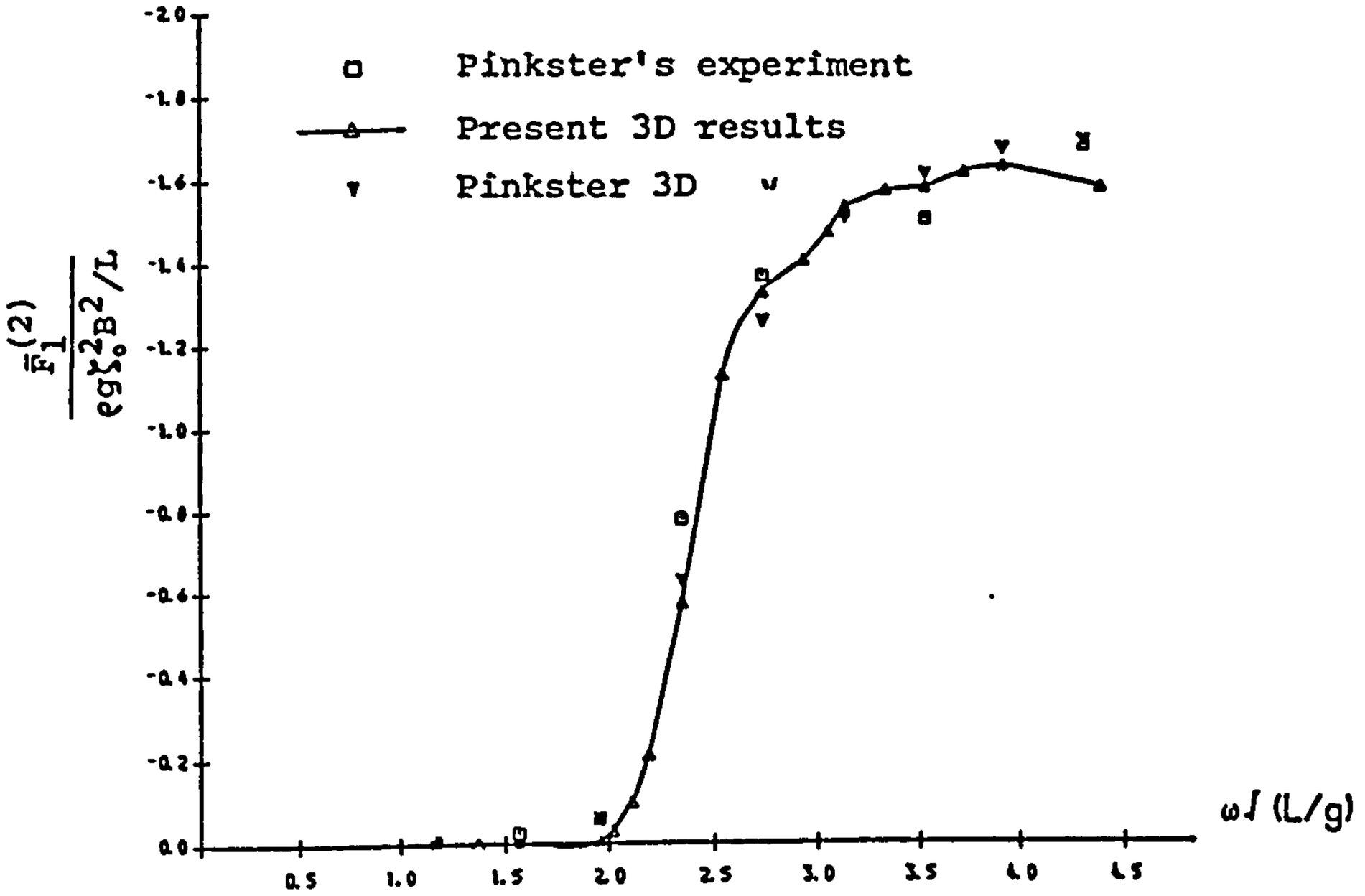

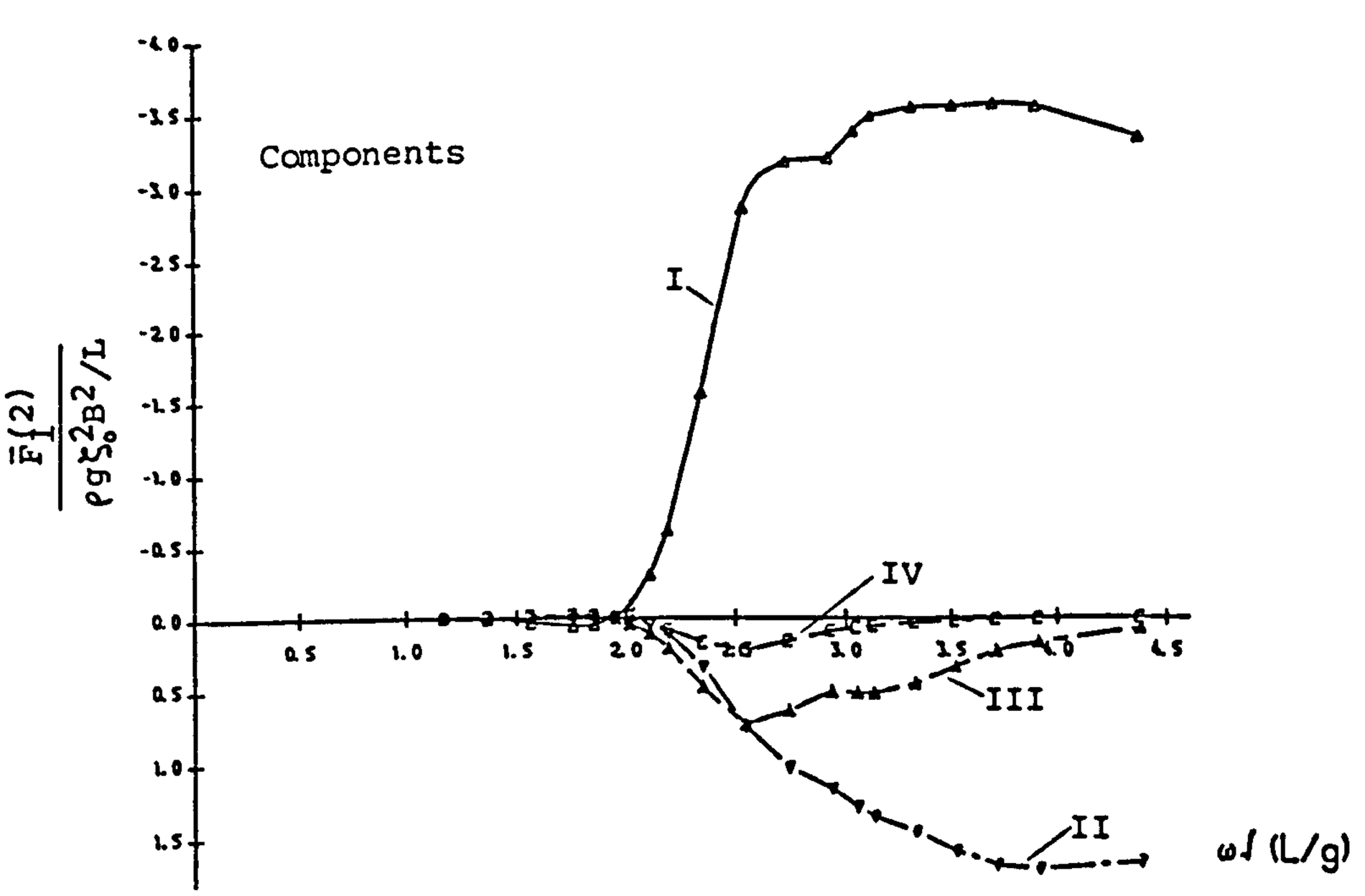

Fig.7.2 ZERO SPEED LONGITUDINAL DRIFTING FORCE OF A BARGE AT WATER DEPTH OF 50M IN HEAD WAVES.

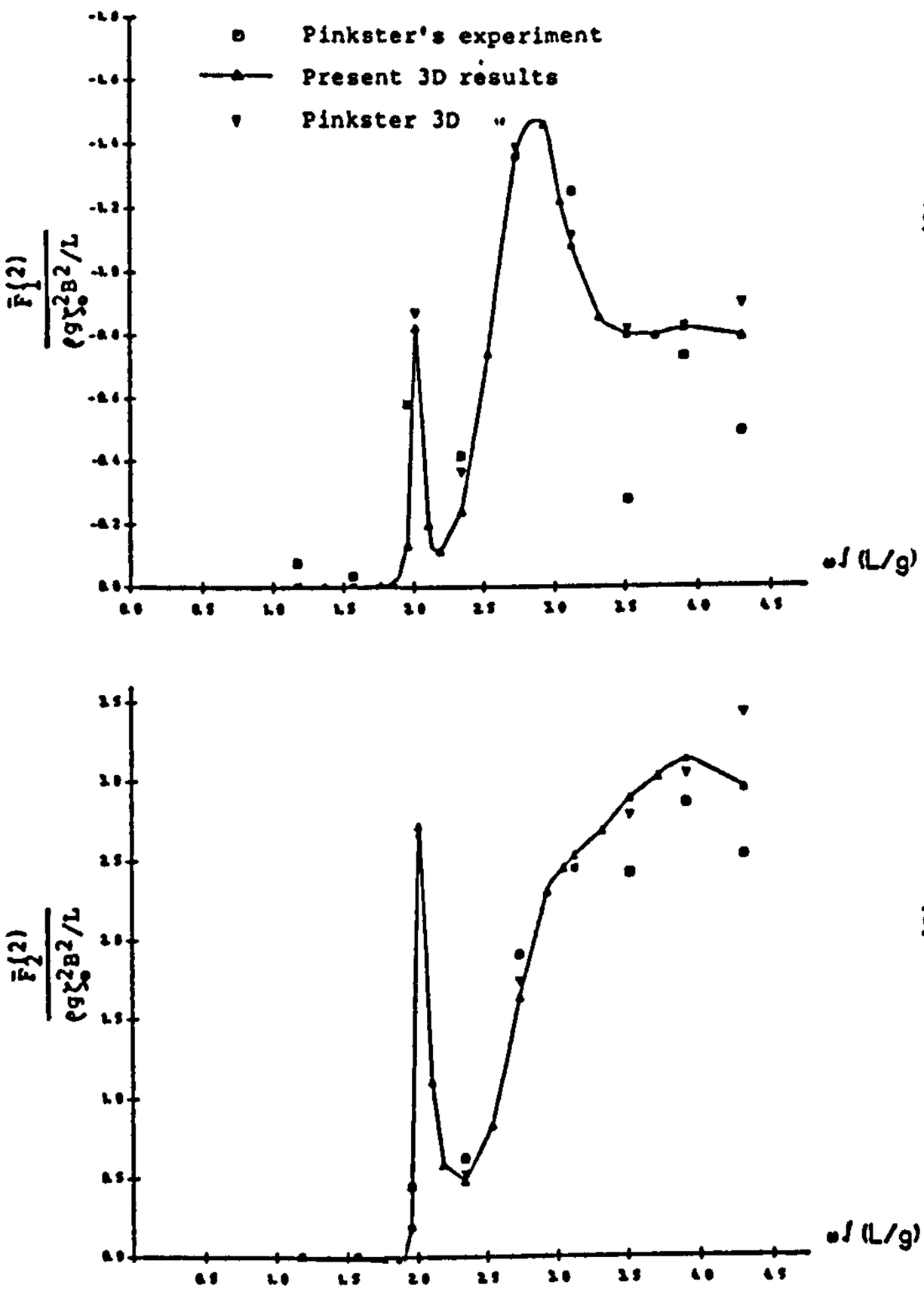

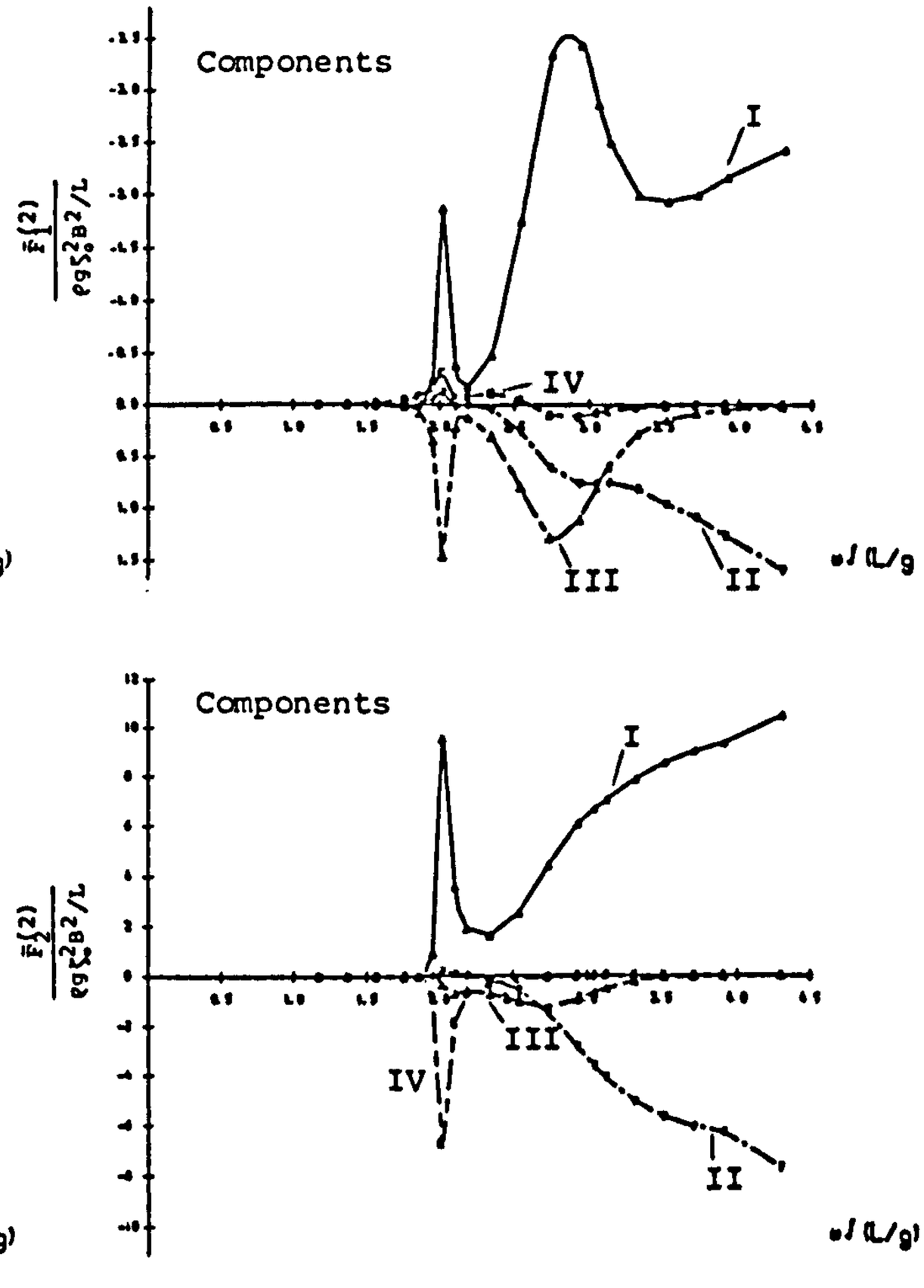

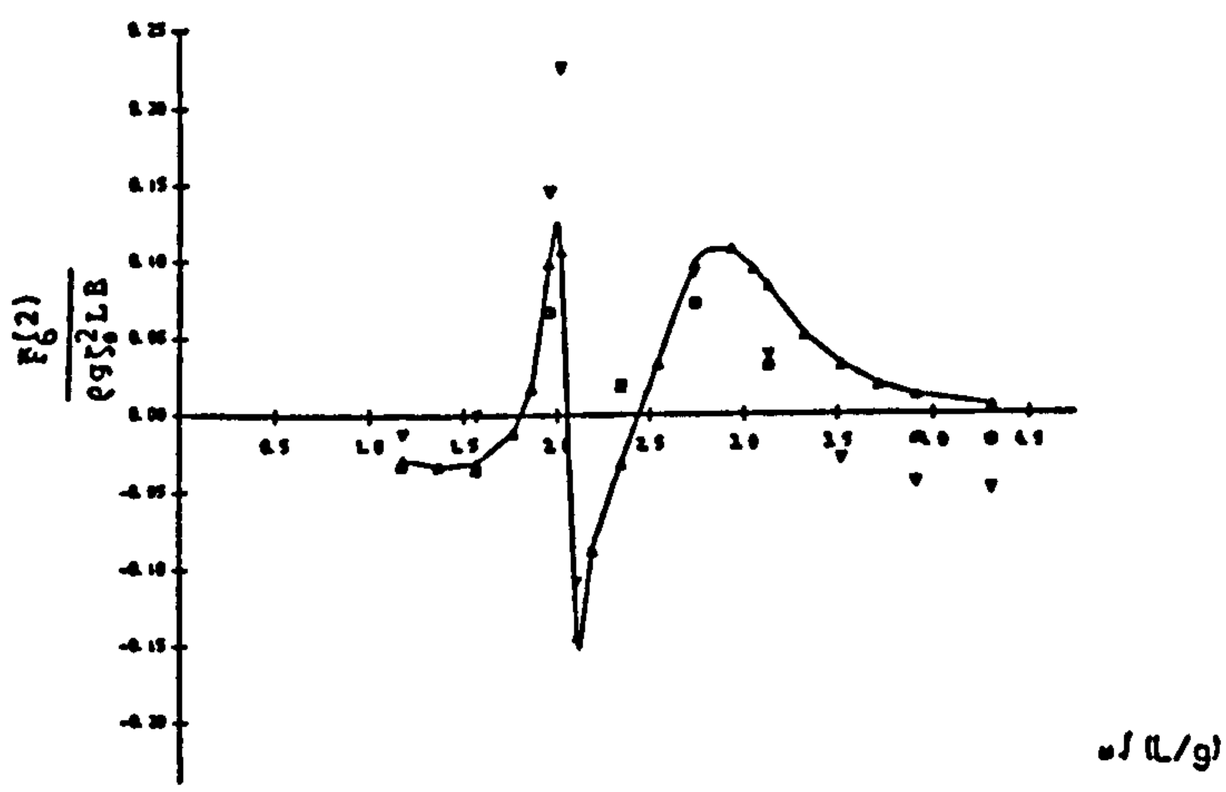

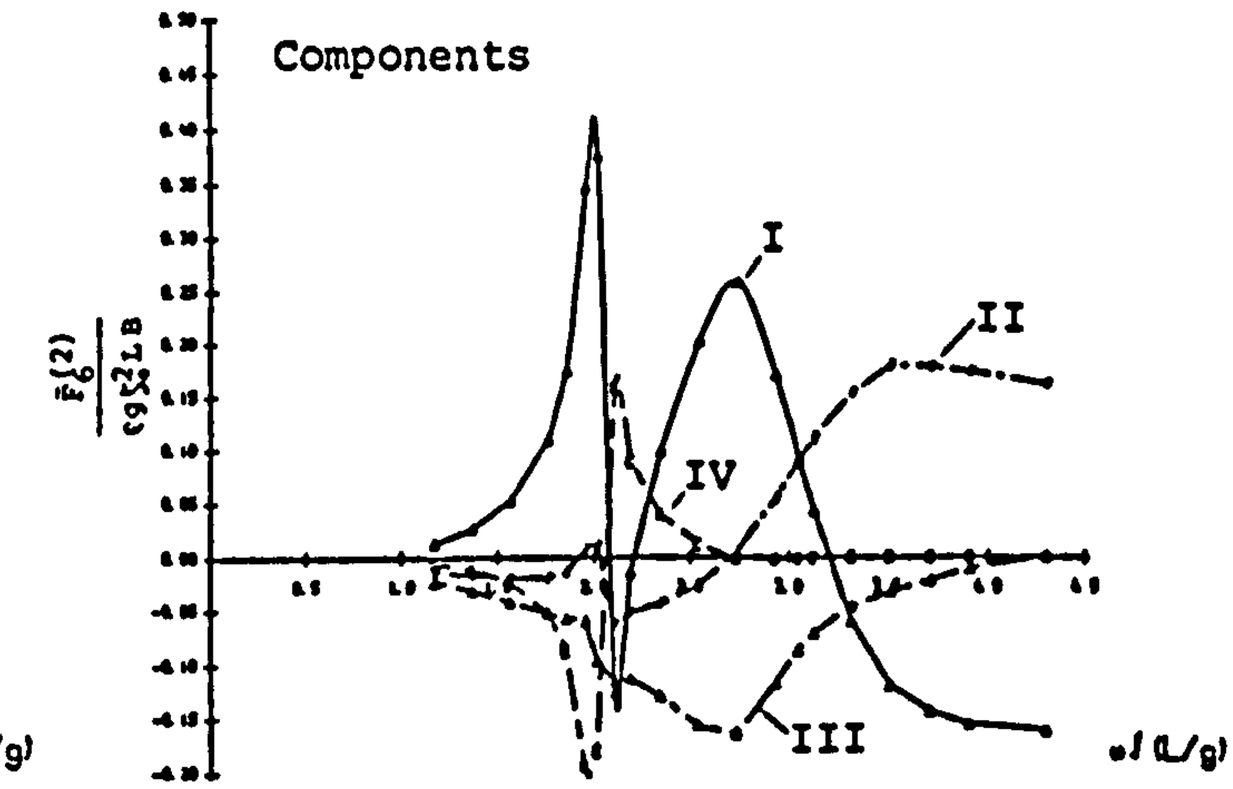

Fig.7.3 ZERO SPEED DRIFTING FORCES AND MOMENT OF A BARGE AT WATER DEPTH OF 50M IN BOW QUARTERING WAVES.

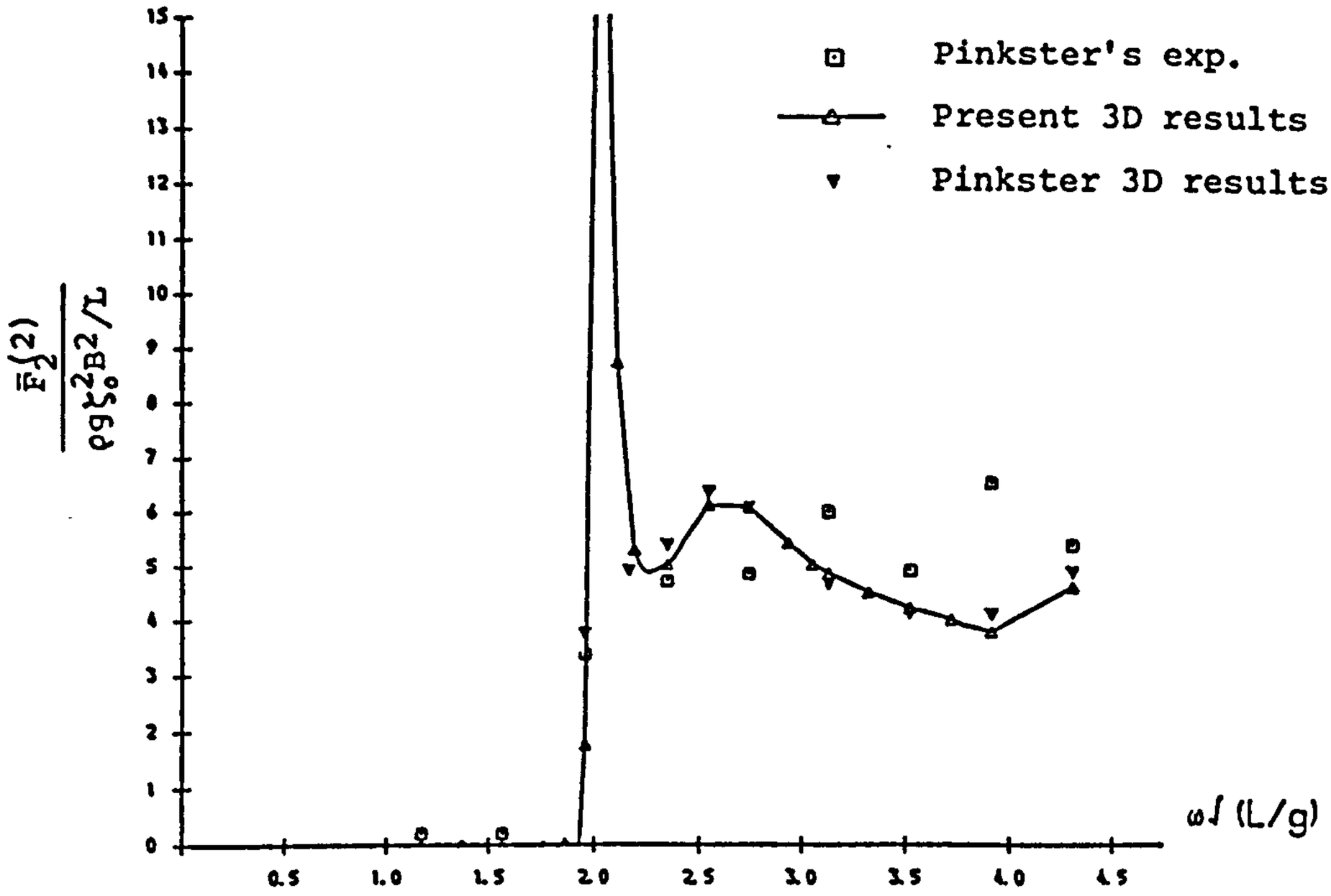

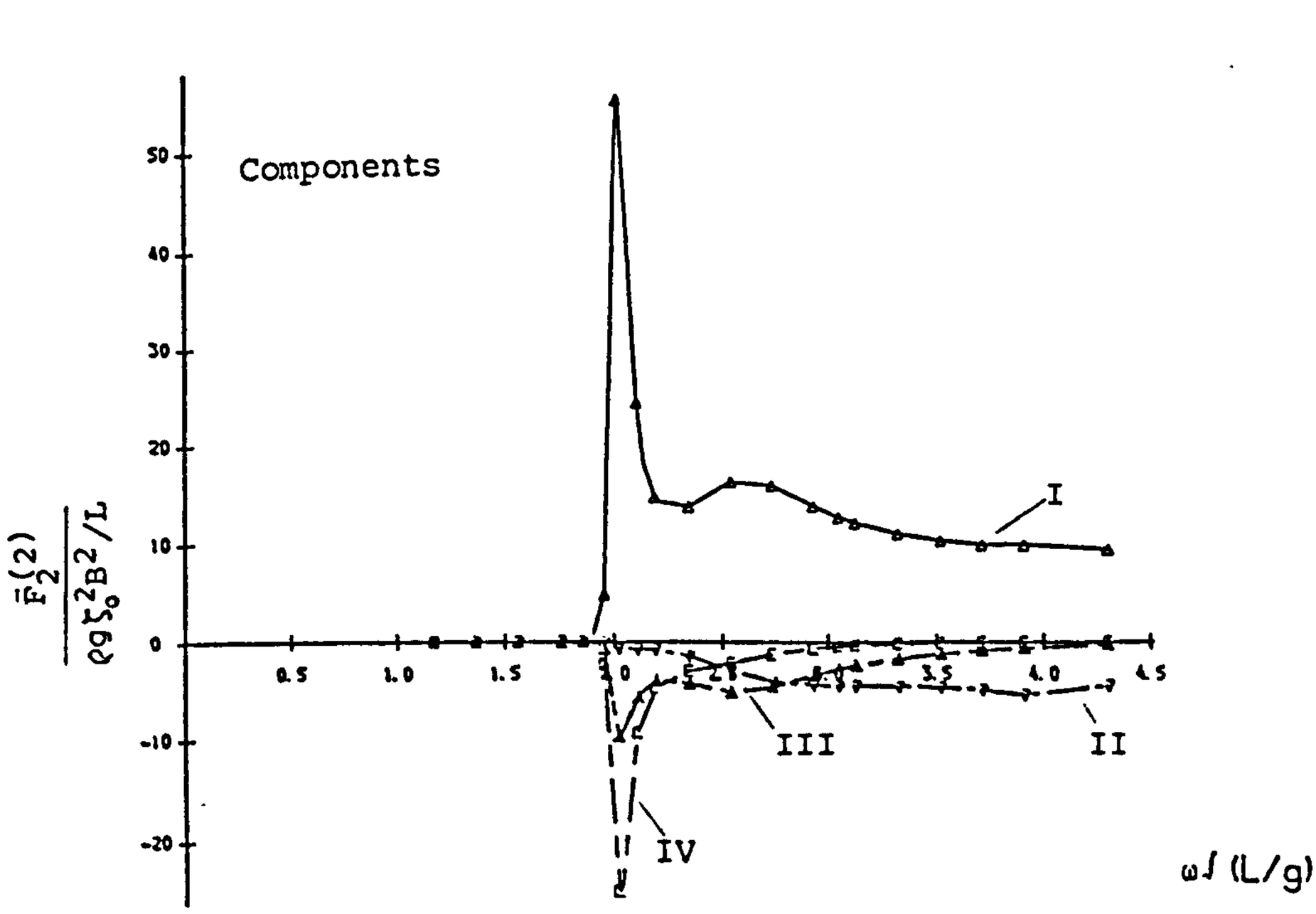

Fig.7.4 ZERO SPEED TRANSVERSE DRIFTING FORCE OF A BARGE AT WATER DEPTH OF 50M IN BEAM WAVES.

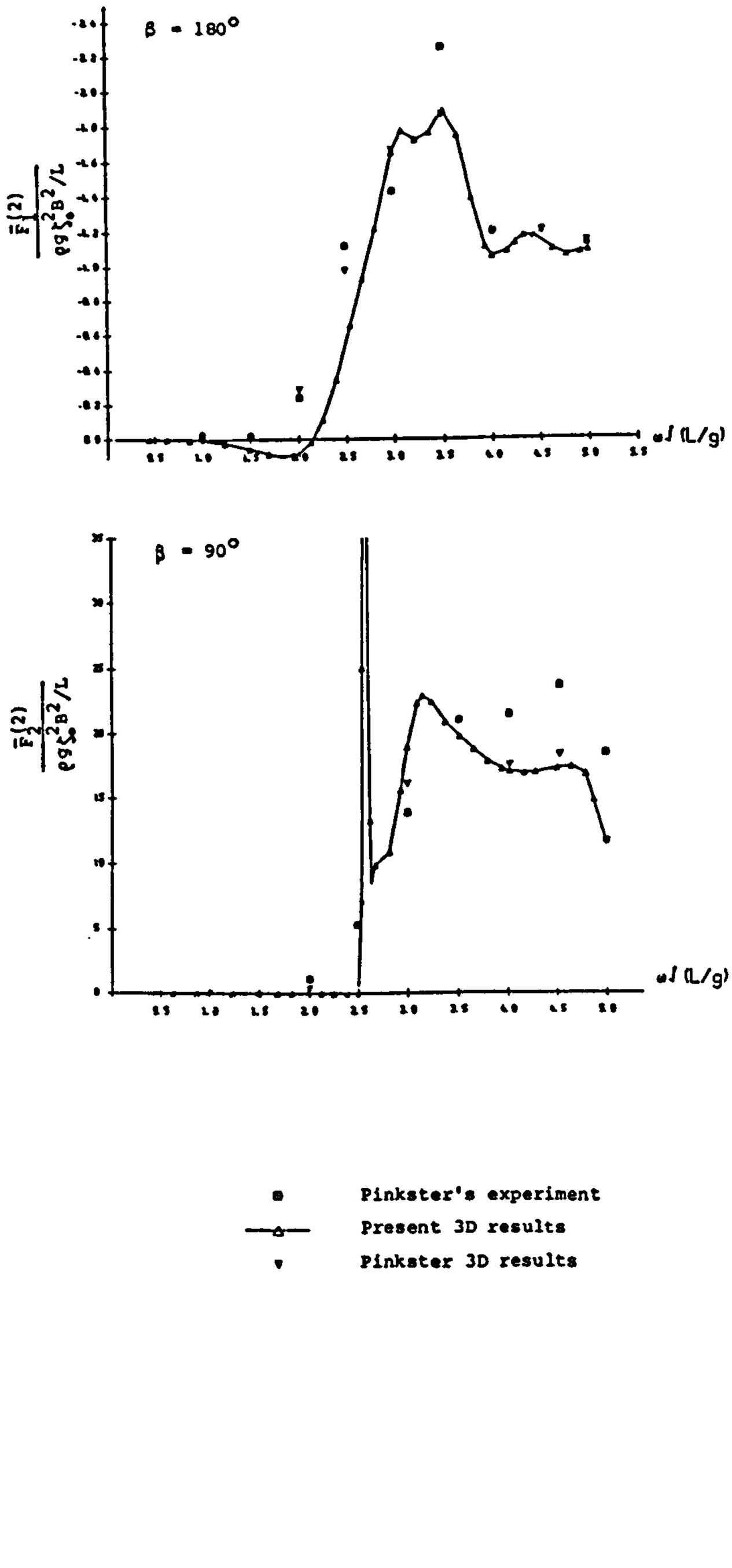

Fig.7.5 ZERO SPEED DRIFTING FORCES AND MOMENT FOR 200,000 DWT TANKER AT WATER DEPTH OF 82.5M IN HEAD WAVES, BEAM WAVES AND BOW QUARTERING WAVES.

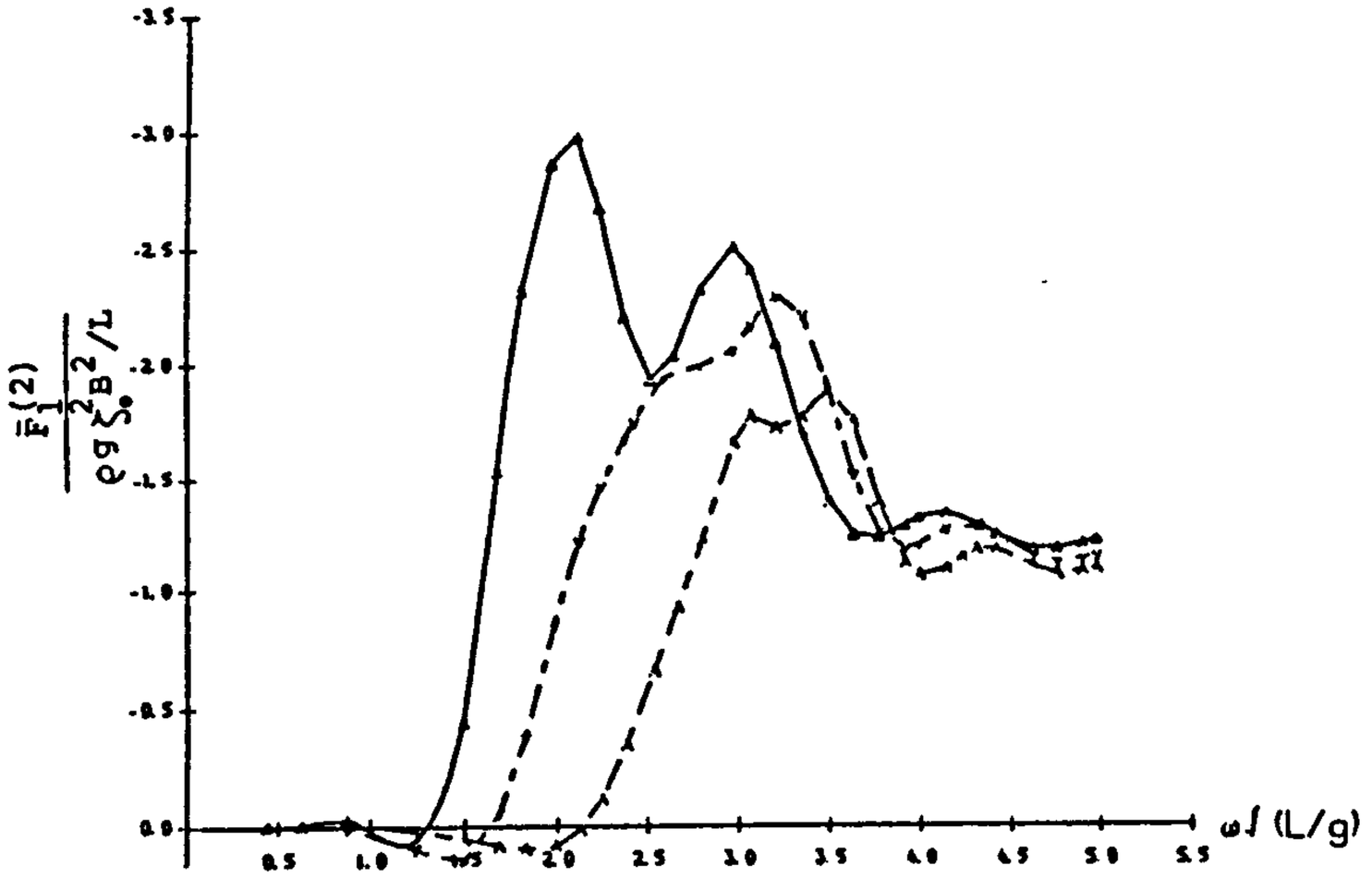

H/D	3D theory
1.200	—△—
1.600	- - ▽ - -
4.365	— ∧ —

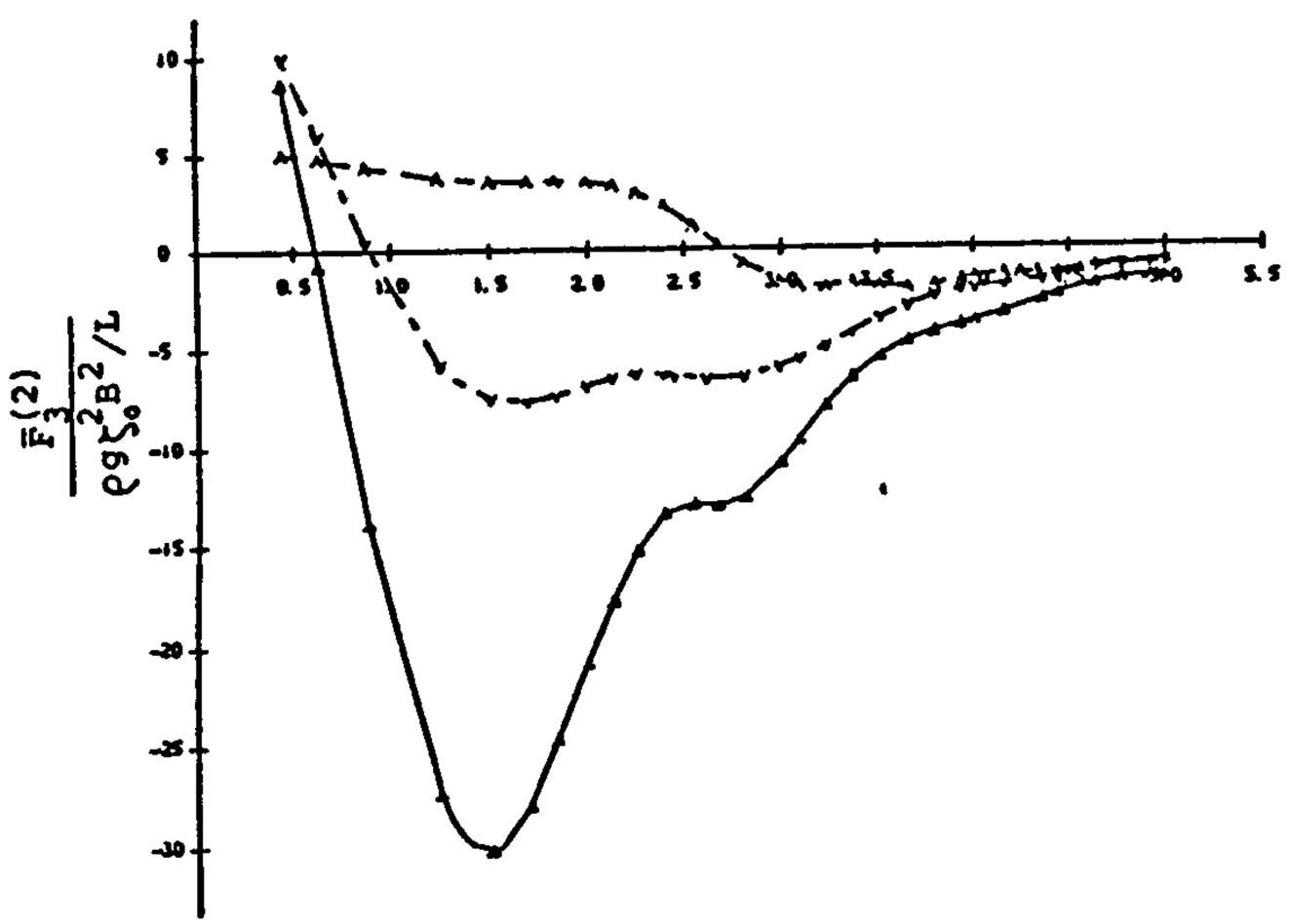

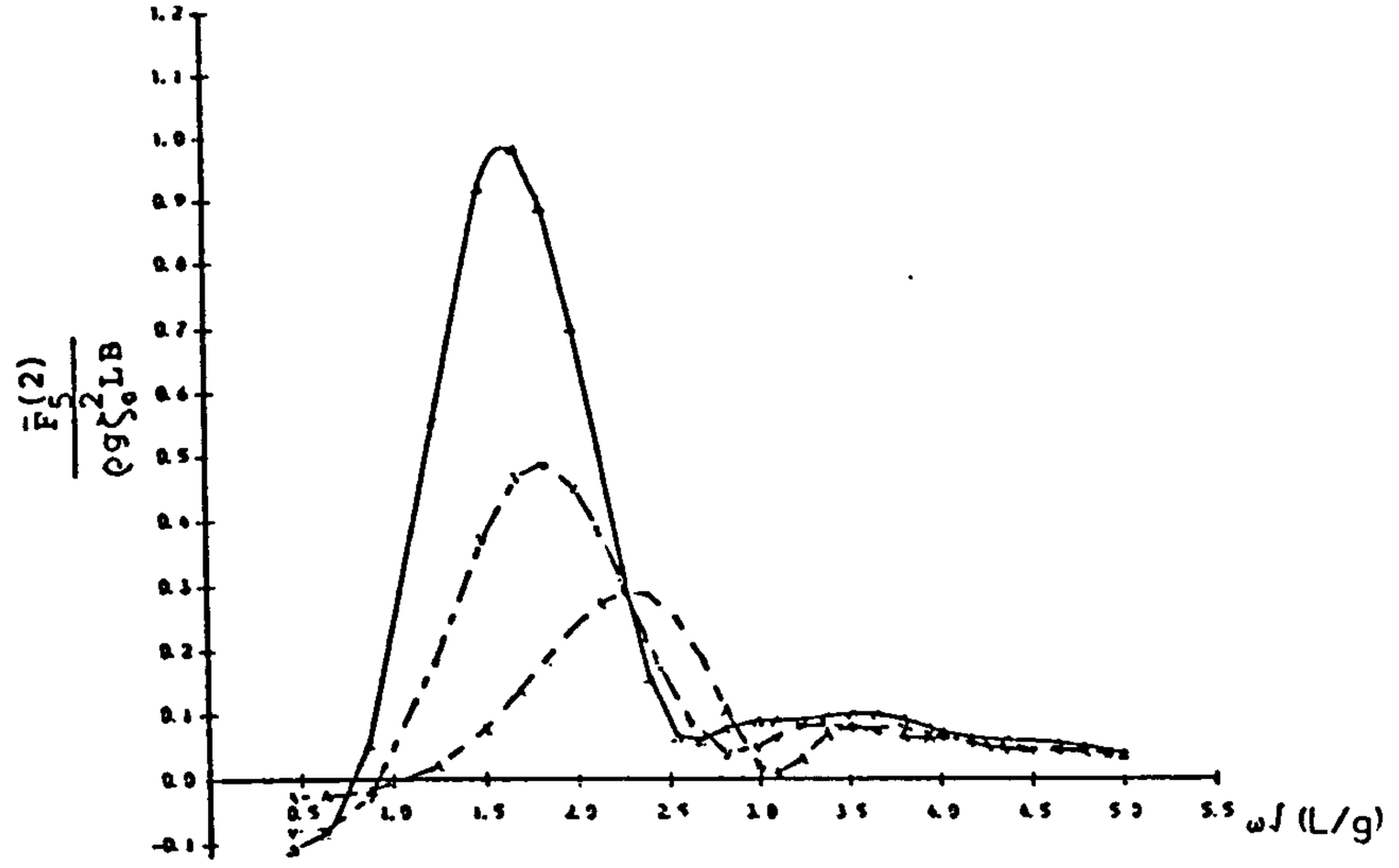

Fig.7.6 ZERO SPEED DRIFTING FORCES AND MOMENT FOR 200,000 DWT TANKER AT VARIOUS WATER DEPTHS IN HEAD WAVES.

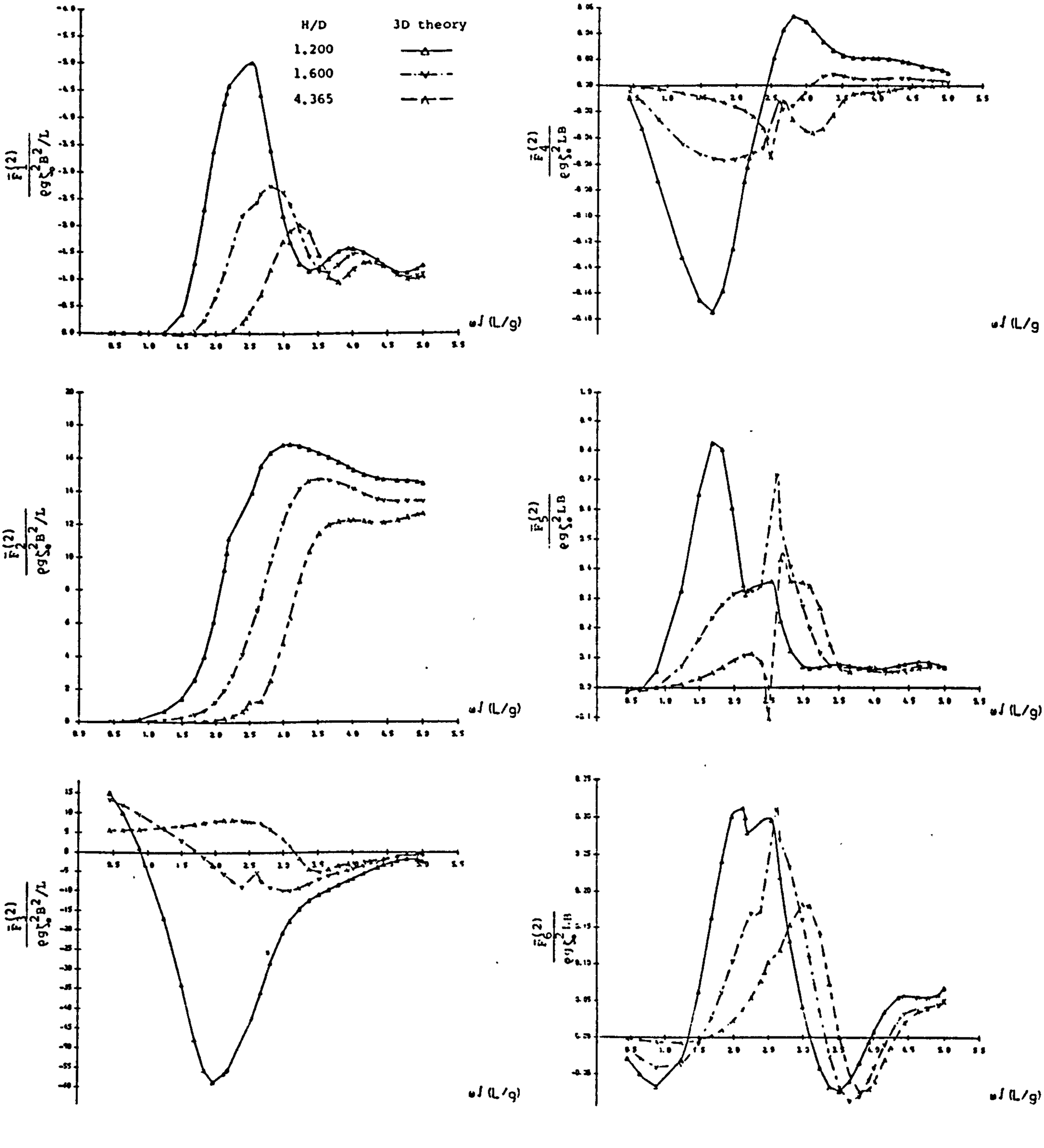

Fig.7.7 ZERO SPEED DRIFTING FORCES AND MOMENTS FOR 200,000 DWT TANKER AT VARIOUS WATER DEPTHS IN BOW QUARTERING WAVES.

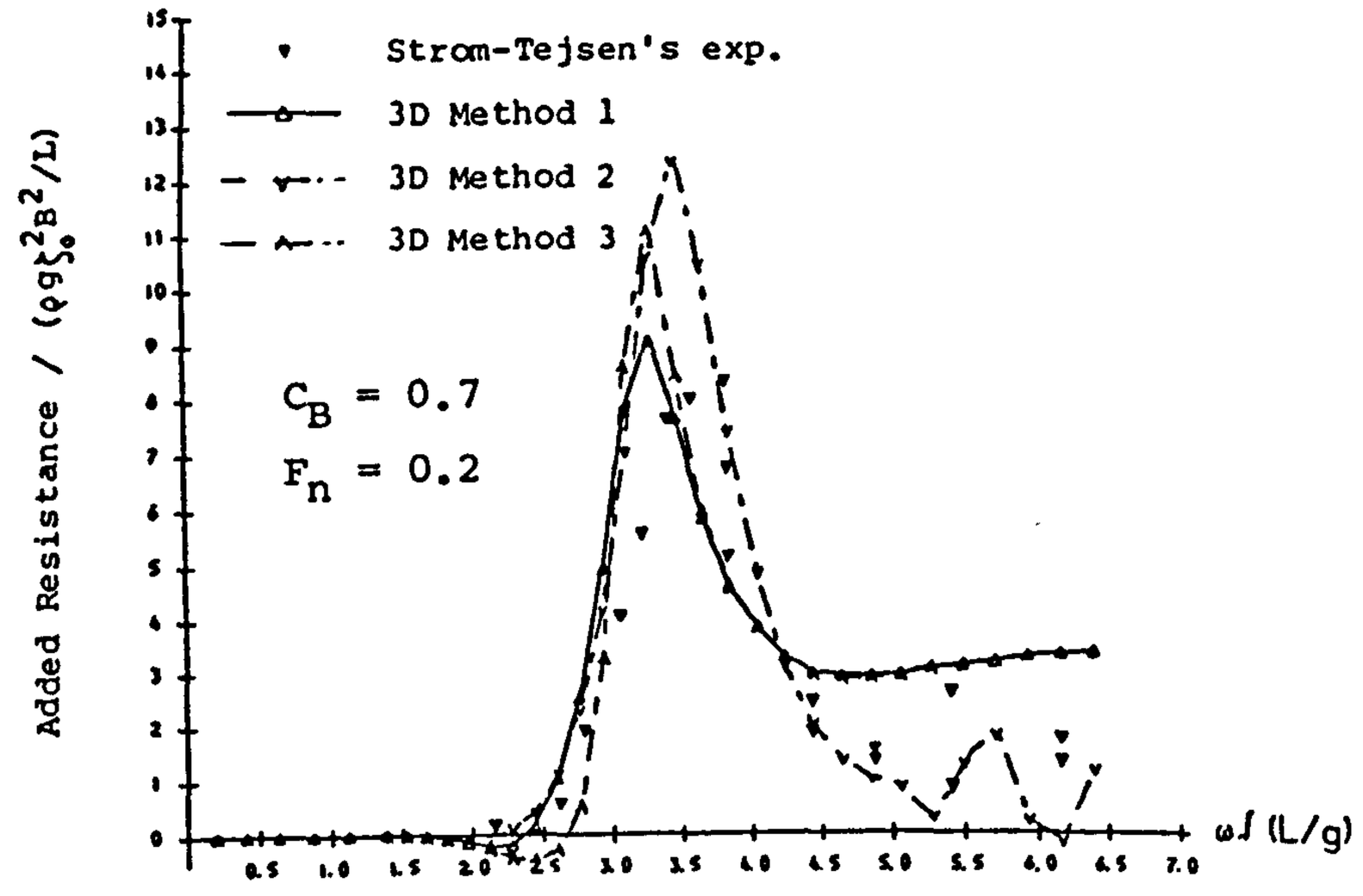

Method 1 - three dimensional translating pulsating source modelling* with high pitch damping coefficient

Method 2 - three dimensional oscillating source modelling

Method 3 - three dimensional translating pulsating source modelling

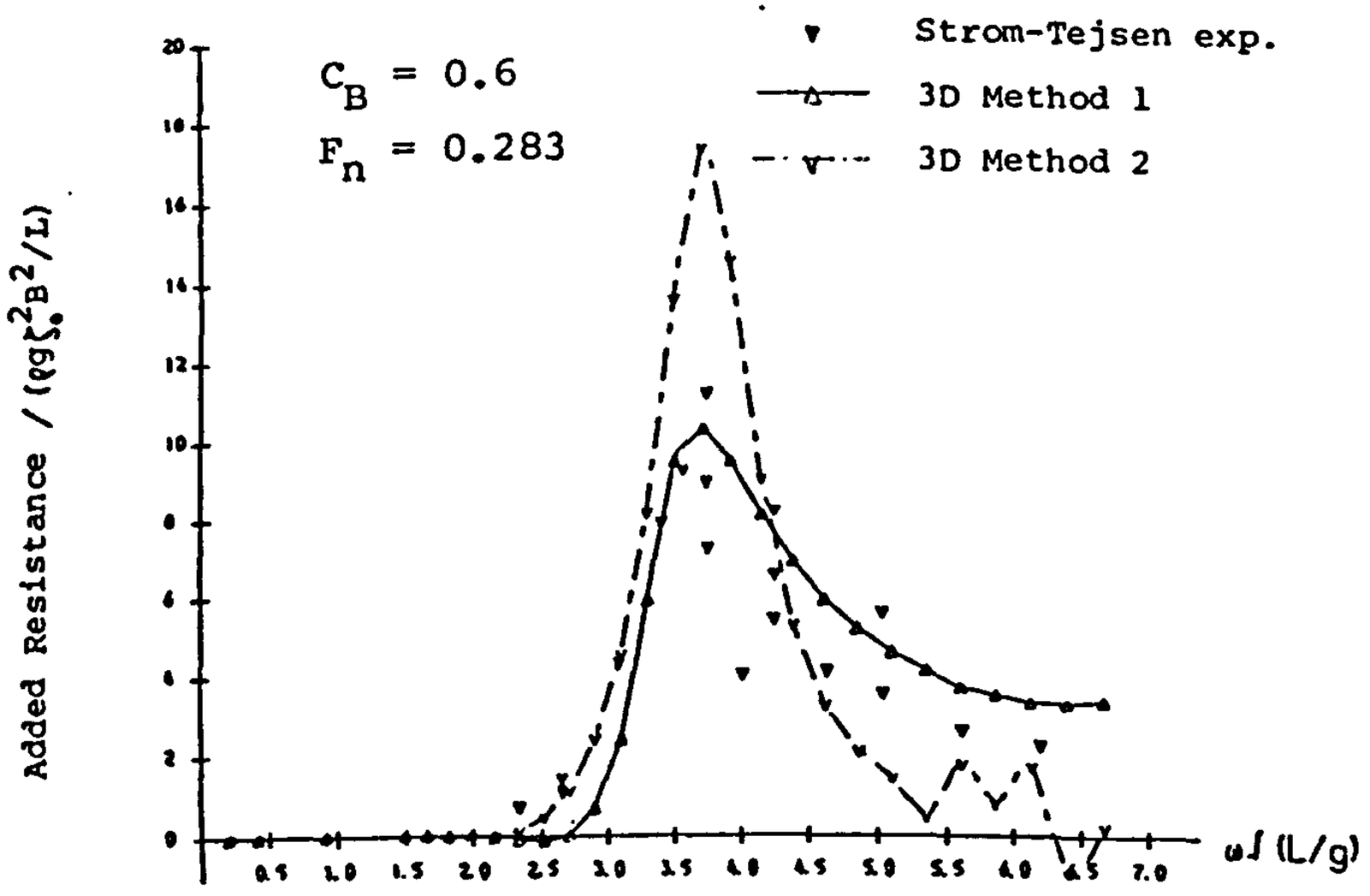

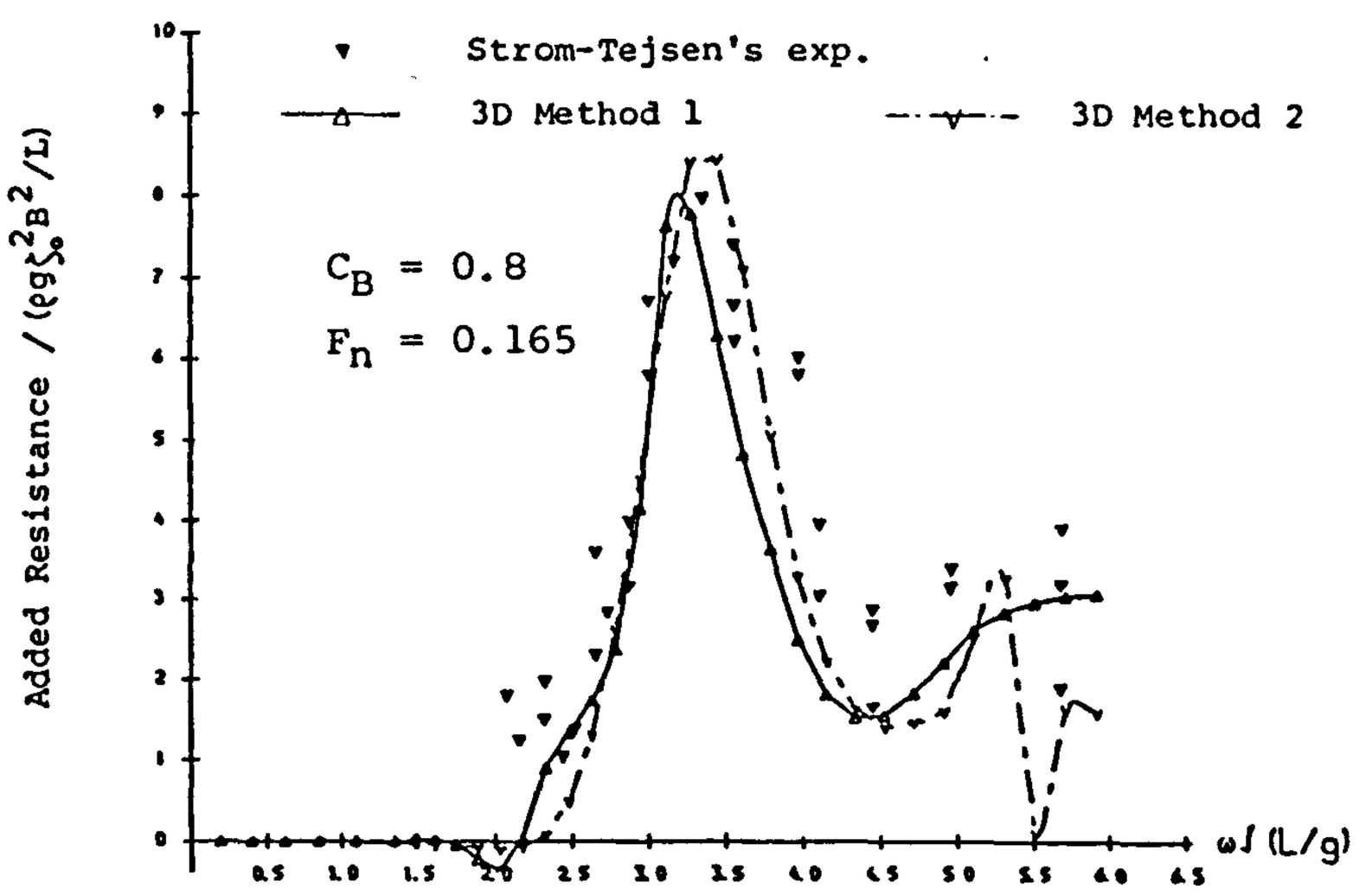

Fig.7.9 Added Resistances for three Series-60 ships advancing in head waves at infinite water depth

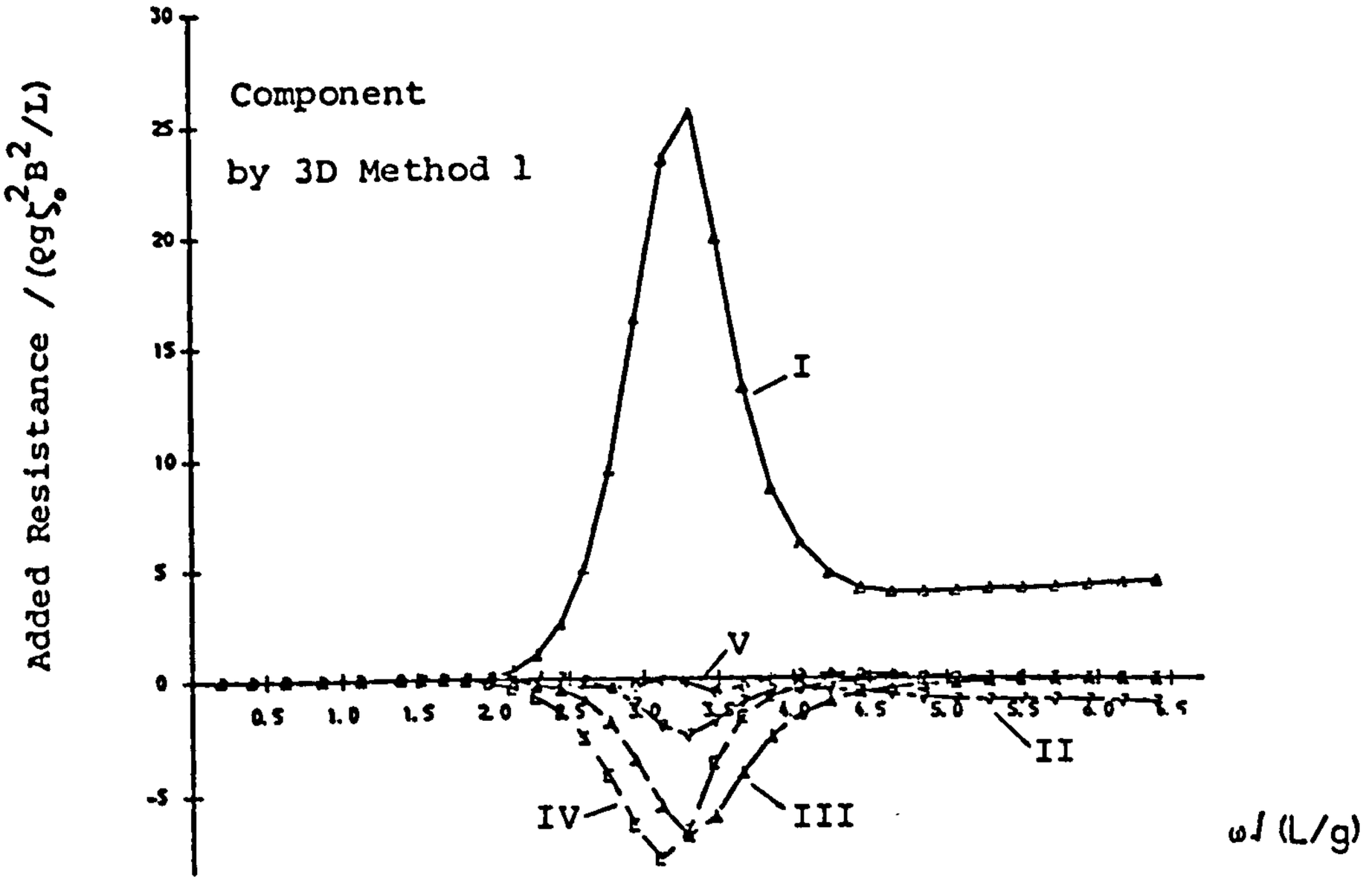

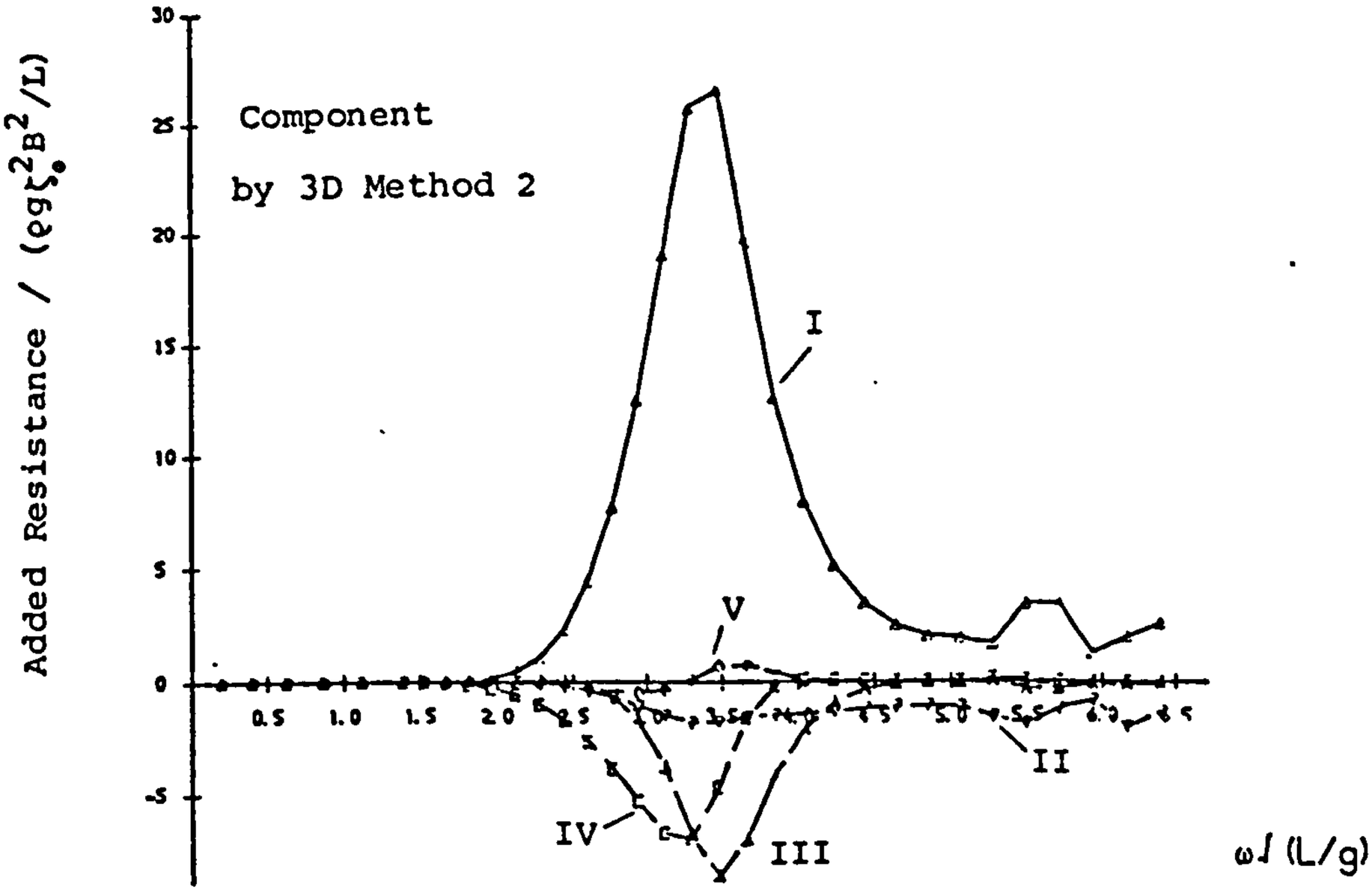

Fig.7.10 ADDED RESISTANCES FOR A SERIES-60 SHIP OF C_B=0.7 AT F_n=0.2 AT INFINITE WATER DEPTH IN HEAD WAVES

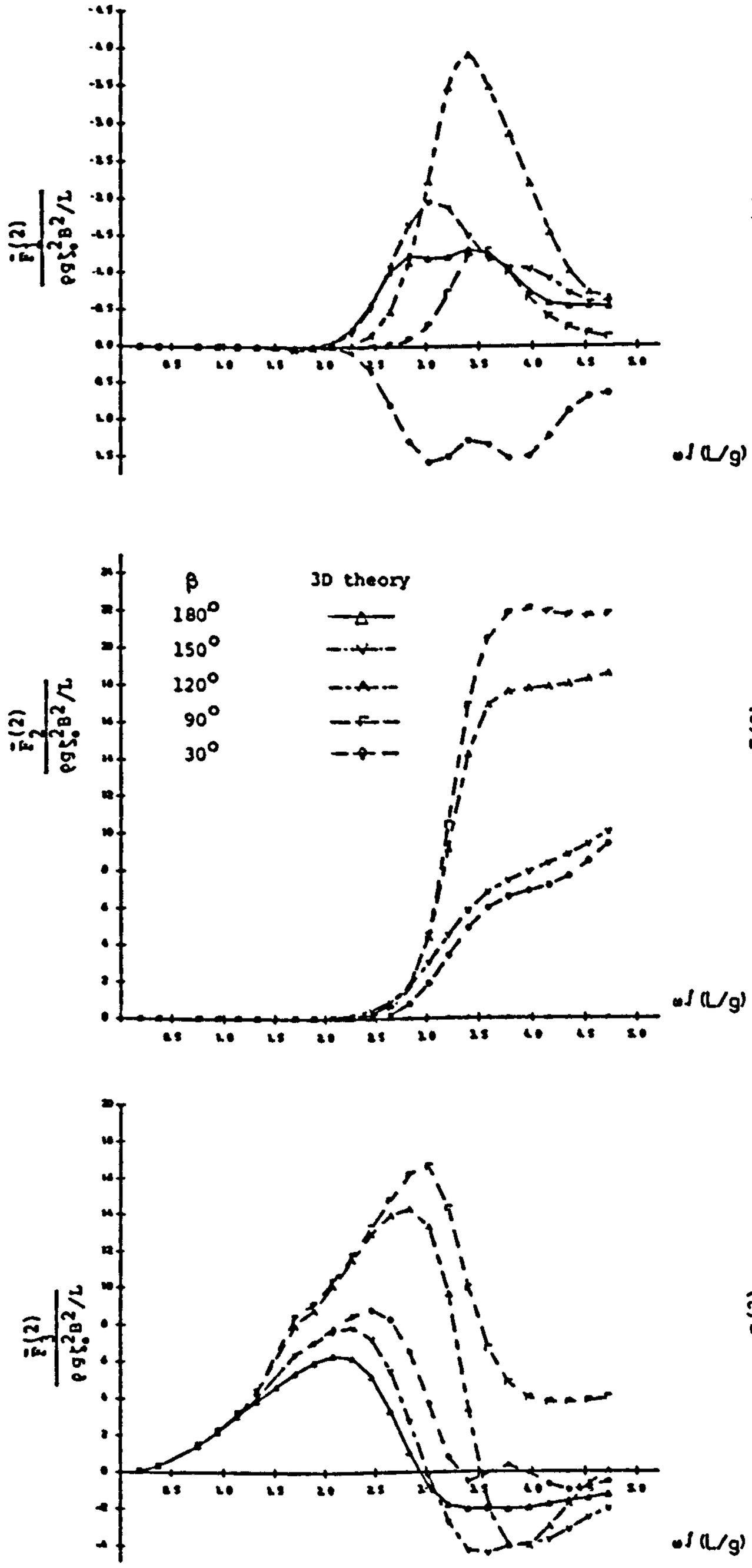

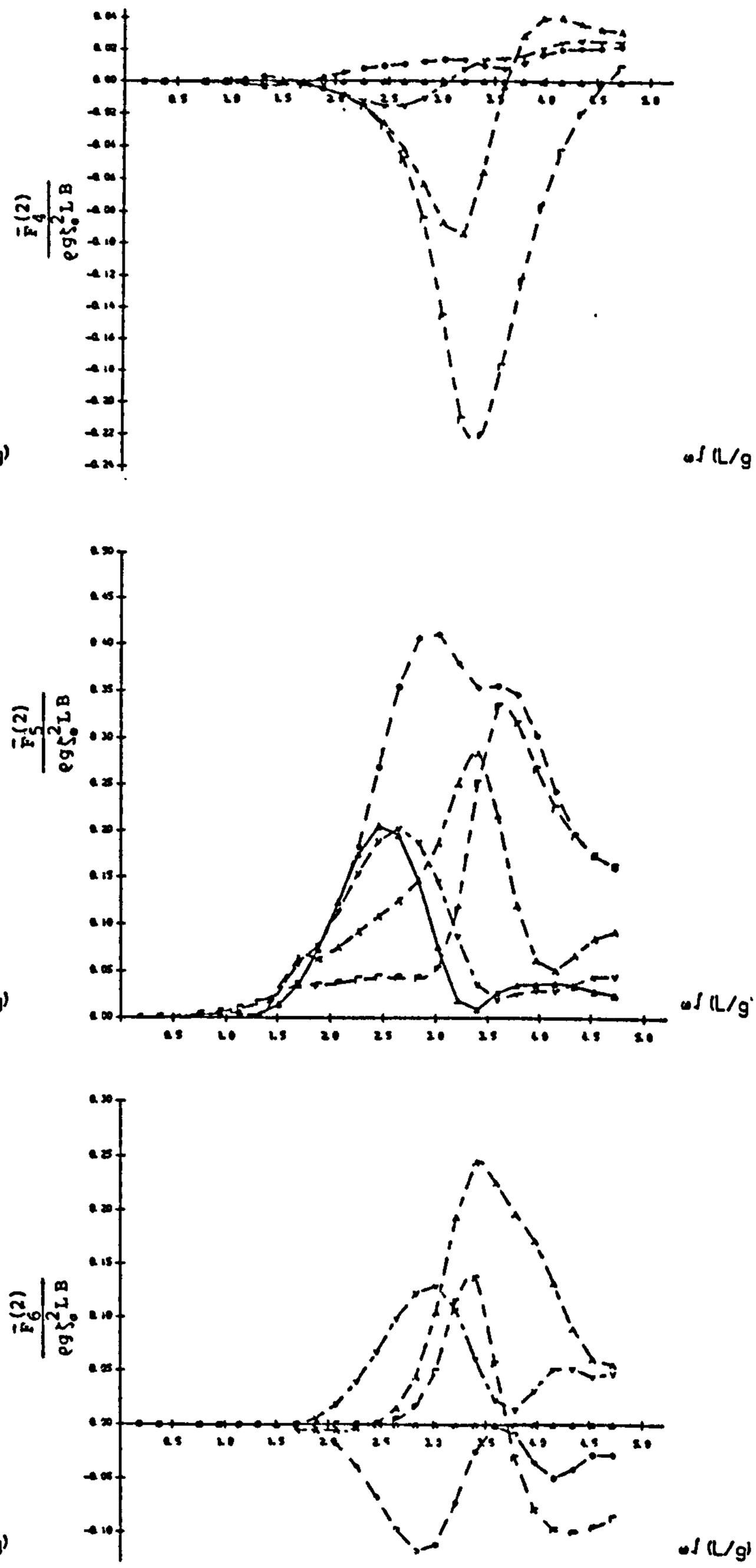

Fig.7.11 ZERO SPEED DRIFTING FORCES AND MOMENTS FOR A SERIES-60 SHIP OF C_B=0.7 AT INFINITE WATER DEPTH AT VARIOUS ANGLES OF WAVE INCIDENCE

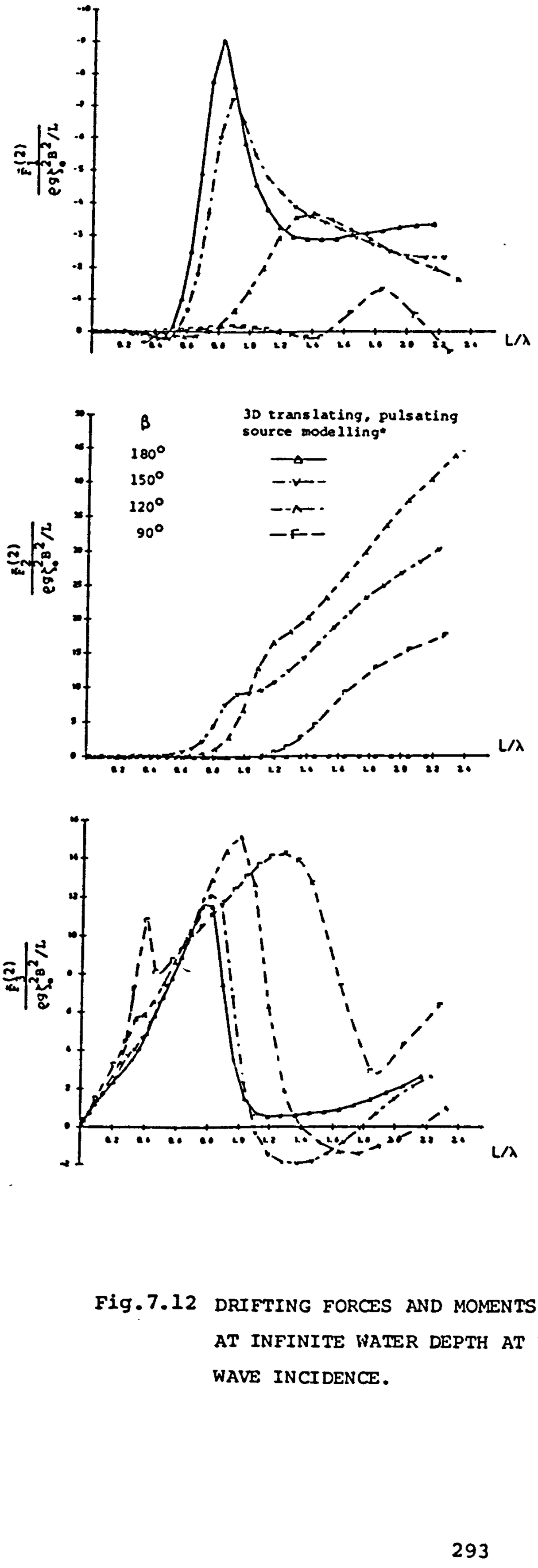

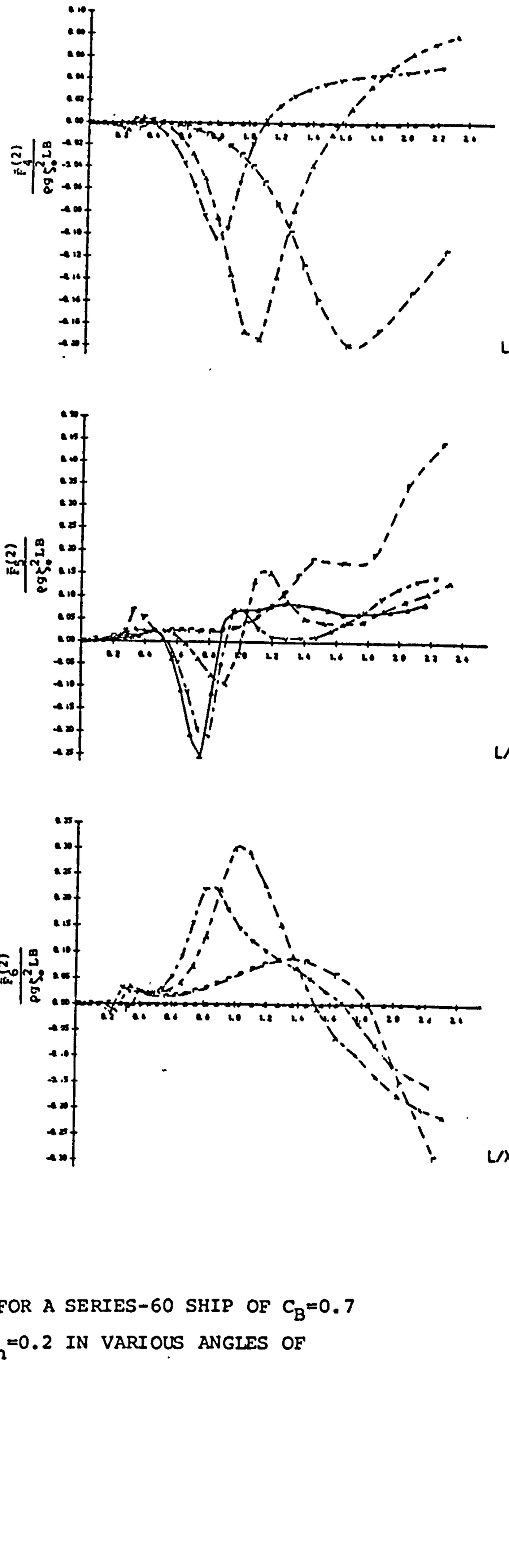

Fig.7.12 DRIFTING FORCES AND MOMENTS FOR A SERIES-60 SHIP OF C_B=0.7 AT INFINITE WATER DEPTH AT F_n=0.2 IN VARIOUS ANGLES OF WAVE INCIDENCE.

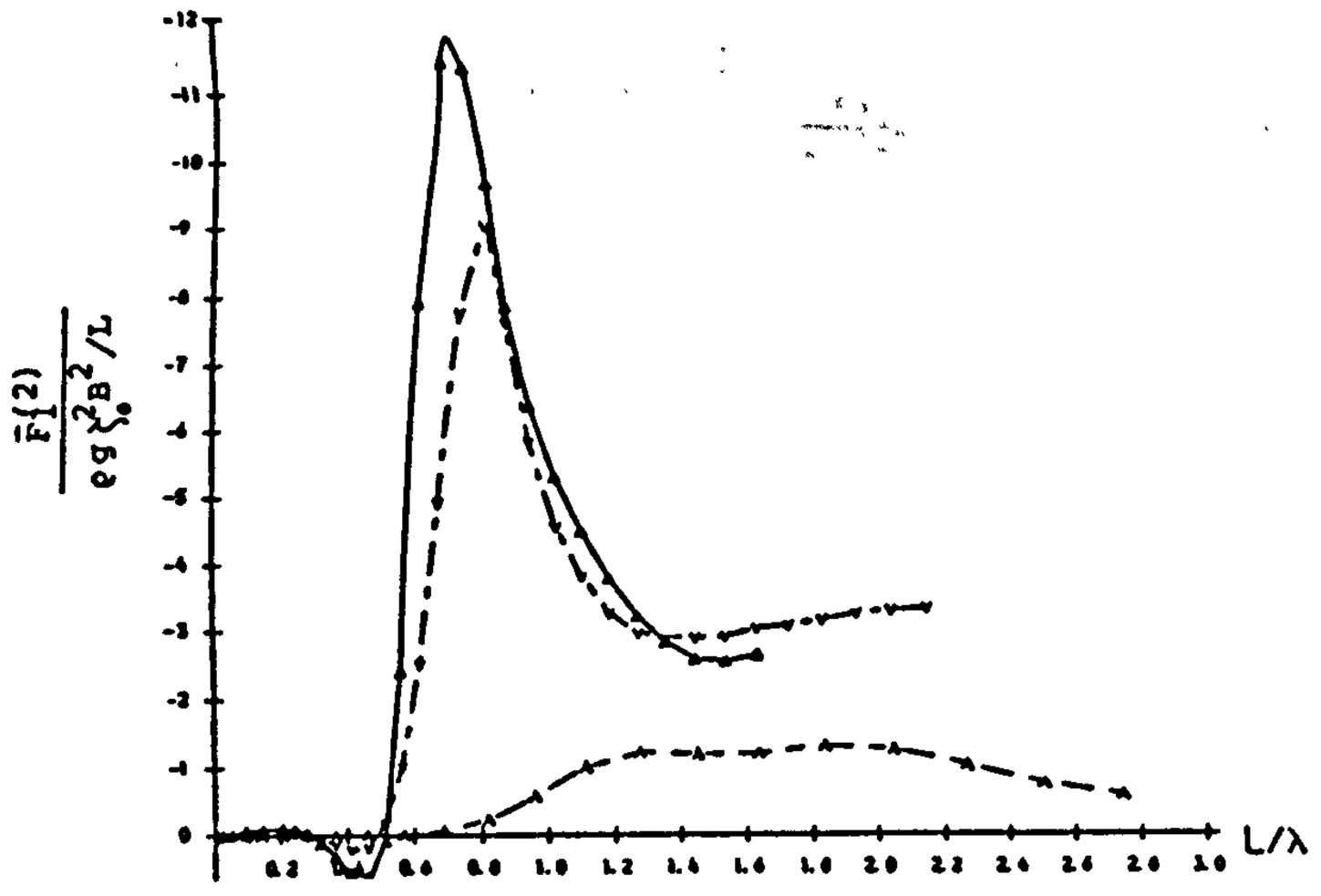

Froude No.	3D translating, pulsating source modelling*
0.3	—△—
0.2	—▽—
0.0	—∧—

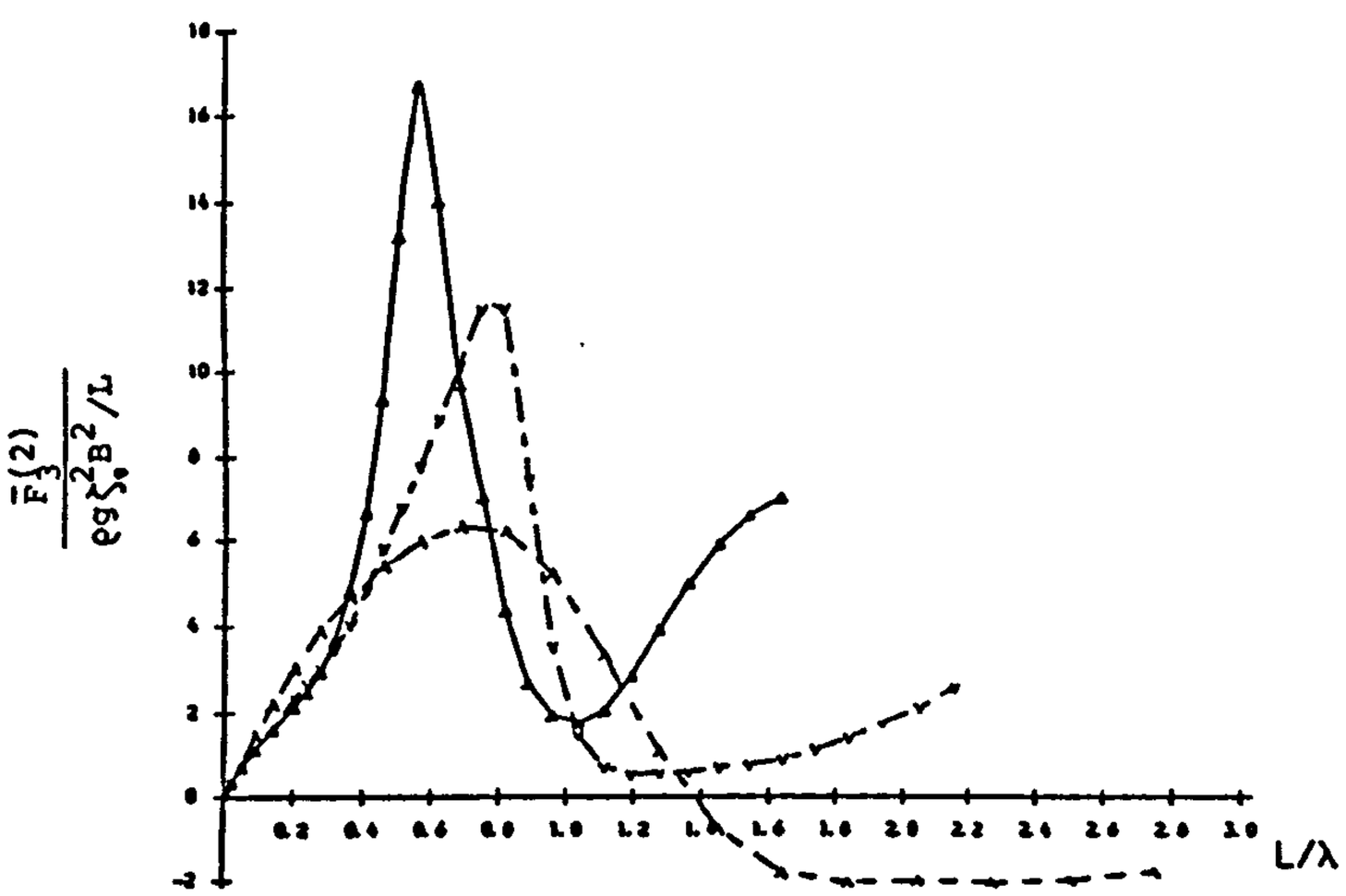

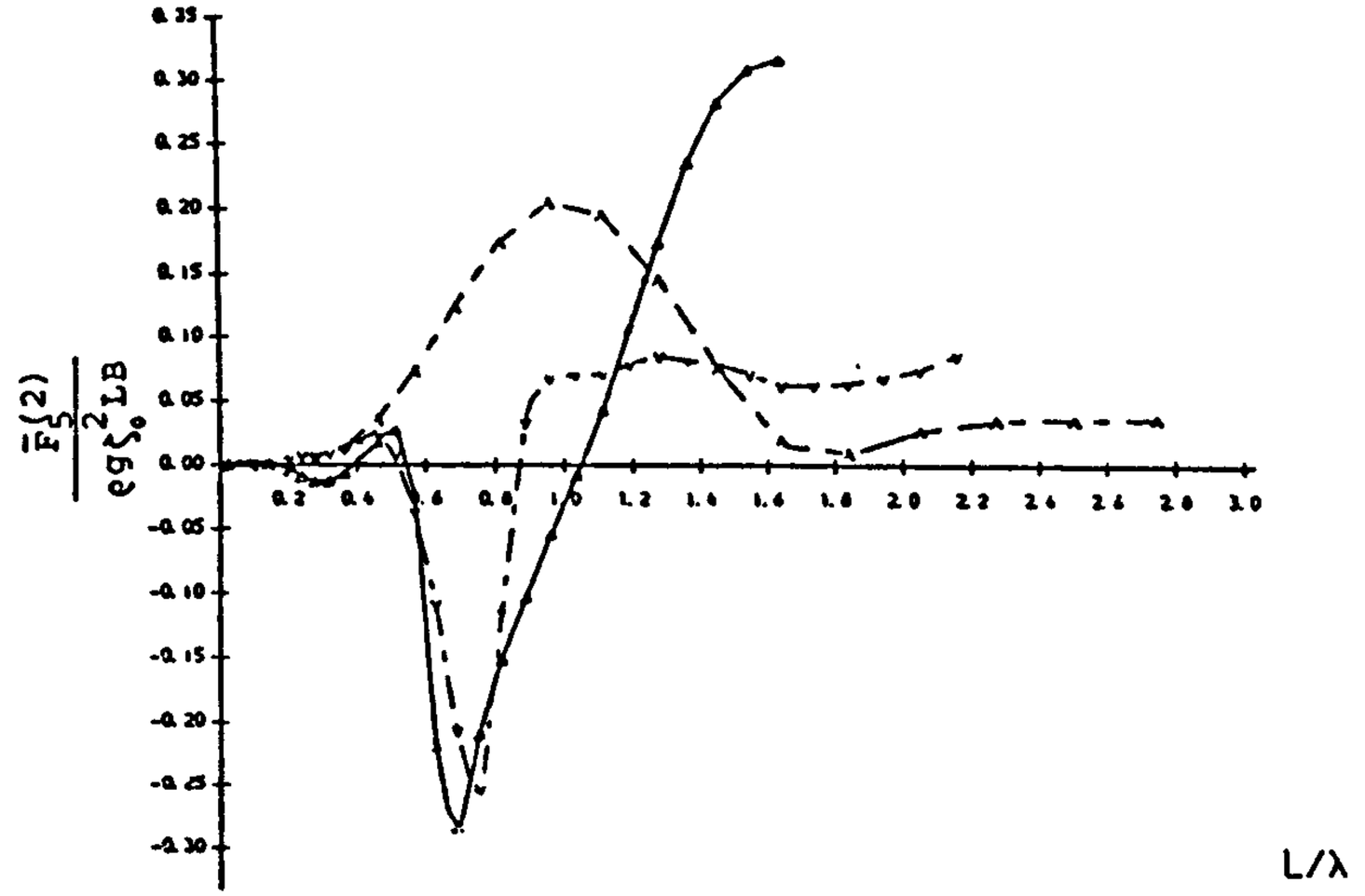

Fig.7.13 DRIFTING FORCES AND MOMENT FOR A SERIES-60 SHIP OF C_B=0.7 AT INFINITE WATER DEPTH AT VARIOUS FROUDE NUMBERS IN HEAD WAVES.

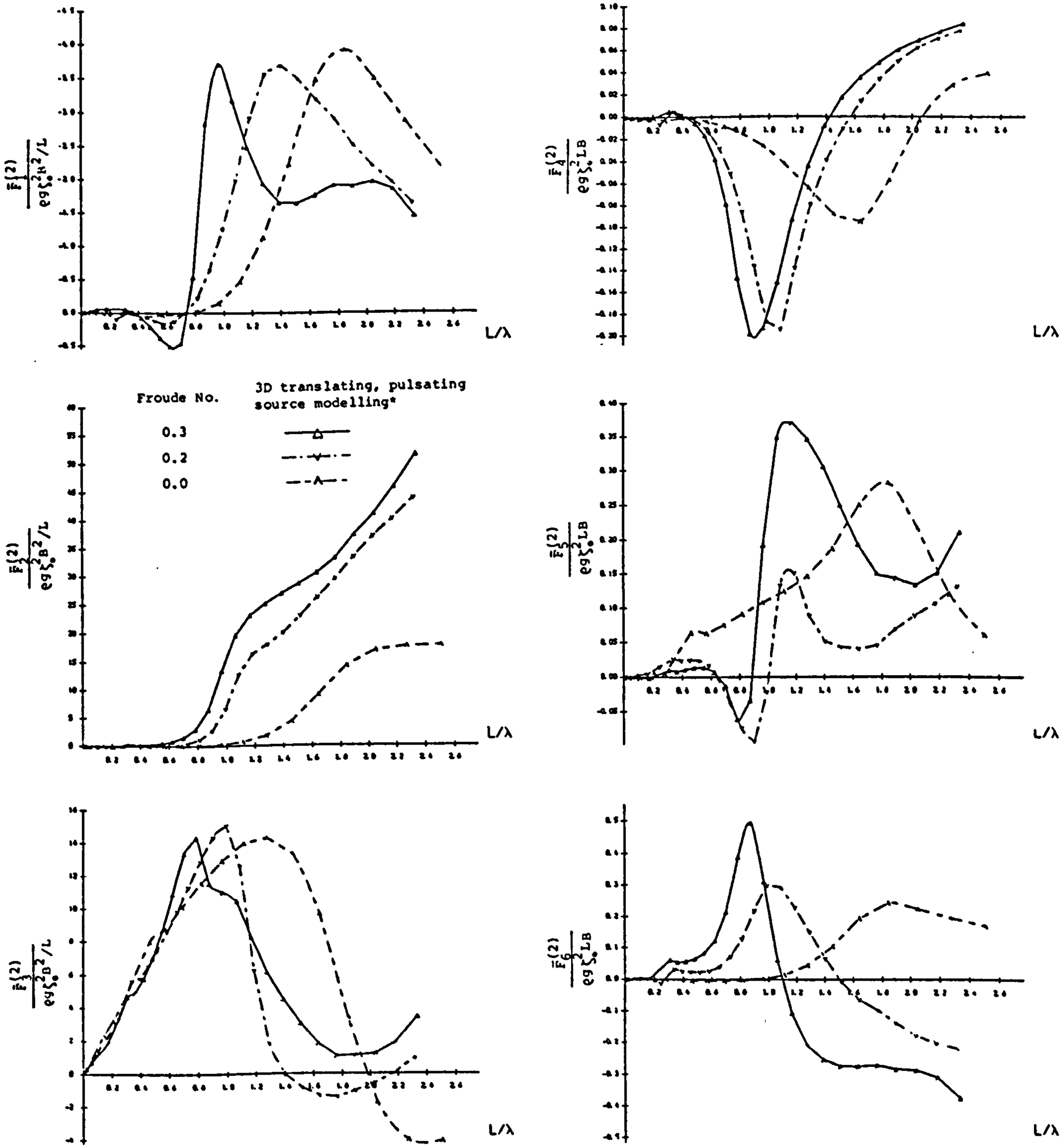

Fig.7.14 DRIFTING FORCES AND MOMENTS FOR A SERIES-60 SHIP OF C_B=0.7 AT INFINITE WATER DEPTH AT VARIOUS FROUDE NUMBERS IN ANGLE 120° OF WAVE INCIDENCE.

CHAPTER 8

CONCLUDING REMARKS

It has been noted in the theoretical formulation of the unsteady forward motion problem that the non-linear free surface and body boundary conditions make the problem unamenable to obtain analytical or numerical solutions because not only these two conditions are non-linear but also the exact free surface and wetted body surface are unknown beforehand. Therefore these two conditions are systematically transformed from the exact surface to the mean surface under the context of perturbation analysis. Nevertheless the first-order free surface condition for the unsteady forward motion problem is expressed in terms of the unsteady potential and steady potential. This first-order free surface condition is still difficult to solve analytically. A further simplification can be made to reduce the effects of the steady perturbation flow on the free surface by making an assumption that the body is slender or fully submerged. This results in a linearised free surface condition in terms of the forward speed and the frequency of oscillation. Under the assumption of small oscillatory motions, the unsteady forward motion problem can be decomposed into diffraction and radiation problems. The linearised body boundary condition for the radiation problem also contains various convective effects of steady perturbation flow due to forward speed. As long as the steady perturbation flow around the hull is as small as on the free surface, the linearised body boundary condition is reduced to a simple forward speed correction on the pitch and yaw motions.

The solution of the linearised unsteady forward motion problem is constructed by means of the Green function integral equation method. Thus the domain of the problem is reduced from the infinite fluid domain to the body surface on which source singularities are distributed. In the free surface wave field the convective effects of the forward speed are such that the free surface disturbances produced at the bow region

are convected downstream. In order to accommodate the three-dimensional convective effects in the free surface, the complete linearised free surface condition is used. This leads to the use of a translating pulsating source which is a function of the forward speed, frequency of oscillation and spatial coordinates. A distinct feature of the three-dimensional free surface flows due to the interactions of the forward speed U and the frequency of oscillation ω is the critical point $\tau=\omega U/g=1/4$. In the subcritical regime $\tau<1/4$, one wave group is progressing upstream and three wave groups are trailing behind the source. In the supercritical regime $\tau>1/4$, the wave group advancing in front of the source disappears and all wave groups are swept downstream. The wave patterns are strongly dependent on the forward speed and the frequency of oscillation. If the Froude number is low in comparison with the dimensionless frequency, the wave patterns are moon-like in the subcritical region or cut moon-like in the supercritical region. On the other hand a low frequency number associated with a high Froude number produces the Kelvin wave patterns. If the frequency of oscillation is zero, the translating source is a Kelvin source function which generates pure Kelvin wave groups. In the limit of zero forward speed the source becomes pure oscillatory and the wave patterns are ring waves radiating in all horizontal directions. At shallow water depths, the depth effect on the wave patterns makes the wave length shorter and so the flow regime is shifted towards supercritical.

The numerical computations for the fully submerged and semi-submerged ellipsoids show that their hydrodynamic coefficients are strongly speed dependent. The forward speed cross coupled hydrodynamic coefficients satisfy the Timman-Newman relationships very well for the fully submerged ellipsoid but not so well for the semi-submerged ellipsoid where discrepancies may be attributed to weak singularities on the free surface line integral. The forward speed hydrodynamic coefficients in symmetrical modes of motion are singular at a localised frequency corresponding to $\tau=1/4$. This singular behaviour is due to the singularity in the forward speed free surface Green function at the critical point $\tau=1/4$. However those coefficients in anti-symmetrical modes of motion are not noticeably affected by this singularity.

Comparisons of the calculated and measured principal hydrodynamic coefficients and wave excitation forces display excellent agreement for the stationary Series-60 ship in deep water and the stationary 200,000 dwt tanker in shallow water. However, for the roll damping, there are some unresolved discrepancies between the potential theory and experiments. The calculated cross coupled hydrodynamic coefficients for zero speed case agree very well with the Timman-Newman's symmetry relationship. When the hydrodynamic coefficients calculated by the three-dimensional translating pulsating source modelling and three-dimensional oscillating source modelling with simple speed correction in pitch and yaw motions for the Series-60 ship advancing in deep water are compared with the available experimental results, the correlations are not so good as those for the zero speed case. Both mathematical models do not predict a reasonable roll damping and pitch damping for the Series-60 ship with forward speed. Nevertheless the results obtained from the translating pulsating source modelling show the same trends as the measurements but those obtained from the oscillating source modelling do not. Forward speed wave excitation forces predicted by both models for head waves agree with each other and with the experimental data. However the translating pulsating source modelling gives better phase predictions.

Numerical calculations for the mean second-order forces and yaw moment on an ocean-going barge and a 200,000 dwt tanker without forward speed show that the three-dimensional source distribution technique combined with near-field method show good agreement with the measured values. The evaluations of the forward speed surge drifting forces (added resistances) on three Series-60 ships, with various block coefficients, advancing in head waves demonstrate that the results obtained from the three-dimensional translating pulsating source modelling agree better with the measurements than those obtained from the oscillating source modelling. The former shows a similar asymptotic trend as the measurements in short waves and predicts well the peaks of added resistances for these three ships but the latter underpredicts the measured added resistance values at high frequencies and overpredicts the peak of added resistance for the fine form ship with high speed.

In general the effects of water depth on the first-order and second-order wave forces are significant at water depth to ship's draught ratio less than 4.0. When the water is shallow these hydrodynamic forces are very sensitive to change in water depth at low frequencies. In very short waves the water depth effects are not important, even in shallow water.

Recommendation for future work

The three-dimensional source distribution technqiue has been shown to be a powerful tool to solve the unsteady forward motion problem. Continued efforts in this line of research are a very worthwhile. These efforts include a development of efficient algorithms to replace the numerical evaluation of the integrals in the expression for the translating pulsating source potential and its derivatives. The full expressions for m-terms in the body boundary condition which results from consistent linearisation of the body motions within the steady velocity field should be used in future development. The m-terms are difficult to implement since one needs to solve the Neumann-Kelvin problem. In order to overcome this difficulty efficient algorithms for computing a translating source potential and its derivatives up to second order are needed.

REFERENCES

Abramowitz,M. and Stegun,I.A. (1972)
Handbook of Mathematical Functions, Dover Publications, New York.

Ankudinov,V.K. (1969)
"Non-peridical Forces and Moments on a Ship in Waves", International Shipbuilding Progress, Vol. 16, pp. 199-204.

Ankudinov,V.K. (1972)
"The Added Resistance of a Moving Ship in Waves", International Shipbuilding Progress, Vol.19, pp.402-414.

Baar,J.J.M. and Price,W.G. (1988)
"Evaluation of the Wavelike Disturbance in the Kelvin Wave Source Potential", Journal of Ship Research, Vol.32, No.1, pp.44-53.

Beukelman,W. and Gerritsma,J. (1982)
"The Distribution of Hydrodynamic Mass and Damping of an Oscillating Shipform in Shallow Water", International Shipbuilding Progress, Vol.29, pp.297-315.

Beukelman,W., Huijsmans,R.H.M. and Keuning,P.J. (1984)
"Calculation methods of Hydrodynamic Coefficients of Ships in Shallow Water", International Shipbuilding Progress, Vol.31, pp.209-223.

Børresen,R. and Faltinsen,O.M. (1984)
"Ship Motions in Shallow Water by Unified Theory", Proceedings of 15th Symposium on Naval Hydrodynamics, pp.51-65.

Bowers,E.C. (1976)
"Long Period Oscillations of Moored Ships Subject to Short Wave Seas", Trans.RINA, Vol. 118, pp.181-191.

Brand,L. (1957)
Vector Analysis, John Wiley & Sons, Inc.

Breit,S.R. (1985)
"A Higher-Order Panel Method for Surface Wave Radiation and Diffraction by A Spheroid", Proceedings of 4th International Conference on Numerical Ship Hydrodynamics, Washington D.C., pp.200-215.

Burton,A.J. and Miller,G.F. (1971)
"The Application of Integral Equation Methods to the Numerical Solution of Some Exterior Boundary-value Problems", Proceedings of the Royal Society of London, Series A, Vol.323, pp.201-220.

Chan,H.S. (1989)
"Green function in the Theory of Steady Forward Motion", Report No.NAOE-89-21, Dept.NAOE, University of Glasgow.

Chang,M.S. (1977)
"Computations of Three-Dimensional Ship-Motions with Forward Speed", Second International Conference on Numerical Ship Hydrodynamics, University of California, Berkeley, pp.124-135.

Chang,M.S. and Pien,P.C. (1976)
"Velocity Potentials of Submerged Bodies Near a Free Surface - Application to Wave-Excited Forces and Motions", Proceedings of 11th Symposium on Naval Hydrodynamics, London, pp.545-554.

Chapman,R.B. (1977)
"Survey of Numerical Solutions for Ship Free-Surface Problems", Second International Conference on Numerical Ship Hydrodynamics, University of California, Berkeley

Clauss,G. and Sukan,M. (1982)
"Drift forces and compact offshore structures in regular and irregular waves", Applied Ocean Research, Vol.4, No.4, pp.208-218.

Dawson,C.W. (1977)
"A Practical Computer Method for Solving Ship-Wave Problems", Second International Conference on Numerical Ship Hydrodynamics, University of California, Berkeley, pp.30-38.

De Jong,B. (1969)
"Computation of the Hydrodynamics Coefficients of Oscillating Cylinders", Delft University of Technology, Shipbuilding Lab., Report No. 174A.

Doctors,L.J. and Beck R.F. (1987)
"Numerical Aspects of the Neumann-Kelvin Problem", Journal of Ship Research, Vol.31, No.1, pp.1-13.

Endo H. (1987)
"Shallow-Water Effect on the Motions of Three-Dimensional Bodies in Waves", Journal of Ship Research, Vol.31, No.1, pp.34-40.

Faltinsen,O.M. (1974)
"A Numerical Investigation of the Ogilvie-Tuck Formulas for Added-Mass and Damping Coefficients", Journal of Ship Research, Vol.18, No.2, pp.73-84.

Faltinsen,O.M. and Løken,A.E. (1979)
"Slow Drift Oscillations of a Ship in Irregular Waves", Det norske Veritas Publication No.108.

Faltinsen,O.M. and Michelsen,F.C. (1974)
"Motions of Large Structures in Waves at Zero Froude Number", International Symposium on Dynamics of Marine Vehicles and Structures in Waves, University of College, London, pp.91-106.

Faltinsen,O.M. and Børresen,R. (1984)
"Ship Motions in Shallow Water by Unified Theory", Proceedings of 15th Symposium on Naval Hydrodynamics, Hamburg, pp.51-65.

Faltinsen,O.M., Minsaas,K.J., Lispis,N. and Skjordal,S.O. (1980)
"Prediction of Resistance and Propulsion of a Ship in a Seaway", Proceedings of 13th Symposium on Naval Hydrodynamics, pp.505-529.

Faltinsen,O.M. and Sortland,B. (1987)
"Slow drift eddy making damping of a ship", Applied Ocean Research, Vol.9, No.1, pp.37-46.

Faltinsen,O.M. and Zhao,R. (1989)
"Slow-Drift Motions of a Moored Two-Dimensional Body in Irregular Waves", Journal of Ship Research, Vol.33, No.2, pp.93-106.

Frank,W. (1967)
"Oscillation of Cylinders in or below the Free Surface of Deep Fluids", NSRDC, Report No. 2375, Washington D.C.

Froude,W. (1861)
"On the Rolling of Ships", Trans.INA, Vol.2, p.180.

Fujii,H. and Takahashi,T. (1975)
"Experiment study on the resistance increase of a ship in regular oblique waves", Proceedings 14th ITTC, Vol.4, pp.351-360.

Garrison,C.J. (1978)
"Hydrodynamic Loading of Large Structures: Three-Dimensional Source Distribution Methods", Chapter 3 of "Numerical methods in Offshore Engineering", pp.87-140.

Gerritsma,J. and Beukelman,W. (1964)
"The Distribution of the Hydrodynamic Forces on a Heaving and Pitching Ship Model in Still Water", Report No.61 S, Netherlands' Research Centre T.N.O. for Shipbuilding and Navigation.

Gerritsma,J. and Beukelman,W. (1967)
"Analysis of the Modified Strip Theory for the Calculation of Ship Motions and Wave Bending Moments", International Shipbuilding Progress, Vol. 14, pp.319-337.

Gerritsma,J. and Beukelman,W. (1972)
"Analysis of the Resistance Increase in Waves of a Fast Cargo Ship", International Shipbuilding Progress, Vol.19, pp.285-293.

Guevel,P. and Bougis,J. (1982)
"Ship-Motions with Forward Speed in Infinite Depth", International Shipbuilding Progress, Vol.29, pp.103-117.

Haskind,M.D. (1946)
"The Hydrodynamic Theory of Heaving and Pitching of a Ship", Translated in SNAME Tech. & Res. Bull. No.1-12, 1953.

Havelock,T.H. (1932)
"The Theory of Wave Resistance", Proceedings Royal Society of London, Series A, Vol.138, pp.339-348.

Havelock,T.H. (1940)
"Waves produced by the Rolling of a Ship", Philosophical Magazine, Vol.29, Series 7, p.407.

Havelock,T.H. (1942)
"The Damping of the Heaving and Pitching Motion of a Ship", Philosophical Magazine, Vol.33, Series 7, p.666.

Havelock,T.H. (1942a)
"The Drifting Force on a Ship among Waves", Philosophical Magazine,Vol.33.

Havelock,T.H. (1958)
"The effect of speed of advance upon the damping of heave and pitch", Trans.RINA.,Vol.100, pp.131-135.

Hearn,G.E. (1977)
"Alternative Methods of Evaluating Green's Function in Three-Dimensional Ship-Wave Problems", Journal of Ship Research, Vol.21, No.2, pp.89-93.

Hearn,G.E., Tong,K.C. and Lau,S.M. (1987)
"Sensitivity of Wave Drift Damping Coefficient Predictions to the Hydrodynamic Analysis Models used in the Added Resistance Gradient Method", Proceeding of 6th Symposium International Offshore Mechanics and Artic Engineering, Vol.2, pp.213-225.

Hearn,G.E. and Tong,K.C. (1988)
"Added Resistance Gradient Versus Drift Force Gradient - Based Predictions of Wave Drift Damping", International Shipbuilding Progress, Vol.35, pp.155-181.

Hess,J.L. and Smith,A.M.O. (1962)
"Calculation of Nonlifting Potential Flow About Arbitrary Three-Dimensional Bodies", Douglas Aircraft Company Report No.ES 40622. Also see Journal of Ship Research, Vol.8, No.2, pp.22-44, 1964.

Hess,J.L. and Smith,A.M.O.(1967)
"Calculation of Potential Flow about Arbitrary Bodies", Progress in Aeronautical Sciences, Vol.8, pp.1-136.

Hogben,N. and Standing R.G. (1974)
"Wave Loads on Large Bodies", International Symposium on Dynamics of Marine Vehicles and Structures in Waves, University of College, London, pp.258-277.

Hong,Y.S. (1983)
"Drift forces and moment on SWATH ship in oblique waves", Proceedings of International Workshop on Ship and Platform, University of California, Berkeley, pp.266-281.

Hong,Y.S. (1986)
"Heave and Pitch Motions of SWATH Ships", Journal of Ship Research, Vol.30, No.1, pp.12-25.

Hosoda,R. (1973)
"The Added Resistance of Ships in Regular Oblique Waves", Journal of the Society of Naval Architects of Japan, Vol.133, pp.1-20.

Hu,P.N. and Eng,K. (1966)
"Drifting Force and Moment on Ships in Oblique Waves", Journal of Ship Research, Vol. 10, No.1, pp.18-24.

Huijsmans,R.H.M. and Dallinga,R.P. (1983)
"Non-Linear Ship Motions in Shallow Water", Proceedings of International Workshop on Ship and Platform Motions, University of California, Berkeley, pp.321-339.

Inglis,R.B. and Price,W.G. (1980)
"Motions of Ships in Shallow Water", Trans.RINA.,Vol.122, pp.269-284.

Inglis,R.B. and Price,W.G. (1980a)
"Comparison of calculated responses for arbitrary shaped bodies using two and three-Dimensional Theories", International Shipbuilding Progress, Vol.27, pp.86-95.

Inglis,R.B. and Price,W.G. (1981)
"Calculation of the Velocity Potential of a Translating, Pulsating Source", Trans.RINA., Vol.123, pp.163-175.

Inglis,R.B. and Price,W.G. (1981a)
"The influence of speed dependent boundary conditions in three dimensional ship motion problems", International Shipbuilding Progress, Vol.28, pp.22-29.

Inglis,R.B. and Price,W.G. (1981b)
"Irregular frequencies in three dimensional source distribution techniques", International Shipbuilding Progress, Vol.28, pp.57-62.

Inglis,R.B. and Price,W.G. (1982)
"A Three Dimensional Ship Motion Theory Comparison between Theoretical Predictions and Experimental Data of the Hydrodynamic Coefficients with Forward Speed", Trans. RINA., Vol.124., pp.141-156.

Jensen,S.P. (1987)
"On the Numerical Radiation Condition in the Steady-State Ship Wave Problem", Journal of Ship Research, Vol.31, No.1, pp.14-22.

John,F. (1949)
"On the Motion of Floating Bodies. I", Communications on Pure and Applied Mathematics, Vol.2, pp.13-57.

John,F. (1950)
"On the Motion of Floating Bodies. II. Simple Harmonic Motions", Communications on Pure and Applied Mathematics,Vol.3, pp.45-101.

Kaplan,P. (1983)
"Simplified Three-Dimensional Method for Calculating Drift Forces on Ships and Semisubmersibles in Waves", Proceedings of International Workshop on Ship and Platform Motions, University of California, Berkeley, pp.305-320.

Kelvin, Lord (1887)

"On the waves produced by a single impulse in water of any depth, or in a dispersive medium", Proceedings of the Royal Society of London, Series A, Vol.42, pp.80-85.

Kim,C.H. and Bao,W. (1985)

"A Strip Method for Lateral Drift Force of a Semi-submersible", Journal of Energy Resources Technology, Vol.107, pp.329-334.

Kim,C.H. and Chou,F. (1973)

"Prediction of Drifting Force and Moment on an Ocean Platform Floating in Oblique Waves", International Shipbuilding Progress, Vol.20, pp.388-401.

Kim,C.H., Chou,F.S., Tien,D. (1980)

"Motions and Hydrodynamic Loads of a Ship Advancing in Oblique Waves", SNAME Transactions, Vol.88, pp.225-256.

Kim,M.H. and Yue,K.P. (1988)

"The Nonlinear Sum-Frequency Wave Excitation and Response of a Tension-Leg Platform", BOSS.

Kim,W.D. (1965)

"On the harmonic oscillations of a rigid body on a free surface", Journal of Fluid Mechanics, Vol.21, Part 3, pp.427-451.

Kim,W.D. (1966)

"On a Free-Floating Ship in Waves", Joural of Ship Research, Vol.10, No.3, pp.182-200.

Kinsman,B. (1965)

Wind Waves, Dover Publications, Inc., 1984.

Kochin,N.E. (1939)

"The Two-Dimensional Problem of Steady Oscillations of Bodies under the Free-Surface of a Heavy Incompressible Fluid", Translated in SNAME Tech. & Res. Bull. No.1-9., 1952.

Korvin-Kroukovsky,B.V. (1955)
"Investigation of Ship Motions in Regular Waves," Trans.SNAME, Vol.63, pp.386-435.

Korvin-Kroukovsky,B.V. and Jacobs,W.D. (1957)
"Pitching and Heaving Motions of a Ship in Regular Waves", Trans.SNAME, Vol.65, p.590-632.

Krylov,A.N. (1896)
"A New Theory of Pitching of Ships on Waves and of Stress produced by this Motion", Trans.INA, Vol.37, pp.326-368.

Lamb,H. (1932)
Hydrodynamics, Dover Publications, New York, 1945.

Lau,S.M. (1987)
"Three-Dimensional Hydrodynamic Analysis of First & Second Order Forces on Free Floating Structures with Forward Speed", Ph.D. Thesis, Department of Naval Architecture and Shipbuilding, University of Newcastle Upon Type, England.

Lee,C.M. and Newman,J.N. (1971)
"The Vertical Mean Force and Moment of Submerged Bodies Under Waves", Journal of Ship Research, Vol. 15, No.3, pp.231-245.

Lenoir,M. and Richer,J. (1985)
"A Localized Finite Element Method Applied to The 3-D Seakeeping Problem", Proceedings of 4th Fourth International Conference on Numerical Ship Hydrodynamics, Washington D.C., pp.164-174.

Lewis,F.M. (1929)
"The Inertia of Water Surrounding a Vibrating Ship", Trans.SNAME, Vol.37.

Liapis,S. and Beck,R.F. (1985)
"Seakeeping Computations using Time-Domain Analysis", Proceedings of 4th International Conference on Numerical Ship Hydrodynamics, Washington D.C., pp.34-55.

Lighthill,J. (1978)

Waves in Fluids, Cambridge University Press.

Lighthill,M.J. (1967)

"On waves generated in dispersive systems by travelling forcing effects, with applications to the dynamics of rotating fluids", Journal of Fluid Mechanics, Vol.27, pp.725-752.

Lin,W.C. and Reed,A.M. (1976)

"The Second Order Steady Force and Moment on a Ship Moving in an Oblique Seaway", Proceeings of 11th Symposium on Naval Hydrodynamics, London, pp.333-351.

Lockwood-Taylor,J. (1930)

"Some Hydrodynamical Inertia Coefficients", Philosophical Magazine, Vol.9, Series 7, p.161.

Loeser,D.J., Yue,D.K. and Salvensen,N. (1982)

"Slender-Body Calculations of Large-Amplitude Ship Motions", Proceedings of 14th Symposium on Naval Hydrodynamics, University of Michigan, pp.383-414.

Lunde,J.K. (1952)

"On the Linearized Theory of Wave Resistance for Displacement Ships in Steady and Accelerated Motion", Trans.SNAME.,Vol.59, pp.25-85.

Manning,G.C. (1939)

"The Motions of Ships Among Waves", Principles of Naval Architecture, Vol.2, p.1, SNAME, New York.

Marthinsen,T. (1983)

"Calculation of slowly varying drift forces", Applied Ocean Research, Vol.5, No.3, pp.141-144.

Maruo,H. (1960)

"The Drift of a Body Floating on waves", Journal of Ship Research, Vol.4, No.3, pp.1-10.

Maruo,H. (1963)
"Resistance in Waves", the Society of Naval Architects of Japan, 60th Anniversary Series, Vol.8, Chapter 5.

Maruo,H. (1985)
"A Method of Computation for Steady Ship Waves with Non-linear Free Surface Conditions", Proceedings of 4th International Conference on Numerical Ship Hydrodynamics, Washington D.C., pp.218-233.

Maruo,H. and Iwase,K. (1980)
"Calculation of Added Resistance in Oblique Waves", Journal of the Society of Naval Architects of Japan, Vol.147, pp.36-43.

Matsui,T. (1988)
"Computation of Slowly Varying Second Order Hydrodynamic Forces on Floating Structures in Irregular Waves", Proceeding of 7th International Offshore Mechanics and Artic Engineering Symposium, Vol.2., pp.117-124.

Mavrakos,S.A. (1988)
"The vertical drift force and pitch moment on axisymmetric bodies in regular waves", Applied Ocean Research, Vol. 10, No.4, pp.207-218.

Mei,C.C. (1987)
"Numerical Methods in Water-Wave Diffraction and Radiation", Annual Review of Fluid Mechanics, Vol.10, pp.393-416.

Michell,J.H. (1898)
"The Wave Resistance of a Ship", Philosophical Magazine,Vol.45,pp.106-123.

Milne-Thomson,L.M. (1968)
Theoretical Hydrodynamics, The Macmillan Press Ltd.

Molin,B. (1979)
"Secon-order diffraction loads upon three-dimensional bodies", Applied Ocean Research, Vol.1, No.4, pp.197-202.

Molin,B. (1983)
"On Second-Order Motion and Vertical Drift Forces for Three Dimensional Bodies in Regular Waves", Proceedings of International Workshop on Ship and Platform, University of California, Berkeley, pp.344-362.

Monacella,V.J. (1966)
"The Disturbance due to a Slender Ship Oscillating in Waves in a Fluid of Finite Depth", Journal of Ship Research, Vol.10, pp.242-252.

Newman,J.N. (1961a)
"A Linearised Theory for the Motion of a Thin Ship in Regular Waves", Journal of Ship Research, Vol.3, pp.34-55.

Newman,J.N. (1961b)
"The Damping of an Oscillating Ellipsoid Near a Free Surface", Journal of Ship Research, Vol.3, pp.44-58.

Newman,J.N. (1962)
"The Exciting Forces on Fixed Bodies in Waves", Journal of Ship Research, Vol.5, pp.10-17.

Newman,J.N. (1965)
"The Exciting Forces on a Moving Body in Waves", Journal of Ship Research, Vol.9, pp.190-199.

Newman,J.N. (1967)
"The Drift Force and Moment on Ships in Waves", Journal of Ship Research, Vol.11, No.1, pp.51-60.

Newman,J.N. (1970)
"Applications of Slender-Body Theory in Ship Hydrodynamics", Annual Review of Fluid Mechanics, Vol.2, pp.67-94.

Newman,J.N. (1974)
"Second-order, Slowly-varying Forces on Vessels in Irregular Waves", International Symposium on Dynamics of Marine Vehicles and Structures in Waves, University of College, London, pp.182-186.

Newman,J.N. (1977)
Marine Hydrodynamics, MIT press, Cambridge, Massachusetts.

Newman,J.N. (1978)
"The Theory of Ship Motions", Advances in Applied Mechanics, Vol.18, pp.221-283.

Newman,J.N. (1983)
"Three-Dimensional Wave Interactions with Ships and Platforms", Proceedings of International Workshop on Ship and Platform Motions, University of California, Berkeley, pp.418-442.

Newman,J.N. (1984a)
"Approximations for the Bessel and Struve Functions", Mathematics of Computation, Vol.43, No.168, pp.551-556.

Newman,J.N. (1984b)
"Double-Precision Evalustion of the Oscillatory Source Potential", Journal of Ship Research, Vol.28, No.3, pp.151-154.

Newman,J.N. (1984c)
"An expansion of the oscillatory source potential", Applied Ocean Research, Vol.6, pp.116-117.

Newman,J.N. (1985a)
"Algorithms for the free-surface Green function", Journal of Engineering Mathematics, Vol.19, pp.57-67.

Newman,J.N. (1985b)
"The evaluation of Free-Surface Green Functions", Proceedings of 4th International Conference on Numerical Ship Hydrodynamics, Washington D.C., pp.4-23.

Newman,J.N. (1987a)
"Evaluation of the Wave-Resistance Green Function: Part 1 - The Double Integral", Journal of Ship Research, Vol.31, No.2, pp.79-90.

Newman,J.N. (1987b)

"Evaluation of the Wave-Resistance Green Function: Part 2 - The Single Integral on the Centerplane", Journal of Ship Research, Vol.31, No.3, pp.145-150.

Newman,J.N. (1989)

"The Numerical Towing Tank - Fact or Fiction ?", 11th Georg Weinblum Memorial Lecture, Schiffstechnik Bd.36, pp.155-168.

Newman,J.N. and Sclavounos,P.D. (1980)

"The Unified Theory of Ship Motions", Proceedings of 13th Symp. Naval Hydrodynamics, Tokyo, Japan.

Newman,J.N. and Sclavounos,P.D. (1988)

"The Computation of Wave Loads on Large Offshore Structures", pp.605-619.

Newman,J.N. and Tuck,E.O. (1964)

"Current Progress in the Slender-Body Theory of Ship Motions", Proceedings of 5th Symp.Naval Hydrodynamics, ACR-112, pp.129-167, Washington D.C.

Noblesse,F. (1977)

"The Fundamental Solution in the Theory of Steady Motion of a Ship", Journal of Ship Research, Vol. 21, No.2, pp.82-88.

Nobesse,F. (1978a)

"The Steady Wave Potential of a Unit Source, at the Centerplane", Journal of Ship Research, Vol.22, No.2, pp.80-88.

Noblesse,F. (1978b)

"On the Fundamental Function in the Theory of Steady Motion of Ships", Journal of Ship Research, Vol.22, No.4, pp.212-215.

Noblesse,F. (1981)

"Alternative integral representations for the Green function of the theory of ship wave resistance", Journal of Engineering Mathematics, Vol.15, No. 4, pp.241-265.

Nobesse,F. (1982)
"The Green function in the theory of radiation and diffraction of regular water waves by a body", Journal of Engineering Mathematics, Vol.16, pp.137-169.

Noblesse,F. (1983a)
"A Slender-Ship Theory of Wave Resistance", Journal of Ship Research, Vol.27, No.1, pp.13-33.

Noblesse,F. and Triantafyllou,G. (1983b)
"Explicit Approximations for Calculating Potential Flow About a Body", Journal of Ship Research, Vol.27, No.1, pp.1-12.

Odabasi,A.Y. and Hearn,G.E. (1977)
"Sea Keeping Theories: What is the Choice?", North East Coast Institution of Engineers and Shipbuilders Transactions, Vol.94, pp.53-84.

Ohmatsu,S. (1975)
"On the Irregular Frequencies in the Theory of Oscillating Bodies", Papers of Ship Research Institute, No.48.

Ogawa,A. (1967)
"The Drifting Force and Moment on a Ship in Oblique Regular Waves", International Shipbuilding Progress, Vol.14, pp.34-40.

Ogilvie,T.F. (1974)
"Fundamental Assumptions in Ship-motion Theory", International Symposium on Dynamics of Marine Vehicles and Structures in Waves, University of College, London, pp.135-145.

Ogilvie,T.F. (1983)
"Second-Order Hydrodynamic Effects on Ocean Platforms", Proceedings of International Workshop on Ship and Platform Motions, University of California, Berkeley, pp.205-265.

Ogilvie,T.F. and Shin,Y.S. (1978)
"Integral equation solutions for time-dependent free surface problems", Journal of Society of Naval Architects of Japan, Vol.143, pp.41-51.

Ogilvie,T.F. and Tuck,E.O. (1969)
"A Rational Strip Theory for Ship Motions," Part 1, Report No.013, Dept.NAME, University of Michigan.

Patterson,T.N.L. (1968)
"The Optimum Adddition of Points to Quadrature Formulae", Mathematics of Computation, Vol.22, pp.847-856.

Peters,A.S. and Stoker,J.J. (1957)
"The Motion of a Ship, as a Floating Rigid Body, in a Seaway", Communications on Pure and Applied Mathematics, Vol.10, pp.399-490.

Pinkster,J.A. (1974)
"Low Frequency Phenomena Associated with Vessels Moored at Sea", Paper SPE 4837, European Spring Meeting of SPE-AIME, Amsterdam.

Pinkster,J.A. (1979)
"Mean and Low Frequency Wave Drifting Forces on Floating Structures", Ocean Engineering, Vol.6, pp.593-615.

Pinkster,J.A. (1980)
"Low frequency second order wave exciting forces on floating structures",NSMB, Wageningen, publication no.650.

Porter,W.R. (1960)
"Pressure Distributions, Added Mass and Damping Coefficients for Cylinders Oscillating in a Free Surface", University of California, Inst. of Eng. Res., Series No.82, Issue No. 16.

Rahman,M. (1984)
"Wave diffraction by large offshore structures: an exact second-order theory", Applied Ocean Research, Vol.6, No.2, pp.90-100.

Remery,G.F.M. and Hermans,A.J. (1972)
"The Slow Drift Oscillations of a Moored Object in Random Seas", Society of Petroleum Engineers Journal 1972, pp.191-198.

Salvesen,N. Tuck,E.O. and Faltinsen,O.M. (1970)
"Ship Motions and Sea Loads", Trans.SNAME, Vol.78, pp.250-287.

Salvesen,N. (1974)
"Second-order Steady-state Forces and Moments on Surface Ships in Oblique Regular Waves", International Symposium on Dynamics of Marine Vehicles and Structures in Waves, University of College, London.

Sayer,P. and Ursell,F. (1976)
"On the Virtual Mass, at Long Wavelengths, of a Half-Immersed Circular Cylinder Heaving on Water of Finite Depth", Proceedings of 11th Symposium on Naval Hydrodynamics, London, pp.529-532.

Sayer,P. and Ursell,F. (1977)
"Integral-Equation Methods for Calculating the Virtual Mass in Water of Finite Depth", Second International Conference on Numerical Ship Hydrodynamics, University of California, Berkeley, pp.176-184.

Schmitke,R.T. (1978)
"Ship Sway, Roll, and Yaw Motions in Oblique Seas", Trans.SNAME, Vol.86, pp.26-46.

Sclavounos,P.D. (1983)
"Energy Relations in Slender-Ship Theory", Proceedings of International Workshop on Ship and Platform Motions, University of California, Berkeley, pp.467-490.

Sclavounos,P.D. (1984a)
"The Unified Slender-Body Theory : Ship Motions in Waves", Proceedings of 15th Symposium on Naval Hydrodynamics, Hamburg, pp.177-193.

Sclavounos,P.D. (1984b)
"The Diffraction of Free-Surface Waves by a Slender Ship", Journal of Ship Research, Vol.28, No.1, pp.29-47.

Sclavounos,P.D. (1985)
"Forward-Speed Vertical Wave Exciting Forces on Ships", Journal of Ship Research, Vol.29, No.2, pp.105-111.

Sclavounos,P.D. and Lee,C.M. (1985)
"Topics on Boundary-Element Solutions of Wave Radiation-Diffraction Problems", Proceedings of 4th International Conference on Numerical Ship Hydrodynamics, Washington D.C, pp.175-184.

Shen,H.T. and Farell,C. (1977)
"Numerical Calculation of the Wave Integrals in the Linearized Theory of Water Waves", Journal of Ship Research, Vol.21, No.1, pp.1-10.

Smith,W.E. (1967)
"Computation of Pitch and Heave Motions for Arbitrary Ship Forms", International Shipbuilding Progress, Vol.14, pp.267-291.

Sommerfeld,A. (1949)
Partial Differential Equations in Physics, Academic Press Inc.

St. Denis,M and Pierson,W.J. (1953)
"On the motions of ships in confused seas", Trans.SNAME, Vol.61, pp.280-357.

Stoker,J.J. (1957)
Water Waves, Interscience Publishers.

Standing,R.G. Dacunha,N.M.C. and Matten,R.B. (1981a)
"Mean Wave Drift Forces : Theory and Experiment", National Maritime Institute Report No.R124.

Standing,R.G. Dacunha,N.M.C. and Matten,R.B. (1981b)
"Slowly-Varying Second-Order Wave Forces : Theory and Experiment", National Maritime Insitute Report No.R138.

Strom-Tejsen,J. Yeh,H. and Moran,D.D. (1973)
"Added Resistance in Waves", Trans.SNAME, Vol. 81, pp.109-143.

Stuntz,G.R. and Taylor R.J. (1964)
"Some Aspects of Bow Thruster Design", Trans.SNAME,Vol.72, pp.336-373.

Suyehiro,K. (1924)
"On the Drift of Ships caused by Rolling among Waves", Trans.INA., Vol.66.

Suzuki,K. (1985)
"Boundary Integral Equation Method For The Linear Wave Resistance Problem", Proceedings of the Fourth International Conference on Numerical Ship Hydrodynamics, Washington D.C., pp.308-323.

Takagi,M., Furukawa,H. and Takagi,K. (1983)
"On the Precision of Various Hydrodynamic Solutions of Two-Dimensional Oscillating Bodies", Proceedings of International Workshop on Ship and Platform Motions, University of California, Berkeley, pp.450-466.

Tanaka,H. and Kitagawa,H. (1962)
"On the study of characteristics of ship motions by a forced oscillation method (Part 1)", Journal ZK, Vol.111, p.92.

Tasai,F. (1959)
"On the Damping Force and Added Mass of ships Heaving and Pitching", Report of Research Inst. for Appl. Mech., Kyushu University, Vol. 7, No.26.

Telste,J.G. and Noblesse,F. (1986)
"Numerical Evaluation of the Green Function of Water-Wave Radiation and Diffraction", Journal of Ship Research, Vol.30, No.2, pp.69-84.

Telste,J.G. and Noblesse,F. (1988)
"The Non-oscillatory Near-field Term in the Green Function for Steady Flow about a Ship", Prceedings of 17th Symposium on Naval Hydrodynamics, Hague, Netherlands, pp.33-46.

Timman,R. and Newman,J.N. (1962)
"The Coupled Damping Coefficients of a Symmetric Ship", Journal of Ship Research, Vol.5, pp.1-7.

Ursell,F. (1949)
"On the heaving motion of a circular cylinder on the surface of a fluid", Quart. Joural of Mech. Appl. Math. Vol.2, pp.218-231.

Ursell,F. (1953)

"Short surface waves due to an oscillating immersed body, Proceedings of the Royal Society of London, Series A, Vol.220, pp.90-113.

Ursell,F. (1953a)

"Mass transport in gravity waves", Proceedings of the Cambridge Philosophical Society, Vol.49, pp.145-150.

Ursell,F. (1962)

"Slender oscillating ships at zero forward speed", Joural of Fluid Mechanics, Vol.19, pp.496-516.

Ursell,F. (1973)

"On the exterior problems of accoustic", Proceedings of the Cambridge Philosophical Society, Vol.74, pp.117-125.

Ursell,F. (1981)

"Irregular Frequencies and the Motion of Floating Bodies:, Journal of Fluid Mechanics, Vol.105, pp.143-156.

Van Leeuwen,G. (1964)

"The Lateral Damping and Added Mass of an Oscillating Shipmodel", Shipbuilding Laboratory, Delft, Publication No.23.

Van Oortmerssen,G. (1976)

"The Motions of a Moored Ship in Waves", NSMB,Wageningen, publication no. 510.

Vugts,J.H. (1971)

"The Hydrodynamic Forces and Ship Motions in Oblique Waves", Netherlands Ship Research Centre TNO, Report No.150 S.

Watanabe,Y. (1938)

"Some contribution to the theory of rolling", Trans.INA., Vol.80.

Webster,W.C. (1975)

"The Flow About Arbitrary, Three-Dimensional Smooth Bodies", Journal of Ship Research, Vol.19, No.4, pp.206-218.

Wehausen,J.V. (1971)
"The Motion of Floating Bodies", Annual Review of Fluid Mechanics, Vol.3, pp.237-268.

Wehausen,J.V. and Laitone,E.V. (1960)
"Surface Waves", Handbuch der Physik, Vol.9, Springer-Verlag, Berlin.

Wu,G.X. and Eatock-Taylor,R. (1987)
"A Green's Function Form for Ship Motions at Forward Speed", International Shipbuilding Progress, Vol.34, pp.189-196.

Wu,G.X. and Eatock Taylor,R. (1988)
"Reciprocity Relations for the Hydrodynamic Coefficients of Bodies with Forward Speed", International Shipbuilding Progress, Vol.35, pp.145-153.

Wu,G.X. and Eatock Taylor,R. (1989)
"On the Radiation and Diffraction of Surface Waves by Submerged Spheroids", Journal of Ship Research, Vol.33, No.2, pp.84-92.

Wu,X.J. and Price,W.G. (1986)
"An equivalent box approximation to predict irregular frequencies in arbitrarily-shaped three-dimensional marine structures", Applied Ocean Research, Vol.8, No.4, pp.223-231.

Yeung,R.W. (1982)
"Numerical Methods in Free-Surface Flows", Annual Review of Fluid Mechanics, Vol.14, pp.395-442.

Yeung,R.W. and Kim,S.H. (1984)
"A New Development in the Theory of Oscillating and Translating Slender Ships", Proceedings of 15th Symposium on Naval Hydrodynamics, Hamburg, pp.195-218.

Zhao,R. and Faltinsen,O.M. (1988)
"Interaction between waves and current on a two-dimensional body in the free surface", Applied Ocean Research, Vol.10, No.2, pp.87-99.